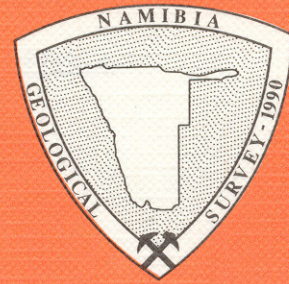


GEOLOGICAL SURVEY OF NAMIBIA

MINISTRY OF MINES AND ENERGY



**THE GEOLOGY AND GEOCHEMISTRY OF THE PROTEROZOIC
AWASIB MOUNTAIN TERRAIN, SOUTHERN NAMIBIA**

by

B.G. HOAL



MEMOIR 11

1990

Front cover: View southwards from the southern locality of the predominantly volcanic Haiber Flats Formation, Awasib Mountain terrain. This mountain rises some 500 m above the adjacent Namib sand sea (Quaternary in age) and constitutes one of the westernmost outcrops of the Proterozoic Sinclair Sequence. The Quiver tree in the foreground is rooted in scree from the cliff-like cooling unit of "rhyolite porphyry" (high-silica crystal-lithic tuff). Gneisses, schists and amphibolites of the underlying Kairab Complex form the ridges in the middle distance, while the mountains in the far distance constitute part of the Konipberg Formation (deformed correlate of the Sinclair Sequence?) and the Namaqualand Metamorphic Complex. The Cretaceous Dikker Willem carbonatite is barely visible in the left background.

MINISTRY OF MINES AND ENERGY
GEOLOGICAL SURVEY OF NAMIBIA

Director: R. McG. Miller

MEMOIR 11

**The geology and geochemistry of the Proterozoic
Awasib Mountain terrain, southern Namibia**

by

B.G. Hoal

Typesetting and layout: J. Angermund, B.G. Hoal

Obtainable from the Geological Survey
P.O. Box 2168, Windhoek, 9000, Namibia

	Price
Local (+ GST)	R 20.00
Abroad Post Free	R 25.00

ISBN 0 86976 233 8

Copyright reserved
1990

ABSTRACT

The middle to late Proterozoic Awasib Mountain terrain (AMT) straddles the boundary between the Rehoboth and Gordonia subprovinces in southern Namibia. The AMT is made up of two major crustal components, the older of which is correlated with the Namaqualand Metamorphic Complex (NMC), and the younger with the Sinclair Sequence.

The oldest part of the early-stage crust is represented by the amphibolite-grade Kairab Complex which has undergone three episodes of deformation (D_1 - D_3). Within this complex, high-alumina pillow-bearing basalts form part of a bimodal volcanic succession and yield an age of *ca.* 1460 Ma (Rb-Sr, Pb-Pb) with a low $^{87}\text{Sr}/^{86}\text{Sr}$ initial ratio (R_0) of 0.7027 ± 1 . While these basalts are characterised by the low contents of Ti, Nb, Zr, Y, Ni and Cr typical of island-arc or back-arc settings, low- and high-silica rhyolites display chondrite-normalised patterns (especially negative Th anomalies) which are also consistent with a subduction-related environment.

Younger metaluminous granitoids and gabbroids in the early-stage crust have undergone D_3 deformation and low-medium grade metamorphism. There is a close spatial and compositional association between the metavolcanic succession and these younger intrusive rocks. The association between gabbro, a mafic dyke swarm, pillow-bearing basalt, pyroclastic rhyolite and tonalite-trondhjemite resembles that of a dismembered ophiolite complex. Progressive intrusion of tonalite (Aunis Tonalite Gneiss; age 1271 ± 62 Ma, $R_0 = 0.7029 \pm 3$) to granite (Khorasib Granite Gneiss) reflects juvenile magma input followed by an increasing contribution from subcontinental within-plate mantle lithosphere and heterogeneous crust. Ocean-ridge granite (ORG)-normalised trace element patterns for the granitoid gneisses are typical of arc granites (i.e. enrichment in K, Rb, Ba and Th relative to Nb, Zr and Y) and suggest that the change in granitoid compositions records a progression from a primitive to mature (continental) arc or post-orogenic environment.

The late-stage crust of the AMT comprises both trough-hosted volcano-sedimentary successions and high-level intrusions which have undergone four episodes of deformation (D_4 - D_7), the most intense phase (D_5) being associated with greenschist facies metamorphism. Late bimodal dyke swarms constitute the youngest expression of magmatism in the AMT, but these dykes have been affected by the 07 phase of folding. In contrast, similar lithologies in the type area of the Sinclair Sequence are relatively undeformed and unmetamorphosed in comparison with the late-stage AMT crust.

The oldest sediments in the late-stage crust are represented by immature and poorly sorted clastic sediments of the Urusib Formation. Clasts (granitic and volcanic) are locally derived and sedimentary features suggest the intercalation of braided streamflow fans with lacustrine deposits. This typical rift succession reaches a maximum thickness of 2400 m.

The predominantly volcanic Haiber Flats Formation (HFF) overlies the Urusib Formation disconformably and has a minimum thickness of 3000 m. This bimodal succession occurs at three localities, or centres, all of which are dominated by rhyolites. Basaltic andesites are volumetrically important at an early stage, but andesites, dacites and rhyodacites are poorly represented. While porphyritic textures are characteristic of all volcanic types, pyroclastic textures are most common in the rhyolites. Stratified tuffites and volcanoclastic and clastic rocks typically make up $< 10\%$ of the HFF. Barby Formation basaltic andesites and tuffites are lithologically and compositionally similar to their counterparts in the HFF, but only occur in the eastern part of the AMT and are not in contact with the latter. Eruptive rocks of the HFF therefore constitute the most westerly occurrence of Sinclair volcanism and appear to be situated close to a palaeomargin.

Despite the presence of metamorphic biotite, compositions of relict plagioclase, pyroxene and titanomagnetite phenocrysts in HFF basaltic andesites are similar to their counterparts in orogenic basaltic andesites. Whole-rock compositions likewise show a strong similarity to calc-alkaline or high-K (not shoshonitic) volcanic suites from active continental margins such as western North America and Chile. These distinctive compositional features include high abundances of K, Rb, LREE, Th and 'h: (and sometimes Nb and Y), and low abundances of the high field strength elements (except Nb and Y in the rhyolites). Rhyolites reveal typical A-type characteristics which are compatible with a significant crustal contribution in their petrogenesis.

HFF basaltic andesite yields an age of 1086 ± 44 Ma and R_0 of 0.7030 ± 2 indicating derivation from a mantle source region which is slightly depleted relative to "Bulk Earth". However, a relatively high $^{238}\text{U}/^{204}\text{Pb}$ ratio (μ) of 10.2 suggests a crustal (slab?) component undetected by the Rb-Sr system. An errorchron age of 1038 ± 74 Ma for rhyolite porphyry is within error of that deduced for the basaltic andesite, while a high R_0 of 0.718 ± 15 is consistent with the inferred crustal origin. Petrogenetic modelling suggests that basaltic andesite (including high-Mg types) has evolved from a mantle-derived basaltic parent by fractional crystallisation and has sub-

sequently undergone assimilation-fractional crystallisation and mixing to form andesite. Rhyolites represent near-minimum partial melts of a basic to intermediate source in the lower to middle crust which have undergone fractional crystallisation, volatile transfer involving late-stage magmatic fluids, and possibly thermogravitational diffusion. Rhyodacite magmas have a similar origin to the rhyolites, but possibly also underwent mixing with basic magmas.

The post-HFF calc-alkaline Haisib Intrusive Suite (HIS) and slightly peralkaline Awasib Granite show close spatial and compositional associations with the volcanics, despite relative enrichment of the former in K, Rb, LREE, Th, Zr, Nb, Ni and Cr at intermediate silica levels. The HIS-Awasib “suite” compositional range reflects the increasing influence of both sub-continental within-plate mantle lithosphere and continental crust at an active continental margin. The A-type Awasib Granite yields an errorchron age of 957 ± 50 Ma and R_0 of 0.717 ± 8 , both features being compatible with field relationships and an inferred crustal source. The Saffier Intrusive Suite (formerly intrusive rocks of the “Barby Formation” and “Spes Bona Syenite”) and Bushman Hill Quartz Diorite are broadly contemporaneous with the HIS, while the Chowachasib Granite Suite represents the youngest pre-dyke plutonism. The change in composition from calc-alkaline to alkali-calcic of the late-stage granitoids is compatible with an overall increase in arc maturity.

Crustal evolution of the AMT took place in two major tectonomagmatic events. Formation of the early-stage crust started around 1460 Ma ago as a primitive oceanic arc or continental back-arc and ended as a relatively mature arc or active continental margin about 1270 Ma ago. Continental collision (coinciding with D_2 , and possibly D_3 , in the Central Zone of the NMC) initiated the second event by causing the formation of a new subduction zone. Subduction, oblique to the new continental margin, resulted in both compressional (“ice-floe”) and tensional (“pull-apart”) tectonics close to 1200 Ma ago. While mafic and felsic magmatism were related to the alternation of compressional and tensional regimes, overall development formed part of three major pulses of sedimentation, magmatism and tectonic activity in the Sinclair Sequence. During back-arc development prior to 957 Ma old granite plutonism in the AMT, synchronous transcurrent movements resulted in the slicing-up and removal of part of the arc and accretionary complex. Extensional tectonics enabled the preservation of thick volcano-sedimentary successions and the intrusion of bimodal dyke swarms, provisionally dated at 844 ± 35 Ma ($R_0 = 0.7064 \pm 2$).

TABLE OF CONTENTS

PART A: GENERAL INTRODUCTION		3. MINERAL CHEMISTRY AND METAMORPHISM ... 19
1. PREAMBLE	1	3.1 INTRODUCTION..... 19
1.1 LOCATION.....	1	3.1.1 General..... 19
1.2 PREVIOUS WORK.....	1	3.1.2 Kairab metabasalt..... 19
1.3 PRESENT STUDY	1	3.1.3 Kairabmetagabbro..... 19
1.4 ACKNOWLEDGEMENTS	1	3.1.4 Aunis Tonalite Gneiss
2. REGIONAL GEOLOGY	2	19
2.1 REGIONAL SETTING.....	2	3.2 PLAGIOCLASE
2.2 LITHOSTRATIGRAPHY.....	3	3.2.1 Kairab metabasalt..... 20
2.3 STRUCTURE AND METAMORPHISM.....	6	3.2.2 Kairabmetagabbro..... 20
2.4 SUMMARY	10	3.2.3 Aunis Tonalite Gneiss
		21
		3.3 AMPHIBOLE..... 21
		3.3.1 Kairab metabasalt..... 21
		3.3.2 Kairabmetagabbro..... 22
		3.3.3 Aunis Tonalite Gneiss
		23
		3.4 BIOTITE
		3.4.1 Kairab metabasalt..... 24
		3.4.2 Aunis Tonalite Gneiss
		24
		3.5 EPIDOTE
		3.5.1 Kairab metabasalt..... 25
		3.5.2 Kairabmetagabbro..... 25
		3.6 CHLORITE
		3.6.1 Kairab metagabbro..... 25
		3.7 SUMMARY
		26
		4. WHOLE-ROCK CHEMISTRY
		4.1 INTRODUCTION..... 26
		4.2 ASSESSMENT OF ALTERATION
		27
		4.3 GEOCHEMICAL CHARACTERISATION
		27
		4.3.1 Kairab Complex
		4.3.1.1 Metavolcanic succession
		(i) Classification
		27
		(ii) Comparison with modern volcanic suites.....
		29
		(iii) Comparison with ancient volcanic suites.....
		33
		4.3.1.2 Meta-intrusive suites..... 35
		4.3.2 Early-stage granitoids
		(i) Introduction..... 36
		(ii) Classification..... 36
		(iii) Comparison with modern and ancient granite
		suites
		38
		4.4 SUMMARY
		4.4.1 Kairab Complex
		4.4.2 Early-stage granitoids
		42
		5. GEOCHRONOLOGY
		5.1 INTRODUCTION..... 43
		5.2 ISOTOPE RESULTS
		5.2.1 Kairab Complex metabasalt..... 43
		5.2.2 Aunis Tonalite Gneiss
		43
		5.3 DISCUSSION
		43
PART B: EARLY-STAGE CRUST		
1. INTRODUCTION	11	
2. LITHOSTRATIGRAPHY.....	11	
2.1 KAIRAB COMPLEX	11	
2.1.1 Introduction.....	11	
2.1.2 Undifferentiated basement	11	
2.1.2.1 Garub Sequence	11	
(i) Granofels.....	11	
(ii) Aluminous gneiss.....	11	
(iii) Biotite and biotite-hornblende schist	11	
(iv) Quartzofeldspathic metamorphites.....	12	
(v) Quartzose metamorphites.....	12	
(vi) Mafic metamorphites.....	12	
(vii) Magnesian metamorphites	12	
(a) Anthophyllite fels.....	12	
(b) Chlorite schist.....	12	
2.1.2.2 Magnet tafelberg serpentinite	12	
2.1.2.3 Biotite gneiss	12	
2.1.3 Metavolcanic succession.....	13	
2.1.3.1 Metabasalt.....	14	
(i) Field character.....	14	
(ii) Petrography	14	
2.1.3.2 Metafelsite	14	
(i) Field character	14	
(ii) Petrography.....	14	
2.1.4 Meta-intrusive suite	16	
(i) Field character	16	
(ii) Petrography.....	16	
2.2 AUNIS TONALITE GNEISS	16	
(i) Field character.....	16	
(ii) Petrography	17	
2.3 KHORASIB GRANITE GNEISS.....	17	
(i) Field character.....	17	
(ii) Petrography	19	
2.4 SUMMARY	19	

PART C: LATE-STAGE CRUST	
1. INTRODUCTION	45
2. LITHOSTRATIGRAPHY	45
2.1 URUSIB FORMATION	45
(i) Field character	45
(a) Section southwest of DiaR10	45
(b) Section southwest of Piekniekkoppe	45
(c) Urusib section	45
Conglomerate member	47
Siltstone member	47
Pebbly sandstone member	47
Shale member	47
(d) Section southwest of Chowachasib Mountain	47
(e) Stellarine section	47
(ii) Petrography	47
(iii) Provenance and palaeoenvironment	47
2.2 HAIBER FLATS FORMATION (HFF)	48
2.2.1 General description	48
2.2.1.1 Distribution	48
2.2.1.2 Thickness	48
2.2.1.3 Field relationships	48
2.2.1.4 Volcanic types	48
2.2.2 Structure and metamorphism	50
2.2.3 Lithostratigraphy	52
2.2.3.1 Introduction	52
2.2.3.2 Southern locality	52
2.2.3.3 Central locality	54
2.2.3.4 Northern locality	54
2.2.4 Petrography	56
2.2.4.1 Introduction	56
2.2.4.2 Basaltic andesite	56
2.2.4.3 Andesite and dacite	56
2.2.4.4 Rhyodacite	58
(i) Southern locality rhyodacite	58
(ii) Northern locality rhyodacite	58
2.2.4.5 Rhyolite	58
(i) Pyroclastic rhyolite	58
(ii) Non-pyroclastic rhyolite	61
2.3 BARBY FORMATION	61
(i) Field character	61
(ii) Petrography	62
2.4 HAISIB INTRUSIVE SUITE (HIS)	62
(i) Field character	62
(ii) Petrography	62
2.5 SAFFIER INTRUSIVE SUITE (SIS)	62
(i) Field character	62
(ii) Petrography	65
(a) Gabbro-monzogabbro series	65
(b) Monzonite-syenite series	65
2.6 BUSHMAN HILL QUARTZ DIORITE	66
(i) Field character	66
(ii) Petrography	66
2.7 AWASIB GRANITE	67
(i) Field character	67
(ii) Petrography	67
2.8 CHOWACHASIB GRANITE SUITE (CGS)	68
(i) Field character	68
(ii) Petrography	68
2.9 MAFIC AND FELSIC DYKES	69
(i) Basic dykes	69
(ii) Intermediate dykes	69
(iii) Acid dykes	69
(iv) Alkaline dykes	69
2.10 SUMMARY	69
2.10.1 Late-stage volcano-sedimentary successions	69
2.10.2 Late-stage intrusive suites	70
3. MINERAL CHEMISTRY AND METAMORPHISM	71
3.1 INTRODUCTION	71
3.1.1 General	71
3.1.2 Haiber Flats Formation (HFF) and Barby Formation	71
(i) Basaltic andesite-andesite	71
(ii) Rhyolite-rhyodacite	71
3.1.3 Late-stage (“Sinclair-type”) granitoids	71
3.2 FELDSPAR	71
3.2.1 HFF and Barby Formation	71
3.2.2 HIS, Awasib and Chowachasib Granites	72
3.3 PYROXENE	73
3.3.1 HFF and Barby Formation	73
3.3.2 Chowachasib Granite	74
3.4 AMPHIBOLE	74
3.4.1 HFF and Barby Formation	74
3.4.2 HIS, Awasib and Chowachasib Granites	76
3.5 BIOTITE	76
3.5.1 HFF and Barby Formation	76
3.5.2 HIS, Awasib and Chowachasib Granites	77
3.6 CHLORITE	78
3.6.1 HFF and Barby Formation	78
3.6.2 HIS	78
3.7 EPIDOTE	79
3.7.1 HFF and Barby Formation	79
3.7.2 HIS	79
3.8 OXIDE MINERALS	79
3.8.1 HFF and Barby Formation	79
3.8.2 HIS, Awasib and Chowachasib Granites	79
3.9 METAMORPHISM IN THE HFF	79
3.10 SUMMARY	80
3.10.1 Late-stage volcanic successions	80
3.10.2 Late-stage intrusive suites	80
4. WHOLE-ROCK CHEMISTRY	81
4.1 INTRODUCTION	81
4.2 ASSESSMENT OF ALTERATION	81
4.3 GEOCHEMICAL CHARACTERISATION	81
4.3.1 Late-stage (“Sinclair-type”) volcanics	81
4.3.1.1 Classification	81
(i) Alkali - silica variation	83

(ii) Iron enrichment	83	4.4.2 Late-stage (“Sinclair-type”) intrusive suites.....	107
(iii) Alkali-lime index	83	5. GEOCHRONOLOGY	108
4.3.1.2 Major element variation	84	5.1 INTRODUCTION.....	108
(i) Introduction.....	84	5.2 ISOTOPE RESULTS	110
(ii) Systematic description	84	5.2.1 Haiber Flats Formation (HFF) basaltic andesite	110
(a) Titanium	84	(i) Whole-rock Rb-Sr data	110
(b) Aluminium	85	(ii) Whole-rock Pb-Pb data.....	110
(c) Iron.....	85	5.2.2 HFF rhyolite	110
(d) Magnesium.....	86	5.2.3 Awasib Granite.....	110
(e) Calcium and the alkalis.....	86	5.2.4 “Barby Formation” trachyandesite	110
(f) Manganese and phosphorus	86	(i) Whole-rock Rb-Sr data	110
4.3.1.3 Trace element variation.....	86	(ii) Whole-rock Pb-Pb data.....	111
(i) Variation diagrams.....	86	5.3 DISCUSSION	111
(a) K-group: Ba, Cs, Rb and Sr	86	5.3.1 HFF volcanic succession	111
(b) LREE Group: 1a, Ce and Nd	89	5.3.2 Awasib Granite.....	112
(c) Th-group: Th, U and Pb	89	5.3.3 “Barby Formation” trachyandesite	112
(d) HFSE-group: Zr, Nb and Y	90	5.4 SUMMARY	112
(e) Compatible Group: Ni, Co, Cr, V and Sc	90	6. PETROGENESIS OF THE HAIBER FLATS	
(f) Chalcophile Group: Cu, Zn and Mo	90	FORMATION VOLCANIC SUCCESSION	113
(ii) REE	90	6.1 INTRODUCTION.....	113
(a) Description	90	6.1.1 General	113
High-Mg basaltic andesite (BH 598).....	90	6.1.2 Petrogenetic models.....	113
Acid basaltic andesite (BH 690B).....	90	6.1.3 Whole-rock model compositions.....	113
High-silica pyroclastic rhyolite (BH 669)	90	6.1.4 Model mineral compositions	114
(b) Comparison of REE between lavas of the Haiber Flats, Barby and Guperas Formations.....	91	6.1.5 Crystal-liquid distribution coefficients	114
4.3.1.4 Comparison of Haiber Flats Formation (HFF) lavas with younger volcanic suites.....	91	6.2 CLOSED SYSTEM FRACTIONAL CRYSTALLISATION (FC).....	115
(i) The HFF volcanic suite.....	91	6.2.1 Basaltic andesite to andesite (BA-A)	115
(a) Major and trace element abundances	91	6.2.2 Andesite to rhyodacite (A-RD).....	116
Major elements.....	91	6.2.3 Rhyodacite to rhyolite (RD-R1, RD-R2).....	119
Trace elements	91	6.2.4 Discussion.....	119
(b) Trace element trends	93	6.3 ASSIMILATION-FRACTIONAL CRYSTALLISATION (AFC).....	122
(c) Trace element abundance patterns	93	6.3.1 Basaltic andesite to andesite (BA-A)	122
(ii) HFF mafic lavas.....	94	6.3.2 Andesite-rhyodacite (A-RD)	125
(a) Trace element “spidergrams”	94	6.3.3 Rhyodacite to rhyolite (RD-R1; RD-R2)	125
(b) REE patterns	94	6.3.4 Discussion.....	125
(iii) HFF felsic lavas.....	95	6.4 MAGMA MIXING	127
(a) Trace element “spidergrams”	95	6.4.1 Mixing to generate andesite (A).....	128
(b) REE patterns	96	6.4.2 Mixing to generate rhyodacite (RD).....	128
(iv) Summary.....	96	6.4.3 Discussion.....	128
4.3.2 Late-stage (“Sinclair-type”) intrusive suites.....	97	6.5 PARTIAL MELTING (PM).....	131
4.3.2.1 Introduction.....	97	6.5.1 Basaltic andesites.....	131
4.3.2.2 Classification	97	(i) Basaltic andesite as a primary magma	131
4.3.2.3 Comparison of the HIS and Awasib Granite with the HFF volcanic suite	99	(ii) Basaltic andesite derived from a parental melt.....	133
(i) Introduction	99	(iii) REE considerations	133
(ii) Major element variation	99	(iv) Discussion	134
(iii) Trace element variation	99	6.5.2 Rhyolites.....	135
(a) K-group	99	(i) General	135
(b) LREE Group	99	(ii) Quantitative modelling.....	136
(c) Th-group.....	99	(iii) Discussion.....	139
(d) HFSE Group	99	6.6 GENERAL DISCUSSION.....	140
(e) Compatible Group.....	99	6.6.1 Petrogenesis of the basaltic andesites and andesites	140
(iv) REE patterns.....	100	6.6.2 Petrogenesis of rhyolite and rhyodacite	140
4.3.2.4 Comparison of late-stage granitoids with Modern and ancient intrusive suites.....	102	6.6.3 Petrogenesis of the HFF volcanic succession	141
4.4 SUMMARY	106		
4.4.1 Late-stage (“Sinclair-type”) volcanics.....	106		

6.7 SUMMARY	142	4. SUMMARY	153
		5. CONCLUDING REMARKS	155
PART D: SYNTHESIS		REFERENCES	
1. INTRODUCTION	143	APPENDIX	
2. ISOTOPIC EVOLUTION.....	143	I. SAMPLE LOCALITIES.....	I
2.1 STRONTIUM ISOTOPES.....	143	II. ANALYTICAL TECHNIQUES.....	I
2.2 LEAD ISOTOPES	144	i. SAMPLE PREPARATION	I
3. GEOTECTONIC SETTING.....	146	ii. WHOLE-ROCK ANALYSES.....	I
3.1 BACKGROUND.....	146	a. X-ray fluorescence spectrometry.....	I
3.2 EARLY- TO LATE-STAGE CRUSTAL		b. Rare earth element (REE) analyses.....	I
EVOLUTION OF THE NMC	147	c. Radiogenic isotope analyses.....	I
3.3 GEOTECTONIC EVOLUTION OF LATE-STAGE		iii. MINERAL ANALYSES	IV
CRUST IN THE AMT AND THE TYPE AREA		III. DATABASE DESCRIPTION	IV
OF THE SINCLAIR SEQUENCE.....	148	i. WHOLE-ROCK DATA	IV
3.3.1 A model of anorogenic rifting.....	148	ii. MINERAL DATA.....	IV
3.3.2 A subduction-related model.....	149	iii. DISTRIBUTION COEFFICIENT DATA.....	IV
(i) Geotectonic features.....	149		
(ii) Geochemical and isotopic features.....	151		
3.4 DISCUSSION.....	151		



Landsat image (170 x 180 km) of the Proterozoic Awasib Mountain terrain (AMT) and adjacent areas in southwestern Namibia - see simplified geological map on p. 4 (Fig. A.4).
Photo: Satellite Applications Centre, MIKOMTEK, CSIR.

PART A: GENERAL INTRODUCTION

1. PREAMBLE

1.1 LOCATION

The middle to late Proterozoic Awasib Mountain terrain (AMT) is situated within the Namib Desert to the south-west of Maltahöhe and is bounded by latitudes 25°00'S and 26°00'S, and longitudes 15°00'E and 16°00'E (Fig. A.1). The area is approximately 11 200 km² in extent but out-crop is concentrated largely in the central-eastern portion and makes up a relatively small part of the total area. The topography of the study area is characterised by rugged inselbergs which rise steeply above sand- and scree-covered plains.

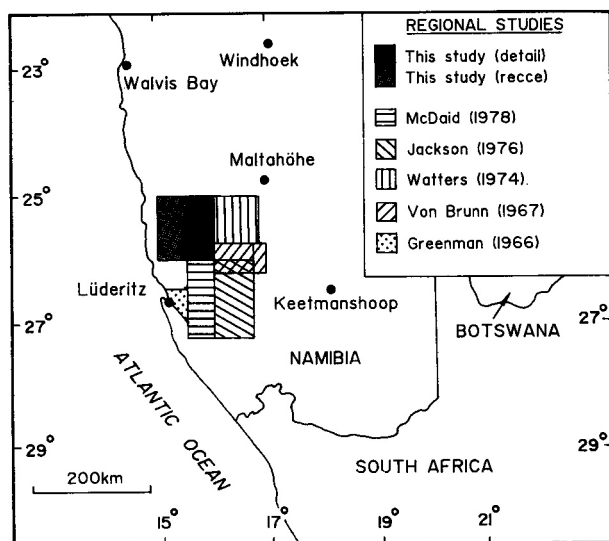


Fig. A.1: Locality map of regional geological studies undertaken in southern Namibia.

1.2 PREVIOUS WORK

Initial mapping of the AMT was carried out in 1963 by geologists of Consolidated Diamond Mines, but these maps remain unpublished. Martin (1965) identified several rock types within the AMT which he correlated with lithologic units of the Sinclair "Series" in the neighbouring region. Amongst these were felsites of the Nagatis Formation, reddish Tumuab Granite and sediments of the Kunjas Formation.

Watters (1974), after completing a regional study to the east of the AMT, produced a generalised geological map of the Sinclair, Helmeringhausen and Awasib areas in which he depicted the AMT as underlain almost entirely by the Sinclair Sequence. While this depiction was largely corroborated by the reconnaissance work of Harrison (1979), the South African Committee for Stratigraphy (SACS, 1980) has shown that a larger portion of the AMT is underlain by pre-Sinclair metamorphic basement than previously indicated.

Areas adjacent to the AMT have been subject to several major regional mapping projects which have been under-

taken since the mid-sixties (Fig. A.1). Studies which dealt mainly with the cover rocks and high-level intrusions of the Sinclair Sequence are those of Von Brunn (1967) and Watters (1974), while the neighbouring, largely underlying, Namaqualand Metamorphic Complex (NMC) has been studied by Greenman (1966), Jackson (1976) and McDaid (1976, 1978). Details of earlier work carried out in these areas is contained in Range (1910, 1912), Beetz (1923, 1924), Kaiser (1926) and Martin (1965).

1.3 PRESENT STUDY

Although several reconnaissance studies have been conducted since the early sixties, the present study is the first detailed geological investigation of both early-stage crust (or "basement" of possible NMC affinity) and late-stage crust (or "cover") in the AMT (map - Appendix I). Despite the broad scope of this study, the aims have been specific and are listed below.

(i) To extend mapping from adjacent areas (Fig. A.1) into the AMT and to attempt correlation between these areas.

(ii) To provide and interpret data on the mineral, whole-rock and isotope compositions of volcanic and associated intrusive rocks in the early- and late-stage crust of the AMT.

(iii) To investigate possible petrogenetic models for the derivation of eruptive rocks of the Haiber Flats Formation (HFF), a formation that is lithologically similar to the Barby Formation of the Sinclair Sequence.

(iv) To determine basement-cover relationships in the AMT and to attempt to use these relationships to solve the current enigma of radiometrically older Sinclair Sequence rocks overlying an apparently younger metamorphic basement.

(v) To evaluate the importance of the AMT in a model for the crustal evolution of the Sinclair Sequence and the adjacent NMC.

1.4 ACKNOWLEDGEMENTS

I would like to thank Roy McG. Miller, Director of the Geological Survey of Namibia, for arranging this project and for introducing me to the Sinclair Sequence in the Helmeringhausen area. Karl Schalk acted as my mentor in the Awasib Mountains and tried his best to instill scepticism in me with regard to all geological observations which were not based on field evidence. John Ward guided me through the Namib sand sea to the God-forsaken Uri Hauchab and Hauchab inselbergs.

In the Department of Geochemistry at Cape Town, I am indebted to my Ph.D. supervisors Dave Reid and Tony Erlank for their energy in wading through bulky manuscripts, to Simon Milner for his patient demonstration of XRF techniques, to Marshall Otter and Dick Rickard for their help in using the microprobe, to Andy Duncan and Dave Hill for imparting a small part of their computer skills to me, and to Chris Harris for arranging a much needed Antarctic

interlude.

In gaining hands-on experience in the use of Rb-Sr and Pb-Pb isotope techniques, I wish to thank all the personnel of the Geochronology Division of the National Physical Research Laboratory, Pretoria. In particular Jock Harmer and Bruce Eglinton showed tolerance beyond the call of duty.

I also acknowledge useful discussions with Survey colleagues, particularly Karl Hoffmann, and the following persons: Chris Hartnady, Tony Ewart, Bill Collins, Ian Plimer, Peter Floyd, Gavin Brown and Gregor Borg.

I am further grateful to Simon Cloete and Petite Badenhorst of the Geological Survey for the employment of their draughting skHIS and Annatjie Maree of Hirt and Carter for her generous advice and help in the art of Desktop Publishing. I also owe a great debt of gratitude to my parents for their constant encouragement, without which I might still be suffering the affliction of part-time study.

Lastly, I would like to point out that although this memoir overlaps significantly with my Ph.D. dissertation (Hoal, 1989a), it has benefited greatly from the penetrating comments of Andrew Glikson, Brian Watters and Allan Wilson.

2. REGIONAL GEOLOGY

2.1 REGIONAL SETTING

The major tectonic provinces and subprovinces of southern Africa are illustrated in Fig. A.2 (after Hartnady *et al.*, 1985). The situation of the AMT across the proposed boundary between the Rehoboth and Gordonia subprovinces is important with regard to two problems:

- (i) the actual position of this boundary, and
- (ii) the relationship between these subprovinces. Work on this boundary has previously been restricted to the Excelsior-Lord Hill shear zone (e.g. Von Brunn, 1967; Blignault *et al.*, 1974; Jackson, 1976, Tankard *et al.*, 1982) and has not been extended to the northwest (Fig. A.4).

Metamorphic basement to the Sinclair Sequence has been grouped both with the Kheis Group (Von Brunn, 1967; Blignault *et al.*, 1974) and the Namaqualand Metamorphic Complex (Jackson, 1975; Kröner, 1977), while SACS (1980) proposed separate groupings of these "floor rocks" into the Mooirivier Metamorphic Complex and Neuhof Formation.

With regard to the Sinclair Sequence (which includes the

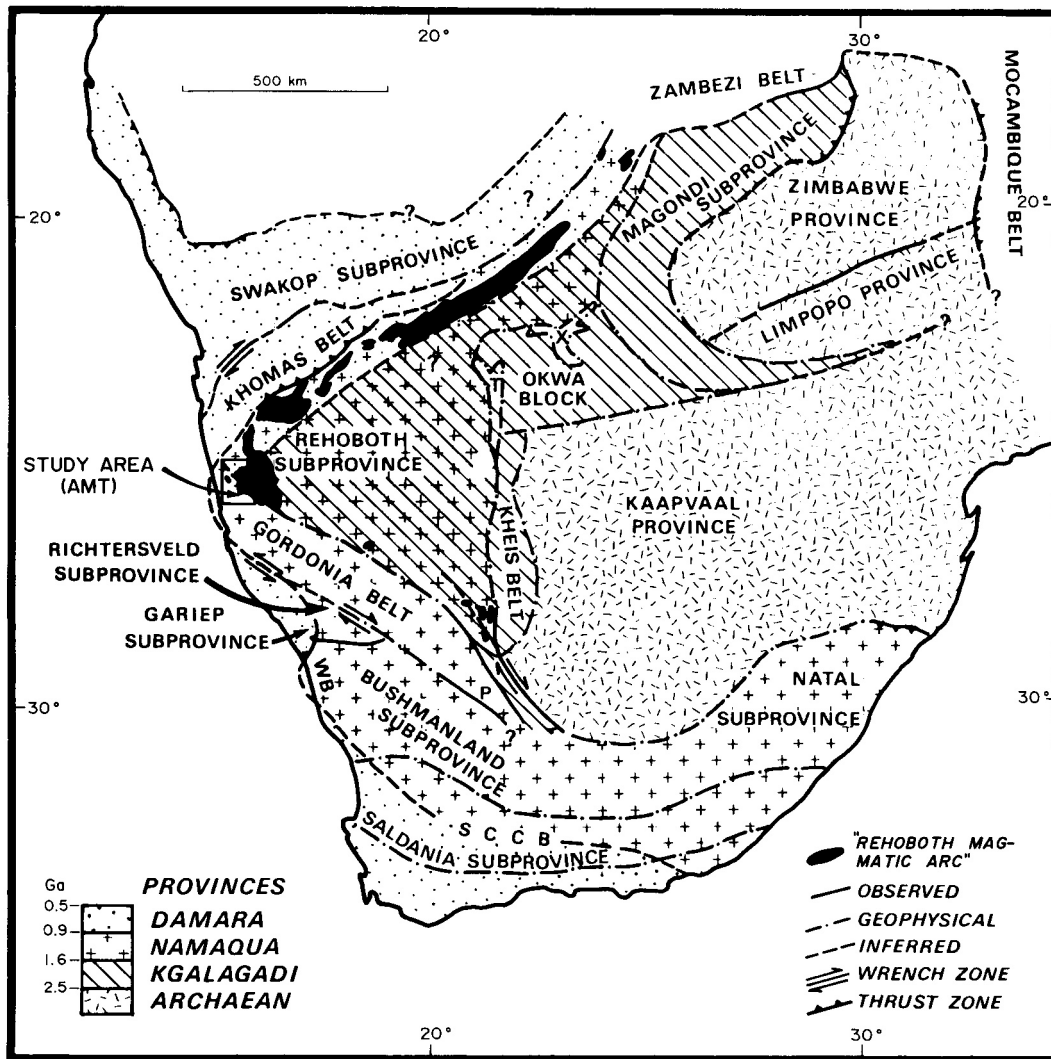


Fig. A.2: Regional setting of the "Rehoboth Magmatic Arc" in the tectonic framework of southern Africa (after Hartnady *et al.*, 1985). The situation of the Awasib Mountain terrain (AMT) is also illustrated relative to the Rehoboth and Gordonia subprovinces.

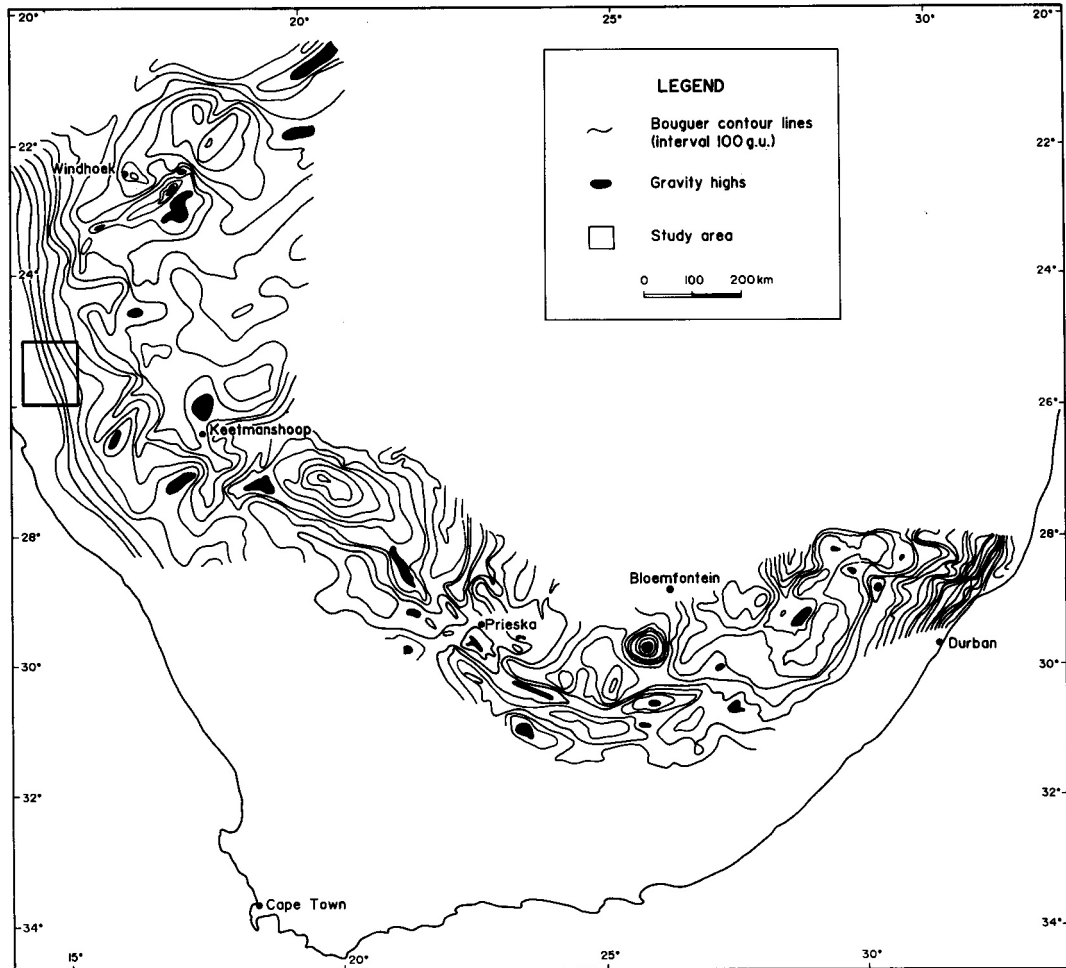


Fig. A.3: A simplified Bouguer anomaly map compiled from data for the northern boundary of the Namaqua-Natal Belt (after De Beer and Meyer, 1984) and southern Namibia (after Kleywegt, 1967).

late-stage crust of the AMT), the regional setting is seen as part of a curvilinear association of Irumide-age rocks (the so-called “Rehoboth Magmatic Arc”, Fig. A.2) which extends from the Koras Group near Upington to the Goha Hills in northern Botswana (Watters, 1974 and subsequent workers). The geotectonic setting of this association has been variously interpreted as an ancient active continental margin (Watters, 1974; Hoal, 1987), an aulacogen (Kröner, 1977), an intracontinental rift similar to the East African rift (Mason, 1981; Borg, 1988) and a collision-related rift (Hoal, 1987).

Geophysical studies, on a regional scale, have provided useful information with regard to some of the major structures at the boundary of the Gordonia and Rehoboth sub-provinces, e.g. Bouguer gravity anomalies (Kleywegt, 1967; SWA/Namibia Geological Map, 1980) and aeromagnetic lineaments (CDM Mineral Surveys, 1981). Gravity contours (with dark-shaded highs) indicate a continuation of the line of anomalies identified by De Beer and Meyer (1984) along the margin of the Kaapvaal Craton (Fig. A.3). This feature is important with regard to the northwestward continuation of the proposed *ca.* 1.3 Ga old active continental margin (after De Beer and Meyer, 1984). Possible further extension of this ancient margin into South America (Fig. D.3) provides an alternative interpretation to the extrapolation of this line along the younger Irumide belt (e.g. Borg, 1988). The paucity of

gravity stations between the Sinclair and Rehoboth areas does not allow for a confident choice between these options.

Aeromagnetic lineaments in the Sinclair and adjacent NMC have been interpreted from aeromagnetic contours (Hoal, 1987) and show strong northwesterly and, to a lesser degree, northeasterly trends (Fig. AA). These trends appear to be related to faults (frequently transcurrent) which allow for significant offsets or branching of the major Excelsior-Lord Hill shear belt and its possible northwestward continuation towards Hauchab as a complex fault zone. This “Excelsior-Hauchab Lineament” (EHL; Hoal, 1987) also has associated with it several serpentinite and metagabbroid (including diorite) bodies in a relationship similar to that of the better known Tantalite Valley Shear Zone (e.g. Tankard *et al.*, 1982).

In the regional context, the AMT consists of both early-stage crust of possible NMC affinity and late-stage crust which forms, together with the Konipberg Formation, the most westerly occurrence of the Sinclair Sequence.

2.2 LITHOSTRATIGRAPHY

While individual units in early-stage crust of the AMT have been studied in some detail, the stratigraphic succession remains uncertain and will only be dealt with briefly in

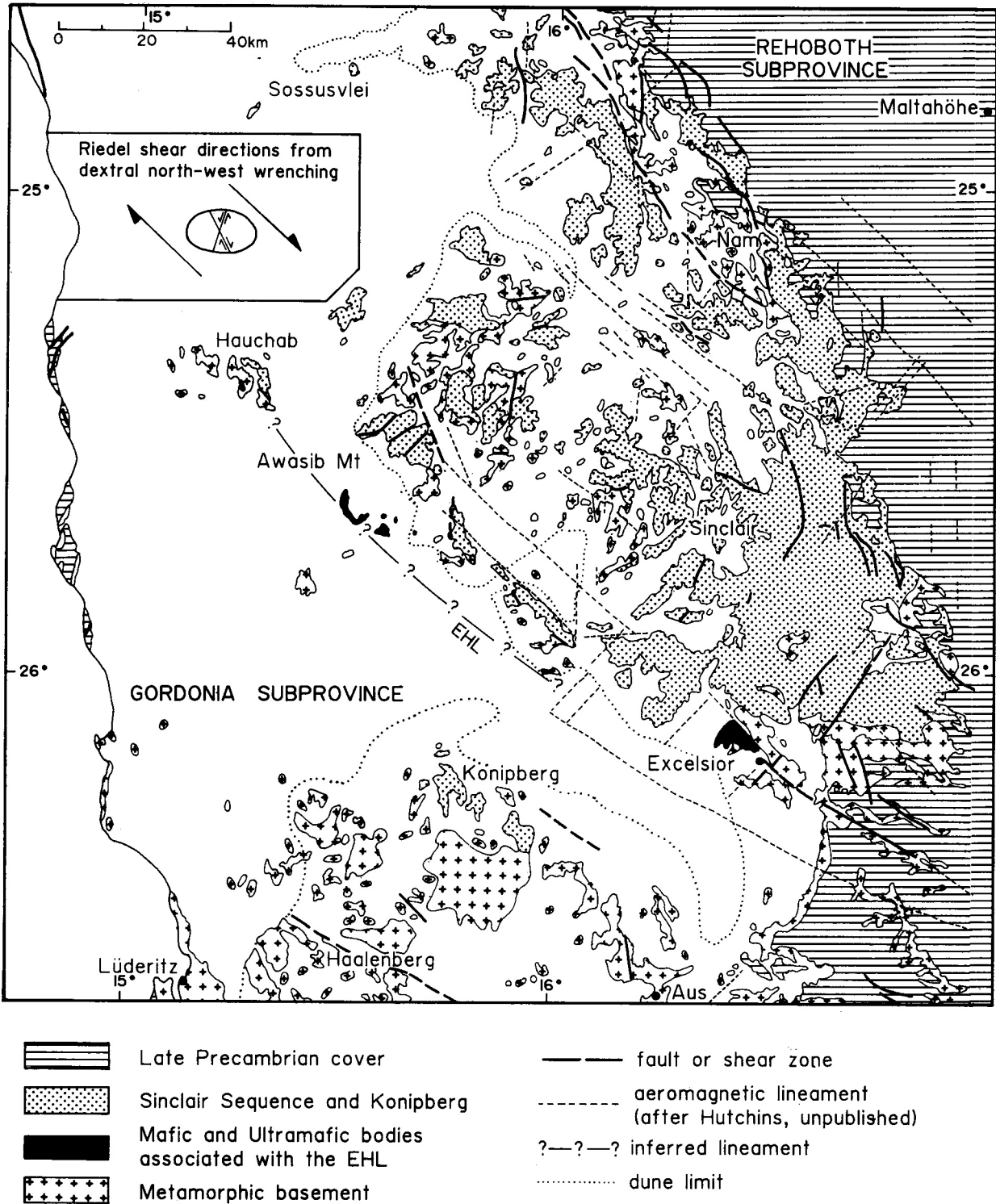


Fig. A.4: A simplified geological map of portion of the Rehoboth and Gordonia subprovinces indicating major structural trends inferred from aeromagnetic data (EHL: Excelsior - Hauchab Lineament).

conjunction with the associated metamorphic and structural history in Section 2.3 (Table A.3). A more comprehensive breakdown of individual units forms part of the legend to the 1:100 000 scale geological map of the AMT (Appendix I). This study is primarily concerned with the late-stage crust in the AMT and its relationship to the type area of the Sinclair Sequence as established by SACS (1980) and revised by Hoal (1985).

Table A.1 compares the stratigraphic succession in the type area of the Sinclair Sequence with the succession observed

in the AMT. This comparative table is based on field observations and not radiometric data, the latter having produced conflicting results (see discussion in Section C.5). An example of this dilemma is provided by the petrographic and geochemical similarities between the Haiber Flats and Barby Formations, yet Rb-Sr data indicate a difference of *ca.* 100 Ma in their ages of extrusion.

Mafic to intermediate intrusions of the “Barby Formation” and “Spes Bona Syenite” now form part of the “Saffier Intrusive Suite” (Hoal, 1989b) and, where recognised in the AMT,

TABLE A.1: Lithostratigraphy of late-stage crust in the Awasis Mountain terrain (AMT) compared with the lithostratigraphy of the Sinclair Sequence (modified from SACS, 1980).

TYPE AREA OF THE SINCLAIR SEQUENCE			AREA OF PRESENT INVESTIGATION		
Formation	Lithology	Intrusion	Formation	Lithology	Intrusion
AUBURES	Red quartzite, arkose, conglomerate, minor shale.				
				Mafic and felsic (dolerite, gabbro, quartz porphyry).	Dykes, sills and plugs.
	Red, fine- to medium-grained granite.	SONNTAG and GAMSBERG GRANITES		Red, medium-grained monzogranite to alkali feldspar granite.	CHOWACHASIB GRANITE
GUPERAS	Quartz porphyry lavas. Quartz porphyry lava, agglomerate, minor basic lava. Sandstone, siltstone, conglomerate, minor orthoquartzite, shale.	Quartz porphyry intrusive. Quartz porphyry dykes. Basic stocks and plugs. Basic dykes.	GUPERAS	Mafic and felsic.	Dykes, sills and plugs.
	Red, fine- to medium-grained, porphyritic granite.	NUBIB and ROOIKAM GRANITES		Red, very fine- to medium-grained granite porphyry.	AWASIB GRANITE
				Quartz diorite, tonalite and diorite Monzonite, quartz monzonite, quartz syenite, granodiorite, monzogranite	BUSHMAN HILL QUARTZ DIORITE HAISIB INTRUSIVE SUITE
	Gabbro, norite, picrite, anorthosite, monzonite, diorite, syenite	SAFFIER INTRUSIVE SUITE		Gabbro, norite, picrite, anorthosite, troctolite, monzonite, diorite, syenite	SAFFIER INTRUSIVE SUITE
BARBY	Sandstone, conglomerate, grit, tuffaceous sandstone. Basic and intermediate lava and agglomerate, minor acid lava; interbedded quartzite, conglomerate and bands of felsic lava. Acid lava, ignimbrite, tuff.		HAIBER FLATS BARBY	Acid welded ash-flow tuff, volcaniclastics, lava. Basic to intermediate lava, ash-flow and airfall tuff. Interbedded sandstone and conglomerate. Basic to intermediate lava, volcaniclastic sediment, airfall.	
KUNJAS	Arkose, shale, grit, quartzite, conglomerate.		URUSIB	Arkose, grit, sandstone, conglomerate, quartz arenite, shale.	
	Granite, granite porphyry.	TUMUAB and KOTZERUS GRANITES, OKARUS GRANITE PORPHYRY			
NAGATIS	Acid lavas and ignimbrites, conglomerate, grit, arkose, shale, minor basic lava.				

these intrusions have been mapped as such. The mutual relationship between the Haisib Intrusive Suite, Bushman Hill Quartz Diorite and Saffier Intrusive Suite is not well established but these units are depicted as broadly contemporaneous. Table A.1 also indicates the post-Sinclair status of the Aubures (previously "Auborus") Formation on the following grounds:

(i) The Aubures Formation is hosted in fault-bounded

troughs which cut across the regional trend of typical Sinclair-age basins.

(ii) The Aubures Formation is younger than the latest granite magmatism in the Sinclair Sequence, which represents the closing off of the last volcano-sedimentary episode (Table A.2).

(iii) Correlation of the Aubures Formation with the Doornpoort Formation in the Rehoboth area is significant in view

TABLE A.2: Comparison of evolutionary schemes for the Sinclair Sequence and late-stage crust in the Awasisb Mountain terrain (AMT).

Proposed Evolution of the Sinclair Sequence (Watters, 1974)		Observed Evolution of the Sinclair Sequence (SACS, 1980; this study)		Proposed Evolution of late-stage crust in the AMT (this study)	
3rd cycle	Auborus Formation <i>sandstone, conglomerate</i>	Post-Sinclair (early Damara?)		3rd cycle	Chowachasib Granite and dyke swarms
	Rooiberg granite (now Sonntag Granite)	3rd cycle	Sonntag/Gamsberg Granite and dyke swarms		
2nd cycle	Guperas Formation <i>rhyolitic intrusives and extrusives, basic lava and intrusives</i>	3rd cycle	Guperas Formation <i>rhyolitic extrusives, basic lava</i>	2nd cycle	Awasisb Granite Saffier Intrusive Suite, Haisib Intrusive Suite, Bushman Hill Quartz Diorite.
	Guperas Formation <i>sandstone, conglomerate</i>		<i>sandstone, conglomerate</i>		
2nd cycle	Nubib/Rooikam/Tumuab Granite Spes Bona syenite	2nd cycle	Nubib/Rooikam/Haremub Granite Saffier Intrusive Suite <i>gabbro, norite, monzonite, diorite, syenite</i>	2nd cycle	Barby Formation and Haiber Flats Formation
	Barby Formation <i>basic lava and intrusives, rhyolitic extrusives</i>	2nd cycle	Barby Formation <i>basic lava and rhyolitic extrusives</i>		
1st cycle	Kunjas Formation <i>arkose, grit shale</i>		Kunjas Formation <i>arkose, grit shale</i>		Urusib Formation
	Haremub/Kotzerus Granite	1st cycle	Tumuab/Kotzerus Granite	1st cycle	
1st cycle	Nagatis Formation <i>rhyolitic extrusives and minor basic lava, arkose, grit, shale</i> (?Unexposed basic intrusives and extrusives)	1st cycle	Nagatis Formation <i>rhyolitic extrusives and minor basic lava, arkose, grit, shale</i>	1st cycle	

of the post-Gamsberg Granite age of the latter. Hoffmann (1989) considers the Doornpoort Formation to be of early Damaran age.

(iv) A palaeomagnetic age of *ca.* 1000 Ma led Kröner (1977) to suggest that the Aubures Formation was younger than the Sinclair Sequence.

Most of these problems of correlation reflect the deposition of volcano-sedimentary successions of the Sinclair Sequence in isolated basins which have developed both synchronously and diachronously. Coupled to the episodic nature of the magmatism, contemporaneous faulting and vertical movement, it is hardly surprising that the resultant stratigraphy is difficult to unravel.

Watters (1974, 1976) viewed the Sinclair Sequence as having evolved in three cycles, each cycle being initiated by the emplacement of basic magma and terminated by sedimentation. Table A.2 presents a reinterpretation of this cyclical evolution which is more compatible with field evidence, i.e. artificial boundaries are not created within formations, and places the evolution of the late-stage AMT predominantly within the second cycle of activity. In this revised model, each cycle is initiated by sedimentation, followed by volcano-sedimentary activity, and terminated by plutonism. Each cycle represents an episode of both extension and vertical tectonics, with accompanying sedimentation and pulses of magmatism. The final stage of plutonism in the third cycle

terminates the development of the Sinclair Sequence and excludes the Aubures Formation.

2.3 STRUCTURE AND METAMORPHISM

Table A.3 compares the geologic history of the AMT with that of the neighbouring NMC ("Central Zone") and possible Sinclair-type supracrustals within the latter province. The type area of the Sinclair Sequence is excluded from this table due to its relatively undeformed and unmetamorphosed nature. The controversial Nam Shear Zone appears to have affected Sinclair-type lithologies (Watters, 1974), but Schalk (pers. comm., 1985) regards this zone as part of the older Neuhoof Formation which suffered only minor reactivation in Sinclair times.

Within the early-stage crust of the AMT, the Kairab Complex shows many similarities to the "pre-tectonic" Garub Sequence described by Jackson (1976). The oldest regional fabric (s_1) is present in grey gneisses as a gneissic or migmatitic layering which is inferred to be parallel to the lithologic layering (s_0). The foliation s_1 is the result of transposition or overprinting of so during the D_1 deformational event (Plate A.1a). Tight, often overturned folds (f_2) are typical of D_2 , but their orientation does not appear to have any regional consistency. A penetrative mineral lineation is usually present and designated l_2 . Distinction between s_1 and s_2 foliations is

TABLE A.3: Comparison between geological histories of the Awasis Mountain terrain (AMT) and the adjacent Central Zone of the Namaqualand Metamorphic Complex (NMC).

AMT (THIS STUDY)		CENTRAL ZONE OF THE NMC (TANKARD ET AL., 1982)	
LITHOLOGIC UNIT	STRUCTURAL & METAMORPHIC FEATURES	LITHOLOGIC UNIT	STRUCTURAL & METAMORPHIC FEATURES
	Faults causing dyke offsets and brittle deformation (Aubures age?)		
	D ₇ : Open folds and warps		
Mafic and felsic dykes.	Utilisation of conjugate fractures.		
	D ₆ : Crenulation folds, kinkbands, crenulation lineation, conjugate fractures (NW-SE & NE-SW). Retrograde metamorphism.		
	D ₅ : Dextral and sinistral shearing (NW-SE, NE-SW, E-W), shear-related folds, stretching lineation, localised thrusting. Greenschist metamorphism.		D ₆ : Dextral shearing (NW-SE) Excelsior, Tantalite Valley, Nam (D ₄ /D ₅) - McDaid (1978)
Chowachasib Granite?			D ₅ : Open folding, trends NW-SE and E-W. Retrograde metamorphism.
	D ₄ : Open folds (NW-SE), fracture cleavage, block tilting, faulting.		D ₄ : Open folding, trends NW-SE, N-S, NE-SW.
Mafic to felsic intrusions (Haisib and Saffier Intrusive Suites, Bushman Hill Quartz Diorite, Awasis Granite). Volcano-sedimentary successions (Urusib, Haiber Flats and Barby Formations).		Granitoid batholiths (Glockenberg Granite) Volcano-sedimentary successions (Konipberg Formation)	D ₃ : Fabric in cover, tight E-W folding (McDaid, 1978).
		Granitoid batholiths (Tumuab and Kotzerus) Volcano-sedimentary successions (Nagatis Formation) Naisib River Igneous Suite	D ₃ *: Regional fabric N-S to NW-SE, isoclinal to open folding, local refoliation. Amphibolite metamorphism. * not identified by McDaid (1978).
Khorasib Granite, Aunis Tonalite Gneiss Kairab Complex gabbro, diorite. Khorasib Granite Gneiss (?)	D ₃ : Regional fabric (s ₃) in granitoid gneisses which contain schist xenoliths bearing earlier fabric (s ₁ /s ₂), mineral lineation.	Jakkalskop charnockite, alaskitic batholiths (Aus, Kubub, Anib), granitoid batholiths (Kunguib, Tschauchaib), gabbroids (Konip).	
	D ₂ : Close asymmetric folds in layered gneiss and schists, local refoliation of s ₁ by s ₂ , mineral lineation. Amphibolite metamorphism, migmatization.		D ₂ : Regional fabric, isoclinal to tight folding, local refoliation. Amphibolite metamorphism, metatexis.
Kairab Complex (basal portion). Volcano-sedimentary succession. Intrusive augen gneiss and ultramafic plugs (pre-tectonic).	D ₁ : Regional fabric (s ₁) parallel to lithologic layering (s ₀). Isoclinal folds (f ₁) in grey gneiss. Amphibolite metamorphism, migmatization.	Garub Sequence volcano-sedimentary succession with significant carbonate. Tsirub augen gneiss (pre-/post-D ₁). Magnetafelberg serpentinite (pre-tectonic).	D ₁ : Regional fabric, isoclinal to tight folding. Amphibolite metamorphism, metatexis.

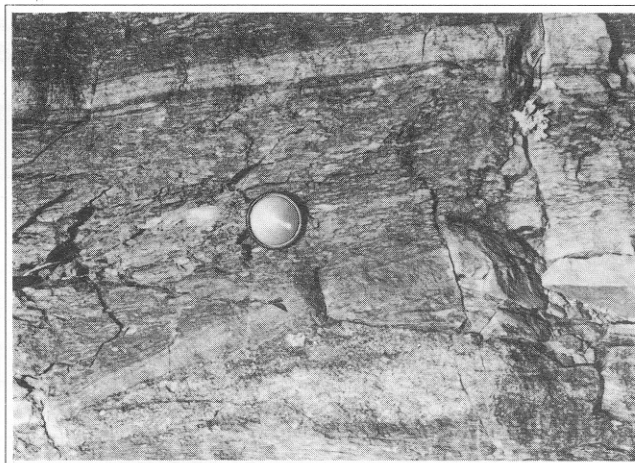
difficult on a regional scale, since refoliation is only locally observed (Plate A.1b). The deformational episodes D₁ and D₂ both appear to be characterised by high-grade metamorphism (upper amphibolite facies) and associated metatexis.

The regional fabric (s₃) typical of syn- to late-tectonic granitoids in the AMT "basement" is widespread but shows vari-

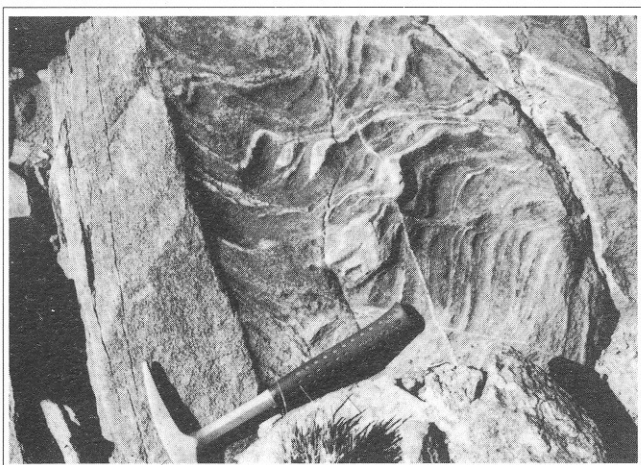
able development (Plate A.1c). Metasedimentary (and possibly amphibolitic) xenoliths may also show earlier fabrics (s₁/s₂) despite flattening in the plane of s₃. A mineral lineation (l₃) is occasionally developed. The extent of this D₃ phase of deformation is difficult to ascertain, but associated dextral shears may be the earliest manifestation of transcurrent



A.1a: Isoclinal f_1 folds defined by migmatite neosomes in garnet-biotite gneiss of the Kairab Complex. Flattening and boudinage of the early layering (s_0) have resulted in the development of transposed layering (s_1). 6 km south of Piekniekkoppe. (Map - Appendix I).



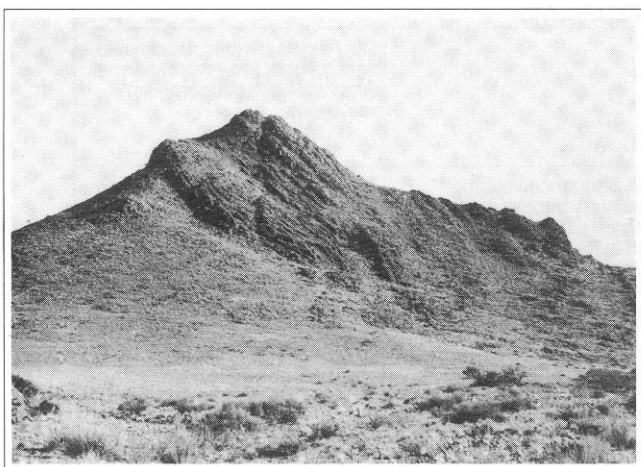
A.1b: Regional s_1 foliation in biotite-hornblende gneiss which has been refoliated in a narrow zone (s_2) between the lens cap and patchy neosome. Kairab Complex, 7 km west of Diar 11.



A.1c: Migmatized biotite gneiss of the Kairab Complex which has been intruded by a dyke of Khorasib Granite Gneiss. Earlier s_1 and s_2 fabrics in the migmatite are clearly cross-cut by the s_3 foliation within the granite gneiss. Corner boundary between farms Springbokvlakte 166 and Kumbis 55.



A.1d: Eastern limb of upright fold in lithic arenite of the Urusib Formation. Axial-plane cleavage is defined by pebble flattening and illustrates a high angle to the more moderately dipping bedding planes, here defined by heavy mineral concentrations. Core of Urusib synclinorium.



A.1e: Steeply-dipping to overturned western limb of Urusib synclinorium. Immediately west of thrust contact indicated on 1:100 000 map (Appendix I).



A.1f: Isoclinal S-told defined by "quartz porphyry" dyke in sheared metaandesite of the Haiber Flats Formation. Inferred sense of movement is sinistral. Shear zone 7 km southeast of Haiber Hill.

movements which culminated in the creation of pull-apart basins in late-stage (or "Sinclair-age") crust. Later movement (D_5 ?) has occurred along these faults and resulted in shear zones at several basin margins in the AMT.

The recognition of several phases of deformation in late-stage crust of the AMT constitutes a significant departure from the generally accepted idea of minimal tilting and gentle folding in the Sinclair Sequence (e.g. Watters, 1974; Kröner, 1977; Mason, 1981). Harrison (1979) identified two post-"Guperas Formation" deformational phases as well as a late phase of normal and reverse faulting in the AMT. This deformational sequence was revised and expanded by Hoal (1985) and is now considered to comprise four recognisable phases of deformation as well as a late phase of faulting (Hoal, 1989b).

The D_3 event recognised by McDaid (1978) in the Sinclair-age Konipberg Formation appears to be restricted to the syn- to late-tectonic "basement" granitoids in the AMT. The first recognisable phase of deformation in late-stage crust of the AMT affected all units except the Chowachasib Granite Suite. This event (D_4) is represented by open northwest to north-northwest-trending folds (f_4) which have been intersected by an axial-plane cleavage (s_4 ; Plate A.1d) and display a mineral lineation (l_4). These folds are both upright and more rarely overturned, while coaxial warps of the limbs were observed in the synclinorium north of Urusib waterhole (Plate A.1e). Associated with this phase of deformation are widespread fracture cleavage and block tilting, possibly as a result of sliding on listric or detachment faults.

The following deformational event (D_5) probably followed shortly after D_4 and is characterised by widespread shearing along s_4 planes of weakness. The conjugate shear couple represented by the northwest-trending Haiber Flats Shear Zone (HFSZ, first named by Harrison, 1979) and a smaller north to northeast-trending shear zone to the southeast of Haiber Hill (map - Appendix I) may represent Riedel shears in response to overall dextral wrenching. Hence the sense of movement in the shear zone southeast of Haiber Hill is sinistral (Plate A.1f), while sense of movement in the HFSZ is inferred to be dextral (Fig. A.4). Associated with this widespread shearing event are a number of tight, often reclined, folds (f_5), local thrusts, and a well-defined stretching lineation (l_5). The latter indicates both strike-slip and dip-slip movement. The presence of prograde biotite in basaltic andesites of the Haiber Flats Formation (Part C.3) reflects medium to upper greenschist facies metamorphism.

A late phase of deformation (D_6) is suggested by crenulation folding and kinking (f_6) of s_5 shear planes and the common occurrence of a crenulation lineation (l_6). Conjugate fractures associated with D_6 rather than D_5 (cf. Hoal, 1985) define a pattern which corresponds to the orientation of late- to post-tectonic basic and acid dyke swarms. Retrograde metamorphism in the form of widespread alteration is probably associated with this episode of deformation. A subsequent phase of folding and warping (f_7) about an east-northeast-trending axis has resulted in the bending of both shear planes and the s_3 fold axial plane of the Urusib synclinorium.

Late-stage faults show a variable orientation, but are commonly parallel or transverse to basin margins, i.e. north-west- or northeast-trending. North-trending faults may be

younger and possibly of post-Sinclair (Aubures or Nama) age. The brittle nature of these faults is indicated by commonly associated breccia, while quartz veining is a characteristic feature. In the absence of stratigraphic marker horizons, older faults can usually be distinguished from their younger counterparts by the transcurrent rather than vertical sense of movement.

The degree of deformation and associated metamorphism within the Sinclair Sequence increases further to the west and south of the Awasis Mountains. This is indicated by the intense shearing of the Urusib Formation at Hauchab and the medium to high-grade deformation and metamorphism within the Konipberg Formation (correlated with the Barby Formation by McDaid, 1978). The influence of the Pan-African Damaran Orogeny on the NMC has been severe along the coast of Namibia (Kröner and Jackson, 1974) and has resulted in low angle thrusts to the east. Possible effects of the Pan-African orogeny on the AMT must, therefore, be taken into account.

The degree to which Pan-African metamorphism is evident in the AMT may be assessed by interpolation between illite crystallinity isolines and extrapolation of the biotite isograd established for Pan-African outcrops by Ahrendt *et al.* (1977). Fig. A5 illustrates that the AMT lies close to the $Hb_{rel} > 130$ isoline which suggests that the grade of metamorphism attributable to the Pan-African orogeny did not exceed "very low grade" (i.e. $Hb_{rel} \approx 130$, which is equivalent

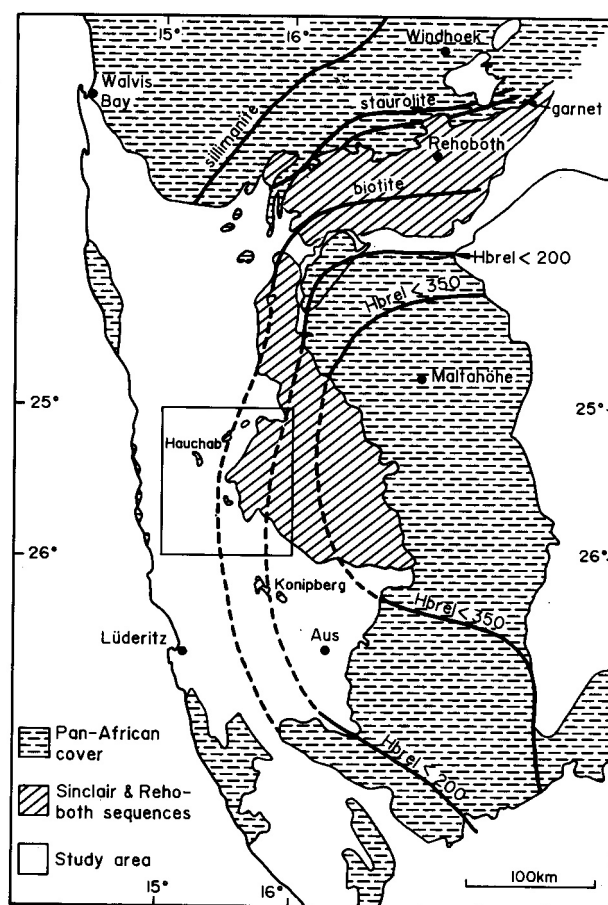


Fig. A.5: Illite crystallinity isolines and metamorphic isograds for the Pan-African Orogeny in southern Namibia. Solid lines after Ahrendt *et al.* (1977); dashed lines interpolated or extrapolated.

to temperatures lower than 300- 360°C). Extrapolation of the biotite isograd - is less easily achieved but was assumed to be sub-parallel to the Hb_{rel} isolines. According to this interpretation, biotite-grade metamorphism during the Pan-African should be confined to the AMT outliers (Hauchab and Uri Hauchab) and not recorded further east within the AMT proper or the Konipberg Formation. The presence of metamorphic biotite within the HFF basaltic andesites and Urusib Formation sediments suggests that the late-stage AMT crust has undergone an episode of metamorphism unrelated to the Pan-African event.

2.4 SUMMARY

(i) The middle to late Proterozoic Awasib Mountain terrain (AMT) comprises two major crustal components that are correlated with the Namaqualand Metamorphic Complex (NMC) and Sinclair Sequence respectively.

(ii) The metamorphic Kairab Complex forms an important constituent of the early-stage crust of the AMT and comprises a mixed gneiss and amphibolite terrain. Within the Kairab Complex, a relatively well-preserved volcano-sedimentary succession bears a lithologic resemblance to the Garub Sequence in the Central Zone of the NMC.

(iii) The post-Kairab Aunis and Khorasib granite (*sensu lato*) gneisses in the AMT appear to have counterparts amongst the numerous granitoid batholiths in the NMC (Table A.3).

(iv) The early-stage crust has undergone at least three episodes of deformation, the earliest of these being characterised by amphibolite-grade metamorphism and migmatitisation.

(v) The late-stage crust of the AMT is characterised by trough-hosted volcano-sedimentary successions (Urusib, Haiber Flats and Barby Formations) and a host of high-level intrusive rocks (Saffier and Haisib Intrusive Suites, Bushman Hill Quartz Diorite, and Awasib and Chowachasib Granites) which together bear a strong resemblance to lithologies in the middle part, or second cycle, of the Sin-

clair Sequence (Tables A.1 and A.2).

(vi) In comparison to the Sinclair Sequence, late-stage AMT rocks are strongly deformed (four episodes of deformation) and metamorphosed (greenschist facies) as a result of events which pre-dated the Pan-African orogeny and appear to be closely related to tectonic (and possibly also magmatic) activity in the adjacent Central Zone of the NMC. Southwest of the AMT, the even more highly deformed and metamorphosed Konipberg Formation may lie close to a palaeomargin of the Sinclair Sequence.

(vii) Late bimodal dyke swarms represent the youngest magmatism in the AMT and may be correlated with similar dyke swarms in the Sinclair Sequence. The Aubures Formation, formerly part of the Sinclair Sequence, post-dates this late magmatism and therefore probably formed during early Pan-African rifting.

The close spatial association of early- and late-stage crust in the AMT provides an opportunity to solve the enigma of a radiometrically older Sinclair Sequence that stratigraphically overlies a younger NMC "basement". While the apparent location of the AMT across the boundary of the Rehoboth and Gordonia tectonic subprovinces has an important bearing on the palaeoenvironments of both early- and late-stage crust in the AMT, conclusions arrived at for the AMT should provide general explanations for the evolution of the adjacent NMC and Sinclair Sequence. The more regional problem of a "Rehoboth Magmatic Arc" incorporating Irumide-age rocks of the AMT and Sinclair Sequence will not be addressed in any detail in this memoir.

The early- and late-stage crust of the AMT are treated separately (in Parts B and C, respectively) with regard to those regional and petrological aspects which best provide a framework for the discussion of the Proterozoic crustal evolution of the AMT (in Part D). Taking into account the greater degree of deformation and metamorphism evident in the early-stage crust of the AMT, a greater emphasis will be placed on the late-stage crust, in particular the volcanic succession of the HFF. It will be shown that data from the latter succession have an important bearing on the "orogenic versus anorogenic" origin of the Sinclair Sequence.

PART B: EARLY-STAGE CRUST

1. INTRODUCTION

The term “basement” refers, in the broad sense, to those lithologic units which underlie Sinclair-type rocks in the AMT. However, the division between an older “basement” and overlying “cover” is not rigorous in a regional context in view of widespread overlap in radiometric ages. Accordingly, reference is made to an early- and late-stage crust which better reflects the progression from an early orogeny in the floor rocks to a later event which records synchronous magmatic and tectonic activity in the Sinclair Sequence and parts of the adjacent NMC, respectively. In this respect, it is important to determine whether the early-stage crust in the AMT shows affinity with the NMC or forms, instead, part of an older craton (KAAPVAAL CRATON?).

The main aims in Part B are to provide both data and discussion on the following aspects of the early-stage crust of the AMT:

(i) Field character and petrography of the most prominent rock types in order to establish the early lithostratigraphy of the AMT.

(ii) Mineral chemistry of selected lithologic units with a view to determining the nature of the precursors and the degree and extent of subsequent metamorphism.

(iii) Whole-rock chemistry of a variety of rock types for the purpose of geochemical characterisation and comparison with modern and ancient analogues in the literature.

(iv) Geochronology of selected lithologic units in order to determine both the age and source characteristics of these units.

2. LITHOSTRATIGRAPHY

The aim of this section is to provide brief descriptions of the distribution, field character and petrography of the major lithologic units which form part of the early-stage crust in the AMT. Limited detail is provided in the case of lithologic units which have been previously described in areas adjacent to the AMT. Localities referred to in the text are illustrated on the accompanying geological map (Appendix I).

2.1 KAIRAB COMPLEX

2.1.1 Introduction

The pre-Sinclair basement in the AMT consists of a large variety of metamorphic rocks or “metamorphites” of both igneous and sedimentary origin. While some lithologic units have identical counterparts in the NMC as mapped by Jackson (1976) and McDaid (1976, 1978), there exists also a variety of associated metavolcanic and meta-intrusive units which appear to be distinct from neighbouring “basement” lithologies. Accordingly, a threefold division of the Kairab Complex into undifferentiated basement, a metavolcanic succession and a meta-intrusive suite was applied.

2.1.2 Undifferentiated basement

Many of the lithologies which make up the undifferentiated part of the Kairab Complex fall into the “pre-tectonic” category defined by Jackson (1976, p. 12) and comprise metamorphic rocks of diverse origin. Previously described lithologic units in the NMC which correspond to units within this succession include the Garub Sequence, layered biotite gneiss, Magnet tafelberg serpentinite and biotite granite gneiss. These units, although recognised in outcrop, have generally not been differentiated at the 1: 100 000 scale of the regional geological map (Appendix I).

2.1.2.1 Garub Sequence

The Garub Sequence, as described by Jackson (1976, p. 15-70), comprises fourteen different rock types which can be differentiated in the field. Although only nine of these rock types can be recognised in the AMT, they cover much of the previously described compositional range from “calcic” to “magnesian” (Jackson, 1976, p. 15). Brief descriptions of the major Garub Sequence-type lithologies that occur in the AMT are given below.

(i) Granofels

Lenticular rafts of carbonate-free granofels occur in a layered mafic intrusion of the Saffier Intrusive Suite which is situated on the farm Wolwedans in the northeastern part of the AMT. The granofels are characterised by a dark, banded appearance which is the result of diopside-rich layers alternating with plagioclase-rich layers. In addition to plagioclase and diopside, the granofels are composed of opaque minerals and secondary chlorite, biotite, epidote, actinolite and sphene. The fine-grained granoblastic polygonal texture is not unusual for outcrops of basement situated this far north in the AMT.

(ii) Aluminous gneiss

Layered gneisses which reflect an original “pelitic” character are restricted to a raft of muscovite-biotite-stauroilite gneiss in Awasi Granite at Guinasib Mountain, and to several outcrops of muscovite-biotite gneiss in the proximity of Haiber Hill which appear to contain needles of Sillimanite. Although these lithologies are quite unlike the typical aluminous gneisses of the Garub Sequence, many of the differences in character may be attributed to the lower metamorphic grade in the AMT basement.

(iii) Biotite and biotite-hornblende schist

Biotite schists constitute the most common Garub Sequence-type lithology in the AMT, but may differ from the type locality in containing significant amounts of muscovite. The remaining mineralogy is made up of plagioclase, quartz, minor K-feldspar, occasional garnet and hornblende. Accessory phases include apatite, zircon, sphene and opaque minerals, but several of these minerals appear to be secondary in origin. Epidote, like muscovite, is more

abundant than in the type locality and this may be attributed to a lower metamorphic grade in the AMT. Hornblende may be present in sufficient amounts to refer to the rock as a biotite amphibolite rather than a biotite-hornblende schist. The distribution of biotite schists is widespread, while hornblende-bearing schists are not as common and appear to be restricted to the southern part of the AMT. Together, these schists suggest derivation from a “semi-pelitic” protolith.

(iv) *Quartzofeldspathic metamorphites*

Jackson (1976, p. 37) assigned to this category all quartzfeldspar rocks of the Garub Sequence which contained < 5% mafic minerals. In the AMT this category includes pink quartzofeldspathic gneisses of arkosic character as well as white pegmatoids and garnet-bearing granite-aplites which are together associated with mafic schists and amphibolites in the southern most part of the area.

(v) *Quartzose metamorphites*

Metaquartzite occurrences are rare, the only body of and prominence being a magnetite metaquartzite outcrop situated 2.5 km west of the DiaR10 trigonometrical beacon. This metaquartzite exhibits a distinctive grey to red colour and inequigranular texture. Magnetite makes up 10-15% of the rock and is the only mineral of any prominence besides quartz. The magnetite metaquartzite overlies garnet-biotite schist and schistose amphibolite of the Garub Sequence.

(vi) *Mafic metamorphites*

“Metabasites” described in the area around Aus (Jackson, 1976, p. 41-52) include granulites, amphibolites and epidote schists. Granulite facies granulites, which are typically hypersthene-bearing, have not been recorded anywhere in the AMT and this may reflect a northward decrease in metamorphic grade. This observation is borne out by the rarity of diopside-bearing amphibolites in the AMT, since such amphibolites commonly occur in areas adjacent to granulite occurrences. A single outcrop of diopside-bearing amphibolite was noted 2 km to the northwest of the DiaR10 trigonometrical beacon. The more widespread diopside-free amphibolites in the AMT are characterised by several features which suggest a lower metamorphic grade than the diopside-bearing amphibolites, viz. a green colour and poikiloblastic nature of the hornblende, the presence of epidote and the subordinate nature of granoblastic polygonal textures. The range in mineralogy and texture of the diopside-free amphibolites differs little from that already described by Jackson (1976, p. 48-51), but many of the lower grade ortho-amphibolites have been mapped separately as part of a metavolcanic succession or meta-intrusive suite of rocks. These ortho-amphibolites are described in some detail in the following section. Quartz-epidote-chlorite schists, or so-called “epidote schists”, are better described in the AMT as epidote-rich biotite and hornblende schists which have suffered retrograde metamorphism.

(vii) *Magnesian metamorphites*

Anthophyllite fels and chlorite schist occur together in the southern most part of the AMT. This association of

magnesian metamorphites, resembles the cummingtonite and chlorite schist association described by Jackson (1976, p. 52). However, the different mineralogy merits the independent description given below.

(a) *Anthophyllite fels*

This lithology occurs as pods, possibly dykes originally, in the chlorite schist and is closely associated with lenses of serpentinite. Anthophyllite-gedrite makes up almost 60% of the rock with lesser amounts of tremolite (30%) and chlorite (10%). Large laths of porphyroblastic anthophyllite may define a schistose fabric, but are more commonly randomly oriented. Tremolite and chlorite are typically intergrown in fibrous aggregates to form a “groundmass” to the anthophyllite laths. The medium-grained and dark green character of the anthophyllite fels is distinctive.

(b) *Chlorite schist*

Chlorite is the major constituent but appears to form a fibrous replacement product of tremolite; together these intergrowths define a crenulated foliation. Occasional anthophyllite laths have grown across this foliation and appear to have a preferred orientation orthogonal to the latter trend. These fine-grained chlorite schists may have formed by the retrogression of associated poikiloblastic amphibolites which are typically made up of tremolite-actinolite (60%), plagioclase (20%) and chlorite (20%).

2.1.2.2 *Magnettafelberg serpentinite*

Several lenticular bodies of green serpentinite in the southern most part of the AMT bear a strong resemblance to the Magnettafelberg serpentinite described by Jackson (1976, p. 86-88). These bodies are small, generally less than 300 m by 100 m, and occur as pods and lenses in the host anthophyllite-tremolite-chlorite schist of the Garub Sequence. Antigorite is the predominant mineral and forms fibrolamellar aggregates which have been cross-cut by finely banded veins of chrysotile. Associated trails of opaque minerals typically enhance this layering, while minor laths of anthophyllite are randomly oriented. Numerous irregular and cross-cutting veins of white magnesite have intruded along fractures and shears which post-date the regional foliation.

Scree cover has obscured the age relationship between the serpentinites and their host, but the pod-like nature and ultrabasic composition of the serpentinite bodies suggests that they were emplaced as ultramafic intrusions at an early stage in the history of the AMT.

2.1.2.3 *Biotite gneiss*

“Biotite gneiss” has been used as a “sack-term” in the AMT and incorporates various lithologies designated separately by Jackson (1976) as “layered biotite gneiss” (*ibid.*, p. 71-73) and “biotite granite gneiss” (*ibid.*, p. 95-97). Megacrystic augen gneisses of granodioritic to tonalitic composition have also been included in this category despite their superficial similarity to typical Tsiirub gneiss in the

area around Aus. This correlation has not been made for the following reasons:

(i) Tabular K-feldspar megacrysts in the biotite gneisses of the AMT are commonly a distinctive pink colour and the rock more leucocratic in appearance than the Tsirub gneiss.

(ii) Garnet, which is not an uncommon phase in the Tsirub gneiss, has not been observed in the megacrystic gneisses of the AMT.

(iii) The megacrystic gneisses of the AMT usually form diffuse zones within larger outcrops of biotite gneiss and are difficult to map as separate units.

Outcrops of “layered biotite gneiss” are confined to the southern part of the AMT. They differ from similar biotite gneisses of the Aus area in containing muscovite as a prominent mineral and rarely any garnet. Layering is most commonly defined by varying proportions of biotite, but some discordant quartzofeldspathic layers are clearly the result of migmatitisation. Although intercalations of biotite schist and amphibolite of the Garub Sequence with layered biotite gneiss are not common, the continuous nature of the very fine scale layering suggests a sedimentary protolith for these gneisses.

More commonly biotite gneisses in the AMT have a “streaky” rather than a layered texture, and the widespread occurrence of megacrystic augen is indicative of an igneous rather than a sedimentary origin (cf. Vernon and Williams, 1988). While Jackson (1976) refers to a group of lithologically homogeneous biotite gneisses as “biotite granite gneiss”, the biotite orthogneisses in the AMT differ in the following aspects:

(i) Lithological heterogeneity is reflected in a variation in composition from tonalitic to granitic.

(ii) Hornblende is not uncommon in the more mafic granitoids.

(iii) Garnet is very rare.

2.1.3 Metavolcanic succession

Metavolcanics of basaltic and rhyolitic composition occur both separately and together throughout the AMT, but metavolcanics of intermediate composition are rare. The fragmentary, deformed and metamorphosed nature of these volcanic outcrops precludes any rigorous stratigraphic analysis. However, together with subordinate volcanoclastic sediments, these basalts and felsites form an extensive volcano-sedimentary succession underlying the Sinclair Sequence and not, as previously mapped by Watters (1974, Fig. 33), of equivalent age to the Barby Formation. Significantly, several of the basalts bear a petrographic resemblance to metabasites within the Garub Sequence.

To the southwest of Chowachasib Mountain (map - Appendix I) there is an estimated thickness of 4000 m of plagioclase-phyric basalts interbedded with porphyritic, occasionally flow-folded, rhyolites (Fig. B.1). In the upper part of this steeply-dipping succession porphyritic and amygdaloidal basalts exhibit well-formed pillow structures (Plate B.1a), while the rhyolites are typically pyroclastic in character. The volcanic succession has been intruded by coarse-grained Aunis Tonalite Gneiss and possibly also by layered metagabbro. Very similar eruptive rocks underlie the Urusib Formation sedimentary succession in the central part of the AMT, but felsites are intercalated here with plagioclase-phyric basalts which are not obviously pillow-bearing. Further prominent outcrops of these metavolcanics form part of Bushman

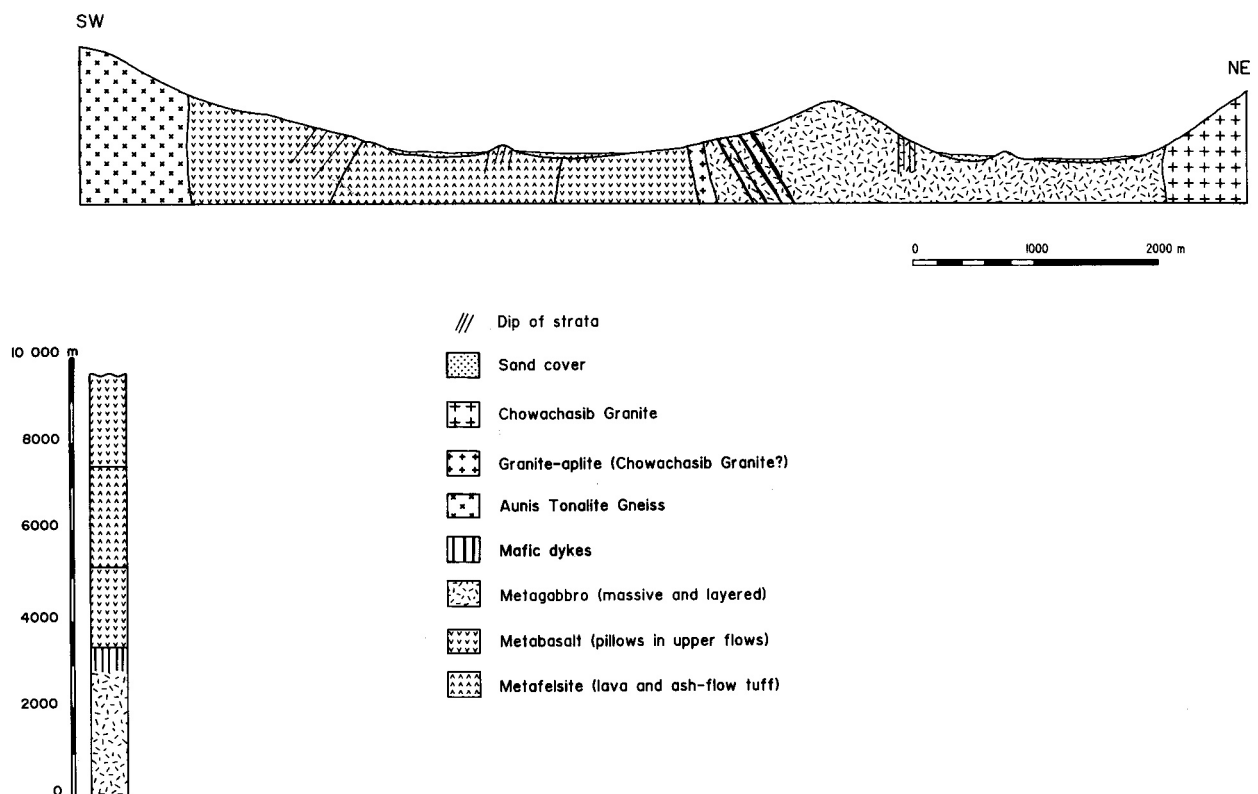


Fig. B.1: Horizontal and vertical sections through the Kairab Complex to the southwest of Chowachasib Mountain. The absence of upper sedimentary and lower ultramafic units in this succession is atypical of modern ophiolites (Section 2.1.4), but may reflect dismembering by tectonic emplacement and later intrusive activity.

Hill and the mountainous region immediately to the south of it.

2.1.3.1 Metabasalt

(i) Field character

Although deformation and recrystallisation of the basalts have adversely affected the recognition of primary textures and the determination of way-up criteria, several outcrops have, nevertheless, preserved important palaeoenvironmental indicators. Relatively undeformed flows allow the recognition of both pillows and pillow-fragment breccias (Plate B.1 b). While pillow structures provide evidence for subaqueous extrusion, either submarine or sub-lacustrine, pillow-fragment breccias suggest that such extrusion took place on a steep slope or escarpment (Fisher and Schmincke, 1984, p. 268). Alternatively, such breccias may indicate high volatile pressures in the magma, with subsequent fragmentation at shallow water depths (Glikson, pers. comm., 1989).

Row tops and bases are not easily identified and can often only be inferred from the presence of volcanoclastic interbeds. Such interbeds may be characterised by a dark carbonate-rich matrix which weathers negatively between light-coloured metafelsite clasts. Individual flow units can usually only be traced for a limited extent laterally, a distance of 2 km for a pillow-bearing basalt being exceptional.

(ii) Petrography

Plagioclase phenocrysts, sometimes glomerocrysts, make up 32% of the rock on average (range 20-40%) and may exceed 9 mm in length (plate B.1c). Despite widespread alteration and strain, plagioclase phenocrysts have retained subhedral to euhedral forms and calcic compositions (bytownite to anorthite). The patchy appearance and fractured nature of many plagioclase crystals is attributed to metamorphic recrystallisation and later alteration to aggregates of epidote, sericite, actinolite, albite and carbonate.

The original presence of mafic phenocrysts is difficult to assess in view of the high proportion (nearly 30%) of poikiloblastic hornblende. The strongly pleochroic (yellow-brown to dark green) poikiloblasts of hornblende rarely exceed 2 mm in size (average 0.3 mm) and contain inclusions of plagioclase and quartz of groundmass affinity. Alteration of hornblende to carbonate, epidote and chlorite is not uncommon and is probably the result of retrograde reaction, but elsewhere hornblende, biotite and euhedral epidote appear to be in equilibrium. Reddish-brown biotite may constitute a significant part of the rock (up to 8%; average 3%), particularly where there is a high proportion of blue-green amphibole or actinolite.

Amygdales, where present, make up 3-4% (maximum 8%) of the rock, and are characterised by a rounded, but strained, appearance. Quartz and epidote are the main constituent minerals. The groundmass, although largely replaced by poikiloblastic hornblende, is made up essentially of plagioclase and biotite, with scattered alteration products (epidote, carbonate, sericite, quartz, chlorite and opaque minerals).

2.1.3.2 Metafelsite

(i) Field character

The porphyritic and amygdaloidal nature of many felsites is an indication of volcanic origin. Compositionally these flows range from dacite to rhyolite, the more acidic varieties often showing evidence of secondary silicification. The thickest succession of felsites is exposed to the southwest of Chowachasib Mountain where it reaches an estimated thickness of 1600 m, but individual flows appear laterally discontinuous due to the paucity of outcrop.

The occurrence of flow folds in the felsites and the limited extent of individual flow units together suggest that many of the felsites were lava flows (Plate B.1d). However, widespread fragmental textures indicate that pyroclastic flows also make up a significant part of the volcanic succession. Pyroclastic debris are often difficult to recognise due to metamorphic recrystallisation and tectonic flattening of both pumice clasts and crystal fragments. Individual flows of felsite are difficult to recognise and flow tops and bases are invariably obscured, either by scree cover or intense deformation.

(ii) Petrography

Phenocrysts constitute an average of 10% (range 5-25%) of the rock and are made up predominantly of quartz, plagioclase and perthite. Poikiloblasts of biotite and hornblende may further indicate the original presence of ferromagnesian phenocrysts. Opaque minerals could also constitute original phenocrysts, but their xenoblastic form in association with biotite suggests a secondary origin.

Quartz, in general, makes up over 35% of the rock (range 20-75%) and is a prominent constituent of the quartzofeldspathic groundmass. Quartz phenocrysts average 0.5 mm in size (maximum 4.0 mm) and are commonly highly strained and recrystallised, often forming polycrystalline aggregates of amygdaloidal appearance.

Feldspars, both plagioclase and K-feldspar, constitute between 20 and 60% of the rock (average 50%). Feldspar phenocrysts are of similar size to quartz phenocrysts and plagioclase is generally dominant over perthitic K-feldspar. Feldspar phenocrysts are typically porphyroclastic and cloudy with alteration products of epidote, muscovite, carbonate, chlorite, biotite, quartz and opaque minerals. Original twinning (Carlsbad and albite) and low relief (RI < quartz) of plagioclase suggest sodic compositions largely (albite to oligoclase). Fragmentation of feldspar phenocrysts has occurred in response to deformation and resultant grains are usually strongly zoned or exsolved and intensely altered.

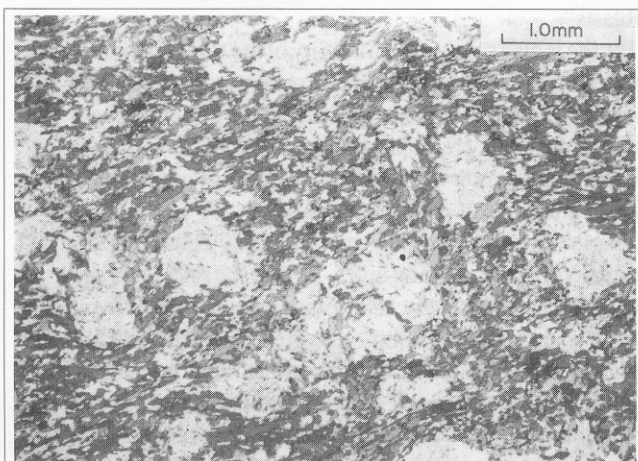
Poikiloblasts of blue-green to green hornblende and brown biotite occur both separately and as intergrowths, but are restricted to felsites in the central part of the area. These poikiloblasts average 0.8 mm in size (maximum 3.0 mm) and may form equilibrium intergrowths with epidote, garnet and opaque minerals. An opaque mineral, probably magnetite, forms idioblastic "phenocrysts" which average 0.4 mm in size. A metamorphic origin is indicated for the latter by its occasional xenoblastic form and disequilibrium undergrowth with biotite.



B.1a: Pillow structures in a plagioclase-porphyrific metabasalt flow in the Kairab Complex, 7 km southwest of Chowachasib Mountain. Downward-facing pillow cusps indicate that this flow unit is the right way up.



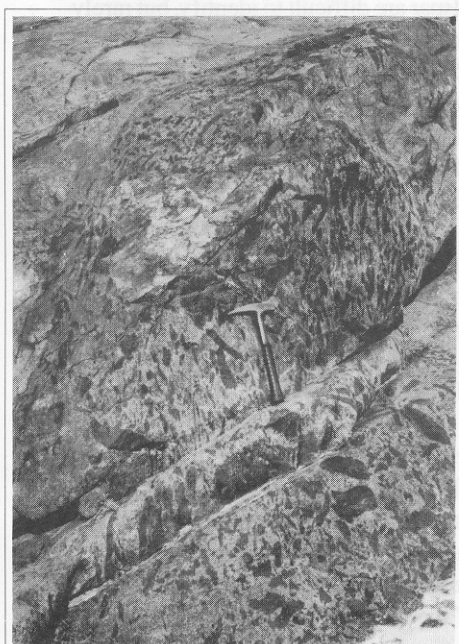
B.1b: Pillow fragment breccia in Kairab Complex metabasalt 10 km southeast of Awasib Fountain. This breccia suggests extrusion of the basalt on a steep slope or as shallow water depths if volatile pressures in the magma were high.



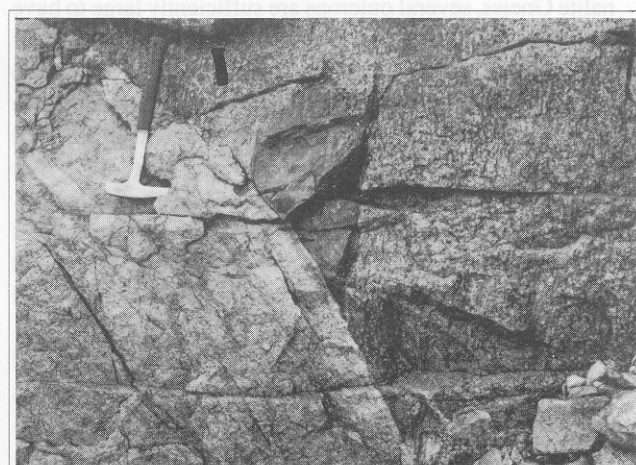
B.1c: Kairab Complex metabasalt (BH 883) - 3 km north-west of Satanskop. PPL. Anhedral plagioclase phenocrysts (porphyroclasts) set in a foliated "matrix" of metamorphic hornblende. [PPL = Plane Polarised Light]



B.1d: Irregular folds in Kairab Complex metafelsite which are attributed to primary viscous flow rather than tectonic activity. 5 km southwest of Chowachasib Mountain.



B.1e: Profusion of country-rock xenoliths (mainly Kairab Complex orthoamphibolite) in the Aunis Tonalite Gneiss which suggests magmatic stoping during emplacement. 5 km northwest of Urusib waterhole.



B.1f: Early and late phases of the Khorasib Granite Gneiss: mafic xenolith-bearing tonalite-granodiorite gneiss has been intruded by sheet-like granite gneiss. Note the difference in orientation of the gneissic fabrics (s₂ and s₃?), here inferred to indicate a protracted history of emplacement. 6 km south of Awasib Fountain.

The groundmass is typically a very fine-grained (< 0.5 mm) intergrowth of quartz and feldspar (perhaps originally devitrified glass) which is usually extensively recrystallised and occasionally exhibits pervasive silicification. Subcircular myrmekitic intergrowths resemble spherulites which suggest the presence of original volcanic glass. The groundmass mineralogy also comprises disseminated grains and “flakes” of biotite (3-10%), chlorite (2-7%), hornblende (< 7%), muscovite (1-7%) and epidote (< 5%). Very minor amounts (< 1 %) of garnet, carbonate, apatite and opaque minerals are usually present in addition.

The anastomosing fabric is best defined by trails of mica - flakes, particularly biotite, and epidote. Additional features which both define and accentuate this fabric include granular trails of quartz, feldspar and opaque minerals, streaked out and flattened quartz phenocrysts and amygdales, and flattened poikiloblasts of biotite and hornblende.

2.1.4 Meta-intrusive suite

(i) Field character

Intrusive amphibolite and metafelsite bodies are commonly associated with what appear to be their extrusive equivalents in the metavolcanic succession. While the metafelsite bodies are usually sheet-like in appearance and differ little in their field character and petrography from previously described felsic metavolcanics, massive amphibolite bodies display textures which clearly indicate plutonic precursors. These gabbroic rocks have been intruded by the Aunis Tonalite Gneiss, but the contact relationship between the latter and intrusive felsites is less certain. The compositional relationship between the Aunis Tonalite Gneiss and intrusive felsites (Section B.4) indicates sufficient geochemical similarities to suggest the possibility of a genetic association. Accordingly, this section will deal only with the gabbroic rocks.

Gabbro, diorite and minor peridotite crop out as relict bodies which range in dimensions from a few metres to several kilometres across. While these bodies may commonly be described as rafts within the younger Aunis Tonalite Gneiss, several outcrops are sufficiently large to have suffered little physical or chemical transformation by later intrusive activity. In particular, the large gabbroic outcrop situated southwest of Chowachasib Mountain occupies an important stratigraphic position with respect to adjacent pillowed basalts and a mafic dyke swarm (Fig. B.1). The association here is conceivably that of a dismembered ophiolite in which the lower most ultramafic and uppermost sedimentary members are absent. Numerous dykes and bodies of aplite, quartz porphyry and felsite have intruded the gabbroids.

The melanocratic appearance of the gabbroids makes it difficult to distinguish at a distance between these bodies and the equally dark-coloured basalts. Consequently volumetric estimates are difficult to make and these lithologies have commonly been grouped together on the map (Appendix I). Several good exposures allow the recognition of cumulate layering in the gabbroids. Elsewhere a more mottled appearance is prevalent due to aggregates or “clots” of mafic minerals.

(ii) Petrography

The metagabbroids are typically fine- to medium-grained and inequigranular, occasionally displaying well-preserved ophitic and subophitic textures. Hornblende and tremolite-actinolite make up 35-60% of the rock (average 50%). Hornblende, typically pleochroic from yellow-brown to dark green or blue-green, forms both small xenoblastic to subidioblastic grains (average size 0.3 mm) and larger (up to 4.0 mm in size), often poikiloblastic, intergrowths with tremolite-actinolite and less commonly biotite. The original alteration of primary pyroxene (augite?) to actinolite followed by prograde metamorphism may provide a general explanation for the paragenesis of hornblende except for those localities (e.g. southwest of Chowachasib Mountain) where tremolite-actinolite has clearly overprinted earlier hornblende. The distribution of hornblende is generally uniform and rarely shows any preferred orientation. Subhedral to fractured augite was observed in noteworthy amounts (7-25%) at only two localities where it occurs both as inclusions in plagioclase and more skeletal remnants (0.3 mm, maximum 1.0 mm) in amphibole “poikiloblasts”.

Biotite is also present in a minority of the samples, where it makes up 7-15% of the rock and occurs as both skeletal xenoblasts and flakes (average 0.8 mm) and decussate intergrowths with tremolite-actinolite. Biotite exhibits widespread alteration to chlorite, inclusions of plagioclase, and rims and trails of opaque granules.

Plagioclase is usually present in roughly equal proportions to hornblende, making up 15-50% of the rock (average 40%). Subhedral plagioclase grains show a significant range in size (average 0.8 mm, maximum 3.5 mm) and are frequently indeterminate due to alteration to epidote, sericite and occasionally chlorite. Twinning (commonly albite, but often combined with Carlsbad and/or pericline) and normal zoning, where preserved, indicate fairly calcic compositions, viz. An₄₅ to An₈₈ (extinction angle determination). While the effects of deformation are not widespread in plagioclase, some grains do show clear evidence of having recrystallised to smaller, often polygonal, subgrains.

Quartz and K-feldspar are difficult to identify, but rarely exceed 10% of the rock. Alteration (or retrograde) products include chlorite (< 12%), epidote (< 10%), sericite, sphene, carbonate and opaque minerals. The latter constitute up to 5% of the rock and are present as large skeletal grains of both magnetite and ilmenite. Accessory apatite grains are typically prismatic (0.5 mm long) and usually constitute a late phase.

Preferred orientation, where present, is defined by elongate aggregates of hornblende alternating with discontinuous, strained quartzofeldspathic layers.

2.2 AUNIS TONALITE GNEISS

(i) Field character

Much of the AMT is underlain by granitoid gneisses of tonalitic to granitic composition. Amongst the more intermediate members is a distinctive unit of medium- to coarse-grained leucotonalite gneiss which has clearly intruded ortho-amphibolites of the Kairab Complex. Although the

Aunis Tonalite Gneiss crops out over a wide area, the major part of this unit forms a single body which underlies Urusib Formation sediments in the central portion of the AMT (map - Appendix I). The shape of this pluton is ellipsoidal with a northwest-trending long axis and an inferred outcrop area of almost 500 km². Xenolith-choked contacts with the country rock (Plate B.Le) indicate that magmatic stoping was an important mechanism during emplacement. The Haiber Flats Shear Zone is situated along the western margin of the Aunis Tonalite Gneiss and may represent remobilisation of an older country rock fracture which was initially utilised by the tonalite. Irregular pluton margins are the result of subsequent intrusive activity.

The Aunis Tonalite Gneiss is characterised by a foliation defined by quartz-rich layers and trails of mafic minerals which wrap around porphyroclasts of feldspar. The weathered surface is usually a buff, rusty-brown colour with typical weathering-resistant quartz ribs. Mafic xenoliths, largely orthoamphibolite and biotite schist, are commonly flattened in the plane of the foliation and vary greatly in size from centimetre to metre scale. In some cases the streaky and disaggregated nature of the xenoliths may be the result of magmatic corrosion and/or later deformation.

Apart from the spatial association between the Aunis Tonalite Gneiss and metafelsites of the Kairab Complex, there are geochemical similarities between them which suggest a genetic association as well (Section BA).

(ii) Petrography

The Aunis Tonalite Gneiss is a rock of relatively uniform appearance and mineralogy, but the non-uniform response to deformational stress has resulted in heterogeneous textures.

Plagioclase typically forms anhedral to subhedral porphyroclasts (average size 2.0 mm, maximum 7.0 mm) which make up 35-50% of the rock (average 42%). While a xenoblastic nature is not common, plagioclase margins may be highly irregular and crenulate in form. Features which indicate deformation include bent twin lamellae and mineral fragmentation (subgrains 0.3 mm in size), the latter commonly giving rise to a "sieve" texture when accompanied by quartz blebs. Despite widespread alteration of plagioclase, strong normal zoning (core An₄₅, rim An₂₅) and twinning (usually albite) maybe preserved.

K-feldspar (microcline and microperthite) rarely exceeds 5% and may be entirely absent. K-feldspar usually forms small xenoblastic (average size 0.4 mm) intergrowths with plagioclase which can be distinguished from the latter by both microcline twinning and a relatively unaltered appearance. Rims and patches of K-feldspar in plagioclase appear to be the result of microclinisation or exsolution.

Quartz makes up 25-45% of the rock (average 37%) and typically forms a mortar texture in which large strained porphyroclasts (average size 2.0 mm) are surrounded by relatively strain-free and equidimensional sub grains (average size 0.2 mm). Aspect ratios of strained quartz may be high, while margins are usually highly irregular. A gneissic fabric is formed where quartz aggregates have segregated into anastomosing layers. Quartz also occurs as tiny granules in cross-cutting trails and along grain boundaries, as small

inclusions in other minerals (particularly hornblende), and occasionally as myrmekitic intergrowths. The variable nature of quartz is due to the interaction of deformation and recrystallisation which has resulted in strain, granulation and blastesis.

Strongly pleochroic brown biotite makes up around 8% (range 7 -1 0%) of the rock and occurs either as small "flakes" (average size 0.2 mm) or large, occasionally poikiloblastic, xenoblasts (average size 1.5 mm). Hornblende, where present, makes up approximately equal proportions to biotite and shows strong pleochroism from light yellow-green to dark green or blue-green. Hornblende, like biotite, occurs as both small, sometimes subhedral, grains (average size 0.3 mm) and large ragged poikiloblasts (up to 3.0 mm in size). Biotite is typically intergrown with hornblende in large aggregates (up to 5 mm in size) which may be slightly elongated in the plane of the foliation.

Accessory phases include sphene, apatite, zircon, allanite, muscovite, epidote and opaque minerals. The most widespread alteration products are epidote, sericite, chlorite and carbonate.

2.3 KHORASIB GRANITE GNEISS

(i) Field character

This unit comprises a heterogeneous group of grey to pink granitoid gneisses which range in composition from tonalite to syenogranite. While it is clear that some of the more granitic members post-date the Aunis Tonalite Gneiss, the age relationship between the latter and the bulk of the Khorasib Granite Gneiss remains obscure. It seems probable that this unit covers a broad time span as indicated by the variation in both intensity and orientation of the gneissic fabric (Plate B.1f).

For the purpose of lithologic description, the Khorasib Granite Gneiss can be subdivided into the following categories:

- (a) Tonalite to granodiorite gneiss
- (b) Granite gneiss
- (c) Foliated granite

These compositional categories are, however, difficult to apply rigorously in the field and a simpler twofold division into "gneisses" and "granites" was adopted on the map (Appendix I). Within the "gneisses", an age progression from tonalite to granite is generally, but not always, true.

All the different rock types within the Khorasib Granite Gneiss appear to be randomly distributed throughout the area with little suggestion of a zoned batholithic complex. Individual plutons are commonly irregular in shape but tend to be better preserved than the earlier Aunis Tonalite Gneiss due to fewer subsequent intrusions. Contacts with country rock other than the Aunis Tonalite Gneiss are rare, but a characteristic feature of the more gneissic members is the profusion of biotite schist and amphibolite xenoliths which are typically less flattened than similar xenoliths in the Aunis Tonalite Gneiss.

Despite similarities in appearance between the intermediate members of the Khorasib Granite Gneiss and the Aunis Tonalite Gneiss, the latter may be distinguished on petro-

TABLE B.1: Petrography of the Khorasib Granite Gneiss (% = vol. % of rock).

	TONALITE AND GRANODIORITE GNEISS	GRANITE GNEISS	FOLIATED GRANITE
TEXTURE	Medium-grained, augen (K-feldspar megacrysts). Refoliation, mineral segregation and recrystallisation where affected by later mylonitisation.	Medium-grained, augen (K-feldspar and plagioclase megacrysts). Refoliation similar to tonalite-granodiorite.	Fine- to medium-grained, massive to foliated. Aplites are allotriomorphic-granular. K-feldspar megacrysts occur, but are not common.
MINERALOGY			
Plagioclase	50% (40-60%). Av. size 2.0 mm, max. size 6.0 mm. Anhedral to subhedral porphyroclasts. Albite and Carlsbad twinning. Strong normal zoning (andesine-labradorite cores). Breakdown and recrystallisation into subgrains. Undulose extinction, bent twin lamellae, quartz-filled fractures. Commonly altered to sericite + epidote + carbonate ± albite.	28% (10-40%). Anhedral to subhedral porphyroclasts (av. size 2.0 mm) and megacrysts (>10 mm). Albite and Carlsbad twinning. Similar deformation and alteration to tonalite-granodiorite. Not as fractured as K-feldspar.	26% (10-35%). Anhedral to subhedral, smaller than K-feldspar. Subgrains (av. size 0.3 mm). Tiny granules in quartzofeldspathic intergrowths. Distinguished from K-feldspar by albite twinning, normal zoning (oligoclase-albite) and altered appearance.
K-feldspar	15% (< 5-25%). Av. size range 0.3 mm (matrix) to 4.0 mm (porphyroclasts). Megacrysts up to several cm. Anhedral to subhedral. Microcline microperthite. Distinguished from plagioclase by less altered nature, microcline twinning and poikilitic character. Rims of quartz-plagioclase intergrowths resemble mortar texture.	35% (20-45%). Anhedral to subhedral porphyroclasts (av. size 2.0 mm), megacrysts (up to 12 mm). Poikilocrysts of microperthite are fractured and rimmed by myrmekite.	38% (20-55%). Anhedral microcline (av. size 1.5 mm) and subgrains (av. size 0.2 mm). Occasional megacrysts (up to 14 mm). Microcline microperthite. Porphyroclasts rimmed by myrmekite and/or plagioclase subgrains. Larger grains are fractured, zoned and occasionally poikilitic. Some equidimensional intergrowths with plagioclase.
Quartz	20% (15-25%). Bimodal size: strained porphyroclasts (av. size 1.0 mm, max. 4.0 mm), strain-free polygonal grains and anhedral granules (av. size 0.1 mm). Mortar texture. Aggregates and trails define strong fabric.	30% (20-45%). Strained porphyroclasts/xenoblasts (up to 9.0 mm in size). Grains in interstitial aggregates either strain-free and equant (0.2-1.0 mm) or strained and stretched. Mortar texture. Quartzofeldspathic patches formed by comminution.	28% (20-35%). Interstitial aggregates of strained xenoblasts (av. size 1.0 mm) which are typically stretched. Less commonly, quartz occurs in mortar texture, as tiny granules in anastomosing trails, and as exsolution blebs and inclusions in K-feldspar and plagioclase.
Biotite	15% (8-25%). Bimodal size: xenoblastic/subidioblastic crystals (av. size 1.0 mm, max. 3.0 mm), small subhedral "flakes" (< 0.2 mm in size). Pleochroic from yellow- to green-brown or dark brown. Aligned to define fabric. Usually some chloritisation.	6% (2-15%). Bimodal size: xenoblasts/poikiloblasts (up to 2.0 mm in size), small subhedral "flakes" (0.1 mm in size). Pleochroic from light to dark brown. Aligned to define fabric. Apatite and zircon inclusions. Chloritised.	4% (2-15%). Similar to granite gneiss but differs in being coarser grained, subhedral and more commonly replaced by chlorite.
Other	Decussate intergrowths of muscovite + sphene + epidote + opaques with biotite form anastomosing fabric. Allanite (up to 1.2 mm) is accessory.	Similar decussate intergrowths to tonalite-granodiorite. Allanite more abundant.	Similar decussate intergrowths to gneisses. Widespread albitisation and silicification in aplites. Garnet subidioblasts in latter.

graphic (a lower content of ferromagnesian minerals) and geochemical criteria (Section B.4).

(ii) *Petrography*

The petrography of the Khorasib Granite Gneiss is discussed in terms of the abovementioned compositional categories in Table B.1.

2.4 SUMMARY

(i) The Kairab Complex is made up of several lithologic units that can be directly correlated with components of the NMC, namely the Garub Sequence, “biotite gneiss” and Magnet tafelberg serpentinite.

(ii) Apparently distinct from the NMC, a 6000 m thick bimodal volcanic succession in the Kairab Complex comprises feldspar-phyric basaltic flows (ortho-amphibolites) and hornblende ± biotite poikiloblastic rhyolites which are closely associated spatially, temporally and compositionally with cumulate metagabbro and sheet-like metafelsite intrusions. Preserved features in this succession include pillow structures and pillow breccias in the basalts and pyroclastic textures and flow folds in the rhyolites. Together with the presence of a mafic dyke swarm, the metavolcanic succession and associated intrusives are conceivably representatives of a dismembered ophiolite complex.

(iii) The post-Kairab Complex Aunis Tonalite Gneiss forms a pluton with an inferred area of some 500 km² which is situated adjacent to a major shear zone in the Haiber Flats. Numerous mafic xenoliths (some of metabasalt) suggest magmatic stoping during emplacement. This granitoid shows a close spatial association with the metafelsites of the Kairab Complex. Biotite and hornblende constitute the most important mafic phases which, together with plagioclase porphyroclasts, define a strong gneissic fabric.

(iv) The Khorasib Granite Gneiss comprises tonalite-granodiorite gneiss, granite gneiss and granite, but there is no systematic zonation to suggest a zoned batholithic complex. While the “gneisses” are of uncertain age with regard to the Aunis Tonalite Gneiss, “granites” typically post-date the latter. Biotite is the dominant mafic phase by far and shows a progressive depletion from tonalite to granite. Megacrystic feldspars are most common in the gneisses where they occur as augen.

3. MINERAL CHEMISTRY AND MET AMORPHISM

3.1 INTRODUCTION

3.1.1 General

Mineral assemblages were selected from three lithologic units in the early-stage crust of the AMT for electron microprobe (EMP) analysis. These analyses have extended Jackson's (1976) database for metamorphic “basement” of the NMC around Aus and provided new insight with respect to the extent and grade of amphibolite facies metamorphism in the region. Analyses of primary phases, where preserved,

have further enabled a better understanding of the early-stage protoliths. Since textural evidence does not always allow the unequivocal identification of igneous mineralogy, compositional characteristics of phases are important in any discussion of their original formation.

The following sections describe the mineral chemistries of the common phases encountered in selected lithologic units. All EMP analyses are tabulated on the accompanying Microfiche card and discussed in Appendix III.

3.1.2 Kairab metabasalt

The assemblage plagioclase + hornblende + epidote ± biotite is widespread in metabasaltic rocks of the Kairab Complex as illustrated on an ACF diagram (Fig. B.2a). As mentioned in the previous section, the Kairab metabasalt may bear a strong petrographic resemblance to Garub metabasites described from the Aus area by Jackson (1976). Accordingly, mineralogical comparisons will be made wherever possible. All mineral analyses were derived from a single, relatively undeformed and homogeneous, flow unit to the southwest of Chowachasib Mountain, the two sample sites (BH 770 and BH 901) being situated approximately 300 m apart. Pillow structures are well-preserved in the eastern part of the flow, especially at the site of sample BH 770.

3.1.3 Kairab metagabbro

Garub metabasites near Aus include several intrusive amphibolites (Jackson, 1976, p. 46) which may be equivalent to metagabbros in the Kairab Complex. This section compares analyses between the Kairab metagabbro and metabasalt as well as between these lithologies and “meta-basites” in the vicinity of Aus. While the metagabbros frequently retain original igneous textures (e.g. ophitic), several major phases such as hornblende exhibit a metamorphic texture. The evidence for a retrograde metamorphic imprint in the metagabbros is better developed than in the metabasalts, and takes the form of both chloritisation and epidotisation. The mineral parageneses are illustrated in an ACF diagram (Fig. B.2b) to facilitate comparison with the metabasalts. Accordingly, this diagram is not strictly applied to metamorphic phases and also includes relict igneous phases.

3.1.4 Aunis Tonalite Gneiss

Despite the spatial association between the Aunis Tonalite Gneiss and Kairab Complex, this granitoid appears to have preserved much of its primary mineralogy. The gneissic character is the result of a deformational event (including metamorphism) which could be late- or post-tectonic with respect to the major event which affected much of the Kairab Complex. Assessment of the grade of metamorphism in the Aunis Tonalite Gneiss is important with regard to assessing the timing of its emplacement into metabasalt and metagabbro. The major mineral assemblage, discussed in detail in Section 2, may be summarised as follows:

plagioclase + quartz + biotite ± hornblende ± K-feldspar

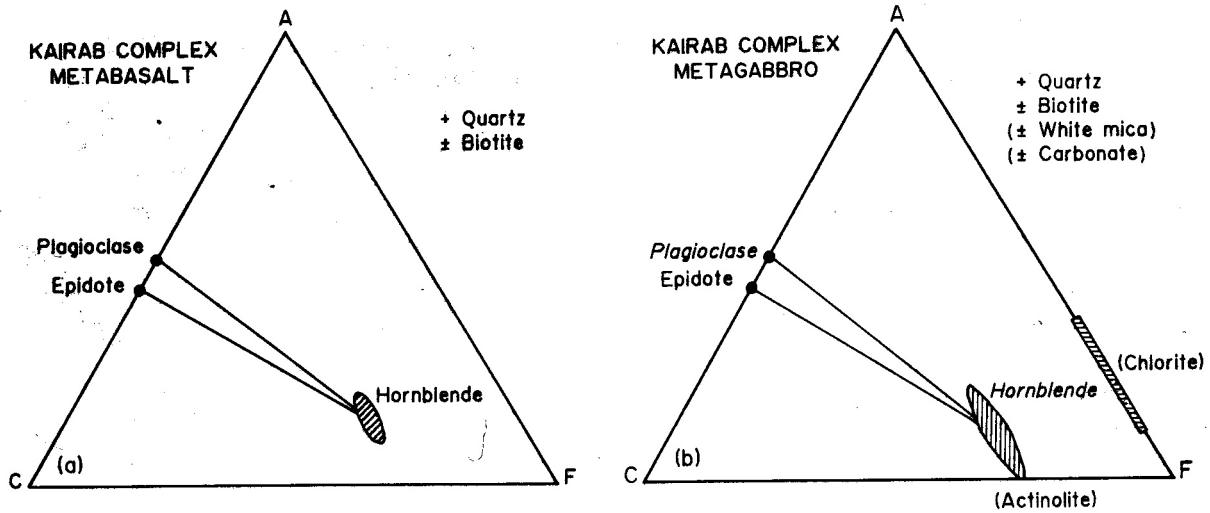


Fig. B.2: ACF diagrams illustrating mineral parageneses in metabasalts and metagabbros of the Kairab Complex. While largely relict igneous phases are written in italics, retrograde phases are presented in parentheses. A = $Al_2O_3 + Fe_2O_3 - (Na_2O + K_2O)$, C = $CaO - 3.3P_2O_5$, F = $FeO + MgO + MnO$, mole%.

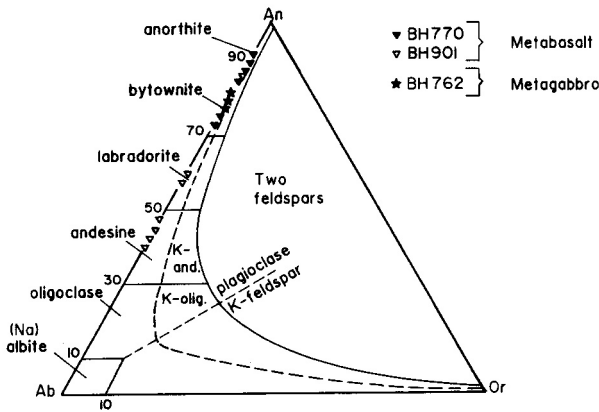


Fig. B.3: Plagioclase compositions in metabasalt and metagabbro from the Kairab Complex. An (Anorthite), Ab (Albite), Or (Orthoclase). Field boundaries after Smith (1974).

3.2 PLAGIOCLASE

3.2.1 Kairab metabasalt

The range in anorthite content from An_{40} to An_{92} is illustrated in Fig. B.3 and broadly corresponds to the epidote-hornblende or hornblende zones within the Garub metabasites. While the presence of epidote is more compatible with the former zone, the average anorthite content of An_{69} indicates a closer affinity to the higher grade hornblende zone (average An_{67} after Jackson, 1976, p. 127). However, plagioclase in sample BH 770 yields an average An_{84} composition in comparison to only An_{54} in sample BH 901. While the latter composition agrees well with Jackson’s value of An_{55} determined for the epidote-hornblende zone, the more calcic composition of An_{84} is typical of metabasites which form part of the granulite facies. Since petrographic observation precludes the latter possibility, it may be concluded that such high anorthite contents in the Kairab metabasalt represent primary compositions.

The mineral parageneses in the Kairab metabasalt suggest a metamorphic grade typical of the epidote amphibolite or

amphibolite facies. In metabasalts of amphibolite grade from the Llano Uplift in central Texas, Garrison (1978) observed eight discrete compositional domains in plagioclase ranging from An_{38} to An_{91} . He suggested several explanations for this phenomenon, but favoured an extremely complex immiscibility region which allowed more than four metastable end member compositions to exist. While the demarcation of similar compositional domains in the Kairab metabasalt has not been attempted, it can be demonstrated that individual plagioclase phenocrysts are made up of complex intergrowths of varying anorthite content in the range An_{44} to An_{86} . Such intergrowths may also span the range between Bøggild (An_{47} and An_{58}) and Huttenlocher (An_{67} and An_{90}) intergrowths in a region which is widely considered “homogeneous” (Goldsmith, 1982). Braun and Müller (1975) have reported that the homogenisation of plagioclase is initiated only at temperatures greater than 600°C (upper amphibolite facies).

The above observations suggest that disequilibrium probably existed during lower amphibolite facies metamorphism of the Kairab metabasalt but do not argue convincingly for either a prograde or retrograde origin for the plagioclase intergrowths. On the available evidence, the possibility that highly calcic plagioclase represents a relict phase cannot be excluded.

3.2.2 Kairab metagabbro

The average anorthite content of An_{81} ($\pm An_2$) shows little variation and is close to the average value of An_{84} ($\pm An_8$) exhibited by the pillow-bearing metabasalt (Fig. B.3). Again, such calcic compositions are typical of what Winkler (1976, p. 168) has termed “labradorite/bytownite-amphibolites”, but the absence of metamorphic diopside allows for the possibility that these calcic compositions are primary in origin. The presence of intergrowths of varying anorthite contents, as seen in some of the metabasalts, was not observed in any of the metagabbros. This observation is somewhat contrary to that of Grove (1977) who regards “Huttenlocher plagi-

oclases" as useful indicators of a slower cooling history. It is, however, possible that the plagioclases in the metagabbro demonstrate local disequilibrium and compositional variation on a submicroscopic scale.

3.2.3 Aunis Tonalite Gneiss

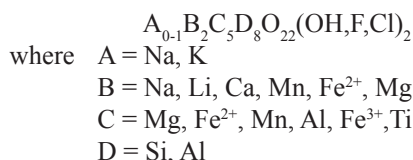
Plagioclase is the predominant mineral phase and is characterised by strong normal zonation (An_{46} core, An_{25} rim) in the southern part of the pluton near Aunis waterhole, but more sodic compositions (An_{38} - An_{18}) in the northern part. This could reflect the more differentiated nature of the northern part of the pluton as indicated by its relative enrichment in bulk-rock silica and alkalis and depletion in magnesium. CIPW normative proportions reveal further that whereas the southern sample (BH 746) is tonalitic in composition, the northern sample (BH 759) has a more trondhjemitic affinity (Section 4).

While the porphyroclastic nature and recrystallised textures exhibited by plagioclase provide clear evidence of elevated pressures and temperatures, the core compositions recorded are inferred to be primary in origin. More sodic compositions may, like K-feldspar rims and patches, be the result of deuteric effects rather than metamorphism.

3.3 AMPHIBOLE

3.3.1 Kairab metabasalt

The blue-green to green colour of amphibole in the metabasalts is in agreement with both the paragenesis epidote + quartz and the lower amphibolite facies grade inferred for these rocks from the anorthite content of plagioclase. The general amphibole formula may be written as follows (Hawthorne, 1981):



On the basis of their B group cation occupancy, all amphib-

oles within the Kairab metabasalt may be described as calcic ($[Ca + Na]_B \geq 1.34$). In order to chemically classify these amphiboles, the scheme of Leake (1968) was followed (Fig. B.4). The advantage of this scheme is that it does not require the determination of Fe^{2+} and Fe^{3+} , neither of which may be obtained by using the EMP. Amphibole formulae have, in addition, been calculated on an anhydrous basis (23 oxygens) as suggested by Borg (1963).

By comparison with hornblendes from the Garub metabasites in Fig. B.4, several features of interest are apparent:

(i) Most of the analysed hornblendes display similar or lower Mg/(Mg + Fe) ratios than their counterparts in the Garub metabasites.

(ii) A greater range in Si content is displayed by hornblendes from the Kairab metabasalt.

(iii) Two compositional types are unique to the Kairab metabasalt, viz. Mg-hastingsite and Fe-tschemakite.

Both tschermakitic substitution (aluminium for silica) and edenitic substitution (alkali occupancy of the A-site) have traditionally been related to variations in metamorphic grade. While a decrease in tschermakitic substitution with increasing metamorphic grade has been observed by several workers (e.g. Leake, 1965; Binns, 1965; Jackson, 1976; Albat, 1984), other workers find no such correlation (e.g. Engel and Engel, 1962; Bard, 1970). The compositions of amphiboles are plotted according to the classification scheme of Miyashiro (1973) in Fig. B.5, which illustrates the overall similarity of hornblendes in the Kairab metabasalt to hornblendes of the epidote-hornblende and hornblende zones (zones A and B, respectively) in Garub metabasites. However, the lower Si contents of the former are distinctive and typical of low-pressure amphiboles according to Raase (1974).

The very high values of Al^{VI} in hornblendes of the Kairab metabasalt (Fig. B.6) cannot be the result of high pressure formation as advocated by Leake (1965), since this is incompatible with the low Si contents illustrated in Fig. B.5. High Al^{VI} is accordingly attributed to the high alumina bulk compositions of these metabasalts.

The relationship between alkali enrichment in the A-site of hornblendes, or edenitic substitution, and increasing metamorphic grade has been well established by a number of workers (e.g. Shido, 1958; Engel and Engel, 1962; Binns,

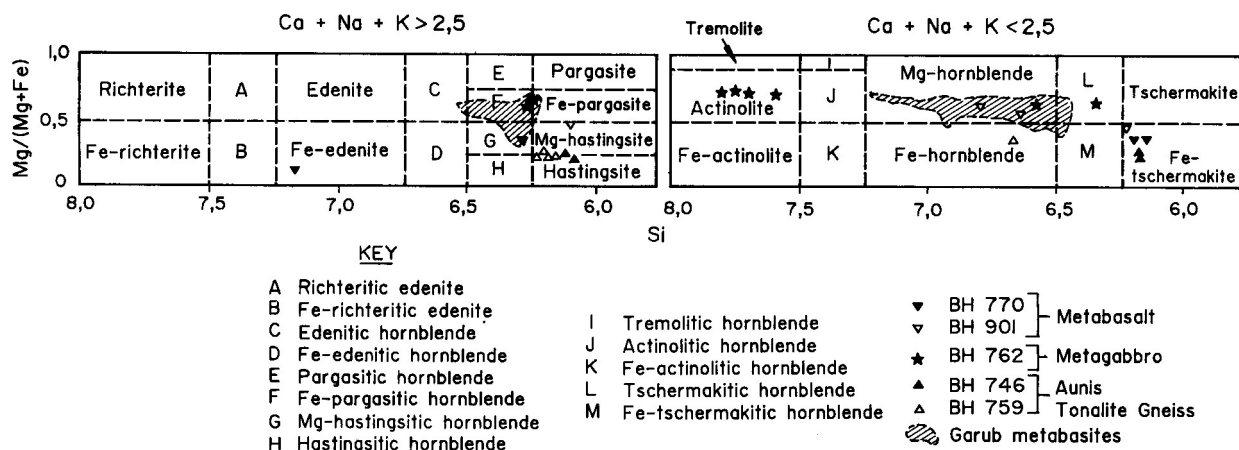


Fig. B.4: Hornblende compositions in Kairab metabasalt, Kairab metagabbro and Aunis Tonalite Gneiss plotted in terms of the classification of Leake (1968). The field of hornblendes from Garub metabasites is after Jackson (1976). All data were normalised to 23 oxygens with all iron considered as Fe^{2+} .

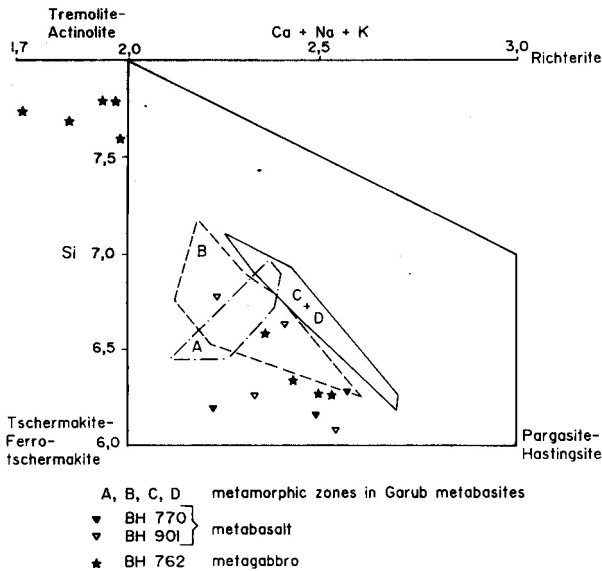


Fig. B.5: Hornblende compositions in metabasalt and metagabbro from the Kairab Complex plotted according to the classification of Miyashiro (1973). Metamorphic zones in the Garub metabasites are after Jackson (1976). All data normalised to 23 oxygens.

1965). Jackson (1976, Fig. 32) has shown that despite a wide variation in alkali content of hornblende within the different metamorphic zones in the Aus area, there is a steady enrichment from the epidote-hornblende (zone A) to the diopside-hornblende zone (zone C). The mean of 0.444 ± 0.118 for $(\text{Na} + \text{K})$ in hornblendes of the Kairab metabasalt once again indicates a grade transitional between Jackson's zone A (mean = 0.432 ± 0.071) and zone B (mean = 0.517 ± 0.101).

The titanium content of hornblende has been reported by Engel and Engel (1962) and Binns (1965) to increase with increasing metamorphic grade irrespective of the titanium content of the host rock. Raase (1974) also reported an increase from 0.08 to 0.29 ions per formula (on the basis of 23 oxygens) from the greenschist-amphibolite transition to the granulite facies. Jackson (1976, Fig. 33) showed that hornblendes of zone A have a significantly lower concentration of Ti (mean = 0.056 ± 0.027) than hornblendes of the higher grade zones. The hornblendes of the Kairab metabasalt show even lower contents of Ti (mean = 0.038 ± 0.012), but it appears likely that biotite (up to 8% by volume) has preferentially accommodated much of the Ti. Enrichment of Ti in hornblende may, therefore, not be solely dependent on metamorphic grade, despite coexistence with the Ti phase ilmenite.

3.3.2 Kairab metagabbro

The amphiboles analysed exhibit a range in colour from essentially colourless, through blue-green and green, to a distinct brownish-green. These calcic amphiboles ($[\text{Ca} + \text{Na}] \geq 1.34$) are similar in composition to the amphiboles of the Kairab metabasalt, but may be intergrown with, or overprinted by, amphiboles of actinolitic composition (Figs B.4 and B.5). Such intergrowths could represent equilibrium assemblages indicative of a miscibility gap between actinolite and horn-

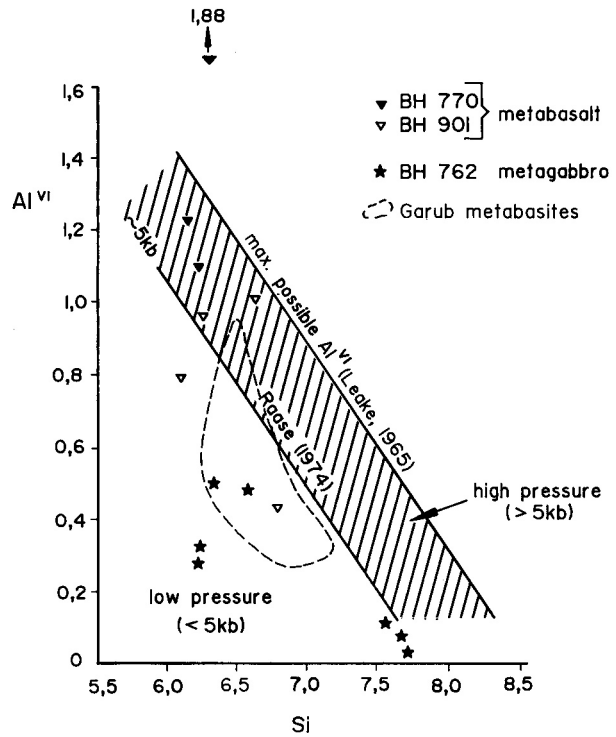


Fig. B.6: Relationship between Si and Al^{VI} contents in hornblendes from Kairab metabasalt and metagabbro. Diagonal boundaries indicate high- and low-pressure environments as well as the maximum possible Al^{VI} concentration in hornblende. Data sources as indicated. The field of hornblendes from Garub metabasites is after Jackson (1976).

blende (e.g. Shido and Miyashiro, 1959) or disequilibrium assemblages resulting from recrystallisation (e.g. Grapes, 1975; Grapes and Graham, 1978). However, according to Laird (1982), actinolite is typical of the greenschist facies and this is borne out by the occasional overprinting of chlorite by actinolite in the metagabbro.

Fig. B.5 illustrates that hornblendes in the metagabbro are similar in composition to hornblendes from both the Kairab metabasalt and the epidote-hornblende and hornblende zones within the Garub metabasites. Unlike hornblendes in the metabasalt, however, hornblendes in the metagabbro have the low contents of Al^{VI} and Si typical of low-pressure amphiboles reported by several workers (e.g. Leake, 1965; Raase, 1974) and illustrated in Fig. B.6. A plot of total Al versus Ti for all of the amphiboles in the metagabbro (Fig. B.7) reveals that while pale green actinolites display characteristically low contents of Al and Ti, green to brown hornblendes exhibit relatively high Ti contents.

Hynes (1982) stated that "the clearest distinction between amphiboles from medium- and low-pressure terrains is on the basis of Ti content". The relatively high Ti contents in hornblendes from the metagabbro may, therefore, reflect a lower pressure of formation in comparison with hornblendes from the metabasalt (Fig. B.7). While Ti/Al ratios vary significantly between the different groups of hornblendes illustrated in Fig. B.7, actinolites from the metagabbro display the lower Ti/Al ratios characteristic of the metabasaltic rocks. It is possible that these actinolites represent a metamorphic overprint unrelated to earlier hornblendes of higher grade,

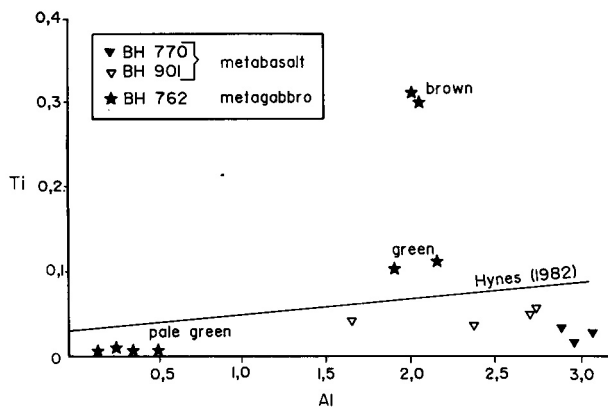


Fig. B.7: Total Al vs. total Ti (cations per 23 oxygen anions) in amphiboles from Kairab metagabbro and metabasalt. The straight line (after Hynes, 1982) is for purposes of comparison only and emphasises the relatively high Ti contents in hornblendes from the metagabbro. While brown hornblendes in the latter are probably magmatic in origin, green hornblendes are not as compositionally distinct from hornblendes in the metabasalt and may, therefore, be metamorphic in origin.

but still low-pressure, origin. Alternatively, the hornblendes in the metagabbro have retained their primary igneous compositions and the actinolites form part of the same, or a later, metamorphic event that resulted in hornblende formation in the metabasalts.

In support of a relict igneous origin for the hornblendes in the metagabbro are their high contents of Ti and alkalis ($\text{Na} + \text{K} = 0.686 \pm 0.083$) and low contents of Mn (0.024 ± 0.003). Metamorphic hornblendes with these compositional abundances are usually restricted to high-grade rocks, commonly in the granulite facies (e.g. Engel and Engel, 1962).

Bulk-rock composition and oxygen fugacity are factors which may also play an important role in determining the compositions of amphiboles. Bulk-rock oxidation ratios ($2\text{Fe}_2\text{O}_3/100/[2\text{Fe}_2\text{O}_3 + \text{FeO}] \text{ mole\%}$; Reid, 1977) in the metabasalt are significantly lower than those in the metagabbro, viz. 28.4 and 39.8 respectively, while whole-rock chemistries also show a marked difference, e.g. Ti/Al of 0.021 in metabasalt relative to 0.054 in metagabbro. These observations are compatible with those of Hietanen (1974) who finds no systematic variation in Mg/Fe or Ti in amphiboles independent of rock composition and oxygen fugacity.

3.3.3 Aunis Tonalite Gneiss

Bulk-rock compositional differences between the southern and northern portions of the Aunis Tonalite Gneiss are also reflected in the hornblende compositions (Fig. B.4). Using the classification scheme of Miyashiro (1973), it can be further seen that these hornblendes show a compositional overlap with hornblendes from both metabasalt and metagabbro in the Kairab Complex (Fig. B.8). Plutonic hornblende does, however, show a relative enrichment in Ti in comparison with metamorphic hornblende from Kairab metabasalt (despite higher bulk-rock Ti in the latter) and Ti contents in hornblendes from the Aunis Tonalite Gneiss are similar to those in several primary hornblendes in intrusive rocks from

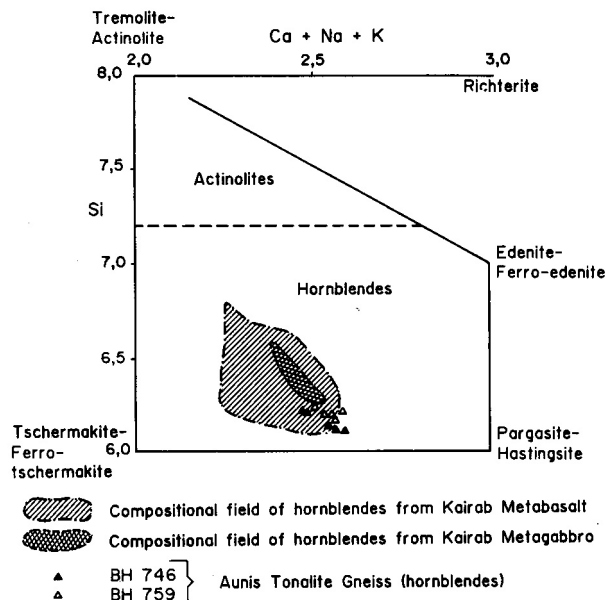


Fig. B.8: Hornblende compositions in the Aunis Tonalite Gneiss plotted according to the classification scheme of Miyashiro (1973). Compositional fields of hornblendes (mainly primary?) from the Kairab metagabbro and metamorphic hornblendes from the Kairab metabasalt are included for comparison. All data normalised to 23 oxygens.

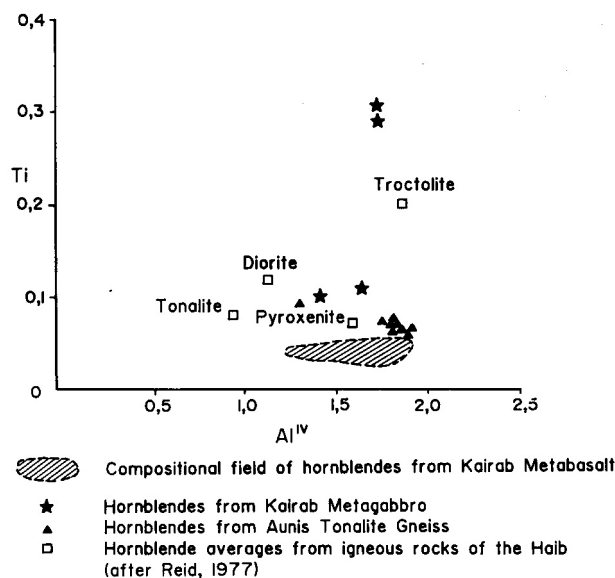


Fig. B.9: Plot of Al^{IV} vs. Ti for hornblendes from the Aunis Tonalite Gneiss compared with primary hornblendes in igneous rocks of the Haib (after Reid, 1977) and hornblendes (mainly primary?) from the Kairab metagabbro. The field occupied by metamorphic hornblendes in the Kairab metabasalt is also shown. All data normalised to 23 oxygens.

the Haib (Fig. B.9). Hornblendes of the Kairab metagabbro which contain the highest Ti contents are typically brownish-green to brown in colour compared with the more bluish-green to green colour of hornblendes in the Aunis Tonalite Gneiss. The generally higher Al^{VI} and lower (Na + K) contents of the latter could indicate that crystallisation took place at lower temperatures than in the metagabbro. The high values of Al^{VI} are illustrated by comparison with average

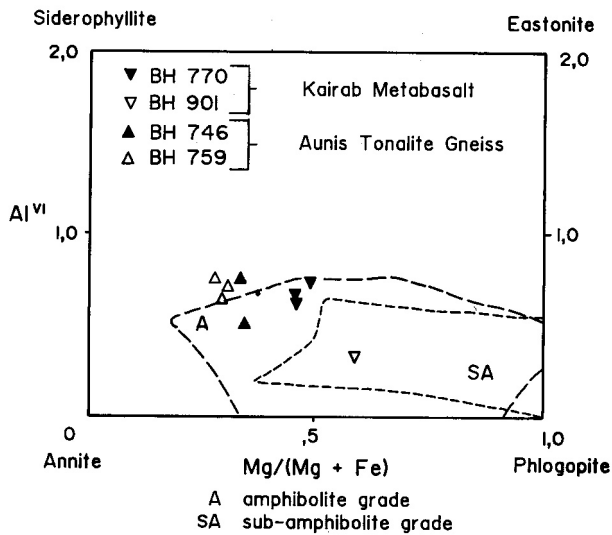


Fig. B.11: Biotite compositions from the Kairab metabasalt and Aunis Tonalite Gneiss projected onto the "ideal biotite plane" (Deer *et al.*, 1966). Fields of metamorphic grade (after Guidotti, 1984) indicate that biotites from the Kairab metabasalt are largely compatible with amphibolite grade. Biotites from the Aunis Tonalite Gneiss form a distinct compositional field which is inferred to be largely magmatic in origin. All data normalised to 22 oxygens.

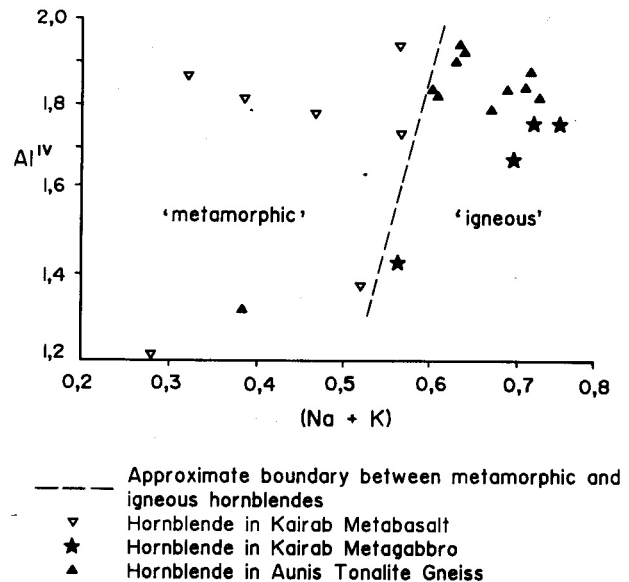


Fig. B.10: Plot of $(Na + K)$ vs. Al^{IV} for hornblendes from the Kairab Complex (metabasalt and metagabbro) and Aunis Tonalite Gneiss. The diagonal line defines the approximate boundary between hornblendes of metamorphic and igneous origin. All data normalised to 23 oxygens.

values of hornblendes from the Haib intrusive rocks (after Reid, 1977, Fig. 53) and the lower Al^{VI} values reported for hornblendes from granitic rocks of the central Sierra Nevada batholith (Dodge *et al.*, 1968).

While Al^{VI} contents of hornblendes from the Aunis Tonalite Gneiss are similar to hornblendes in the Kairab Complex, $(Na + K)$ contents are generally higher than the metabasalt but similar to the metagabbro (Fig. B.10). Together with the high Ti contents, these compositional features suggest a primary origin for most of the hornblende in the Aunis Tonalite Gneiss. The single hornblende composition which plots within the "metamorphic" field in Fig. B.10 may represent a xenocryst derived from the meta-basaltic country rock.

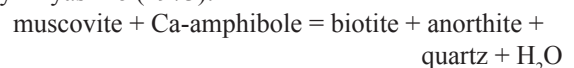
3.4 BIOTITE

3.4.1 Kairab metabasalt

Biotite analyses obtained from the Kairab metabasalt are illustrated in Fig. B.11 in terms of the "ideal biotite plane". Al^{VI} contents and $Mg/(Mg + Fe)$ ratios of these biotites fall in the range 0-1 and 0.3-1, respectively, which is regarded by Guidotti (1984) as characteristic of amphibolite-grade biotites. The mean Al^{VI} content of 0.600 ± 0.170 is, however, close to the maximum of 0.6 inferred by the same author to be typical of biotites from amphibolites and sub-amphibolites.

Titanium enrichment in biotite, like hornblende, has been correlated with prograde metamorphism (Engel and Engel, 1960). Again the coexistence of biotite with ilmenite in the metabasalt has ensured that the former is saturated with Ti. A mean Ti content of 0.209 ± 0.013 is within the range of greenschist-grade metapelites and semi-pelites, but Guidotti (1984) admits that the specific values for metabasites are not

yet well established. The relatively high content of Al^{VI} in biotites of the Kairab metabasalt may well be related to the low Ti content, since Ti increase at the expense of Al^{VI} has been alluded to by Guidotti (1984). The occasional presence of reddish-brown biotite with "lamellae" of white mica in the metabasalt may further suggest the following reaction proposed by Miyashiro (1973):



3.4.2 Aunis Tonalite Gneiss

Biotite is always present in the Aunis Tonalite Gneiss and coexists with hornblende in both samples analysed by EMP. Although hornblende-biotite mineral pairs have not been analysed, $Fe/(Fe + Mg)$ values for the two phases suggest that, at the one sigma level of confidence, more iron-rich pairs characterise the northern, more differentiated, part of the pluton. Compositional characteristics of biotite are consistent with a magmatic origin, although textural features are often ambiguous.

The relatively high Al contents of primary hornblende are also reflected by biotite compositions projected onto the siderophyllite-annite-phlogopite-eastonite quadrilateral (Fig. B.11), especially when compared with biotite compositions of Sinclair-type granitoids (Section C.3). Biotite compositions display lower $Mg/(Mg + Fe)$ ratios compared with metamorphic biotites in the Kairab metabasalt. Enrichment in Al_2O_3 in biotite is further illustrated relative to the bulk-rock composition in Fig. B.12, with data points plotting close to the outer limit of the overall range reviewed by Spear (1984).

With increased aluminium activity, biotite is commonly accompanied by aluminous minerals such as garnet and

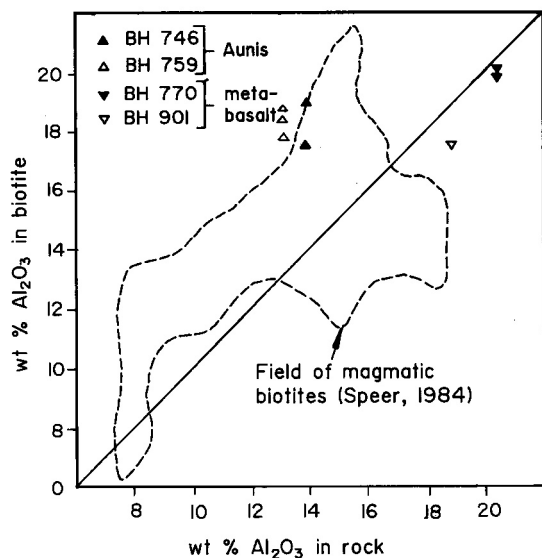


Fig. B.12: Variation in wt.% Al_2O_3 between biotite and host Aunis Tonalite Gneiss. Biotites plot in the vicinity of the most Al_2O_3 -rich part of the field of magmatic biotites (after Speer, 1984). Biotites in metabasalts are plotted for comparison.

cordierite as reported by de Albuquerque (1973) and Speer (1981). The absence of such phases typical of S-type granites may be attributed to a variety of factors such as temperature, pressure, oxygen fugacity and water fugacity (Speer, 1984). Additional factors may be the post-crystallisation history (e.g. deformation and metamorphism) and the influence of coexisting phases. The composition of biotite will itself be affected by all of these factors.

3.5 EPIDOTE

3.5.1 Kairab metabasalt

Several euhedral crystals of epidote were analysed in order to determine whether this phase is compatible with lower amphibolite facies grade or represents a later retrograde phase of metamorphism. While certain workers (e.g. Holdaway, 1965; Maruyama *et al.*, 1983) have observed a decrease in the Fe content of epidote with an increasing grade of metamorphism, other workers (e.g. Sethuraman and Moore, 1973; Jamieson, 1981) report the opposite trend. Cooper (1972) has reported that epidote compositions in metabasic rocks from the Haast Schist Group show no systematic variation with the progression from greenschist to amphibolite facies. He does, however, relate epidote composition to the iron content of the rock and the oxidation state maintained during metamorphism.

The epidotes of the Kairab metabasalt show a compositional range of pistacite from $\text{Ps}_{23.5}$ to $\text{Ps}_{26.7}$, with a bulk-rock oxidation ratio of 28.4. Very similar pistacite contents in epidotes from metabasalts of the Yap Islands in the western Pacific are shown by Maruyama *et al.* (1983) to be typical of the amphibolite facies (Fig. B.13). In conclusion it can be stated that the compositions of well-formed epidote crystals are compatible with an origin in the lower amphibolite facies. More patchy aggregates of epidote (not analysed in

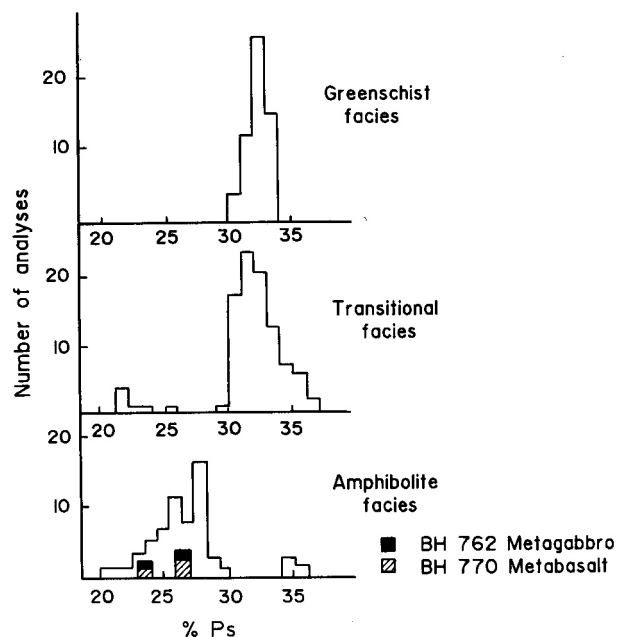


Fig. B.13: Frequency diagram of epidote compositions from Kairab metabasalt and metagabbro compared with epidote compositions from metabasalts of different metamorphic facies in the Yap Islands (Maruyama *et al.*, 1983). The low pistacite contents in epidotes of the Kairab Complex are most compatible with amphibolite facies metamorphism.

this study) may, however, represent a later retrograde metamorphic imprint.

3.5.2 Kairab metagabbro

Epidote is usually present as small scattered granules but also forms larger crystals in aggregates with amphibole. The pistacite content is very similar to that of epidote in the amphibolite facies metabasalt (Fig. B.13). However, the bulk-rock oxidation ratio of 39.8 (compared to 28.4 in the metabasalt) should result in a more iron-rich epidote according to Cooper (1972). The use of epidote composition as an indicator of metamorphic grade has, at least in this case, proved to be unsatisfactory. Clearly a greater number of analyses is required to establish what factors control the composition of epidote in the metagabbro.

3.6 CHLORITE

3.6.1 Kairab metagabbro

Although present mainly as scattered "flakes" throughout the groundmass, chlorite has, on occasion, been overprinted by actinolite. Laird (1982) reported that actinolite is distinctly more Mg-rich than coexisting chlorite, but that hornblende and chlorite have about the same Mg cationic content. Chlorite in the Kairab metagabbro has a Mg content of 5.73 ± 0.30 , which is distinctly higher than the Mg content of both hornblende (2.95 ± 0.07) and actinolite (3.69 ± 0.16). These discrepancies imply that the assemblage hornblende + actinolite + chlorite is in disequilibrium and that it may represent an arrested stage of read-justment to a higher, or lower, grade

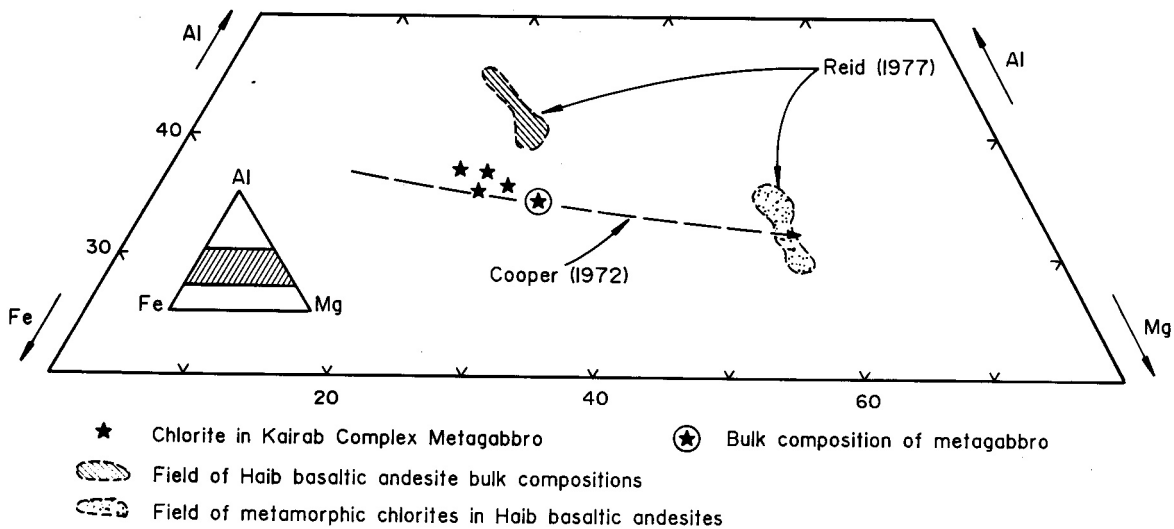


Fig. B.14: Al-Mg-Fe plot of metamorphic chlorites in the Kairab metagabbro. Compositions are compared with metamorphic chlorites from the Haast metabasites (dashed line after Cooper, 1972) and from the Haib basaltic andesites (after Reid, 1977). All data normalised to 28 oxygens.

of metamorphism. This disequilibrium is consistent with a primary origin for hornblende.

An Al-Mg-Fe plot of chlorites in the metagabbro (Fig. B.14) illustrates compositional similarities to biotite zone chlorites in the Haast metabasites (Cooper, 1972). Upper greenschist facies metamorphic chlorites from the Haib (Reid, 1977) are illustrated in Fig. B.14 for comparison. The widespread alteration of biotite to chlorite may provide support for a retrograde overprint in the metagabbro, possibly as a result of intrusive activity related to the emplacement of Kairab Complex metafelsites and Aunis Tonalite Gneiss.

3.7 SUMMARY

(i) While metabasic rocks in the Kairab Complex show a metamorphic mineralogy similar to low-medium grade amphibolites in the Garub Sequence, the presence of relict plagioclase phenocrysts (high An contents) in metabasalt and relict plagioclase and hornblende (high Ti and alkali contents) in metagabbro indicate preservation of the primary mineralogy.

(ii) The amphibolite facies grade of metamorphism is best illustrated by the Kairab metabasalts which are characterised by low Si, Ti and alkali contents in hornblende, Al^{VI} contents and $Mg/(Mg + Fe)$ ratios of biotite in the range 0-1 and 0.3-1, respectively, and epidotes in the range Ps_{23-27} .

(iii) A retrograde metamorphic imprint is represented by chlorite and actinolite growth in the Kairab metagabbro and may be related to the emplacement of younger granitoids.

(iv) Although porphyroclastic and recrystallised textures are widespread, the Aunis Tonalite Gneiss has preserved much of its primary mineralogy and compositional changes are inferred to be the result of deuteric effects rather than metamorphism.

(v) The primary nature of hornblende in the Aunis Tonalite Gneiss is suggested by relatively high contents of Ti and alkalis, and high Al^{VI} relative to the ratio $Mg/(Mg + Fe)$. Al-

though enriched in Al_2O_3 relative to the whole-rock compositions, biotite compositions plot within the field of magmatic biotites reviewed by Speer (1984).

4. WHOLE-ROCK CHEMISTRY

4.1 INTRODUCTION

Whole-rock analyses are presented on the accompanying Microfiche cards and in Table V (Appendix m) for a total of 190 samples from the AMT, 78 of which represent early-stage crust. Sample localities are illustrated on a 1: 100 000 scale geological map (Appendix I). This section concentrates on those suites for which Sr isotope and/or REE data have been obtained, viz. Kairab metabasalt and Aunis Tonalite Gneiss. Data from associated lithologic units provide an important frame of reference for discussion of the tectonomagmatic evolution of the early-stage crust.

Analyses are reported on Microfiche with total Fe expressed as Fe_2O_3 . However, an estimate of the Fe_2O_3/FeO ratio is required in order to accurately calculate both the CIPW norm and Mg# (molecular $MgO/[MgO + FeO]$) values. Le Maitre (1976) proposed the calculation of an oxidation ratio ($FeO/[FeO + Fe_2O_3]$) based on multiple regression formulae for volcanic and plutonic rocks:

$$Ox_{(volcanic)} = 0.93 - 0.0042 SiO_2 - 0.022 (Na_2O + K_2O)$$

$$Ox_{(plutonic)} = 0.88 - 0.0016 SiO_2 - 0.027 (Na_2O + K_2O)$$

This method is favoured for the calculation of Fe_2O_3/FeO ratios in early- and late-stage AMT rocks for the following reasons:

(a) The oxides used in the formulae are assumed to be largely unaffected by alteration (see following discussion).

(b) The oxidation ratios are based on a statistical database of nearly 26000 analyses which provide more realistic mean values as opposed to the maximum values ($Fe_2O_3 = TiO_2 + 1.5$ wt. %) suggested by Irvine and Baragar (1971).

(c) Where titrimetric determinations have been carried out on FeO contents, these values compare favourably with those

calculated by the method of Le Maitre (1976).

Occasionally the stability of the major oxides is in question and in these cases the use of $\text{Fe}_2\text{O}_3/\text{FeO}$ ratios typical of modern magma type equivalents is preferable. Mg# values in particular are sensitive to the $\text{Fe}_2\text{O}_3/\text{FeO}$ ratio and the selection of so-called "unrupted" ratios has been resorted to in the calculation of these values (cf. Gill, 1981).

The degree of alteration in igneous rocks of the early-stage crust is discussed in the following section and is of particular importance where comparisons are made between ancient and modern rock suites. Alteration is considered here to represent any process, generally post-consolidation, which has changed the original chemical composition of an igneous rock. While the effects of weathering may be excluded to some extent by careful sample selection, the influence of such processes as metamorphism and metasomatism may be more subtle and the effects less easily avoided during sampling.

4.2 ASSESSMENT OF ALTERATION

The most severe alteration in the early-stage crust of the AMT probably occurs in metabasalts of the Kairab Complex. The presence of pillows in these basaltic rocks suggests the possibility of both sub-aqueous weathering and hydrothermal alteration caused by subvolcanic igneous intrusions. However, the amphibolite grade of metamorphism is too high to use LOI (volatile content) as a measure of any hydrous alteration, since prograde reactions typically result in significant dehydration.

Although some evidence for element mobility should be expected in metabasic rocks (Floyd, 1976; Beswick and Soucie, 1978), alteration during metamorphism may give rise to the redistribution of elements on the scale of the sample rather than a complete change in element concentrations (Smith, 1968). The possibility of nearly isochemical metamorphism may be considered in the case of the Kairab metabasalts in view of the large sample masses (± 6 kg) taken. In order to test this possibility, the approach of Beswick and Soucie (1978) was used and is illustrated in Fig. B.15. This approach compares major oxide molecular proportion ratios in metavolcanic rocks to the same ratios in essentially unaltered post-Mesozoic suites. The common denominator in these ratios is K_2O , which is retained in the liquid phase until late stages of fractionation prior to the crystallisation of K-feldspar.

In general, deviations from unaltered trends in Fig. B.15 are not significant in terms of vertical and horizontal displacements. However, considerable displacement is indicated for three samples along a 45° positively sloping line as a result of their extremely low K_2O contents. Potassium depletion may be the result of metamorphism in these samples, since mobility of both Sr and K has been reported in low-grade basaltic rocks (Smith and Smith, 1976) and could, therefore, reflect a retrograde metamorphic overprint in the case of the medium-grade Kairab metabasalts.

When compared with the metabasalts, metafelsites in the Kairab Complex plot closer to the origin and show greater deviation from the unaltered trends in Fig. B.15. The data

scatter is compatible with some silicification and lesser Ca depletion in these lavas. Accordingly, mobile elements (e.g. LILE) must be used with caution in any geochemical classification. However, the degree of scatter is not extreme and no correction procedure was considered necessary.

In conclusion, nearly isochemical metamorphism may be assumed for the majority of eruptive rocks in the Kairab Complex provided that obviously sheared and altered zones are avoided during sampling. If similar constraints are applied to associated meta-intrusive rocks in the Kairab Complex, then an assumption of only limited mobility of the major elements may be considered reasonable.

4.3 GEOCHEMICAL CHARACTERISATION

4.3.1 Kairab Complex

4.3.1.1 Metavolcanic succession

(i) Classification

The metavolcanics of the Kairab Complex display a wide range in composition from "basalt" to "rhyolite" on the total alkali-silica (TAS) diagram (Fig. B.16) in which compositional fields are defined according to Le Bas *et al.* (1986). The paucity of compositions in the "basaltic andesite" to "dacite" range is noteworthy and illustrates the bimodal nature of this succession (Table B.2). A limited effect of post-consolidation processes such as alteration and metamorphism is suggested by the similar compositional fields (according to Winchester and Floyd, 1977) illustrated for these lavas in immobile element ratio plots (e.g. Zr/TiO_2 versus SiO_2 ; Fig. B.30). These plots do, however, suggest that some of the basaltic rocks show well-defined alkaline tendencies, a characteristic which is not well illustrated in Fig. B.16. This alkaline tendency is also not borne out by the low TiO_2 concentrations, particularly when plotted on the widely used $\text{Zr}/\text{P}_2\text{O}_5$ versus TiO_2 plot (Fig. B.17) in which magma types are defined according to Floyd and Winchester (1975).

In order to differentiate between the two subalkalic series, tholeiitic and calc-alkaline, several criteria may be used, viz. alkali contents, iron-enrichment, groundmass mineralogy and normative mineralogy (Gill, 1981, p. 8). Some of these criteria have been employed in the TAS (Fig. B.16) and AFM (Fig. B.18) diagrams and provide good evidence for the tholeiitic nature of the bulk of the metavolcanic succession. The apparent calc-alkaline classification of several samples in these diagrams may, however, be attributed to enhanced concentrations of total alkalis as a result of alteration. By contrast, concentrations of the "stable" oxide Al_2O_3 in the Kairab basalts are generally high when compared with typical tholeiitic series reported by Irvine and Baragar (1971). So-called high-alumina basalt was originally defined by Kuno (1960, p. 122) as basalt having a "higher content of Al_2O_3 (generally higher than 17 per cent and rarely as low as 16 per cent) than that of the tholeiite with the corresponding SiO_2 and total alkalis, and by lower alkali content than that of the alkali basalt, provided only aphyric rocks are compared".

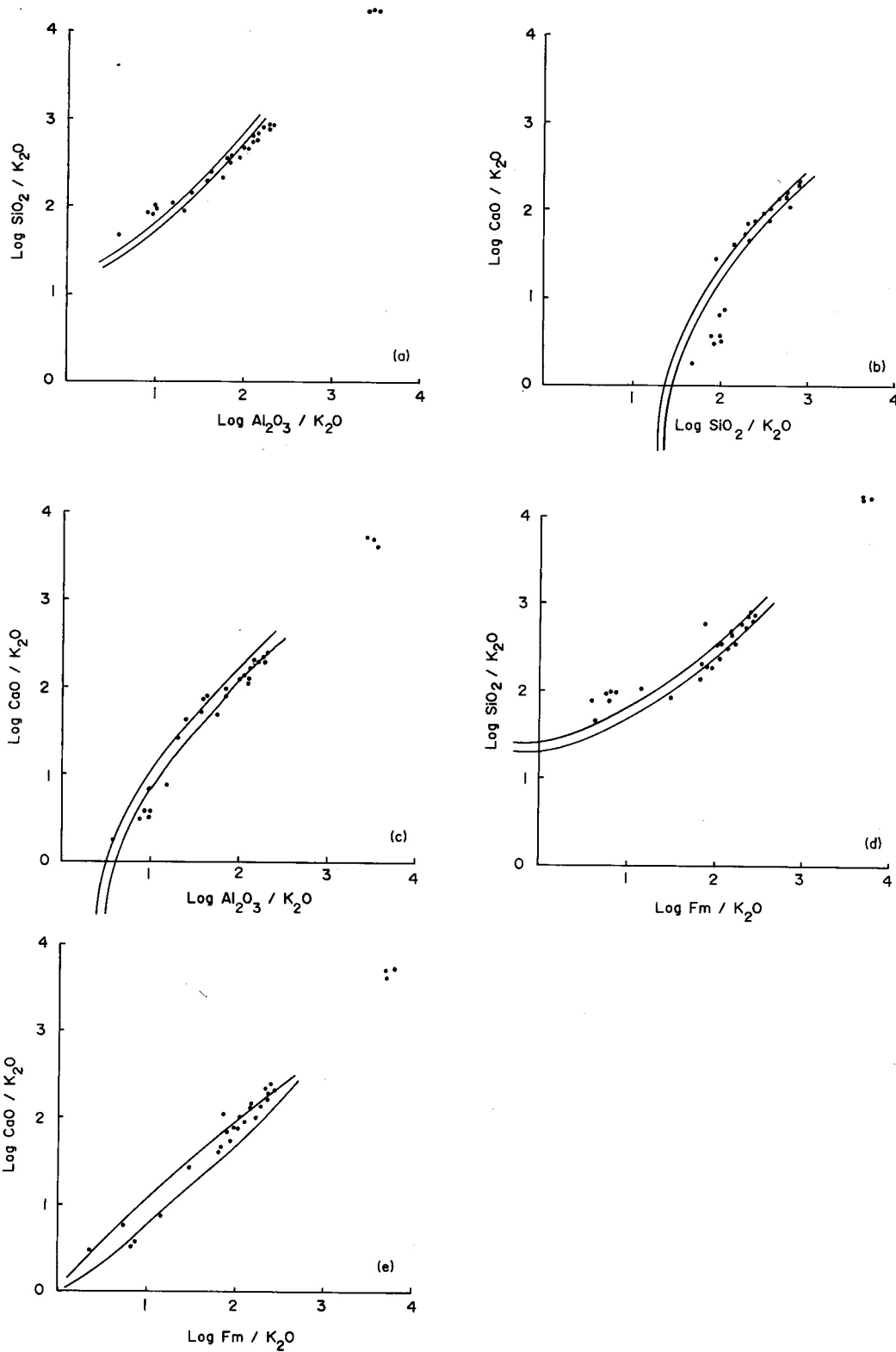


Fig. B.15: Logarithmic oxide molecular ratio plots for the Kairab metavolcanic succession compared with trends for modern suites (after Beswick and Soucie, 1978). Fm = FeO + MgO + MnO.

Using the abovementioned chemical characteristics, Middlemost (1975) devised a plot of Al₂O₃ versus alkali-index ($[\text{Na}_2\text{O} + \text{K}_2\text{O}] / \{[\text{SiO}_2 - 43] * 0.17\}$) in order to separate high-alumina basalts from other more common sub-alkalic basalts. This plot is illustrated in Fig. B.19, where it is used to differentiate between basalts in the Kairab Complex. The high-alumina basalts are typically rich in plagioclase

phenocrysts and hence do not satisfy Kuno's original stipulation that only aphyric rocks be compared. However, the term "high-alumina" basalt has been applied extensively to plagioclase-porphyrific lavas in the Aleutian Arc (Brophy, 1986, 1987; Brophy and Marsh, 1986; Gust and Perfit, 1987; Myers *et al.*, 1986), although the primary (and non-accumulative) nature of these lavas is the subject of much

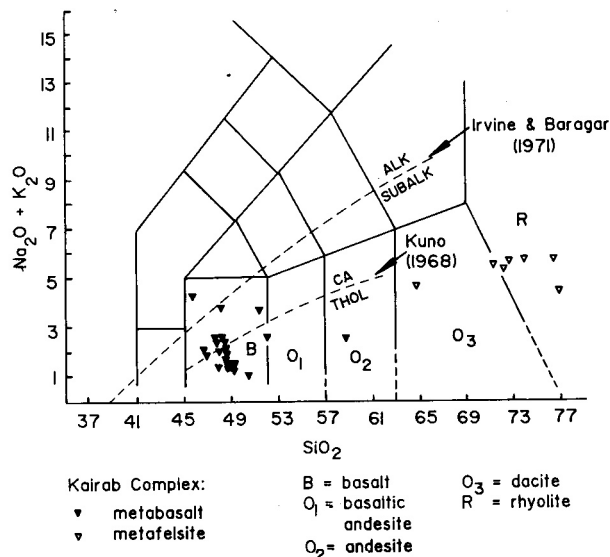


Fig. B.16: Total alkali-silica (TAS) diagram showing distribution of data for the Kairab metavolcanic succession. Rock group subdivision is according to Le Bas *et al.* (1986). Boundaries between tholeiitic (THOL) and calc-alkaline (CA), and sub-alkaline (SUBALK) and alkaline (ALK) fields are according to Kuno (1968) and Irvine and Baragar (1971), respectively.

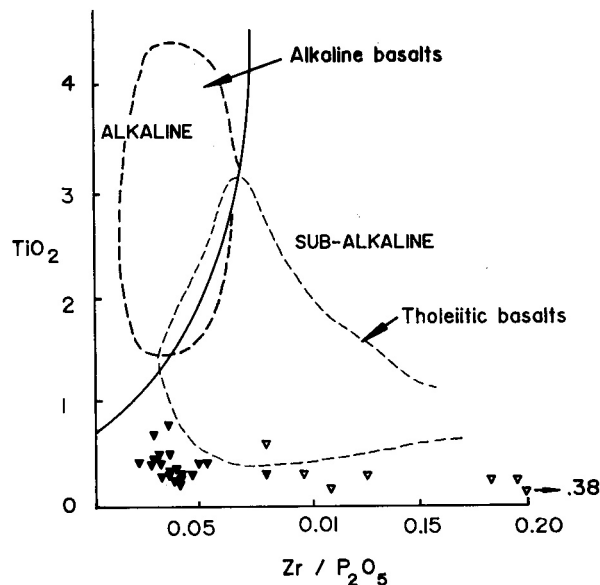


Fig. B.17: Zr/P₂O₅ vs. TiO₂ plot illustrating the subalkaline character of the Kairab metavolcanic succession. Magma type divide and fields are from Floyd and Winchester (1975).

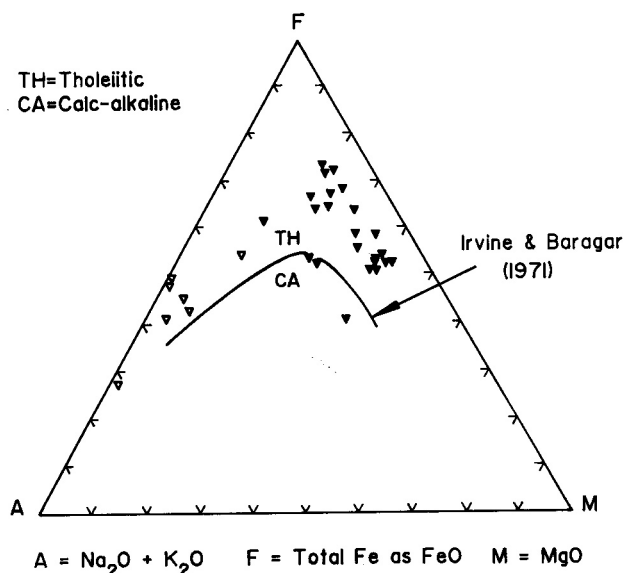


Fig. B.18: AFM diagram showing compositional variation of the Kairab metavolcanic succession. Boundary between tholeiitic and calc-alkaline fields is according to Irvine and Baragar (1971).

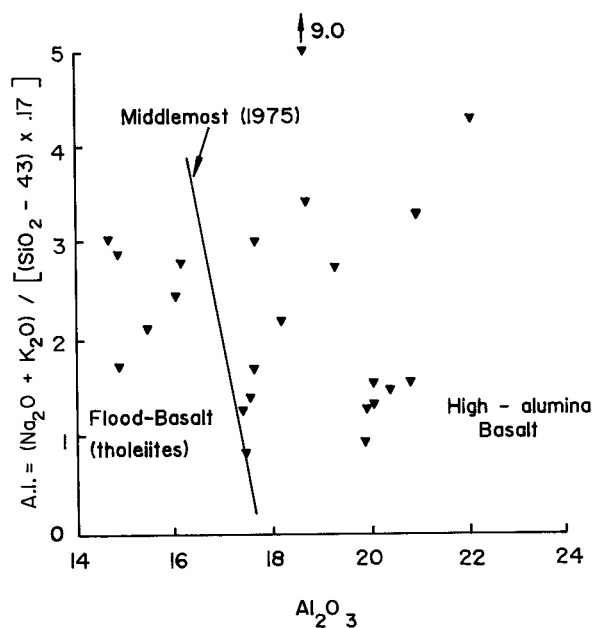


Fig. B.19: Alumina vs. alkali index (A.I.) diagram showing the high-alumina to tholeiitic character of the Kairab metabasalts. Boundary line and fields after Middlemost (1975).

debate.

Kairab metafelsites are typically rhyolitic and form both a low-silica (71-75% SiO₂) and high-silica (> 75% SiO₂) group. From Table B.2, comparison of these two groups indicates that the high-silica group is characterised by lower contents of all oxides except SiO₂ and total alkalis. However, total alkalis never reach levels out of the subalkaline and calc-alkaline fields (Figs B.16 and B.18) of Irvine and Baragar (1971). High field strength element (HFSE) contents are broadly similar in both rhyolite groups, but slightly higher in the high-silica group, whereas light rare earth elements (LREE) are slightly lower in the latter group.

(ii) Comparison with modern volcanic suites

The average compositions listed in Table B.2 are not ideal for comparative purposes since both boundary conditions and statistical significance vary considerably for averages reported in the literature. Accordingly, Fig. B.20 better illustrates the averages and ranges of several diagnostic and relatively stable elements in the Kairab basalts as compared with data for modern basalts compiled by MacLean *et al.* (1982). This figure indicates that the so-called immobile elements Ti, Y, Zr and Nb in Kairab basalts differ from recent flows in two main aspects:

(a) Element abundances occupy a relatively narrow range

TABLE B.2: Average chemical compositions of metavolcanics in the Kairab Complex.

	THOLEIITE		DEPLETED THOLEIITE		HIGH-AL BASALT		ANDESITE DACITE		RHYOLITE			
	(n=6)		(n=2)		(n=14)		(n=1)	(n=1)	LOW-SiO ₂		HIGH-SiO ₂	
	mean	s.d.	mean	s.d.	mean	s.d.	mean	mean	mean	s.d.	mean	s.d.
SiO ₂	47.98	.61	49.60	.96	48.49	1.51	58.62	64.78	72.52	1.00	76.59	.43
TiO ₂	.38	.04	.33	.12	.40	.13	.67	.58	.24	.08	.17	.10
Al ₂ O ₃	15.30	.64	17.48	.16	19.35	1.43	19.89	16.00	12.60	.76	11.64	1.15
Fe ₂ O ₃ *	12.11	1.04	9.41	2.37	12.35	1.21	6.71	8.08	5.33	.71	3.63	1.73
MnO	.26	.05	.16	.03	.24	.05	.13	.08	.16	.06	.14	.13
MgO	7.64	.61	7.01	.77	4.37	1.19	1.18	1.56	.47	.37	.07	.10
CaO	14.14	1.53	13.51	.48	12.63	1.43	10.08	4.21	3.11	1.04	2.68	.01
Na ₂ O	1.78	.30	2.28	1.75	1.89	.84	2.38	3.62	4.29	.25	3.04	1.69
K ₂ O	.31	.18	.20	.05	.18	.19	.15	.93	1.20	.12	1.99	.78
P ₂ O ₅	.11	.03	.02	.01	.10	.03	.19	.16	.08	.02	.05	.02
Nb	6.4	2.7	1.8	.5	7.2	1.9	.9	4.7	5.1	2.1	6.5	5.1
Zr	38	12	12	5.0	38	4.2	56	125	95	5.9	112	2.6
Y	12	1.9	7.9	.1	9.4	3.2	25	36	37	11	38	26
Sr	245	83	212	40	264	47	301	251	150	51	136	98
Rb	9.3	3.0	1.7	1.0	6.8	3.2	1.0	30	24	6.8	35	23
Th	1.0	1.1	n.a.		.8	.8	2.7	2.6	2.0	1.0	1.4	1.3
Pb	13	4.8	n.a.		8.9	4.3	3.0	2.9	4.6	3.6	6.8	6.1
Zn	88	31	78	23	89	19	68	116	59	14	57	30
Cu	63	72	113	150	84	57	84	5.6	3.9	3.5	1.9	2.0
Ni	110	68	50	16	18	12	4.8	2.5	1.5	.8	1.4	1.2
Co	44	12	n.a.		35	6.7	16	5.6	6.3	5.8	14	14
Cr	324		144	13	13		15	9.8	15	4.5	16	
V	341	46	299	66	376	48	173	23	8.9	10.7	18	2.5
Ba	106	30	15	9.5	112	60	33	174	360	205	367	58
Sc	52		51	.7	38		34	26	15	2.1	6.6	
La	3.8		2.2	1.4	6.6		1.3	11	10	1.4	8.2	
Ce	3.1		n.a.		9.9		9.5	24	25	3.5	20	
Nd	2.0		n.a.		8.7		9.6	18	18	4.5	13	
Cs	1.8		n.a.		1.6		1.4	3.4	2.8	1.6	1.1	
Mg#	60	2	64	3.0	45	8	29	31	16	12	6	8

Major oxide concentrations in wt.%; trace element concentrations in ppm

All Fe expressed as Fe₂O₃*

n.a. = not analysed; s.d. = standard deviation (1σ)

of values.

(b) Element concentrations are generally close to the lower limit displayed by modern basalts.

Although absolute abundances of these elements may be subject to variation as a result of a variety of both open and closed system magmatic and metamorphic processes, the low overall contents of Ti, Y, Zr and Nb in Kairab basalts do not

favour within-plate settings such as ocean islands and continental interiors. Abundances of Ti, Y and Zr are also low relative to typical mid-ocean ridge basalts. Together with the tholeiitic character demonstrated in the previous section, it is clear that the trace element abundances of the Kairab basalts most closely resemble those of island-arc or back-arc tholeiites.

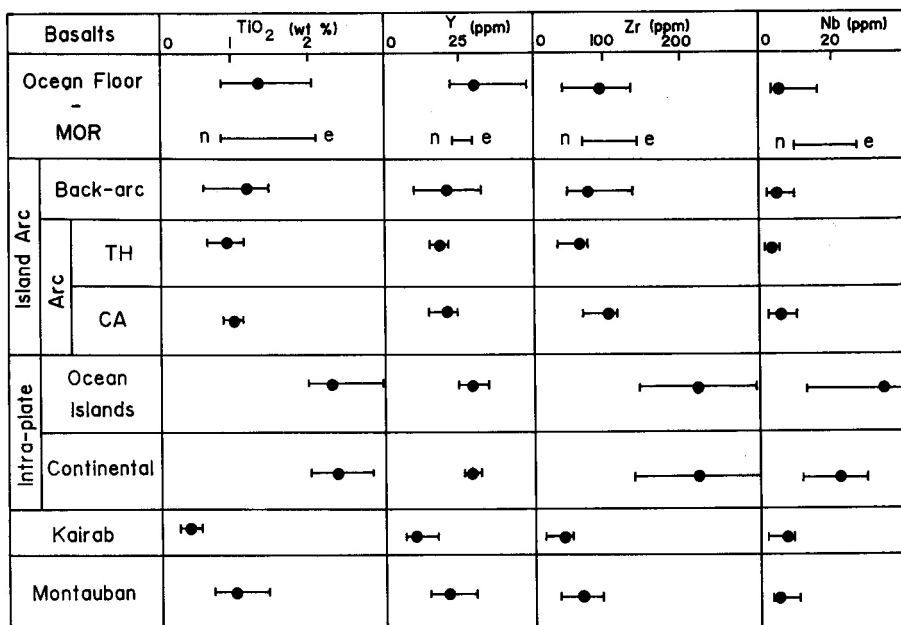


Fig. B.20: Comparison of “immobile” elements in Kairab metabasalts with modern basalts and Montauban metabasalts. Data ranges and averages (filled circles) compiled by MacLean *et al.* (1982) for modern and Montauban basalts.

The generally low abundances of the compatible elements Ni (mean = 46 ppm) and Cr (mean = 103 ppm) in the Kairab basalts are also fairly typical of island-arc tholeiites (< 50 ppm for both according to Jakeš and Gill, 1970, and Jakeš and White, 1972), although high values have been reported in the literature (Brown *et al.*, 1977). A plot of Y versus Ni (Crawford and Keays, 1978) provides a useful means of illustrating the contrasting abundances of HFSE and compatible elements in tholeiites from the ocean-floor as opposed to island arcs (Fig. B.21).

Shervais (1982) has demonstrated that Ti/V ratios of volcanic rocks reflect the oxygen fugacities of the magma and are typically lowest in tholeiites from island arcs compared

with MORB, continental flood basalts and alkali basalts of ocean islands. This ratio may also be used in altered rocks since Ti and V behave coherently during alteration. Analyses of the Kairab basalts show an average Ti/V ratio of about 6, but a range from less than 5 to around 20 (Fig. B.22). While Ti/V ratios of less than 10 are most characteristic of boninites, a wide range in Ti/V ratios in samples from a restricted geographical area may be diagnostic of a back-arc setting (Shervais, 1982).

The amphibolite facies grade of metamorphism typical of basalts of the Kairab Complex does not, in general, appear to have disturbed the incompatible elements as witnessed by their narrow compositional ranges. Although the evidence

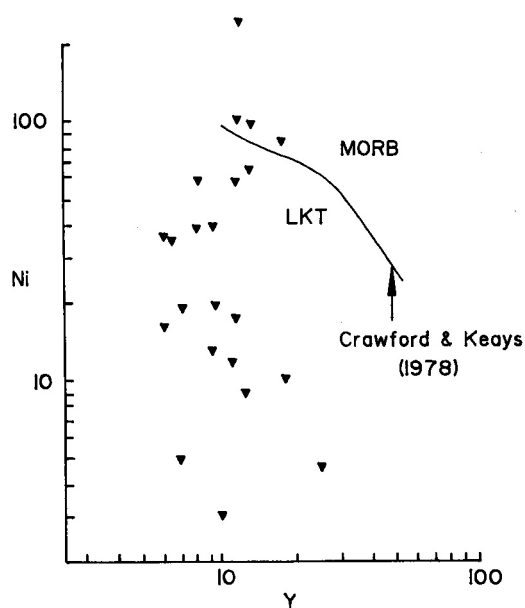


Fig. B.21: Y vs. Ni diagram illustrating that the bulk of the data for Kairab basalts plot within the low-K tholeiite (LKT) field. Field boundary taken from Crawford and Keays (1978).

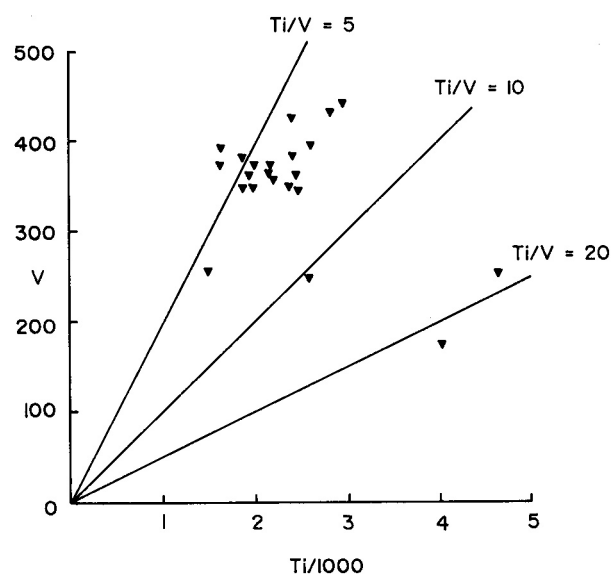


Fig. B.22: Ti vs. V plot of Kairab basalts, showing trend lines of constant Ti/V ratios = 5, 10 and 20 for reference (modified from Shervais, 1982). See text for discussion.

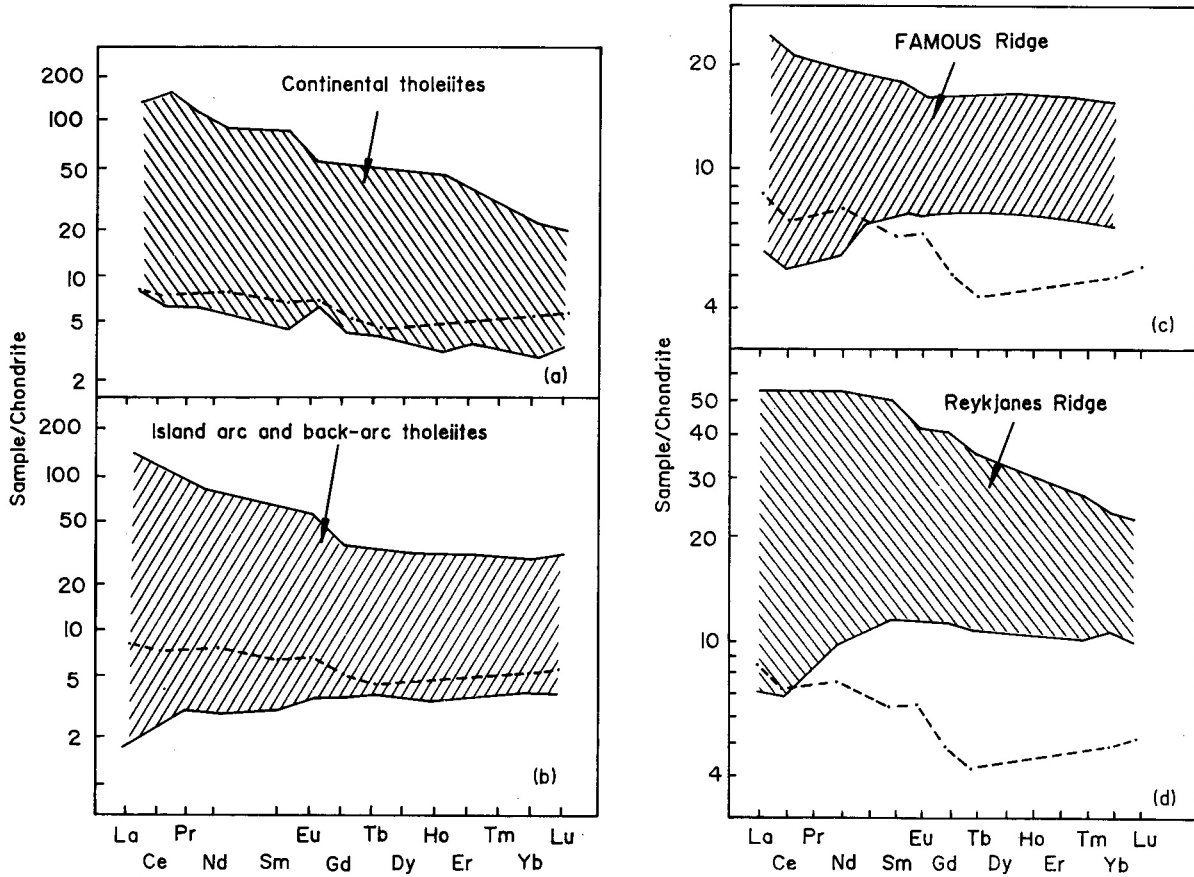


Fig. B.23: Comparison between the chondrite-normalised REE pattern for pillow-bearing high-alumina basalt in the Kairab Complex (broken line) and REE distributions (shaded areas) from (a) continental tholeiites, (b) island-arc and back-arc tholeiites, (c) & (d) transitional mid-ocean ridge segments. Data compilations: (a) & (b) from Cullers and Graf (1984), (c) & (d) from Saunders (1984).

for element immobility is largely qualitative, compositional stability appears to be borne out by the only slightly LREE-enriched pattern ($La_N/Yb_N = 1.7$) of pillow-bearing high-alumina basalt (Fig. B.23). Comparative fields for continental tholeiites as well as island-arc and back-arc tholeiites indicate that the profile of this basalt is more typical of the latter group. The slightly positive Eu anomaly, as also shown by the lower margin of the field, is certainly atypical of continental tholeiites and is not sufficiently pronounced to suggest plagioclase accumulation. While slight LREE enrichment is not uncommon in transitional ridge segments, the patterns displayed are distinctly different from that of the Kairab basalt (Fig. B.23). The latter pattern is similar to high-alumina Atka basalts in the Aleutian Arc (Myers *et al.*, 1986), although overall enrichment is not as great (Fig. B.24).

Further trace element characterisation of the Kairab basalts can be achieved by using MORB-normalised abundance patterns (Pearce, 1982). Three sample groups were chosen for display in Fig. B.25, viz. tholeiites, “depleted” tholeiites and high-alumina basalts. Since MORB-normalised patterns are thought to reflect source region characteristics independent of magmatic processes such as fractional crystallisation and partial melting, the following observations can be made by comparison of patterns in Fig. B.25 with those typical of a range of modern sources (Pearce, 1982, 1983):

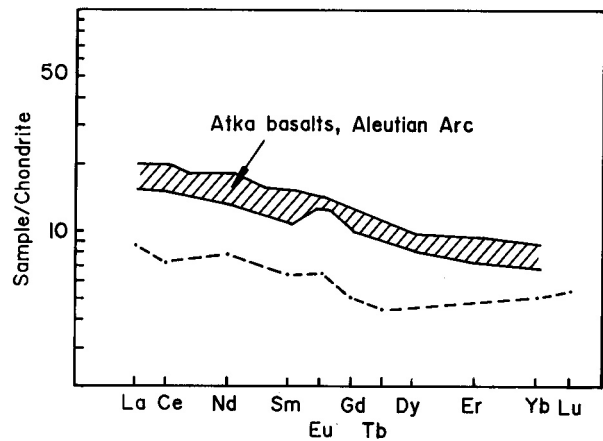


Fig. B.24: Comparison between the chondrite-normalised REE pattern for pillow-bearing Kairab basalt (broken line) and patterns for the high-alumina Atka basalts from the Aleutian Arc (after Myers *et al.*, 1977).

(a) Both tholeiitic and high-alumina basalts show features in common with volcanic-arc magma types, viz. an enrichment in the elements Sr, K, Rb, Ba and Th, and a depletion in the elements Ce, P, Zr, (Sm), Ti, Y and (Yb).

(b) The slight enrichment in Nb and sometimes Sc and Cr in the tholeiitic and high-alumina basalts is, however, somewhat anomalous and resembles patterns displayed by transitional volcanic-arc basalts.

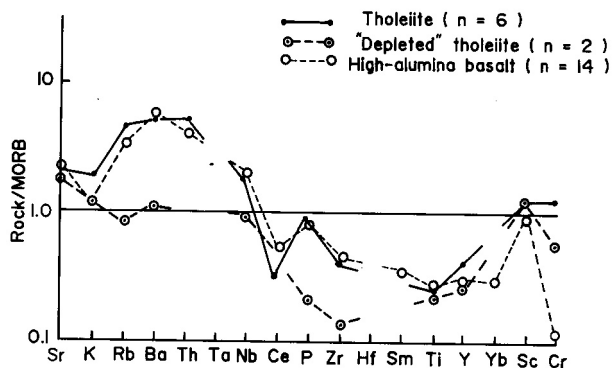


Fig. B.25: MORB-normalised minor and trace element variation diagram for Kairab tholeiites, "depleted" tholeiites and high-alumina basalts. Normalising abundances according to Pearce (1982, 1983).

(c) While patterns obtained in the first two groups are largely similar, the "depleted" tholeiitic basalts are characterised by MORB-like abundances for several of the LIL elements (K, Rb, Ba), but significant depletion in the elements P, Zr, Ti, and Y. The continuity of depletion in these elements suggests that this is a primary feature.

Pyroclastic rhyolites, although volumetrically subordinate to associated basalts, form an important part of the metavolcanic succession in the Kairab Complex. The compositional characteristics of both low- and high-silica rhyolites are best illustrated in "spidergrams" (Fig. B.26) using the procedure of Thompson *et al.* (1984). These spidergrams incorporate comparative data from rhyolites of both intra-continental rifts and intra-arc regions of Cenozoic age (compiled by Sylvester

et al., 1987), and illustrate that the Kairab rhyolites most closely resemble the rhyolites of subduction-related suites. This similarity is further borne out by the wide range in SiO_2 (71-77 wt. %), relatively high concentrations of $\text{Al}_2\text{O}_3 + \text{CaO}$ (mean > 14.33 wt. %) and low total alkalis (mean < 5.5 wt. %) in the Kairab rhyolites.

Both low- and high- SiO_2 Kairab rhyolites show overall chemical similarities to high- SiO_2 oceanic island-arc rhyolites in a chondrite-normalised spidergram (Fig. B.27). Of particular interest are the pronounced negative Th anomalies, since Th depletion is regarded as typical of high- SiO_2 oceanic island-arc rhyolites as opposed to rhyolites formed in continental arcs and intracontinental rifts (Sylvester *et al.*, 1987).

(iii) Comparison with ancient volcanic suites

Many of the geochemical characteristics of the Kairab basalts discussed in the previous section are notably similar to Proterozoic amphibolites at Montauban-les-Mines in the Grenville Province of Quebec (MacLean *et al.*, 1982). This comparison is particularly applicable since it involves rocks of similar origin and composition (pillow-bearing basalts), metamorphic grade (amphibolite facies), age (Proterozoic), and tectonic situation (adjacent to broadly contemporaneous, relatively undeformed, rift-related volcanics). The geochemical similarities are illustrated in Figs B.20 and B.28 and MacLean *et al.* (1982) conclude that the data for the metabasalts and other amphibolites at Montauban are most compatible with tholeiitic volcanism in an island-arc environment. Cr and Ni contents are, however, relatively high compared with Kairab basalts and more typical of a back-arc environment.

Proterozoic amphibolites in the Bushmanland Group of

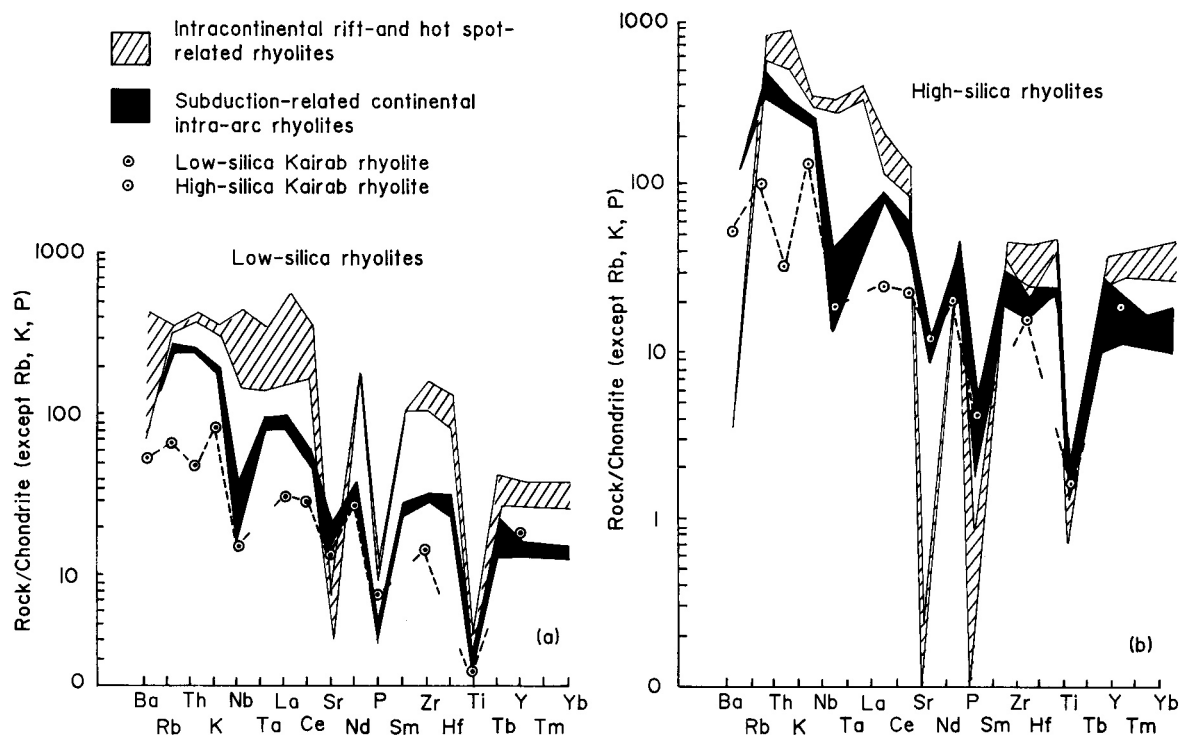


Fig. B.26: Chondrite-normalised minor and trace element variation diagrams for (a) average low-silica (70-75 wt.%) and (b) average high-silica (>75 wt.%) Kairab rhyolites following the procedure of Thompson *et al.* (1984). Data compilations for intracontinental and subduction-related rhyolites are from Sylvester *et al.* (1987).

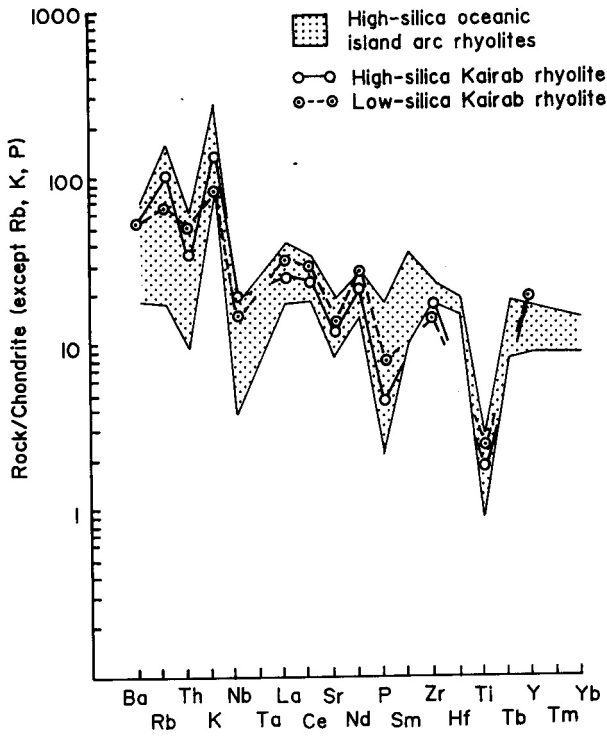


Fig. B.27: Chondrite-normalised minor and trace element variation diagram for high-silica (> 75 wt.%) Kairab rhyolites compared with high-silica oceanic island-arc rhyolites. Plotting procedure and data compilation as for Fig. B.26.

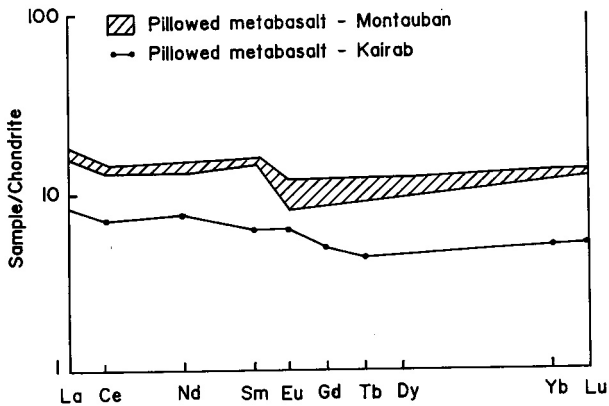


Fig. B.28: Comparison between chondrite-normalised REE patterns for the Kairab and Montauban (after MacLean *et al.*, 1982) pillowed metabasalts.

the Namaqualand Metamorphic Complex have been studied in detail by Reid *et al.* (1987). These workers show that the Bushmanland amphibolites contain tholeiitic basalts which are enriched in Ni relative to modern basalts. When compared with the Bushmanland basalts in a plot of Mg# (molecular $MgO/[MgO + FeO]$ adjusted to wt. % $Fe_2O_3/FeO = 0.2$) versus Ni (Fig. B.29), it is clear that the Kairab basalts are generally characterised by considerably lower Ni contents. While Gill (1979) regards relatively high Ni contents as typical of Archaean tholeiites, the comparatively low Ni contents in the Kairab basalts are more typical of modern analogues, especially island-arc tholeiites. Relatively high Ni contents and high Mg# values in the Kairab basalts are generally restricted to those samples which are not characterised by high-alumina compositions and show in Fig. B.29

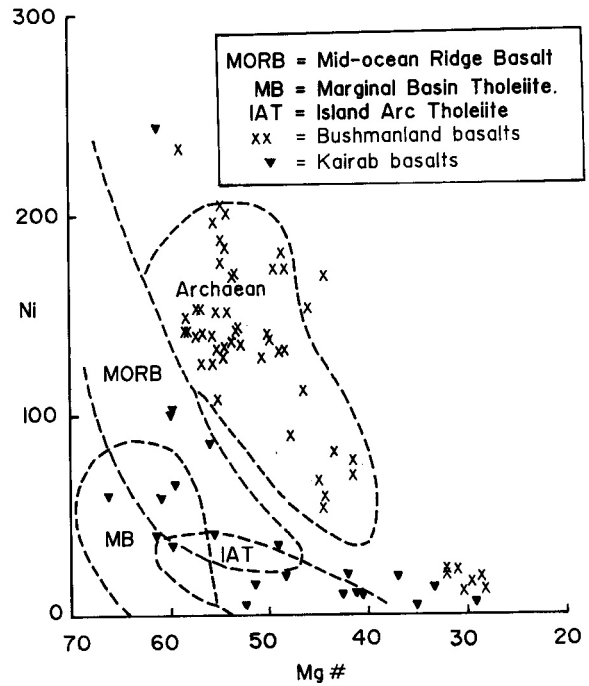


Fig. B.29: Mg# vs. Ni diagram comparing Kairab basalts with Proterozoic Bushmanland basalts (after Reid *et al.*, 1987). Modern and Archaean basalt fields are from Gill (1979).

a close resemblance to tholeiites from mid ocean ridges and marginal basins.

The overall chemical similarity of the Kairab basalts to amphibolites of the Areachap Group in South Africa has important geotectonic implications. Situated some 700 km to the southeast of the AMT and along the eastern margin of the NMC, massive amphibolites of the Bokspuits sequence (within the Areachap Group) chemically resemble low-K arc tholeiites (Geringer, *et al.*, 1986). A more detailed discussion on the regional significance of this similarity is given in Part D.

The bimodal nature of the Kairab metavolcanics together with the low-K tholeiitic character of many of the basalts bear similarities to several Archaean greenstone belts described from the Canadian Shield, e.g. Michipicoten (Sylvester *et al.*, 1987) and the Huronian (Jolly, 1987). The compositional characteristics of the Kairab rhyolites compare favourably with those of the Michipicoten rhyolitic ash-flow tuffs, e.g. similar patterns in chondrite-normalised spidergrams, the latter having been interpreted as subaerial to submarine arc eruptions. LILE and LREE contents of the calc-alkaline rhyolites in the Huronian rift are, however, generally higher than the Kairab rhyolites and are interpreted by Jolly (1987) to have been erupted in a developing continental rift zone. In both the Michipicoten and Huronian greenstones, the compositional characteristics of the rhyolites clearly depend on the nature of the crustal sources which have undergone partial melting/anatexis.

Bimodality alone does not provide sufficient evidence for a continental rift setting and may be attributed to several causes:

(a) In ancient back-arc basins, bimodal volcanics may reflect felsic input from the arc and mafic input in the basin (Condie, 1986).

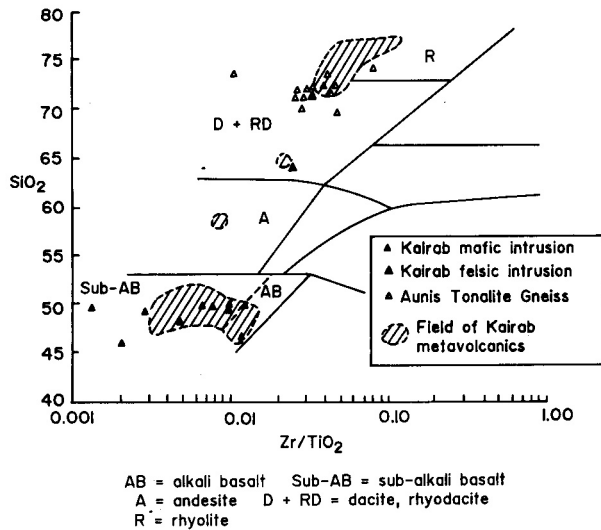


Fig. B.30: Zr/TiO_2 vs. SiO_2 diagram showing the similarities in composition between early-stage intrusive units and the Kairab metavolcanic succession. Rock group divisions are according to Winchester and Floyd (1977).

(b) Paucity of andesitic magma along an immature oceanic island arc, e.g. Kermadec-Tonga arc, or along a predominantly rhyolitic continental arc, e.g. Taupo volcanic zone, may result in bimodal volcanic successions (Sylvester *et al.*, 1987).

(c) Liquidus surfaces have shallow slopes at shallow depths (< 10 km), so that fractional crystallisation may give rise to bimodal magmas (Grove and Donnelly-Nolan, 1986).

(d) A dual source such as concomitant partial melting in the mantle and in overlying crust (Glikson, pers. comm., 1989).

4.3.1.2 Meta-intrusive suites

While not discussed in any detail here, selected major and trace element data of metagabbroic and metafelsitic intrusive rocks are presented in Figs B.30 and B.31 in order to illustrate their relationship to associated metavolcanics in the Kairab Complex. The plot of Zr/TiO_2 versus SiO_2 (Fig. B.30) indicates a close compositional association between the volcanics and later intrusive rocks. The relatively wide spread in Zr/TiO_2 ratios for the metagabbroids is possibly due to their wider regional distribution compared with the metabasalts.

The bimodality of the metavolcanics is also reflected in the meta-intrusive suite in both Fig. B.30 and on an AFM diagram (Fig. B.31). The displacement of the meta-intrusive rocks towards more MgO -rich compositions (and higher $Mg\#$ values) compared with the metavolcanics is probably the result of their cumulate origin rather than indicative of a more primitive nature. Substantial compositional variability exists within the suite of metagabbros (Appendix III - Table V), especially for the more mobile elements such as the alkalis. Such variation is not uncommon in Proterozoic metagabbros from bimodal suites, e.g. Salida gabbros in central Colorado (Boardman and Condie, 1986). While broadly similar compositional variation is displayed by the

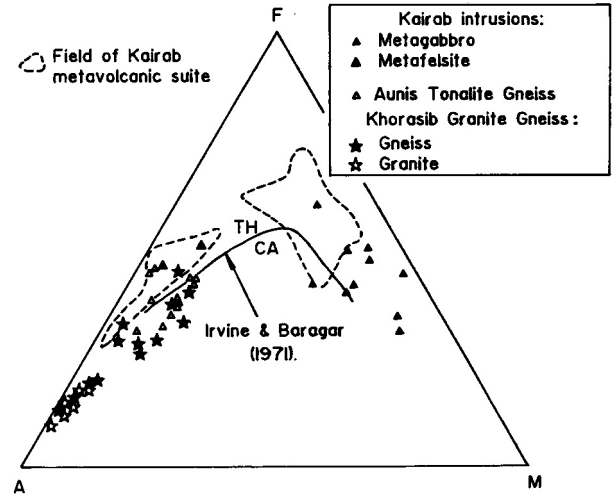


Fig. B.31: AFM diagram showing compositional variation of intrusive rocks which make up the early-stage crust of the AMT. The fields occupied by the Kairab metavolcanic succession are plotted for comparison.

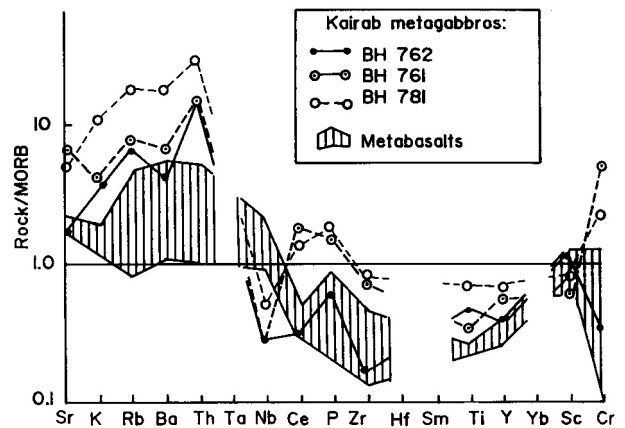


Fig. B.32: MORB-normalised minor and trace element variation diagram for Kairab metagabbros compared with the envelope of patterns obtained for associated metabasalts. Normalising procedure according to Pearce (1982, 1983).

associated metavolcanics, certain compositional types are unique to the lavas, e.g. high-alumina basalt.

A more rigorous comparative treatment would be to consider only those gabbros which are unequivocally associated with eruptive rocks both spatially and, probably, temporally. Potentially of greatest importance are those gabbros which are stratigraphically associated with the high-alumina pillow-bearing basalts to the southwest of Chowachasib Mountain (see Section B.2). MORB-normalised plots are presented in Fig. B.32 for three of these gabbros together with the envelope of patterns obtained for the basalts in Fig. B.25. The most noteworthy feature here is that MORB-normalised patterns for these gabbros indicate greater enrichment compared with associated basalts for all elements except Nb, although some overlap does occur. These patterns also most closely resemble those displayed by volcanic-arc basalts (Pearce, 1982, 1983), a feature consistent with the interpretation for the Kairab basalts in the previous section.

The implication of a more enriched source for the gabbros suggests either a separate source relative to the basalts or a later period of metasomatism resulting in enrichment of the same source. Alternatively, enrichment may have been produced by a smaller degree of partial melting of the same source that produced the basalts. In view of the relatively high oxidation state of the gabbros, the higher LIL elements may signify intra-plutonic fractionation or secondary addition related to alteration and metamorphism (Glikson, pers. comm., 1989).

The paucity of data available for the intrusive metafelsites precludes any detailed discussion of their chemical character. The two samples taken show compositions similar to those for “dacite” and “low-silica rhyolite” in Table B.2. Perhaps of more importance, however, is the compositional similarity between the “low-silica” metafelsites and the Aunis Tonalite Gneiss illustrated in Figs B.30 and B.31. A genetic relationship between intrusive metafelsite and Aunis Tonalite Gneiss would suggest a much greater volume of felsic intrusive activity associated with the metavolcanic succession.

4.3.2 Early-stage granitoids

(i) Introduction

Selected major and trace element data are presented in this section for a range of predominantly felsic granitoids and gneisses which make up a significant proportion of the early-stage crust. These granitoids may be broadly divided into the Aunis Tonalite Gneiss and Khorasib Granite Gneiss, the latter comprising both gneiss and granite (Section B.2). Occasional reference will be made to intrusive rocks in the Kairab Complex which were briefly discussed in the previous section. In view of the many uncertainties inherent in the field relationships of these “basement” granitoids, this section will attempt to establish geochemical parameters by which these granitoids may be discriminated from each other as well as reveal any subtle relationships between them. In particular, it

is intended to provide the necessary geochemical background for further discussions on the petrogenesis of late-stage successions, specifically the vol-canics of the HFF.

(ii) Classification

Generally smooth trends obtained on Harker diagrams (not presented here) suggest that subsolidus alteration is not significant for the granitoid suites selected and that these trends probably reflect primary igneous processes. Accordingly, the use of major and trace elements in the classification of these granitoids is considered valid.

On a normative An-Ab-Or diagram (Fig. B.33), data for the Aunis Tonalite Gneiss plot predominantly in the tonalite field of Barker (1979) with some overlap into the trondhjemite field. While samples of the Khorasib gneiss straddle the granodiorite and granite fields, the younger Khorasib granite samples plot entirely within the granite field. The data scatter in an AFM diagram (Fig. B.31) infers a calc-alkaline character for most of the early-stage granitoids. Associated gabbros of the Kairab Complex are, however, typically tholeiitic in character and hence difficult to relate to the more felsic granitoids. A normative Qz-Ab-Or diagram (Fig. B.33) suggests that only data for the Khorasib Granite Gneiss follow a calc-alkaline trend, whereas data from the Aunis Tonalite Gneiss lie closer to a gabbro-trondhjemite trend (after Barker and Arth, 1976). Data for the gabbros may, however, lie on either of these trends.

A widely used first order classification of granitoids is the degree of alumina saturation (Shand, 1927; Chappell and White, 1974) which refers to the molecular proportion of Al₂O₃ relative to the alkalis and CaO. This classification is illustrated in Fig. B.34, which shows that the early-stage granitoids are predominantly metaluminous to slightly peraluminous. Peraluminous tendencies are largely restricted to the Khorasib Granite Gneiss, especially the younger granites. In general, however, the ratio A/CNK (*molecular%* Al₂O₃ / (CaO + Na₂O + K₂O)) does not exceed 1.1 and is therefore unlike the strongly peraluminous granites derived from “S-

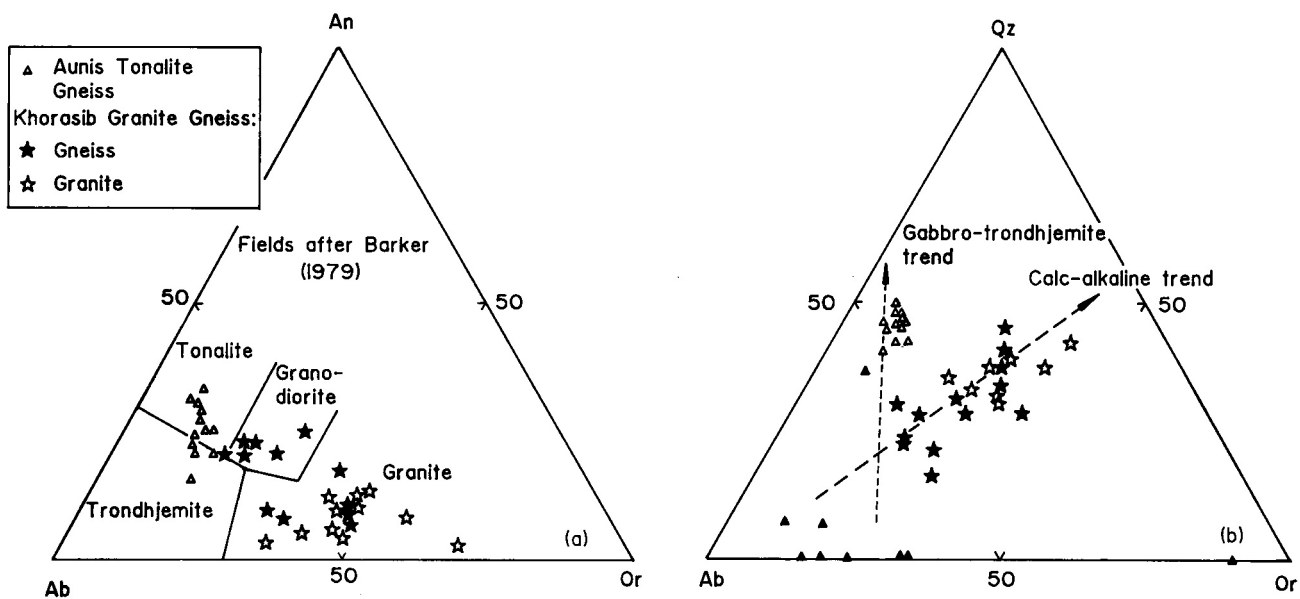


Fig. B.33: Ternary plots for early-stage granitoids in the AMT. (a) Normative An-Ab-Or; (b) normative Qz-Ab-Or. Chemical trends from Barker and Arth (1976).

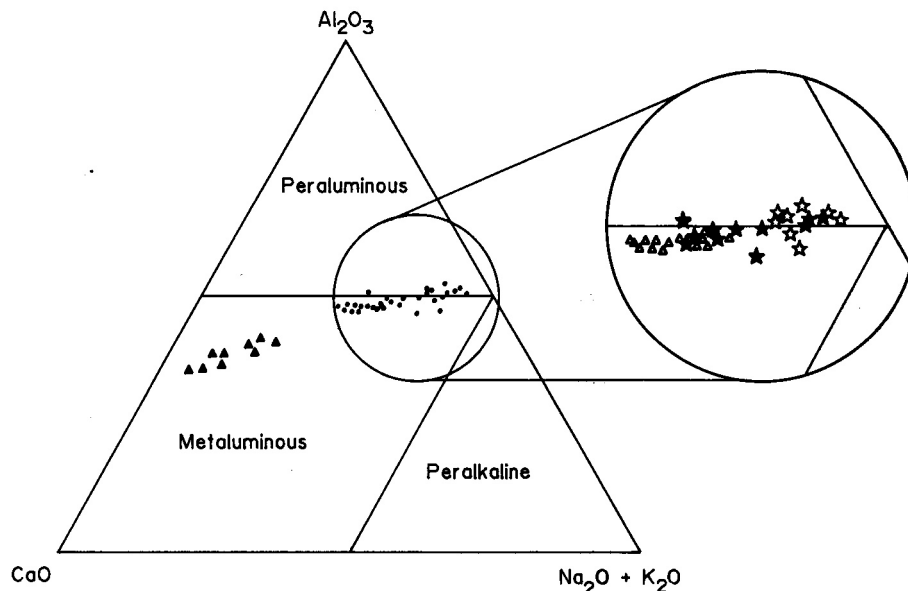


Fig. B.34: Molecular alumina-calcium-alkalis ternary diagram showing the metaluminous to slightly peraluminous character of early-stage intrusive units. Classification based on Shand (1927). Symbols as before.

type” sources (Chappell and White, 1974). Nevertheless, the ratio A/CNK (Shand Index) is a useful measure of alumina saturation and may be used further as a crude indicator of the “S-type” component involved in the derivation of anatectic granites.

In addition to alumina saturation, enrichment in HFSE has been used by Pearce *et al.* (1984) to infer the degree to which a given granite demonstrates a “within-plate” character. However, only partial discrimination is achieved between different early-stage granitoids by plotting the parameters Nb + Y and A/CNK against each other (Fig. B.35). Samples of the Aunis Tonalite Gneiss show low levels of HFSE and moderate levels of A/CNK, both features typical of calc-alkaline granitoids. While data for the Khorasib granites exhibit

relatively high values of A/CNK and a wide range in HFSE, data for the Khorasib gneisses appear to be transitional between the two groups and may represent both calc-alkaline and crustal-melt granitoids. While it is possible that the Khorasib gneisses contain some unrelated rock types, an alternative explanation is that the chosen geochemical parameters are not able to achieve a meaningful separation of granitoids within this suite. Accordingly, one may question the usefulness of discriminant plots which are based on the application of simple geochemical parameters (e.g. Pearce *et al.*, 1984).

In general, geochemical discrimination between the Aunis Tonalite Gneiss and Khorasib Granite Gneiss (especially the Khorasib granite) is easily achieved, e.g. Fig. B.36. However, distinction between older gneiss and younger granite

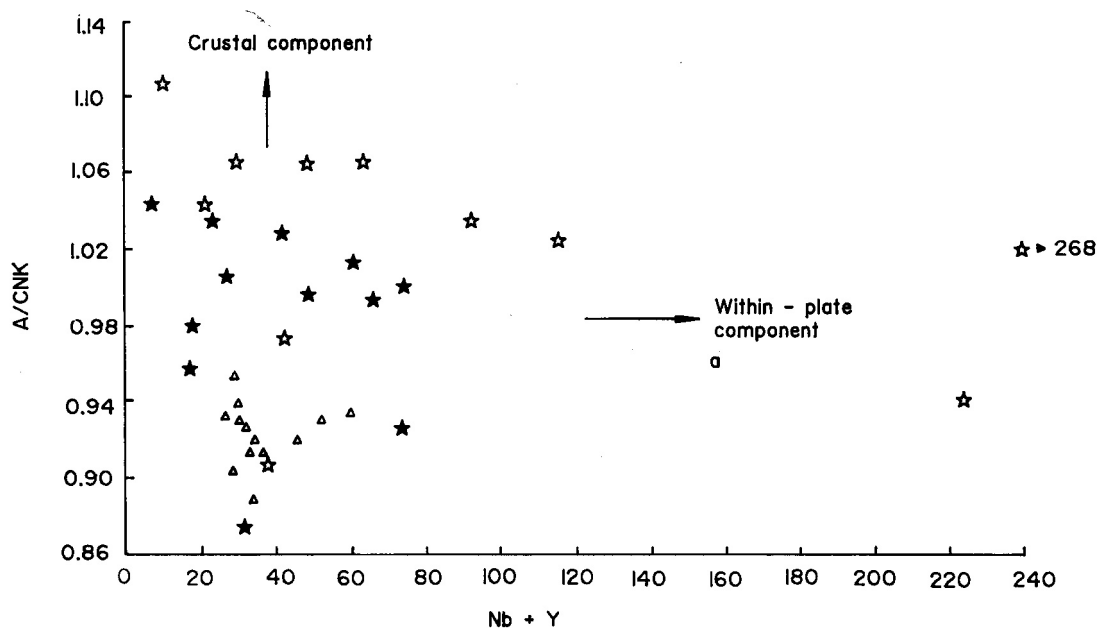


Fig. B.35: (Nb + Y) vs. Shand Index (A/CNK) diagram showing compositional variation in the early-stage granitoids. Symbols as before.

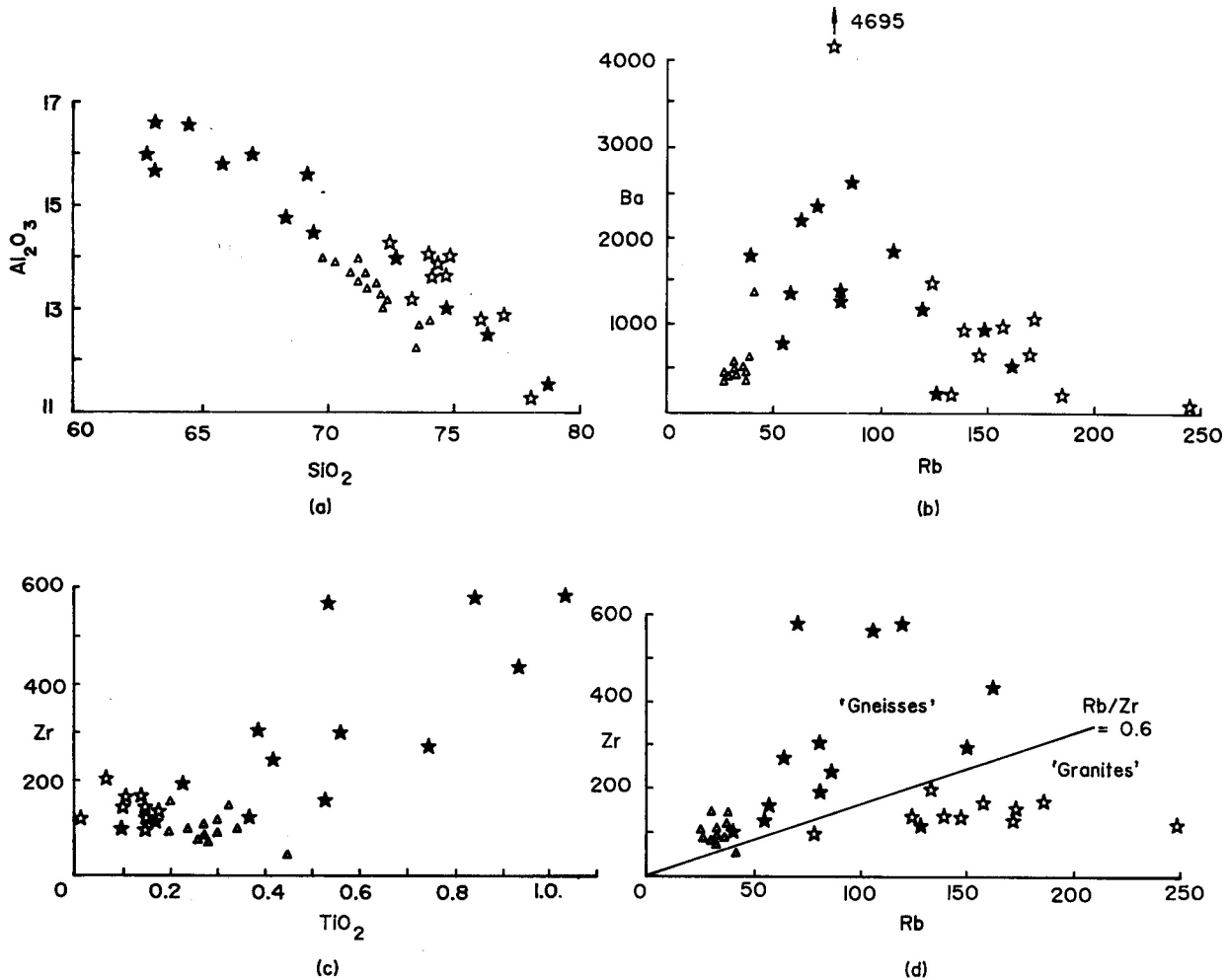


Fig. B.36: Geochemical discrimination between early-stage granitoids using variation diagrams (a) $\text{SiO}_2\text{-Al}_2\text{O}_3$, (b) Rb-Ba , (c) $\text{TiO}_2\text{-Zr}$ and (d) Rb-Zr . Symbols as before.

within the latter suite is less easy to make. Granite (*sensu stricto*) gneisses within this suite are compositionally similar to the granites and may, therefore, imply that field distinction on the basis of fabric development is not a useful criterion. Certain element ratios do, however, appear to support this criterion, e.g. Rb versus Zr (Fig. B.36d) which indicates that the Rb/Zr ratio typically exceeds 0.6 in the granites, but rarely does in the gneisses.

(iii) *Comparison with modern and ancient granite suites*

The suggested calc-alkaline and gabbro-trondhjemitic trends displayed by the early-stage granitoids in Fig. B.33 warrant further comparison with better studied and preserved intrusive suites reported in the literature. Rogers and Greenberg (1981) used a diagram of $\log(\text{K}_2\text{O}/\text{MgO})$ versus SiO_2 to obtain maximum separation of calc-alkaline and alkaline granite suites from a variety of suites of Pan-African to Recent age. These fields, together with the trend for the Sierra Nevada batholith and data for the early-stage AMT granitoids, are illustrated in Fig. B.37. This diagram illustrates the following features:

(a) A broad correspondence between data for the Khorasib Granite Gneiss and the Sierra Nevada batholith trend, with a gradual displacement of the former towards relatively high SiO_2 contents with increasing alkalinity.

(b) Poor correspondence between data for the Aunis Tonalite Gneiss and the field of "calc-alkalic batholiths".

(c) An approximate clustering of gabbros of the Kairab Complex at the lower end of the field of "calc-alkalic batholiths", indicating that these basic rocks may form part of a bimodal association with either the Aunis Tonalite Gneiss or Khorasib Granite Gneiss in view of the general contemporaneity of these units.

The close spatial and compositional association between the Aunis Tonalite Gneiss and metavolcanic succession of the Kairab Complex is noteworthy. In particular, it is conceivable that these tonalities represent the end product of differentiation within a possible ophiolite sequence southwest of Chowachasib Mountain. In order to test this possibility, data for the Aunis Tonalite Gneiss have been plotted on a semilog diagram of SiO_2 versus K_2O (Fig. B.38). Compositional fields (according to Coleman, 1977) indicate that an extremely low K_2O content is the most important chemical characteristic of ophiolite sequences. Fig. B.38 shows several important features, viz. the similarity of the Aunis Tonalite Gneiss to "continental trondhjemitites", the good correlation between "continental granophyres" and the Khorasib Granite Gneiss and the wide range in K_2O for Kairab Complex gabbros. However, Coleman (1977) cautions against such comparisons in view of widespread low-grade metamorphism

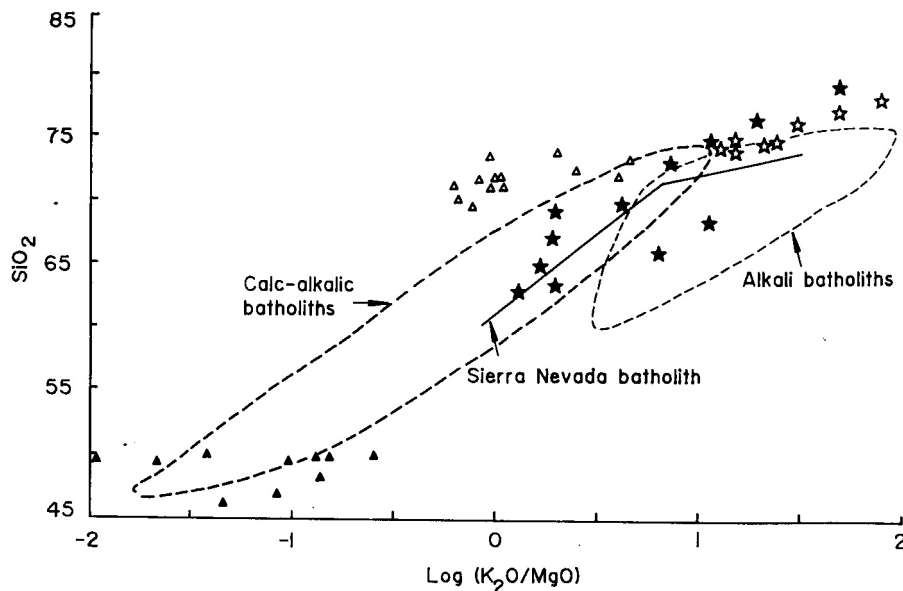


Fig. B.37: Log (K_2O/MgO) vs. SiO_2 diagram showing the relationship between early-stage AMT intrusions and fields of “calc-alkalic” and “alkali” batholiths for a variety of suites of Pan-African to Recent age (after Rogers and Greenberg, 1981). Note the occurrence of the Sierra Nevada batholith trend in both fields. Symbols as before.

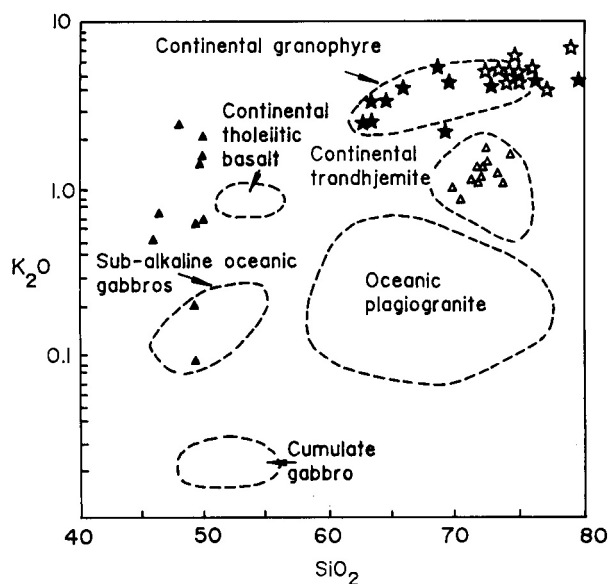


Fig. B.38: Semilog plot of SiO_2 vs. K_2O illustrating the compositional affinities of early-stage AMT granitoids and Kairab gabbros according to the classification scheme of Coleman (1977). Symbols as before.

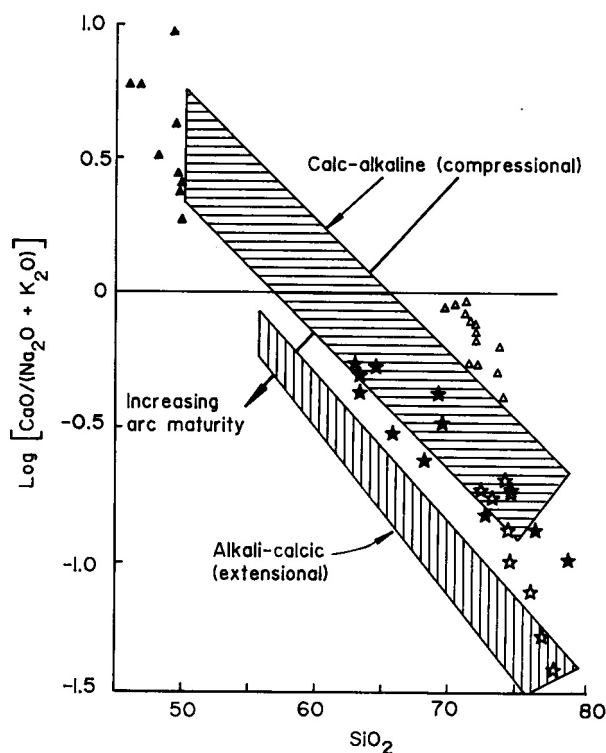


Fig. B.39: Silica vs. calc-alkaline ratio plot for early-stage AMT granitoids and Kairab gabbros. Calc-alkaline (compressional) and alkali-calcic (extensional) fields are modified from Brown (1982). Symbols as before.

and possible metasomatism in ophiolites.

The differentiation trends that give rise to oceanic plagiogranites are typically tholeiitic rather than calc-alkaline (Coleman, 1977). By plotting SiO_2 against the calc-alkali ratio $\log(CaO/Na_2O + K_2O)$ in Fig. B.39, trends for the early-stage AMT granitoids may be compared with trends for both modern magmatic arcs and intrusive suites (Brown, 1982). From this illustration it appears that the Aunis Tonalite Gneiss is calcic rather than calc-alkaline, whereas data for the Khorasib gneisses are predominantly calc-alkaline but also plot between the calc-alkaline and alkali-calcic fields. Samples of the Khorasib granite also tend to scatter between these fields and indicate some affinity with extensional al-

kali-calcic suites. Kairab gabbros show significant scatter in Fig. B.39 and do not demonstrate any clear association with the felsic granitoids.

The general decrease in logarithmic calc-alkali ratios from Aunis Tonalite Gneiss through Khorasib gneiss to Khorasib granite may reflect a transition from a compressional to extensional regime (cf. Brown, 1982). Coupled with this increase in logarithmic calc-alkali ratio is a general decrease

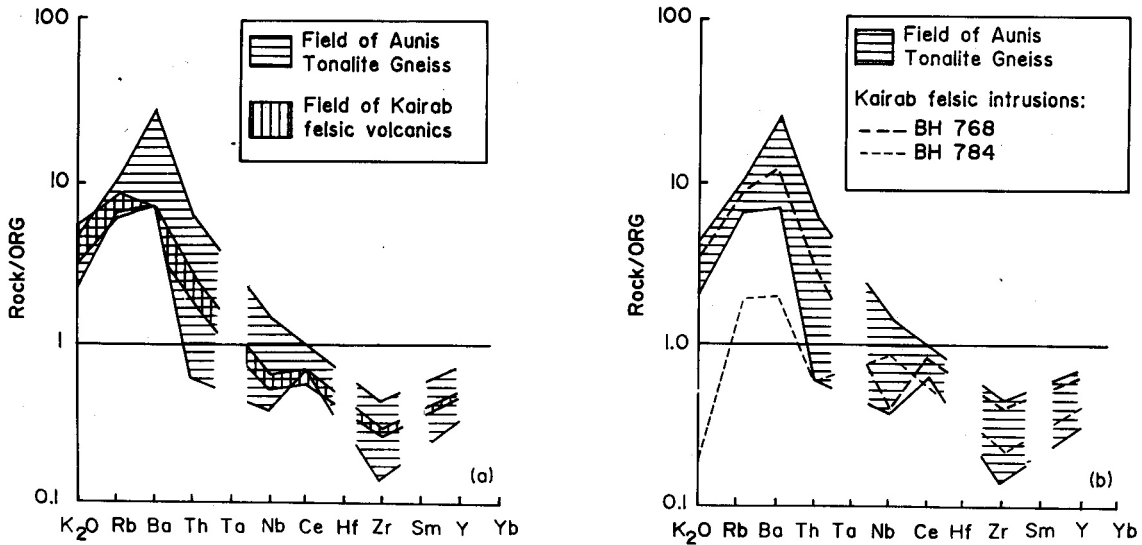


Fig. B.40: Ocean-ridge granite (ORG)-normalised trace element variation diagrams illustrating overlapping patterns between (a) the Aunis Tonalite Gneiss and Kairab felsic volcanics, and (b) the Aunis Tonalite Gneiss and Kairab felsic intrusions. Normalising procedure according to Pearce *et al.* (1984).

in silica from the Aunis Tonalite Gneiss to the more mafic Khorasib gneisses, a trend which could suggest increasing arc maturity (Fig. B.39). The possibility, then, that the early-stage granitoids may record a history of arc development and subsequent intraplate extension is strongly dependent on the temporal relationships between these rock types. Intra-suite variation is difficult to constrain where field relationships are lacking (see Section B.2) and so the above assertion must remain somewhat speculative.

Field relationships, regional considerations and geochemistry of metavolcanics in the Kairab Complex all appear to be consistent with the existence of an active continental margin in pre-Sinclair times. Accordingly, the geochemistry of related early-stage granitoids should lead to a similar conclusion. These granitoids and metavolcanics can best be compared by normalising their trace element abundances to the trace element composition of a hypothetical ocean-ridge granite (ORG) according to the method of Pearce *et al.*, (1984). These authors have calculated the trace element abundances of ORG by assuming 75% Rayleigh fractional crystallisation of a magma with the composition of a mid-ocean ridge basalt.

Fig. B.40 illustrates the overall compositional similarity between the Aunis Tonalite Gneiss and felsic volcanic and intrusive rocks in the Kairab Complex. The relative depletion in K, Rb and Ba in one of the felsic intrusions (BH 784) is possibly the result of alteration. ORG-normalised patterns for the Khorasib Granite Gneiss are less useful for comparative purposes due to intra-suite compositional variation, and are not illustrated here. Despite the considerable spread in patterns for the Khorasib Granite Gneiss, correspondence is poor between these patterns and those for Kairab Complex felsites (*sensu lato*).

Nevertheless, most of the early-stage granitoids show certain features in common, viz. enrichment in K, Rb, Ba and Th relative to Nb, Zr and Y. Where these features are combined with low values of Y relative to ORG, the resultant patterns

strongly resemble those obtained for typical volcanic-arc granites (cf. Pearce *et al.*, 1984). However, within the upper range of values obtained for the Khorasib Granite Gneiss, it is important to note that Nb, Zr and Y levels may be close to their normalising values and together with the LILE enrichment already mentioned, such overall abundances may be considered characteristic of “crust-dominated” patterns (Thirlwall and Jones, 1983, Pearce *et al.*, 1984).

The implication of these normalised abundance patterns is that there exists a variety of potential sources for the various granitoids and that field classification may well be oversimplified. The complexity of the situation is illustrated in Fig. B.41 which attempts to discriminate between granitoids of different tectonic affinity (fields after Pearce *et al.*, 1984). The large spread in values from VAG to WPG is particularly well developed in the Khorasib Granite Gneiss, the Aunis

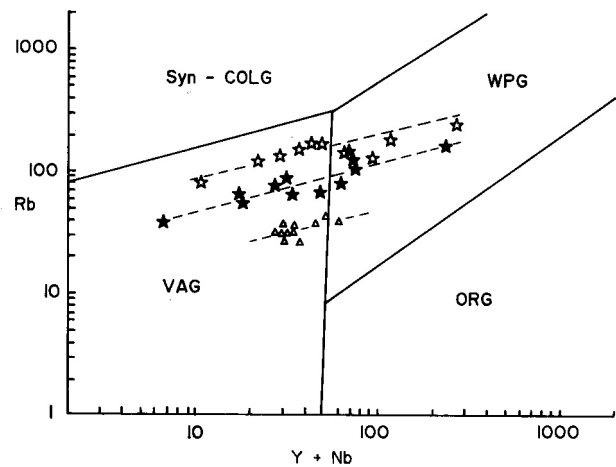


Fig. B.41: (Y + Nb) vs. Rb discriminant diagram for early-stage AMT granitoids. Fields of syn-collision (Syn-COLG), volcanic-arc (VAG), within-plate (WPG) and ocean-ridge (ORG) granites are from Pearce *et al.* (1984). Dashed lines link similar granitoid types within the AMT. Symbols as before.

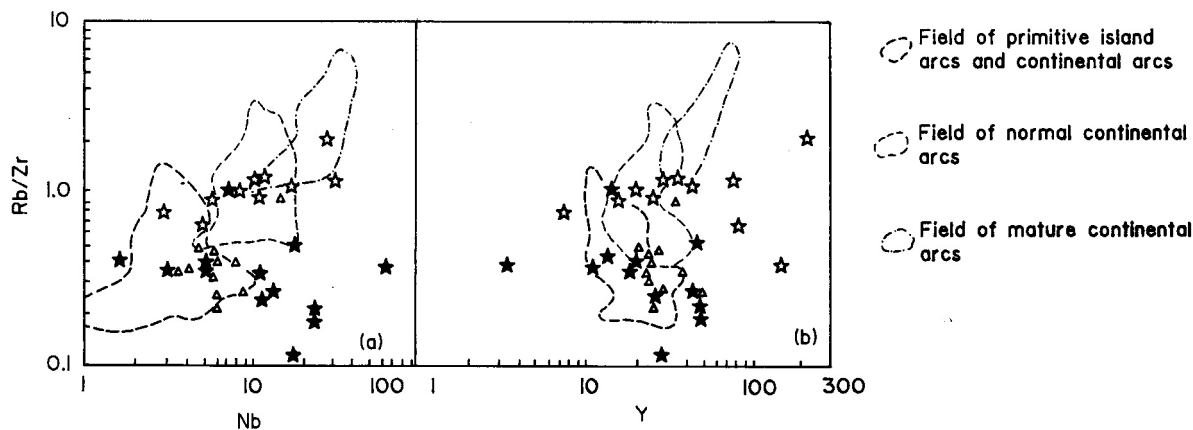


Fig. B.42: Plots of Nb and Y against Rb/Zr for early-stage AMT granitoids. Fields are modified from Brown *et al.* (1984).

Tonalite Gneiss showing relatively little scatter. Of interest here is the general increase in Rb from the Aunis Tonalite Gneiss (33 ppm) through Khorasib gneiss (82-102 ppm) to Khorasib granite (147 ppm). Pearce *et al.* (1984) consider such progressive enrichment in Rb to represent the selective introduction of Rb from the subduction zone into the mantle source region. Within the VAG field at least, the relatively steep increase in Rb content may be due to the importance of amphibole as a crystallising phase (Pearce *et al.*, 1984). The spread in Y + Nb values does, however, suggest that petrogenetic modelling of granitoids of the Khorasib Granite Gneiss cannot be well constrained and this feature is consistent with the involvement of con-tinental crust in their genesis. Superimposed alteration (sufficient to enrich Rb), crystal accumulation and volatile fluxing have probably all influenced the petrogenesis of these ancient granitoids and thereby contributed to the data scatter.

The source heterogeneity implied by the compositional variability of the early-stage granitoids is further illustrated in plots of Rb/Zr against Nb and Y (Fig. B.42). Brown *et al.* (1984) have used these parameters to illustrate trends of increasing arc maturity, but such trends are less evident here due to data scatter. Nevertheless, Fig. B.42 does illustrate a general increase in Nb and Y with increasing Rb/Zr ratio and it is clear that the youngest "basement" granitoids, viz. the Khorasib granites, display consistently higher Rb/Zr ratios than the older gneisses. Furthermore, there exists a general correspondence between data fields of the Aunis Tonalite Gneiss and "primitive island arcs" as well as between the Khorasib granite and "normal to mature island arcs" in Fig. B.42 (compositional fields modified after Brown *et al.*, 1984). Samples, typically of Khorasib Granite Gneiss, show HFSE enrichments at given levels of Rb/Zr which may reflect the source contribution from "within-plate" mantle lithosphere (cf. Brown *et al.*, 1984). However, the superimposed contribution by the continental crust (enrichment and melting) is a probable cause of scatter in these diagrams and tends to obscure an overall trend of increasing arc maturity from the Aunis Tonalite Gneiss to the Khorasib granite.

4.4 SUMMARY

4.4.1 Kairab Complex

(i) The Kairab Complex volcanic succession shows a range in composition from basalt to rhyolite with a paucity of intermediate compositions.

(ii) While TAS and AFM diagrams indicate a tholeiitic affinity for much of this succession, the low Ti abundances in the basalts suggest that these flows are wholly sub-alkaline rather than demonstrating any alkaline tendencies as indicated by the slightly elevated contents of total alkalis. Consideration of the Al_2O_3 content relative to the alkali-index of Middlemost (1975) reveals that the majority of basalts, especially pillow-bearing flows, are high-alumina types.

(iii) Low abundances of Ti, Y, Zr and Nb in Kairab basalts resemble those of modern island-arc or back-arc tholeiites, although low abundances of Ni and Cr are more typical of the former. The range in Ti/V ratio from < 5-20 for the Kairab basalts and the only slightly LREE-enriched pattern ($La_N/Yb_N = 1.7$) for high-alumina basalt are, however, more diagnostic of a back-arc setting. High-alumina basalts from the Aleutian Arc (Myers *et al.*, 1977) display REE patterns not unlike those of pillow-bearing Kairab basalt.

(iv) MORB-normalised trace element patterns (Pearce, 1982) reveal that both tholeiitic and high-alumina basalts in the Kairab Complex show features in common with volcanic-arc magma types, namely, an enrichment in the elements Sr, K, Rb, Ba and Th, and a depletion in the elements Ce, P, Zr, Sm, Ti, Y and Yb. Slight enrichment in Nb and sometimes Sc and Cr are, however, more typical of patterns displayed by transitional volcanic basalts. Volumetrically minor "depleted" tholeiites show MORB-like abundances for K, Rb and Ba, but significant depletion in P, Zr, Ti and Y.

(v) Ancient analogues for the Kairab metabasalts are found in Proterozoic amphibolites at Montauban-les-Mines in the Grenville Province (Maclean *et al.*, 1982). The latter differ in their slightly higher contents of Cr and Ni but otherwise show remarkable similarity for the HFSE and REE patterns

and reinforce the idea that the Kairab basalts are subduction-related.

(vi) In the regional context, the Kairab basalts show an overall compositional similarity to low-K arc tholeiites (amphibolites) of the Proterozoic Areachap Group (Geringer *et al.*, 1986) situated 700 km to the southeast of the AMT along the eastern margin of the NMC.

(vii) Kairab metafelsites are typically rhyolitic and are represented by both low- and high-silica types. Comparison of both groups of rhyolites with Cenozoic analogues suggests a broad compositional affinity with subduction-related suites, but good agreement for the elements Nb, Sr, Nd, P, Ti, Y and Zr in the high-silica rhyolites. The negative Th anomalies are believed to be particularly characteristic of high-silica oceanic island-arc rhyolites rather than continental arcs or intracratonic rifts (Sylvester *et al.*, 1987).

(viii) Ancient analogues of the Kairab rhyolites are best represented by the Archaean Michipicoten rhyolitic ash-flow tuffs (Sylvester *et al.*, 1987), the latter having been interpreted as subaerial to submarine arc eruptions.

(ix) The bimodal nature of the Kairab volcanic succession may be a consequence of selective preservation (Condie, 1986), paucity of magma of intermediate composition (Sylvester *et al.*, 1987), fractional crystallisation at shallow depth (Grove and Donnelly-Nolan, 1986), or a dual source (Glikson, pers. comm., 1989).

(x) Metagabbros show compositional similarities to the Kairab basalts, but high-alumina compositions are unique to the latter. More MgO-rich compositions in the gabbros reflect their cumulate origin, while greater enrichment of elements (excluding Nb) in MORB-normalised plots suggests a more enriched source, or a smaller degree of partial melting of the same source, for the gabbros.

(xi) Metafelsite intrusions are poorly represented but show, along with their volcanic counterparts, a compositional similarity to Aunis Tonalite Gneiss on AFM, Zr/TiO₂ versus SiO₂ and ORG-normalised diagrams. Although not studied in any detail, a genetic relationship between metafelsite and Aunis Tonalite Gneiss would greatly increase the volume of felsic magmatism associated with the Kairab basalt.

(xii) Geochemical data for the Kairab gabbros do not show any clear association with the Aunis Tonalite or Khorasib Gneisses.

4.4.1 Early-stage granitoids

(i) Data for the Aunis Tonalite Gneiss show some overlap into the trondhjemite field on a normative An-Ab-Or diagram (Barker, 1979), while the Khorasib Granite Gneiss is contained within the granodiorite and granite fields on the same diagram.

(ii) Although a calc-alkaline character is inferred for these granitoids on an AFM diagram, the Aunis Tonalite Gneiss lies closer to a gabbro-trondhjemite trend on a normative Qz-Ab-Or diagram.

(iii) Early-stage granitoids are typically metaluminous in the classification of Shand (1927), although several of the Khorasib granites show a peraluminous tendency.

(iv) Low levels of HFSE in the Aunis Tonalite Gneiss are typical of calc-alkaline granitoids and contrast strongly with the “within-plate” character demonstrated by HFSE enrichment in Khorasib granites. While the latter may be regarded as typical crustal melts, the associated gneisses are transitional between the two groups and represent both calc-alkaline and crustal-melt granitoids.

(v) Geochemical discrimination between Khorasib gneiss and granite is best achieved using a Rb/Zr ratio of 0.6, the latter being characterised by values greater than this.

(vi) The Aunis Tonalite Gneiss, despite its close association with the metavolcanic succession of the Kairab Complex, shows the higher K₂O contents typical of continental trondhjemites rather than oceanic plagiogranites (Coleman, 1977). The Khorasib Granite Gneiss shows even higher K₂O contents diagnostic of continental granophyres but a broad correspondence to the calc-alkaline to alkaline Sierra Nevada batholith trend on a diagram of log(K₂O/MgO) versus SiO₂ (Rogers and Greenberg, 1981).

(vii) Comparison of trends for the early-stage granitoids with trends for modern magmatic arcs and intrusive suites on a SiO₂ versus calc-alkali ratio diagram (Brown, 1982) shows that the Aunis Tonalite Gneiss is calcic rather than calc-alkaline whereas the Khorasib Granite Gneiss exhibits a calc-alkaline to alkali-calcic tendency. Notwithstanding the problems of correlation between the early-stage granitoids, the trend from calcic to alkali-calcic is considered to reflect a history of arc development and subsequent intra-plate extension.

(viii) LILE enrichment relative to HFSE is common to most early-stage granitoids and resultant patterns on ORG-normalised plots are typical of volcanic-arc granites (Pearce *et al.*, 1984). Where the HFSE Nb, Zr and Y are close to their normalising values in addition (as shown by several Khorasib granites), the patterns are considered characteristic of “crust-dominated” patterns (Thirlwall and Jones, 1983).

(ix) The tectonic discriminant diagram Y + Nb versus Rb (Pearce *et al.*, 1984) confirms a volcanic-arc environment for the Aunis Tonalite Gneiss but shows a spread of data for the Khorasib Granite Gneiss across the volcanic-arc and within-plate fields. A general increase in Rb from Aunis Tonalite Gneiss via Khorasib gneiss to Khorasib granite may reflect the selective introduction of Rb from the subduction zone into the mantle source region, but the spread in Y + Nb values is indicative of involvement of the continental crust in the genesis of the Khorasib Granite Gneiss.

(x) HFSE enrichments at given levels of Rb/Zr in the latter further suggest a source contribution from within-plate subcontinental lithosphere (Brown *et al.*, 1984). An overall trend of increasing arc maturity from Aunis Tonalite Gneiss to Khorasib granite is partly obscured by the involvement of continental crust.

5. GEOCHRONOLOGY

5.1 INTRODUCTION

Correlation of the early-stage crust in the AMT with the NMC would infer an age range from middle to late Proterozoic. Accordingly, isotopic measurements have been carried out on the Kairab Complex metabasalt (Rb-Sr and Pb-Pb) and Aunis Tonalite Gneiss (Rb-Sr) in order to determine both absolute ages and the duration of activity in the Proterozoic (see also Hoal *et al.*, 1986, 1989). A more detailed discussion on the source characteristics is presented in Part D.

A description of the chemical and analytical methods and experimental uncertainties is presented in Appendix II. Sample localities in the AMT are illustrated on a 1: 100000 scale geological map (Appendix I).

5.2 ISOTOPE RESULTS

Rb-Sr and Pb-Pb results are shown in Table B.3 and on conventional isochron diagrams in Fig. B.43.

5.2.1 Kairab Complex metabasalt

The ten analysed samples of the Kairab Complex Metabasalt define an isochron (MSUM = 2.48) with an age of 1461 ± 169 Ma and an initial $^{87}\text{Sr}/^{86}\text{Sr}$ ratio (R_0) of 0.70269 ± 12 . The separation of sample BH 774 from the main cluster of data points in Fig. B.43 clearly exerts a significant control on the slope of the regression line. Consequently, Pb separates were measured for four samples which fall within the main sample cluster on the Rb-Sr isochron. The inset in Fig. B.43 illustrates that these samples define a Pb-Pb isochron (MSUM = 1.1) with an age of $1467 +201/-215$ Ma and $\lambda = 9.87 \pm 0.14/-0.15$. The λ value is slightly higher than the value of 9.74 preferred by Stacey and Kramers (1975) for the second stage of their two-stage model of Pb isotope evolution. The R_0 estimate for this unit is low, an indication that the source material of this metabasalt had a Rb/Sr ratio similar to, or slightly lower than, a "Bulk Earth" mantle composition.

5.2.2 Aunis Tonalite Gneiss

Nine samples of the Aunis Tonalite Gneiss define an isochron (MSUM = 1.3) with an age of 1271 ± 62 Ma and R_0 of 0.7029 ± 3 . Sample BH 745 was excluded from the regression as it appears slightly weathered in thin section and deviates from the isochron line by more than three times the

analytical uncertainty (Fig. B.44). Exclusion of this datum has little effect on the age and R_0 estimates. Again the R_0 estimate for the Aunis Tonalite Gneiss is low, an indication that the source material of this granitoid had a Rb/Sr ratio similar to a "Bulk Earth" or "Uniform Reservoir" mantle composition. This precludes a significant crustal pre-history or "residence time" for this unit, and implies that the estimated age reflects the time of primary derivation and crystallisation of the Aunis Tonalite Gneiss.

5.3 DISCUSSION

The age of *ca.* 1460 Ma obtained for the Kairab Complex metabasalt is considered to represent the time of extrusion of these flows in view of the agreement between Rb-Sr and Pb-Pb systems. A minimum age for the Kairab Complex basement is provided by the age of 1271 ± 62 Ma obtained for the Aunis Tonalite Gneiss, since this age is considered to represent a primary crystallisation event. This age coincides with a likely maximum age of 1300 Ma for the D₂ Namaqua event (Cahen and Snelling, 1984, p. 65) and is consistent with a previous correlation between the Kairab Complex and the NMC (Hoal, 1985).

Low R_0 values in both Kairab metabasalt and Aunis Tonalite Gneiss imply juvenile additions of magma from the mantle. This event may be compared with volcanism dated at between 1300 and 1100 Ma (Barton and Burger, 1983) along the eastern margin of the NMC near Upington. These workers have shown that tholeiitic metabasalts of the Wilgenhoutsdrif Group and calc-alkaline volcanic rocks of the Jannelsepan Formation exhibit R_0 values which infer mantle derivation, but λ values indicative of enriched mantle or crustal recycling. Barton and Burger (1983) further interpreted the isotopic data to reflect an active continental margin related to the convergence and subsequent collision which characterises the Namaqua tectogenesis. Similar conclusions may be drawn for the Kairab metabasalt and Aunis Tonalite Gneiss, which suggests that this active continental margin can be extended from near Coperton in South Africa to the northern part of the AMT, a distance of nearly 850 km.

In the Rehoboth area to the northeast of the AMT, Reid *et al.* (1988) have reported Rb-Sr isochron ages of 1442 ± 32 Ma ($R_0 \approx 0.7018$) for the Alberta Mafic Complex and 1238 ± 13 Ma ($R_0 \approx 0.7041$) for the Biesiepoort Granite/Weener Quartz Diorite. These ages and R_0 values are broadly similar to those obtained for the Kairab metabasalt and Aunis Tonalite Gneiss, respectively, and may provide evidence for the northeast ward extension of this ancient active margin.

Lithology and Sample number **Rb (ppm)** **Sr (ppm)** **⁸⁷Rb/⁸⁶Sr (atomic)** **⁸⁷Sr/⁸⁶Sr (atomic)** **²⁰⁶Pb/²⁰⁴Pb** **²⁰⁷Pb/²⁰⁴Pb** **²⁰⁸Pb/²⁰⁴Pb**

Kairab Complex Metabasalt

BH 770	2.01	307	0.0189	0.70297 ± 2			
BH 774	12.1	254	0.1372	0.70565 ± 1			
BH 783	1.37	384	0.0103	0.70286 ± 1			
BH 901	1.10	265	0.0120	0.70340 ± 1	20.931	15.858	38.205
BH 902	0.89	290	0.0089	0.70280 ± 1	17.840	15.565	37.515
BH 903	0.75	328	0.0067	0.70289 ± 1			
BH 904	7.92	395	0.0579	0.7040 ± 1			
BH 905	3.92	313	0.0362	0.70315 ± 1	17.870	15.584	37.569
BH 906	2.30	274	0.0243	0.70323 ± 1			
BH 907	5.38	360	0.0433	0.70337 ± 1	18.689	15.660	38.494

Aunis Tonalite Gneiss

BH 727	29.8	121	0.713	0.71609 ± 1			
BH 745	30.1	205	0.425	0.71131 ± 1			
BH 746	25.3	214	0.342	0.70912 ± 1			
BH 747	19.9	227	0.254	0.70766 ± 1			
BH 748	25.9	193	0.388	0.70977 ± 1			
BH 749	25.1	200	0.368	0.70951 ± 1			
BH 750	25.4	208	0.353	0.70915 ± 1			
BH 751	28.9	190	0.440	0.71082 ± 1			
BH 752	24.6	181	0.393	0.71015 ± 1			
BH 753	19.7	210	0.271	0.70782 ± 1			

Rb-Sr: Quoted errors at 2σ level; sample Sr ratios reproducible to 0.01%
 Pb-Pb: Average errors listed in Appendix II; 206/204 and 207/204 reproducible to 0.09%

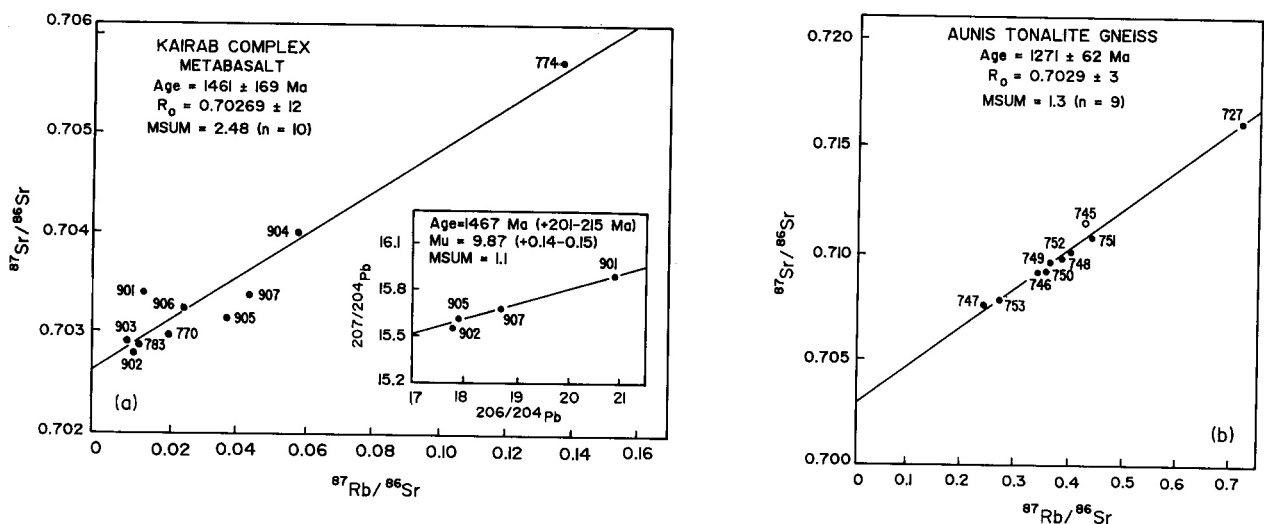


Fig. B.43: Whole-rock isochron plots for early-stage lithologic units in the AMT:
 (a) Kairab Complex metabasalt: Rb-Sr isochron and Pb-Pb isochron (inset) for selected samples.
 (b) Aunis Tonalite Gneiss: Rb-Sr isochron. Open symbol BH 745 excluded from regression.

PART C: LATE-STAGE CRUST

1. INTRODUCTION

Late-stage crust in the AMT is correlated with the Sinclair Sequence and comprises both “cover” rocks and high-level intrusions which are typically less deformed and metamorphosed than lithologies in the early-stage crust. A greater emphasis is placed on the eruptive rocks of the Haiber Flats Formation (HFF) in view of their relatively well-preserved nature and suitability for geochemical and petrogenetic studies. Localities referred to in the text are illustrated on the accompanying regional map (Appendix I). Where applicable, the reader’s attention will be drawn to similarities between the units discussed and their counterparts in the Sinclair Sequence.

The main aims in Part C are to provide both data and discussions on the following aspects of the late-stage crust of the AMT:

(i) Field character and petrography of the major lithologic units in order to establish the lithostratigraphy of the late-stage AMT and, where possible, the provenance and palaeoenvironment of the units in question.

(ii) Mineral chemistry of selected lithologic units with a view to determining igneous compositions as well as the degree of metamorphism and/or alteration.

(iii) Whole-rock chemistry of a variety of rock types, including the Barby Formation of the Sinclair Sequence, for the purpose of geochemical characterisation, regional correlation, and comparison with modern and ancient analogues in the literature.

(iv) Petrogenesis of the HFF eruptive rocks in view of their relatively well-preserved nature and significance in the evolution of the late-stage crust and the Sinclair Sequence.

(v) Geochronology of selected lithologic units, including the Barby Formation (type area), in order to determine both the age and source characteristics of these units.

2. LITHOSTRATIGRAPHY

This section provides brief descriptions of the distribution, field character and petrography of the major lithologic units which form part of the late-stage crust in the AMT.

2.1 URUSIB FORMATION

The sedimentary Urusib Formation (now thought to incorporate the Tsaurob Formation; Hoal, 1985) has been variously correlated with the Kunjas Formation (Martin, 1965; SACS, 1980) and the Guperas Formation (Watters, 1974; Harrison, 1979) in the Sinclair Sequence. These problems of correlation are the result of a lack of continuity between sediments in the AMT and those in the Sinclair Sequence type area to the east. Available field evidence suggests that the Urusib Formation occupies a stratigraphic position closer to the Kunjas Formation than the Guperas Formation. This evidence is based largely on the following observations:

(a) Arkoses of the Urusib Formation have been intruded by gabbros of the Saffier Intrusive Suite on State Land adjacent to the farm Gorrasis.

(b) Basal conglomerates of the Urusib Formation only overlie early-stage crust in the AMT.

Lithologic descriptions of the Urusib Formation are given in Harrison (1979) and Hoal (1985), and will not be repeated in detail here. Some discussion is, however, given on selected lithostratigraphic sections and on the provenance and palaeoenvironment of this succession, since these have a direct bearing on the setting of the overlying Haiber Flats Formation;

(i) Field character

Sediments of the Urusib Formation unconformably overlie, or are faulted against, metamorphic rocks of the Kairab Complex, Aunis Tonalite Gneiss and Khorasib Granite Gneiss (Plate A.Le). This sedimentary succession is made up predominantly of immature and poorly sorted clastic rocks which reach an estimated thickness of 2400 m within the Urusib synclinorium. Regional facies variations are best represented by five selected lithostratigraphic sections which are described below and illustrated in Fig. C.1:

(a) Section southwest of DiaR10

In the southeastern part of the AMT, the Urusib Formation is in tectonic contact with underlying basement gneisses and younger monzogranite of the Haisib Intrusive Suite. The basal part of this succession consists of polymict breccia which grades upwards into petromict conglomerate and cross-bedded lithic arenite. The latter, which commonly carries well-rounded quartz pebbles, attains a thickness of approximately 1600 m before grading upwards into the predominantly volcanic succession of the Haiber Flats Formation. The upper contact zone is obscured by a swarm of northwest-trending rhyolite dykes, but is arbitrarily demarcated by the lower most volcanic flow of the Haiber Flats Formation.

(b) Section southwest of Piekniekkoppe

The sedimentary succession in this section forms the northwestward extension of the previous one and attains a similar minimum thickness. In the basal part quartz pebbles and lithic fragments (volcanic and granitic in composition) define a down-dip pebble-stretching lineation. Large cobbles of basement gneisses are also present, but the basal contact is a sedimentary unconformity rather than tectonic in nature as seen further south. Although there is no evidence of intercalated volcanics of the Haiber Flats Formation in the upper part, plugs of intrusive andesite may represent feeders to such volcanics.

(c) Urusib section

This section is the type locality of the Urusib Formation and will accordingly be described in more detail than the other sections. The estimated thickness of 2400 m is made up of four informal members which are discussed below.

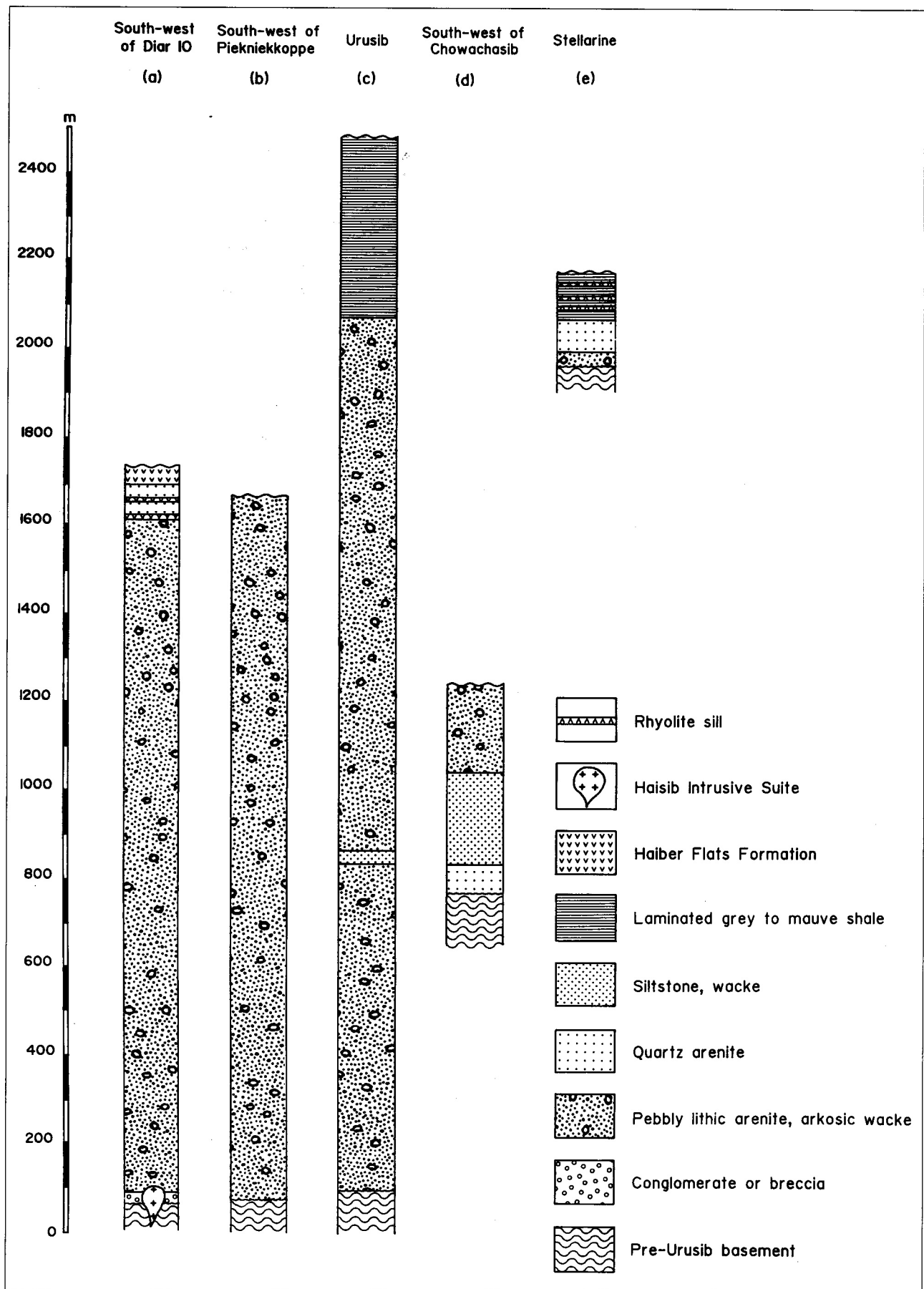


Fig. C.1: Lithostratigraphic sections of the Urusib Formation.

Conglomerate member

This 700 to 800 m thick member is made up predominantly of grey to brown petromict conglomerate, pebbly lithic arenite and subarkose. Clasts are typically quartz with subordinate feldspar, while lithic fragments are predominantly granitic and volcanic (mainly felsic in composition). Planar and trough cross-bedding are widespread throughout this member, although more massive upward-fining beds are also developed, particularly at the base of the succession.

Siltstone member

Although only 50 to 100 m thick, this member is remarkably persistent laterally and is made up predominantly of dark grey siltstone and laminated quartz wacke. Minor, but important, grey carbonate (sandy limestone) and red chert crop out on the western limb of the Urusib synclinorium. Sedimentary structures include nearly vertical fluid-escape channels which have disrupted the laminations, groove casts which indicate a palaeocurrent direction from northwest to southeast, and ripple marks.

Pebbly sandstone member

With a minimum thickness of 1200 m, this member consists primarily of grey to brown pebbly lithic arenite, lithic and arkosic wacke, and subordinate petromict conglomerate. The pebbly sandstone member contains similar sedimentary structures to the conglomerate member, but displays, in addition, characteristic slump structures and ripple marks. Much of this member resembles cross-bedded lithic arenite situated to the southwest of the DiaR10 trigonometrical beacon, but pebbles define an extremely strong stretching lineation in the core of the Urusib syncline (Plate C.1a).

Shale member

Laminated dark grey carbonaceous shale occupies the core of the Urusib synclinorium and may exceed 300 m in thickness. An accurate estimate of the thickness is, however, difficult to make in view of disruption of the sequence by mafic dykes and poor outcrop.

(d) Section southwest of Chowachasib Mountain

The sequence here has been intruded by the Chowachasib Granite and is unique in that there is no development of a basal conglomerate. A basal pink to white quartz arenite member overlies metagabbro of the Kairab Complex and reaches an estimated thickness of 80 m. Pebbles are rare and the quartz arenite displays a mature and well-sorted nature. The overlying grey siltstone member may attain a thickness in excess of 200 m and laminated portions are similar to siltstones in the Urusib section. The uppermost part of this succession is made up of grey to brown lithic arenite and subarkose which together constitute a minimum thickness of about 200 m.

(e) Stellarine section

This section, only 200 m thick, is made up of unusual lower beds of dark grey conglomerate and grey lithic sandstone with occasional interbeds of grey shale. The clasts in the basal conglomerate are typically subangular felsic and

mafic volcanics, while clasts in the overlying conglomerate are almost entirely angular quartz. Trough and planar cross-bedding are well-developed and upward fining is evident in several of the beds. Overlying this lower portion is a succession of grey to white quartzite which is in turn overlain by an estimated thickness of 100 m of grey shale. The vertical continuity of this shale is interrupted by several SHIS of rhyolite.

(ii) Petrography

Petrographic study of the Urusib Formation is hampered by widespread deformation, particularly shearing (Plate C.1a), and greenschist grade of metamorphism (Plate C.1b). Volumetric estimates of matrix are particularly difficult in some cases due to the breakdown of feldspars and growth of white micas. The variability in the nature and composition of the sediments precludes a detailed discussion here, but the reader is referred to Harrison (1979, p. 23-31) for petrographic descriptions of the major lithologies.

(iii) Provenance and palaeoenvironment

The predominance of granitic lithic fragments in the basal part of the Urusib Formation suggests a largely granitic source for these arkosic sediments. Furthermore, the syenogranitic nature of many of the fragments indicates a proximal source such as the Khorasib granite. Elsewhere clasts of tonalite gneiss and metaquartzite may be correlated with the Aunis Tonalite Gneiss and Kairab Complex, respectively.

Higher up in the succession, but still within the coarser-grained clastic sediments, lithic fragments comprise both quartzofeldspathic clasts (volcanic or sedimentary in origin) as well as dark siltstones and shales. Whereas the latter are thought to represent intraformational rip-up clasts, the source of the volcanic and sedimentary fragments remains uncertain.

Despite obliteration of many primary sedimentary structures by shearing, Harrison (1979, p. 52-54) proposed a braided stream environment for much of the succession on the basis of the following observations:

- (a) The widespread occurrence of petromict conglomerates, arkoses and lithic sandstones.
- (b) Sedimentary structures such as planar and trough cross-bedding, ripple marks, parallel laminations, scour surfaces, longitudinal bars and channel fill sequences.
- (c) Poor sorting and a predominantly upward-fining sequence.
- (d) Sheetlike deposits of sand and gravel.
- (e) The absence of features indicative of low gradient meandering streams, e.g. point-bar sequences.
- (f) Graded cross-strata.

The above proposal is further supported by such features as pebble imbrication and rip-up clasts.

Harrison (1979, p. 56) further suggested that the "siltstone member" was lacustrine in origin on the basis of such features as parallel laminations, ripple marks and wavy bedding, and the presence of a carbonate-chert association which he regarded to be of playa lake origin. However, the occurrence of quartz and lithic wacke in much of this member indicates that clastic material must have formed a

significant proportion of the fluvial load discharged into the proposed lake. Finely laminated grey carbonaceous shales may similarly be of lacustrine origin but reflect more quiescent conditions than the siltstones.

From the above considerations, it is possible to recognise two sedimentary cycles in the Urusib Formation at the type locality. The first cycle was initiated by uplift of a predominantly granitic source area leading to rapid fluvial deposition of coarse clastic material, and was terminated by relatively stable crustal conditions resulting in a lacustrine environment with occasional fluvial discharges. The second cycle was initiated by uplift of a similar granitic source area to the first cycle, but with a larger volcano-sedimentary component, and was terminated by more stable conditions resulting in the establishment of a lacustrine environment.

Parts of each cycle may be recognised in the section southwest of Chowachasib Mountain, but only part of the first cycle is preserved in the sections southwest of DiaR10 and Piekniekkoppe. The Stellarine section appears to record only part of the second cycle. While palaeocurrent directions for the Urusib section suggest a source to the northwest or west (Harrison, 1979, p. 31), similar data are not available for the other sections. However, the regional distribution of coarse-grained clastic rocks suggests that these sections represent independent depocentres which existed contemporaneously with the Urusib basin.

It is concluded that the Urusib Formation is made up of several fault-bounded troughs which reflect separate, but broadly synchronous, periods of uplift and quiescence. While braided streamflow fans reflect such tectonically active periods, associated lake deposits are the result of more stable crustal conditions.

2.2 HAIBER FLATS FORMATION (HFF)

2.2.1 General description

2.2.1.1 Distribution

The Haiber Flats Formation volcano-sedimentary succession, hereafter referred to as the HFF, has its major outcrop adjacent to the Haiber Flats in the central part of the AMT. Similar lithologic associations can be traced to the southeast of Awasib Mountain in what probably constitutes a lateral continuation of this formation. Despite the disruptive effects of deformation and metamorphism, significant lateral variations in the original nature and composition of the volcanics suggest that these rocks are the eruptive products of several, possibly overlapping, volcanic centres.

The HFF has an outcrop area of between 70 and 80 km² which is confined to a series of northwest-trending linear troughs within the early-stage crust (map - Appendix I). However, the combination of extensive movement along the margins of these troughs (Plate C.1 c) and widespread intrusive activity suggests that the original outcrop area of the HFF may have been substantially greater than the estimate given here. This contention is supported by the pyroclastic nature of many of the HFF volcanics as well as lithologically similar outcrops as far west as Hauchab (Fig. A.4).

Furthermore, the overall compositional and stratigraphic similarity of the HFF to the Barby Formation may support a correlation between them. In this event the original area of outcrop would be increased dramatically, since Watters (1974, p. 23) has estimated that the Barby Formation probably covered an area in excess of 40000 km².

2.2.1.2 Thickness

The total thickness of the HFF is difficult to estimate due to discontinuous exposures and the disruptive effect of younger intrusions. Minimum thickness estimates range from around 3000 m in the south of the AMT to almost 7000 m in the north. The latter estimate is, however, poorly constrained by the available field evidence and may well represent a maximum thickness for the HFF. In addition, it is difficult to assess the possibility of stratigraphic repetition in the HFF, since any step-faults, as observed in the Barby Formation by Von Brunn (1967, p. 139), have been obscured by pervasive fracture cleavage (Plate C.1d).

2.2.1.3 Field relationships

The basal contact of the HFF is best exposed in the southern part of the AMT where this predominantly volcanic succession overlies the Urusib Formation. Here the uppermost pebbly lithic arenites of the latter formation have been intensely intruded by rhyolite dykes and sHIS, the contact between these sediments and the overlying HFF being placed at the lower most volcanic flow. This constitutes a somewhat arbitrary boundary since it is not always possible to distinguish between rhyolite sHIS and flows. The possibility of a disconformable relationship between these two formations in the southern most portion of the AMT is partly borne out by the angular unconformity observed to the west of Piekniekkoppe.

Widespread intrusions of the Haisib Intrusive Suite and the younger Awasib Granite are closely associated, both spatially and chronologically, with the HFF. These intrusions, particularly the former, are typically located along the margins of the troughs which host the HFF.

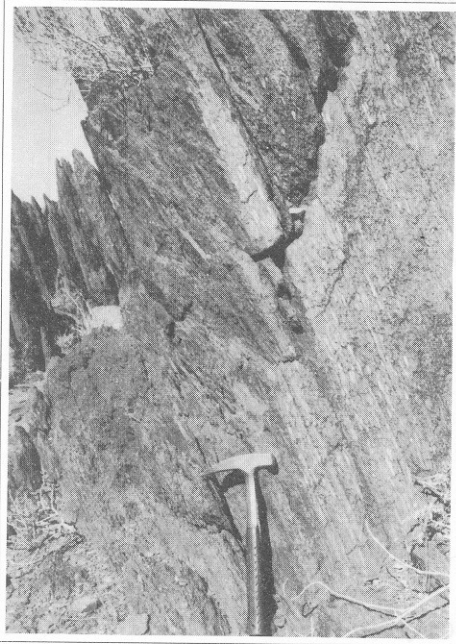
2.2.1.4 Volcanic types

The different volcanic types in the HFF are distinctive and can be grouped into two broad categories:

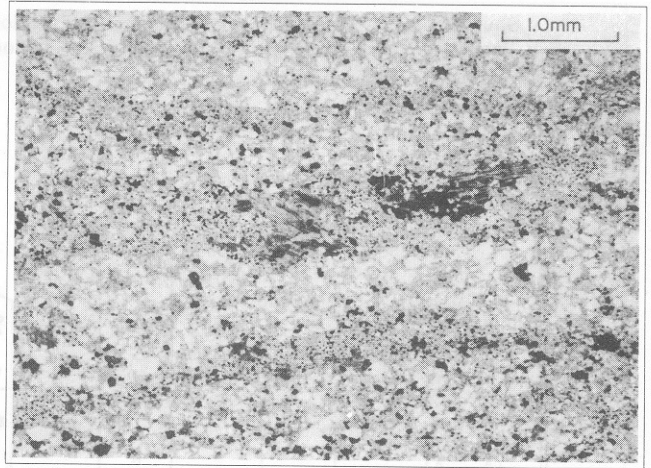
(a) Basaltic andesite and andesite: pyroxene- and/or feldspar-porphyrific lavas, aphyric lavas, pyroclastic flows, stratified tuffites (as defined by Bates and Jackson, 1980) and volcanoclastics.

(b) Rhyolite and rhyodacite: quartz- and feldspar-porphyrific lavas, pyroclastic flows, stratified tuffites and volcanoclastics.

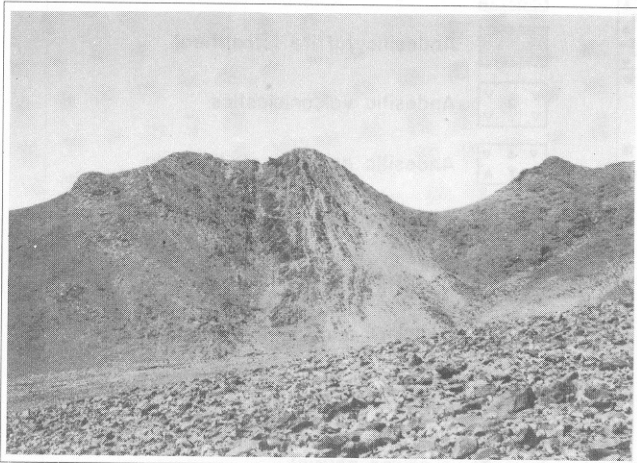
Although there is a virtual continuum in compositions from basaltic andesite to rhyolite, the intermediate members (siliceous andesite-dacite-rhyodacite) are volumetrically insignificant. While the nature and type of the earliest volcanic activity show significant regional variation, basaltic andesites and andesites are more voluminous than rhyolites at this early stage. Rhyolites do, however, increase



C.1a: Steep southwest-dipping shear planes in pebbly lithic arenite of the Urusib Formation. Note stretched clasts to right of hammer. Core of Urusib synclinorium; 2 km northeast of Urusib.



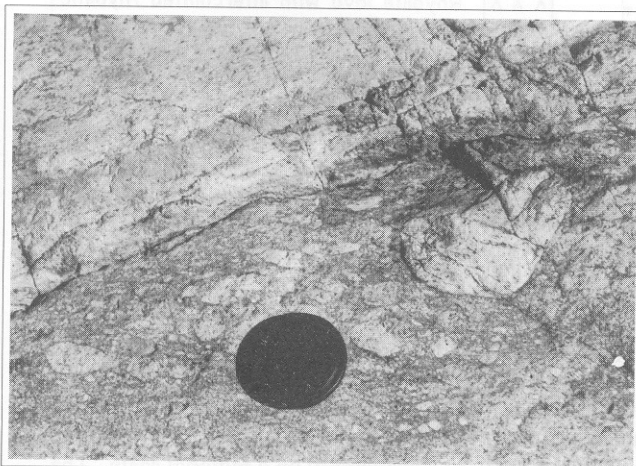
C.1b: Urusib Formation greywacke (BH 871). PPL. Prominent biotite poikiloblast in centre-right of photomicrograph indicates greenschist facies metamorphism. State Land southwest of Gor-rasis.



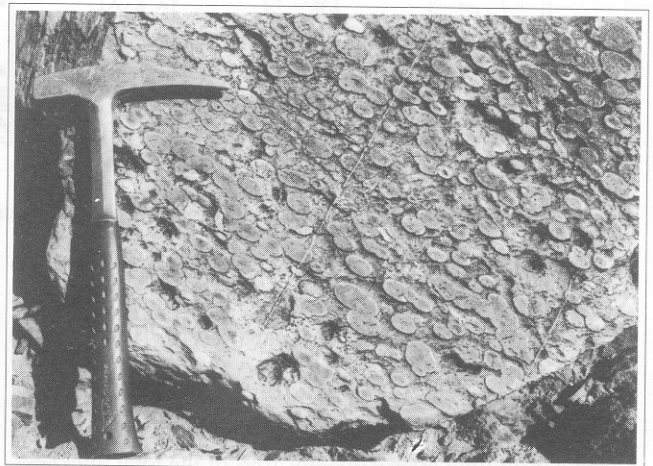
C.1c: Sheared northeast margin of fault trough at the "southern locality" of the HFF. Shear zone separates early-stage crust on the left from HFF eruptive rocks on the right. Section about 300 m high and approximately 15 km south of Diar 10 beacon.



C.1d: Layering-parallel fracture cleavage with a vertical to steep northeast dip in rhyolite flows and ash-flow tuff of the HFF. The ash-flow tuff (≈ 3 m thick) exhibits a more weathered and fractured appearance due to its less competent nature. Southern locality of the HFF. (Map - Appendix I).



C.1e: Volcanic conglomerate made up largely of rounded clasts derived from the underlying rhyolite lava. Lens cap for scale. Southern locality of the HFF.



C.1f: Globular rhyodacite (BH 512-type). Globules may be the result of vapour separation, liquid immiscibility or devitrification. Southern locality of the HFF.

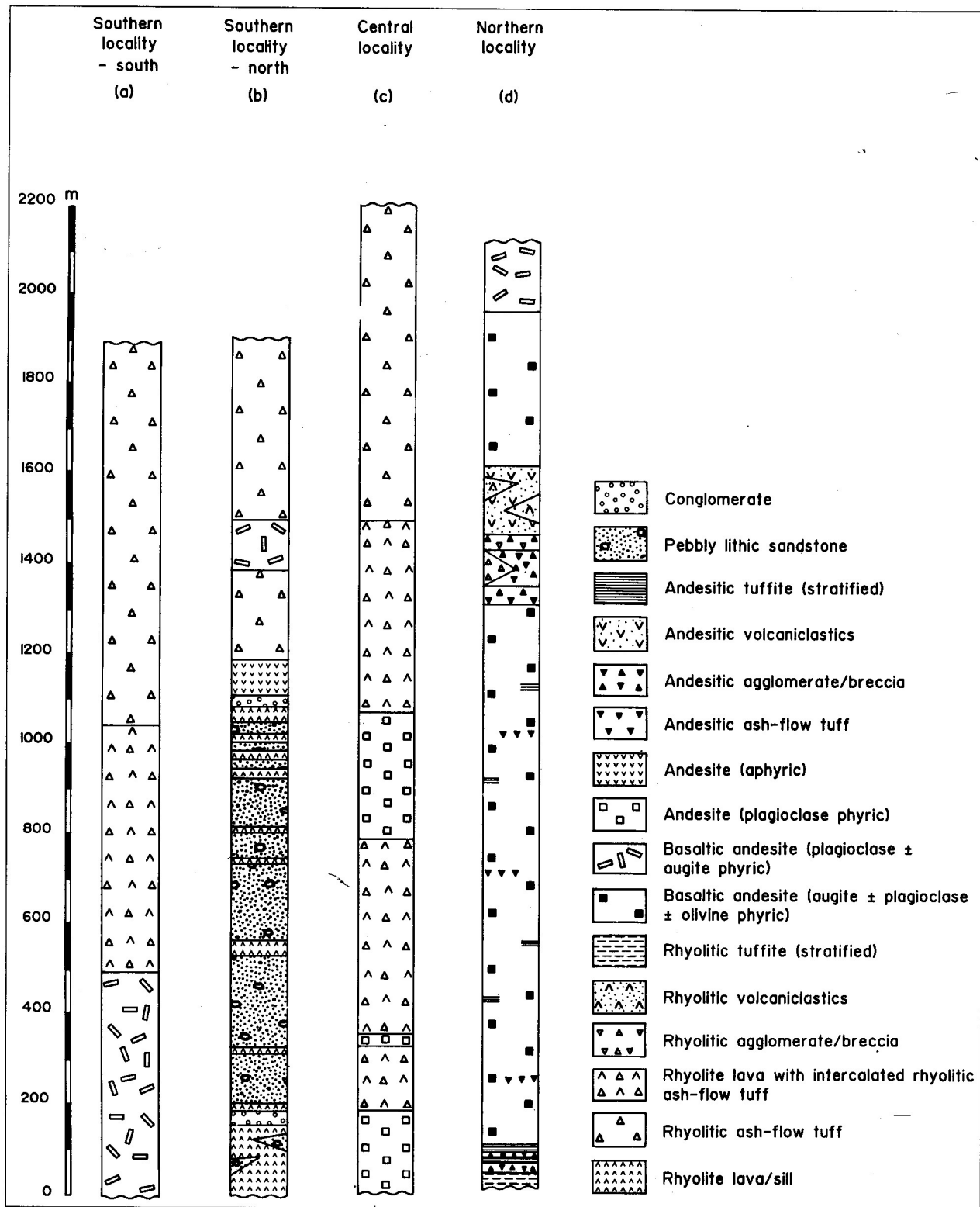


Fig. C.2: Lithostratigraphic sections of the different volcanic localities, or centres, of the Haiber Flats Formation (HFF).

in importance with time and the overall volumetric ratio of rhyolite to andesite (*sensu lato*) ranges from 3:1 in the south of the AMT to 4:1 in the north.

Sediments are a relatively minor constituent of the HFF, reaching a maximum development south of latitude 25°45'S and constituting approximately 10% of the total thickness. However, epiclastic rocks appear to be absent from the thickest part of the formation at Awasis Mountain.

2.2.2 Structure and metamorphism

As discussed in Section A2.3, the HFF has been subjected variously to tilting, folding, shearing and low-grade metamorphism. The intensity of deformation and grade of metamorphism vary considerably on a regional scale. The earliest period of deformation is probably related to the forceful intrusion of the Haisib Intrusive Suite. Plutons of this suite,

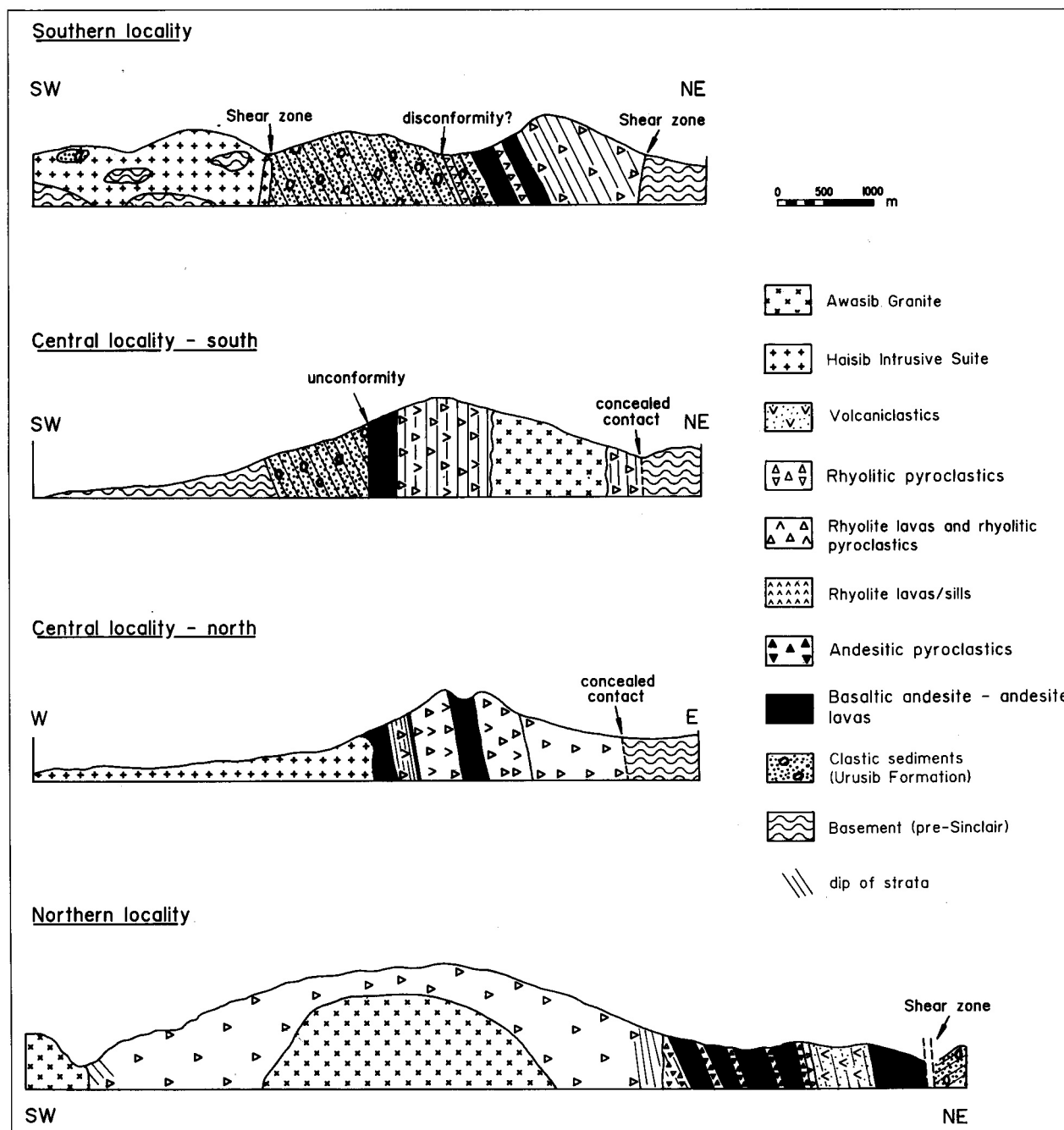


Fig. C.3: Schematic horizontal sections of the different volcanic localities, or centres, of the Haiber Flats Formation (HFF).

together with the Awsasib Granite, resulted in the updoming and tilting of the overlying strata, commonly in an easterly direction. Contact metamorphic effects are difficult to evaluate in the light of subsequent regional metamorphism, but may be indicated by the highest contents of green-brown biotite being associated with those andesites which are most intensely intruded by the Haisib Intrusive Suite.

The large open folds (f_4) observed in the Urusib Formation, are difficult to detect in the younger HFF, possibly as a result of subsequent shearing. However, it appears likely that the pervasive fracture cleavage, which is commonly layering-parallel (Plate C.1d), is axial planar to such folds and hence forms part of the D_4 phase of deformation. Widespread sericitisation and subordinate silicification are probably the result of accompanying as well as subsequent

metamorphism.

A later episode of more ductile deformation (D_5) produced cataclastic, protomylonitic and mylonitic textures. Folds associated with this shearing are usually tight and reclined (Plate A. If). Mineral and stretching lineations are associated with the ss foliation and display a highly variable plunge from subhorizontal to steeply down dip. The mineral assemblage albite + epidote + chlorite + sericite + quartz \pm actinolite \pm biotite \pm calcite associated with this widespread shearing event is typical of the greenschist facies and indicates a higher grade of metamorphism in volcanics of the HFF than in similar Sinclair Sequence rock types to the east of the AMT.

The layering-parallel shear planes were folded into north-west and northeast-trending kink bands and crenulations during a phase of deformation which occurred subsequent to the

shearing, but was probably related to it. A well-developed axial-plane cleavage and crenulation lineation are associated with this D_6 phase of deformation.

The last major episode of deformation (D_7) suffered by the HFF resulted in large scale warping about an east to east-northeast-trending axis. This folding is best illustrated in the southern part of the AMT by the northward change in the trend of fracture cleavage and shear planes from northwest to north (map - Appendix I).

2.2.3 Lithostratigraphy

2.2.3.1 Introduction

The lateral variability in the nature and composition of the HFF requires that description of this formation be based on geographical as well as lithologic criteria. Accordingly, the HFF has been divided into three localities which may correspond to separate, but broadly contemporaneous, volcanic centres. Lithostratigraphic columns and schematic sections for these localities are illustrated in Figs C.2 and C.3. The legends to these figures are based on an informal member subdivision which can be readily applied in the field. However, attempts to correlate these members between sections suggest that lateral interfingering must have occurred and that lateral variations in thickness and composition are significant.

2.2.3.2 Southern locality

The earliest evidence of volcanic activity is in the form of relatively thin rhyolite flows which are intercalated with clastic sediments. The red to grey colour, porphyritic texture and occasionally flow-banded character of the rhyolite lavas are features which are also common to numerous dykes and sHIS within the succession. However, pebbly lithic arenites which are intercalated with the rhyolites have clearly derived their volcanic clasts from immediately underlying flows (plate C.1e). In addition, contorted flow folds within some of the flow-banded rhyolites suggest that these flows were originally lavas. Flow-top breccias are rarely preserved, probably due to active fluvial processes.

Clastic sediments are laterally discontinuous and suggest deposition by debris flows and braided streams. Conglomerates contain a variety of clasts, viz. mafic schist, granite gneiss, quartzite, shale and rhyolite. Sedimentary structures include planar and trough cross-bedding, pebble imbrication and size grading. Although these HFF clastic sediments differ little in appearance from the underlying Urusib Formation, there is a notable increase in the proportion of volcanic clasts.

Within this zone of intercalated rhyolite and sediment, occasional pyroclastic flows form uniformly thin but laterally continuous layers. Globular rhyodacites of greenish-grey colour are often associated with the latter (Plate C.1f). The term "globular" is used non-genetically here to describe round to oval-shaped structures which vary greatly in size from less than a millimetre to several centimetres. These structures differ from the classic lithophysae described by Ross and Smith (1961) in that they are neither

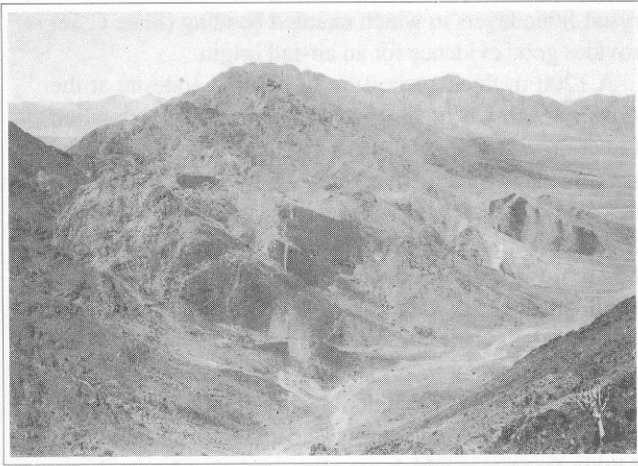
hollow nor show evidence of having been filled with vapour-phase minerals. While similar in texture and composition to the groundmass, these globules are distinguished by their lighter colour and concentric shell structures. In parts the globules have coalesced to form wavy bands, elsewhere they concentrate to form subcircular "nests". Similar features have been described in globular ignimbrite sheets from Kenya (Hay *et al.*, 1979), but their origin remains unexplained.

Dark green basaltic andesite conformably overlies the intercalated rhyolite and sediment, and varies from plagioclase-porphyritic and amygdaloidal flows in the south to aphyric and sparsely amygdaloidal flows in the north. Lateral continuity is difficult to establish due to faulting, scree cover and the rugged terrain (Plate C.2a). Basaltic andesites attain an estimated thickness of 500 m in the southern portion, but the base is not exposed. While boundaries to individual flows tend to be obscured by pervasive fracture cleavage, the uppermost part of the basaltic andesite succession exhibits a varying degree of brecciation. Portions of this flow-top breccia have been infilled by felsitic tuffite of possible air-fall origin.

Overlying reddish rhyolites are predominantly welded crystal-lithic tuffs (plate C.2b) in which pyroclasts range in size from lapilli to blocks (after the classification of Schmid, 1981). Dark grey streaks within the lighter-coloured groundmass are interpreted as collapsed pumice fragments, and the overall texture may commonly be described as eutaxitic (Plate C.2c). Widespread fracture cleavage, which is particularly well developed in the pyroclastic layers, has facilitated severe weathering (Plate C.1d). More weathering-resistant rhyolite lavas which are intercalated with the pyroclastic horizons are typically flow-banded and occasionally exhibit striking flow folds (plate C.2d). Although flow boundaries are difficult to locate, it is clear that individual flows, or cooling units, of rhyolite (*sensu lato*) range in thickness from less than a metre to several hundred metres.

The thicker felsic horizons probably represent single cooling units which were made up of several independent flows. These large cooling units have a massive appearance and typically form weathering-resistant mountain crests. Originally mapped as rhyolite porphyry (Hoal *et al.*, 1986), this massive unit is made up of crystal-rich ash-flow tuff which forms an easily recognisable pyroclastic member that can be followed for a distance of nearly 20 km along strike, but which appears to thin towards the northwest. Similar outcrops of this unit occur in both the central and northern localities (Plate C.2e).

The coarsest agglomerates at the southern locality were recorded to the southeast of the mapped area in the vicinity of the Diar II trigonometrical beacon. Here blocks and bombs commonly exceed 15 cm in size, with some boulders of up to 1 m in diameter, and such deposits are inferred to be proximal to a volcanic centre. While angular lithic fragments often provide one of the best clues in the field to a pyroclastic origin, vapour phase crystallisation has produced light-coloured streaks which are not observed in the lavas. "Exotic" lithic fragments, mostly comprising earlier andesite flows (cognate origin) or sedimentary clasts (acci-



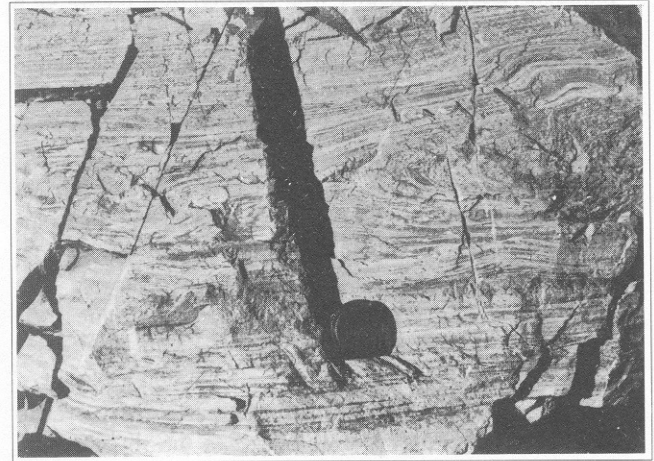
C.2a: View southwards of the southern locality of the HFF showing the interbedded and discontinuous nature of basaltic andesite (dark layers) and rhyolite (light layers) flows. This mountain range rises 550 m above the surrounding plains.



C.2b: Welded ash-flow tuff containing an abundance of lapilli-size lithic fragments of rhyolitic composition. Grey matrix is porphyritic and carries dark fragments of flattened pumice. Southern locality of HFF. Coin for scale.



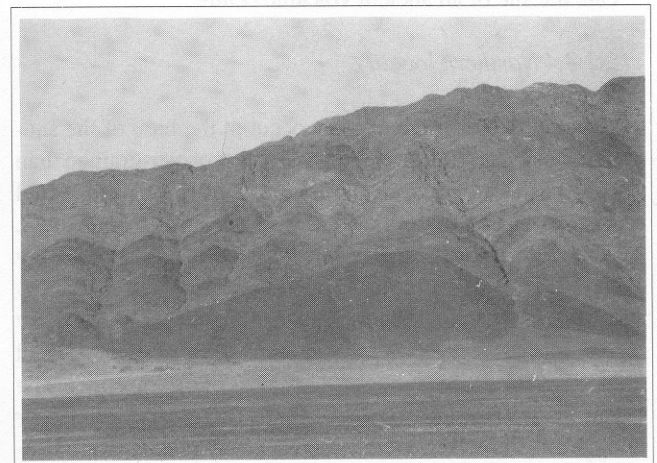
C.2c: Flow fold in fiammé-textured rhyolite. Dark streaks represent collapsed pumice fragments which have partly coalesced to form a eutaxitic layering. Stretching of these fragments may be the result of rheomorphism. Southern locality of HFF. Coin for scale.



C.2d: Contorted flow banding in rhyolite lava. Continuous nature of layers of uniform thickness and absence of pyroclastic textures contrast markedly with C.2c. Northern locality of HFF. Lens cap for scale.



C.2e: Block (0.7 m high) of rhyolite porphyry carrying flattened lithic fragments of phenocryst-rich rhyolite. Fragments may be of juvenile or cognate origin. Southern locality of HFF.



C.2f: View eastwards of the central locality of the HFF showing the intercalated nature of lower andesite (dark layers) and upper rhyolite (light portion). The lowermost dark dome-shaped outcrop is made up of quartz monzonite of the younger Haisib Intrusive Suite. Total height of the section is approximately 400 m.

dental origin), are not prominent in the pyroclastic deposits. Rare stratified tuffite consists of alternating fine- to coarser-grained layers composed of both angular crystals (mainly feldspar and quartz) and rhyolite fragments. Admixtures of epiclastic material are suggested by the pronounced rounding exhibited by several of the clasts.

2.2.3.3 Central locality

Basaltic andesites (including a high- Mg flow) are largely restricted to the northern part of this locality where they have been intensely intruded by plutons of the Haisib Intrusive Suite. Subsequent shearing has transformed many of the original flows into mylonitic greenschists (Plate A.1f), but primary textures are preserved along the flanks of the main shear zone. Plagioclase and a ferromagnesian mineral (replaced pyroxene and/or olivine) constitute widespread phenocrysts in these flows.

Andesites within the main shear zone have preserved their original plagioclase-phyric character despite a strong foliation. Biotite, together with epidote, now makes up a significant proportion of the andesite and has imparted a dark green colour to the rock. Secondary silicification is widespread in the form of patches and veins and dacitic compositions may, therefore, not be primary. The interfingering of the andesite with flow-banded rhyolite and crystallitic tuff is illustrated in Plate C.2f. The rhyolite-andesite association occurs over several hundred metres in stratigraphic height with rhyolite, made up largely of ash-flow tuffs, becoming dominant in the upper part.

While rhyolites (*sensu lato*) closely resemble their southern locality counterparts, so-called rhyolite porphyries are less prominent. An apparently sub-circular intrusion of microgranite porphyry, which forms part of the Awasis Granite, bears a strong resemblance to the rhyolite porphyries. As a result of this similarity, and because of the near vertical attitude of the rhyolite layers, it is difficult to ascertain the original shape of the granite pluton. Nevertheless, available evidence suggests that the granite could represent a subvolcanic pluton and may, therefore, demarcate the site of an ancient volcanic centre.

2.2.3.4 Northern locality

Stratified rhyolitic tuffites occur at the base of the succession (Plate C.3a) and are somewhat coarser-grained than tuffites described from the southern locality. Individual units rarely exceed more than a few metres in thickness. Although a small degree of sedimentary reworking may have taken place, these tuffites were probably originally air-fall or ash-flow tuffs and hence indicate rhyolitic activity at an early stage. Epiclastic material appears to be restricted to the upper, more poorly welded, parts of these tuffites. The tuffites are overlain by thicker beds of volcanic breccia or agglomerate which are characterised by abraded and fractured rhyolite pyroclasts.

The earliest manifestation of basaltic andesitic eruptions is marked by the occurrence of stratified tuffites approximately 100 m above the base of the succession (Fig. C.2). These tuffites are characterised by a fine stratification of

crystal-lithic layers in which mantled bedding (Plate C.3b) provides good evidence for an air-fall origin.

A 1200 m thick succession of basaltic andesite at the northern locality is made up of a monotonous intercalation of lava flows, fragmental rocks and stratified tuffites. The lava flows are typically pyroxene porphyritic with subordinate plagioclase phenocrysts and amygdaloids. Although fresh in appearance, a greenish tint to the dark grey colour of these flows indicates moderate alteration. The thickness of individual flows varies from several metres to almost 140 m, the boundaries between flows usually being demarcated by fragmental layers (Plate C.3c). The latter may be broadly classified as volcanoclastic in origin, but commonly exhibit the grading (both normal and inverse) and angularity of lithic fragments which are characteristic of pyroclastic flow deposits. These layers are rarely more than a few metres in thickness. However, in the uppermost part of this succession, andesitic volcanic breccia or agglomerate takes on a more acidic character due to the increased proportion of felsic clasts.

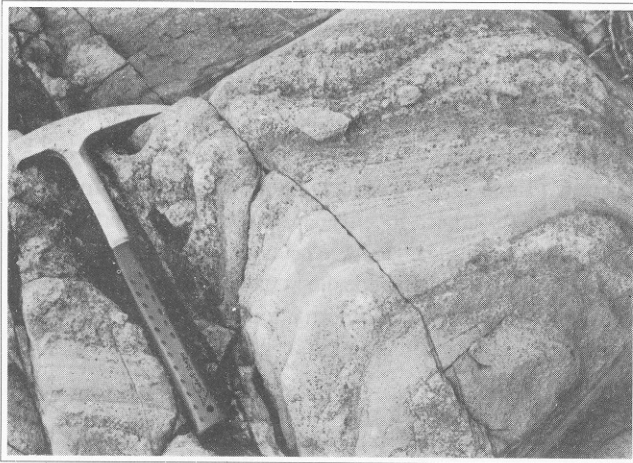
A zone of both rhyolitic and andesitic volcanoclastics overlies this mixed agglomeratic horizon, but the original nature of these deposits is obscured by shearing. The volcanoclastics appear to be overlain by a massive outcrop of mainly pyroxene-porphyritic basaltic andesite which occurs adjacent to the shear zone. These massive beds are in turn overlain by more plagioclase-porphyritic and amygdaloidal basaltic andesites which have been subjected to intense shearing reminiscent of the central locality. The contact between these massive flows is, unfortunately, not exposed.

This overall succession of predominantly andesitic (*sensu lato*) volcanics on the eastern flank of Awasis Mountain has been tilted to the east by the intrusive Awasis Granite and probably also by rhyolite plugs (Fig. C.3 and Plate C.3d). In the central northern part of this locality, the granite has caused the updoming of a considerable thickness of acid pyroclastic rocks. Most of these pyroclastics are massive beds of ash-flow tuff and agglomerate which rarely allow their attitude to be ascertained. However, several widely separated flows do indicate eastward dips of 60-80°, which suggest an approximate thickness of rhyolite (*sensu lato*) in excess of 6000 m. This estimate is difficult to evaluate in the light of widespread intrusion by rhyolite plugs and the Awasis Granite, together with the rugged nature of the terrain. The major part of the rhyolitic volcanism post-dates the andesitic phase. This is well illustrated by contaminated rhyolite tuffs which contain a profusion of exotic mafic volcanic fragments (Plate C.3e). The intrusive rhyolite plugs represent a still later phase of acid volcanism or a period of resurgence.

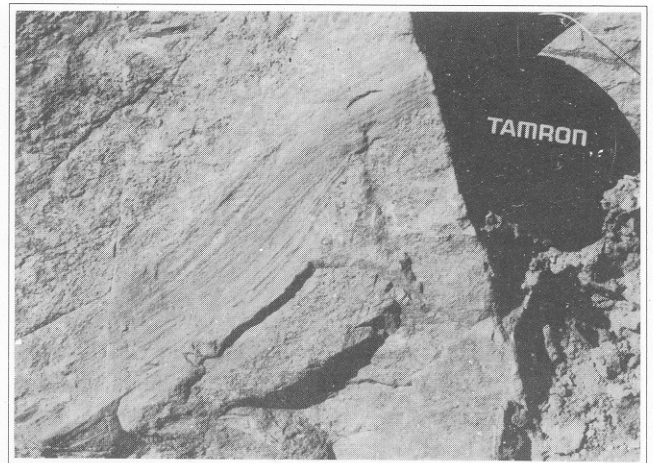
A small outcrop of porphyritic and sparsely amygdaloidal rhyodacite in the southern part of Awasis Mountain is different in appearance and composition from the globular rhyodacite recorded in the southern locality.

The possibility of a volcanic centre being located within the northern locality is suggested by several independent lines of evidence:

- (i) The presence of coarse-grained proximal agglomerate deposits in the northern part of Awasis Mountain.
- (ii) Several dome-shaped rhyolite plugs which are close-



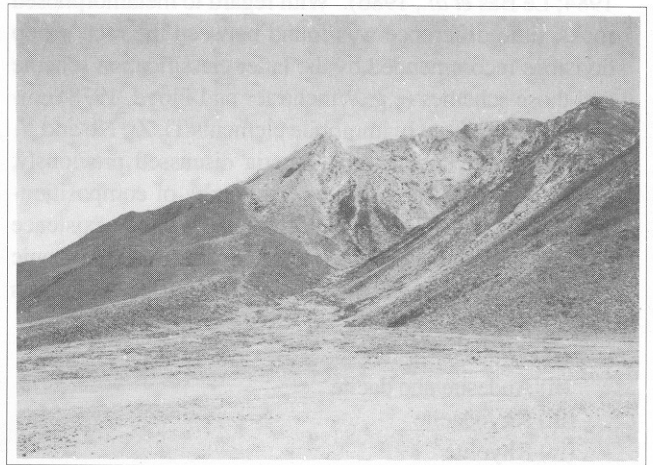
C.3a: Stratified rhyolitic tuffite showing normal and inverse grading. Low-angle truncations suggest that this deposit is the result of ash-flow surge rather than air fall. Some sedimentary reworking may, however, have taken place. Basal part of section at northern locality of HFF.



C.3b: Planar fabric and mantled bedding indicate an air-fall origin for the thin basaltic andesite layer. Adjacent layers are of similar composition, but represent pyroclastic-flow deposits. Northern locality of HFF. Lens cap for scale.



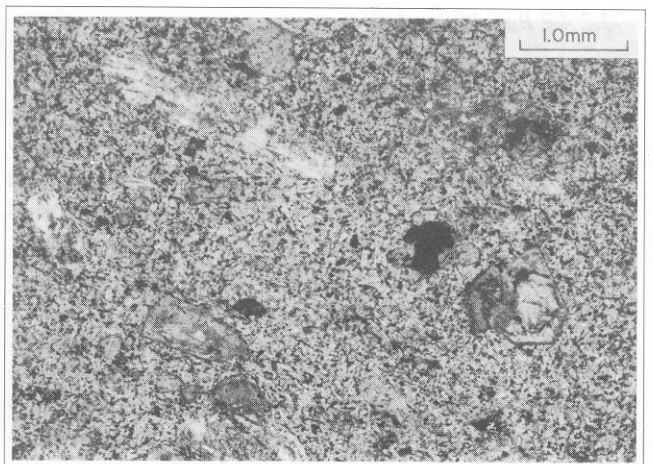
C.3c: Fragmental and multiply-graded layer of basaltic andesite which occurs between flows of similar composition. Origin is uncertain, but may represent a mixed pyroclastic-epiclastic deposit. Northern locality of HFF. Lens cap for scale.



C.3d: View southwards of the northern locality of the HFF showing the earlier basaltic andesites (dark portion on left) in contact with later rhyolites in the central portion of the photo. Dark scree within the latter is typically associated with rhyolite porphyry plugs. Northeastern part of Awasis Mountain - section approximately 500 m high.



C.3e: Welded rhyolitic ash-flow tuff containing abundant dark fragments (cognate?) of basaltic andesite. The streaky nature of these clasts suggests that mixing of the two magma types has occurred. Northern locality of HFF in the vicinity of Nos Numabis.



C.3f: HFF basaltic andesite (BH 690) - northern locality. PPL. Phenocrysts of augite (pseudomorphed by actinolite) and tabular plagioclase in a pilotaxitic groundmass. Titanomagnetite is scattered throughout the section as a groundmass phase and as large "amoeboid" replacement products.

ly associated, spatially and temporally, with the rhyolite flows.

(iii) The subvolcanic Awasi Granite crops out over an area of approximately 30 km² and is intimately associated with the felsic phase of volcanism.

2.2.4 Petrography

2.2.4.1 Introduction

Petrographic properties usually allow the classification of individual volcanic members in the HFF without recourse to whole-rock chemistry. Hence, rhyodacites can be distinguished from both dacites and rhyolites by their intermediate petrographic character. However, in very fine-grained aphyric rocks it is usually necessary to resort to chemical analyses in order to accurately classify them. The classification scheme used is that of TAS (Total Alkalis versus Silica) which has been recommended by IUGS (Le Maitre, 1984; Le Bas *et al.*, 1986). With regard to metamorphosed rocks, little difference was found between the rock group divisions recommended by the latter classification scheme and those schemes (e.g. Winchester and Floyd, 1978) employing the relatively immobile elements Ti, Zr, Nb and Y.

Together with the field criteria discussed previously, significant differences in the petrography of compositionally similar volcanics are in accordance with the existence of three separate volcanic centres. The major volcanic groups which can be discussed petrographically are as follows:

- (i) Basaltic andesite
- (ii) Andesite and dacite
- (iii) Rhyodacite
- (iv) Rhyolite

The first and last groups are volumetrically most important in the HFF and are represented at all of the different localities. Accordingly, petrographic data is presented in comparative form for these two groups in Tables C.1 and C.2, but will also be discussed below along with the petrography of the andesite-dacite and rhyodacite groups.

2.2.4.2 Basaltic andesite

Porphyritic textures are characteristic of all three localities, only a single aphyric flow having been observed at the southern locality. The latter flow is, however, strongly altered and characterised by intergrowths of epidote and actinolite which make up 5-10% of the rock and could represent replacement products of original phenocrysts. Plagioclase and augite constitute easily recognised phenocryst phases in many basaltic andesites (Plate C.3f), although augite is typically pseudomorphed by actinolite. Relict cores of augite are, however, well preserved in the northern locality (Plate C.4a) and their arrangement suggests original glomeroporphyritic texture in which individual crystals display both twinning and zoning.

Pseudomorphous replacement products (actinolite, biotite, chlorite and magnetite) suggest that olivine constituted a major phenocryst in basaltic andesite at the central and possibly also the northern locality (Plate C.4b). Less common-

ly, these pseudomorphs exhibit outlines more indicative of original hornblende. In view of the degree of alteration, it is difficult to sustain any suggestion that magnetite constitutes a primary phenocryst phase.

Phenocryst proportions show considerable regional variation (Table C.1) in which plagioclase is dominant mainly in the southern locality and augite in the northern locality. Olivine appears to have been the dominant phenocryst in high-Mg basaltic andesite at the central locality, but the degree of alteration and deformation here does not allow easy distinction between pseudomorphs after pyroxene and olivine.

Amygdales, although present, are only widespread in the southern locality, but even here rarely exceed 15 % of the rock. In deformed flows, amygdales have undergone recrystallisation and redistribution to form trails and patches of disseminated quartz, a texture difficult to distinguish from the effects of secondary silicification. These trails occasionally have a vein-like appearance and brecciated texture which appears to be of secondary origin.

The groundmass of basaltic andesites is typically cryptocrystalline and composed of a pilotaxitic to trachytic intergrowth of plagioclase laths together with pseudomorphed pyroxene and interstitial K-feldspar. The cloudy appearance of the groundmass is due to scattered opaque and secondary minerals, viz. epidote, sericite, actinolite, biotite (green to brown) and sphene.

While alteration and recrystallisation are evident in virtually all basaltic andesites, eruptive rocks of the central locality show the greatest degree of metamorphic reconstitution. Hence porphyroblasts of carbonate (often associated with green biotite) and mafic aggregates (biotite ± epidote ± carbonate ± opaque minerals) are particularly well developed at this locality. Bladed to subhedral tourmaline (pink to blue-grey pleochroism) forms a rare component of these aggregates. Although greenschists are typical of the central locality, evidence for deformation at the southern and northern localities is generally restricted to bending of cleavage planes or fracturing of mineral phases. However, a weak to moderate tectonic fabric may be defined variously by the subparallel arrangement of ellipsoidal amygdales, by elongate aggregates of intergrown biotite and actinolite which may be folded and strained, and by anastomosing trails of secondary minerals.

2.2.4.3 Andesite and dacite

Andesitic and dacitic flows are best developed at the central locality and differ little in appearance and petrography. These intermediate flows are typically plagioclase phyric (average 15% of the rock) with individual phenocrysts having an average size of 0.7 mm (maximum size 4.5 mm). Plagioclase forms anhedral to subhedral porphyroclasts which may be granulated at their margins and show complete replacement by albite or the assemblage epidote + biotite ± actinolite. Polysynthetic twinning is usually well developed in albite, but may be partly obscured by the alteration assemblage epidote + sericite + chlorite + biotite. Deformation has resulted in recrystallisation of several feldspars into irregular subgrains with an accompanying exsolution

TABLE C.1: Petrography of basaltic andesites from the southern, central and northern localities of the Haiber Flats Formation (HFF).

	SOUTHERN LOCALITY	CENTRAL LOCALITY	NORTHERN LOCALITY
TEXTURE	Porphyritic (up to 20% phenocrysts). Amygdaloidal (usually <15% amygdalae). Occasionally pilotaxitic. Secondary fabric due to growth of biotite \pm actinolite.	Porphyritic (10-30% phenocrysts). Schistose in proximity of shear zones due to alignment of biotite.	Porphyritic to glomeroporphyritic (5-15% phenocrysts). Occasionally amygdaloidal. Pilotaxitic to trachytic. Weak secondary fabric due to growth of biotite + actinolite.
PHENOCRYSTS			
Plagioclase	Dominant. Av. size 1.5 mm, max. 5.0 mm. Subhedral to euhedral. Carlsbad and albite twinning. Andesine composition. Fractured and altered (saussuritisation and sericitisation).	Subordinate. Av. size 1.1 mm, max. 5.0 mm. Microphenocrysts (av. size 0.2 mm). Anhedral to subhedral. Deformed albite twin lamellae. Severe alteration (often albitisation) and complete replacement in high-Mg andesite by chlorite + sericite \pm actinolite \pm epidote \pm opaques.	Subordinate. Av. size <1 mm, max. 1.5 mm. Subhedral. Carlsbad and albite twinning. Normal zoning (labradorite cores). Altered to sericite + chlorite + epidote \pm opaques.
Augite	Rare relict cores. Replacement by aggregates of actinolite + epidote (av. size 0.5 mm).	Dominant, except in high-Mg andesite. Av. size 1.0 mm, max. 2.5 mm. Anhedral to subhedral. Pseudomorphed by actinolite \pm biotite \pm epidote \pm chlorite \pm sericite \pm opaques.	Dominant. Av. size 0.8 mm, max. 3.0 mm. Subhedral to euhedral. Twinned and zoned. Relict cores in pseudomorphs of actinolite.
Other	Biotite and actinolite may have replaced a ferromagnesian mineral other than augite.	Olivine suggested by opaque-filled fractures in actinolite/chlorite pseudomorphs, dominant phenocrysts in high-Mg andesite (av. size 1.5 mm). Microphenocrysts of opaques are probably secondary.	Olivine suggested by opaque-filled fractures in biotite/chlorite pseudomorphs. Subhedral. Size 0.5-5.0 mm. Possible microphenocrysts of titanomagnetite. Presence of hornblende uncertain.
AMYGDALES	Rounded or ellipsoidal. Up to 6 mm in size. Quartz-filling occasionally forms mortar texture. Other phases are chlorite, biotite, epidote, actinolite, opaques, sphene and carbonate. Recrystallisation results in a patchy and vein-like occurrence.	Granoblastic quartz aggregates may represent recrystallised amygdalae (or secondary silicification).	Patchy aggregates of quartz \pm epidote \pm chlorite (up to 4 mm in size). Uncommon. Strained appearance. May resemble strained quartz xenocrysts.
GROUNDMASS	Aphanitic intergrowth of feldspar (mainly plagioclase), quartz and opaques (haematite and/or magnetite). Alteration products are epidote, biotite, sericite, chlorite, sphene and oxide.	Aphanitic intergrowth of mainly plagioclase laths and opaques. Secondary assemblage similar to southern locality, but quartz also prominent. Biotite alignment defines a strong fabric.	Crypto- to microcrystalline intergrowth of tabular plagioclase (labradorite) laths, pseudomorphs of actinolite after augite, and interstitial K-feldspar. Scattered titanomagnetite granules. Secondary assemblage as for southern locality but lacking in chlorite.

of quartz blebs.

Biotite, pleochroic from light yellow to brownish green, forms small flakes which have a high aspect ratio and are aligned, sometimes in continuous layers, to define a strong foliation. Intergrowths of biotite with epidote granules and skeletal opaque minerals are widespread, but particularly dense in the pressure shadows of plagioclase porphyroclasts. Together, biotite and epidote make up in excess of one third of the rock volume.

Ubiquitous silicification is present both as patchy intergrowths in the groundmass and as veins. The groundmass is aphanitic and consists of strongly aligned plagioclase laths, flakes of green biotite, and granules of quartz, epidote, sphene and opaque minerals. Granular-textured plagioclase may be the result of comminution, while the subparallel orientation of both plagioclase porphyroclasts and their replacement products further accentuates the mylonitic fabric in these andesites. The more biotite-rich rocks usually show evidence for a crenulation cleavage in addition to the main mylonitic fabric.

2.2.4.4 Rhyodacite

(i) Southern locality rhyodacite

Unique to this rhyodacite are large ellipsoidal “globules” (average 20 mm in length) which resemble much smaller structures (less than 0.2 mm in size) that have been described from ignimbrites in Kenya (Hay *et al.*, 1979). The rhyodacite is typically aphyric and consists of a micro- to cryptocrystalline intergrowth of quartz and feldspar with widespread secondary phases such as epidote, green biotite, chlorite, sphene and sericite. “Globules” are compositionally and texturally similar to the “host” groundmass; both consist of allotriomorphic, inequigranular intergrowths of quartz and feldspar together with approximately equal proportions of the abovementioned secondary minerals. Globules differ from the groundmass, however, in the following characteristics:

(a) A finer-grained nature which is especially well demonstrated by the profusion of tiny epidote granules.

(b) A more leucocratic appearance due to a relative depletion in biotite and chlorite.

(c) A more pronounced tabular shape of plagioclase which is aligned parallel to the foliation.

The darker colour of many of the globule cores is related to an increase in the content of epidote, while the outer rims may also contain a particularly dense concentration of epidote. The latter feature, together with an inner rim which is essentially epidote-free, forms a distinct margin (about 0.2 mm wide) to these structures.

The presence of tabular plagioclase phenocrysts (average 0.5 mm long) is suggested by pseudomorphs of granoblastic quartz \pm biotite.

(ii) Northern locality rhyodacite

A porphyritic nature is characteristic of this rhyodacite, with phenocrysts of plagioclase, K-feldspar, quartz and clinopyroxene constituting approximately 10% of the rock. The presence of amygdals is indicated by elongated aggregates of quartz (up to 0.5 mm in size), actinolite and opaque

minerals, surrounded in turn by a quartzofeldspathic shell and an outer rim of opaque granules.

Quartz phenocrysts are typically large (average size 1.8 mm), rounded and resorbed. Evidence for strain in quartz is usually restricted to undulose extinction, although occasional recrystallisation has resulted in granoblastic polygonal aggregates. Plagioclase forms tabular phenocrysts (average size 1.0 mm) and microphenocrysts (less than 0.5 mm in size) which display both twinning (albite and Carlsbad) and strong normal zoning (An_{35} cores), despite widespread saussuritisation. K-feldspar occurs as altered, sieve-like, phenocrysts (average size 1.0 mm), but is a relatively minor component in the rhyodacite. Clinopyroxene, probably augite, forms anhedral to subhedral crystals (average size 0.5 mm) which are typically altered, sometimes intensely, to the assemblage actinolite \pm green biotite \pm opaque minerals.

The intergranular groundmass is an aphanitic undergrowth of the same phases as the phenocrysts but contains, in addition, a high content of opaque and secondary minerals. An opaque mineral, possibly magnetite, may reach microphenocryst size (up to 0.3 mm) but has a secondary appearance. Occasional patchy areas of quartz are probably also secondary in origin. A trachytic texture has been preserved in portions of the rhyodacite.

2.2.4.5 Rhyolite

While rhyolitic volcanics are predominantly pyroclastic in origin, lavas may occasionally be recognised by their apparent lack of pyroclastic textures.

(i) Pyroclastic rhyolite

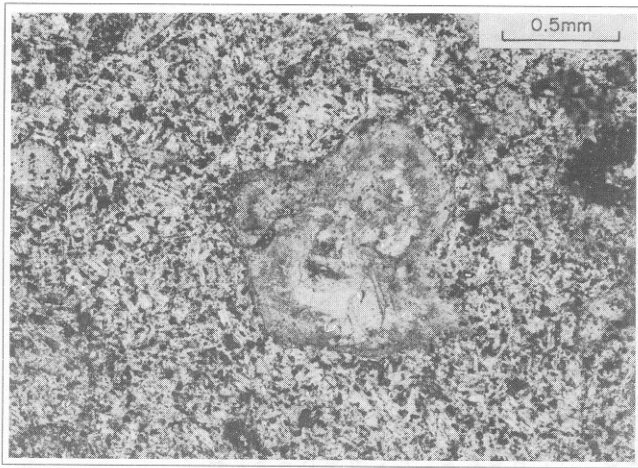
The term “pyroclastic rhyolite” is applied to lithic-crystal tuff of rhyolitic composition which is usually made up of easily recognisable phenocrysts (commonly K-feldspar, plagioclase and quartz) and lithic fragments (*sensu lato*). The ratio of lithic to crystal components varies from about 0.5 in the central locality rhyolites to 2.0 in the northern locality rhyolites, while the ratio in the southern locality is about 1.0 (Table C.2).

Perthitic K-feldspar is always the dominant phenocryst, but widespread albitisation (Plate C.4c) does not allow a reasonable estimate of the original K-feldspar/plagioclase ratio. Primary plagioclase can usually be distinguished from secondary albite by its more altered nature and polysynthetic (as opposed to “chessboard”) twinning. The fractured nature of many of the feldspar phenocrysts together with such features as undulose extinction, granulation and recrystallisation, clearly indicate that the rock has undergone greater strain than would be expected from pyroclastic processes alone.

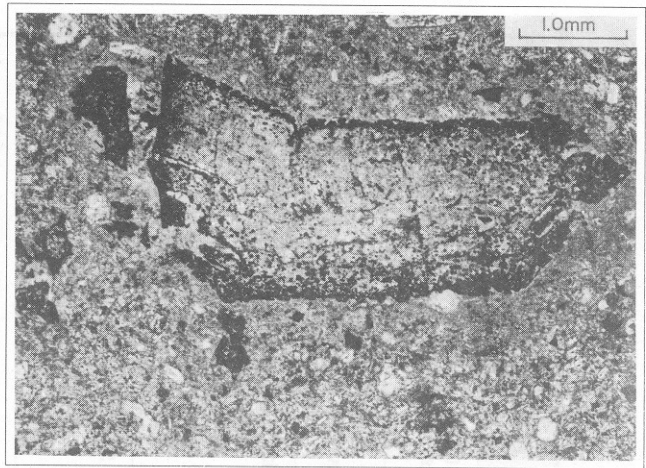
Quartz phenocrysts are usually rounded and resorbed, sometimes with deep embayments, but occasionally exhibit bipyramidal outlines and a poikilitic nature. Angular “chips” of quartz may represent pyrogenic crystals which fractured during eruption. In addition to the strain-related features expected from pyroclastic processes, quartz phenocrysts exhibit widespread evidence of tectonic deformation, e.g. well-developed mortar texture in rhyolites of the

TABLE C.2 : Petrography of pyroclastic rhyolites from the southern, central and northern localities of the Haiber Flats Formation (HFF).

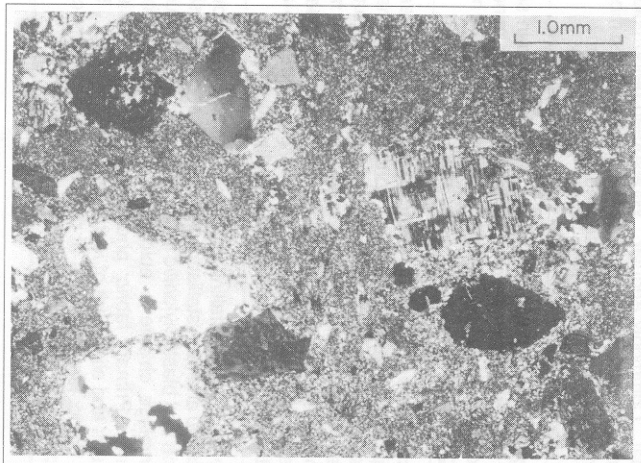
	SOUTHERN LOCALITY	CENTRAL LOCALITY	NORTHERN LOCALITY
TEXTURE	Porphyritic to glomeroporphyritic (15-30% phenocrysts, av. 23%); fragmental (10-35% lithics, av. 19%); massive and eutaxitic.	Porphyritic (10-35% phenocrysts, av. 18%); fragmental (av. <10% lithics); massive and eutaxitic; commonly mylonitic.	Porphyritic (10-25% phenocrysts, av. 15%); fragmental (15-50% lithics, av. 30%); massive and eutaxitic.
PHENOCRYSTS	K-feldspar \geq quartz > plagioclase	K-feldspar \geq quartz \geq plagioclase	K-feldspar \geq quartz > plagioclase
K-feldspar	Dominant. Size 0.2-3.5 mm. Anhedral to subhedral. Mesoperthite. Fractured and resorbed. Angular chips reflect pyroclastic process. Recrystallisation due to tectonic stress. Replacement by albite ("chessboard" twinning) and alteration to sericite + epidote + carbonate + oxide.	Dominant. Size 0.2-2.0 mm. Anhedral to subhedral. Mesoperthite. More fractured than at southern locality. Resorption difficult to recognise. Angular chips. Widespread recrystallisation. Replacement by albite ("chessboard" twinning) and alteration to oxide \pm epidote \pm sericite \pm sphene.	Dominant. Size 0.2-3.0 mm. Similar nature to southern locality.
Plagioclase	Subordinate. Size 0.2-3.5 mm. Anhedral to subhedral. Albite, Carlsbad and pericline twins; composition albite to rare oligoclase (av. An ₉). Fractured and resorbed. Similar alteration to K-feldspar.	Subordinate. Size 0.2-2.0 mm. Anhedral to subhedral. Albite and pericline twins common. Albite composition. Commonly fractured (angular chips), occasionally resorbed. Similar alteration to K-feldspar.	Subordinate. Size 0.2-3.0 mm. Similar nature to southern locality.
Quartz	Size <0.2 (microphenocrysts) - 1.8 mm. Rounded and resorbed. Occasionally bipyramidal. Angular fragments not uncommon. Stress-related features: undulose extinction, stretching and mortar texture. Latter not widespread.	Size up to 3.0 mm. Rounded and resorbed. Rarely bipyramidal. Commonly angular. Widespread deformational features: undulose extinction, severe stretching and mortar texture. Lenticular zones of secondary silicification.	Large subhedral or rounded poikilocrysts (up to 4.0 mm in size) have undergone severe resorption. Otherwise similar to southern locality.
Other	Secondary assemblage opaques + biotite \pm chlorite \pm sericite may have replaced an original ferromagnesian mineral phenocryst.	Intergrowths of epidote \pm opaques (up to 20 mm in size) may have replaced an original ferromagnesian mineral phenocryst. Magnetite of phenocryst dimensions (0.2 mm) is largely secondary.	Apart from possible replacement products of an original ferromagnesian phase (see southern locality), several minerals reach phenocryst dimensions, viz. biotite, magnetite and zircon (up to 0.2 mm).
LITHIC FRAGMENTS	Size highly variable. Accidental fragments rare. Typically opaque- or crystal-rich. Spherulitic. Usually coarser-grained than groundmass and insets less deformed in comparison with "host". High aspect ratios (30:1) partly due to tectonic stress. Flammé difficult to recognise due to extreme welding and additional tectonic shortening.	Typically large (10 cm in size) and characterised by coarsely (up to 0.4 mm) devitrified, spherulitic groundmass. Similar characteristics to southern locality where undeformed. Elsewhere lithics difficult to distinguish from patches of recrystallised groundmass, fragmented phenocrysts and lensoid zones of silicification. Break-up and redistribution of lithic fragments is partly tectonic.	More abundant than at other localities, but of variable size. Typically coarser-grained and more cloudy than groundmass. Ellipsoidal devitrification centres are unlike spherulitic elsewhere. Quartz phenocrysts partly recrystallised and patchy nature of lithic fragments may resemble zones of secondary silicification. Mafic lithic fragments are of uncertain origin but resemble flammé.
GROUNDMASS	Micro- to cryptocrystalline quartzfeldspathic intergrowth. Devitrified and recrystallised. Fabric defined by trails of opaques, lenticular patches of recrystallised phases, flattened lithic fragments and linear intergrowths of sericite. Flow banding defined by alternation of layers rich and poor in opaques.	Micro- to cryptocrystalline quartzfeldspathic intergrowth. Devitrified and recrystallised. Widespread secondary silicification and blastomylonitic in shear zones. Cloudy due to assemblage chlorite \pm epidote \pm opaques \pm sericite \pm sphene. Primary fabric: phenocryst alignment, trails of opaques and alignment of lenticular lithic fragments. Tectonic fabric: lensoid zones of recrystallisation, phenocryst stretching and sericite intergrowths.	Similar to southern locality.



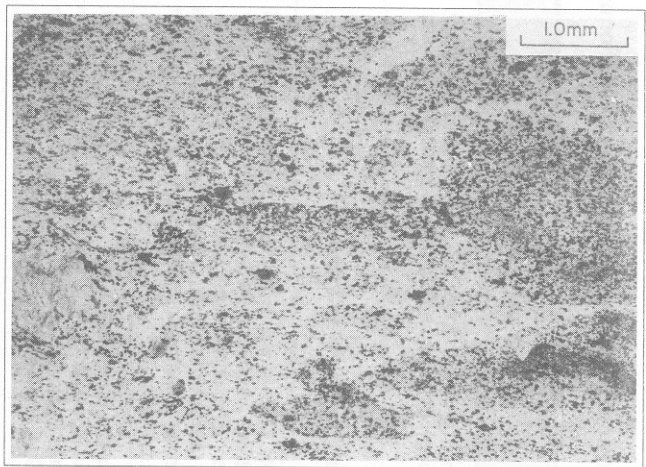
C.4a: HFF basaltic andesite (BH 690) - northern locality. PPL. Close-up view of adjoining augite phenocrysts showing clear core of augite and a more turbid replacement rim of actinolite set in a pilotaxitic groundmass. The secondary magnetite patch on the right is associated with biotite intergrowths.



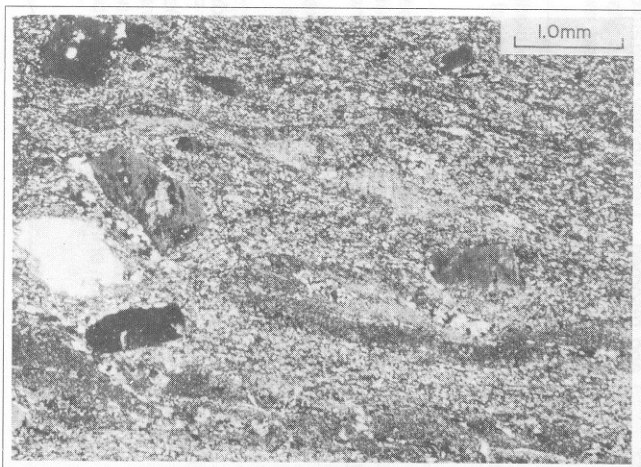
C.4b: HFF basaltic andesite (BH 687) - northern locality. XPL. Biotite-magnetite pseudomorph after olivine phenocryst. Magnetite-filled fractures in surrounding microphenocrysts are especially reminiscent of olivine. [XPL = Cross Polarised Light]



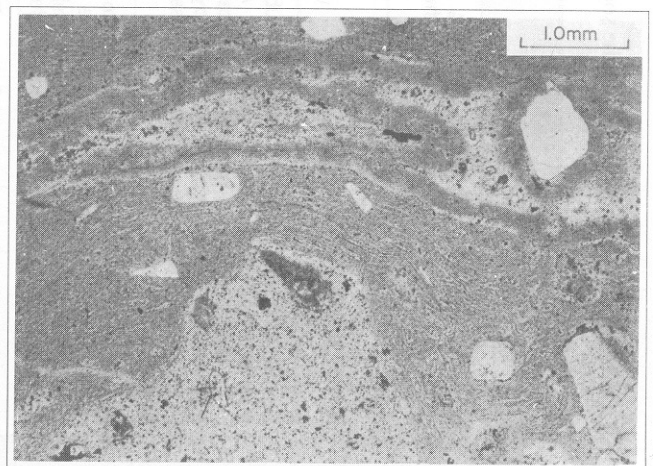
C.4c: HFF rhyolite porphyry (BH 611) - central locality. XPL. Recrystallisation of quartz phenocrysts (lower left) has resulted in irregular margins and a domainal structure. An albite pseudomorph after K-feldspar (centre-right) shows characteristic "chess-board" twinning.



C.4d: HFF pyroclastic rhyolite (BH 53) - southern locality. PPL. Slightly flattened lithic fragments are distinguished from the quartzofeldspathic groundmass by their higher concentrations of opaque minerals. Phenocrysts of feldspar and quartz (lower left) are subordinate to lithic fragments.



C.4e: HFF pyroclastic rhyolite (BH 188A) - central locality. XPL. Dark wavy bands and flattened fragments are interpreted as devitrified glass or juvenile clasts. Phenocrysts are feldspar and quartz. Foliation is partly tectonic in origin and some secondary silicification has taken place.



C.4f: HFF pyroclastic rhyolite (BH 236) - northern locality. PPL. Welded ash-flow tuff showing resorbed and angular phenocrysts and lithic fragments in a devitrified groundmass. Compression and stretching of original shards has resulted in a flow foliation which is moulded around the phenocrysts and the lowermost lithic fragment. The curved feature in the upper part of the photomicrograph is a spherulitic fragment of juvenile origin.

central locality. Where deformation has been severe, quartz aggregates are typically streaked out in the plane of the foliation and resemble lenticular zones of secondary silicification.

Sparse aggregates of the secondary assemblage opaque minerals \pm biotite \pm chlorite \pm sericite \pm epidote may be pseudomorphous after a ferromagnesian mineral phenocryst. Brown biotite, magnetite and zircon occasionally reach phenocryst dimensions and possibly constitute primary phases.

The groundmass is a micro- to cryptocrystalline undergrowth of granular quartz and feldspar which is charged with small opaque minerals. Lithic fragments can usually be distinguished from the groundmass by their darker, opaque mineral-rich appearance (Plate C.4d). A primary fabric, where present, is usually defined by the alignment of elongate groundmass phases and may be accentuated by such features as trails of opaque minerals, subparallel alignment of phenocrysts, elongate patches of more coarsely crystalline groundmass phases, and flattened lithic or pumice fragments (Plate C.4e). Where significant mineral segregation has taken place, e.g. opaque mineral-rich and opaque mineral-poor layers, the texture is fluidal and probably primary in origin.

The pyroclastic nature of these flows is best indicated by an appreciable content of angular lithic fragments and, less commonly, by the presence of collapsed pumice fragments or "fiammé" (after Ross and Smith, 1961). The high aspect ratios (up to 30) of both lithic and pumice fragments may give rise to a eutaxitic fabric, but it should be noted that some of the flattening is probably the result of tectonic stress. Although the appearance of lithic fragments varies considerably, one feature common to all is the more coarse-grained and spherulitic nature of the groundmass relative to the host. The combined effect of devitrification, recrystallisation and silicification has completely destroyed any evidence of vitroclastic texture, or shard structure, in the groundmass (Plate C.4f).

Lithic fragments are usually porphyritic, with an identical phenocryst assemblage to the host, although individual phenocrysts are typically larger. While it is clear that in some rhyolites the lithic fragments, particularly the larger ones, have shielded their insets from stress, elsewhere entire fragments have suffered considerable deformation as indicated by such features as fractures, quartz-filled pressure shadows adjacent to feldspar porphyroclasts, and isoclinal folds. Some lithic fragments are rimmed by intergrowths of quartz and carbonate; this may suggest disequilibrium between "host" and "pyroclast" and possibly a cognate origin. In general, however, it is difficult to distinguish between clasts of juvenile and cognate origin.

The hybrid nature of tuffs in the northern part of Awasis Mountain (Plate C.5a) suggests that these tuffs are the result of mixed pyroclastic eruptions. Although compositionally distinct from the rhyolitic "host", the mafic (possibly andesitic) lithic fragments resemble compressed pumice clasts and could be cognate in origin.

As in the case of the basaltic andesites, the central locality rhyolites show the greatest degree of deformation and metamorphism. A mylonitic fabric is best expressed by alignment of recrystallised lensoid aggregates of quartz \pm

carbonate \pm muscovite together with anastomosing trails of intergrown sericite flakes. On occasion the degree of recrystallisation relative to comminution may be sufficient to refer to the texture as blastomylonitic (Plate C.5b). Owing to the intensity of deformation, it is usually difficult to distinguish lithic fragments from coarser-grained patches of recrystallised groundmass, disaggregated phenocrysts and lensoid zones of silicification.

(ii) Non-pyroclastic rhyolite

Phenocrysts make up 10-20% of the rock and comprise plagioclase predominantly with lesser, but important, K-feldspar and quartz. Plagioclase, both albite (An_8) and subordinate oligoclase (An_{25} ?), forms anhedral to subhedral microphenocrysts and phenocrysts (average size 0.9 mm, maximum size 5.0 mm) which occasionally show significant resorption. Zoning is usually strong and both albite and pericline twins are commonly developed. Glomeroporphyritic aggregates of plagioclase, and more rarely K-feldspar, may be widespread. The effects of deformation, where present, are particularly noticeable in plagioclase phenocrysts, viz. bent twin lamellae, fracturing, quartz exsolution and disaggregation. Cloudy interiors in plagioclase are the result of replacement by the secondary assemblage epidote + sericite \pm chlorite \pm carbonate.

K-feldspar phenocrysts are present as both orthoclase microperthite and microcline, but recognition is difficult due to widespread albitisation. K-feldspar is mostly anhedral in form, fractured and less altered than plagioclase.

Phenocrysts of quartz, where present, are both rounded and bipyramidal in form (average size 0.04 mm). Angular outlines are less common, possibly as a result of widespread resorption.

"Poikiloblasts" of an opaque mineral (average size 0.3 mm) are usually altered to sphene \pm chlorite and may be associated with large epidote grains (up to 0.5 mm).

The cloudy groundmass is either a cryptocrystalline intergrowth of granular quartz and feldspar, as in pyroclastic rhyolite, or it exhibits an unusual devitrification texture which is made up of sieve-like ellipsoids (average size 0.5 mm) of quartzofeldspathic composition. The long axis alignment of these ellipsoids defines a fabric which may be primary in origin. However, elsewhere the alignment of secondary phases such as opaque minerals, epidote, chlorite, green biotite and sericite, is more compatible with a tectonic origin.

2.3 BARBY FORMATION

(i) Field character

Mafic flows of the Barby Formation are restricted to the eastern part of the AMT (map - Appendix I) where they have commonly been intruded by members, gabbro to syenite, of the Saffier Intrusive Suite. Thickness estimates do not exceed several hundred metres and are uncertain as a result of disruptive intrusive activity. While minor stratified tuffites are found near the base of these mafic lavas at Gorrasis Mountain, evidence for intercalated sediments and/or rhyolitic volcanic activity is generally lacking. The nature and mineralogy of the best exposed mafic flows sug-

gest their correlation with the Barby Formation “basaltic andesite member” (after Watters, 1974, p. 34).

(ii) *Petrography*

Petrographic similarity to the Barby Formation “basaltic andesite member” (as described by Watters, 1974, p. 34-35) precludes any detailed discussion here. In summary, phenocrysts constitute approximately 8% of the rock and are made up predominantly of clinopyroxene and plagioclase in a pilotaxitic to trachytic groundmass. Zoisite, rather than epidote, is widespread and forms patchy aggregates together with biotite and opaque minerals. The unusual yellow-brown colour and subhedral form of biotite appears to be the result of hydrothermal alteration related to syenite intrusion. Strain-related features include occasional granoblastic polygonal intergrowths of K-feldspar and quartz which form rims to phenocrysts, particularly within pressure shadows. Lensoid zones which consist of quartz \pm zoisite may represent original amygdaloids, although these zones also exhibit an “interstitial”, or secondary, appearance.

2.4 HAISIB INTRUSIVE SUITE (HIS)

(i) *Field character*

Plutons which make up the Haisib Intrusive Suite (HIS) range in composition from quartz monzonite to quartz syenite, with the possible inclusion of several bodies of more granodioritic to monzogranitic affinity. The distribution of the suite indicates a close spatial association with the HFF. Compositional differences between the plutons associated with the different volcanic “localities” or centres are not systematic on a regional scale and do not, therefore, reflect any batholithic zonation.

The area underlain by the HIS is only about 15 km² in total, but is clearly confined to structural weaknesses within, or at the margins of, northwest-trending troughs which also host the HFF and, in part, the Urusib Formation. Relative proportions of the major rock types within the HIS are difficult to estimate due to only slight variations in field appearance. However, it is clear that while quartz monzonite is the dominant rock type at the northern and central localities, granodiorite and monzogranite characterise the southern locality.

Usually grey to green in colour, granitoids of the HIS typically contain an abundance of xenoliths which have both subangular and diffuse outlines (Plate C.5c). The partial assimilation of these xenoliths, although locally quite common, is not usually the cause of the blotchy appearance of the granitoids. This hybrid character also occurs where xenoliths are uncorroded in appearance, a clear indication that the heterogeneous nature was derived prior to emplacement. While a large proportion of these xenoliths have been derived from the volcanics of the HFF, many granite and amphibolite xenoliths can be related to early-stage crust in the AMT.

Shearing has been widespread in the HIS and large lateral displacements can sometimes be inferred. This is well illustrated at the southern locality by the truncation of several mafic dykes at the sheared boundary between monzogranite of the HIS and adjacent sediments of the Urusib Formation

(map - Appendix I). In the southern part of Awasib Mountain, foliated quartz monzonite has been intruded by relatively undeformed Awasib Granite.

The HIS appears to occupy a similar stratigraphic position to gabbroic and syenitic rocks of the Saffier Intrusive Suite, and a tentative correlation of volcanics of the HFF with the Barby Formation would certainly support this. However, the distinctive appearance and composition of granitoids of the HIS advise against any premature correlation of this suite with the Saffier Intrusive Suite.

(ii) *Petrography*

The main petrographic features of the HIS are summarised in Table C.3.

Despite the widespread occurrence of strain-related features such as fractures, bent twin lamellae and undulose extinction, the development of a moderate foliation is relatively rare. However, in the proximity of shear zones there is a significant change in the nature and composition of the average quartz monzonite. The major features typical of such sheared rocks are as follows:

- (a) Albitisation is often intense and may result in the complete replacement of K -feldspar.
- (b) Feldspars constitute porphyroclasts in a granulated, recrystallised and silicified “groundmass”.
- (c) Quartz is completely recrystallised to form small subgrains and skeletal patches which are typically elongate, highly strained, and intergrown to form trails or “ribbons”.
- (d) A strong foliation is primarily defined by the alignment and intergrowth of both biotite laths and elongate quartz and feldspar crystals.

2.5 SAFFIER INTRUSIVE SUITE (SIS)

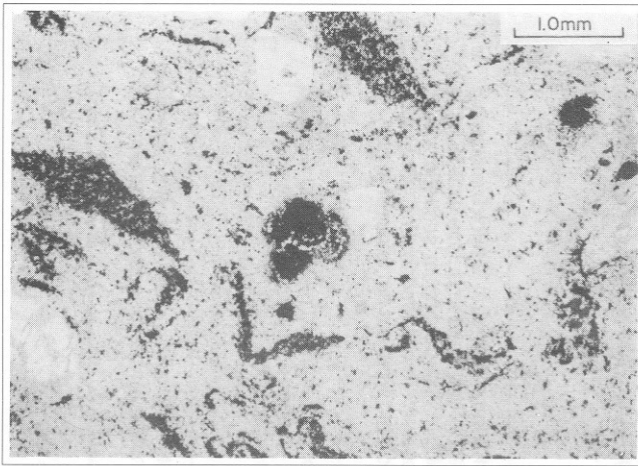
(i) *Field character*

Mafic to intermediate plutonic rocks which belong to the Saffier Intrusive Suite (SIS) have previously been mapped as “Barby Formation intrusive units” and “Spes Bona Syenite” (Watters, 1974). The latter syenite was subsequently included in the Barby Formation by Watters (1982) due to compositional and isotopic similarities between these two rock units. However, not only is the incorporation of intrusive rocks in a formation contrary to the guidelines of SACS (1980, p. 1-5), but the geographic locality of greatest abundance of these plutonic rocks is the farm Saffier. Accordingly, it is proposed that plutonic rocks previously regarded as “Barby Formation” and “Spes Bona Syenite” now be incorporated into the “Saffier Intrusive Suite”.

Comprehensive descriptions of intrusive units in this suite have been presented by Watters (1974, p. 49-57) and will not be repeated here. Within the AMT, these units can be grouped into two broad series:

- (a) Gabbro-monzogabbro series
- (b) Monzonite-syenite series

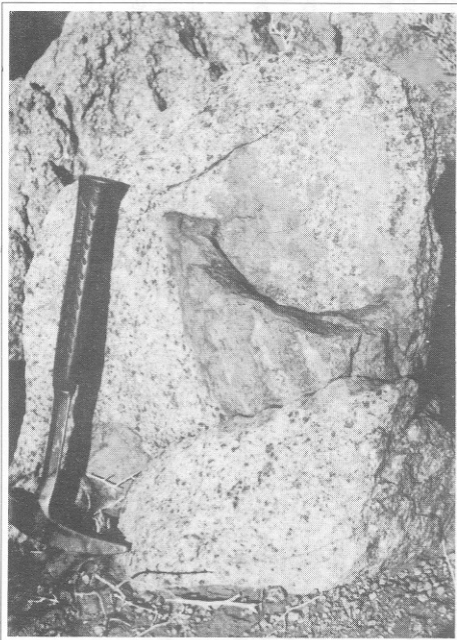
The peripheral arrangement of “monzonites” relative to a central body of syenite, as noted by Watters (1974, p. 54), is largely substantiated by this study. However, it should be stressed that the gradational nature of contacts between the various textural and mineralogical types is indicative of a



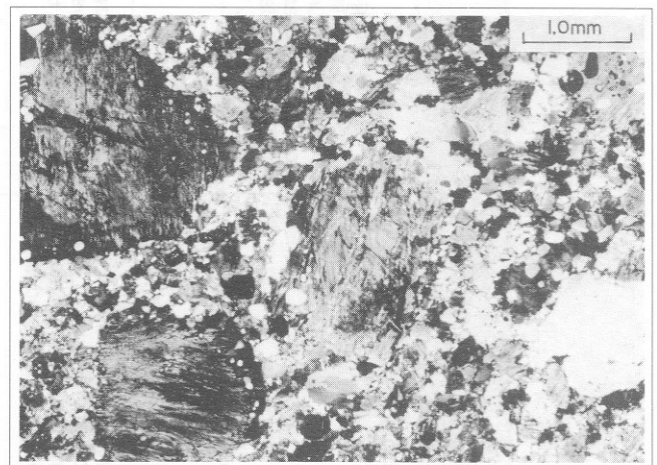
C.5a: HFF hybrid ash-flow tuff (BH 701) - northern locality. PPL. Flattened and contorted lithic/pumice fragments (cognate basaltic andesite?) set in a devitrified rhyolitic groundmass with the phenocryst assemblage quartz, K-feldspar, plagioclase and hornblende.



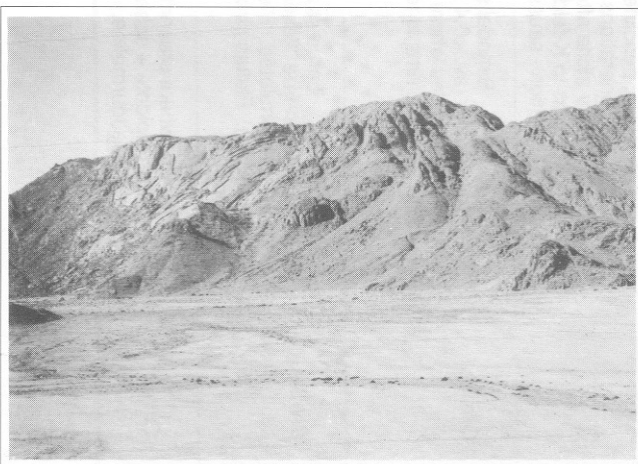
C.5b: HFF rhyolite (BH 186) - central locality shear zone. PPL. Segregation of quartz- and mica-rich layers in folded blastomylonite. Folds form part of the D₅ deformational event.



C.5c: Xenoliths of HFF andesite in quartz monzonite of the Haisib Intrusive Suite. The xenoliths show irregular and diffuse margins due to partial assimilation by the quartz monzonite. 6 km southeast of Haiber Hill.



C.5d: Awasis Granite - microgranite porphyry (BH 678). XPL. Phenocrysts of perthitic K-feldspar and quartz set in a recrystallised groundmass consisting predominantly of the same phases. Note blebs of quartz in later growth rims around K-feldspar.



C.5e: View eastwards of Awasis Mountain (850 m above the plain) showing the huge “whalebacks” typical of the Chowachasib Granite Suite. Coarse-grained granite of the latter has intruded the more fractured outcrop of Awasis Granite.



C.5f: Xenoliths of both early- and late-stage crust in coarse-grained syenogranite of the Chowachasib Granite Suite. The major country-rock types visible here are cross-bedded lithic arenite of the Urusib Formation (top left below hammer) and orthoamphibolites of the Kairab Complex (dark blocks). 3 km southwest of Chowachasib Mountain beacon (2063 m).

TABLE C.3: Petrography of the Haisib Intrusive Suite (HIS) and Awasis Granite.

	HAISIB INTRUSIVE SUITE	AWASIB GRANITE
TEXTURE	Medium- to coarse-grained, inequigranular to hypidiomorphic granular. Widespread strain but foliation only near shear zones: protomylonitic to mylonitic.	3 types: a) Fine-grained allotropic seriate, rare fluidal structure. b) Very fine-grained porphyritic (phenocrysts $\geq 50\%$). c) Medium-grained hypidiomorphic granular. Granophytic occasionally in b) and c). Rapakivi in some porphyries. Where present, deformational textures correspond to "Nubib granite and gneiss" (Watters, 1974, p. 64-67).
MINERALOGY		
K-feldspar	42% (30-65%). Av. size 3.5 mm, max. 20.0 mm. Anhedral to subhedral. String and bead perthite. Large poikilocrysts and commonly twinned (Carlsbad, subtle microcline). Replacement by secondary microcline and albite. Differs from plagioclase in occasionally megacrystic and less altered nature. Marginal fractures and quartz intergrowths.	(50-60%). Av. size 2.0 mm, max. 8.0 mm. Anhedral to subhedral. String and patch mesoperthite. Rapakivi in porphyries. Carlsbad and microcline twinning. Quartz blebs in margins.
Plagioclase	27% (15-45%). Av. size 2.1 mm, max. 7.0 mm. Subhedral; widespread twinning (albite, pericline, Carlsbad). Strong normal zoning (andesine to oligoclase). 3 generations: inclusions in K-feldspar, exsolved in K-feldspar, and secondary albite after K-feldspar and earlier plagioclase. Albite and myrmekite rims to K-feldspar. Fracturing and recrystallisation (subgrains). Severe alteration - saussuritisation and biotite + sphene + opaques.	<10% (max. 20%). Size generally <2.0 mm. Subhedral, euhedral inclusions in K-feldspar. Albite twinning (<Ans). Widespread saussuritisation, but secondary albite is less altered.
Quartz	13% (5-30%). Bimodal size: porphyroclasts (av. 1.0 mm, max. 2.0 mm) and subgrains (av. <0.4 mm). Fractured and strained. Granoblastic polygonal aggregates where recrystallised. Strain-free aggregates occur as fracture fillings, rims to feldspar and quartz (mortar texture) and interstitially.	(25-35%). Av. size 2.0 mm, max. 4.5 mm. Anhedral in hypidiomorphic type to subhedral in porphyritic type. Widespread undulose extinction, but mortar texture rare. Patches of blebs in feldspar appear secondary in general, but may represent inclusions where confined to rims. Granophytic intergrowths interstitial in hypidiomorphic type, but rim feldspar in porphyritic type.
Biotite	14% (5-25%). Large strained laths (av. size 2.5 mm, max. 8.0 mm) and smaller strain-free "flakes" (av. size 0.2 mm). Large laths typically poikilitic and bent/crenulated. Pleochroic light yellow to green or brownish green (chloritised). Flakes strongly aligned and intergrown to form fabric in shear zones.	<5%. Where present, biotite is strongly chloritised/oxidised and replaced by aggregates of chlorite + epidote + sphene + opaques. Occasional poikiloblasts form intergrowths with muscovite.
Other	Actinolite, where present, is associated with the assemblage biotite + chlorite + epidote + sphene + opaques. Accessory apatite, zircon and rare pink to blue tourmaline.	Poikilitic green hornblende - possibly xenocrystic. Alteration of opaques to sphene suggest original titanomagnetite. Accessory apatite and zircon.

comagmatic origin. The “link” between the monzonite-syenite and gabbro-monzogabbro series may be provided by a dyke of monzonite porphyry in monzogabbro on State Land adjacent to the farm Gorrasis. This porphyry resembles a much coarser-grained variety of the “large-feldspar trachyandesite” member of the Barby Formation.

Although widely distributed, members of the SIS are primarily concentrated in the eastern part of the AMT. A notable exception to this pattern is a layered mafic intrusion situated to the southwest of Awasis Mountain within the Namib sand sea (map - Appendix I). The association of gabbro-norite with troctolite in this intrusion is unusual for the AMT, but has been recorded amongst the so-called “black bodies” of the NMC. The nearest of these mafic bodies is the Konip Mafic Complex (after McDaid, 1978) which is situated approximately 60 km to the south. Considerable uncertainty, therefore, surrounds the stratigraphic position of this layered intrusion. Significantly, however, there appears to be an overlap in age between the SIS (inferred age range between 957 and 1190 Ma; Section C.5) and the NMC noritoids (1017± 110 Ma after Stumpfl *et al.*, 1976).

Cumulate layering is not uncommon in members of the SIS and is typically found in small layered intrusions, e.g. plutons on the farms Wolwedans and Springbokvlakte, and also on State Land adjacent to the farm Gorrasis. Nevertheless, massive textures are widespread, particularly in the coarser-grained syenites. Evidence for chilling against the country rock is rare, although fine-grained porphyritic textures are more typical of the margins than the interiors of plutons.

Awasis Granite has intruded gabbro of the SIS at Awasis Mountain, while various members of this suite have intruded sediments of the Urusib Formation on State Land adjacent to the farm Gorrasis as well as flows of the Barby Formation at Gorrasis Mountain. The only occurrence of picrite was found as a raft in Chowachasib Granite situated on the northern side of Gorrasis Mountain.

Basaltic andesite of the Barby Formation shows evidence of potassic metasomatism and reconstitution where it has been intruded by syenite at Gorrasis Mountain. More commonly, however, contact metamorphic effects are restricted to slight recrystallisation and the growth of low-grade mineral assemblages. Syenite has itself been subjected to severe shearing at its northern contact with the Chowachasib Granite at Gorrasis Mountain.

(ii) Petrography

While detailed petrographic descriptions of individual rock types are given in Watters (1974, p. 50-56), the following descriptions are more general and comparative in nature.

(a) Gabbro-monzogabbro series

This series includes gabbros (sometimes anorthositic), gabbro-norites, olivine gabbro-norites and norites; essential constituents being plagioclase and clinopyroxene (mainly augite).

Plagioclase makes up 55-80% of the rock (average 64%) and is not uncommonly of cumulus origin. While twinning, zonation and habit of plagioclase differ little relative to the

type locality, individual crystals tend to be larger (average 2.5 mm, maximum 16 mm), more rarely euhedral (generally subhedral, sometimes with highly irregular margins) and may show a greater degree of deformation (undulose extinction, severely bent twin lamellae, fracturing and recrystallisation to form subgrains, patchy exsolution of quartz blebs). Similar features appear to be restricted to the monzonite-syenite series within the type locality.

Clinopyroxene, predominantly augite, is present in amounts of 4 to 40% (average 19%) and is of similar form (anhedral to subhedral) and size to the type locality. However, poikilitic “intercumulus” plates may reach much larger dimensions (up to 20 mm) in the anorthositic gabbros and twinning (both simple and polysynthetic) is not uncommon. Alteration to actinolite, while rarely advanced, is usually present to some degree along the crystal margins where it may be associated with greenish-brown biotite. In some cases, however, clinopyroxene has been completely replaced by aggregates of the assemblage actinolite + chlorite + opaque minerals + epidote ± carbonate ± biotite ± hornblende which lend the rock a spotted appearance in hand specimen.

Orthopyroxene (pleochroic pink hypersthene) makes up 0-25% of the rock and forms crystals of similar habit and size to augite. While hypersthene may form large poikilitic crystals (up to 14 mm in size), it occurs most commonly as rims to olivine crystals or in clusters with augite. Strain-related features in hypersthene crystals include fractures and bent ex solution lamellae, while the nature and composition of alteration products are similar to those of augite.

Olivine, where present, constitutes up to 9% of the rock and may form fairly large crystals (up to 4.5 mm). Olivine is characterised by an anhedral form, opaque mineral-filled fractures and a clear colour. With the exception of occasional plagioclase inclusions, olivine appears to be early-formed. Alteration to serpentine is rarely prominent.

K-feldspar, although commonly absent or present only in accessory amounts, may constitute as much as 20% of the monzogabbros. The K-feldspar is usually perthitic microcline (fractured and slightly cloudy) and has an interstitial or intergranular appearance. In addition to some replacement by myrmekite and perthite at its margins, K-feldspar (perthite) has itself replaced plagioclase in part.

Biotite (< 5% of the rock) usually exhibits a distinctive red-brown pleochroism, more rarely greenish brown, and occurs as both primary intergranular or interstitial “flakes” (average size 0.5 mm) and as part of secondary intergrowths after clinopyroxene. Opaque minerals (< 4%) occur either in association with biotite or as small granules in many of the ferromagnesian phases. Both biotite and opaque minerals are more widespread in monzogabbros than gabbros.

Quartz, where present, rarely exceeds 2% of the rock, is typically interstitial and occasionally forms leucocratic zones parallel to the primary layering.

Accessory phases include apatite (< 2% of the rock) and rare Zircon.

(b) Monzonite-syenite series

Monzonite corresponds to the “poikilitic medium-grained porphyritic” type described by Watters (1974, p. 56), hav-

ing roughly equal proportions of plagioclase and K-feldspar (about 70% total feldspar). Both clinopyroxene- and plagioclase-phyric types are present, with olivine constituting a more rare phenocryst phase. In general the texture is finer-grained than that observed in the type area, but this may be due, in part, to a more marginal situation. The effect of peripheral chilling appears to have resulted in a very fine-grained granular groundmass in outcrops within the central part of the farm Gorrasis.

Coarse-grained grey syenite differs little from type locality description for the "Spes Bona Syenite" (Watters, 1974, p. 55-56). However, towards the margins of the main syenite body, i.e. eastern Gorrasis and northwestern Aandster, the syenite is finer-grained, sometimes porphyritic, and may take on a "monzosyenitic" character. The presence of coarse-grained quartz syenite xenoliths in finer-grained syenite indicates a complex marginal zone.

Fine-grained syenite contains a slightly higher proportion of plagioclase than the coarse-grained type, but otherwise both the nature and amount of the ferromagnesian phases are remarkably similar. The texture varies from seriate to porphyritic (up to 30% K-feldspar phenocrysts), the groundmass typically containing subparallel laths of both K-feldspar and plagioclase (average size 1.0 mm). Perthite appears to rim and overprint well-twinned plagioclase laths. Aggregates of the assemblage clinopyroxene + biotite ± apatite ± opaque minerals are fairly common and in the case of clinopyroxene (diopsidic augite), the aggregates may represent recrystallisation into subgrains, although poikilitic textures are also common. The distinctive red-brown pleochroism and irregular form of biotite are much like biotite in the monzogabbro.

Within the border facies of the syenite, a group of fine-grained (average grain size 0.7 mm) olivine-bearing "monzosyenites" appears to be characterised by a relatively high plagioclase/K-feldspar ratio (about 0.2). The presence of olivine in amounts exceeding 2% (up to 8%) may be diagnostic of this group, but subsequent replacement of the olivine renders this an unreliable criterion. Biotite may constitute in excess of 5% of the rock. The texture is seriate to porphyritic, with phenocrysts comprising plagioclase, poikilitic clinopyroxene (diopsidic augite) and K-feldspar. Olivine is not uncommonly rimmed by the assemblage clinopyroxene ± red-brown biotite ± opaque minerals ± apatite. This assemblage may form aggregates which have a granoblastic polygonal form and often completely replace olivine. Together with similar granular textures in K-feldspar, these aggregates appear to indicate extensive recrystallisation in response to strain. Within very fine-grained members (average grain size 0.3 mm), sheaf-like granophyric intergrowths resemble devitrification textures, but are here attributed to recrystallisation.

2.6 BUSHMAN HILL QUARTZ DIORITE

(i) Field character

Although widely distributed, quartz diorite plutons are primarily situated in the northeastern part of the AMT in the vicinity of the 1690 m high Bushman Hill. The term "quartz diorite", as used here, is slightly misleading, since

more tonalitic and dioritic rocks have also been included. Stratigraphically these plutons can usually only be assigned a "post-basement, pre-Chowachasib Granite" status. However, a single pluton of quartz diorite near to Numabis (map - Appendix I) contains volcanic xenoliths which belong to the HFF and has itself been intruded by the Awasis Granite. A stratigraphic equivalence of the Bushman Hill Quartz Diorite to the SIS seems likely, despite the petrographic similarity to some of the Guperas Formation "basic intrusives" described by Watters (1974, p. 71-73).

The appearance of the quartz diorite is massive and even-grained, although large amphiboles may be associated with later veins and apophyses of both Awasis and Chowachasib Granite. Where such granite intrusion has been intense, the diorite tends to take on a hybrid and/or brecciated appearance.

(ii) Petrography

The texture is fine- to medium-grained (average grain size 1.0 mm) and not uncommonly intergranular. Plagioclase (average size 1.5 mm, maximum size 4.0 mm) constitutes 50-60% of the rock (average 57%). Widespread zoning (normal to oscillatory with cores of An_{45-50}) and twinning (albite mainly) of plagioclase laths are usually preserved despite often pervasive alteration (especially in the cores). In addition, plagioclase crystals have retained a subhedral to euhedral habit and may form a loosely-packed network.

K-feldspar, where present (< 7%), occurs predominantly as small interstitial grains of fractured microcline micropertite (average size 0.2 mm), but also forms granophyric intergrowths with quartz. K-feldspar may either rim large plagioclase grains or completely enclose smaller ones, although poikilocrysts are rare.

Quartz is present as both large, strained, anhedral grains (average size 1.5 mm, maximum size 5.0 mm) and smaller, more strain-free, interstitial grains (average size 0.2 mm). These grains and aggregates together make up 20-30% of the quartz diorites (*sensu stricto*), but < 7% of the diorites. Exsolution blebs of quartz in plagioclase or K-feldspar are rare.

Ferromagnesian minerals, which constitute up to 30% of the rock, often show significant alteration and comprise amphibole (hornblende and/or hornblende-actinolite intergrowths), biotite and more rarely clinopyroxene. Brown hornblende, where present, occurs variously as interstitial crystals, skeletal and ragged poikilocrysts (up to 7 mm in size) and prismatic or euhedral crystals. More typically, however, hornblende pleochroism is from light brownish-green to green. The appearance of hornblende suggests a late magmatic origin with subsequent alteration to, or undergrowth with, patchy light green or blue-green actinolite. Aggregates of alteration products associated with hornblende are typically made up of the assemblage actinolite ± carbonate ± epidote ± sphene ± chlorite. Inclusions in the hornblende are primarily quartz, plagioclase and opaque minerals.

Biotite occurs as both subhedral "flakes" (average size 0.2 mm) and much larger xenoblasts (average size 1.4 mm, maximum size 3.0 mm) which are strongly pleochroic from

light brown to dark brown but usually display tints of green. Biotite makes up 8-15% of the rock (average 11%) and, although always present, it may be strongly chloritised (often pseudomorphed by the assemblage chlorite \pm epidote \pm opaque minerals \pm sphene). Secondary actinolite occasionally forms intimate intergrowths with biotite, sometimes cross-cutting, but is usually subordinate. Large xenoblasts of biotite, where present, typically display a poikiloblastic, and occasionally kink-banded, nature. Aggregates of biotite “flakes” are widespread and are distinguished with some difficulty from biotite schist xenoliths.

Clinopyroxene, mostly augite, forms anhedral and twinned phenocrysts (up to 15% of the rock) which are commonly glomerocrysts (aggregates up to 4 mm in size, individuals up to 2 mm). These phenocrysts typically show alteration along their margins to the assemblage actinolite + biotite + chlorite + opaque minerals. “Groundmass” augite is widely pseudomorphed by actinolite.

Associated with the mafic minerals are a number of accessory phases, viz. sphene, apatite, zircon, epidote and opaque minerals. These accessory minerals vary from anhedral and skeletal secondary phases to euhedral crystals and inclusions. Sphene forms secondary rims to opaque minerals, but also occurs as large (0.7 mm in size) subhedral crystals. Secondary opaque minerals, usually small (average size 0.2 mm, maximum size 0.5 mm) and cubic in form, may constitute as much as 5% of the rock.

2.7 AWASIB GRANITE

(i) Field character

The Awasisb Granite, like members of the HIS, is largely confined to the same northwest-trending troughs occupied by volcanics of the HFF (map - Appendix I). Furthermore, the Awasisb Granite closely resembles rhyolites (*sensu lato*) of the HFF in composition; a similar comparison has been drawn between plutonic rocks of the Haisib Intrusive Suite and intermediate volcanics of the HFF. The likelihood of this granite being subvolcanic in origin is further explored in Sections C.4 and C.5.

The Awasisb Granite underlies an area of approximately 55 km² with its major exposure in the rugged, 1752 m high Awasisb Mountain. The granite here is closely associated with rhyolites of the HFF and there is some difficulty in distinguishing between rhyolite porphyry plugs of the latter formation and microgranite porphyry of the Awasisb Granite. A similar relationship can be seen west of Piekniekkoppe, but in the southern most part of the AMT, outcrops of Awasisb Granite are volumetrically insignificant when compared with their “host” volcanics. By contrast, the 1327 m high Guinasib Mountain consists predominantly of Awasisb Granite, apparently with no associated volcanics.

The Awasisb Granite is reddish in colour and can most commonly be termed a “microgranite porphyry” (plate C.5d). However, there are several different textural varieties which may indicate different phases of intrusion and can usually be allocated to one of three categories presented in Table C.3.

While the Awasisb Granite shows evidence for having intruded both the Haisib and Saffier Intrusive Suites at Awa-

sib Mountain, it has itself been intruded at the same locality by coarse-grained Chowachasib Granite (Plate C.5e). In addition, volcanic xenoliths of the HFF are not uncommon in the Awasisb Granite. Furthermore, this granite has steeply tilted sediments of the Urusib Formation on the southwestern flank of Guinasib Mountain.

Intrusive contacts are characteristically sharp with scant evidence of chilling, although broad (metre scale) marginal zones of finer-grained nature were noted in the southwestern portion of Awasisb Mountain. The effect of intrusion has often been brittle, resulting in breccias at the contacts and utilisation of fractures in the country rock by apophyses of granite. Rounded xenoliths are rare in the proximity of intrusive contacts, although occasional streaking out of mafic xenoliths does occur. However, hybridisation as a result of such assimilation (as described by Von Brunn, 1967, p. 102-107, and Watters, 1974, p. 59-60) is a rare feature in the Awasisb Granite.

Apart from the mechanical effects of intrusion, the Awasisb Granite may be responsible for a limited degree of contact metamorphism. Evidence for this is restricted to the slightly more altered appearance of the HFF volcanics which are now situated adjacent to outcrops of the Awasisb Granite. These effects are, however, difficult to evaluate in the light of a more regional metamorphic imprint as well as the more pervasive influence of the higher temperature mafic granitoids of the Haisib Intrusive Suite.

Many of the granites incorporated in the “Awasisb Granite” correspond to rocks which have been described by Watters (1974, p. 64-67) as “Nubib granite and gneiss”. The latter group is, however, very broad in its coverage and appears to incorporate both pre- and post-Sinclair Sequence lithologies. Accordingly, the term “Awasisb Granite” is retained for a group of distinctive micro granite porphyries in the AMT.

A gneissic texture is rarely developed in the Awasisb Granite and there is not always an obvious spatial association between strain-related features and known shear zones. Granular “recrystallisation” textures are commonly restricted to the marginal portions of plutons and may, therefore, owe some of their appearance to chilling rather than deformation.

(ii) Petrography

The different textural varieties within the Awasisb Granite do not differ markedly in their mineralogy and have, therefore, been collectively described in Table C.3.

The following strain-related features are widespread in the Awasisb Granite, particularly in proximity to shear zones, but also on a more regional scale:

- (a) A predominance of clear perthite and strained quartz over cloudy orthoclase perthite and unstrained quartz.
- (b) Bent twin and ex solution lamellae in feldspars.
- (c) Fractures and marginal granulation in feldspars and quartz.
- (d) Mortar texture in quartz.
- (e) Strong zoning and undulatory extinction in feldspars.
- (f) Comminution of feldspars to form a seriate texture.
- (g) Protomylonitic textures illustrated by streaked-out quartz crystals and trails of granulated minerals.

(h) A leucocratic appearance possibly due to the replacement and removal of ferromagnesian minerals.

2.8 CHOW ACHASIB GRANITE SUITE (CGS)

(i) Field character

With the exception of mafic and felsic dykes, the Chowachasib Granite Suite, hereafter termed the "Chowachasib Granite" or CGS, constitutes the youngest phase of intrusive activity within the AMT. Since the total outcrop area does not exceed 120 km², individual bodies can usually be classed as "stocks" (after Bates and Jackson, 1980). The largest stock is about 55 km² in areal extent and forms the 2063 m high Chowachasib Mountain. However, it is conceivable that this stock links up below sand cover with a 28 km² outcrop at the 1690 m high Bushman Hill and a smaller outcrop of only 2 km² to the northwest (map - Appendix I). The projected form of this mass would be subcircular and underlie an area of approximately 450 km² in extent, thereby constituting a body of batholithic dimensions. Smaller outcrops of the Chowachasib Granite are situated in the eastern part of the AMT on the farms Gorrasis and Stellarine, as well as a more prominent mass of about 15 km² which forms the 1763 m high Satanskop Mountain. In the western part of the area, the largest body of granite has an areal extent of about 12 km² where it underlies a considerable part of the 1752 m high Awasib Mountain. The outcrop pattern indicates that individual plutons usually conform to a regional northwest trend.

The Chowachasib Granite, as described above, forms an integral part of many of the highest and most rugged mountains in the AMT. At a distance this granite can often be identified by huge "whale backs" which have formed through exfoliation (Plate C.5e). The texture of the granite is typically medium- to coarse-grained and hypidiomorphic granular, although coarsely porphyritic varieties are widespread in the northwestern part of Bushman Hill. While most plutons are reddish in colour, granites in the vicinity of Satanskop exhibit a whitish-grey colour which appears to indicate a less potassic nature. These differences are clearly primary, since there is no evidence for hybridisation by assimilation of basic material as described by Von Brunn (1967, p. 102-107) for the Rooikam Granite.

Xenoliths are, in general, not common in the Chowachasib Granite except for the southwestern part of Chowachasib Mountain where the granite is characterised by a xenolith-choked zone adjacent to outcrops of the Urusib Formation and Kairab Complex (Plate C.5f). The effects of intrusion by the Chowachasib Granite are mostly restricted to tilting of the country-rock strata, although there are some spectacular examples of elevated rafts, e.g. sediments of the Urusib Formation in the southern part of Chowachasib Mountain, and mafic bodies of the SIS to the southeast of Satanskop.

Contacts with the country rock are mostly sharp, with only occasional evidence of chilling and even more rarely the assimilation of sedimentary xenoliths. As for the Awasib Granite, the effect of any contact metamorphism is usually difficult to recognise. However, sediments adjacent to granite in the southwestern portion of Chowachasib Moun-

tain have undergone deformation, recrystallisation and even occasional assimilation. Since this is by far the largest individual granite mass in the AMT, it can be assumed that sufficient heat was retained during emplacement for the observed transformation of the country rock. The relatively warm country rock was further able to accommodate a greater number of granite apophyses here than elsewhere.

(ii) Petrography

Mineral chemistry (Part C.3) suggests that the Chowachasib Granite Suite comprises at least three distinct plutons. Petrographically, however, this distinction is not easily made and it is therefore best to describe these members collectively. Relative to the Awasib Granite, this granite suite is characterised by its much coarser-grained nature (average grain size of 4.0 mm) and widespread hypidiomorphic granular texture.

K-feldspar, both microcline and orthoclase mesoperthite, constitutes 30-60% of the rock (average 44%) and is commonly of anhedral or subhedral form. The latter form predominates in the more porphyritic granites, where large K-feldspar phenocrysts may reach 26.0 mm in length. Carlsbad twinning and strong zoning are not unusual in K-feldspar and a poikilitic texture is occasionally developed. Perthite is of the patch and string type and cloudy in appearance, exsolved albite apparently in optical continuity with less cloudy, secondary albite rims. More rarely, secondary albite has completely pseudomorphed original K-feldspar.

Plagioclase makes up 4-30% of the rock (average 23%) and consists of subhedral laths (up to 5.0 mm in length and An₁₈ in composition) and patchy replacement rims to both K-feldspar and more calcic plagioclase. Saussuritisation is usually more advanced in the primary plagioclase, but has rarely obscured the polysynthetic twinning. Normal zoning and bent twin lamellae are fairly common features near Satanskop.

Quartz typically forms large interstitial aggregates (commonly > 10.0 mm in size) or rounded crystals (up to 9.0 mm in size) which together constitute 28% of the rock on average. Quartz invariably exhibits undulose extinction, but may form incipient mortar texture where it has undergone greater strain. Small quartz blebs are fairly common in the marginal zones of K-feldspar and in the groundmass of porphyritic granite. Quartz also forms part of interstitial granophyric intergrowths with K-feldspar, but these intergrowths are not as widespread as in the Awasib Granite.

Biotite is usually present and occurs as both intergrown flakes and larger brown to green-brown laths (up to 3.0 mm in size). Kink bands and undulose extinction constitute occasional features of the biotite, while chloritisation is usually present to some degree. Biotite is typically interstitial and may be poikilitic in appearance. Small flakes of biotite are commonly associated with mafic aggregates of the assemblage opaque minerals + sphene + epidote ± apatite ± zircon.

Hornblende only predominates over biotite in K-feldspar-rich granite at Bushman Hill and in the northern part of the farm Gorrasis. Together these two mafic minerals constitute an average of 5% of the rock and are not uncommonly inter-

grown in mafic aggregates. Hornblende is green to green-brown in colour (sometimes with reddish-brown cores) and forms both prismatic crystals and poikilitic plates up to 3.5 mm in size. Incipient alteration of hornblende to chlorite is a widespread feature.

Clinopyroxene, probably augite, forms subhedral to rounded crystals (average size 0.3 mm) in K-feldspar granite on the farm Gorrasis, but its occurrence is rare and may represent a xenocryst phase. Clinopyroxene, which usually occurs in clusters, is typically rimmed, and partly replaced, by blue-green hornblende.

Accessory phases include sphene, allanite, apatite and zircon.

Marginal portions of the Chowachasib Granite tend to be relatively fine-grained (average grain size 1.2 mm) or coarsely porphyritic. Strain-related features also appear to be more widespread in these marginal zones. Such features include undulose extinction, fractures, bent twin lamellae, kink bands, granulation and disaggregation of grain margins, and trails of incipient comminution.

2.9 MAFIC AND FELSIC DYKES

The majority of dykes in the AMT resemble their counterparts in the Sinclair Sequence type locality with respect to both trend and composition. Both individual dykes and dyke swarms are strikingly bimodal in composition and detailed petrographic descriptions have been provided by Von Brunn (1967, p. 125-138) and Watters (1974, p. 73-75, p. 97-101). However, the latter author's correlation of the majority of both "basic" and "quartz porphyry" dykes with the "Guperas Formation" may be in need of revision if the "pre-dyke" Chowachasib Granite is younger than the Guperas Formation of the Sinclair Sequence.

Dyke swarms appear to have utilised a conjugate fracture system which may be related to major shear movement in the AMT (Hoal, 1985). Mafic and felsic dykes within the AMT can be accommodated by a four-fold division into basic, intermediate, acid and alkaline compositions.

(i) Basic dykes

(a) Basic dykes comprise a range of rock types, viz. gabbro, diorite, monzonite, dolerite, basalt and andesite.

(b) Dyke swarms follow two major trends, viz northeast to north-northeast and east to east-southeast. Where basic dykes intersect, the former trend is later.

(c) Deformation in the basic dykes is restricted to occasional shearing (D_5 ?) and later warping (D_7).

(d) The general lack of any metamorphic character, except in shear zones, suggests that these dykes formed late in the history of the AMT.

(e) Individual basic dykes can be traced for up to 9 km along strike and are usually vertical or steeply-dipping in attitude. The width of dykes is highly variable, but usually between 1 and 30 m.

(f) The east-southeast-trending swarm of dykes at Chowachasib Mountain is characterised by a more moderate dip to the northeast and common "swelling" along strike to form plug-like masses.

(g) While the finer-grained porphyritic basic dykes differ

little in appearance from their counterparts in the Sinclair, the medium-grained dykes (typically northeast to north-northeast-trending) bear a distinct resemblance to dykes within the Gannakouriep Suite to the south (Reid, pers. comm., 1986).

(ii) Intermediate dykes

(a) Dykes of intermediate composition are restricted to a few occurrences of quartz monzonite within the HFF and even more rare quartz microdiorites.

(b) While intermediate dykes do not occur in swarms, trends of individual dykes are most commonly north, north-east and east-southeast.

(c) Porphyritic textures are widespread in intermediate dykes, plagioclase being the most common phenocryst.

(d) Xenoliths and xenocrysts are particularly common in quartz microdiorite dykes.

(iii) Acid dykes

(a) Acid dykes comprise a variety of rock types, viz. rhyolite, micro granite, granite and granodiorite.

(b) Dyke swarms follow similar, but more variable, trends to the basic dykes, viz. north-northeast, east and northwest to north-northwest.

(c) Where acid dykes intersect basic dykes, they are usually younger.

(d) Evidence for deformation and metamorphism indicates that acid dykes, like the basic dykes, were emplaced late in the history of the AMT.

(e) Individual dykes may be traced for up to 12 km along strike and are usually steep in attitude. A swarm of flow-banded rhyolite dykes on the farm Aandster does, however, dip at an angle of 40° to the east. Dyke width is variable, but mostly between 1 and 20 m.

(f) "Swelling" of dykes along strike is a widespread feature, especially in the central part of the AMT.

(g) Porphyritic rhyolite sHIS are considerably more common than their mafic counterparts.

(h) Acid dykes in the AMT have been mapped in adjacent areas as "granite porphyry", "hybrid granophyre" and "quartz porphyry" (Von Brunn, 1967, p. 26-28; Watters, 1974, p. 97-101).

(iv) Alkaline dykes

A single east-southeast-trending dyke of porphyritic phonolite crops out to the west of Awasib Fountain where it has cut across several north-northeast-trending gabbro dykes. While this dyke may represent a much younger phase of intrusion (possibly Karoo?), it should be noted that the east-southeast trend is the same as that of the major basic dyke swarm at Chowachasib Mountain.

2.10 SUMMARY

2.10.1 Late-stage volcano-sedimentary successions

(i) The 2400 m thick sedimentary succession of the Urusib Formation forms the basal portion of the late-stage stratigraphy in the AMT and occupies a stratigraphic position similar to that of the Kunjas Formation in the Sin-

clair Sequence. Trough-hosted sediments are made up predominantly of immature and poorly-sorted clastic rocks that grade upwards into eruptive flows of the HFF and are characterised by sedimentary features typical of braided streamflow fans. While the latter are attributed to periods of uplift, associated lacustrine deposits (shale and siltstone) are thought to reflect more stable crustal conditions.

(ii) The Haiber Flats Formation (HFF), despite an estimated thickness of between 3000 and 7000 m, has a small outcrop area (< 80 km²) confined to three northwest-trending linear troughs termed the southern, central and northern localities. These localities, or volcanic centres, are characterised by predominantly bimodal volcanic successions (basaltic andesite:rhyolite \approx 1:3-1:4) but andesitic-rhyodacitic compositions are represented. Porphyritic and pyroclastic textures are widespread in the flows, particularly in the more felsic compositions. Minor deposits of stratified tuffite and volcanoclastics are associated with these flows.

(iii) Although subjected to the effects of four episodes of regional deformation and associated greenschist facies metamorphism, the HFF appears to have undergone early local tilting and possibly contact metamorphism as a result of the forceful intrusion of the HIS and Awasib Granite.

(iv) Evidence for the presence of volcanic centres at the different regional localities of the HFF includes the localised occurrence of coarse agglomerates (southern and northern localities), the presence of resurgent rhyolitic plugs/domes (northern locality), the subvolcanic nature of microgranite porphyry (central and northern localities), and the difficulty in correlating flow units between the different localities.

(v) Basaltic andesite flows of the HFF are typically porphyritic (5-20% phenocrysts), the phenocryst assemblage (where preserved) usually comprising plagioclase, clinopyroxene (\pm olivine) and possibly titanomagnetite in a pilotaxitic to trachytic groundmass. Plagioclase is the dominant phenocryst in southern locality flows, but is subordinate to clinopyroxene in northern locality flows. While amygdalae are only widespread in the southern locality, pyroclastic textures (including mantled bedding) appear to be restricted to the northern locality basaltic andesites. Andesite and dacite flows are unique to the central locality, where mylonitisation has transformed these flows into greenschists. Only plagioclase forms an easily recognisable phenocryst, but biotite, clinopyroxene and titanomagnetite may be present in addition.

(vi) Rhyodacites are rare in the HFF and occur as both globular ignimbrite (southern locality) and porphyritic flows in which the phenocrysts are plagioclase, K-feldspar, quartz and clinopyroxene. Rhyolite flows are often highly porphyritic (10-35% phenocrysts of K-feldspar, quartz and plagioclase) and comprise both welded crystal-lithic tuffs (10-50% lithic fragments) and flow-banded lavas (10-20% phenocrysts). Thick ash-flow tuff horizons appear to represent single cooling units made up of several independent flows. Rhyolitic air-fall deposits are rare and were only observed at the southern and northern localities. While the presence of fiammé is not unusual in the rhyolites, any evidence of vitro clastic texture has been destroyed by devitrification, recrystallisation and silicification.

(vii) Mixed pyroclastic eruptions (rhyolite-basaltic an-

desite) and composite dykes, though not widespread, suggest that magma mingling has occurred in the HFF.

(viii) Basaltic andesites of the Barby Formation crop out in the eastern part of the AMT where they have been intruded by gabbros and syenites of the Saffier Intrusive Suite (SIS). These flows are porphyritic (8% phenocrysts of plagioclase and clinopyroxene) and characterised by a pilotaxitic to trachytic groundmass.

2.10.2 Late-stage intrusive suites

(i) The Haisib Intrusive Suite (HIS) shows a close spatial association with the HFF and is typically confined to the sheared margins of the troughs that host the latter. The quartz monzonite to quartz syenite compositions of the HIS are intermediate relative to the basaltic andesite-rhyolite end members of the HFF. The abundance of xenoliths in the HIS can be related to both the HFF and early-stage crust. The HIS is older than the Awasib Granite and occupies a similar stratigraphic position to that of the SIS.

(ii) The SIS incorporates Watters' (1974) previously mapped "Barby Formation intrusive units" and "Spes Bona Syenite". This suite comprises a gabbro-monzogabbro and monzonite-syenite series which are typically confined to the eastern part of the AMT. A layered gabbro-norite-troctolite body in the western part of the AMT may show an affinity with the Konip Mafic Complex (McDaid, 1978) or the NMC noritoids. Cumulate textures are most common in the layered rocks, while marginal portions of the plutons are typically finer grained and porphyritic.

(iii) The Bushman Hill Quartz Diorite comprises diorites, quartz diorites and tonalities of uncertain stratigraphic position, but which bear a compositional similarity to the SIS.

(iv) The Awasib Granite, like the HIS, is largely confined to the same troughs occupied by the HFF. This granite is also compositionally similar to the rhyolites of the HFF and its close spatial association with the latter and similarity in texture to rhyolite porphyry suggest a subvolcanic relationship. While clearly younger than the HIS and SIS, the Awasib Granite has been intruded by the Chowachasib Granite. Although intrusive contacts are typically sharp, recrystallisation textures at the margins may be the result of chilling.

(v) The Chowachasib Granite Suite is made up of several exposed stocks, some of which may be linked below the surface to form a single mass of batholithic dimensions (450 km²) in the northern part of the AMT. Typically medium-to coarse-grained, this monzo- to K-feldspar granite constitutes the latest phase of pre-dyke magmatism. While generally devoid of xenoliths, the Chowachasib Granite does carry large rafts of sediment of the Urusib Formation. Mafic phases are typically biotite \pm hornblende \pm rare clinopyroxene.

(vi) Bimodal dyke swarms appear to have utilised a conjugate fracture system (essentially northeast and east-southeast-trending) related to regional shear movement. Compositionally these dykes are basic, intermediate, acid and alkaline. Metamorphic effects are minimal, while deformation is restricted to occasional shearing and late phase

warping. Swelling of basic and acid dykes along strike is a common feature. A single east-southeast-trending phonolite dyke may represent a much younger phase of intrusion, possibly of Karoo age.

3. MINERAL CHEMISTRY AND METAMORPHISM

3.1 INTRODUCTION

3.1.1 General

Mineral assemblages were selected from a number of lithologic units in the late-stage crust of the AMT for EMP analysis. Analyses of both primary and secondary phases have provided new insight with respect to the igneous and metamorphic evolution of Sinclair-type rocks in the AMT. The following sections describe the mineral chemistries of the common phases encountered in the selected lithologic units. All EMP analyses are tabulated on the accompanying Microfiche card and discussed in Appendix III.

Although this study aims primarily at determining igneous compositions, metamorphic effects are widespread and must be investigated in order to assess the degree of alteration prior to geochemical study. Furthermore, metamorphic phase compositions enable determination of the grade of metamorphism and allow comparison of late-stage crust with early-stage crust in the AMT and with the type area of the Sinclair Sequence.

3.1.2 Haiber Flats Formation (HFF) and Barby Formation

(i) Basaltic andesite-andesite

In contrast to the more acidic flows, andesites (*sensu lato*) of the HFF are better characterised by relict igneous phases due to less pervasive secondary effects. A single sample of basaltic andesite from the Barby Formation on the farm Gorrasis has been included for comparative purposes. The mineral assemblage in these mafic rocks varies from an essentially primary one to a wholly metamorphic assemblage typical of the greenschist facies. The variation in mineral parageneses is illustrated on an ACF diagram in Fig. CA.

(ii) Rhyolite-rhyodacite

Rhyolitic flows of the HFF have been studied in very little analytical detail compared with their andesitic counterparts. However, mutual interbedding and intercalation suggest that conclusions arrived at for the latter should, although incomplete, hold true for the entire volcanic pile. EMP analytical work on the rhyolites was largely carried out to test petrographic observations and is considered under "Metamorphism of the HFF" (Section 3.9).

3.1.3 Late-stage ("Sinclair-type") granitoids

The major intrusive suites which post-date the extrusion of the HFF volcanics may be broadly grouped into compo-

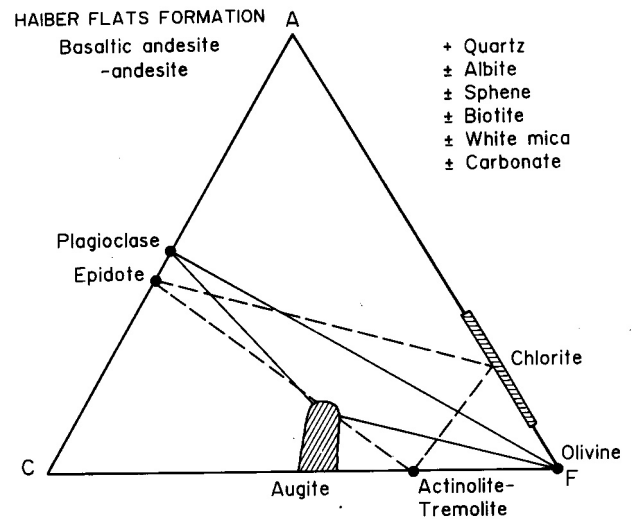


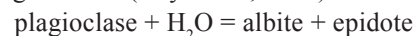
Fig. C.4: ACF diagram illustrating primary igneous (solid lines) and metamorphic (dashed lines) mineral assemblages in "andesites" of the Haiber Flats Formation.

sitional categories of mafic (Saffier Intrusive Suite), intermediate (Haisib Intrusive Suite) and felsic (Awasi Granite and Chowachasib Granite Suite) affinities. The type locality of the Saffier Intrusive Suite is not located in the AMT and this suite, although well represented in the eastern part of the study area, will not be discussed here.

3.2 FELDSPAR

3.2.1 HFF and Barby Formation

Plagioclase phenocrysts vary in composition from labradorite or andesine in weakly metamorphosed flows of the northern and southern localities to albite or oligoclase in their more strongly metamorphosed equivalents at the southern and central localities (Fig. C.5a). While an apparent paucity of compositions in the range An_3 - An_{38} may reflect the existence of the peristerite gap, no statistically significant study has been made. Much of the calcic plagioclase is primary, the more sodic compositions probably representing varying degrees of response to metamorphism, possibly as a function of associated water fugacity. Albite is wholly metamorphic in origin and derived from the following reaction (Miyashiro, 1973):



The general absence of exsolution features in plagioclase has been reported by Grove (1977) to be characteristic of rapidly cooled volcanic rocks. This observation appears to hold true for much of the HFF as well.

Plagioclase compositions in the Barby Formation basaltic andesite are primary, but slightly more sodic than in the weakly metamorphosed HFF volcanics (Fig. C.5b). Approximate correlations between anorthite contents of plagioclases and whole-rock CaO contents and $\text{CaO}/\text{Na}_2\text{O}$ ratios in Fig. C.6 illustrate that bulk magma composition exerts a measure of control on the plagioclase composition. Similar correlations have been reported by Ewart (1976) for very calcic plagioclases in orogenic basalts and andesites and these compositional fields allow a broad distinction between igneous and metamorphic plagioclase compositions

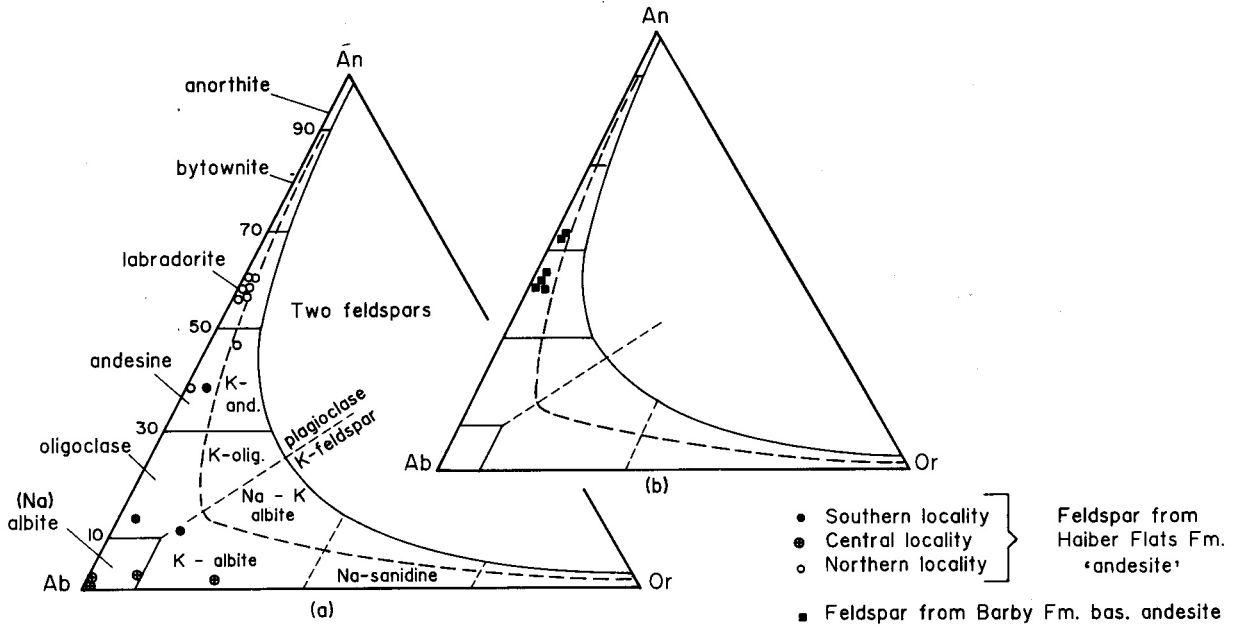


Fig. C.5: Plagioclase phenocryst compositions in (a) andesites (*sensu lato*) of the Haiber Flats Formation, and (b) basaltic andesite of the Barby Formation. The more sodic compositions (albite-oligoclase) are secondary in origin.

in the HFF (Fig. C.6).

K-feldspar is a groundmass phase in these mafic-intermediate flows and was not analysed.

3.2.2 HIS, Awasisb and Chowachasib Granites

Despite widespread albitisation in these granitoids, it is clear that original plagioclase in the HIS is relatively anorthitic in comparison with plagioclase in the younger Awasisb Granite and Chowachasib Granite Suite (CGS). The decrease in anorthite content can be broadly correlated with an increase in the differentiation index (DI), especially

when the most calcic plagioclase is considered from each of several plutons (Fig. C.7). Plagioclase in the Awasisb Granite is typically more sodic (< An₅) than in the late CGS (An₅-An₂₀), although the general tendency towards more sodic compositions in the higher silica members of this suite is not well defined.

K-feldspar is generally more abundant than plagioclase in the HIS and is present predominantly as microcline microperthite and microcline. It is difficult to determine whether these two phases represent the discrete phases typical of subsolvus granites, since much of the microcline has a secondary appearance. Accordingly, it seems most likely that

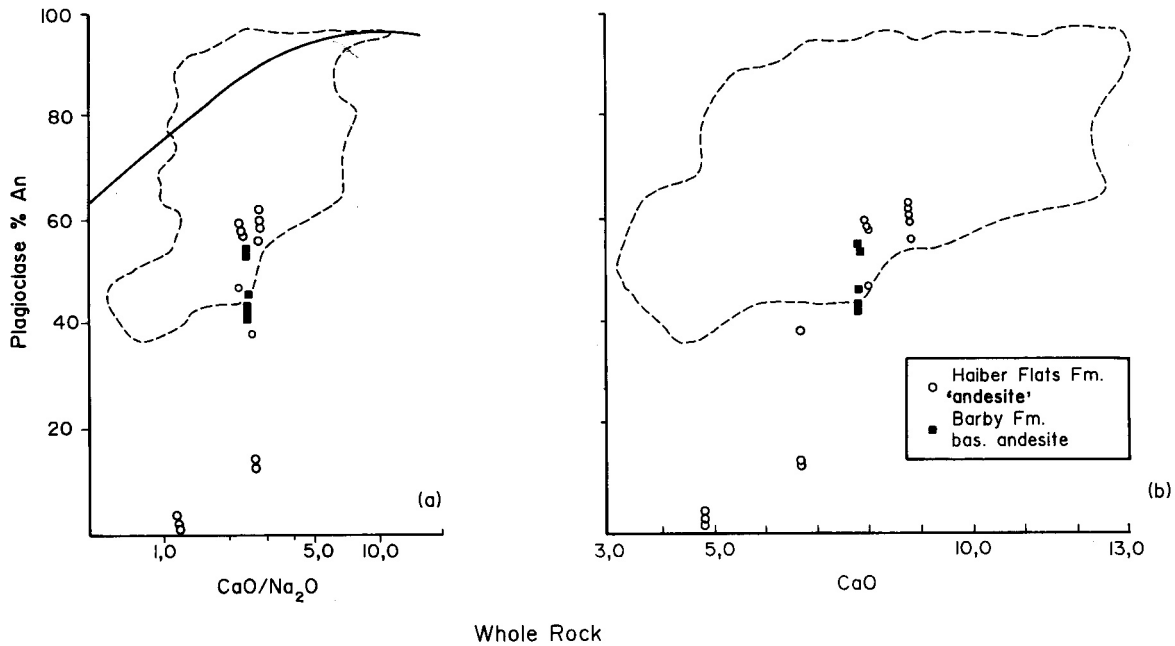


Fig. C.6: An contents of plagioclase phenocryst compositions in “andesites” of the HFF and Barby Formation plotted against (a) whole-rock CaO/Na₂O, and (b) whole-rock CaO. Liquidus curve in (a) and compositional fields in (a) and (b) are from (Ewart, 1976). Note separation of primary (>An₃₅) and metamorphic (<An₁₅) plagioclase phases.

3.3 PYROXENE

3.3.1 HFF and Barby Formation

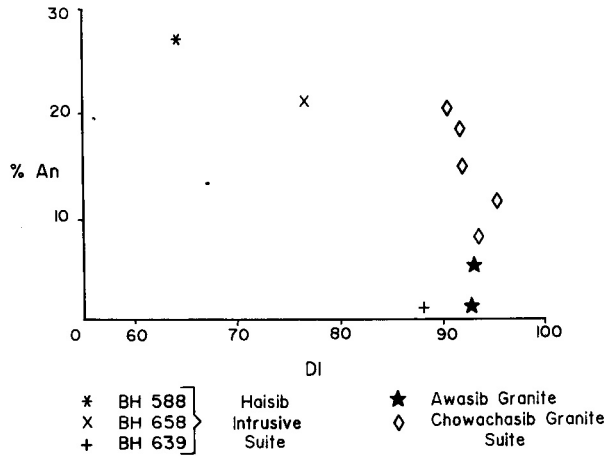


Fig. C.7: Compositional variation of the most calcic plagioclases as a function of Differentiation Index (DI) for different plutons within the late-stage granitoid suites.

the granites of the HIS were originally hypersolvus but were subsequently subjected to an increase in p_{H_2O} , perhaps as a result of the influx of water (Martin and Bonin, 1976). If the hypersolvus granites were previously consolidated, then these authors suggest that the introduction of meteoric water could cause the solidus to drop sufficiently to initiate partial refusion. In the case of the HIS, the common proximity of shear zones may mark the sites of fluid pathways necessary for the required introduction of H_2O to increase p_{H_2O} .

K-feldspar in the Awasib Granite is typically micropertthitic, but is also associated with plagioclase in occasional Rapa-kivi texture (average: core Or_{97} , rim Ab_{98}). K-feldspars in the CGS commonly contain a high proportion of exsolved albite and are best termed "mesopertthites". In general, the feldspars of the CGS are better preserved than their counterparts in the Awasib Granite, largely as a result of widespread albitisation, silicification and recrystallisation in the latter.

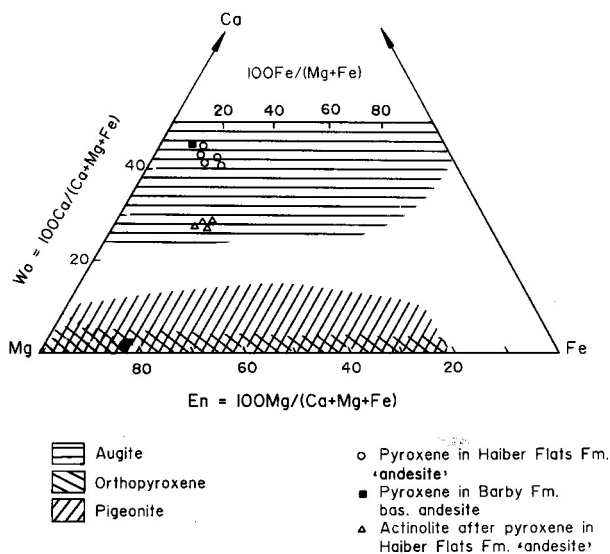
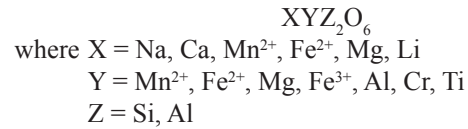


Fig. C.8: Pyroxene phenocryst compositions in "andesites" of the HFF and Barby Formation according to the simplified nomenclature of Ross and Huebner (1979). Also plotted are compositions of actinolite pseudomorphs after augite in the HFF.

Relict clinopyroxene (augite) cores in actinolite pseudomorphs are petrographically distinct from metamorphic diopside in Kairab Complex amphibolites. Augite is often the only primary ferromagnesian phase preserved in andesites (*sensu lato*) of the HFF. The general pyroxene formula may be written as follows (Cameron and Papike, 1980):



Using the simplified system of pyroxene nomenclature adopted by Ross and Huebner (1979), pyroxene phenocryst compositions of the HFF and Barby Formation are illustrated in Fig. C.8. Clinopyroxenes in both formations are typical augites which show a relatively small range in composition, while orthopyroxenes in the Barby Formation are bronzites and emphasise the Mg-rich (En_{83}) compositions regarded as typical of "orogenic" pyroxenes by Ewart (1982). Despite the limited compositional variation exhibited by augites, there is a slight tendency towards Ca depletion and Fe enrichment which may reflect magma crystallisation.

The presence of non-quadrilateral components (e.g. Ti, Al, Cr, Fe^{3+} , Mn, Na) in the pyroxene structure has been reported by Lindsley (1983) to affect the activities of Wo, En and Fs components. The substitution of Mn^{2+} for Fe^{2+} is illustrated by the positive correlation between MnO and FeO content in Fig. C.9. However, pyroxenes of the HFF and Barby Formation occupy different parts of the diagram which illustrates that the former are usually less MnO-rich for the same FeO content. Furthermore, relatively high TiO_2 abundances in HFF pyroxenes are associated with low ratios of $MgO/(MgO + FeO)$, thereby suggesting a more differentiated nature compared with the Barby Formation.

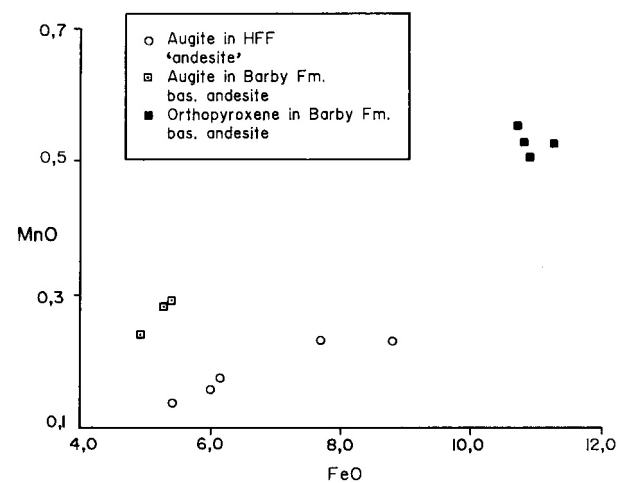


Fig. C.9: FeO vs. MnO diagram for pyroxene phenocrysts in "andesites" of the HFF and Barby Formation.

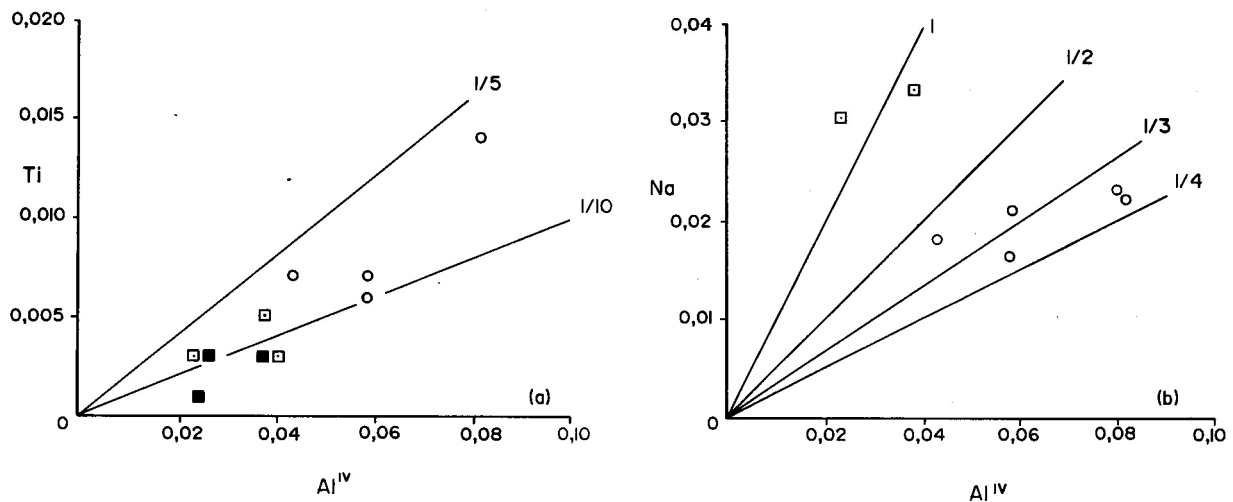


Fig. C.10: Plots illustrating (a) Ti-Al and (b) Na-Al substitution in pyroxenes of the HFF and Barby Formation.

Relative constancy of the inter element ratios Ti/Al^{IV} and Na/Al^{IV} indicate that Ti- Al^{IV} and Na- Al^{IV} are important substitution couples in pyroxenes of the HFF and Barby Formation (Fig. C.10). The Na/Al^{IV} ratio also separates the clinopyroxenes into their respective formations, viz. HFF ($Na/Al^{IV} = 1/4 - 1/2$) and Barby Formation ($Na/Al^{IV} \approx 1$). Comparison with relict clinopyroxenes of the Bitterwater metalavas (correlated with the Barby Formation; Williams-Jones, 1984) shows an overall similarity in Ti/Al ratios. However, Na/Al^{IV} ratios are generally higher in the HFF, and especially the Barby Formation, when compared with the Bitterwater clinopyroxenes ($Na/Al^{IV} = 1/4 - 1/8$ most commonly).

The studies of Kushiro (1960) and Le Bas (1962) have demonstrated that the compositions of clinopyroxenes vary according to the chemistry of their host lavas. Relict clinopyroxenes of both the HFF and Barby Formation do not generally contain the high Al and Ti contents typical of alkalic parentage, but do exhibit a depletion in Cr and Ti displayed by many calc-alkaline lavas. However, clinopyroxenes from these formations plot within the field of overlap between volcanic-arc and ocean-floor basalts in the discriminant function diagram of Nisbet and Pearce (1977). Leterrier *et al.* (1982) attribute the inconclusive results obtained using the latter diagram to the following limitations:

- (i) A small database of only 329 clinopyroxenes
- (ii) The use of mainly groundmass clinopyroxenes
- (iii) The use of oxides such as TiO_2 , MnO and Na_2O in concentrations which are often close to the detection limit of the EMF.
- (iv) The incorporation of all major basalt types in a single diagram.

Leterrier *et al.* (1982) have devised three magmatic discriminant diagrams based on a data file of 1225 clinopyroxene analyses (706 from phenocrysts) selected from basalts or basic andesites on the criterion that Thornton and Tuttle's (1960) differentiation index be lower than 50. The elements used (Ti, Cr, Ca, Al and Na) are able to discriminate between three strongly contrasted magma types, viz. "orogenic basalts", "tholeiites from distensive areas or non-

orogenic tholeiites", and "alkali basalts and related rocks".

Fig. C.11(a-c) illustrates the application of these discriminant diagrams to clinopyroxenes of the HFF and Barby Formation. The inferred non-alkaline and orogenic character of these lavas agrees well with whole-rock compositions (Section C.4), but the discrimination between calc-alkaline and tholeiitic affinities is inconclusive.

3.3.2 Chowachasib Granite

Rare "xenocrysts" of clinopyroxene occur in a "host" of titanium-rich hornblende (2.82% TiO_2) in K-feldspar granite of the CGS. The average clinopyroxene composition of $WO_{45.5}En_{41.0}Fs_{13.5}$ is slightly more Fe-rich than is typical for clinopyroxenes of the HFF or Barby Formation, but is otherwise sufficiently similar to have been inherited from xenoliths of these formations.

3.4 AMPHIBOLE

3.4.1 HFF and Barby Formation

The alteration of clinopyroxene to pale green amphibole is particularly widespread in the HFF. The compositions of the secondary amphiboles vary from actinolitic hornblende to tremolite in terms of Leake's (1968) classification (Fig. C.12) and all fall within the field of actinolites using Miyashiro's (1973) scheme (Fig. C.13). Even where pyroxene has been completely replaced, actinolite pseudomorph compositions plot within the augite field of the pyroxene quadrilateral (Fig. C.8).

The relatively low Ti/Al ratios (mean = 0.035 ± 0.017) of secondary amphiboles in the HFF are not compatible with a low-pressure origin, but may resemble the atypical low-pressure amphiboles reported by Grapes *et al.* (1977) from metabasites of the Hidaka Mountains. Hynes (1982) suggested that the absence of sphene as a phase buffering the Ti content of amphibole in these metabasites may have given rise to their low Ti contents. Sphene, although present as a secondary phase in the HFF, may post-date the amphibolitisation of the pyroxenes.

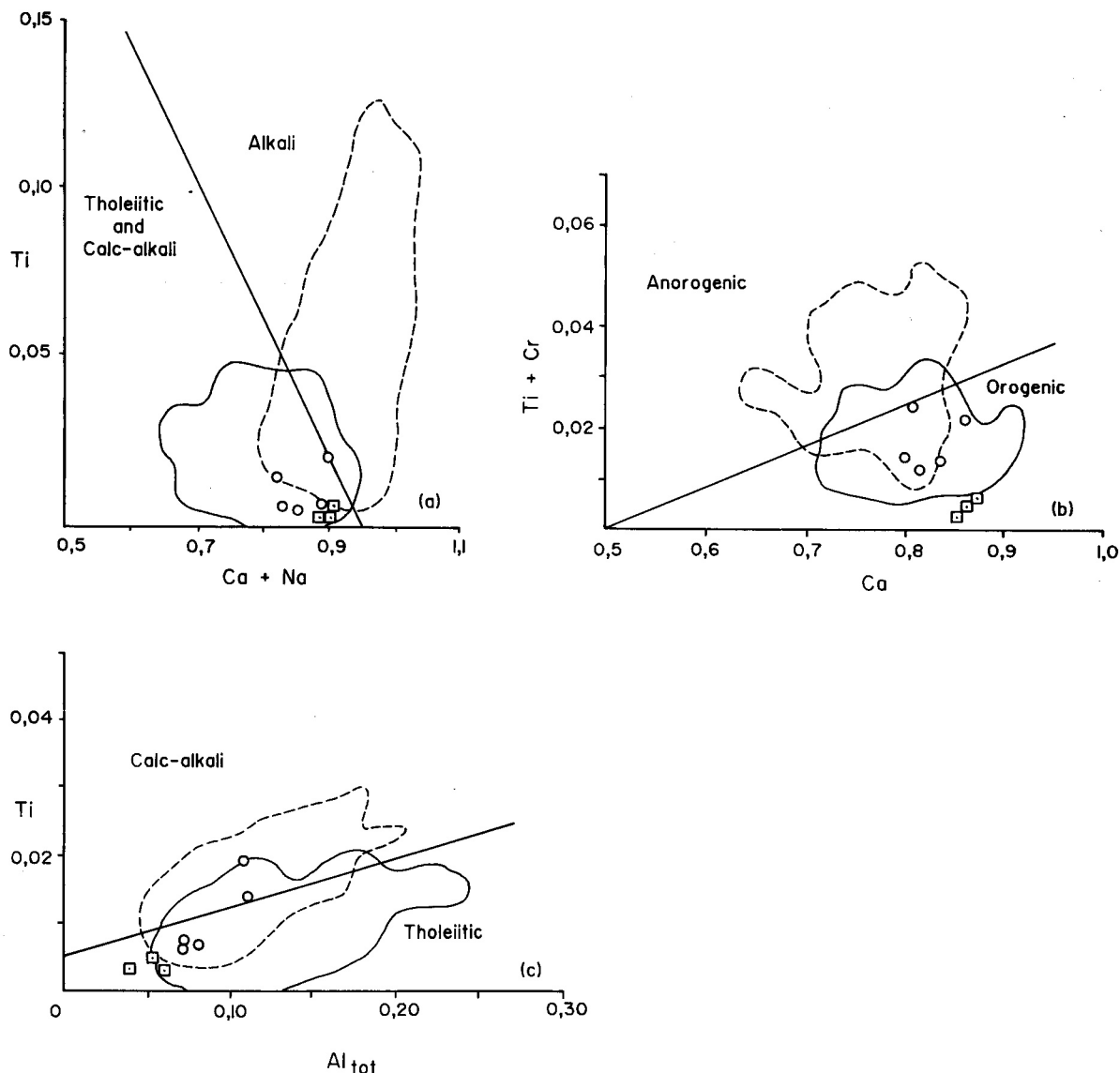


Fig. C.11: Magmatic affinities of clinopyroxene phenocrysts in the HFF and Barby Formation according to the discrimination diagrams of Leterrier *et al.* (1982). Each diagram shows the dividing line between, and outermost contours of, the fields distinguished.

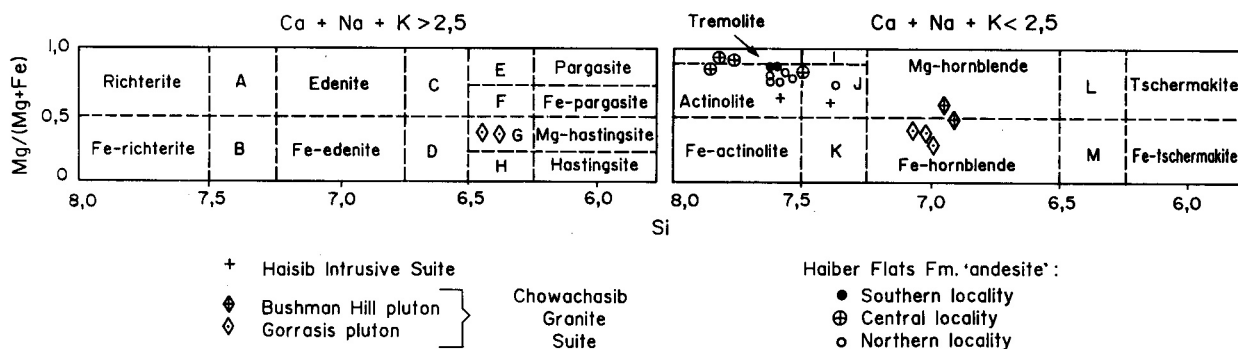


Fig. C.12: Amphibole compositions in HFF "andesite" and post-HFF granitoids plotted in terms of the classification of Leake (1968). All data normalised to 23 oxygens. Only hornblendes from the Chowachasib Granite Suite are igneous in origin. Fields as in Fig. B.4.

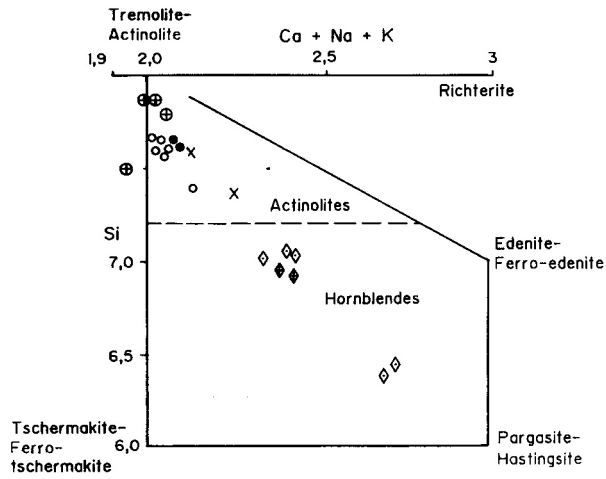


Fig. C.13: Amphibole compositions in HFF "andesite" and post-HFF granitoids plotted according to the classification of Miyashiro (1973). All data normalised to 23 oxygens. Note separation into igneous hornblende and metamorphic actinolite. Symbols as indicated previously.

3.4.2 HIS, Awasib and Chowachasib Granites

The few amphibole analyses available from a quartz syenite of the HIS indicate that the green amphibole present is actinolitic hornblende and actinolite (Fig. C.12). While the actinolite is compositionally similar to the actinolite pseudomorphs after augite in the HFF (Fig. C.13), actinolitic hornblende is considerably more enriched in TiO_2 (1.91 %) and could, therefore, reflect a relict igneous origin (cf. Reid, 1977, p. 173). Such high Ti contents are generally more typical of amphiboles of the Saffier Intrusive Suite and may, therefore, suggest a relationship between the latter and the HIS.

Amphiboles are extremely rare in the Awasib Granite and, where present, appear to have been inherited from mafic xenoliths. The dark green hornblendes in the CGS are, by contrast, typically igneous in composition, as shown by their high TiO_2 contents (mean 1.71 ± 0.78 %).

Amphiboles in the CGS are largely Fe-hornblendes according to Leake's (1968) classification scheme, with Mg-hastingsitic hornblende only occurring in K-feldspar granite which contains no coexisting biotite (Fig. C.12). In general, amphiboles are only common in the more alkaline granites of the CGS, possibly as a result of enhanced stability due to Na and Al (rather than Ca) substitution (cf. Wones and Gilbert, 1982). The tendency of these amphiboles towards more edenitic and hastingsitic compositions is illustrated in Miyashiro's (1973) scheme (Fig. C.13).

Amphiboles from K-feldspar granite of the CGS at Goraris tend to display higher Fe/(Fe + Mg) ratios (≥ 0.6) at Si contents of ≈ 7.0 compared with their counterparts in syenogranite at Bushman Hill. This relative iron enrichment is probably largely due to increased oxygen fugacity, since some of the hornblendes in the K-feldspar granite display relatively low Si contents (< 6.5) which clearly do not reflect an increase in silica activity in the crystallising magma. By contrast, the relatively high Al^{IV} contents of these iron-enriched amphiboles (Al^{IV} of 1.22 in K-feldspar granite com-

pared with 1.08 in syenogranite) may, as proposed by Wones and Gilbert (1982), have been influenced by the activities of Na_2O , Al_2O_3 and SiO_2 in the melt.

3.5 BIOTITE

3.5.1 HFF and Barby Formation

Biotite analyses provide a means of distinguishing between the different volcanic groups on the basis of the following criteria:

(i) Titanium content, which is considerably higher in the igneous biotites of the Barby Formation compared with the metamorphic biotites of the HFF. This feature is well illustrated in Fig. C.14, with comparative fields (after Reid, 1977, Fig. 30) of upper greenschist-grade biotites from the Haib basaltic andesite and igneous biotites of the Vioolsdrif diorite.

(ii) FeO^*/MgO ratios, which appear to be unique to each group and may be correlated with the host-rock composition (Fig. C.14).

Titanium content combined with the FeO^*/MgO ratio further enables an inter-group discrimination between the different volcanic localities, or centres, of the HFF.

The grade of metamorphism in the HFF volcanics is probably lowest at the northern locality, slightly higher at the southern locality and highest at the central locality. However, as can be seen from Figs C.14 and C.15, there is no accompanying compositional trend which confirms the regional pattern. While this observation is in contrast to studies which show systematic compositional variation in biotite as a function of increasing or decreasing metamorphic grade (e.g. Engel and Engel, 1960; Miyashiro, 1953), other workers (e.g. Cooper, 1972) have reported the absence of any such correlation.

While the composition of biotite probably depends on factors other than metamorphic grade (e.g. host-rock composition, composition of coexisting phases), the paragenesis of this phase in the HFF implies temperatures close to the maximum of 400–450°C likely to be encountered in "regional burial metamorphism" (Winkler, 1976, p. 4).

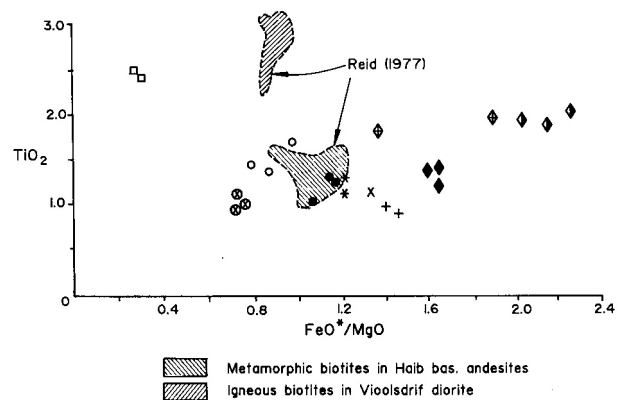


Fig. C.14: Plot of FeO^*/MgO vs. TiO_2 for biotites of the HFF, Barby Formation and post-HFF granitoids. All data normalised to 22 oxygens. Reference fields are from Reid (1977). Symbols as before.

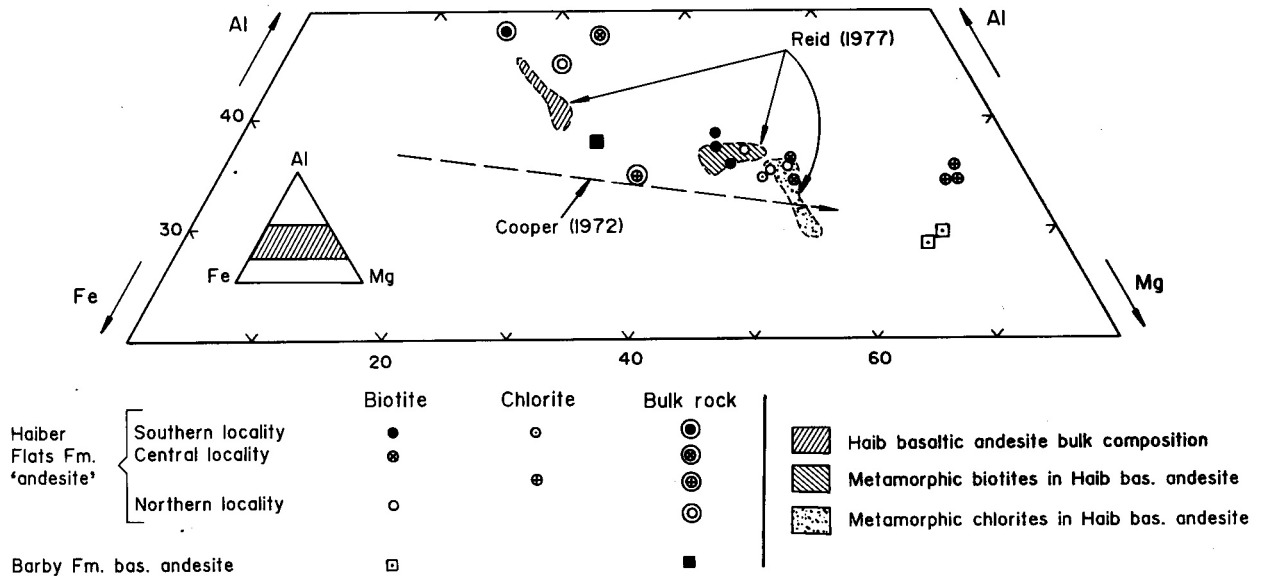


Fig. C.15: Al-Mg-Fe plot of metamorphic biotites and chlorites from different volcanic localities, or centres, in the HFF. Comparative fields from Reid (1977). Dashed line reflects change in chlorite composition in Haast metabasites with increasing metamorphic grade (Cooper, 1972). Biotite data normalised to 22 oxygens, chlorite data to 28 oxygens.

3.5.2 HIS, Awasib and Chowachasib Granites

The siderophyllite-annite-phlogopite-eastonite quadrilateral illustrates the compositional groupings of biotites from both the HIS and younger granites (Fig. C.16). Positive correlations between compositions of biotite and their host rocks (e.g. wt.% Al_2O_3) suggest that factors such as metamorphism, coexisting phases and physical conditions of crystallisation have not exerted any significant influence on the mineral-rock relationship (cf. Speer, 1984).

By comparison with metamorphic biotites of the HFF, biotites of the HIS exhibit higher FeO^*/MgO ratios, but similar TiO_2 contents (Fig. C.14). The relatively low TiO_2 contents in HIS biotites are probably the result of chloriti-

sation, as biotites do occasionally contain TiO_2 contents of up to 5.7%. Since the kinked appearance of large biotites in the HIS indicates a pre-tectonic nature, it is concluded that these crystals were originally igneous in origin but have subsequently undergone greenschist metamorphism.

In order to further explore the possibility of a metamorphic origin for at least some of the biotites analysed from the HIS, compositions of biotites are compared with the HFF in Fig. C.17. Despite the differences in bulk-rock composition between the HIS and HFF, biotites of the former plot close to their counterparts in the latter. This implies that controls other than bulk-rock composition have influenced the composition of these phases, e.g. metamorphism, oxygen fugacity and water fugacity. Contact metamorphism of the HFF on a regional scale by the HIS is considered unlikely in view of the metamorphosed nature of the HIS itself.

Widespread chloritisation of biotite in the Awasib Granite precludes any reliable analysis of this phase. However, dark brown biotite is still well preserved in the CGS and the generally high TiO_2 contents (mean $1.94 \pm 0.36\%$) are consistent with a primary igneous character. Biotites tend to display distinct compositional characteristics for the different plutons in the CGS (Fig. C.16). Particularly distinctive are the low Al^{VI} contents of biotites from the Bushman Hill syenogranite as well as low $\text{Mg}/(\text{Mg} + \text{Fe})$ ratios of biotites from syenogranite at Awasib Mountain.

There appears to be a systematic increase in both Ti content and $\text{Fe}/(\text{Fe} + \text{Mg})$ ratio with differentiation index (m) in the CGS, i.e. from monzogranite at Satanskop to syenogranite at Awasib Mountain (Fig. C.18). While this trend may relate to differences in the temperature of crystallisation, the range in m is very small and consequently such factors as oxygen and water fugacity may be more important. However, fractional crystallisation of small amounts of mafic phases would not greatly affect the DI, but could produce the observed pattern due to the low abundances of Ti, Fe and Mg in the granites.

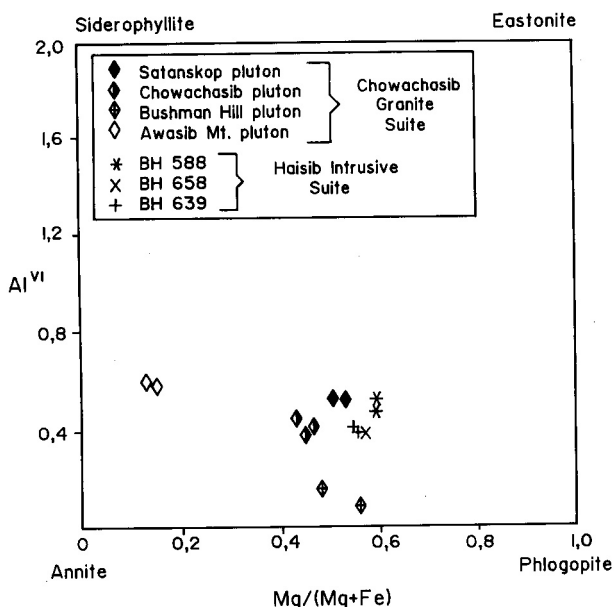


Fig. C.16: Biotite compositions from the post-HFF granitoids projected onto the "ideal biotite plane" (Deer *et al.*, 1966). All data normalised to 22 oxygens.

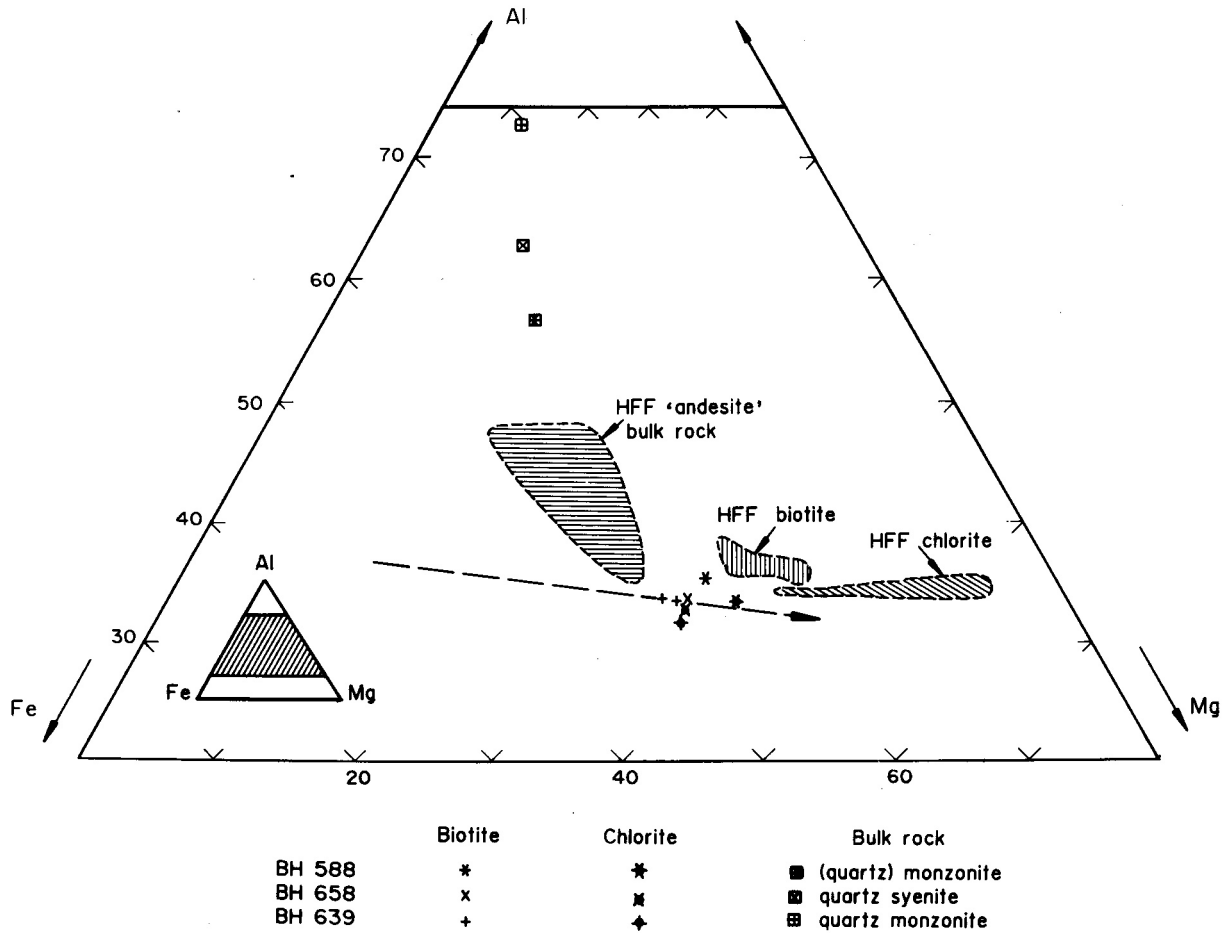


Fig. C.17: Al-Mg-Fe plot of metamorphic biotites and chlorites in the Haisib Intrusive Suite compared with compositional fields for the HFF "andesites". Data normalised as in Fig. C.15.

3.6 CHLORITE

3.6.1 HFF and Barby Formation

Chlorite analyses indicate compositions ranging from ripidolite to sheridanite or clinocllore using Hey's (1954) nomenclature (Fig. C.19). The more Mg-rich chlorite compositions (Fig. C.15) reflect their high-MgO andesite host in part, but are sufficiently extreme to suggest a higher grade of metamorphism for the central locality. This suggestion is supported by both field and petrographic observations. The central locality chlorites are colourless compared with their light green counterparts at the other localities.

Chlorites from the southern locality exhibit slightly higher Mg/Fe ratios relative to the host rock and are similar in composition to chlorites from the oligoclase zone, or upper greenschist facies, of the Haast Schist Group studied by Cooper (1972).

3.6.2 HIS

Only chlorites from the HIS were analysed and these reveal compositions which are generally more Fe- and less Mg-rich than their counterparts in the HFF (Figs C.17 and C.19).

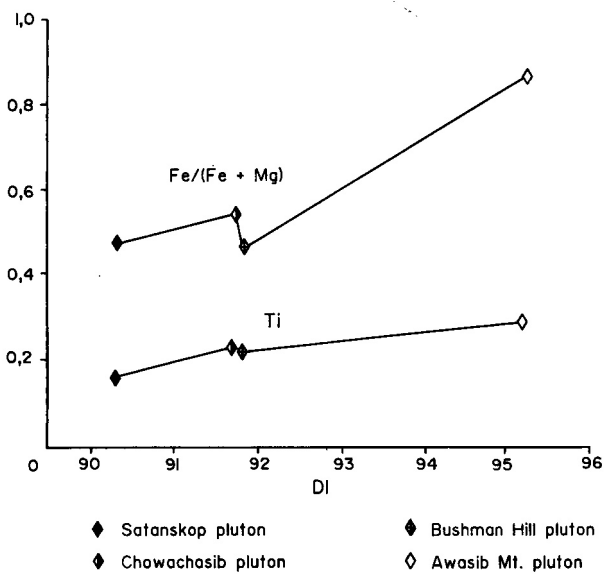


Fig. C.18: Compositional variation of biotite in the Chowachasib Granite Suite. Data normalised to 22 oxygens.

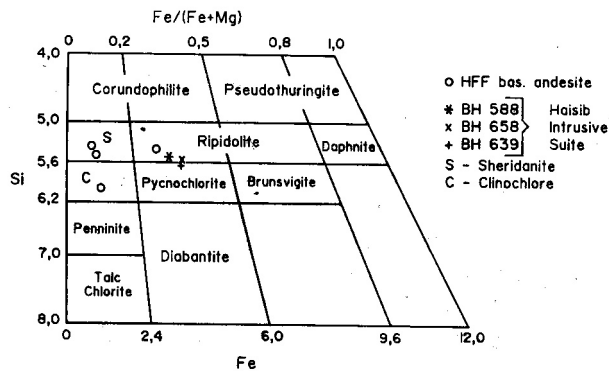


Fig. C.19: Chlorite compositions in the HFF "andesite" and Haisib Intrusive Suite plotted according to the classification of Hey (1954). Data normalised to 28 oxygens.

3.7 EPIDOTE

3.7.1 HFF and Barby Formation

Epidotes from the central and northern localities of the HFF occur as replacement products of plagioclase and ferromagnesian minerals. Epidote compositions may be related to a variety of different factors such as bulk-rock composition, oxygen fugacity and possibly metamorphic grade.

Epidotes of the HFF show a compositional range from $Ps_{27.2}$ to $Ps_{30.5}$ which is more iron rich than the range of $Ps_{23.5}$ to $Ps_{26.7}$ exhibited by epidotes of amphibolite-grade metabasalts from the Kairab Complex. Maruyama *et al.* (1983) have also shown that more iron-rich epidotes tend to characterise lower grade assemblages in the metabasaltic rocks of the Yap Islands. However, the intermediate host-rock compositions in the HFF are typically more oxidised and hence suggest that oxygen fugacity could have played an important role in determining the iron content of the epidotes (cf. Liou, 1973). This suggestion is supported by the relatively high average bulk-rock oxidation ratio of 42.4 in the HFF compared with only 28.4 in the Kairab metabasalt.

3.7.2 HIS

Epidote in the HIS is secondary in origin and varies in composition from $Ps_{22.3}$ in quartz syenite to $Ps_{26.6}$ - $Ps_{28.3}$ in quartz monzonite, the latter range agreeing well with the range $Ps_{27.2}$ - $Ps_{30.5}$ determined for epidotes of the HFF. The bulk-rock oxidation ratios of the quartz monzonite and quartz syenite are similar, namely 54.7 and 52, 1, respectively; hence oxygen fugacity may not be an important control on the iron content of epidote in this case.

3.8 OXIDE MINERALS

3.8.1 HFF and Barby Formation

Fe-Ti oxide minerals are usually completely oxidised and made up of magnetite and exsolved ilmenite. This exsolution texture suggests the presence of an original homogeneous titanomagnetite phase. The common association of rims

of biotite and sphene with the oxide minerals supports the latter suggestion. Secondary haematite and magnetite (porphyroblasts) are also present, but more common in highly altered (or metamorphosed) HFF andesites. While totals are usually close to 100% when Fe^{3+} and Fe^{2+} are calculated assuming perfect stoichiometry, totals as low as 95% are probably the result of alteration.

Although the variable proportion of exsolved ilmenite does not allow accurate estimation of the original Ti content in the oxide minerals, relatively homogeneous titanomagnetites of the Barby Formation contain a maximum TiO_2 of about 14% which corresponds to an approximate composition of $Mt_{60}Usp_{40}$. This composition compares favourably with the average value of Usp_{38} reported by Ewart (1982) for Fe-Ti oxides in orogenic basalts, basaltic andesites and andesites.

3.8.2 HIS, Awasib and Chowachasib Granites

Limited EMP analyses indicate that despite widespread oxidation and alteration to haematite \pm sphene \pm chlorite, oxide minerals in these granitoids can be identified as mainly magnetite and ilmenite. The original phase was probably titanomagnetite which has now exsolved intersecting lamellae of ilmenite. The latter is subordinate, thereby suggesting a low Usp content in the original phase.

3.9 METAMORPHISM IN THE HFF

EMP analyses of HFF rhyolites show that:

(i) Plagioclase is predominantly albite ($An_{0.6} \pm An_{0.2}$), both in primary and secondary phases. This observation supports widespread albitisation in these volcanics.

(ii) Secondary white micas exhibit the higher K, Si and (Mg + Fe) contents typical of muscovite as opposed to margarite or paragonite (Guidotti, 1984).

(iii) Chlorites are classified as pycnochlorites according to the scheme of Hey (1954), which indicates a more Fe-rich character than their counterparts in the andesites.

(iv) Oxide minerals are largely secondary and made up of magnetite, haematite and ilmenite.

The widespread occurrence of secondary albite, muscovite and chlorite in the rhyolites of the HFF is entirely compatible with the greenschist-grade of metamorphism deduced from the secondary mineral parageneses of the andesites. This metamorphic event represents a regional imprint which has not been recognised in Sinclair-type rocks to the east as indicated by the absence of the requisite mineral parageneses in the sample of Barby Formation basaltic andesite from eastern Gorrasis.

A variation in the degree of metamorphic recrystallisation within the greenschist facies is evident between the different volcanic localities, or centres, of the HFF. While it may be possible to relate such variation to differences in the depth of burial, both the overall grade of metamorphism (which is close to the limit of so-called "regional burial metamorphism") and accompanying deformation suggest that additional factors must be considered. One possibility is that the closely related Haisib Intrusive Suite may repre-

sent, in part, the subvolcanic magma chambers which have provided additional heat and fluids to facilitate metamorphic recrystallisation. A variation in the proximity of such magma chambers to overlying volcanics would clearly result in a variation in the degree of recrystallisation which could further be manifested on a regional scale. The availability of water may also play an important role (cf. Winkler, 1976, p. 165).

Such regional "contact metamorphism" does not, however, account for the accompanying deformation and it is further significant that members of the Haisib Intrusive Suite display a similar degree of metamorphism and deformation to that experienced by the HFF. A more regional and dynamic event must, therefore, be looked to in order to explain the observed variation in response to greenschist facies metamorphism in the HFF.

3.10 SUMMARY

3.10.1 Late-stage volcanic successions

(i) Plagioclase phenocrysts in basaltic andesites of the HFF display both primary (labradorite-andesine) and secondary (albite-oligoclase) compositions, the former showing an approximate correlation with the bulk composition. Plagioclase phenocrysts in the Barby Formation are rarely affected by metamorphism and display similar primary compositions to the HFF.

(ii) Relict augite phenocrysts in HFF basaltic andesites differ from the Barby Formation by displaying lower MnO contents at a given FeO content, higher Ti abundances and lower Na/Al^{IV} ratios. Depletion in Cr and Ti for clinopyroxenes from both formations is typical of a calc-alkaline and orogenic character (Le Terrier *et al.*, 1982). Bronzite phenocrysts are unique to Barby Formation basaltic andesite and emphasise the Mg-rich compositions typically found in orogenic pyroxenes (Ewart, 1982).

(iii) Actinolite pseudomorphs after augite are most common in the HFF and show enrichment in Mg and Fe and depletion in Ca relative to the primary phase.

(iv) Biotite compositions in the HFF are typically metamorphic as shown by their similarity in terms of TiO₂ and FeO*/MgO to compositions of the upper greenschist facies Haib basaltic andesites (Reid, 1977). By contrast, biotite compositions in the Barby Formation are typically primary as shown by their high Ti contents.

(v) Metamorphic chlorite compositions in the HFF basaltic andesites are typical of greenschists (e.g. Haib basaltic andesite, Reid, 1977) and Mg enrichment in chlorites at the central locality may reflect a locally higher grade of metamorphism.

(vi) Epidote compositions of Ps₂₇₋₃₀ in the HFF are similar to compositions of Ps₂₇₋₂₈ in quartz monzonite of the HIS, possibly in response to similar metamorphic conditions.

(vii) In the HFF, the association of oxide minerals with rims of biotite and sphene suggests that the original oxide phase was titanomagnetite. In Barby Formation basaltic andesite, titanomagnetite corresponds to a composition of Mt₆₀Usp₄₀, which compares favourably with the average value of Usp₃₈ reported by Ewart (1982) for Fe-Ti oxides in orogenic basaltic andesites.

(viii) EMP analyses show that HFF rhyolites are characterised by primary and secondary albite, secondary muscovite (as opposed to margarite and paragonite), pycnochlorite and magnetite, haematite and ilmenite.

3.10.2 Late-stage intrusive suites

(i) A decrease in An content of plagioclase shows a correlation with increasing DI in the Haisib Intrusive Suite (HIS). Granites of the HIS were originally hypersolvus, but a subsolvus appearance may be attributed to the influx of water via proximal shear zones and the consequent depression of the solidus. Plagioclase in the Awasis Granite is typically sodic (An < 5), while K-feldspars are micropertthitic and more rarely rimmed by albite to form Rapakivi texture. Plagioclase in the Chowachasib Granite Suite (CGS) varies from An₅₋₂₀ and is less altered than counterparts in the Awasis Granite.

(ii) Actinolite in the HIS is similar in composition to actinolite in the HFF, but actinolitic hornblende exhibits high Ti contents more typical of a primary origin. Primary hornblendes in the CGS are only common in the more alkaline granites, possibly as a result of enhanced stability due to Na and Al (rather than Ca) substitution. Iron enrichment in these hornblendes is attributed to oxygen fugacity since a corresponding trend in silica enrichment is not evident.

(iii) Biotite compositions in the HIS exhibit similar TiO₂ contents to metamorphic biotites in the HFF, but higher FeO*/MgO ratios. Occasionally high contents of TiO₂ in biotites from the HIS suggest that the original phase was magmatic in origin and that subsequent changes in composition were the result of metamorphism. Biotites in the CGS display compositional characteristics which enable discrimination between the different plutons, e.g. low Al^{VI} at Bushman Hill and low Mg/(Mg + Fe) at Awasis Mountain. With an increase in DI, biotites show a systematic increase in Ti content and Fe/(Fe + Mg) as a result of fractional crystallisation or oxygen/water fugacity.

(iv) Chlorite compositions in the HIS are generally more Fe- and less Mg-rich than their counterparts in the HFF basaltic andesites, while epidote compositions are similar to the latter.

(v) Compositions of occasional clinopyroxenes in K-feldspar granite of the CGS are similar to those obtained in the HFF or Barby Formation and suggest that these are inherited phases.

4. WHOLE-ROCK CHEMISTRY

4.1 INTRODUCTION

Whole-rock analyses are tabulated on the accompanying Microfiche card (discussion in Appendix III) for a total of 103 samples from the late-stage crust of the AMT and 9 samples from the Barby Formation (Sinclair Sequence type area). This section places emphasis on the eruptive rocks of the HFF and their associated intrusions, viz. the HIS and Awasisb Granite. The volcanic rocks are of particular interest, since variation diagrams show reasonable coherence and may, therefore, approximate a liquid line-of-descent.

As explained in Section BA, the $\text{Fe}_2\text{O}_3/\text{FeO}$ ratios for analyses have been estimated according to the method of Le Maitre (1976) for use in calculation of CIPW norms and Mg# (molecular $\text{MgO}/[\text{MgO} + \text{FeO}]$) values. Where rocks are relatively altered and suggest oxidation, an "unrupted" $\text{Fe}_2\text{O}_3/\text{FeO}$ ratio has been estimated (e.g. 0.3 for andesites; Gill, 1981).

4.2 ASSESSMENT OF ALTERATION

The low grade of metamorphism (greenschist facies or lower) in late-stage crust of the AMT is unlikely to be isochemical with respect to the volatile components H_2O and CO_2 . The histogram in Fig. C.20 illustrates the range in "loss on ignition" (LOI) for lithologic units in the late-stage crust. The LOI values used are minimum values due to incomplete oxidation of Fe during the ashing of sample powders. However, a corrected LOI can only be calculated if the actual FeO and Fe_2O_3 contents are known as well as the amount of unoxidised Fe. By estimating Fe_2O_3 and FeO according to the method of Le Maitre (1976) and assum-

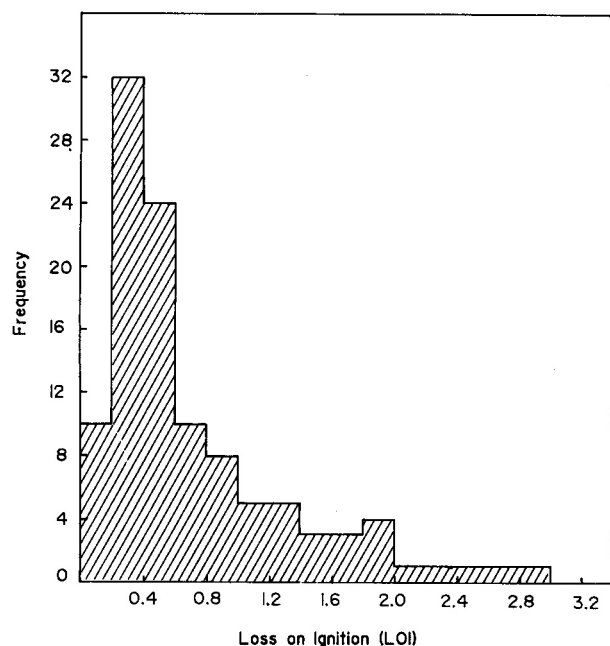


Fig. C.20: Frequency histogram illustrating the range in "loss on ignition" (LOI) in lithologic units within the late-stage crust of the AMT.

ing that about 20% Fe is unoxidised, the corrected LOI is found to be slightly higher than the calculated LOI. Use of the latter value does, however, enable a crude measure of the volatile content which, in turn, allows an approximate assessment of alteration.

LOI, as a measure of hydration (and minor carbonation in the case of the HFF), increases with an increase in hydrous minerals during greenschist facies metamorphism (up to 3% H_2O ; Jolly, 1972) and weathering (Miyashiro *et al.*, 1969). While Irvine and Baragar (1971) have considered Precambrian greenstones with greater than 2.5% H_2O^+ to be unacceptably altered, Smith (1968, 1969) has found a favourable comparison between volcanics and their altered equivalents (recalculated on a water-free basis) having up to 12% H_2O^+ . The implied lack of any direct relationship between volatile content and alteration (especially in greenschist facies volcanics) has been reported by other workers, e.g. Reid (1977), Williams-Jones (1984).

Despite the latter considerations, it is clear from Fig. C.20 that the bulk of analyses from Sinclair-age rocks contain LOI values which are acceptably low according to Irvine and Baragar (1971). The implied lack of alteration may once again be tested using the approach of Beswick and Soucie (1978). Figs C.21a-e illustrate that data for the HFF volcanic suite are comparable to the unaltered Phanerozoic trends used as references by these workers. Nevertheless, data scatter is sufficient to suggest some alteration of the rhyolites, e.g. silicification (Figs C.21a and d), Ca depletion possibly as a result of albitisation (Figs C.20b and e) and potassium metasomatism (Fig. C.21 e). Data for the mafic lavas are generally less aberrant but do suggest some silica and Ca depletion (Figs C.21d and e).

While the approach of Beswick and Soucie (1978) clearly indicates some element mobility in the HFF eruptive rocks, this assessment is dependent on the reference database used by these workers. Compared with post-Mesozoic volcanic suites, the rhyolites of the HFF exhibit low levels of Ca and high levels of silica and potassium. Such chemical characteristics may be considered primary if these rhyolites are the product of extreme fractionation or derived from a crustal (A-type) source (see discussion in Section 4.3.2). Accordingly, the alteration present in the HFF volcanic suite is not considered to be sufficiently intense to preclude the employment of geochemical techniques on these rocks. This view is supported by the "unaltered" nature of the data when plotted in the ternary diagram $\text{MgO}/10\text{-CaO}/\text{Al}_2\text{O}_3\text{-SiO}_2/100$ (Davis *et al.*, 1978) - Fig. C.22.

4.3 GEOCHEMICAL CHARACTERISATION

4.3.1 Late-stage ("Sinclair-type") volcanics

4.3.1.1 Classification

Volcanic rocks of the Haiber Flats Formation (HFF) are discussed in this section, with comparative reference being made to compositionally similar extrusives in the Barby Formation. The former are volumetrically more important in the AMT and represent the western most occurrences of Sinclair-age volcanism. The data for the HFF volcan-

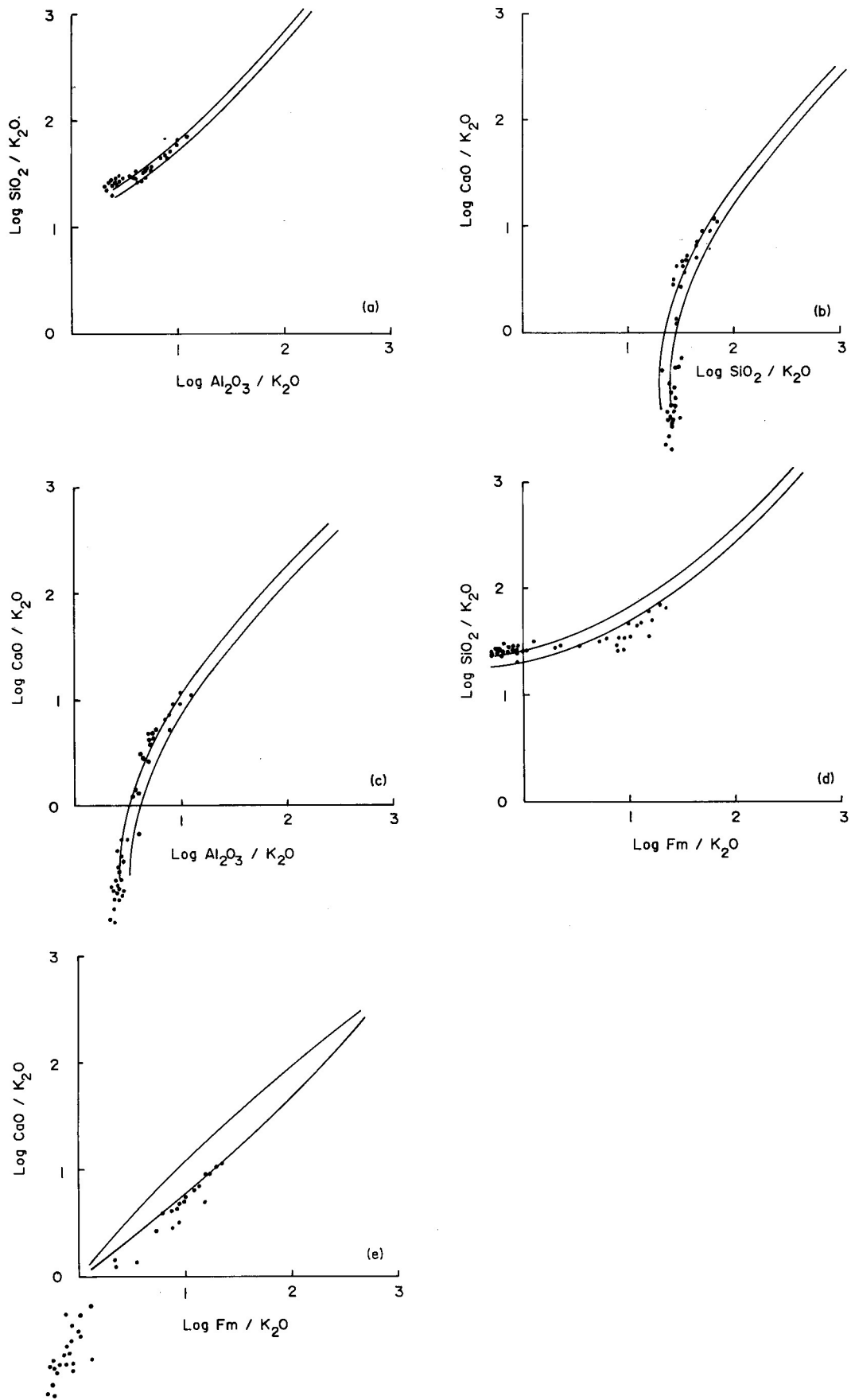


Fig. C.21: Logarithmic oxide molecular ratio plots for the HFF volcanic succession compared with trends for modern suites (after Beswick and Soucie, 1978). $\text{Fm} = \text{FeO}^* + \text{MgO} + \text{MnO}$.

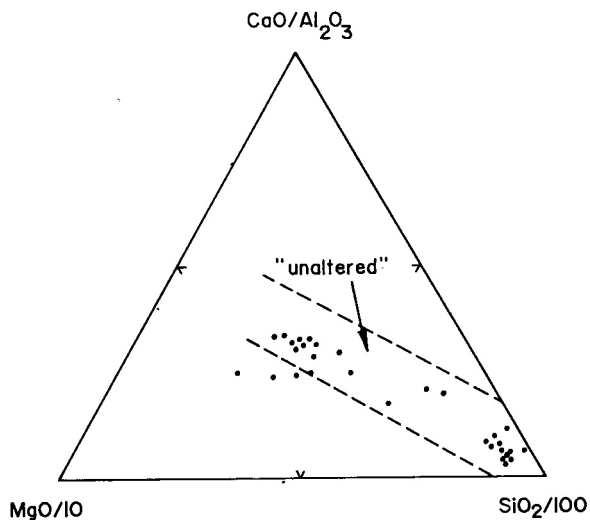


Fig. C.22: Plot of HFF data in the ternary system MgO/10-CaO/Al₂O₃-SiO₂/100 (Davis *et al.*, 1978). "Unaltered" compositions fall within the dashed lines.

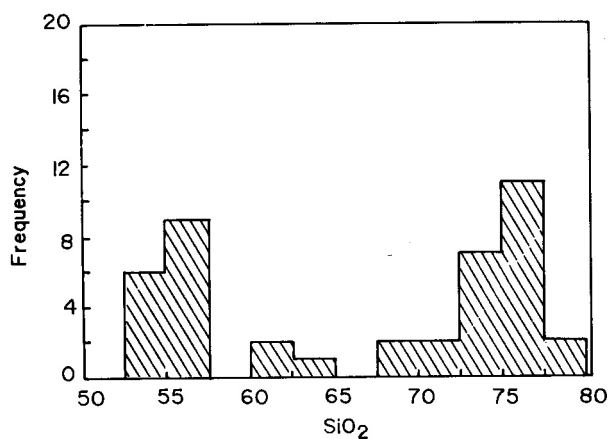


Fig. C.23: Frequency histogram illustrating the bimodal distribution of silica contents in HFF eruptive rocks.

ics have been tabulated into eight of the twelve chemical groupings advocated by Ewart (1979, 1982), viz. 52-54, 54-56, 56-58, 60-63, 63-66, 66-69, 69-73, and > 73% SiO₂ (Table C.4). The distribution between these groupings is essentially bimodal (Fig. C.23) with a paucity of compositions in the intermediate compositional range, especially 58-66% SiO₂.

(i) Alkali - silica variation

The wide range of compositions displayed by volcanics of the HFF is illustrated in a total alkali - silica plot (Fig. C.24) where fields are defined according to Le Bas *et al.* (1986). This diagram emphasises the calc-alkaline (after Kuno, 1968) or sub-alkalic (after Irvine and Baragar, 1971) nature of most of the volcanics, although several samples are clearly alkaline. A relatively potassium-rich nature is indicated for an average trend of the HFF on a plot of SiO₂ versus K₂O (Fig. C.25). Comparison with circum-Pacific trends (after Gill, 1970) illustrates a similar slope but consistently higher K₂O contents for the average HFF trend.

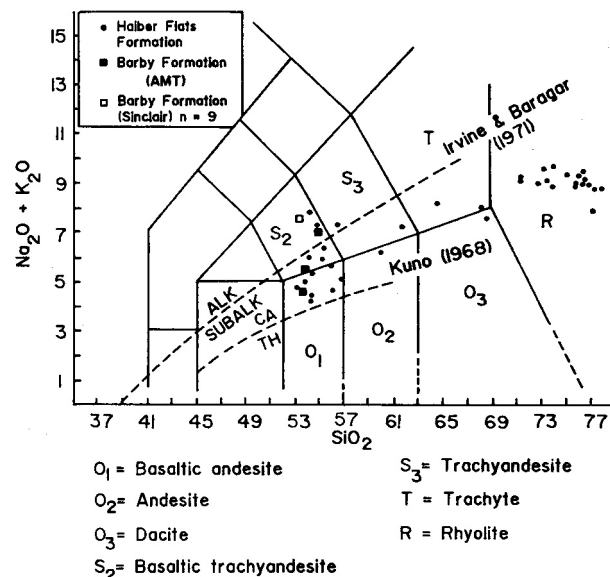


Fig. C.24: Total alkali-silica (TAS) diagram showing distribution of data for the HFF volcanic succession. Rock group subdivision is according to Le Bas *et al.* (1986). Other fields as for Fig. B.16.

This trend is comparable to that of calc-alkaline volcanics from the "southern" Barby Formation in the Sinclair Sequence (after Brown and Wilson, 1986). The shoshonitic trend of some Barby Formation volcanics is, however, clearly much steeper than either of these trends. The HFF trend falls within the "high-K" field of Ewart (1979, 1982), modified from Peccerillo and Taylor (1976), and most closely resembles orogenic volcanic suites from the western zone of the western USA and the Mediterranean region (see Section 4.3.1.4).

(ii) Iron enrichment

The lack in iron enrichment for HFF eruptive rocks is illustrated in plots of FeO* versus MgO (Fig. C.26a) and SiO₂ versus FeO^T/(FeO^T + MgO) (Fig. C.26b). These diagrams show that data for the HFF lavas compare favourably with both the calc-alkaline Cascade volcanics (Carmichael, 1964) and calc-alkaline "southern" Barby Formation volcanics (Brown and Wilson, 1986), and are clearly distinct from the tholeiitic Thingmuli trend (Carmichael, 1964). The AFM trend (Fig. C.55; Section C.6) also compares well with calc-alkaline volcanic suites in general and falls within the "calc-alkaline" field of Irvine and Baragar (1971).

The tendency for HFF rhyolites to plot within the tholeiitic field designated by Miyashiro (1974) is the result of extremely low MgO contents and does not necessarily indicate iron enrichment.

(iii) Alkali-lime index

A convenient method of illustrating Peacock's (1931) alkali-lime index is by plotting SiO₂ versus log(CaO/Na₂O + K₂O), e.g. Brown (1982). Fig. C.27 illustrates that the HFF lavas are calc-alkalic (%SiO₂ ≈ 57) and define an average trend which lies close to the field of "normal calc-alkaline andesites" (after Brown, 1982).

TABLE C.4: Average major and trace element compositions of Haiber Flats Formation eruptive rocks, with silica intervals according to Ewart (1979, 1982).

SiO ₂	52-54%	54-56%	56-58%	60-63%	63-66%	66-69%	69-73%	>73%
n =	2	9	3	2	1	2	3	19
SiO ₂	53.49	54.69	56.54	61.07	64.62	68.46	71.88	75.64
TiO ₂	0.90	1.00	1.08	0.75	0.64	0.49	0.30	0.12
Al ₂ O ₃	14.12	15.33	16.25	15.22	15.35	14.67	14.00	12.10
Fe ₂ O ₃ *	9.73	9.52	8.11	6.85	5.62	4.26	2.90	2.19
MnO	0.16	0.16	0.14	0.10	0.05	0.10	0.14	0.07
MgO	8.62	5.83	5.03	3.69	2.53	1.24	0.44	0.27
CaO	7.85	7.28	6.90	5.47	2.87	2.94	1.09	0.53
Na ₂ O	2.84	3.51	3.61	3.73	4.51	4.01	4.56	4.60
K ₂ O	2.02	2.31	2.04	2.92	3.61	3.69	4.47	4.50
P ₂ O ₅	0.28	0.37	0.30	0.20	0.20	0.14	0.23	0.06
Mo	1.8	2.0	3.0	2.3	2.1	4.0	4.3	3.7
Nb	5.6	7.6	7.0	9.4	10	16	20	20
Zr	118	163	195	206	233	205	361	289
Y	23	29	27	38	36	47	66	95
Sr	525	524	518	405	309	278	100	44
U	1.3	2.0	3.2	3.4	2.0	6.1	3.2	3.5
Rb	62	84	94	126	147	166	165	198
Th	1.7	4.9	7.6	10	13	18	25	27
Pb	21	20	4.1	23	20	19	24	25
Zn	75	73	62	49	39	56	32	29
Cu	10	72	24	1.5	1.4	6.5	3.1	11
Ni	201	66	72	28	23	11	5.1	4.1
Co	40	30	32	24	17	9.2	1.6	0.8
Cr	712	208	128	111	54	27	22	21
V	167	155	156	120	89	50	19	20
Ba	638	714	680	922	1134	706	954	497
Sc	25	23	22	18	11	7.6	5.4	2.9
La	18	28	26	26	29	37	64	52
Ce	32	56	52	49	56	75	127	110
Nd	23	33	30	31	33	39	65	62
Cs	3.6	5.0	5.0	2.9	4.4	4.9	2.0	2.4
DI	37.6	48.6	49.6	61.5	74.7	79.2	90.8	94.1

Major oxides in wt.%; trace elements in ppm. All Fe expressed as Fe₂O₃*

4.3.1.2 Major element variation

(i) Introduction

Variation of major oxides with SiO₂ is illustrated in Fig. C.28 with lavas sampled from the southern, central and northern localities indicated separately on each Harker diagram. Data points which coincide with average trend lines for some oxides are, however, aberrant for others. This may be due to the interplay of several factors such as alteration, fractionation, phenocryst accumulation and regional variation. In addition, Gill (1981, p. 102) notes that a certain "randomness" may be evident within a suite of samples from the same volcano or even the same eruption.

(ii) Systematic description

(a) Titanium

TiO₂ decreases consistently with increasing SiO₂ for all lavas of the HFF. However, southern locality basaltic andesites display relatively high TiO₂ contents which cannot be easily explained by titanomagnetite accumulation. Non-enrichment in Fe₂O₃* for the same samples is consistent with this observation and suggests that the high TiO₂ contents are inherited from a parental magma unique to the southern locality. Spatially-related dacites and rhyolites from the southern locality do not, however, display TiO₂ contents significantly different from the average trend of HFF lavas.

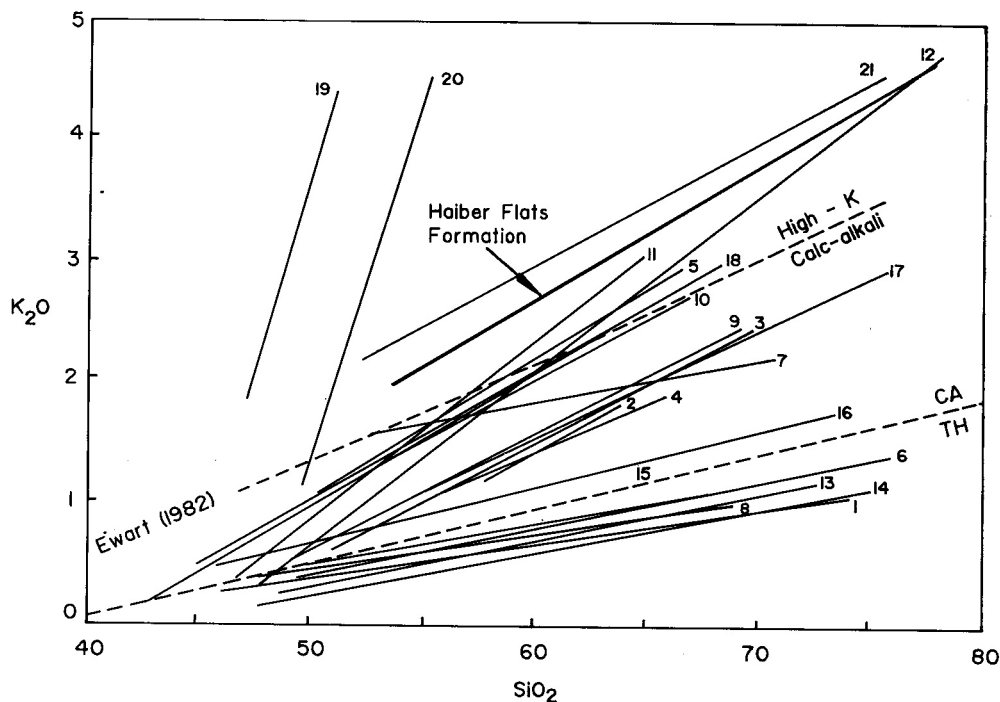


Fig. C.25: Plot of SiO_2 vs. K_2O illustrating average trends for the HFF (bold line) and other volcanic suites. Boundaries between tholeiitic (TH), calc-alkali (CA) and high-K fields are according to Ewart (1982). Trends 1-18 are for Cenozoic suites in the circum-Pacific region (Gill, 1970). 19 = shoshonitic suite of Fiji (Gill, 1970), 20 = shoshonitic lavas of the Barby Formation (Watters, 1974), 21 = "southern area" of the Barby Formation (Brown and Wilson, 1986).

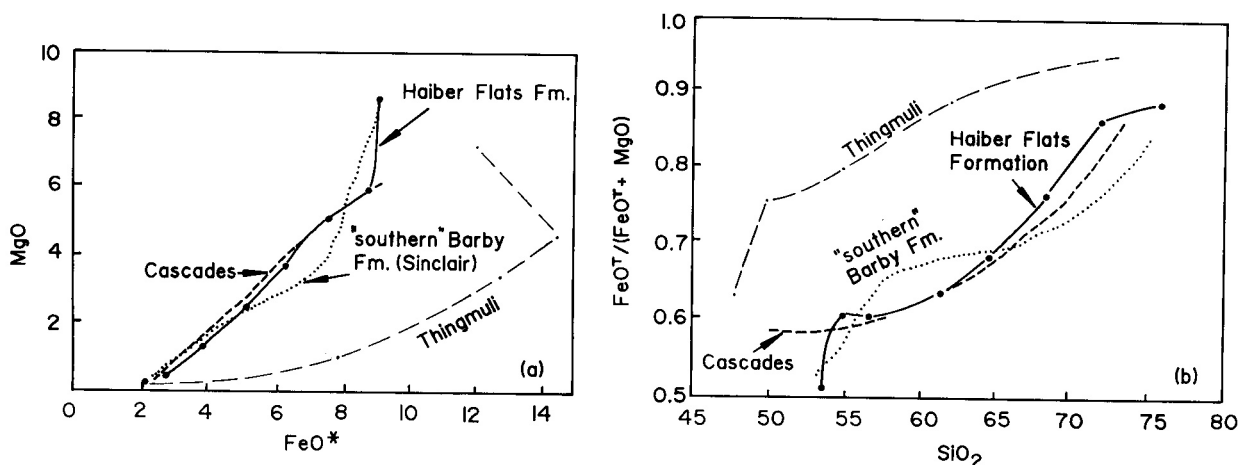


Fig. C.26: Plots of (a) FeO^* vs. MgO , and (b) SiO_2 vs. $\text{FeO}^*/(\text{FeO}^* + \text{MgO})$. FeO^* = total Fe as FeO ; $\text{FeO}^T = \text{FeO} + \text{Fe}_2\text{O}_3$. Filled circles represent averages for HFF data according to the silica categories used by Ewart (1979; 1982). Average trends are also illustrated for the calc-alkaline "southern" Barby Formation (Brown and Wilson, 1986) and Cascades suites (Carmichael, 1964), and the tholeiitic Thingmuli suite (Carmichael, 1964).

(b) Aluminium

Al_2O_3 shows a consistent decrease with increasing SiO_2 for dacites and rhyolites, but significant "scatter" for basaltic andesites. The southern locality basaltic andesites which display TiO_2 enrichment are also characterised by relatively high Al_2O_3 contents. The abundance of plagioclase phenocrysts in these lavas suggests that the observed Al_2O_3 enrichment may be the result of plagioclase accumulation. However, this is not consistent with the absence of sympathetic CaO enrichment and depletion in MgO . The relatively low Al_2O_3 (13.1%) of sample BH 598 from the central locality probably reflects its more primitive nature ($> 10\%$ MgO).

(c) Iron

Fe_2O_3^* decreases consistently with increasing SiO_2 except for a single basaltic andesite sample (BH 509) from the southern locality. This highly plagioclase-phyric sample also shows enrichment in Al_2O_3 and Na_2O , which may suggest dilution of ferromagnesian oxides by plagioclase accumulation. However, the absence of sympathetic enrichment in CaO and depletion in MgO cannot be reconciled with a model of plagioclase accumulation. If the relatively low K_2O content displayed by BH 509 is the result of leaching, then the possibility exists that the Fe_2O_3^* content may have been similarly affected.

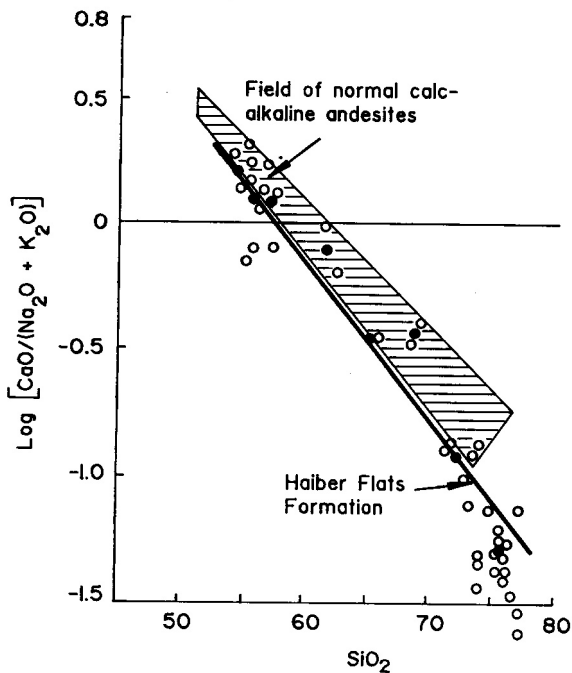


Fig. C.27: Silica vs. calc-alkaline ratio plot for the HFF eruptive rocks. Open circles = all data; filled circles = averages according to silica categories used by Ewart (1979, 1982). Bold line = regression line for HFF data. Field of normal calc-alkaline andesites is from Brown (1982).

(d) Magnesium

While the overall negative correlation of MgO with SiO₂ is well established, it is noted that four samples of basaltic andesite from the central and northern localities may be classified as “high-Mg” (i.e. > 6% MgO according to Gill, 1981, p. 110). Three of these samples are aberrant, viz. BH 692, 604 and 598, and may owe their elevated MgO contents to the accumulation of ferromagnesian minerals. Sample BH 692 from the northern locality shows relict augite cores and enrichment in CaO as well as MgO, but no sympathetic enrichment in Fe₂O₃*. These features may be explained by clinopyroxene accumulation in view of the relatively high MgO/FeO* ratio and CaO content of augite.

Samples BH 604 and 598 from the central locality are metamorphic in character and original ferromagnesian minerals are no longer preserved. However, clinopyroxene is unlikely to be the accumulated phase since only MgO is enriched in these samples and not CaO. Orthopyroxene accumulation would, on the other hand, explain these features due to its relatively high MgO/FeO* ratio and low CaO content. The possible occurrence of pseudomorphs after olivine in BH 598 suggests that olivine may also have been accumulated despite the oversaturated nature of this lava.

(e) Calcium and the alkalis

CaO contents decrease fairly regularly with increasing SiO₂ and vary inversely with alkalis. The scatter in the alkalis, especially Na₂O, may be the result of mobility in response to alteration. Primary variation in K₂O at a particular SiO₂ content has been reported for ejecta from single volcanoes (e.g. Gorton, 1977) and is typically the result of different magma sources. In the HFF lavas K₂O demonstrates a greater rate of increase in the passage from basaltic andesite

to rhyolite than Na₂O, thereby resulting in an increase in K₂O/Na₂O ratios with increasing SiO₂.

(j) Manganese and phosphorus

MnO and P₂O₅ contents both exhibit significant variability with the aberrance of rhyolite sample BH 504 being particularly pronounced. While both MnO and P₂O₅ would be enriched by the accumulation of manganiferous apatite, an accompanying enrichment in CaO is not observed. Similarly, accumulation of ilmenite cannot explain the enrichment in MnO in view of the average contents of Fe₂O₃* and TiO₂ displayed by BH 504. One possible reason for this scatter is that both Mn and P contents in rhyolites are close to 0.1% (1000 ppm) and may, therefore, be acting as dispersed trace elements.

4.3.1.3 Trace element variation

(i) Variation diagrams

A total of 21 trace elements are plotted against SiO₂ in Fig. C.29. While 17 samples have been analysed for only 16 trace elements, REE analyses (apart from La, Ce, and Nd) have been determined for a further 3 samples (Appendix II). The latter are presented in Section (ii).

Some degree of scatter is evident in virtually all of the variation diagrams, which is hardly surprising considering that the HFF lavas have been subjected to both greenschist metamorphism and deformation in their ca. 1000 Ma history. Nevertheless, the database (n=41) is considered sufficient to define average trends for most elements and so provide a means of characterising the magmatic evolution of these lavas.

Systematic description of the trace elements has been organised according to groups of elements which display similar chemical affinities (cf. Gill, 1981).

(a) K-group: Ba, Cs, Rb and Sr

The elements of this group (except Ba and Cs) both increase and decrease in concentration with increasing SiO₂. While the erratic behaviour of Ba may be the result of alteration, the low levels of Cs present do not invite further comment. If K-metasomatism has taken place, the presence of secondary biotite and K-feldspar suggest that one might expect a greater enrichment in Ba due to its ionic similarity to K (Mason, 1966, p. 134). While the generally high contents of green biotite in basaltic andesite samples BH 500 and 501 appear to support this possibility, no obvious petrographic differences can be used in the rhyolites to characterise high- and low-Ba groups. However, silicification and recrystallisation in the rhyolites do appear to be more commonly associated with low Ba contents, e.g. high-silica rhyolites of the central locality.

One indication that the Ba contents of several samples may be original is the much smaller degree of scatter displayed by the same samples on plots of both K₂O and Rb versus SiO₂. Erratic variation of Ba has been reported from modern (unaltered) volcanics, especially acid members of calc-alkaline suites (Arculus, 1976; Gill, 1981), thus confirming that alteration need not be invoked in the case of the HFF.

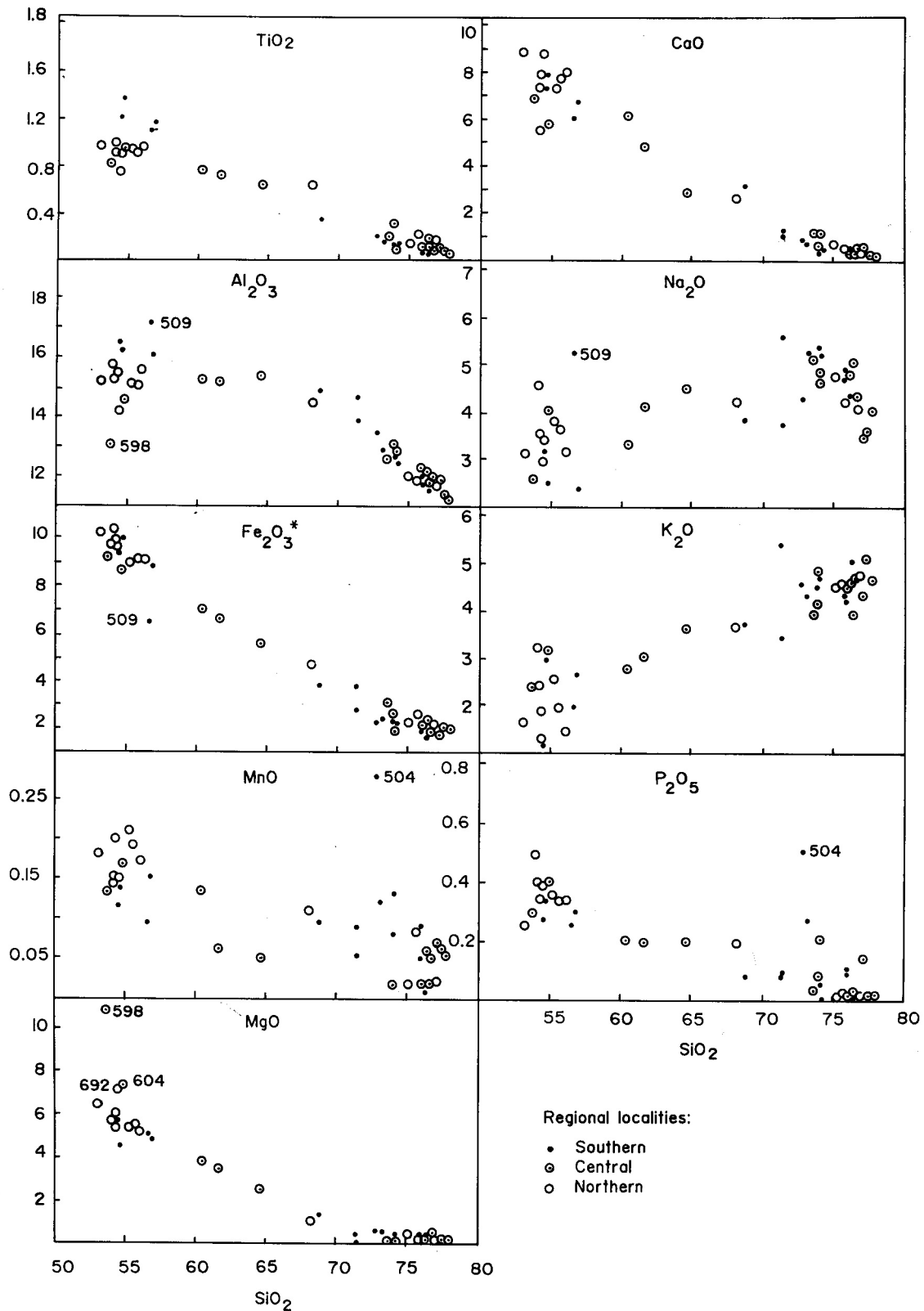
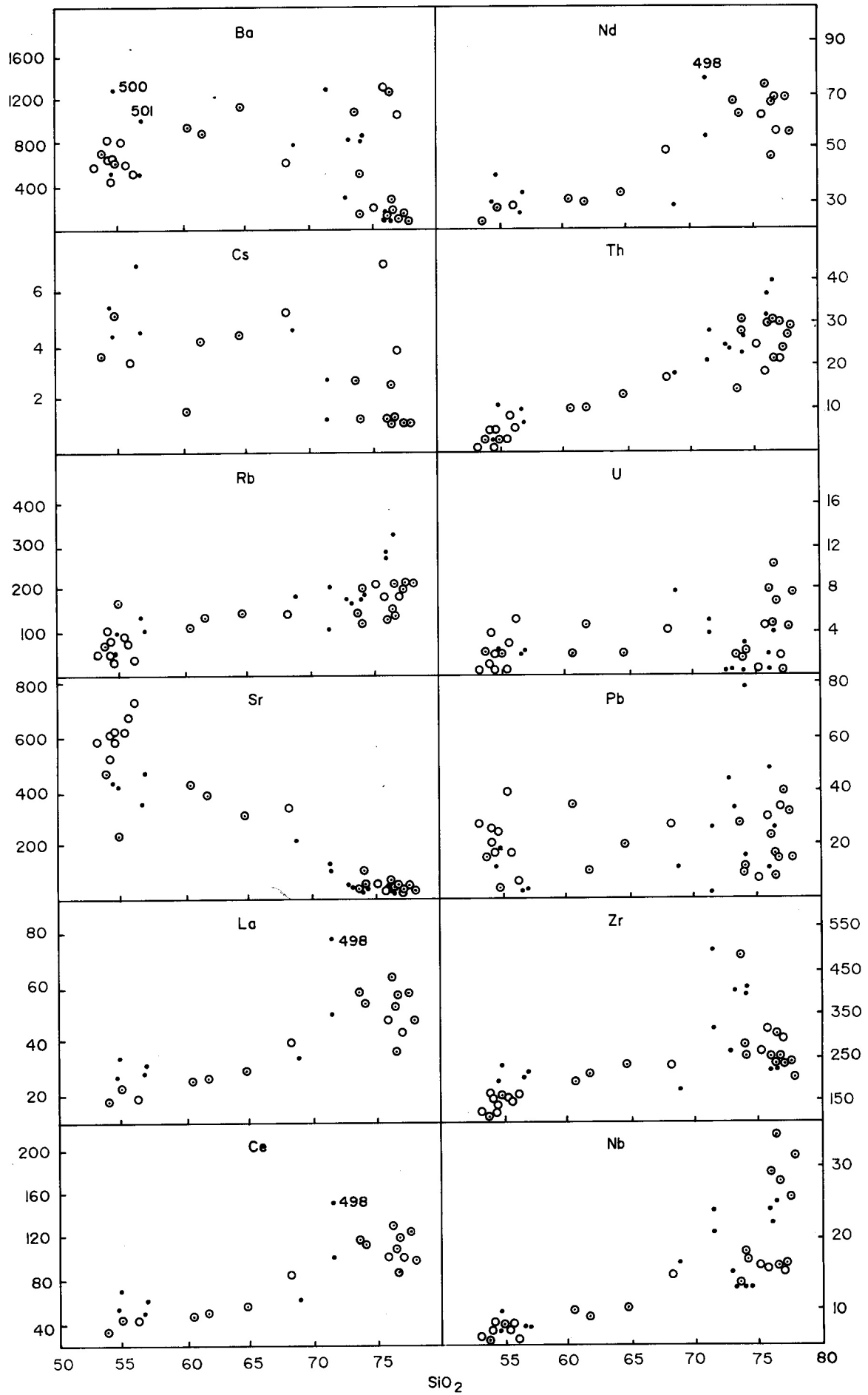


Fig. C.28: Harker diagrams for the HFF volcanic succession with different symbols for the southern, central and northern localities, or centres. Aberrant samples are numbered.

Rb displays a gradual increase from basaltic andesite (50 ppm) to rhyolite (200 ppm) and closely resembles the variation pattern of K_2O .

Sr shows an overall decrease with increasing SiO_2 , despite a steep increase from basaltic andesite to low-silica

andesite in lavas of the northern locality. The latter trend reflects an approximate inverse correlation between Sr and K, but similar trends described by Gunn (1974) are regarded by Gill (1981) as being anomalous and the result of inexplicable Sr enrichment. In general, the significant decrease



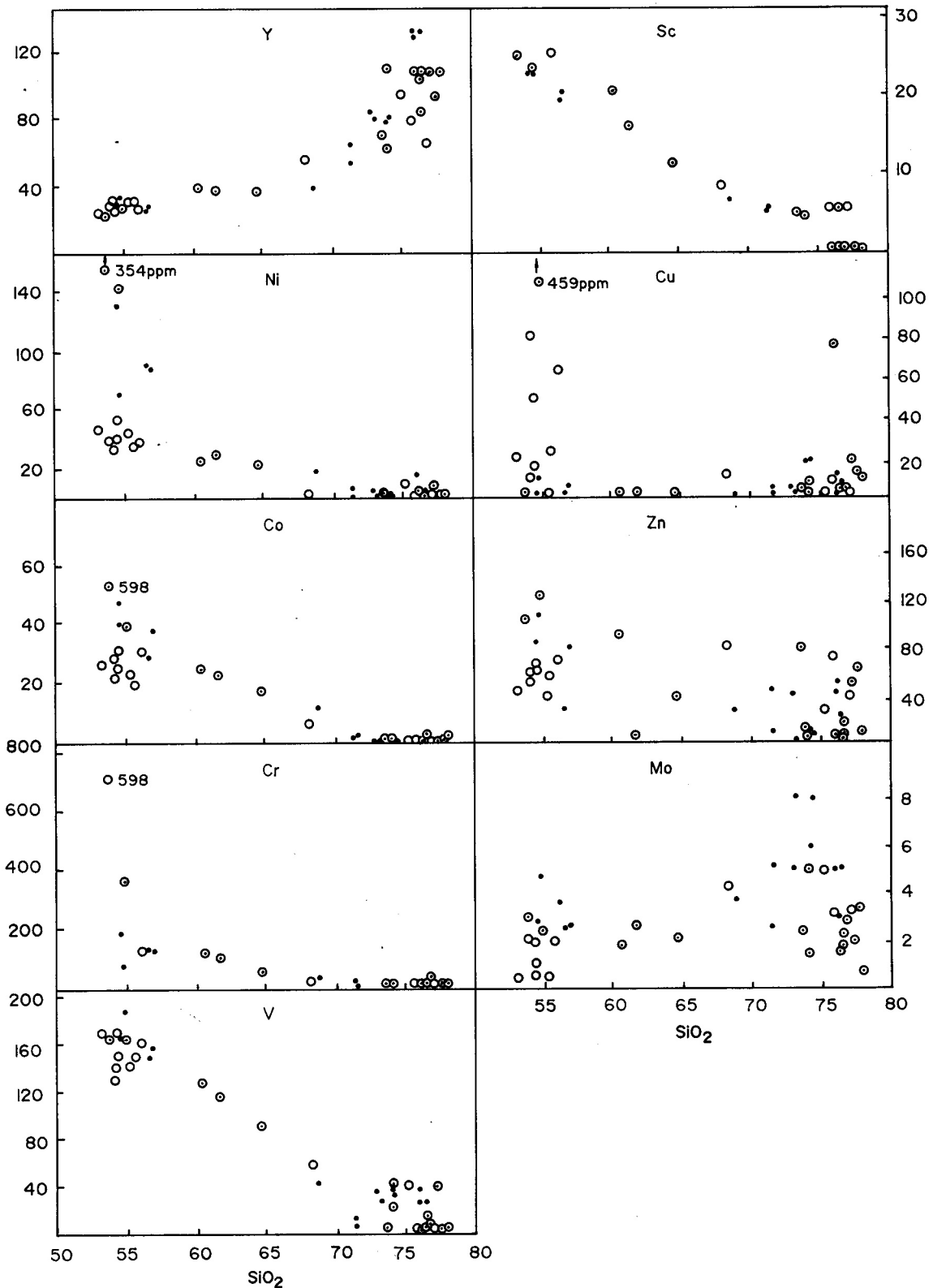


*Fig. C.29: Trace element variation diagrams for the HFF volcanic succession. Silica used as abscissa and symbols as for Fig. C.28. * Continued from previous page.

in concentration of Sr with increasing silica is indicative of advanced magmatic differentiation, typically the result of feldspar fractionation.

(b) LREE Group: La, Ce and Nd

Light REE exhibit similar increases with increasing SiO_2 , the non-pyroclastic rhyolite BH 498 showing abnormal

enrichment in La, Ce and Nd. Such enrichment may be due to an accumulated accessory phase such as sphene or zircon.

(c) Th-group: Th, U and Pb

Th exhibits a significant increase with increasing SiO_2 , while no obvious trend can be seen for either U or Pb. Th

concentrations also increase from northern to southern localities, central locality abundances being typically intermediate in value. U abundances are known to be especially sensitive to crustal thickness (Dupuy *et al.*, 1976) implying that crustal involvement may be responsible for much of the scatter shown by U (and possibly also Pb).

(d) *HFSE-group: Zr, Nb and Y*

Since these elements are characterised by high ratios of charge to ionic size, one would expect their concentrations to increase with increasing SiO₂ due to an incompatible nature with regard to most common minerals. This is indeed the case, although significant scatter tends to occur at high SiO₂ values. At least some of the Zr enrichment in the rhyolites may be the result of zircon accumulation and in this respect it is important to note that the highest Zr abundance occurs in the same sample that also displays significant enrichment in LREE, viz. BH 498. Also of interest is the more Zr-rich nature of southern locality basaltic andesites, a group already distinguished by its relatively high concentrations of Ti, Al, and LREE. Both Nb and Y exhibit pronounced increases with increasing SiO₂, trends being particularly steep in the passage from dacite to high-silica rhyolite.

(e) *Compatible Group: Ni, Co, Cr, V and Sc*

All the compatible elements exhibit a pronounced decrease with increasing SiO₂. Ni, Co and Cr are particularly enriched in the high-Mg basaltic andesite BH 598 and there is an approximate decrease in these elements for basaltic andesites from the central, via the southern, to the northern localities. The regional diversity in Ni for basaltic andesites is difficult to explain in view of current uncertainty with regard to the relative importance of differences in source compositions as opposed to differentiation processes (Gill, 1981, p.135).

Co shows less variation compared with Ni, decreasing from 53 to 0 ppm between high-Mg basaltic andesite and rhyolite.

Cr, like Ni, shows significant enrichment in basaltic andesites of the central locality (362-712 ppm) when compared with the southern (185-78 ppm) and northern (130 ppm) localities.

V decreases regularly with increasing SiO₂, a feature regarded by Gill (1981, p. 137) as typical of suites which are characterised by modest or no iron-enrichment. Considerable variability in V (4-40 ppm) is evident in rhyolites of the HFF, and may be the result of slightly different magnetite contents, possibly due to variation in oxygen fugacity. The slight scatter shown by the major oxides TiO₂ and Fe₂O₃ * at high SiO₂ contents is not inconsistent with the latter observation, since extremely high partition coefficients have been reported for V in magnetite from high-silica rhyolite (e.g. Kd ≈ 500; unpublished compilation by Ewart and Duncan).

Sc shows a regular decrease with increasing SiO₂ from 25 to 0 ppm. Apparent bimodality (scatter?) in Sc abundances at high silica contents in the HFF may be a consequence of mineralogical control, e.g. magnetite in which Kd's for Sc show significant variability.

(j) *Chalcophile Group: Cu, Zn and Mo*

Cu, Zn and Mo all vary irregularly with increasing SiO₂ content, although there is a suggestion of a positive correlation between Mo and SiO₂. The occurrence of malachite staining at the central locality suggests that Cu mineralisation is probably responsible for the relatively high Cu contents obtained for samples of basaltic andesite (459 ppm) and rhyolite (77 ppm) at this locality. Irregular variation of the chalcophile elements contrasts with the relatively coherent trends displayed by the compatible elements and may, therefore, suggest that the former do not owe their distribution to magmatic processes. Similar scatter shown by Pb suggests that hydrothermal processes, possibly magma-driven, may be a common factor controlling the distribution of these elements. Significantly, andesite volcanic provinces are also frequently Cu-Pb-Zn-Mo-Ag-Au metallogenic provinces (Gill, 1981, p. 137).

Mo abundances in the HFF volcanics are difficult to assess in view of the low concentrations (close to the lower limit of detection) and the paucity of published data, but values for "andesites" (*sensu lato*) in the southern and central localities generally exceed the 0.5-2.5 ppm range reported in the literature (Taylor and White, 1966; Taylor *et al.*, 1969; Peccerillo and Taylor, 1976). Mo values for the northern locality "andesites" typically fall within the quoted range for andesites.

(ii) *REE*

(a) *Description*

Chondrite-normalised REE patterns for eruptive rocks of the HFF and Sinclair Sequence are presented in Fig. C.30 (chondritic values after Taylor and Gorton, 1977). The stability of REE patterns in relatively unaltered rocks (Humphris, 1984) permits their use in the characterisation of different magma types represented in the HFF. The three samples analysed for the REE La, Ce, Nd, Sm, Eu, Gd, Tb, Yb and Lu are discussed below.

High-Mg basaltic andesite (BH 598)

This pattern displays LREE enrichment ($La_N/Lu_N = 4.8$; $La_N/Sm_N = 2.3$) and a fairly flat, slightly concave, slope for HREE ($Tb_N/Yb_N = 1.1$; $Yb_N/Lu_N = 0.9$). A slightly negative Eu anomaly is present ($Eu/Sm = 0.69$; $Eu/Eu^* = 0.85$) and HREE enrichment is 10 to 12 times chondritic.

Acid basaltic andesite (BH 690B)

The overall pattern is remarkably similar to that for high-Mg basaltic andesite, but with overall REE enrichment being consistently higher by between 10 and 30%. Normalised inter element ratios indicate LREE enrichment ($La_N/Lu_N = 5.7$; $La_N/Sm_N = 2.2$), a flat slope for HREE ($Tb_N/Yb_N = 1.2$; $Yb_N/Lu_N = 1.0$) and a slightly negative Eu anomaly ($Eu/Sm = 0.68$; $Eu/Eu^* = 0.85$). HREE enrichment is 12 to 15 times chondritic.

High-silica pyroclastic rhyolite (BH 669)

Although the ratios $La_N/Lu_N = 4.4$ and $La_N/Sm_N = 2.8$ for this rhyolite are of a similar order to the andesites (*sensu lato*), overall REE enrichment is between 70 and 120%

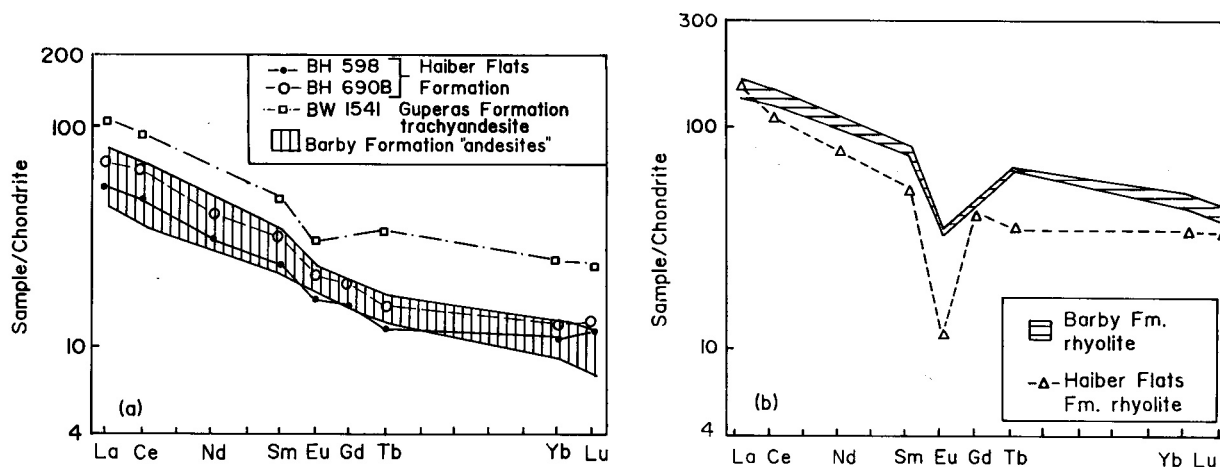


Fig. C.30: Chondrite-normalised REE patterns for the HFF volcanic succession compared with patterns for (a) “andesites” (*sensu lato*) in the Barby and Guperas Formations, and (b) rhyolites in the Barby Formation. Shaded areas represent envelopes of patterns.

higher. The HREE pattern is flat ($Tb_N/Yb_N = 1.0$; $Yb_N/Lu_N = 1.0$), while HREE enrichment is between 33 and 35 times chondritic. The most pronounced feature of this pattern is the large negative Eu anomaly ($Eu/Sm = 0.21$; $Eu/Eu^* = 0.24$).

(b) *Comparison of REE between lavas of the Haiber Flats, Barby and Guperas Formations*

Unpublished REE data from A. Kröner (made available by D.L. Reid, 1987) have been used to compare the REE abundances in lavas of the HFF with those of the Barby and Guperas Formations in the Sinclair Sequence. The following important features are illustrated by Fig. C.30:

- REE patterns for the HFF basaltic andesites generally fall within the envelope of patterns for compositionally similar extrusives in the Barby Formation.
- A single pattern for Guperas Formation trachyandesite displays a similar slope ($La_N/Lu_N = 4.7$) to patterns for the HFF and Barby Formation, but overall enrichment in REE, especially HREE, is more pronounced.
- HFF rhyolite shows a REE pattern which differs in shape and overall enrichment from the envelope of patterns displayed by rhyolites in the northern part of the Barby Formation. By comparison with HFF rhyolite, the latter envelope is not as steep ($La_N/Lu_N = 3.5$ compared with 4.4) and has a less pronounced negative Eu anomaly ($Eu/Sm = 0.43$ compared with 0.21). Significantly, these “northern Barby Formation” rhyolites form part of a bimodal tholeiitic suite which Brown and Wilson (1986) consider to display compositional similarities to the younger Guperas Formation.

4.3.1.4 *Comparison of Haiber Flats Formation (HFF) lavas with younger volcanic suites*

(i) *The HFF volcanic suite*

The different chemical characteristics of mafic and felsic lavas in the HFF and the paucity of lavas of intermediate composition together suggest that bimodality may reflect differences in source derivation. While this aspect forms

the subject of a more detailed discussion in Section C.6 (Petrogenesis of the HFF), mafic and felsic lavas will be discussed separately in sections (ii) and (iii) in order to facilitate their comparison with published data.

(a) *Major and trace element abundances*

Major elements

- Low TiO_2 contents (typically $< 1.0\%$) in the HFF are characteristic of volcanic rocks (especially basalts and andesites) erupted at convergent plate boundaries (Chayes, 1964; Gill, 1981).
- Overall variation in Al_2O_3 for most basaltic andesites and andesites is within the range of “arc tholeiites and orogenic andesites” (Gill, 1981, p. 112).
- K_2O abundances compare favourably with values reported from high-K eruptives in active continental margins of the western USA and Mediterranean (Ewart, 1979, 1982).
- High SiO_2 and alkalis, combined with low MgO and CaO , in the HFF rhyolites resemble rhyolites of anorogenic bimodal associations or orogenic rhyolites of the western USA (Ewart, 1979).

Trace elements

- The absolute abundances of Rb (50 - 200 ppm in basaltic andesite to rhyolite) are typical of high-K calc-alkaline volcanic suites described by Jakeš and White (1972) and Ewart (1979, 1982).
- The decrease in Sr in acid andesites of the central locality is typical of high-K suites (Gill, 1981), while the overall abundances of Sr in basaltic andesites and low-silica andesites are comparable with those reported from medium- to high-K suites.
- Absolute abundances of LREE and La_N/Ce_N ratios (≈ 1.3) in HFF andesites (*sensu lato*) are similar to published values for high-K suites (Masuda *et al.*, 1975; Gill, 1981).
- Despite some scatter, overall abundances of Th-group elements are high, even for high-K suites (Jakeš and Smith, 1970; Gill, 1981).

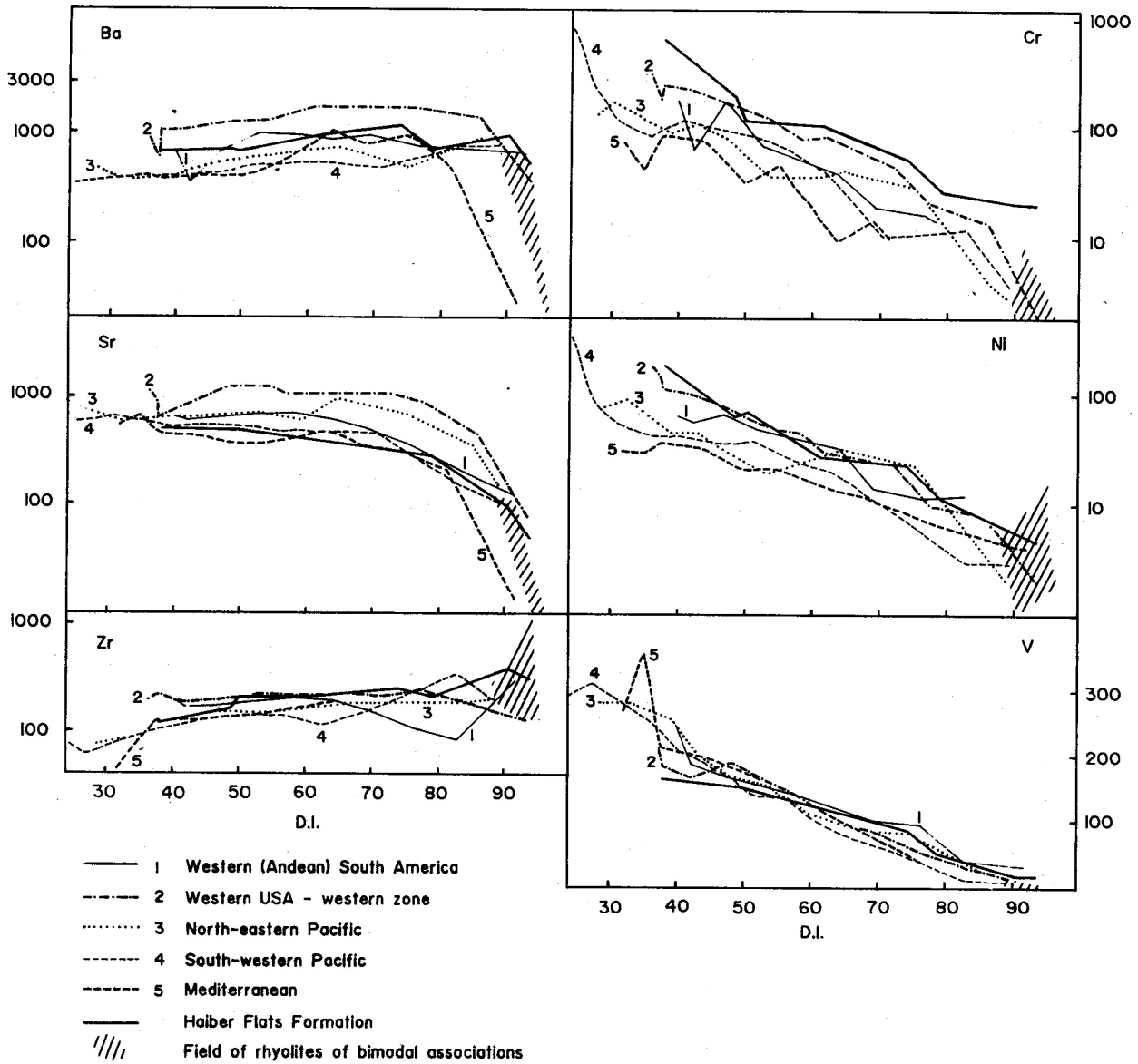


Fig. C.31: Averaged trends (according to Table C.4) of selected trace elements against differentiation index (DI) for the HFF (bold line) compared with various orogenic subregions (Ewart, 1982). Also illustrated are fields for rhyolites of bimodal associations (modified from Ewart, 1979).

- Zr contents for the average trend are high (100- 300 ppm) and comparable with values reported for high-K volcanic suites (Jakeš and White, 1972; Ewart, 1979, 1982).

- While Nb abundances (13-34 ppm) for HFF rhyolites are generally within the range of high-K suites elsewhere (e.g. western belt of the western USA; Ewart, 1979), Y abundances (33-131 ppm) for the same lavas are noticeably higher than for typical "orogenic volcanic suites". Abundances of Nb (5-10 ppm) and Y (22-39 ppm) in the basaltic andesite-andesite range are, however, typical of high-K calc-alkaline volcanic suites reported by the same workers.

- Ni contents for basaltic andesites of the central (143-354 ppm) and southern (71-132 ppm) localities are high compared with Ni contents of calc-alkaline lavas, even high-K suites (cf. Jakeš and White, 1972). Excluding the high-Mg sample BH 598, the overall variation in Ni from basaltic andesite to rhyolite (143 to 0 ppm) is not unlike the varia-

tion reported for other calc-alkaline volcanic suites of Proterozoic age (e.g. 100 to 0 ppm in the Haib lavas; Reid, 1977).

- Average Co contents for the basaltic andesite-andesite range are generally less than 40 ppm and hence within the range of "orogenic andesites" reported by several workers (e.g. Gill, 1981, p. 136; Ewart, 1982).

- With the exception of the high-Mg basaltic andesite, andesites (*sensu lato*) display Cr contents which compare favourably with values reported for medium- to high-K andesites (Gill, 1981, p. 101; Ewart, 1982). Cr contents (16-34 ppm) for the HFF rhyolites are less depleted compared with Ni, but resemble similar values reported by Ewart (1979) for rhyolites from the Mediterranean region.

- V contents for basaltic andesites of the different localities do not vary significantly (159 ± 15 ppm) and fall within the range of values reported for medium- to high-K calc-alka-

line andesites (Gill, 1981).

- Sc values range from 25 to a ppm, the more mafic flows falling within the range 40-10 ppm reported by Gill (1981, p. 137) for basic-acid orogenic andesites.

- Absolute abundances of chalcophile elements are difficult to assess in view of significant scatter, but both Cu and Zn are within the range of values reviewed for calc-alkaline "orogenic" suites (Ewart, 1979, 1982).

(b) Trace element trends

Fig. C.31 illustrates averaged trends (according to Table CA) of Differentiation Index (DI) versus the elements Ba, Sr, Zr, Cr, Ni and V for the HFF compared with averaged trends for orogenic volcanic suites compiled by Ewart (1982). Volcanic suites were selected from western (Andean) South America, the western zone of western USA, northeastern Pacific) southwestern Pacific and the Mediterranean region. Also illustrated are the approximate compositional fields occupied by rhyolites of bimodal basalt-rhyolite associations which have been constructed from data compiled by Ewart (1982) for volcanic centres in the USA, Iceland, western Scotland and northern Ireland, southern Queensland (Australia) and Papua New Guinea.

The grouping of Ba, Sr and Zr is related to the tendency for these elements to follow K during geochemical processes (Ewart, 1982). The HFF displays a general increase in Ba from basaltic andesite to dacite followed by a decrease at higher DI which is similar to trends in both the western USA and western South America while the overall abundances are closer to the latter. Sr in the HFF shows a general decrease which again resembles the trend for western South America, while overall abundances are similar to those of the southwestern Pacific. The marked depletion in Sr at high DI is also typical of both the western USA and Mediterranean rhyolites. Zr exhibits an irregular increase with increasing DI which is similar to the pattern displayed by the western USA at intermediate DI, but only decreases at significantly higher DI. The increase in Zr in the HFF to an abundance peak at $DI \approx 91$ most closely resembles the late-stage increase in Zr (at $DI \geq 85$) displayed by rhyolites

from the northeastern Pacific.

The grouping of Cr, Ni and V is related to the almost universal depletion of these elements with increasing DI in the various orogenic subregions (Ewart, 1982). The HFF trend is characterised by high overall abundances of Ni and Cr which resemble the abundances displayed by lavas of the western USA. The pattern of depletion in these elements with increasing DI is also similar to the western USA, but differs in the less marked depletion of HFF lavas at high DI (≈ 80). V in the HFF lavas displays a pattern with increasing DI which is intermediate between the patterns displayed by lavas of western South America and the western USA.

Rhyolites (*sensu stricto*) of the HFF generally display abundances of the above elements which fall within, or close to, the fields of rhyolites of bimodal associations (Fig. C.31). The major deviations are in the relative enrichments displayed by the HFF for Ba, Sr (to some extent), Cr and V. However, the use of average abundances in compiling trends and the probable mobility of K-group elements under metamorphic conditions allow for the possibility that the HFF rhyolites form part of an anorogenic bimodal association of volcanics. The difficulty in using these compositional fields to determine the magmatic association of rhyolites in general is illustrated by the overlap between these fields and high DI lavas of many orogenic volcanic suites. Furthermore, high-silica biotite rhyolites of the western USA display many of the chemical characteristics of rhyolites of the bimodal associations (Ewart, 1979).

(c) Trace element abundance patterns

While enrichment in K is well established for most lavas of the HFF, certain element abundances are more typical of calc-alkaline lavas, e.g. Sr. Ewart (1982) has shown that low-K, calc-alkaline, high-K and shoshonitic series occupy fairly distinct fields on a diagram of K/Rb ratio against K_2O . In Fig. C.32a, these parameters illustrate that data for the HFF is predominantly high-K in character, with some scatter of data into the calc-alkaline field. The problem of stability of K-group elements during alteration may be partly overcome by using the elements Ti and V, which have been

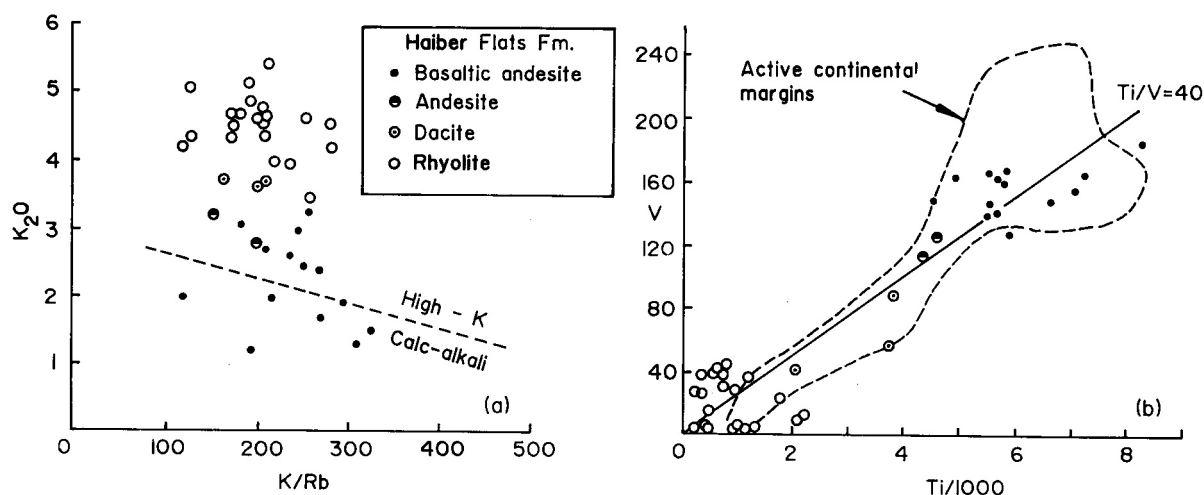


Fig. C.32: Plots of (a) K/Rb vs. K_2O , and (b) Ti vs. V for data of the HFF eruptive rocks. Boundary between calc-alkali and high-K fields in (a) is modified from Ewart (1982); field of active continental margin volcanics in (b) is compiled from data in Shervais (1982).

shown to be stable over a wide range of temperatures and water/rock ratios (Shervais, 1982). On a plot of Ti versus V (Fig. C.32b), data for the HFF show considerable scatter towards the origin (felsic lavas) but away from the origin an approximate trend with $Ti/V \approx 40$ is evident in the more mafic lavas. This ratio is somewhat higher than the calc-alkaline series eruptives reviewed by Shervais (1982), but may be attributed to magnetite fractionation.

(ii) HFF mafic lavas

For convenience three individual samples within the mafic volcanic succession are chosen for discussion, viz. high-Mg basaltic andesite (BH 598), acid basaltic andesite (BH 690B) and andesite (BH 574).

(a) Trace element "spidergrams"

MORB-normalised patterns for these samples are compared with predominantly high-K and calc-alkaline basalts from active continental margins in central Chile, the western USA and Iran (Fig. C.33). Despite the overall similarity between these patterns, the HFF mafic lavas display the following distinctive features:

- A pronounced negative P anomaly which is below the range of most modern continental margin lavas and is also lower than MORB. This depletion may be the result of apatite fractionation.
- A pronounced negative Ti anomaly which is again below the range of the lavas under review, although high-K andesite from Iran does exhibit considerable depletion as well. The low Ti abundance is probably the result of magnetite fractionation.

Not unexpectedly, the HFF basaltic andesitic to andesitic lavas show a more fractionated nature than their basaltic counterparts from Phanerozoic active continental margins. Nevertheless, the overall patterns are similar and by analogy indicate both a within-plate source contribution (high concentrations of Nb relative to Zr and Zr relative to Y and Yb) as well as a subduction component (selective enrichment in Sr, K, Rb, Ba, Th, Ce and Sm) as discussed by Pearce (1983). While the involvement of continental crust cannot be excluded from a genetic model for the more siliceous andesites, a "mantle" isotopic signature (Section C.6) precludes crustal contamination for the basaltic andesites. A similar conclusion was reached with respect to the petro-

genesis of the Chilean basalts (Pearce, 1983).

Sample BH 598 merits special attention in that it is compositionally a high-Mg basaltic andesite which is characterised by several features displayed by so-called "type-E high-Mg andesites" from Cape Vogel, Papua New Guinea (Jenner, 1981), viz. $La_N/Yb_N \approx 3-7$ (BH 598 ≈ 5), $Zr/Nb \approx 19$ (BH 598 ≈ 22) and a marked depletion in Ti relative to Zr and Y. "Boninites", as defined by Bailey (1981), Hickey and Frey (1982) and Bloomer and Hawkins (1987), are characterised by lower TiO_2 ($< 0.6\%$), flatter and less enriched REE patterns, and less enrichment in LILE. However, certain inter element ratios do suggest a boninitic affinity for sample BH 598, e.g. $Ti/Zr \approx 43$ (< 100 in boninites), $Y/Zr \approx 0.2$ (< 0.4 in boninites).

The early eruption of high-Mg basaltic andesite in the HFF and its subsequent deformation and metamorphism are compatible with the timing and occurrence of high-Mg andesites in the Bonin Islands and Marianas Trench. Here these lavas have been associated with the early stages of development of subduction zones or back-arc basins (cf. Karig and Moore, 1975; Cameron *et al.*, 1979). Chemical deviations in sample BH 598 from "typical boninite" could be the result of a within-plate and/or crustal contribution and may consequently provide indirect support for the similarity between the mafic lavas of the HFF and basalts from active continental margins.

(b) REE patterns

Basaltic andesites of the HFF exhibit REE abundances which fall within the range of "orogenic" andesites reviewed by Cullers and Graf (1984), although individual patterns plot within the zone of overlap between continental andesites associated with subduction zones and island-arc andesites.

When compared with specific volcanic suites in Fig. C.34a and b, the REE pattern of HFF acid basaltic andesite most closely resembles those patterns displayed by the high-K San Pedro volcano in the north Chilean Andes (Thorpe *et al.*, 1976). The less enriched nature of high-Mg basaltic andesite is, however, more typical of medium-K "orogenic" andesites from Ancud in central-south Chile (Lopez-Escobar *et al.*, 1976). Significantly, both San Pedro and Ancud are situated along the Andean plate margin and may be regarded as continental andesitic volcanoes associ-

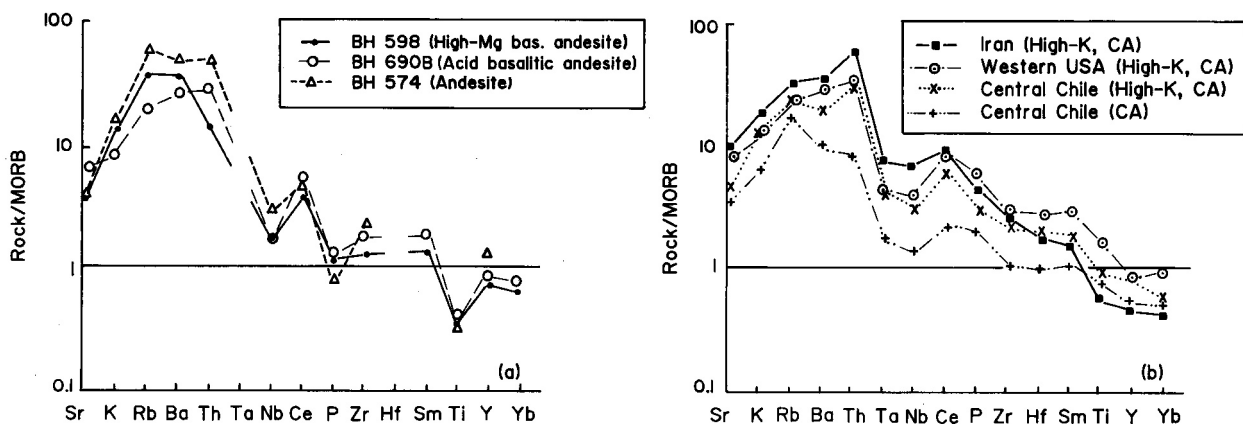


Fig. C.33: MORB-normalised minor and trace element variation diagrams for (a) HFF "andesites", and (b) calc-alkaline and high-K basalts and andesites from various orogenic continental margins. Normalising abundances and comparative data from Pearce (1982, 1983).

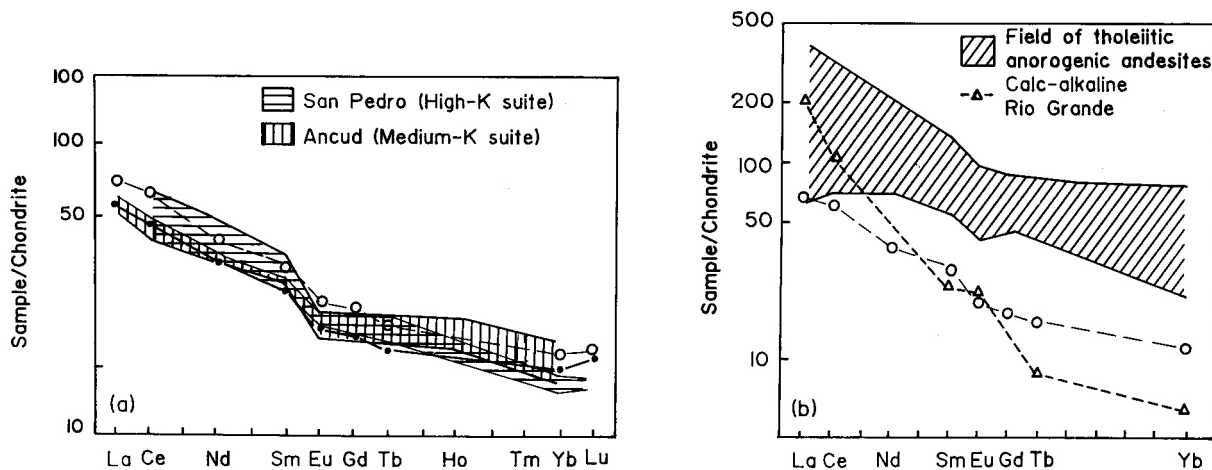


Fig. C.34: Chondrite-normalised REE patterns for HFF basaltic andesites (filled and open circles) compared with patterns from (a) orogenic volcanics at San Pedro (high-K) and Ancud (medium-K) volcanoes in Chile (Lopez-Escobar *et al.*, 1976), and (b) anorogenic tholeiitic and calc-alkaline (Rio Grande) volcanics compiled by Gill (1981). Symbols as in Fig. C.33 (a).

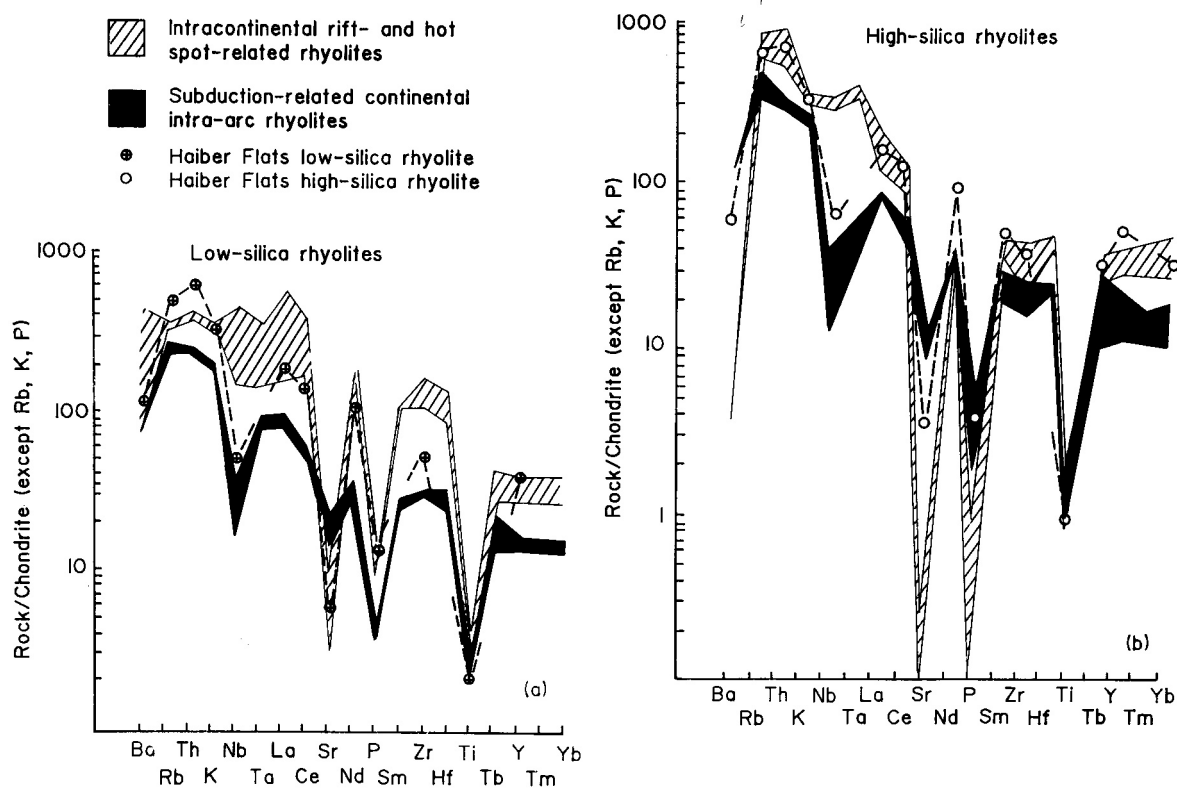


Fig. C.35: Chondrite-normalised minor and trace element variation diagrams for (a) average low-silica (70-75 wt.%), and (b) average high-silica (> 75 wt.%) HFF rhyolites following the procedure of Thompson *et al.* (1984). Envelopes for intracontinental and subduction-related rhyolites are modified from Sylvester *et al.* (1987).

ated with a subduction zone. It is important to note not only the similarities of HFF “andesites” to more recent medium- to high-K “orogenic” andesites, but also their differences when compared with REE patterns for both tholeiitic and calc-alkaline “anorogenic” andesites (Fig. C.34b) reviewed by Gill (1981, p. 129).

(iii) HFF felsic lavas

(a) Trace element “spidergrams”

Averages are considered here for both low- (70-75% SiO₂) and high-silica (> 75% SiO₂) rhyolites in the HFF in

order to facilitate their comparison with rhyolitic ash-flow tuffs from selected Cenozoic terranes reviewed by Sylvester *et al.* (1987). The Cenozoic rhyolites considered by these workers constitute two groups, viz. intracontinental rift- or hot spot-related rhyolites and subduction-related continental intra-arc rhyolites.

Using the procedure of Thompson *et al.* (1984), chondrite-normalised patterns for HFF rhyolites are compared with patterns for Cenozoic rhyolites in Fig. C.35. The following features are illustrated:

- Both low- and high-silica rhyolites in the HFF exhibit an overall chemical similarity to the intracontinental rift- or

hot spot-related rhyolite suites.

- Low-silica rhyolites in the HFF exhibit similarities to subduction-related rhyolites with regard to the elements Ba, Nb, Zr and Ti.

- High-silica rhyolites in the HFF exhibit similarities to subduction-related rhyolites with regard to the elements Ba, Nb, Sr and P.

The difficulty in applying these chemical characteristics may be related to either the highly fractionated nature of the HFF rhyolites or the expected heterogeneity if these rhyolites represent crustal melts. Subtle alteration may be an additional problem with respect to such elements as Ba, Rb, Th and K. In general, however, the relatively low concentrations of alumina plus lime ($\approx 14.0\%$ for low-silica rhyolite and 12.2% for high-silica rhyolite) and high total alkalis ($\approx 9.3\%$ for low-silica rhyolite and 8.9% for high-silica rhyolite) in the HFF rhyolites most closely resemble the major element compositions of rift- or hot spot-related rhyolites.

Significantly there are very close compositional similarities between HFF rhyolites and the Awasib Granite. The latter (discussed in detail in Section 4.3.2) is diagnostic of so-called "A-type" (alkaline or anorogenic) magmas reviewed by Whalen *et al.* (1987). Since "A-type" chemistry has been applied almost exclusively to granites, caution is necessary when applying this concept to rhyolites. Nevertheless, it is important to note that the HFF rhyolites display many of the chemical characteristics of both A-type granites (as defined by Whalen *et al.*, 1987) and within-plate granites (as defined by Pearce *et al.*, 1984). These features are compatible with derivation of the rhyolites from crustal and subcontinental lithospheric sources.

(b) REE patterns

The REE pattern for HFF high-silica rhyolite is compared with patterns for both subduction-related and intraplate rhyolites in Fig. C.36. "Anorogenic" rhyolites represented in this diagram are thought to have originated by partial melting of continental crust, e.g. Kern Plateau (Bacon and

Duffield, 1981) and Monte Arci (Dostal *et al.*, 1982), while "orogenic" rhyolites owe their origins to both partial melting, e.g. Inner Zone of Japan (Terakado and Masuda, 1988), and crystal fractionation, e.g. south Aegean volcanic arc (Innocenti *et al.*, 1981). Despite the overlapping nature of several of these patterns, it is clear that the HFF high-silica rhyolite most closely resembles the pattern for high-silica rhyolite from the Inner Zone of Japan. The relative enrichment in HREE of the HFF is, however, distinct from patterns for both "orogenic" and "anorogenic" rhyolites in Fig. C.36, although a similar HREE enrichment has been reported for non-subduction related rhyolite from the Rio Grande rift (Thompson *et al.*, 1984).

(iv) Summary

Despite moderate deformation and metamorphism, the major and trace element variation in volcanics of the HFF displays the following primary characteristics:

(a) A progression in composition from basaltic andesite to high-silica rhyolite, but with a paucity of compositions ($< 15\%$) in the range andesite to dacite.

(b) The chemical affinity of the HFF volcanic suite is largely calc-alkaline (AFM classification, alkali-lime index), a high- K nature being indicated by the following features:

- K_2O enrichment in the classification of Peccerillo and Taylor (1976).

- High abundances of Rb, LREE, Th, Zr and sometimes Nb and Y. - High ratio of La_N/Ce_N (≈ 1.3).

- REE patterns, especially for the basaltic andesites, which are similar to high-K volcanic suites elsewhere.

(c) An "orogenic" character is suggested for the HFF volcanic suite by a number of compositional features, viz.:

- Calc-alkaline to high- K character

- TiO_2 depletion

- Low abundances of HFSE, except for Nb and Y in the rhyolites

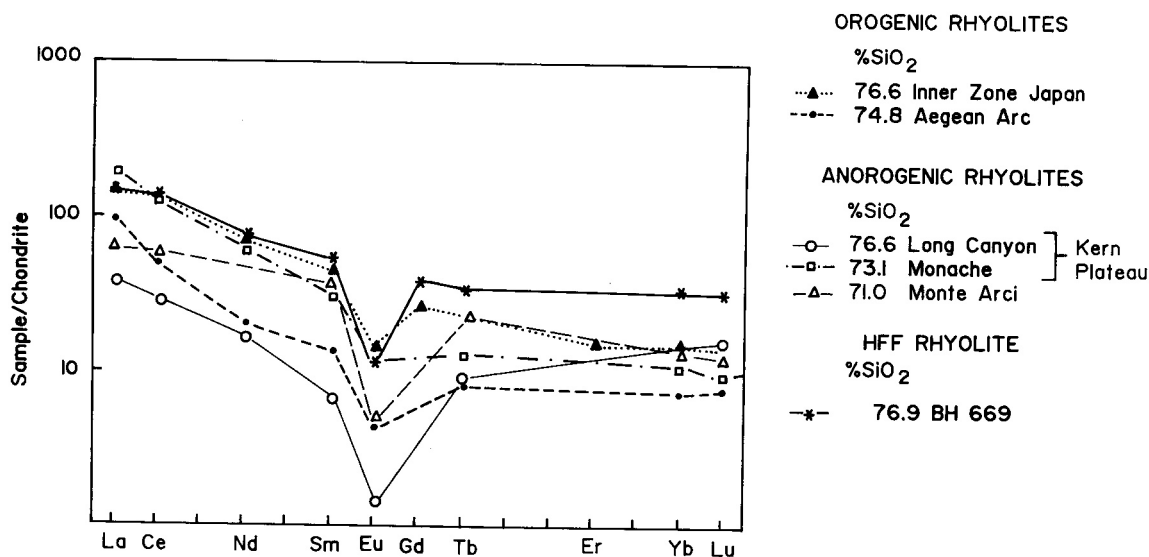


Fig. C.36: Chondrite-normalised REE pattern (bold line) for HFF rhyolite compared with patterns for various orogenic and anorogenic rhyolites. Data sources: Inner Zone Japan (Terakado and Masuda, 1988), Aegean Arc (Innocenti *et al.*, 1981), Kern Plateau (Bacon and Duffield, 1981), Monte Arci (Dostal *et al.*, 1982).

- Eu/Eu* ratio > 0.75 in the basaltic andesites
- Distinctive REE patterns

From the above characteristics it can be concluded that the andesites (*sensu lato*) are “orogenic” as defined by recent workers (e.g. Bailey, 1981; Gill, 1981; Ewart, 1982). Characterisation of the rhyolites is less easily achieved owing to their fractionated nature and A-type features which are almost identical to the Awasib Granite (see section 4.3.2). The presence of both crustal and within-plate components in the HFF rhyolites is implied.

4.3.2 Late-stage (“Sinclair-type”) intrusive suites

4.3.2.1 Introduction

Selected major and trace element data are presented in this section for the following four suites of intrusive rocks, all of which post-date volcanics of the Haiber Flats Formation:

- Saffier Intrusive Suite (SIS)
- Haisib Intrusive Suite (HIS)
- Awasib Granite
- Chowachasib Granite Suite (CGS)

Preliminary data for the Bushman Hill Quartz Diorite indicate significant similarities to the SIS (e.g. Ti/Zr ratios) but will not be discussed in this study. Special attention is, however, given to the HIS and Awasib Granite in view of their close spatial association with, and compositional similarity to, the eruptive rocks of the HFF.

4.3.2.2 Classification

Despite some scatter obtained on variation diagrams (only presented for the HIS and Awasib Granite - Figs C.44 and C.45), the within-suite trends are sufficiently regular to preclude any significant subsolidus alteration. The use of major and trace elements is accordingly considered to be justified in the classification of these intrusive suites.

Overall compositional variation is illustrated in a total al-

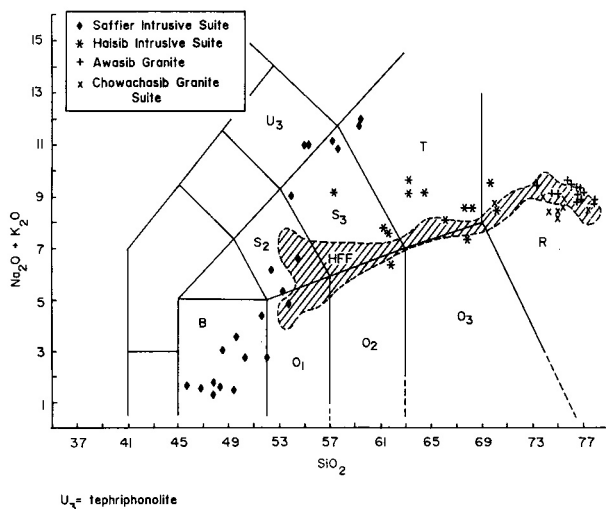


Fig. C.37: Total alkali-silica (TAS) diagram showing distribution of data for the late-stage intrusive suites. Shaded area represents compositional field of the HFF. Rock group subdivision as for Fig. C.24.

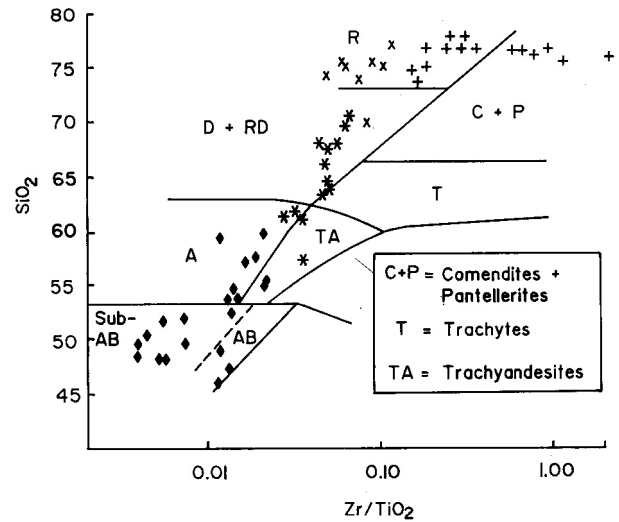


Fig. C.38: The distribution of data for the late-stage intrusive suites in the Zr/TiO₂ vs. SiO₂ diagram devised for altered rocks (Winchester and Floyd, 1977). Annotation of non-alkaline fields is given in Fig. B.30; symbols as in Fig. C.37.

kali-silica plot (Fig. C.37) which shows a steep trend for the SIS and significantly shallower trend for the HIS, Awasib Granite and CGS. The latter trend also coincides approximately with the field of HFF lavas, but is richer in alkalis for the less silica-rich compositions. These divergent trends are primarily defined by alkalinity, a feature which is confirmed by the “alteration-resistant” ratio Zr/TiO₂ in a plot of this ratio against SiO₂ (Fig. C.38).

On a normative An-Ab-Or diagram (Fig. C.39), granites (*sensu lato*) of the Haisib, Awasib and Chowachasib suites plot in the granite field of Barker (1979) with a few data points of the HIS plotting in the granodiorite field.

AFM variation (Fig. C.40a) indicates a calc-alkaline character for most of the intrusive suites except some of the members of the SIS. Brown (1982) has shown that AFM variation may be used as a crude measure of arc maturity in

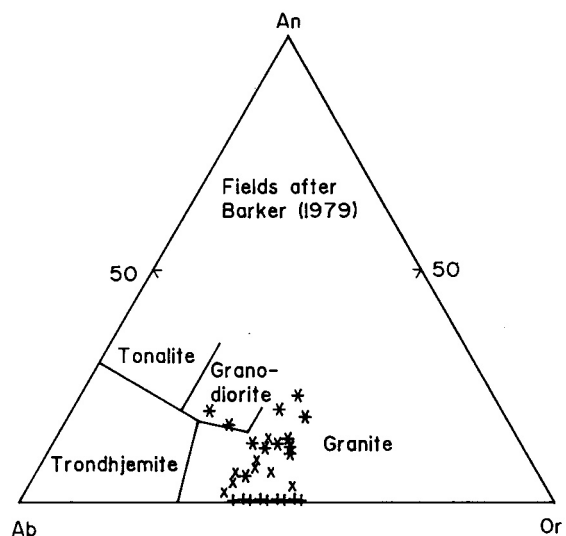


Fig. C.39: Normative An-Ab-Or ternary plot of late-stage granitoids. Compositional fields (Barker, 1979) indicate the “granitic” nature of the HIS, Awasib Granite and CGS. Symbols as indicated previously.

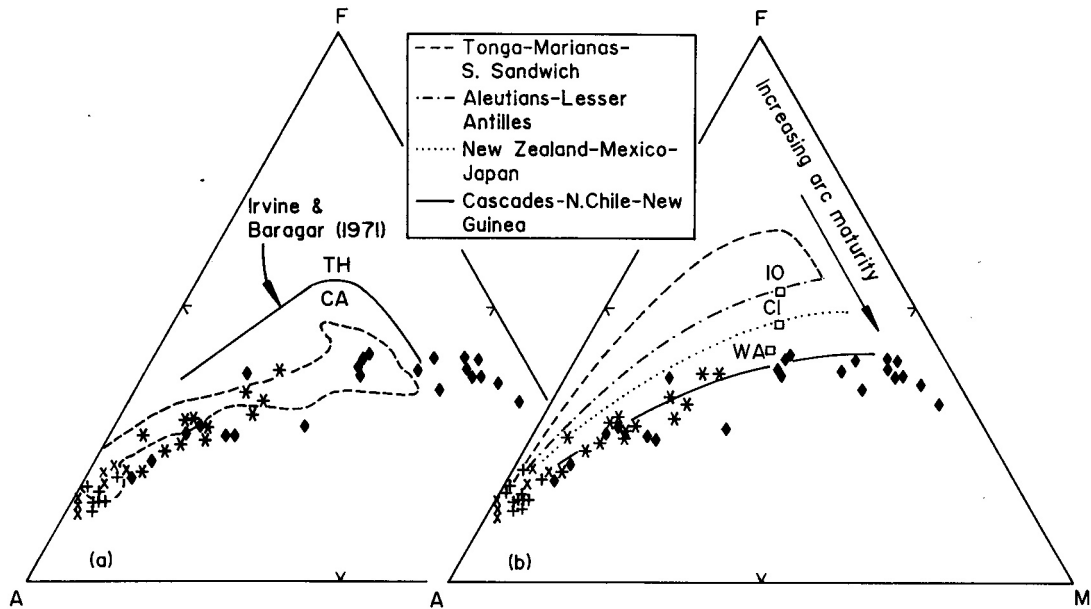


Fig. C.40: AFM variation of late-stage intrusive rocks:
 (a) shows a largely calc-alkaline (CA) as opposed to tholeiitic (TH) character; also shown is the HFF compositional field (dashed boundary)
 (b) compares the late-stage suites with volcanic suites from modern magmatic arcs which show differences due to arc maturity (compilation after Brown, 1982); also shown are Ewart's (1976) averages for western American volcanic arcs (WA), continental island arcs (CI) and intra-oceanic arcs (IO). Symbols as before.

that there exists a family of curves for arc magmas which range from island-arc tholeiites to mature calc-alkaline series of continental margins. Sinclair-age intrusions in the AMT show AFM trends which closely resemble the latter, in particular the Cascades-N.Chile-New Guinea trend illustrated in Fig. C.40b. Features which support this similarity include a high volume ratio of intrusive to extrusive igneous rocks in the AMT, a high volume ratio of acidic and intermediate to basic members in both intrusive and extrusive suites in the AMT, and a close correspondence between the field of HFF lavas and data for the HIS and Awasib Granite. Regression lines in a silica versus calc-alkali ratio plot (Fig. C.41) illustrate that the HIS trend is "alkali-calcic" (i.e. %SiO₂ ≈ 53), although data do overlap significantly with the calc-alkaline field (modified from Brown, 1982). The Awasib Granite data clusters around the lower part of the field occupied by the HFF lavas and also appears to be of "alkali-calcic" affinity. A trend line for both the HIS and Awasib Granite is, however, clearly "calc-alkalic" (%SiO₂ ≈ 58), although the slope is slightly steeper than that displayed by lavas of the HFF. The SIS trend is also clearly alkali-calcic (%SiO₂ ≈ 54) and steeper than the aforementioned trends, while data for the CGS scatters below the lower part of the calc-alkaline field.

The degree of alumina saturation (Shand, 1927; Chappell and White, 1974) displayed by post-HFF granitoids is somewhat less than that shown by granitoids which make up the early-stage crust of the AMT. Fig. C.42 illustrates that these younger granitoids are predominantly metaluminous, with some peralkalinity demonstrated by the Awasib Granite. The degree of peralkalinity is, however, mild (agpaitic index = 1.06) and no undersaturated granitoids have been identified. Reasonable discrimination may be

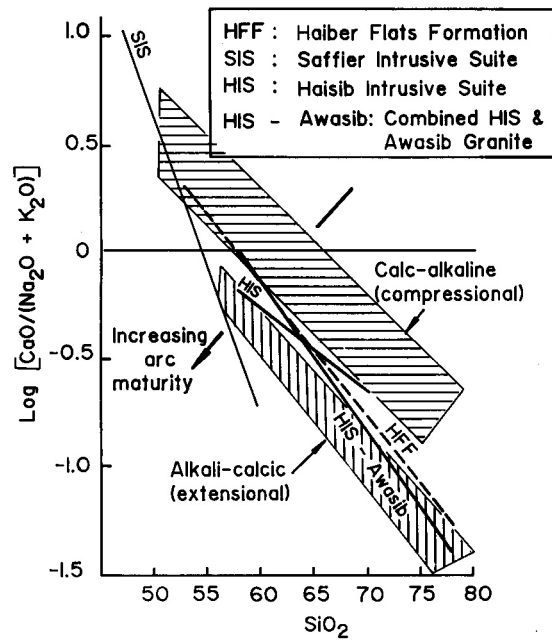


Fig. C.41: Silica vs. calc-alkali ratio plot of regression lines for the late-stage intrusive suites and HFF volcanic succession. The change from calc-alkaline (compressional) to alkali-calcic (tensional) records a trend of increasing arc maturity (Brown, 1982).

achieved between the different granitoid suites by using the ratio A/CNK (*molecular%* Al₂O₃/(CaO + Na₂O + K₂O)) as a measure of alumina saturation and plotting this parameter against the enrichment in HFSE (Fig. C.43). While the considerable range in A/CNK for the SIS is considered to reflect its broad compositional range from gabbro to syenite,

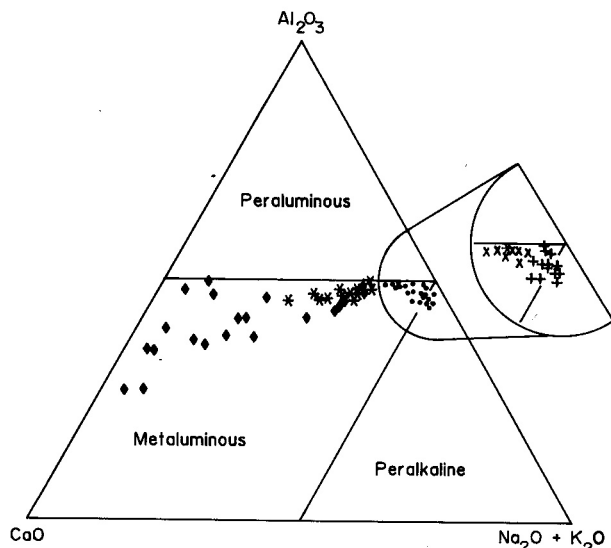


Fig. C.42: Molecular alumina-calcium-alkalis ternary diagram showing the predominantly metaluminous character of late-stage intrusive suites. The enlarged section illustrates the slightly peralkaline nature of the Awasis Granite. Classification based on Shand (1927). Symbols as before.

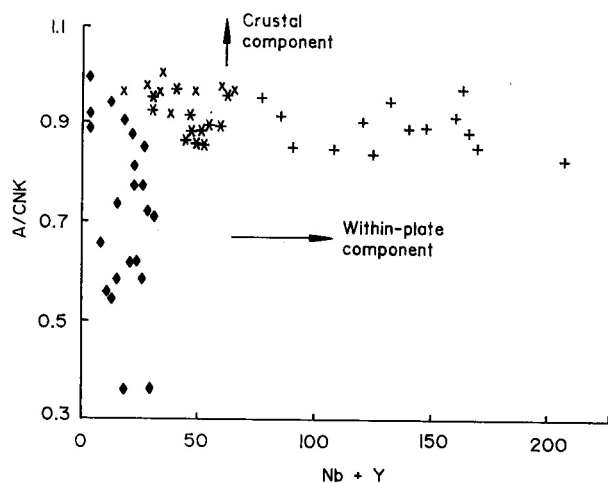


Fig. C.43: (Nb + Y) vs. Shand Index (A/CNK) diagram showing compositional variation of the late-stage intrusive suites. Enrichment in HFSE indicates within-plate character for the Awasis Granite. Symbols as before.

the significant enrichment in HFSE in the Awasis Granite suggests a “within-plate” character (Pearce *et al.*, 1984). This observation is supported by the occurrence of the highest levels of HFSE in the most peralkaline samples.

4.3.2.3 Comparison of the HIS and Awasis Granite with the HFF volcanic suite

(i) Introduction

The close spatial and temporal association between the HIS, Awasis Granite and HFF volcanic suite has been described in Section CO₂. In addition, certain mineralogical similarities have come to light in Section C.3, while the current section has already made reference to the compositional similarities which exist between these rock suites. This section attempts to provide a more rigorous assess-

ment of the geochemical relationships between these rock types, especially since field relationships are often unclear and ambiguous.

(ii) Major element variation

Harker diagrams are illustrated in Fig. C.44 for both extrusive and intrusive suites and the following features are evident:

(a) The HIS-Awasis “suite” exhibits a smaller range in silica compared with the HFF lavas, viz. 57-78% SiO₂ as opposed to 53-78% SiO₂, but is better represented in the range of intermediate compositions.

(b) Smooth trends for the combined data are displayed by all the major oxides except the alkalis, MnO and P₂O₅.

(c) Data scatter differs little between the HFF rhyolites and Awasis Granite, but the HIS shows significant enrichment in K₂O when compared with andesites, dacites and rhyodacites of the HFF.

(iii) Trace element variation

Variation diagrams (Fig. C.45) are again used to illustrate features displayed by selected trace element data for intrusive and extrusive suites. The trace elements are grouped, as in Section 4.3.1.3, according to similar chemical affinities.

(a) K-group

- Ba exhibits considerable scatter in all the suites.
- Rb, like K₂O, is significantly enriched in the HIS compared with HFF andesites, dacites and even many rhyolites.
- Sr shows a regular decrease with an increase in silica from intermediate to acid compositions.

(b) LREE Group

- La is enriched in the HIS relative to HFF andesites and dacites, although it does display considerable scatter.
- Ce shows less scatter than La, but is likewise enriched in the HIS for the same silica range.

(c) Th-group

- Th is enriched in the HIS and to some extent the Awasis Granite when compared with HFF volcanics of similar silica content.

(d) HFSE Group

- Zr tends to be relatively enriched in the HIS, but depleted in the Awasis Granite.
- Nb is also relatively enriched in the HIS, but shows considerable overlap between the Awasis Granite and HFF rhyolites.
- Y exhibits good agreement between much of the HIS and HFF andesites and dacites, although there is a tendency towards greater enrichment in the Awasis Granite relative to the HFF rhyolites.

(e) Compatible Group

- Ni tends to be enriched in the HIS and Awasis Granite relative to HFF andesite-dacite and rhyolite, respectively.

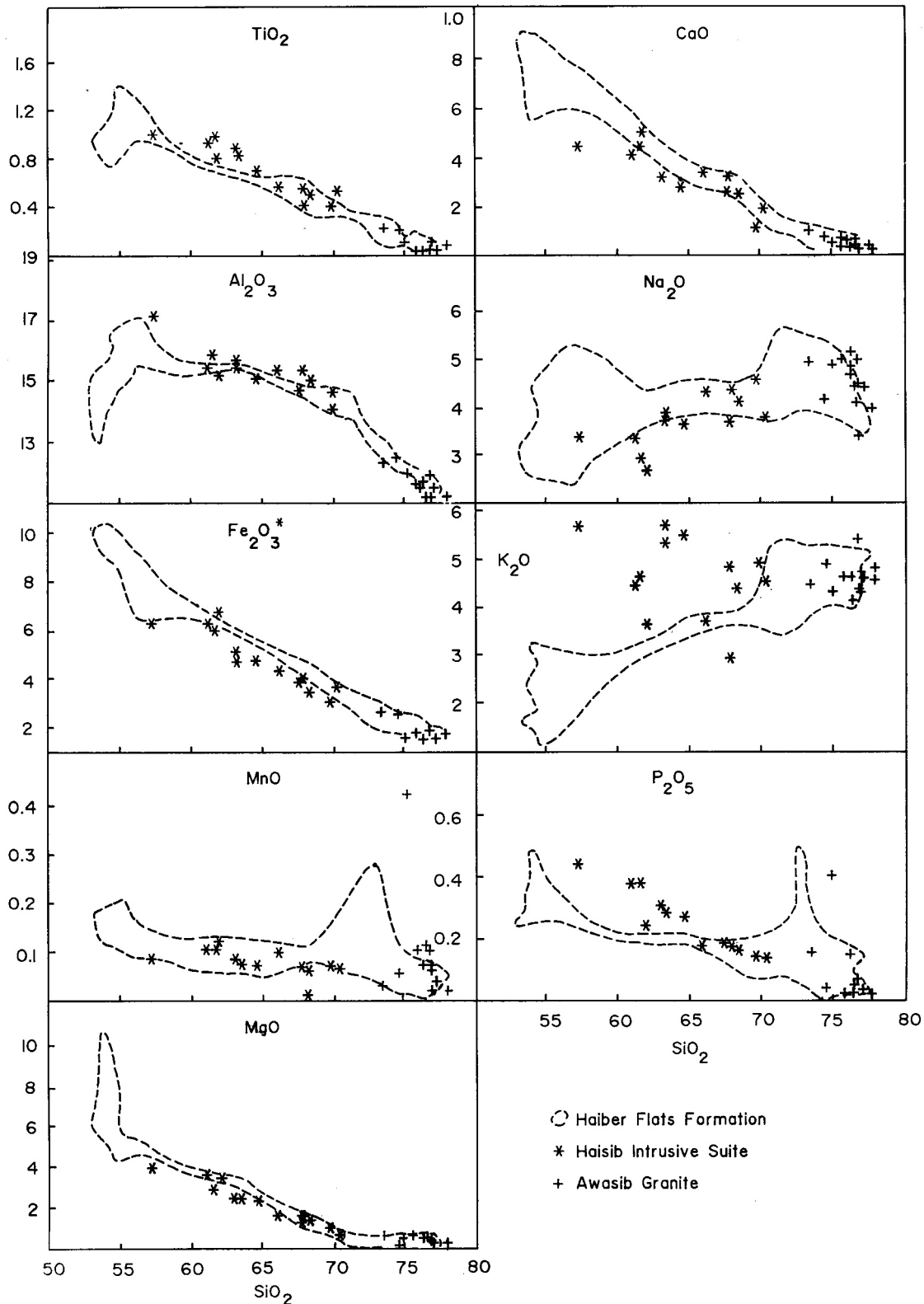


Fig. C.44: Harker diagrams for the HIS and Awasib Granite. Broken lines indicate boundaries for compositional fields of HFF volcanics.

- Cr exhibits relative enrichment for the HIS only.
- V exhibits good agreement between intrusive and extrusive rocks of similar silica content.

(iv) REE patterns

Chondrite-normalised REE patterns are presented in Fig. C.46 for samples of HFF rhyolite and Awasib Granite.

The pattern for the Awasib Granite differs from the HFF rhyolite with respect to its steeper slope ($La_N/Lu_N = 5.4$, compared with 4.4 in the rhyolite), a steeper HREE pattern ($Tb_N/Lu_N = 1.8$, compared with 1.0 in the rhyolite) and a more pronounced negative Eu anomaly ($Eu/Eu^* = 0.05$, compared with 0.24 in the rhyolite).

The different patterns displayed by HFF rhyolite and

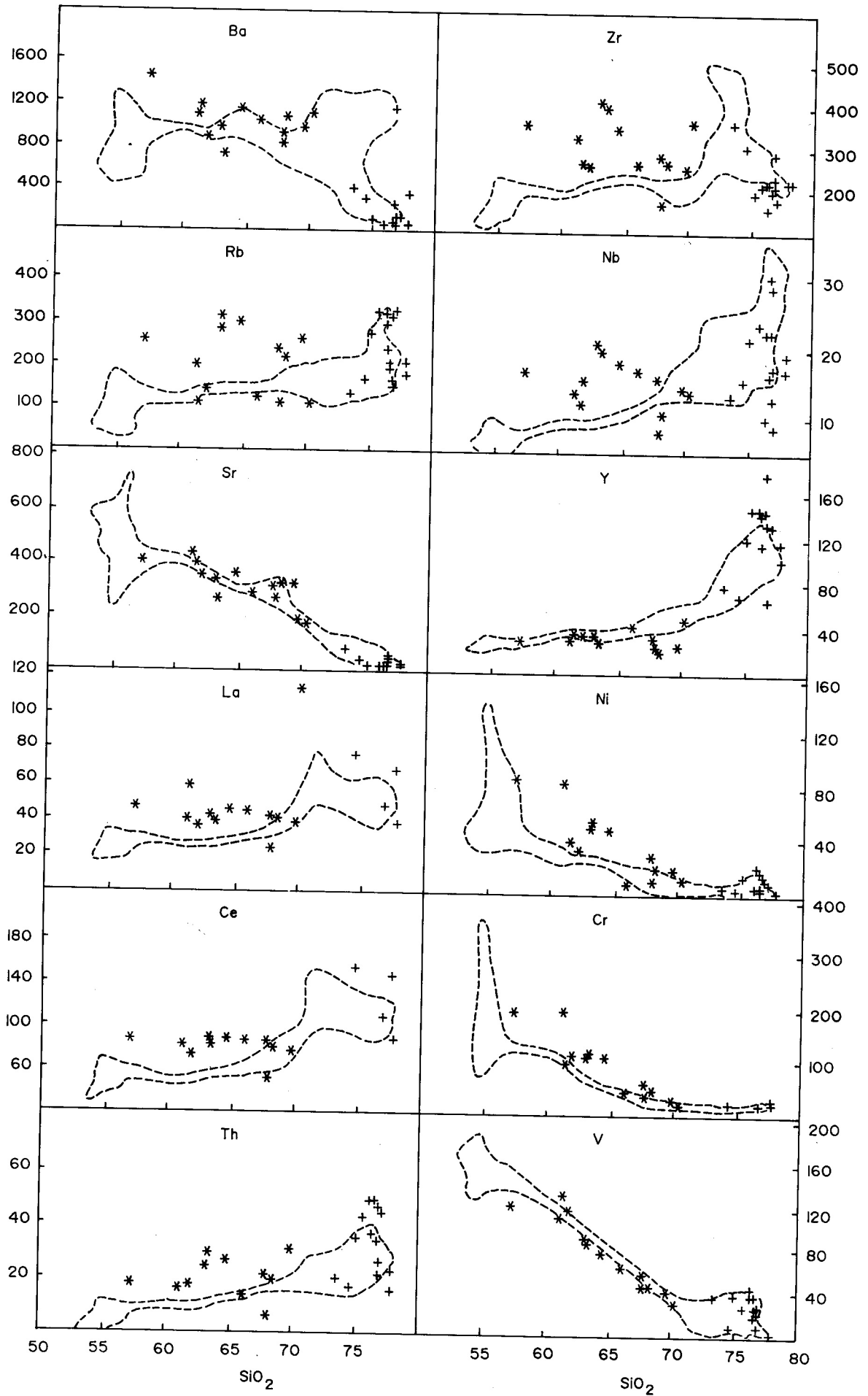


Fig. C.45: Selected trace element variation diagrams for the HIS and Awasib Granite. Broken lines indicate boundaries for compositional fields of HFF volcanics. Silica as abscissa and symbols as for Fig. C.44.

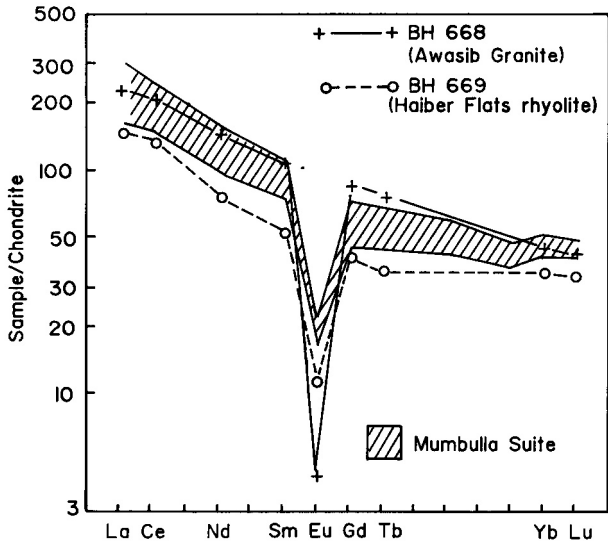


Fig. C.46: Chondrite-normalised REE pattern of HFF rhyolite compared with patterns of the Awasib Granite and A-type Mumbulla Suite from south-eastern Australia (Collins *et al.*, 1982).

Awasib Granite are not consistent with a subvolcanic origin for the latter, although the Eu/Eu^* variations may be explained by different degrees of plagioclase fractionation. However, a database of only two samples cannot be considered conclusive and some heterogeneity may, furthermore, be expected as a natural consequence of crustal melting. REE patterns for the A-type Mumbulla suite in southeastern Australia (Collins *et al.*, 1982) are intermediate between the Awasib Granite and HFF rhyolite patterns (Fig. C.46) implying that both granite and rhyolite are compatible with an A-type origin. The more pronounced negative Eu anomalies in the late-stage AMT rocks (particularly the Awasib Granite) suggest that significant feldspar fractionation has taken place.

4.3.2.4 Comparison of late-stage granitoids with modern and ancient intrusive suites

In a silica versus calc-alkali ratio plot (Fig. C.41), the HIS-Awasib trend exhibits a slope similar to that of the Saudi Arabian Pan-African granitoids (Gass, 1977), but is displaced towards the field of calc-alkaline intrusive suites (modified from Brown, 1982). This intermediate position may reflect a character transitional between the calc-alkaline (compressional) and alkali-calcic (extensional) granitoid suites discussed by Brown (1982). A similar transitional nature is indicated for the HIS-Awasib “suite” in a diagram of $\log(K_2O/MgO)$ versus SiO_2 (Fig. C.47) in which fields have been drawn according to Rogers and Greenberg (1981). This diagram illustrates the following features:

(a) An approximate coincidence between data for the HIS and the calc-alkaline part of the Sierra Nevada batholith trend.

(b) A clustering of data for both the Awasib Granite and CGS above the most silica-rich compositions of the field of “alkali granites” and also above the alkaline part of the Sierra Nevada batholith trend.

(c) A divergent trend towards more potassic and less silica-rich compositions for the SIS.

The transition from the calc-alkaline HIS to more alkaline Awasib Granite may be the result of magmatic differentiation, a change in source characteristics, or a change in tectonic regime. Compositions of associated volcanics of the HFF strongly suggest that they once formed part of a high-K suite of “orogenic” lavas, probably erupted along an active continental margin. The close spatial, temporal and compositional association between the HIS-Awasib “suite” and HFF lavas further suggests that their origins were similar and that the geochemistry of the granitoids should reflect this.

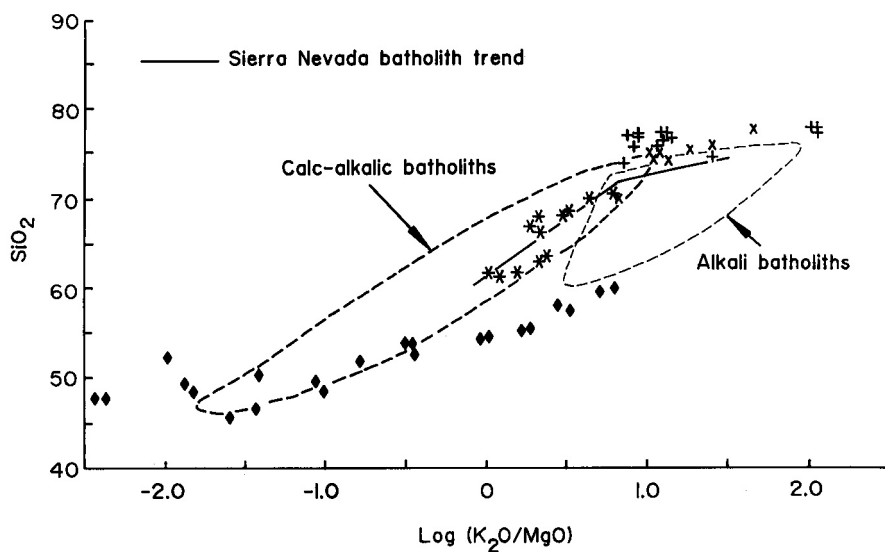


Fig. C.47: $\log(K_2O/MgO)$ vs. SiO_2 showing the relationship between late-stage AMT intrusive suites and fields of “calc-alkalic” and “alkali” batholiths compiled from a variety of Pan-African to Recent suites (Rogers and Greenberg, 1981). There is a broad correspondence between the Sierra Nevada batholith trend and that of the late-stage granitoids (excluding the SIS). Symbols as before.

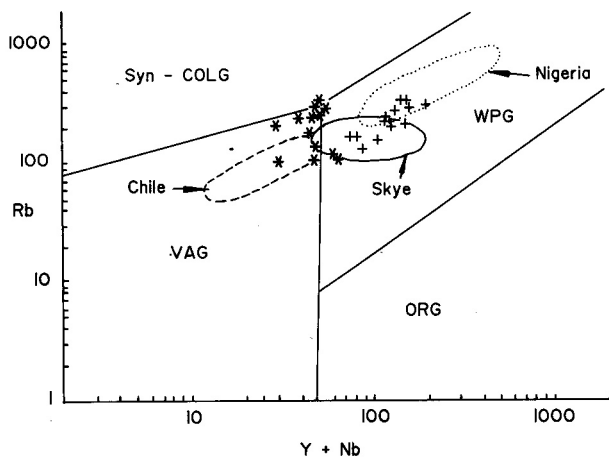


Fig. C.48: $(Y + Nb)$ vs. Rb discriminant diagram for the HIS and Awasib Granite. Field boundaries drawn for volcanic-arc granites (VAG) of central Chile and within-plate granites (WPG) of Skye and Nigeria (Pearce *et al.*, 1984). Annotation as for Fig. B.41; symbols as before.

The tectonic discrimination of the HIS and Awasib Granite in a plot of $Y + Nb$ versus Rb (Fig. C.48) illustrates that data for these granitoids lie in the VAG and WPG fields, respectively (Pearce *et al.*, 1984). A trend from an “arc” to “within-plate” character is only indicated in part, since the majority of data points for the HIS lie above such a trend. The clustering of these data points along the lower boundary of the syn-COLG field indicates a relative enrichment in Rb which clearly reflects the potassic nature of the HIS. Unfortunately, Rb is readily susceptible to alteration processes (Whalen *et al.*, 1987) and so does not allow reliable discrimination between VAG and syn-COLG fields in Fig. C.48.

If, however, the relative enrichment in Rb for the HIS is taken as a primary characteristic, then a likely petrogenetic pathway requires Rb enrichment of the mantle similar to that suggested by Pearce *et al.*, (1984) for the granites of Central Chile. Relatively high values of Rb in the HIS compared with the Chilean granites may be attributed to vari-

able enrichment of the mantle source, late-stage fluid activity or a high degree of crustal contamination (cf. Pearce *et al.*, 1984). The similarity of the data field for the Awasib Granite to within-plate granites of Skye and Nigeria in Fig. C.48 does not indicate an obvious petrogenesis, but -does suggest the possibility of both an enriched mantle source and combined assimilation-fractionation processes.

The $(Y + Nb)$ versus Rb diagram is not well suited to the comparison of different granitoid suites due to the limited number of geochemical parameters. This shortcoming can, to some extent, be overcome by the use of normalised diagrams, in particular the ORG-normalised diagrams employed by Pearce *et al.* (1984). The method for calculating trace element abundances in ORG (hypothetical ocean-ridge granite) has been discussed in Section BA. The normalised pattern obtained for the full range of HIS samples together with their mean value is illustrated in Fig. C.49a. The HIS pattern is characterised by several features displayed by volcanic-arc granites from central Chile, viz. enrichments in K, Rb, Ba, Th and Ce relative to Nb, Zr and Y, and a low value of Y relative to the normalising composition. Although the value of Zr is close to the normalising value, and hence within the range of within-plate granite patterns, the steep decline from Zr to Y is more typical of volcanic-arc granitoids. Enrichment in Zr may, however, be the result of zircon accumulation.

The normalised pattern for Awasib Granite (range and mean) in Fig. C.49b most closely resembles the so-called “crust-dominated” within-plate pattern (after Pearce *et al.*, 1984) exemplified by the Sabaloka complex in the Sudan. Features in common include a well-defined Ba anomaly, enrichment in Rb and Th relative to Nb, and enrichments in Ce and Sm (only available for sample BH 668) relative to adjacent elements. The low values of Nb and Zr are, however, more typical of within-plate granites associated with attenuated continental crust (e.g. Skaergaard and Mull), although the minimum values of these elements are also within the range of volcanic-arc granites. Significantly, the value of Y is close to or higher than the normalising value

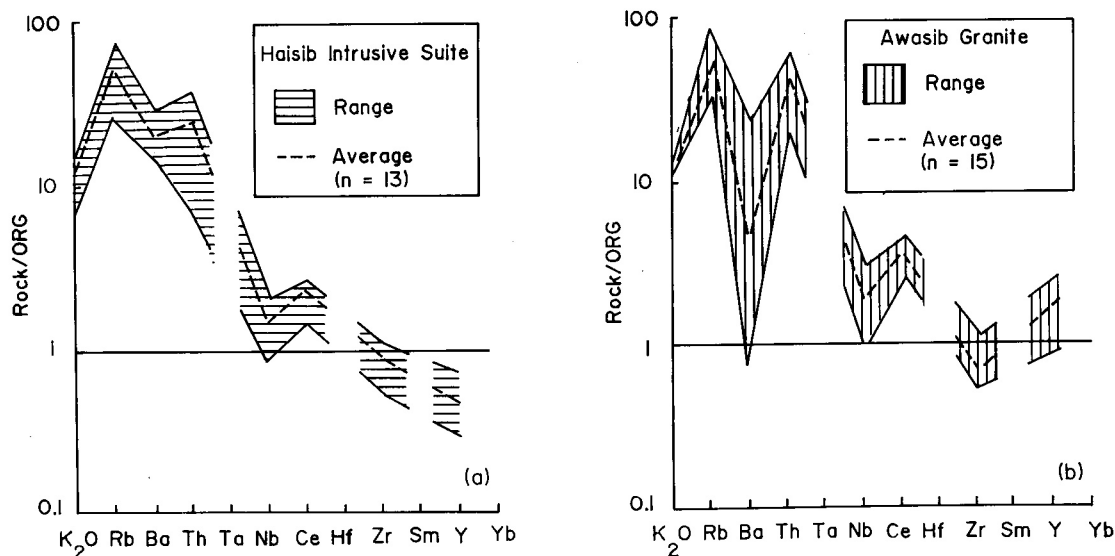


Fig. C.49: Ocean-ridge granite (ORG)-normalised trace element variation diagrams for (a) the HIS, and (b) the Awasib Granite. Average patterns and their ranges in (a) and (b) indicate similarities to “volcanic-arc” and “crust-dominated within-plate” patterns, respectively.

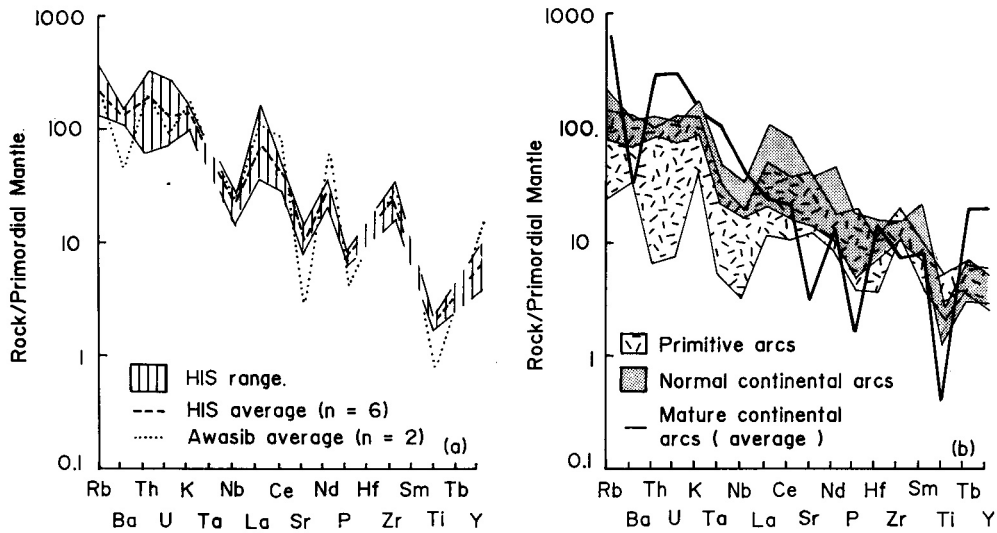


Fig. C.50: Primordial mantle-normalised patterns for (a) the HIS and Awasib Granite, compared with (b) granitoids from Mesozoic and Cenozoic magmatic arcs (compiled by Brown *et al.*, 1984). All data for rocks in the range 66-75% SiO₂.

and would be most unusual in a volcanic-arc granite unless the accumulation of an accessory phase such as zircon had occurred. In addition, it should be noted that the Awasib Granite is generally rich in silica and may consequently represent a more highly fractionated granite than the granitoids in the database of Pearce *et al.* (1984).

The apparent transition from a volcanic-arc to within-plate character recorded by the HIS and Awasib Granite may be a reflection of increasing arc maturity as envisaged by Brown *et al.* (1984). These workers have used Wood's (1979) "primordial mantle" as a normalising value to illustrate element abundance trends with increasing arc maturity. The apparent advantages of this approach over that of Pearce *et al.* (1984) include a greater number of parameters used (18 elements as opposed to 12) and a more specialised application. Primordial mantle-normalised patterns for average HIS and Awasib Granite in the SiO₂ range 66-75% are compared with granitoids from Mesozoic and Cenozoic magmatic arcs (after Brown *et al.*, 1984) in Fig. C.50.

The pattern for the HIS resembles that of normal continental arcs fairly closely despite slight deviations, viz. enrichment in Th, Zr and Y and depletion in Sr. While broadly similar to the HIS, the pattern for low-silica Awasib Granite differs in exhibiting certain similarities to mature island arcs, e.g. greater depletion in Ba, Sr, P and Ti and greater enrichment in Y. Although the low-silica part of the Awasib Granite does not exhibit the more extreme enrichments and depletions typical of peralkaline anorogenic granites, it should be noted that the bulk of the Awasib Granite (not illustrated in Fig. C.50) is high-silica (> 75% SiO₂) in character. This high-silica group is generally characterised by greater enrichment in Y and more significant depletion in the elements Ba, Sr and Ti, all features which may indicate a "within-plate" character. However, these concentrations may equally be the result of increasing arc maturity or simply crystal fractionation.

While averages for the HIS and Awasib Granite do tend to mask intra-suite variation, it is clear from Fig. C.50 that a transition between these suites is accompanied by an in-

crease in LREE and Y and a decrease in Ba, Sr, P and Ti, while Zr remains almost constant. However, if these changes in element abundances are the result of increasing arc maturity, then it is difficult to explain the absence of noteworthy increases in the elements Rb, Th, U and Nb as well as the ratios Nb/Rb and Nb/La (d. Brown *et al.*, 1984). The latter workers make use of plots of Rb/Zr against Nb and Y in order to discuss the effects of fractional crystallisation and source composition on "plutonic" magma types. Representation of these plots in Fig. C.51 illustrates that data for the HIS (total data set) overlaps with data for continental arcs in terms of both Nb and Y concentration at a given Rb/Zr ratio, whereas data for the Awasib Granite (low- and high-silica groups) only corresponds with continental arcs in the plot of Nb versus Rb/Zr. The enrichment in Y displayed by the Awasib Granite occurs at a relatively low Rb/Zr ratio and is clearly aberrant with respect to the trend of increasing arc maturity. The tendency for Nb to increase at a given Rb/Zr ratio in the transition from HIS to Awasib Granite may, however, represent a trend inferred to indicate the involvement of "within-plate" mantle lithosphere by Brown *et al.* (1984). In the case of the Awasib Granite it is possible that Y has acted as a more sensitive indicator of a within-plate source contribution than Nb, unless some form of selective crustal contamination is invoked.

From the above discussion it is clear that the Awasib Granite demonstrates certain trace element characteristics regarded as diagnostic of so-called "A-type" (alkaline or anorogenic) granites (Loiselle and Wones, 1979; Collins *et al.*, 1982; Whalen *et al.*, 1987). In Table C.5 the geochemistry of average Awasib Granite is compared with averages for felsic S-types (granites derived from sedimentary protoliths; Chappell and White, 1974), felsic I-types (granites derived from igneous protoliths; Chappell and White, 1974) and A-types (Whalen *et al.*, 1987). This table illustrates chemical characteristics for A-type granites which are also demonstrated by the Awasib Granite, viz. high SiO₂, Na₂O + K₂O, apgaitic index (A.I.), Fe/Mg, Y and LREE and low CaO, Ba and Sr. Certain "immobile" elements such as Zr

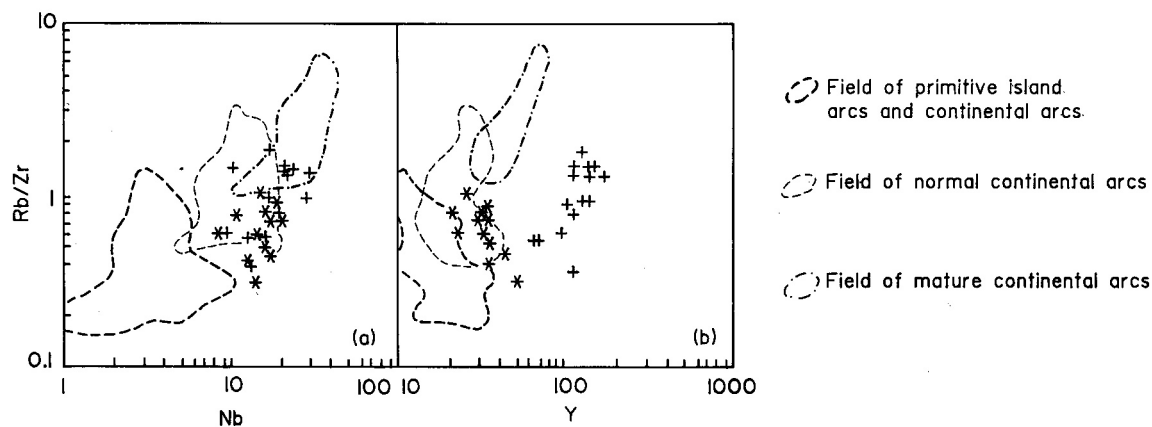


Fig. C.51: Plots of Nb and Y against Rb/Zr for the Haisib and Awasis Granite. Fields reflect a trend of increasing arc maturity (modified from Brown *et al.*, 1984). Symbols as before.

TABLE C.5: Average compositions of the Haisib Intrusive Suite and Awasis Granite compared with various granite types compiled by Whalen *et al.* (1987).

	HAISIB	AWASIB	A-TYPE	FELSIC I-TYPE	FELSIC S-TYPE
n =	13	15	148	421	205
SiO ₂	64.82	76.29	73.81	73.39	73.39
TiO ₂	0.72	0.08	0.26	0.26	0.28
Al ₂ O ₃	15.39	11.67	12.40	13.43	13.45
Fe ₂ O ₃ *	4.81	1.94	3.00	2.07	2.28
MnO	0.08	0.08	0.06	0.05	0.04
MgO	2.26	0.35	0.20	0.55	0.58
CaO	3.25	0.48	0.75	1.71	1.28
Na ₂ O	3.75	4.51	4.07	3.33	2.81
K ₂ O	4.65	4.57	4.65	4.13	4.56
P ₂ O ₅	0.25	0.06	0.04	0.07	0.14
Ba	1032	225	352	510	388
Rb	204	232	169	194	277
Sr	322	31	48	143	81
Pb	27	109	24	23	22
Th	20	34	23	22	18
U	4	4	5	5	6
Zr	306	233	528	144	136
Nb	15	18	37	12	13
Y	33	119	75	34	33
Ce	81	126	137	68	53
Sc	10	2	4	8	8
V	79	25	6	22	23
Ni	38	8		2	4
Cu	43	9	2	4	4
Zn	61	71	120	35	44
K/Rb	189	164	229	177	137
Rb/Sr	0.63	7.48	3.52	1.36	3.42
Rb/Ba	0.20	1.03	0.48	0.38	0.71
A.I.	0.73	1.06	0.95	0.74	0.73

and Nb do not reflect this A-type enrichment and may, therefore, imply that the Awasis Granite is a highly fractionated I- or S-type.

Whalen *et al.* (1987) maintain that plots of Zr + Nb + Ce + Y versus the major element ratios FeO*/MgO and (K₂O +

Na₂O)/CaO may be effectively utilised in identifying A-type granites from a variety of terranes in addition to the well-studied Lachlan Fold Belt of Australia. Application of these plots to the Awasis Granite illustrates fairly well-defined A-type characteristics (Fig. C.52a and b). However, data

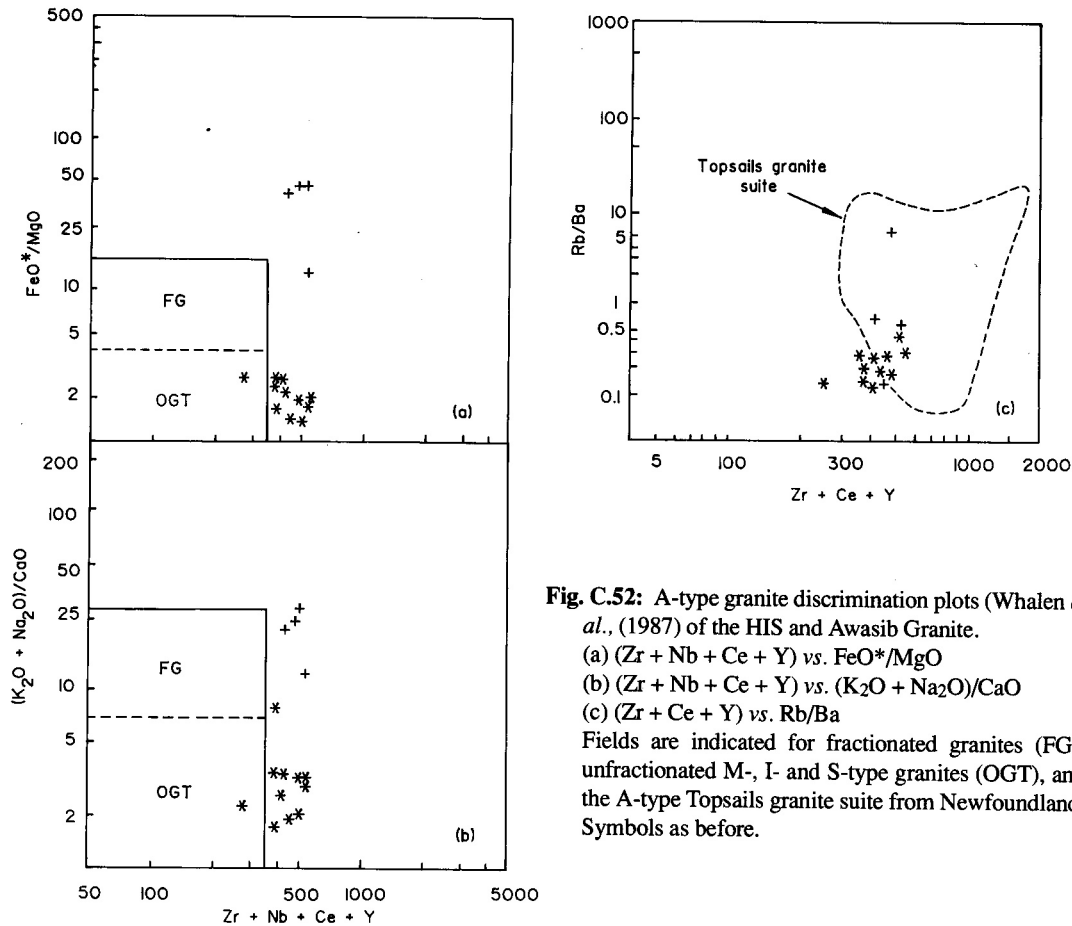


Fig. C.52: A-type granite discrimination plots (Whalen *et al.*, 1987) of the HIS and Awasib Granite.

(a) $(\text{Zr} + \text{Nb} + \text{Ce} + \text{Y})$ vs. FeO^*/MgO

(b) $(\text{Zr} + \text{Nb} + \text{Ce} + \text{Y})$ vs. $(\text{K}_2\text{O} + \text{Na}_2\text{O})/\text{CaO}$

(c) $(\text{Zr} + \text{Ce} + \text{Y})$ vs. Rb/Ba

Fields are indicated for fractionated granites (FG), unfractionated M-, I- and S-type granites (OGT), and the A-type Topsails granite suite from Newfoundland. Symbols as before.

for the “I- to M-type” HIS were also plotted for comparison and indicate that the major difference between the HIS and Awasib Granite in terms of these plots is in the major element ratios and not the summation of trace elements. This is largely due to the enrichment in Zr and Ce in the HIS, although it should be noted that while high Zr contents may be the result of zircon accumulation, high Ce abundances are not unusual in volcanic-arc granites (cf. Chile; Pearce *et al.*, 1984).

The much greater outcrop area of the Awasib Granite compared with the HIS suggests that the former is not the product of advanced crystal fractionation near the roof of a single pluton. This suggestion is partly borne out by the overlap of data between the HIS and Awasib Granite on a plot of $\text{Zr} + \text{Ce} + \text{Y}$ versus Rb/Ba ratio (Fig. C.52c). The latter ratio is a useful index of fractionation, but tends to show considerable variation within individual A-type suites (Whalen *et al.*, 1987). In Fig. C.52c, the similarity between data for the HIS-Awasib “suite” and the Topsails granite suite of western Newfoundland is of more than passing interest. The latter suite has been shown to record a transition from orogenic M-type granite magmatism to voluminous A-type magmatism in the Late Ordovician-Early Silurian (Whalen *et al.*, 1987). The transition from largely I-type HIS of arc affinity to A-type Awasib Granite of within-plate affinity may, by analogy with the Topsails suite, argue for a change in the source of these granitoids from mantle to crust.

4.4 SUMMARY

4.4.1 Late-stage (“Sinclair-type”) volcanics

(i) Volcanics of the HFF are bimodal with a paucity of compositions in the range 58–66% SiO_2 . A calc-alkaline or sub-alkalic nature is shown on the TAS diagram and by Peacock’s alkali-lime index, while a high-K nature is evident in the classification of Ewart (1979, 1982). These characteristics, together with the lack of iron enrichment, compare favourably with the calc-alkaline “southern” Barby Formation volcanics (Brown and Wilson, 1986).

(ii) Variation diagrams illustrate regular trends for most oxides and trace elements when plotted against silica. While rhyolites show little compositional variation on a regional basis, basaltic andesites of the southern locality are relatively enriched in TiO_2 , Al_2O_3 , LREE and Zr. MgO and compatible element enrichment of several basaltic andesites may be the result of ferromagnesian mineral accumulation. Scatter in the alkalis, particularly Na_2O , is attributed to alteration, although variation in K_2O could be primary if different magma sources are involved.

(iii) Apart from Ba, there is an overall increase from basaltic andesite to rhyolite in the abundances of incompatible elements (including the LILE and HFSE) and a decrease in the compatible element concentrations. Ba contents vary significantly in the rhyolites, a primary feature not unusual in calc-alkaline suites (Arculus, 1976). Zircon accumula-

tion may account for the marked enrichment in LREE and Zr in one sample of rhyolite lava. While the regular decrease in V with increasing SiO₂ is typical of suites characterised by moderate or no iron enrichment (Gill, 1981), the considerable variation in V in the rhyolites is attributed to a variation in the magnetite content.

(iv) Chondrite-normalised REE patterns for basaltic andesites show LREE enrichment, flat HREE slopes and slightly negative Eu anomalies (Eu/Eu* = 0.85). The REE pattern for a single high-silica rhyolite shows LREE enrichment and a flat HREE slope, but differs from basaltic andesite in the much higher overall enrichment and large negative Eu anomaly (Eu/Eu* = 0.24). REE patterns for the basaltic andesites compare favourably with those of the Barby Formation, but REE patterns for the rhyolite are distinct from the “northern” Barby Formation.

(v) Comparison of the HFF suite with younger volcanic suites illustrates compositional similarities to high-K eruptives along active continental margins (e.g. western USA and Mediterranean; Ewart, 1979, 1982). These features include low (< 1.0%) TiO₂ contents, high abundances of K₂O, Rb, LREE, Th, Zr, and a high ratio of La_N/Ce_N (≈ 1.3). Low abundances of Nb and Y, and Eu/Eu* > 0.75 in the basaltic andesites. Anomalies are the high Ni abundances in basaltic andesites and high Y abundances in rhyolites. There is no obvious affinity of the latter with anorogenic bimodal associations since high-silica biotite rhyolites of the western USA display many of the same chemical characteristics (Ewart, 1979).

(vi) MORB-normalised trace element patterns for basaltic andesite-andesite show a more fractionated, but generally similar, appearance to patterns for high-K and calc-alkaline basalts from active continental margins in Chile, western USA and Iran (Pearce, 1983). These patterns argue for contributions from both a within-plate (high Nb relative to Zr and Zr relative to Y and Yb) source and subduction component (selective enrichment in Sr, K, Rb, Ba, Th, Ce and Sm).

(vii) High-Mg basaltic andesite shows a boninitic affinity as indicated by the ratios Ti/Zr < 100 and Y/Zr < 0.4.

(viii) Chondrite-normalised REE patterns for basaltic andesites closely resemble those patterns displayed by the high-K San Pedro and medium-K Ancud volcanoes along the Andean plate margin (Chile), and are quite unlike patterns displayed by both tholeiitic and calc-alkaline “anorogenic” andesites.

(ix) Chondrite-normalised element patterns for low- and high-silica rhyolites exhibit an overall similarity to Cenozoic intracontinental rift- or hot spot-related rhyolite suites (Sylvester *et al.*, 1987). However, abundances of the elements Ba, Nb, Zr and Ti in low-silica rhyolites, and Ba, Nb, Sr and P in high-silica rhyolites, are more typical of subduction-related rhyolites. While the chondrite-normalised REE pattern for high-silica rhyolite most closely resembles the pattern for orogenic rhyolite from the Inner Zone of Japan, the relative enrichment in HREE is similar to anorogenic rhyolite from the Rio Grande rift.

(x) The observed compositional heterogeneity and A-type chemistry are indications that the HFF rhyolites are largely derived from a crustal source.

4.4.2 Late-stage (“Sinclair-type”) intrusive suites

(i) The HIS, Awasisib and Chowachasib Granites show a significantly shallower trend (similar to the HFF) on a TAS diagram than that of the SIS. This divergence is defined largely by alkalinity, a feature illustrated on a Zr/TiO₂ versus SiO₂ plot.

(ii) The late-stage granitoids are largely granites, except for a few granodiorites in the HIS, according to the normative An-Ab-Or classification of Barker (1979).

(iii) AFM variation further classifies most late-stage intrusives (except some members of the SIS) as calc-alkaline, typically mature series of continental margins. Although individually alkali-calcic on a silica versus calc-alkali ratio plot (Brown, 1982), the HIS and Awasisib Granite show a combined calc-alkalic trend which is only slightly steeper than that of the HFF.

(iv) The late-stage intrusives are predominantly metaluminous (Shand, 1927) with some peralkalinity shown by the Awasisib Granite (agpaitic index=1.06). While the considerable range in the Shand Index for the SIS is considered to reflect the gabbro-syenite compositional range, the significant enrichment in HFSE (Nb + Y) in the Awasisib Granite suggests a within-plate character (Pearce *et al.*, 1984).

(v) Comparison between the HIS-Awasisib “suite” and HFF lavas on variation diagrams shows that the acidic compositions agree well but that the intermediate compositions of the former are typically more enriched in K₂O, Rb, Th, LREE, Zr, Nb, Ni and Cr.

(vi) REE patterns for the rhyolite and Awasisib Granite differ in that the latter is considerably steeper and displays a more pronounced negative Eu anomaly (Eu/Eu* = 0.05). This discrepancy may reflect crustal heterogeneity if these magmas both represent crustal melts, a feature compatible with the broadly similar REE patterns displayed by the A-type Mumbulla suite in southeastern Australia (Collins *et al.*, 1982).

(vii) The HIS-Awasisib trend on a diagram of log(K₂O/MgO) versus SiO₂ compares favourably with the trend for the Sierra Nevada batholith (Rogers and Greenberg, 1981) although the former is more alkaline. While the Chowachasib Granite occupies a similar position in this diagram to the Awasisib Granite, the SIS shows a divergent trend towards more potassic and less silica-rich compositions. The HIS-Awasisib trend may be the result of magmatic differentiation, a change in source, or a change in tectonic regime (increasingly extensional).

(viii) A trend from an arc to within-plate character on the Y + Nb versus Rb diagram of Pearce *et al.* (1984) is only indicated in part, the aberrant nature of the HIS being due to its enrichment in Rb. Comparison with the granites of Central Chile suggests that this enrichment may be the result of variable enrichment of the mantle source, late-stage fluid activity or a high degree of crustal contamination. The compositional similarity between the Awasisib Granite and within-plate granites of Skye and Nigeria suggests the possibility of an enriched mantle source and an assimilation-fractional crystallisation process in its genesis.

(ix) ORG-normalised patterns for the HIS show several features displayed by volcanic-arc granites from Chile, viz.

enrichments in LILE relative to HFSE and low Y relative to the normalising composition. Patterns for the Awasib Granite most closely resemble the “crust-dominated” within-plate pattern of the Sabaloka complex in Sudan (Pearce *et al.*, 1984) with respect to a negative Ba anomaly, enrichment in Rb and Th relative to Nb, and enrichments in Ce and Sm relative to adjacent elements.

(x) Primordial mantle-normalised patterns (Brown *et al.*, 1984) for the HIS and Awasib Granite illustrate a trend of increasing arc maturity with greater depletion in Ba, Sr, P and Ti and greater enrichment in Y, but high-silica granitic magmas show sufficient enrichment in Y and Nb relative to increasing Rb/Zr to suggest the involvement of subcontinental within-plate mantle lithosphere.

(xi) A-type characteristics of the Awasib granite include high levels of silica, alkalis, apgaitic index, Fe/Mg, Y and LREE and low levels of CaO, Ba and Sr. Relatively low Zr and Nb for the Awasib Granite suggest that these characteristics may be derived by extreme fractionation of I-or S-type sources, although the comparatively low volume of the HIS preclude it as a source. The transition from largely I-type HIS of arc affinity to A-type Awasib Granite of within-plate affinity may, by analogy with the Topsails granite suite of western Newfoundland (Whalen *et al.*, 1984), ar-

gue for a change in source of these granitoids from mantle-dominated to crust.

5. GEOCHRONOLOGY

5.1 INTRODUCTION

While petrographic and geochemical data suggest that the late-stage crust of the AMT is made up of rock types which can be correlated with the Sinclair Sequence, age data from the latter is neither well constrained nor abundant. The relatively undeformed Sinclair Sequence, which apparently overlies the NMC, has yielded ages, determined by a variety of radiometric techniques, that are both similar to and older than ages determined for the NMC (age data reviewed in Caben and Snelling, 1984). In order to determine absolute ages and the duration of magmatic activity for the late-stage crust of the AMT, isotopic measurements were carried out on lithologic units from both the AMT and middle-Sinclair Barby Formation. The units analysed were as follows:

(i) Haiber Flats Formation:

- basaltic andesite (Rb-Sr, Pb-Pb)

- rhyolite (Rb-Sr)

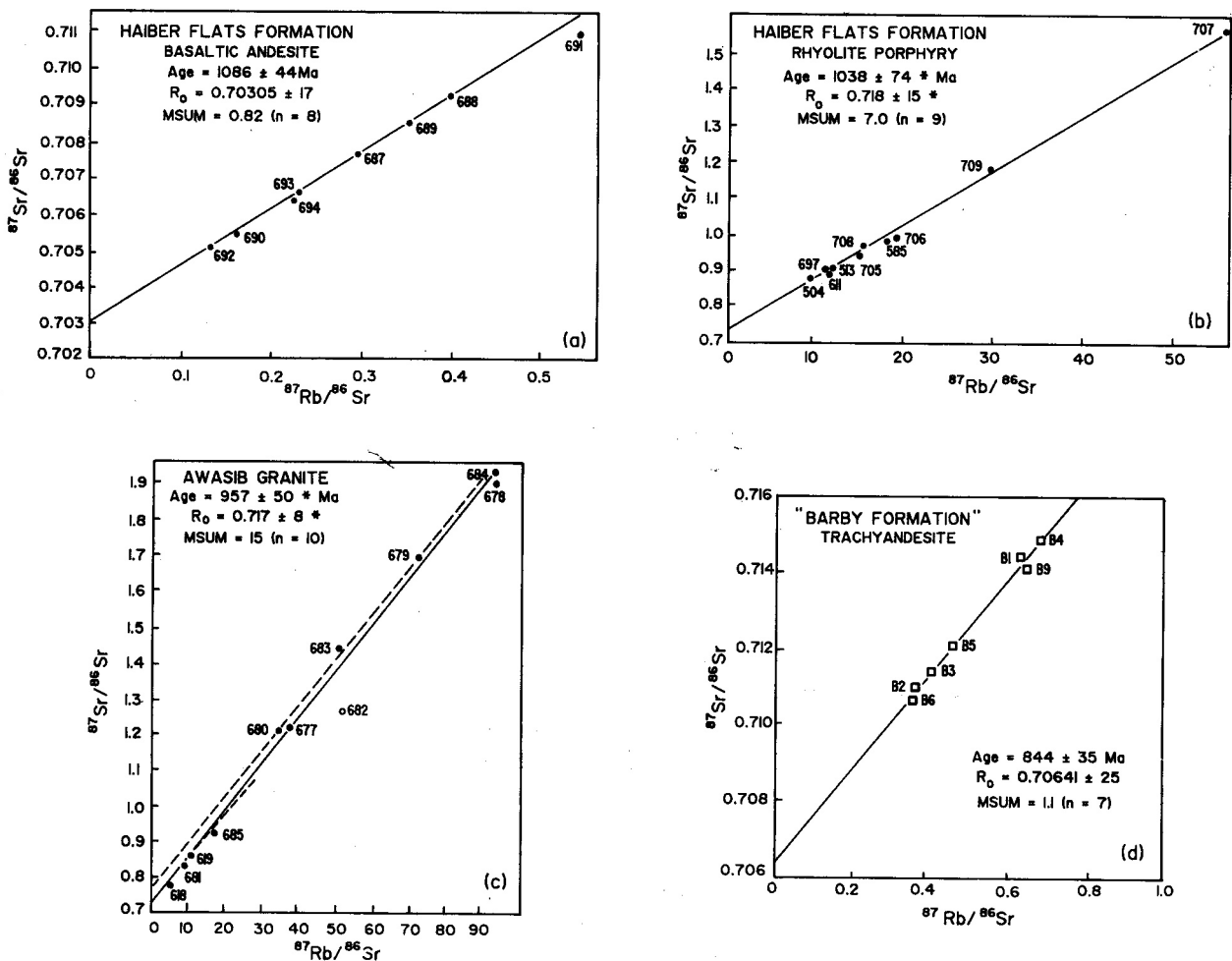


Fig. C.53: Rb-Sr whole-rock data for late-stage AMT and “Sinclair” crust (errors given in Table C.6 and Appendix II):

(a) HFF basaltic andesite: isochron.

(b) HFF rhyolite: errorchron (*).

(c) Awasib Granite: solid line represents an errorchron (*); dashed lines are possible parallel errorchrons of about 895 Ma age (see text). The open symbol BH 682 was excluded from the regression line calculation.

(d) “Barby Formation” trachyandesite: isochron.

TABLE C.6: Isotopic data, late-stage crust.

Lithology and sample number	Rb (ppm)	Sr (ppm)	$^{87}\text{Rb}/^{86}\text{Sr}$ (atomic)	$^{87}\text{Sr}/^{86}\text{Sr}$ (atomic)	$^{206}/^{204}\text{Pb}$	$^{207}/^{204}\text{Pb}$	$^{208}/^{204}\text{Pb}$
Haiber Flats Formation Basaltic Andesite							
BH 687	69.7	699	0.289	0.70763 ± 1			
BH 688	87.1	647	0.390	0.70920 ± 1	19.350	15.768	38.774
BH 689	76.0	639	0.344	0.70846 ± 1	19.147	15.750	38.691
BH 690	38.9	721	0.156	0.70544 ± 1			
BH 691	99.3	533	0.539	0.71122 ± 1	19.173	15.760	38.737
BH 692	28.8	639	0.130	0.70507 ± 1			
BH 693	47.1	606	0.225	0.70657 ± 1	19.528	15.776	39.318
BH 694	46.4	613	0.219	0.70639 ± 1			
Haiber Flats Formation Rhyolite							
BH 504	163	48.7	9.84	0.87197 ± 2			
BH 513	152	37.8	11.8	0.89284 ± 2			
BH 585	182	30.1	14.9	0.97459 ± 2			
BH 611	185	46.9	11.6	0.88677 ± 2			
BH 697	181	46.4	11.5	0.88916 ± 1			
BH 705	162	32.4	14.8	0.93042 ± 1			
BH 706	160	25.0	19.0	0.98562 ± 1			
BH 707	290	16.5	55.0	1.53662 ± 2			
BH 708	249	47.0	15.7	0.96216 ± 1			
BH 709	252	26.0	29.3	1.17164 ± 1			
Awasisb Granite							
BH 618	119	71.7	4.84	0.78325 ± 2			
BH 619	135	40.7	9.74	0.85780 ± 2			
BH 677	269	22.8	35.8	1.21040 ± 2			
BH 678	292	10.3	91.6	1.90512 ± 2			
BH 679	288	12.8	71.4	1.69006 ± 3			
BH 680	296	26.6	33.8	1.20665 ± 2			
BH 681	164	52.2	9.21	0.83989 ± 2			
BH 682	225	13.5	50.8	1.25923 ± 2			
BH 683	247	15.4	49.7	1.4389 ± 6			
BH 684	281	10.0	91.0	1.9284 ± 5			
BH 685	179	31.0	17.1	0.92401 ± 1			
"Barby Formation" trachyandesite							
BH B1	146	657	0.642	0.71429 ± 1			
BH B2	100	797	0.363	0.71082 ± 2	18.416	15.658	38.520
BH B3	101	722	0.406	0.71128 ± 1	18.500	15.686	38.656
BH B4	169	714	0.685	0.71463 ± 1	18.223	15.658	38.272
BH B5	125	796	0.455	0.71197 ± 2			
BH B6	96.4	774	0.361	0.71071 ± 1			
BH B8					17.696	15.610	37.677
BH B9	165	728	0.654	0.71416 ± 1			

All quoted errors given at 2σ ; see Appendix II for detail.

Sample Sr ratios are reproducible to 0.09%; $^{206}/^{204}\text{Pb}$ and $^{207}/^{204}\text{Pb}$ ratios are reproducible to 0.09%.

(ii) Awasisb Granite (Rb-Sr)

(iii) Barby Formation trachyandesite (Rb-Sr, Pb-Pb)

While Rb-Sr work on the AMT lithologic units is discussed in detail in Hoal *et al.* (1986, 1989), it also forms an integral part of this study. Whole-rock Pb-Pb data for the HFF and "Barby Formation" typically show little variation in Pb isotopic composition, hence resulting in large uncertainties in the slopes of regression lines and consequently large uncertainties in the calculated ages. In these instances the data are plotted relative to reference lines, while the $^{238}\text{U}/^{204}\text{Pb}$ ratio (μ) of the source regions can usually be accurately estimated by assuming that the Pb-Pb data emulate secondary isochrons. The μ values are defined

by the intersection of secondary isochrons with Pb growth curves which conform to the second stage of the two-stage Pb isotope evolution model of Stacey and Kramers (1975). Pb data for all suites analysed are compared in Fig. D.2 with both the latter model and the related reservoir growth curves derived from the plumbotectonics model of Zartman and Doe (1981).

The application of isotope tracers in the study of source characteristics is presented in Part D, while chemical and analytical methods (and experimental uncertainties) are given in Appendix n. Sample localities, except for the Barby Formation, are illustrated on the accompanying map (Appendix I).

5.2 ISOTOPE RESULTS

Rb-Sr and Pb-Pb results are presented in Table C.6 and the former also on conventional isochron diagrams in Fig. C.53 (a-d). Since Pb-Pb data on the late-stage crust have little age significance, diagrams form part of the discussion on source characteristics in Part D.

5.2.1 Haiber Flats Formation (HFF) basaltic andesite

(i) Whole-rock Rb-Sr data

The eight analysed samples define a precise isochron (MSUM = 0.8) with an age of 1086 ± 44 Ma and R_0 of 0.70305 ± 17 (Fig. C.53a). The low R_0 indicates a source region having slight time-integrated depletion in Rb/Sr relative to a "Bulk Earth" mantle composition.

(ii) Whole-rock Pb-Pb data

Four of the samples used in the Rb-Sr study define an isochron (MSUM = 0.21) with an age of $563 +2196/-8820$ Ma and $^{238}\text{U}/^{204}\text{Pb}$ (μ) of $10.18 +0.36/-0.62$ (Fig. D.2). Although this "age" and its large uncertainty are of little geochronological significance, the data points do conform to a 1000 Ma reference line. The high μ_2 value for the source region is not easily reconciled with the low R_0 indicative of mantle derivation.

5.2.2 HFF rhyolite

These data, which exhibit significant scatter, define an errorchron (MSUM = 7.0) with an age of $1038 \pm 74^*$ Ma and R_0 of $0.718 \pm 15^*$ (Fig. C.53b). While it may be significant that both of these parameters are within error of those deduced for the basaltic andesite samples, the high R_0 suggests a significant component of melted crust in the genesis of these rhyolites. A choice between these alternatives is precluded by the rather large (augmented) errors on the R_0 estimate. Sample scatter may be attributed to one or more of the following: (a) the samples are not of the same age; (b) the samples have different R_0 ; or (c) the samples did not remain closed systems to Rb and Sr. Field relationships suggest that option (a) is unlikely, but the incorporation of exotic lithic fragments in the rhyolites could possibly account for differences in R_0 during crystallisation of the lavas. However, as the rhyolites show extensive devitrification, the most likely explanation is option (c), i.e. loss of Rb and/or radiogenic Sr during post-crystallisation alteration, particularly during the formation of chlorite and epidote.

5.2.3 Awasis Granite

Ten samples of the Awasis Granite also exhibit significant scatter (MSUM = 15) and the apparent age of $957 \pm 50^*$ Ma and R_0 of $0.717 \pm 8^*$ (Fig. C.53c) needs to be interpreted with caution. Sample BH 682 was excluded from the regression due to its albitised appearance in thin section. Although not conclusive, the age estimate is consistent with field evidence, i.e. the granite is younger than the HFF volcanics. The Awasis Granite is holocrystalline and

contains only minor secondary material (especially when compared with the rhyolites), consequently it is unlikely that the large scatter is due entirely to secondary effects. The high apparent R_0 may thus imply the involvement of pre-existing crustal material in the genesis of the Awasis Granite. It is likely that this material would be compositionally variable and hence incomplete mixing of partial melt fractions extracted from the crustal material would give rise to R_0 heterogeneity in the parent magma. If Awasis Granite data is divided into two groups on the basis of Rb/Sr ratio, i.e. high ratios (samples BH 677, 678, 679, 680, 683, 684) and low ratios (samples BH 618, 619, 681, 685), two sub-parallel errorchrons are apparent (Fig. C.53c). These yield age estimates of $896 \pm 72^*$ Ma (high ratios) and $895 \pm 180^*$ Ma (low ratios), with R_0 estimates of $0.77 \pm 0.05^*$ and $0.72 \pm 0.02^*$, respectively. It is plausible, then, that scatter in this data set is attributable to variation in R_0 at the time of crystallisation. Incomplete mixing can produce misleading ages in whole-rock isotopic dating systems (Juteau *et al.*, 1984) and the deduced age for the Awasis Granite must be viewed with caution.

5.2.4 "Barby Formation" trachyandesite

Ages reported for the Barby Formation in the type area vary significantly (see discussion; Section 5.3) and clearly argued for rigorous sampling, preferably of an individual lithologic unit or member. Accordingly, a single flow of pyroxene-phyric trachyandesite was sampled along a 250 m horizontal profile situated close to the Hahnenkamm trigonometrical beacon on the farm Aubures. A description of the petrography of this flow is given in Watters (1974, p. 38-39). The choice of this lithology was motivated by the following considerations:

(a) Field mapping (Watters, 1974; Brown and Wilson, 1986) indicates that these lavas occupy the stratigraphic position of the Barby Formation, i.e. underlain by sediments of the Kunjas Formation on the farm Klein Haremub and overlain by lavas of the Guperas Formation on the farm Aubures.

(b) Petrography and whole-rock geochemistry reveal mineralogical and compositional similarities between this trachyandesite and basaltic andesite of the HFF.

(c) Previous isotopic work performed on the Barby Formation (see discussion; Section 5.3) has incorporated diverse rocks of volcanic and plutonic origin. Watters (1982) combined Rb-Sr data for a variety of rock types ranging from basalt to syenite, while Kröner (1975, 1977) reported Rb-Sr data from a bimodal basalt-rhyolite association in which the rhyolites show chemical and petrological similarities to the younger Guperas Formation (Brown and Wilson, 1986).

(i) Whole-rock Rb-Sr data

The seven analysed samples define an isochron (MSUM = 1.1) with an age of 844 ± 35 Ma and $^{87}\text{Sr}/^{86}\text{Sr}$ initial ratio (R_0) of 0.70641 ± 25 (Fig. C.53d). This age is considerably younger than expected and the relatively high R_0 may reflect Sr-isotopic homogenisation in the trachyandesite. However, this possibility is not supported by petrographic

evidence which shows these rocks to be largely unaltered. Occasional cross-cutting veins of carbonate do occur, but have been carefully avoided during sampling.

Contamination, if represented by the mixing of two homogeneous sources, should result in a linear array of the data in a simple variation diagram. While the Rb-Sr isochron in Fig. C.53d is compatible with this model, the data scatter in the $1/\text{Sr}$ versus R_0 diagram (Fig. C.54) clearly does not define a mixing line. Still wider data scatter in plots of $^{206}\text{Pb}/^{204}\text{Pb}$ versus $^{87}\text{Sr}/^{86}\text{Sr}$ and $^{208}\text{Pb}/^{204}\text{Pb}$ versus $^{87}\text{Sr}/^{86}\text{Sr}$ is consistent with the absence of simple mixing. Nevertheless, contamination of the magma by a heterogeneous source such as the crust cannot be excluded. This is partly borne out by the relatively high R_0 value of 0.70641 which is inferred to reflect an origin in the lower crust or crustal contamination subsequent to derivation from a mantle source. Assuming the age of 844 Ma to be primary, then the possibility must be entertained that this trachyandesite is younger than the Barby Formation and represents a conformable intrusion or sill.

(ii) Whole-rock Ph-Ph data

Four samples of trachyandesite define an isochron (MSUM = 1.4) with an age of $1271 \pm 836/-1154$ Ma and μ of $10.06 \pm 0.27/-0.33$ (Fig. D.2). Despite the large uncertainty in the calculated age, data points fall close to the 1000 Ma reference line and the calculated age is within error of the Rb-Sr age of 844 ± 35 Ma. The μ_2 value of approximately 10.1 is slightly lower than the value obtained for the HFF, but is more easily reconciled with the relatively high R_0 value, i.e. both Rb-Sr and Pb-Pb data suggest the involvement of crust in the petrogenesis of the trachyandesite.

5.3 DISCUSSION

5.3.1 HFF volcanic succession

The age of the HFF volcanism is provided by the isochron date of 1086 ± 44 Ma for the basaltic andesites. Open system behaviour during devitrification and alteration has given rise to errorchron systematics in the rhyolitic members but the estimated age of 1038 ± 74 Ma is comparable to that of the basaltic andesites. The crustal source of the rhyolites and their interbedded relationship with HFF basaltic andesites may indicate periodic shifts in source region from mantle (\pm crustal component) to crust.

Correlation of the HFF with the Barby Formation of the Sinclair Sequence (Hoal, 1985) would appear to be incorrect in view of the age of 1392 ± 33 Ma inferred for the latter by Watters (1982). However, Watters' (1982) Barby Formation data were recalculated with the NPRL regression program and found to yield an age estimate of 1238 ± 71 Ma and R_0 of $0.7028 \pm 5^*$ with an MSUM of 3.9 (apparently Watters, op. cit., inadvertently quoted one sigma errors on his Fig. 3). Excluding the samples 1557 and 1565, which deviate from the regression line by more than three times the uncertainty (in "X"), the remaining twelve data points yield an isochron estimate (MSUM = 0.9) of 1190 ± 38 Ma and R_0 value of 0.70298 ± 27 . The two deviant samples 1557 and 1565 had R_0 values of 0.7045 and 0.7043, respec-

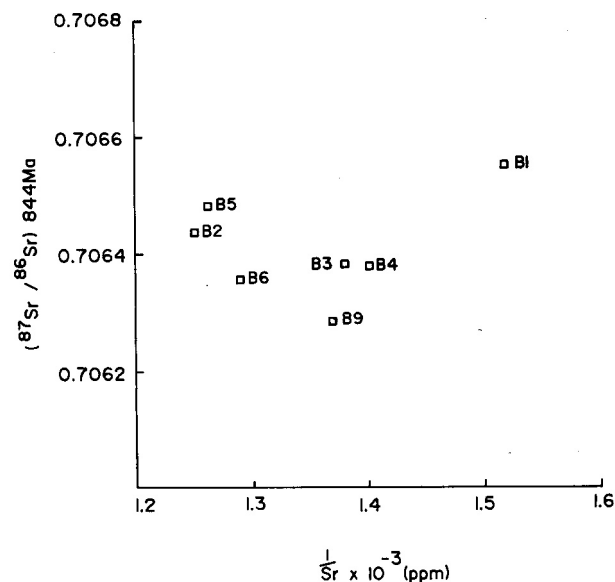


Fig. C.54: $1/\text{Sr}$ vs. $^{87}\text{Sr}/^{86}\text{Sr}$ diagram to illustrate the lack of well-defined mixing in trachyandesite of the "Barby Formation". The $^{87}\text{Sr}/^{86}\text{Sr}$ ratios are calculated for the time of eruption, viz. 844 Ma ago.

tively, at 1190 Ma (i.e. differing by more than the analytical uncertainty) implying that these rocks were derived from a source of different R_0 composition than the bulk of the Barby Formation samples.

Independent support for the age of the Barby Formation is difficult to obtain as several granite bodies which have clearly intruded this formation paradoxically yield much older ages. These ages, which are largely based on U-Pb zircon determinations (reviewed by Watters, 1982), may reflect the existence of relict zircons in the approximate age range 1250 to 1350 Ma. It is further suggested that these inherited zircons were derived from a source of similar age to the early-stage crust in the AMT, e.g. the Kairab Complex or Aunis Tonalite Gneiss.

While the estimate of 1190 Ma for the Barby Formation is also younger than Kröner's (1977) preferred age of 1264 ± 23 Ma (whole-rock Rb-Sr), it is still significantly older than the HFF and a direct time correlation between these formations is not justified. Similarity in R_0 suggests, however, that the basic volcanics of the Barby Formation and HFF were both mantle-derived without any significant contribution from older crust.

The volcano-sedimentary succession of the Koras Group, situated adjacent to the Wilgenhoutsdrif Group, shows petrological and tectonic similarities to the HFF. However, the 1086 Ma age for basaltic andesite of the HFF is significantly younger than the Rb-Sr age of 1176 ± 9 Ma (R_0 of 0.7061 ± 1) reported from basaltic andesite of the middle-Koras Florida Formation by Kröner *et al.* (1977). Better agreement is obtained with Van Niekerk and Burger's (1967) U-Pb zircon age of 1080 ± 70 Ma for the upper Koras quartz porphyry lavas. A syenite associated with the Koras Group has also yielded a Rb-Sr isochron age of 1076 ± 52 Ma with an R_0 of 0.7065 ± 8 (Barton and Burger, 1983), thereby providing supportive evidence for an equivalence between the HFF and upper Koras Group lavas.

While regional and geochronological considerations suggest a similar mode of origin for the HFF (and probably much of the Sinclair Sequence) and the Koras Group, higher R_0 values in the latter argue for a different source or possibly greater crustal influence. The low R_0 value (0.7030 ± 3) of the re-interpreted Barby Formation age of 1190 ± 38 Ma (Hoal *et al.*, 1989) provides additional evidence of regional variation in R_0 between approximately 1200 and 1100 Ma. Significantly, this variation may reflect heterogeneity in the sub-continental mantle of southern Africa during Sinclair times.

The estimated age of $1038 \pm 74^*$ Ma for the HFF rhyolites is also within error of the U-Pb zircon age of 1080 ± 70 Ma obtained by Van Niekerk and Burger (1967) for the upper Koras quartz porphyry lavas, thereby lending support to the overall similarity between these two formations. Slightly younger “feldspar porphyries” in the Goha Hills, Botswana, were extruded from a crustal source at 981 ± 43 Ma (Key and Rundle, 1981) and appear to be consistent with Watters’ (1974) concept of a “Rehoboth Magmatic Arc”.

5.3.2 Awasib Granite

It is not possible to confidently estimate the true age of the Awasib Granite from the available data since wide variations in R_0 are suggested, probably due to incomplete mixing of crust-derived partial melts. However, the calculated age of $957 \pm 50^*$ Ma is within error of the age for the HFF rhyolites and several independent lines of evidence (high R_0 , field relationships and compositional similarities) suggest a close relationship (possibly subvolcanic) between the Awasib Granite and the HFF rhyolites. Somewhat younger ages of approximately 890 Ma have been recorded by Key and Rundle (1981) for magmatic activity subsequent to “intracontinental rifting” in northwestern Botswana. These ages are all younger than the 1100 Ma closing-off of the Namaqua event determined by Barton and Burger (1983).

In their review of tectonothermal events in Africa, Caben and Snelling (1984, p. 434) identify an important event in southwestern Africa at 950 ± 50 Ma. This age is partly defined by late, presumably post-tectonic, pegmatites in the NMC and differs little from the preferred age of the Awasib Granite. The age and A-type chemistry of the Awasib Granite are further compatible with evidence provided by Eglington *et al.* (1986) of significant volumes of A-type granitoids being intruded as recently as 860 Ma ago in the NMC of south-central Natal. Together with extensive metamorphic resetting of undeformed rocks of the Proterozoic Vioolsdrif batholith at between 950 and 920 Ma ago (Reid, 1982), widespread magmatism of A-type affinity in both the NMC and AMT provides evidence for a major tectonothermal event on a regional scale.

5.3.3 “Barby Formation” trachyandesite

The Rb-Sr age of 844 Ma for the “Barby Formation” trachyandesite is difficult to explain unless this unit belongs to a post-Barby intrusive phase, probably a sill judging by its conformable nature. The age is further constrained by the apparent unconformity between this trachyandesite sill

and overlying acid eruptives of the Guperas Formation on the farm Ganaams (Watters, 1974). While there is no available radiometric data for the Guperas Formation, it can be inferred that the age of this formation is older than the *ca.* 1000 Ma estimate for the overlying Aubures Formation (palaeomagnetic data; Kröner, 1977). However, the relatively young age calculated for the trachyandesite is within range of a suspected age of 900 Ma for the post-cratonic Gannakouriep basic dyke swarm (Tankard *et al.*, 1982, p. 273). These uncertainties, compounded by the scatter in the Pb-Pb data, do not allow for a confident interpretation of the 844 Ma age.

5.4 SUMMARY

(i) HFF basaltic andesite defines a Rb-Sr isochron with an age of 1086 ± 44 Ma and R_0 (0.70305 ± 17) indicative of a source region characterised by Rb/Sr similar to “Bulk Earth” mantle. Pb-Pb data have no age significance and the relatively high μ of 10.18 (+.36/-.62) is not easily reconciled with the low R_0 .

(ii) HFF rhyolites define a Rb-Sr errorchron with an age of $1038 \pm 74^*$ Ma and R_0 of $0.718 \pm 15^*$. The age is within error of that for the basaltic andesite, while the high R_0 suggests a component of melted, significantly older, crust in the genesis of the rhyolites.

(iii) The ages of the HFF volcanics are within error of U-Pb zircon and Rb-Sr ages obtained for the upper Koras Group lavas (Van Niekerk and Burger, 1967; Barton and Burger, 1983) and, to a lesser extent, *ca.* 980 Ma old “feldspar porphyries” in the Goha Hills, Botswana (Key and Rundle, 1981).

(iv) A trachyandesite within the type area of the Barby Formation yielded a Rb-Sr isochron age of 844 ± 35 Ma and R_0 of 0.70641 ± 25 . Source mixing is not responsible for the data array and it appears likely that the age is primary, but represents a post-Barby Formation event, e.g. the postcratonic Gannakouriep basic dyke swarm intruded at *ca.* 900 Ma (Tankard *et al.*, 1982). Pb-Pb data correspond to the 1000 Ma reference line and, although poorly constrained, this age is within error of the 844 Ma age. The relatively high μ value of $10.06 +.27/-.33$ is consistent with the R_0 value, both being compatible with crustal involvement in the petrogenesis of the trachyandesite.

(v) Recalculation of previous data for the Barby Formation (Watters, 1982) indicates a preferred age of 1190 Ma and R_0 of 0.70298 ± 27 , hence a direct time correlation with the HFF is not supported.

(vi) The apparent age of $957 \pm 50^*$ Ma and R_0 of $0.717 \pm 15^*$ for the Awasib Granite is within error of the age and R_0 obtained for HFF rhyolite, thereby sustaining the possibility of a subvolcanic relationship. Data scatter may be the result of variation in R_0 at the time of crystallisation as a result of the incomplete mixing of partial melt fractions of the crust. The age of *ca.* 950 Ma defines a widespread tectonothermal event which includes intrusion of late- to post-tectonic pegmatites in the NMC, A-type magmatism in the NMC of south-central Natal and metamorphic resetting of the Vioolsdrif batholith in the Haib.

6. PETROGENESIS OF THE HAIBER FLATS FORMATION VOLCANIC SUCCESSION

6.1 INTRODUCTION

6.1.1 General

Eruptive rocks of the HFF show a compositional range from basaltic andesite to rhyolite and are interbedded in outcrop. Despite deformation and metamorphism, these volcanic rocks define variation trends which are sufficiently regular to allow quantitative petrogenetic modelling. The paucity of intermediate compositions (andesite, dacite and rhyodacite), significant difference in initial $^{87}\text{Sr}/^{86}\text{Sr}$ ratios (R_0 values) between basaltic andesite and rhyolite (Section C.5) and relatively high erupted volume of rhyolite are all factors which argue against magmatic differentiation linking these end members. However, the operation of a crystal fractionation process cannot be excluded for the following reasons:

(i) The intermediate compositions lacking in the HFF may be represented by unerupted equivalents in the Haisib Intrusive Suite (Section C.4).

(ii) The large uncertainty in the R_0 values for the HFF rhyolites (0.718 ± 15) does not preclude the possibility that this ratio could be similar to that of the basaltic andesite (0.70305 ± 17 ; Fig. C.53) and that the rhyolites with lower R_0 could have been derived from a basaltic andesite parent.

(iii) The high volumetric ratio of rhyolite to basaltic andesite may only be apparent in view of the uncertainties in lithostratigraphic correlation and the better preservation of rhyolites due to their more weathering-resistant nature. The occurrence of large volumes of mafic magma in the SIS is important in view of the close temporal (and to some extent compositional- Section C.4) association between the latter and the HFF basaltic andesites.

6.1.2 Petrogenetic models

The petrogenetic processes evaluated in this study as possible processes causing the compositional variation in eruptive rocks of the HFF are as follows:

- (i) Closed system fractional crystallisation (FC)
- (ii) Assimilation and fractional crystallisation (AFC)
- (iii) Magma mixing (MM)
- (iv) Partial melting (PM)

6.1.3 Whole-rock model compositions

Average trend lines may be visually fitted to the data in variation diagrams (Section C.4) and samples can be selected which lie consistently close to these lines. The advantage of using actual whole-rock compositions is that these are, in many cases, complemented by mineral analyses of phenocryst phases.

The following samples have been chosen as representatives of magma compositions which may lie along a calc-alkaline liquid line of descent as illustrated in an AFM diagram (Fig. C.55):

BH 598 High-Mg basaltic andesite MBA

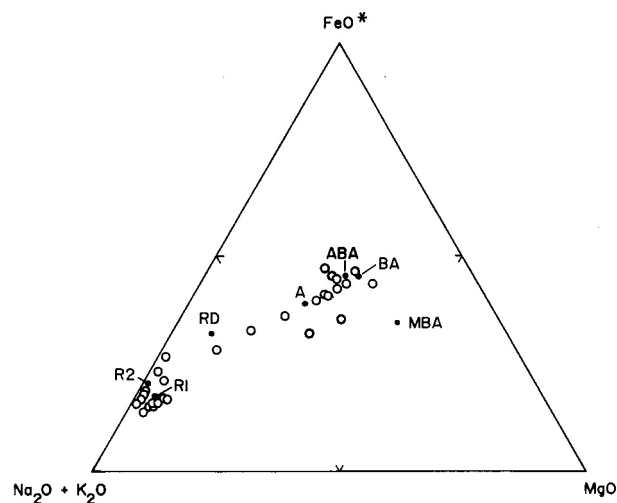


Fig. C.55: AFM diagram showing the calc-alkaline compositional variation of the HFF volcanic suite. Filled circles represent samples chosen for petrogenetic modelling.

BH 694	Basaltic andesite (lowest SiO_2)	BA
BH 690B	Acid basaltic andesite	ABA
BH 574	Andesite	A
BH 660	Rhyodacite	RD
BH 697	Rhyolite (low Ba)	R1
BH 699	Rhyolite (high Ba)	R2

The choice of several samples each of basaltic andesite and rhyolite was influenced by both the compositional variability within these end member groups as well as the lack of data for certain trace elements in the case of analyses performed by the Geological Survey of South Africa, viz. samples BH 694 and BH 697 (comparison of analytical data given in Appendix 11). With the exception of sample BH 574, which comes from the central locality, all the above samples come from the vicinity of Awasis Mountain, or northern locality. The choice of a single sample locality is more likely to exclude the possibility of sampling flows which belong to different volcanic centres. Major and trace element compositions of these samples are listed in Table C.7.

An attempt has been made to relate these compositions (excluding MBA due to its aberrant position in Harker diagrams) to each other by assessing the following stages of magmatic differentiation for both FC and AFC processes, although it is realised that more complicated scenarios are possible:

- (i) Basaltic andesite (BA) - Acid basaltic andesite (ABA)
- (ii) Acid basaltic andesite (ABA) - Andesite (A)
- (iii) Andesite (A) - Rhyodacite (RD)
- (iv) Rhyodacite (RD) - Rhyolite (R1)/(R2)

Various whole-rock compositions have been used in order to assess processes of assimilation. The variation in composition of basement lithologies, although significant, has been represented by the Aunis Tonalite Gneiss due to its volumetric importance, compositional similarity to tonalities and granodiorites of the Khorasib Granite Suite, and the availability of Rb-Sr isotope data. Other potential contaminants considered include the HFF rhyolites BH 697 and BH 699, as well as average continental crust (Taylor and McLennan, 1985).

TABLE C.7: Selected whole-rock compositions used in petrogenetic modelling of the HFF.

	BH 598	BH 694	BH 690B	BH 574	BH 660	BH 697	BH 699	Tonalite Gneiss	Lower Crust	Bulk Crust	Upper Crust	Pyrolite
	MBA	BA	ABA	A	RD	R1	R2	AUNIS	LCRUST	BCRUST	UCRUST	
SiO ₂	54.29	53.74	56.64	60.89	68.50	75.30	76.00	71.95	54.40	57.30	66.00	45.85
TiO ₂	.83	.98	.97	.77	.63	.13	.19	.29	1.00	.90	.50	.20
Al ₂ O ₃	13.17	15.35	15.70	15.35	14.57	12.01	11.89	13.27	16.10	15.90	15.20	3.35
FeO	8.42	9.27	8.27	6.40	4.25	2.05	2.30	4.44	10.60	9.10	4.50	8.13
MnO	.13	.18	.17	.14	.11	.02	.09	.17	.10	.10	.10	.15
MgO	10.94	6.47	5.17	3.87	1.08	.47	.12	1.01	6.30	5.30	2.20	38.73
CaO	6.91	8.95	8.05	6.19	2.74	.72	.55	3.57	8.50	7.40	4.20	3.15
Na ₂ O	2.60	3.14	3.20	3.36	4.25	4.79	4.24	4.00	2.80	3.10	3.90	.41
K ₂ O	2.41	1.66	1.49	2.82	3.68	4.49	4.60	1.22	.34	1.10	3.40	.03
P ₂ O ₅	.30	.25	.34	.21	.19	.01	.02	.09	n.a.	n.a.	n.a.	n.a.
Nb	5.2	6.1	5.6	9.9	14.8	16.1	16.0	6.6	6.0	11	25	.35
Zr	115	123	164	198	234	266	317	95	70	100	190	6.2
Y	23	23	27	39	56	94	78	30	19	20	22	2.2
Sr	470	590	736	427	340	55	29	209	230	260	350	11
Rb	74	51	38	117	146	212	187	33	5.3	32	112	1
Th	2.8	(.5)	5.7	10	18	25	19	1.2	1.1	3.5	10.7	n.a.
Ni	358	48	39	26	2.1	9.0	2.5	0.7	135	105	20	2000
Co	54	26	31	25	6.5	(.5)	(.9)	3.4	35	29	10	110
Cr	718	n.a.	131	119	21	n.a.	21	15	235	185	35	2700
V	166	170	162	127	58	42	4.1	45	285	230	60	75
Ba	709	578	527	959	628	208	1310	519	150	250	550	3.5
Sc	25	n.a.	26	21	8.5	n.a.	5.7	14	36	30	11	20
La	18	n.a.	19	26	40	n.a.	48	8	11	16	30	n.a.
Ce	32	n.a.	44	48	87	n.a.	103	30	23	33	64	n.a.
Nd	24	n.a.	29	31	49	n.a.	62	23	13	16	26	n.a.

Data Sources:

All BH samples analysed at the University of Cape Town except where indicated by an asterisk (Geological Survey); Aunis Tonalite Gneiss is an average of 13 analyses (Appendix III); Crustal averages from Taylor and McLennan (1985); Pyrolite composition based on data from Ringwood (1979) and Frey *et al.* (1978). All Fe expressed as FeO; n.a. = not analysed or not available; parentheses indicate analyses set at detection limit/2.

Magma mixing, which may be viewed as a special case of bulk assimilation, is considered between the end members basaltic andesite and rhyolite in an attempt to yield observed compositions of both andesite and rhyodacite.

Partial melting models address the bimodality of the HFF volcanic suite by considering the petrogenesis of the basaltic andesites and rhyolites separately. Sources in the mantle and crust are considered for mafic and felsic compositions, respectively, and the putative source compositions are listed in Table C.7.

6.1.4 Model mineral compositions

Microprobe analyses of phenocryst phases have been used in all petrogenetic models where possible. Owing to the particularly altered nature of certain phases within flows of the HFF, additional mineral analyses have been used from compositionally similar rocks in the Barby Formation, e.g. olivine, andesine and titanomagnetite. In addition, analyses are supplemented by mineral data, from calc-alkaline rocks where applicable, reported by Deer *et al.* (1966), Reid (1977), Gill (1981), MacGregor (1979), Boyd and Nixon (1973) and Erlank *et al.* (1987). All these mineral compositions are listed in Table C.8.

Mineral abbreviations used in this study are as follows: plagioclase (*plag*), anorthite (*An*), alkali feldspar (*K-spar*), sanidine (*sanid*), olivine (*ol*), forsterite (*Fo*), clinopyroxene (*cpx*), orthopyroxene (*opx*), hornblende (*hbl*), biotite (*biot*), titanomagnetite (*mt*), apatite (*ap*), garnet (*gt*), quartz (*qtz*), phlogopite (*phg*) and ilmenite (*ilm*).

6.1.5 Crystal-liquid distribution coefficients

Distribution coefficients (Kd's) used in this study are listed in Appendix III (Table VI). These values are known to vary as a function of bulk composition (Cox *et al.*, 1979, p. 335) and should, therefore, differ according to the compositional range being evaluated. This study has utilised the most favourable Kd's reported in the literature for compositional ranges which correspond most closely to the bulk compositions under consideration. Unfortunately, independent selection of the most suitable Kd values for individual stages of magmatic differentiation in FC and AFC models has the drawback that the Kd's chosen may not show strong compositional dependence in the passage from basaltic andesite to rhyolite. Nevertheless, adoption of the most favourable Kd's within a specific compositional range generally permits a more conclusive statement to be

TABLE C.8: Mineral composition data used in petrogenetic modelling of the HFF.

	Plagioclase feldspar			K-feldspar	Olivine		Orthopyroxene		Clinopyroxene		
	(An 61)	(An 54)	(An 49)	(Sanid)	(Fo 67)	(Fo 90)	(Opx 1)	(Opx 2)	(Cpx 1)	(Cpx 2)	(Cpx 3)
SiO ₂	53.74	55.79	57.33	67.20	36.03	41.28	52.99	57.33	51.99	53.11	55.20
TiO ₂	n.a.	n.a.	n.a.	n.a.	n.a.	.02	.30	.28	.68	.24	.55
Al ₂ O ₃	28.98	27.84	27.04	18.33	n.a.	.01	1.62	.99	2.71	1.83	2.58
FeO	.69	.44	.34	.83	29.54	9.32	18.64	6.52	7.83	5.51	4.09
MnO	n.a.	n.a.	n.a.	n.a.	.56	.12	.41	.12	.23	.13	.11
MgO	.09	n.a.	n.a.	n.a.	33.69	49.22	23.10	33.57	15.74	16.88	18.48
CaO	12.14	10.72	9.64	.15	.18	.03	2.74	.94	20.50	22.01	16.94
Na ₂ O	4.05	4.86	5.19	6.44	n.a.	n.a.	.20	.26	.31	.29	2.06
K ₂ O	.32	.35	.44	7.04	n.a.	n.a.	n.a.	n.a.	.01	n.a.	n.a.
P ₂ O ₅	n.a.	n.a.	n.a.	n.a.	n.a.	n.a.	n.a.	n.a.	n.a.	n.a.	n.a.

	Hornblende		Biotite		Titano- magnetite	Apatite	Quartz	Garnet	Phlogopite	Ilmenite
	(Hbl 1)	(Hbl 2)	(Biot 1)	(Biot 2)	(Mt)	(Ap)	(Qtz)	(Gt)	(Phg)	(Ilm)
SiO ₂	43.27	48.90	40.44	41.10	n.a.	n.a.	100.00	43.38	43.96	.07
TiO ₂	2.55	1.10	1.16	1.92	14.87	n.a.	n.a.	.50	.60	49.62
Al ₂ O ₃	12.35	8.50	17.62	16.08	.21	n.a.	n.a.	21.65	14.81	.63
FeO	13.06	18.60	12.68	9.68	84.22	.33	n.a.	7.88	3.31	41.16
MnO	.20	n.a.	.22	.11	.57	.02	n.a.	.29	n.a.	n.a.
MgO	14.08	9.50	17.38	20.65	.13	.05	n.a.	21.81	26.73	8.28
CaO	11.33	11.90	.04	.02	n.a.	56.25	n.a.	4.44	n.a.	n.a.
Na ₂ O	2.76	.90	.07	.09	n.a.	.04	n.a.	.06	.05	n.a.
K ₂ O	.41	.50	10.37	10.36	n.a.	.01	n.a.	n.a.	10.08	n.a.
P ₂ O ₅	n.a.	n.a.	n.a.	n.a.	n.a.	43.30	n.a.	n.a.	n.a.	n.a.

n.a. = not analysed or not available

Data Sources:

All microprobe analyses from HFF volcanics and compositionally allied rocks; analyses of Opx 1 and Hbl 1 from orogenic andesites (Gill, 1981); analysis of Hbl 2 from andesite (Reid, 1977); analyses of Sanid and Ap from Deer *et al.* (1966); analyses of Fo 90, Opx 2, Cpx 3 and Gt from garnet peridotite xenolith (MacGregor, 1979); analysis of phlogopite is a GPP average from peridotite nodules (Erlank *et al.*, 1987); ilmenite analysis from sample 2050A - Kao Pipe (Boyd and Nixon, 1973).

made with respect to the viability of a particular petrogenetic model for that compositional range. For this reason two sets of Kd's were considered for the relatively large range of values published for rhyodacitic to rhyolitic magmas. Kd values listed in Appendix m have been compiled from both published work (Frey *et al.*, 1978; Hanson, 1978; Pearce and Norry, 1979; Le Roex, 1980; Henderson, 1984; Nash and Crecraft, 1985) and an unpublished compilation by Ewart and Duncan (pers. comm., 1987).

6.2 CLOSED SYSTEM FRACTIONAL CRYSTALLISATION (FC)

Bulk compositions chosen for modelling closed system fractional crystallisation (FC) match samples which lie consistently close to their average trend lines, here interpreted to be liquid lines of descent, in variation diagrams. Accordingly, these samples are thought to be largely unaffected by crystal accumulation (also see discussion in Section C.4). Fractionating mineral assemblages have been chosen according to petrographic evidence where possible, but this choice has been further influenced by phenocryst assem-

blages typical of more recent eruptive rocks of comparable bulk composition (Ewart, 1976, 1979, 1982; Gill, 1981; Pearce and Norry, 1979). Mineral control lines have played a preliminary role in the selection of fractionating phases, but are difficult to apply to multi-phase assemblages.

The process of closed system fractional crystallisation is here considered to infer the continuous removal of liquidus phases from the melt. The fractionating phases, their proportions and the degree of fractional crystallisation have been calculated using Le Maitre's (1981) least squares mixing approximation (GENMIX). These parameters, obtained by choosing suitable combinations of major oxides, whole-rock and mineral compositions, may be further used to predict trace element concentrations in the derivative melt assuming Rayleigh fractionation. The applicable equations are described in Arth (1976).

6.2.1 Basaltic andesite to andesite (BA-A)

The progression from basaltic andesite (BA) to andesite (A) has been investigated by considering three stages, viz. BA-ABA, ABA-A and BA-A. The observed phenocryst as-

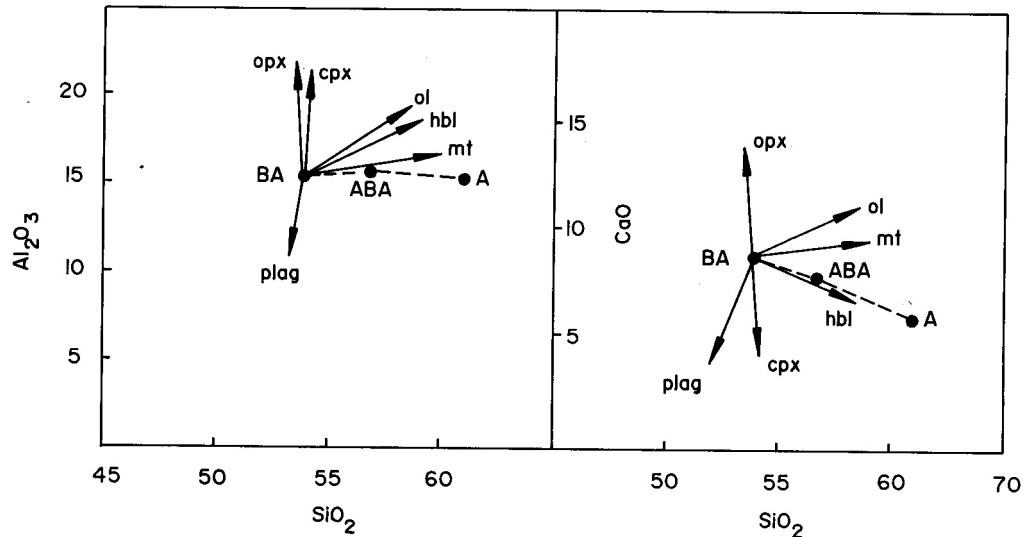


Fig. C.56: Plot of SiO_2 vs. Al_2O_3 and CaO for the progression basaltic andesite (BA) - acid basaltic andesite (ABA) - andesite (A). Vectors represent the path of the residual liquid on removal of different phases from a basaltic andesite magma. Mineral abbreviations are given in the text.

semblage in basaltic andesite is plag + cpx + mt. However, pseudomorphs and pseudomorphic aggregates suggest that an additional ferromagnesian phase(s) was present, probably olivine, or orthopyroxene and hornblende. An additional ferromagnesian phase is also required by consideration of the observed assemblage in the context of mineral control lines (Fig. C.56). Fractional crystallisation of the assemblage plag + cpx + mt indicates that the predominance of plagioclase required to produce the Al_2O_3 - SiO_2 (BA-ABA-A) path would result in a greater depletion in CaO than is displayed by the CaO - SiO_2 path.

In addition, then, to the established assemblage plag + cpx + mt, the phases ol, opx and hbl need to be considered. The likely fractionating assemblage is difficult to constrain by using mineral control lines due largely to the variation in mineral compositions. Olivine is probably only present in the early stage of fractional crystallisation (BA-ABA), thereafter reacting with the increasingly silica-rich liquid to form orthopyroxene. Hornblende is probably absent during the onset of crystallisation (< 56% SiO_2) and is generally thought to be absent in view of petrographic evidence. The most likely additional phases to be considered are, therefore, olivine in the stage BA-ABA and orthopyroxene in the stage ABA-A. The presence of apatite as a fractionating (or accumulating phase) is a further possibility in view of the variation in P_2O_5 from BA to A.

Tables C.9 to C.11 illustrate the best (i.e. lowest residual sum of squares; Le Maitre, 1981) least squares mixing models for three possible stages of fractional crystallisation in the passage from basaltic andesite to andesite. In the progression from BA to A via ABA, the change from a fractionating assemblage of plag + cpx + ol + mt (BA-ABA) to plag + cpx + opx + mt + ap (ABA-A) is accompanied by an increase in the degree of fractional crystallisation from 26% to 41%. An even greater degree of fractional crystallisation (52%) is required if this progression is considered as a single step (BA-A). The fractionating assemblage plag + cpx + ol + mt + ap also indicates that olivine persists despite the high silica content of the liquid. A single-stage evolution

from basaltic andesite to andesite is therefore considered less feasible than that of a changing phase assemblage, but is included here for later comparison with AFC models.

Selected trace elements have been modelled for the stages BA-ABA and ABA-A and the predicted results presented in Tables C.10 (b) and C.11 (b), and Fig. C.57. In the first stage the predicted depletion in compatible elements (Ni, Co, V) is greater than observed, while the degree of enrichment predicted for K-group elements (K, Ba, Rb, but not Sr) is generally too high. However, since we are dealing with metamorphosed rocks, more emphasis should be placed on the predictions of relatively immobile high field strength elements (HFSE) as advocated by Pearce and Norry (1979). Reasonable agreement between actual and modelled trends is evident for the first stage in variation diagrams involving Nb, Y and Zr as well as in plots of Nb, Y and TiO_2 against Zr (Fig. C.57).

In the second stage (ABA-A), it is again evident that both compatible (except V) and K-group elements can not be satisfactorily accounted for by a model of fractional crystallisation alone. HFSE (except Ti) generally display enrichments which are greater than predicted and may suggest crystal accumulation of an accessory phase (e.g. zircon) not accounted for in this model.

6.2.2 Andesite to rhyodacite (A-RD)

A fractionating assemblage was selected with difficulty for this stage owing to pervasive deformation and metamorphism of most andesites in the HFF. The assemblage plag + biot + qtz + mt ± cpx is observed in a few andesites at the central locality and may be considered relevant to any process of fractional crystallisation. Hornblende, although not observed, is considered a likely additional phase in terms of comparison with high-K andesites reported in the literature and in view of compositionally and texturally similar hornblende-phyric trachyandesites in the Barby Formation. The appearance of apatite as a fractionating phase in the previ-

TABLE C.9: Closed system fractional crystallisation: basaltic andesite - andesite (BA - A).

(a) Least squares mixing approximation for FC model.				(b) Predicted trace element abundances in andesite magma using Kd values for "basaltic andesite" (Appendix III), parameters in (a) and the Rayleigh equation.							
Target Composition (A)			Starting Composition (BA)		Fractiona- Propns. ting phases wt.%		BA	A	Magma	% Diff.	Bulk-D
Actual	Estimated	Diff.									
SiO ₂	60.89	60.65	-0.24	An 54	53.89	Nb	6.1	9.9	6.5	-33.9	0.906
TiO ₂	0.77	0.81	0.04	Cpx 2	22.51	Zr	123	198	243	22.8	0.079
Al ₂ O ₃	15.35	15.26	-0.09	Fo 67	15.00	Y	23	39	27	-30.4	0.776
FeO*	6.40	6.22	-0.18	Mt	7.29	Ba	578	959	777	-18.9	0.599
MnO	0.14	0.21	0.07	Ap	1.30	Sr	590	427	711	66.5	0.748
MgO	3.87	3.84	-0.02			Rb	51	117	92	-21.7	0.208
CaO	6.19	6.17	-0.02			Ni	48	26	10	-61.3	3.112
Na ₂ O	3.36	3.64	0.28			Co	26	25	20	-19.9	1.353
K ₂ O	2.82	3.27	0.45			V	170	127	119	-6.4	1.484
P ₂ O ₅	0.21	-0.09	-0.30								
Total	100.00	99.98			F-value = 0.48						

Residual sum of squares = 0.476

TABLE C.10: Closed system fractional crystallisation: basaltic andesite - acid basaltic andesite (BA - ABA).

(a) Least squares mixing approximation for FC model.				(b) Predicted trace element abundances in acid basaltic andesite magma using Kd values for "basaltic andesite" (Appendix III), parameters in (a) and the Rayleigh equation.							
Target Composition (ABA)			Starting Composition (BA)		Fractiona- Propns. ting phases wt.%		BA	ABA	Magma	% Diff.	Bulk-D
Actual	Estimated	Diff.									
SiO ₂	56.64	56.24	-0.40	An 61	49.46	Nb	6.1	5.6	6.3	12.6	0.889
TiO ₂	0.97	0.93	-0.04	Cpx 2	25.68	Zr	123	164	162	-1.1	0.082
Al ₂ O ₃	15.70	15.54	-0.16	Fo 67	17.79	Y	23	27	27	1.1	0.431
FeO*	8.27	7.97	-0.30	Mt	7.08	Ba	578	527	661	25.4	0.556
MnO	0.17	0.18	0.01			Sr	590	736	655	-11.1	0.655
MgO	5.17	5.10	-0.07			Rb	51	38	65	71.1	0.193
CaO	8.05	7.99	-0.06			Ni	48	39	22	-44.4	3.640
Na ₂ O	3.20	3.51	0.31			Co	26	31	22	-27.6	1.490
K ₂ O	1.49	2.19	0.70			V	170	162	147	-9.2	1.480
P ₂ O ₅	0.34	0.34	0.00								
Total	100.00	99.98			F-value = 0.74						

Residual sum of squares = 0.872

TABLE C.11: Closed system fractional crystallisation: acid basaltic andesite - andesite (ABA - A).

(a) Least squares mixing approximation for FC model.				(b) Predicted trace element abundances in andesite magma using Kd values for "andesite"(Appendix III), parameters in (a) and the Rayleigh equation.							
Target Composition (A)			Starting Composition (ABA)								
Actual	Estimated	Diff.	Fractiona- ting phases	Propns. wt.%	ABA	A	Magma	% Diff.	Bulk-D		
SiO ₂	60.89	61.00	0.11	An 54	55.45	Nb	5.6	9.9	8.6	-13.6	0.185
TiO ₂	0.77	0.81	0.04	Cpx 1	18.55	Zr	164	198	256	29.4	0.140
Al ₂ O ₃	15.35	15.33	-0.02	Opx 1	18.23	Y	27	39	35	-10.8	0.512
FeO*	6.40	6.47	0.07	Mt	6.91	Ba	527	959	855	-10.8	0.068
MnO	0.14	0.18	0.04	Ap	0.87	Sr	736	427	543	27.2	1.585
MgO	3.87	3.83	-0.04			Rb	38	117	63	-45.9	0.017
CaO	6.19	6.22	0.03			Th	5.7	10	9.5	-6.2	0.022
Na ₂ O	3.36	3.48	0.12			Ni	39	26	20	-21.7	2.252
K ₂ O	2.82	2.37	-0.45			Co	31	25	25	-1.3	1.440
P ₂ O ₅	0.21	0.32	0.11			Cr	131	119	30	-75.0	3.855
Total	100.00	100.00			F-value = 0.59	V	162	127	127	0.0	1.468
Residual sum of squares = 0.250						Sc	26	21	16	-22.4	1.900
						La	19	26	27	5.1	0.301
						Ce	44	48	55	15.1	0.562
						Nd	29	31	34	9.3	0.701

TABLE C.12: Closed system fractional crystallisation: andesite - rhyodacite (A - RD).

(a) Least squares mixing approximation for FC model.				(b) Predicted trace element abundances in rhyodacite magma using Kd values for "dacite"(Appendix III), parameters in (a) and the Rayleigh equation.							
Target Composition (RD)			Starting Composition (A)								
Actual	Estimated	Diff.	Fractiona- ting phases	Propns. wt.%	A	RD	Magma	% Diff.	Bulk-D		
SiO ₂	68.50	68.50	0.00	An 49	43.78	Nb	9.9	14.8	14.3	-3.1	0.444
TiO ₂	0.63	0.62	-0.01	Cpx 1	18.54	Zr	198	234	243	3.8	0.693
Al ₂ O ₃	14.57	14.57	0.00	Biot 1	15.74	Y	39	56	52	-7.7	0.576
FeO*	4.25	4.25	0.00	Hbl 2	12.41	Ba	959	628	773	23.0	1.325
MnO	0.11	0.18	0.07	Qtz	5.68	Sr	427	340	343	0.9	1.329
MgO	1.08	1.06	-0.02	Mt	3.28	Rb	117	146	131	-10.1	0.828
CaO	2.74	2.75	0.01	Ap	0.57	Th	10.1	17.7	17.5	-1.3	0.178
Na ₂ O	4.25	4.22	-0.03			Ni	26	2.1	5.5	159.8	3.345
K ₂ O	3.68	3.70	0.02			Co	25	6.5	0.8	-88.5	6.275
P ₂ O ₅	0.19	0.17	-0.02			Cr	119	21	6.4	-69.6	5.393
Total	100.00	100.02			F-value = 0.51	V	127	58	3.3	94.3	6.489
Residual sum of squares = 0.007						Sc	21	8.5	5.3	-37.3	3.059
						La	26	40	43	8.2	0.234
						Ce	48	87	77	-11.6	0.293
						Nd	31	49	43	-12.9	0.520

ous stage (ABA-A) is also likely to persist in this stage. The chosen fractionating assemblage $\text{plag} + \text{cpx} + \text{biot} + \text{hbl} + \text{qtz} + \text{mt} + \text{ap}$ is presented in Table C.12 (a) together with a least squares approximation for the major element modelling.

While the low residual sum of squares (0.007) is probably due to the large number of phases in the chosen assemblage, the high degree of fractional crystallisation (49%) is thought to be likely in view of the highly phyric nature of the andesite flows. Trace element modelling (Table C.12 (b); Fig. C.57) reveals reasonable agreement for the K-group elements (except Ba), LREE and HFSE, but poor agreement for most of the compatible elements. The latter deviation is largely the result of the high K_d 's considered likely in the ferromagnesian phases, which causes significant depletion of these elements due to high bulk D 's. When plotted against Zr, it is difficult to relate the depletion of V, itself a relatively immobile element, to alteration. Accordingly, in order to accommodate a FC model it appears necessary to invoke the accumulation of an accessory phase for which V has a high K_d , e.g. zircon. Alternatively, K_d values used for V in the fractionating phases are too high.

6.2.3 Rhyodacite to rhyolite (RD-R1, RD-R2)

The choice of two target compositions for this stage represents an attempt to account for the variability in composition within the rhyolite group. The fractionating assemblages chosen are based only partly on petrography owing to widespread recrystallisation in response to deformation and metamorphism. However, by taking into account the nature of the fractionating assemblage for the previous stage, it is possible to make only slight changes in order to construct an assemblage which differs little from calc-alkaline rhyodacite phenocryst assemblages reported in the literature (e.g. Ewart, 1979, Pearce and Norry, 1979).

The two FC processes investigated here argue for slightly different fractionating assemblages (d. Tables C.13 and C.14). The major changes relative to the previous stage (A-RD) involve the loss of hornblende as a fractionating phase in the stage RD-R1 as opposed to the loss of clinopyroxene in the stage RD-R2, and the appearance of K-spar in both RD-R1 and RD-R2. While both biotite and hornblende compositions (Table C.8) exhibit an expected enrichment in Ti in progressing from rhyodacite to rhyolite, the decrease in Fe/Mg ratios in both phases is not easily explained. The relatively calcic plagioclase (An_{49}) in the fractionating assemblages is questionable in such silica-rich liquids, but adoption of more sodic plagioclase compositions has not proved as effective in modelling the FC process. While the fractionating assemblage used in modelling the stage RD-R1 resembles the petrography more closely, the calculated 56% of fractional crystallisation may be less realistic than only 42.9% fractional crystallisation calculated for the stage RD-R2.

Trace element modelling for these two stages is presented in Tables C.13 and C.14, and Fig. C.57. For the stage RD-R1, acceptable predictions are obtained for both K-group elements (except Th) and HFSE (except Zr). Compatible elements, however, show significantly less depletion than

predicted. For the stage RD-R2, modelling of a greater number of trace elements yields worse predictions for the K-group elements, but slightly improved agreement for the compatible elements if the low levels of abundance are taken into account. The HFSE (except Y) show acceptable agreement. However, examination of the rhyolite data cloud (Fig. C.57) indicates a variation for many elements which is far greater than that of the target samples chosen. Taking this scatter into account suggests that the variation is too great to be accounted for by a FC model. This feature is particularly well illustrated in plots which use Zr as an index of magmatic fractionation (Fig. C.57). The variation in immobile element ratios (e.g. Zr/Y , Zr/Nb) implied by the compositional variation of the rhyolites suggests that another factor or process, rather than fractional crystallisation, was the dominant control.

6.2.4 Discussion

If it is assumed that there is some latitude in the model parameters chosen and allowance is made for the effects of deformation and metamorphism, then it seems reasonable to suggest that closed system fractional crystallisation could have operated in order to produce the compositional variation from basaltic andesite to andesite (and possibly rhyodacite) in the HFF. However, continuation of this process to produce liquids of appropriate rhyolitic composition is not favoured by petrogenetic modelling. It further appears likely that at least some other additional process must have occurred in order to allow for the variation in certain immobile elements, e.g. Zr and V, in the sequence BA to R.

Consideration of the overall trend from basaltic andesite to rhyolite as a function of increasing Zr content illustrates several points by analogy with both observed and modelled fractionation trends reported by Pearce and Norry (1979):

(i) The change in crystallising mafic phases from clinopyroxene-dominated (basaltic andesite-andesite) to amphibole \pm biotite-dominated (andesite-rhyodacite) in the HFF reflects higher $p_{\text{H}_2\text{O}}$ in the magma, possibly as a result of the increasing involvement of continental crust.

(ii) The compositional variation in the rhyolites in terms of Zr and Y may be caused by a varying proportion of zircon and hydrous phases in the fractionating assemblage. Variability in both Y and Zr has been variously attributed to amphibole (Brown *et al.*, 1977) and biotite + zircon (Pearce and Norry, 1979) in fractionating volcanic-arc suites.

(iii) The initial decrease in Ti with increasing Zr may continue to decrease with decreasing Zr in rocks of more acid composition. This trend is shown by several Andean-type arcs (e.g. Chile) and is attributed to increasing amphibole and biotite crystallisation by Pearce and Norry (1979).

(iv) While an overall trend of increasing Nb with increasing Zr is evident for the HFF, scatter within the rhyolites is significant. Complex clusters of points on plots of Zr versus Nb have been recorded for suites from Andean-type margins and are again attributed to the importance of amphibole and biotite + zircon as crystallising phases by Pearce and Norry (1979).

TABLE C.13: Closed system fractional crystallisation: rhyodacite - rhyolite (RD - R1).

(a) Least squares mixing approximation for FC model.				(b) Predicted trace element abundances in rhyolite magma using Kd values for "rhyodacite to rhyolite" (Appendix III), parameters in (a) and the Rayleigh equation.							
Target Composition (R1)			Starting Composition (RD)								
Actual	Estimated	Diff.	Fractiona- ting phases	Propns. wt.%	RD	R1	Magma	% Diff.	Bulk-D		
SiO ₂	75.30	75.28	-0.02	An 49	35.95	Nb	14.8	16.1	16.8	4.6	0.844
TiO ₂	0.13	0.16	0.03	Sanid	31.31	Zr	234	266	321	20.7	0.620
Al ₂ O ₃	12.01	12.00	-0.01	Qtz	18.18	Y	56	94	90	-4.4	0.432
FeO*	2.05	2.02	-0.03	Biot 2	6.48	Ba	628	208	229	10.0	2.213
MnO	0.02	0.20	0.18	Mt	5.74	Sr	340	55	51	-7.9	3.288
MgO	0.47	0.43	-0.04	Cpx 1	1.51	Rb	146	212	204	-4.0	0.600
CaO	0.72	0.72	0.00	Ap	0.84	Th	17.7	25	34	35.7	0.218
Na ₂ O	4.79	4.71	-0.08			Ni	2.1	9.0	2.1	-76.8	1.009
K ₂ O	4.49	4.52	0.03			Co	6.5	(0.5)	0.46	-8.9	4.195
P ₂ O ₅	0.01	-0.03	-0.04			V	58	42	9.9	-76.5	3.131
Total	99.99	100.01		F-value = 0.44							

Residual sum of squares = 0.044 (Value in parentheses represents analysis set at detection limit/2)

TABLE C.14: Closed system fractional crystallisation: rhyodacite - rhyolite (RD - R2).

(a) Least squares mixing approximation for FC model.				(b) Predicted trace element abundances in rhyolite magma using Kd values for "rhyodacite to rhyolite" (Appendix III), parameters in (a) and the Rayleigh equation.							
Target Composition (R2)			Starting Composition (RD)								
Actual	Estimated	Diff.	Fractiona- ting phases	Propns. wt.%	RD	R2	Magma	% Diff.	Bulk-D		
SiO ₂	76.00	75.99	-0.01	An 49	41.39	Nb	14.8	16.0	16.6	3.9	0.789
TiO ₂	0.19	0.22	0.03	Sanid	27.32	Zr	234	317	298	-6.0	0.563
Al ₂ O ₃	11.89	11.89	0.00	Hbl 1	11.45	Y	56	78	55	-29.7	1.038
FeO*	2.30	2.28	-0.02	Qtz	9.80	Ba	628	1310	763	-41.8	0.648
MnO	0.09	0.15	0.06	Mt	5.58	Sr	340	29	57	98.1	4.218
MgO	0.12	0.13	0.01	Biot 2	3.62	Rb	146	187	195	4.4	0.474
CaO	0.55	0.49	-0.06	Ap	0.82	Th	17.7	19	29	50.7	0.130
Na ₂ O	4.24	4.27	0.03			Ni	2.1	2.5	1.2	-49.9	1.934
K ₂ O	4.60	4.53	-0.07			Co	6.5	(0.9)	1.2	32.2	4.074
P ₂ O ₅	0.02	0.07	0.05			Cr	21	21	8.3	-60.6	2.686
						V	58	4.1	1.6	-61.3	7.515
Total	100.00	100.01		F-value = 0.58		Sc	8.5	5.7	4.4	-23.0	2.197
						La	40	48	50	5.2	0.578
						Ce	87	103	116	12.3	0.484
						Nd	49	62	53	-13.8	0.842

Residual sum of squares = 0.016

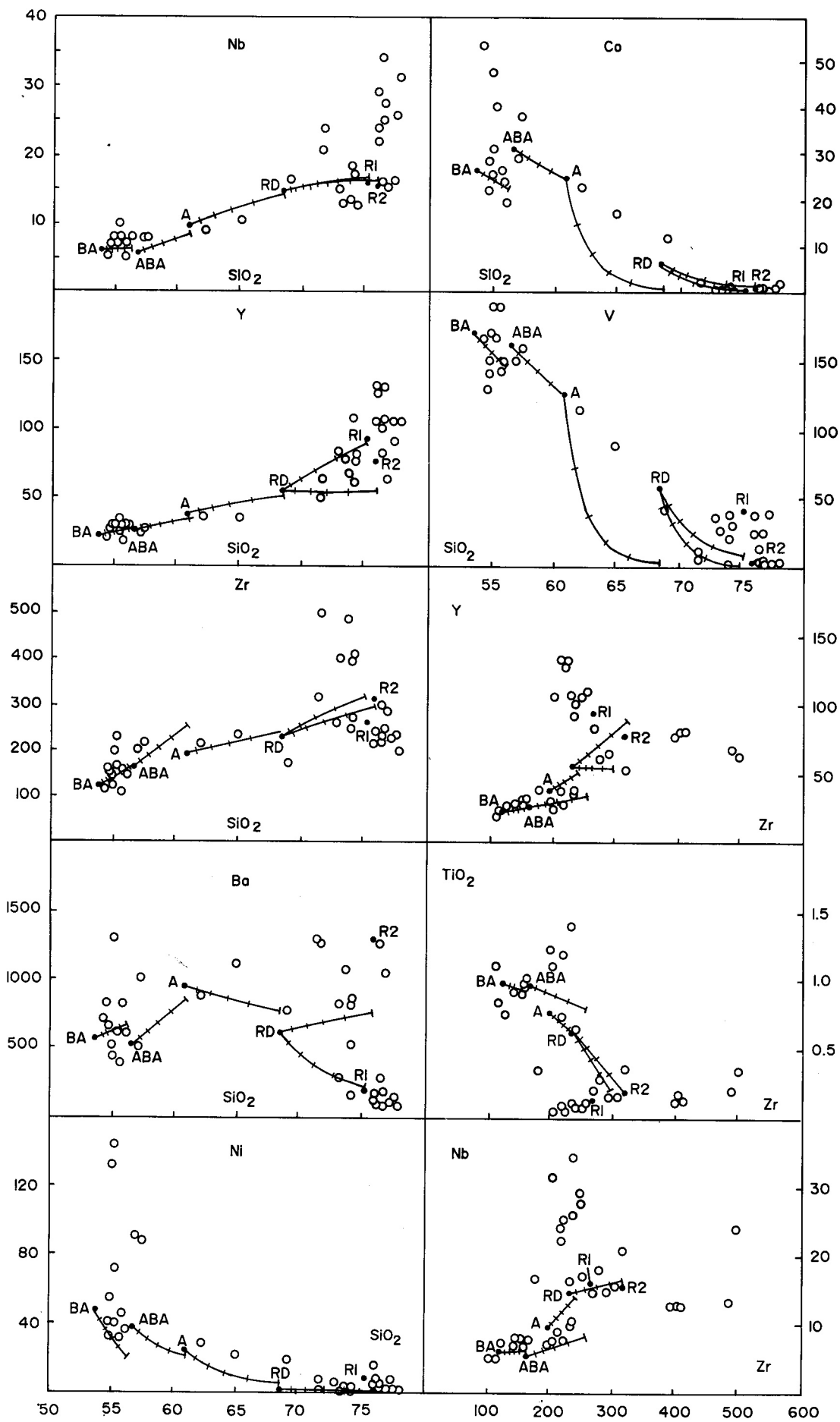


Fig. C.57: Trace element variation diagrams (with SiO_2 and Zr as abscissas) illustrating trajectories calculated for closed system fractional crystallisation (FC) of the HFF volcanics. Bars on the trajectories indicate increments of F for each stage: BA-ABA (0.15), ABA (0.12), A-RD (0.10), RD-RI (0.12) and RD-R2 (0.12). Symbols as in Fig. C.55.

Consideration, then, of both the overall and stage-by-stage evolution of the HFF volcanics suggests that closed system fractional crystallisation (*sensu stricto*) was unlikely to have operated subsequent to the derivative liquid reaching an andesitic composition. Therefore other petro-genetic models need to be evaluated.

6.3 ASSIMILATION-FRACTIONAL CRYSTALLISATION (AFC)

The AFC model considers combined wall-rock assimilation and fractional crystallisation operating simultaneously in a magma chamber. Quantitative modelling of the major elements has been carried out using a modified version of Le Maitre's (1981) GENMIX program (Duncan, pers. comm., 1987) with selected whole-rock, mineral and assimilant compositions as input parameters. Least squares approximation of these parameters enables estimates of the degree of fractional crystallisation (F) and the ratio assimilation rate / crystallisation rate ($M_a/M_c = r$). The trace element composition of the derivative liquid may be calculated by using estimates of these parameters in the equations published by De Paolo (1981).

A wide choice of potential assimilant compositions was considered in order to take account of the lithologic diversity in the AMT (Table C.7). These assimilants included representative compositions from the "basement" (Aunis Tonalite Gneiss) and "cover" (HFF rhyolites R1 and R2; HFF rhyodacite RD) as well as averages for the upper, lower and bulk continental crust (Taylor and McLennan, 1985). Apart from the composition of the assimilant, it is clear that the overall composition of the fractionating assemblage will influence the values of both F and r. The fractionating assemblages utilised in AFC models are the same as those determined for FC models, since these assemblages have a basis in petrography and enable direct comparison between FC and AFC models.

As will be shown, with the exception of the stage from basaltic andesite to andesite (BA-A), consideration of a wide variety of assimilants is generally not able to improve substantially on the predictions of pure FC models. Values

of F, r and the residual sum of squares obtained for preliminary assessment of the stages BA-A, A-RD, RD-R1 and RD-R2 are given in Table C.15. Only data for the more realistic models are presented in Tables C.16 to C.21, while a comparison between AFC and FC models is illustrated for the stage BA-A in Fig. C.58.

6.3.1 Basaltic andesite to andesite (BA-A).

Low initial R_0 values (0.70305 ± 17) for the compositional range BA-ABA suggest that assimilation did not accompany fractional crystallisation at this early stage, although no increase in R_0 would be expected if the assimilant consisted of cogenetic rhyolite of similar age. Consideration of the stage ABA-A yields poor model predictions for all assimilants, often resulting in negative values of r and unrealistic amounts of fractional crystallisation. Accordingly, the more general case of BA-A has been modelled using the same basic parameters determined in the FC model (Table C.9).

The most successful AFC models for this stage have utilised the HFF rhyolites as assimilants. Slightly better results are yielded by the rhyolite sample R1, which indicates an AFC process involving moderate degrees of assimilation ($r = 0.46$) and fractional crystallisation ($\approx 19\%$) and better agreement for most major and trace elements than those predicted by the FC process (Table C.16, Fig. C.58). Consideration of average lower crust as the assimilant ($r = 0.37$; $F = 0.58$) yields a poorer model fit for the HFSE relative to R1, but generally improved predictions for compatible elements (e.g. Ni and V) - Table C.17.

Relative to the predictions of a FC model, the AFC model is better able to account for the trace element concentrations in andesitic derivative liquids. The compositional variation in the rhyolite group allows for considerable latitude in the model predictions, but is not able to account for the relatively high levels of compatible elements in andesites. A possible explanation is that admixtures of an assimilant similar in composition to the lower or bulk crust have been able to contaminate the magma with respect to such elements as Ni, Co and V. Alternatively, some of these varia-

TABLE C.15: Summary of AFC modelling data (abbreviations explained in Table C.7 and text).

Fractionation Stage	Assimilant	F-value	r-value	Residual sum of squares	Fractionation Stage	Assimilant	F-value	r-value	Residual sum of squares	
BA-A	RD	1.03	1.11	0.12	RD-R1	R2	0.43	-1.31	0.03	
	R1	0.81	0.46	0.20		AUNIS	-3.11	-0.56	0.005	
	R2	0.90	0.69	0.10		UCRUST	0.44	0.002	0.04	
	AUNIS	0.61	0.17	0.11		LCRUST	0.68	0.26	0.02	
	UCRUST	1.48	2.88	0.07		BCRUST	0.66	0.29	0.02	
	LCRUST	0.58	0.37	0.02						
	BCRUST	0.67	0.47	0.03						
A-RD	R1	0.93	0.81	0.004	RD-R2	R1	0.55	-0.33	0.01	
	R2	0.49	-0.04	0.007		AUNIS	0.55	-0.15	0.01	
	AUNIS	0.53	0.04	0.006		UCRUST	1.34	4.14	0.003	
	UCRUST	0.55	0.08	0.007		LCRUST	0.66	0.08	0.01	
	LCRUST	0.51	0.03	0.006		BCRUST	0.69	0.14	0.01	
	BCRUST	0.52	0.05	0.006						

TABLE C.16: Assimilation-fractional crystallisation: basaltic andesite - andesite (rhyolite assimilant).

(a) Least squares mixing approximation for AFC model.

(b) Predicted trace element abundances in andesite magma using Kd values for "basaltic andesite" (Appendix III), parameters in (a) and De Paolo's (1981) equations.

	Target Composition (A)			Starting Composition (BA)			BA	R1	A	Magma	% Diff.	Bulk-D
	Actual	Estimated	Diff.	Fractiona- ting phases	Propns. wt.%							
SiO ₂	60.89	60.80	-0.09	An 54	48.66	Nb	6.1	16.1	9.9	7.8	-20.8	0.946
TiO ₂	0.77	0.72	-0.05	Cpx 2	26.43	Zr	123	266	198	197	-0.3	0.086
Al ₂ O ₃	15.35	15.25	-0.10	Fo 67	16.13	Y	23	94	39	37	-6.0	0.788
FeO*	6.40	6.34	-0.06	Mt	7.62	Ba	578	208	959	617	-36.1	0.549
MnO	0.14	0.15	0.01	Ap	1.15	Sr	590	55	427	569	33.2	0.680
MgO	3.87	3.84	-0.03			Rb	51	212	117	98	-16.2	0.192
CaO	6.19	6.17	-0.02	F-value = 0.81		Ni	48	9.0	26	17.2	-34.0	3.387
Na ₂ O	3.36	3.76	0.40			Co	26	(0.5)	25	18.3	-26.7	1.466
K ₂ O	2.82	2.84	0.02	r-value = 0.46		V	170	42	127	120	-5.2	1.579
P ₂ O ₅	0.21	0.10	-0.11	(Ma/Mc)								
Total	100.00	99.99		Assimilant = R1								

Residual sum of squares = 0.196

TABLE C.17: Assimilation-fractional crystallisation: basaltic andesite - andesite ("Lower Crust" assimilant).

(a) Least squares mixing approximation for AFC model.

(b) Predicted trace element abundances in andesite magma using Kd values for "basaltic andesite" (Appendix III), parameters in (a) and De Paolo's (1981) equations.

	Target Composition (A)			Starting Composition (BA)			BA	LCRUST	A	Magma	% Diff.	Bulk-D
	Actual	Estimated	Diff.	Fractiona- ting phases	Propns. wt.%							
SiO ₂	60.89	60.89	0.00	An 54	54.62	Nb	6.1	6.0	9.9	6.3	-36.4	0.952
TiO ₂	0.77	0.73	-0.04	Cpx 2	22.76	Zr	123	70	198	227	14.4	0.079
Al ₂ O ₃	15.35	15.33	-0.02	Fo 67	14.34	Y	23	19	39	31	-20.7	0.550
FeO*	6.40	6.41	0.01	Mt	7.74	Ba	578	150	959	640	-33.3	0.606
MnO	0.14	0.18	0.04	Ap	0.53	Sr	590	230	427	611	43.0	0.735
MgO	3.87	3.87	0.00			Rb	51	5.3	117	76	-35.5	0.210
CaO	6.19	6.20	0.01	F-value = 0.58		Ni	48	135	26	24	-6.6	3.011
Na ₂ O	3.36	3.48	0.12			Co	26	35	25	22	-11.2	1.355
K ₂ O	2.82	2.79	-0.03	r-value = 0.37		V	170	285	127	138	8.9	1.562
P ₂ O ₅	0.21	0.21	0.00	(Ma/Mc)								
Total	100.00	100.08		Assimilant = LCRUST								

Residual sum of squares = 0.018

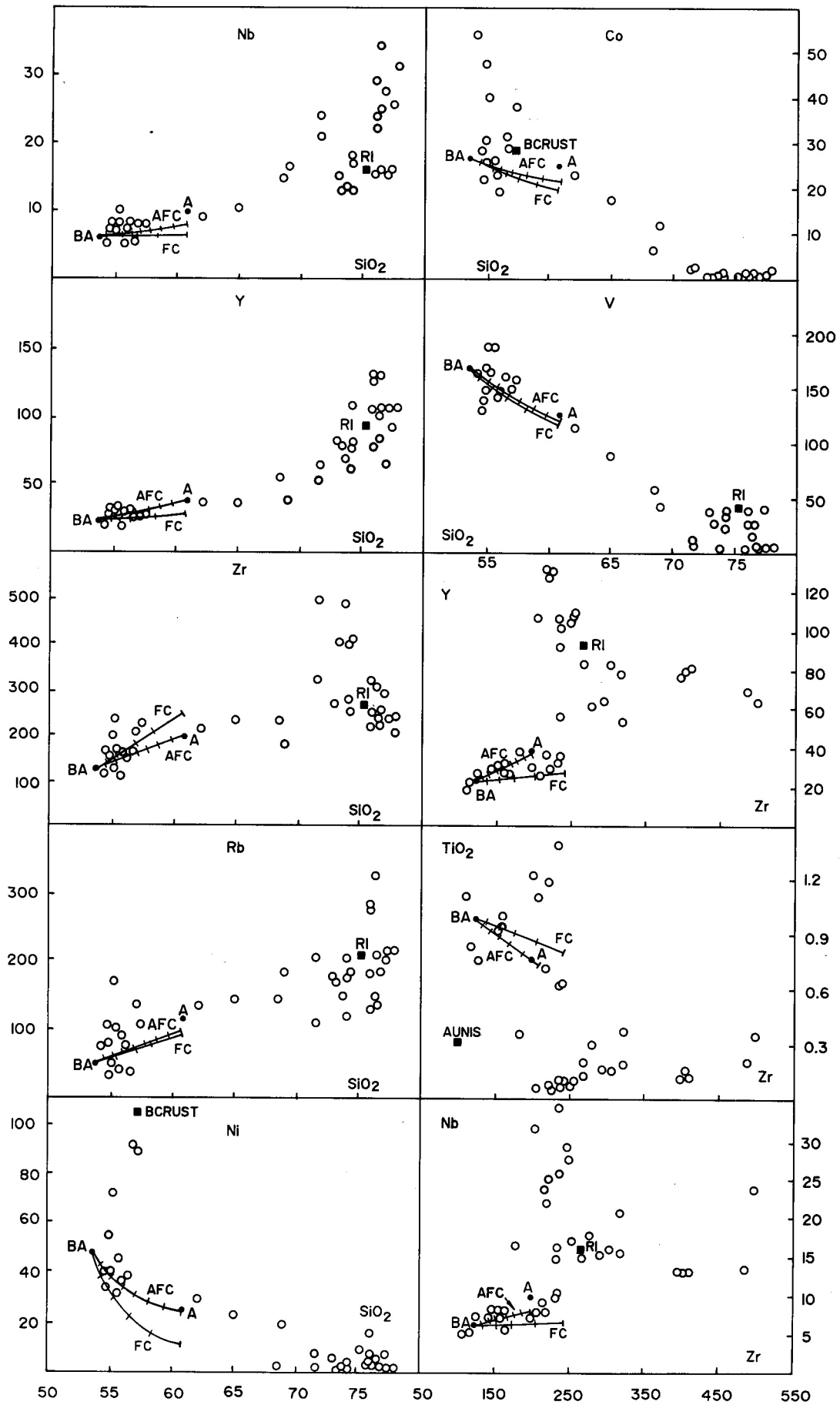


Fig. C.58: Trace element variation diagrams (with SiO₂ and Zr as abscissas) illustrating trajectories calculated for closed system fractional crystallisation (FC) and assimilation - fractional crystallisation (AFC) processes in the compositional range BA-A. Bars on the trajectories indicate increments of 0.10 F for both FC and AFC models. Filled squares represent different assimilants used in AFC modelling (Table C.15). Other symbols as in Fig. C.57.

tions may be due to changing physical conditions, e.g. Kd Ni values for olivine decrease with higher temperature, while Kd V values for magnetite increase with increasing $p_{\text{H}_2\text{O}}$ and oxygen fugacity (Glikson, pers. comm., 1989).

6.3.2 Andesite-rhyodacite (A-RD)

With the exception of the assimilant R1, all other assimilations modelled (including R2) infer around 50% fractional crystallisation and low degrees of assimilation ($r \approx 0.08$) for the stage A-RD. In other words, there is little difference between the bulk of these models and the FC model for this stage. However, by using R1 as an assimilant, the APC model indicates a low degree of fractional crystallisation ($\approx 7\%$) and considerable assimilation ($r \approx 0.8$). Despite this large degree of assimilation, predicted trace element abundances differ little from those obtained where fractional crystallisation is dominant (cf. Tables C.18 and C.19). Such lack of constraint does not allow for a decisive choice between models, but does suggest that the compositional variability of the rhyolites is capable of accounting for substantial variation in the parameters F and r.

Consideration of the HFSE alone indicates that the best model fit is achieved by using average lower crust as an assimilant. Compatible elements remain problematic, however, since small degrees of assimilation of the compatible element-rich lower crust are not able to enrich the derivative liquid sufficiently and in most cases do not fit the data as well as the FC model. The less than predicted Ni abundance is somewhat anomalous in this respect, but it is important to bear in mind the very low concentrations determined (≈ 2 ppm).

6.3.3 Rhyodacite to rhyolite (RD-R1; RD-R2)

Assimilants which best fit an APC model are the upper and bulk crust averages for RD-R1 and lower and bulk crust averages for RD-R2. In the stage RD-R1, using bulk crust as an assimilant requires moderate degrees of both fractional crystallisation ($\approx 44\%$) and assimilation ($r \approx 0.3$), but predicts trace element abundances which are generally less acceptable than those obtained using aFC model. A noteworthy aspect of this model is the significant enrichment achieved in the compatible elements relative to the FC model (cf. Tables C.13 and C.20). Using upper crust as an assimilant in the same stage requires a negligible value of r (≈ 0), thereby indicating a FC process with effectively no contamination.

In the stage RD-R2, neither lower crust nor bulk crust assimilants predict more acceptable trace element abundances compared with FC models. However, once again quite significant enrichment in the compatible elements is achieved and V shows good model fits in both cases (cf. Tables C.14 and C.21).

6.3.4 Discussion

Considering the variety of assimilants used for the APC models tested, and the large degree of fractional crystallisation from andesite to rhyolite in the HFF, it is suggested that AFC models are not able to satisfactorily account for this overall variation. Furthermore, trace element modelling indicates that FC models are in general able to better predict concentrations for a greater variety of trace elements (especially immobile elements) than are APC models. The

TABLE C.18: Assimilation-fractional crystallisation: andesite - rhyodacite (rhyolite assimilant).

(a) Least squares mixing approximation for AFC model				(b) Predicted trace element abundances in rhyodacite magma using Kd values for "dacite" (Appendix III), parameters in (a) and De Paolo's (1981) equations.								
Target Composition (RD)			Starting Composition (A)									
Actual	Estimated	Diff.	Fractionating Phases	Propns. wt. %	A	R1	RD	Magma	% Diff.	Bulk-D		
SiO ₂	68.50	68.50	0.00	An 49	34.38	Nb	9.9	16.1	14.8	13.2	-10.7	0.515
TiO ₂	0.63	0.63	0.00	Hbl 2	25.46	Zr	198	266	234	223	-4.6	0.875
Al ₂ O ₃	14.57	14.57	0.00	Cpx 1	22.63	Y	39	94	56	58	4.5	0.628
FeO*	4.25	4.25	0.00	Biot 1	15.33	Ba	959	208	628	706	12.4	1.256
MnO	0.11	0.12	0.01	Qtz	1.85	Sr	427	55	340	319	-6.3	1.133
MgO	1.08	1.08	0.00	Ap	0.21	Rb	117	212	146	148	1.7	0.816
CaO	2.74	2.73	-0.01	Mt	0.15	Ni	26	9	2.1	6.4	203.9	4.746
Na ₂ O	4.25	4.26	0.01	F-value = 0.93		Co	25	0.5	6.5	2.3	-65.2	6.979
K ₂ O	3.68	3.67	-0.01			V	127	42	58	20	-65.9	6.205
P ₂ O ₅	0.19	0.19	0.00									
Total	100.00	100.01		r-value = 0.81 (Ma/Mc)								
Residual sum of squares = 0.004				Assimilant = R1								

TABLE C.19: Assimilation-fractional crystallisation: andesite - rhyodacite ("Lower Crust" assimilant).

(a) Least squares mixing approximation for AFC model				(b) Predicted trace element abundances in rhyodacite magma using Kd values for "dacite" (Appendix III), parameters in (a) and De Paolo's (1981) equations.								
Target Composition (RD)			Starting Composition (A)									
Actual	Estimated	Diff.	Fractiona- ting Phases	Propns. wt %	A	LCRUST	RD	Magma	% Diff.	Bulk-D		
SiO ₂	68.50	68.50	0.00	An 49	43.69	Nb	9.9	6.0	14.8	14.4	-2.7	0.445
TiO ₂	0.63	0.62	-0.01	Cpx 1	17.87	Zr	198	70	234	241	2.9	0.695
Al ₂ O ₃	14.57	14.57	0.00	Biot 1	15.54	Y	39	19	56	52	-7.3	0.570
FeO*	4.25	4.25	0.00	Hbl 2	13.18	Ba	959	150	628	756	20.4	1.313
MnO	0.11	0.18	0.07	Qtz	5.93	Sr	427	230	340	336	-1.1	1.330
MgO	1.08	1.08	0.00	Mt	3.26	Rb	117	5.3	146	130	11.1	0.817
CaO	2.74	2.74	0.00	Ap	0.53	Th	10.1	1.06	17.7	17.5	-0.9	0.176
Na ₂ O	4.25	4.24	-0.01	F-value = 0.51		Ni	26	135	2.1	6.4	202.9	3.393
K ₂ O	3.68	3.68	0.01	r-value = 0.034		Co	25	35	6.5	0.85	-86.9	6.254
P ₂ O ₅	0.19	0.19	0.00	(Ma/Mc)		Cr	119	235	21	6.2	-70.4	5.651
Total	100.00	100.01		Assimilant = LCRUST		V	127	285	58	4.5	-92.2	6.466
Residual sum of squares = 0.006						Sc	21	36	8.5	5.3	-38.1	3.082
						La	26	11	40	44	9.5	0.228
						Ce	48	23	87	78	-10.5	0.284
						Nd	31	12.7	49	43	-12.1	0.505

TABLE C.20: Assimilation-fractional crystallisation: rhyodacite - rhyolite ("Bulk Crust" assimilant).

(a) Least squares mixing approximation for AFC model				(b) Predicted trace element abundances in rhyolite magma using Kd values for "rhyodacite and rhyolite" (Appendix III), parameters in (a) and De Paolo's (1981) equations.								
Target Composition (R1)			Starting Composition (RD)									
Actual	Estimated	Diff.	Fractiona- ting Phases	Propns. wt.%	RD	BCRUST	R1	Magma	% Diff.	Bulk-D		
SiO ₂	75.30	75.30	0.00	An 49	59.14	Nb	14.8	11	16.1	11.9	-26.3	1.335
TiO ₂	0.13	0.06	-0.07	Qtz	13.50	Zr	234	100	266	218	-18.2	0.964
Al ₂ O ₃	12.01	12.02	0.01	Biot 2	12.95	Y	56	20	94	63	-33.0	0.603
FeO*	2.05	2.07	0.02	Mt	8.31	Ba	628	250	208	490	135.5	1.271
MnO	0.02	0.14	0.12	Cpx 1	3.16	Sr	340	260	55	129	135.1	2.766
MgO	0.47	0.46	-0.00	Sanid	1.96	Rb	146	32	212	164	-22.8	0.570
CaO	0.72	0.74	0.02	Ap	0.98	Ni	2.1	105	9.0	18.2	102.7	0.965
Na ₂ O	4.79	4.75	-0.04	F-value = 0.66		Co	6.5	29	(0.5)	1.5	201.5	6.911
K ₂ O	4.49	4.53	0.04	r-value = 0.029		V	58	230	42	18.0	-57.2	5.234
P ₂ O ₅	0.01	0.00	-0.01	(Ma/Mc)								
Total	99.99	100.07		Assimilant = BCRUST								
Residual sum of squares = 0.023												

TABLE C.21: Assimilation-fractional crystallisation: rhyodacite - rhyolite ("Lower Crust" assimilant).

(a) Least squares mixing approximation for AFC model				(b) Predicted trace element abundances in rhyolite magma using Kd values for "rhyodacite and rhyolite" (Appendix III), parameters in (a) and De Paolo's (1981) equations								
Target Composition (R2)			Starting Composition (RD)		Fractionating Phases		Propns. wt.%					
Actual	Estimated	Diff.			RD	LCRUST	R2	Magma	% Diff.	Bulk-D		
SiO ₂	76.00	76.00	0.00	An 49	51.23	Nb	14.8	6.0	16.0	14.6	-8.8	0.984
TiO ₂	0.19	0.19	0.00	Sanid	15.77	Zr	234	70	266	241	-15.9	0.658
Al ₂ O ₃	11.89	11.89	0.00	Hbl 1	14.98	Y	56	19	78	48	-38.5	1.289
FeO*	2.30	2.29	-0.01	Mt	6.48	Ba	628	150	1310	733	-44.0	0.599
MnO	0.09	0.13	0.04	Qtz	5.63	Sr	340	230	29	86	195.3	4.060
MgO	0.12	0.14	0.02	Biot 2	5.02	Rb	146	5.3	187	183	-2.0	0.424
CaO	0.55	0.50	-0.05	Ap	0.88	Th	17.7	1.06	19	25	32.4	0.154
Na ₂ O	4.24	4.27	0.03			Ni	2.1	135	2.5	4.9	94.2	2.204
K ₂ O	4.60	4.53	-0.07		F-value = 0.66	Co	6.5	35	(0.9)	1.6	76.2	4.999
P ₂ O ₅	0.02	0.08	0.06		r-value = 0.08	Cr	21	235	21	12.5	-40.5	3.248
Total	100.00	100.02			(Ma/Mc)	V	58	285	4.1	3.6	-11.1	9.615
						Sc	8.5	36	5.7	4.4	-23.4	2.864
						La	40	11	48	45	-6.3	0.685
						Ce	87	23	103	103	-0.1	0.572
					Assimilant = LCRUST	Nd	49	12.7	62	48	-23.0	0.999
Residual sum of squares = 0.014												

negligible assimilation implied may not explain some compatible element concentrations which appear to require an additional process or explanation.

The progression of a derivative liquid from a basaltic andesitic ($\approx 54\%$ SiO₂) to andesitic ($\approx 61\%$ SiO₂) composition may be more successfully modelled by assuming an APC as opposed to a FC process. However, the better agreement obtained by APC modelling of the stage BA-A is dependent on an assemblage which requires olivine to persist as a liquidus phase to a fairly siliceous bulk-rock composition. While olivine phenocrysts have been observed in andesites containing 60% SiO₂ at Paracutin, Mexico (Gill, 1981, p.182), it is not clear whether or not these phenocrysts are in equilibrium with their host rocks. Olivine stability in the stage BA -A does, however, appear likely in view of Kushiro's (1975) observation that the stability of olivine is enhanced in high-K suites due to a decrease in the activity of silica as a result of increased water and alkali contents.

While accepting the probable assimilation of rhyolite or rhyolitic crust in the passage from basaltic andesite to andesite, R₀ values (0.70305 ± 17 for basaltic andesite) suggest that such assimilation operated largely in the later stages, viz. acid basaltic andesite to andesite. Although the contamination of andesite by a compatible element-enriched assimilant could explain the relatively high compatible element abundances, it is important to note that both rhyodacitic and rhyolitic derivative liquids are better accommodated by FC models. As noted previously, the broad

compositional variation of the rhyolites is difficult to reproduce by either FC or APC modelling.

6.4 MAGMA MIXING

The interbedded nature of basaltic andesite and rhyolite in the HFF clearly allows for the possibility of simple mixing between these "magma" end members in order to generate the intermediate compositions observed. Data scatter in variation diagrams (Section C.4) is able to accommodate a linear (i.e. mixing) relationship for most major and trace elements. In addition, calculated mixing lines (Langmuir *et al.*, 1978) exhibit close fits to the trend of data on a plot of SiO₂ versus Mg/(Mg + Fe) - Fig. C.59. Significantly, however, mixing cannot easily explain the non-linear trend of data in several variation diagrams, especially those involving relatively immobile elements, e.g. Al₂O₃, Nb and Y. The incorporation of intermediate compositional data from the HIS does, however, widen the data "swathe" sufficiently to allow for mixing in the case of Nb, but not Al₂O₃ or Y.

Magma mixing is here considered to include both the mixing of magmas (so-called hybridisation) and the bulk assimilation of crustal rocks, i.e. without accompanying FC. The process has been modelled according to the general mixing equation of Langmuir *et al.* (1978). The probability of mixing between essentially contemporaneous magmas is considered to be greater than any process involving the bulk assimilation of "cold" country rock, and feasible end mem-

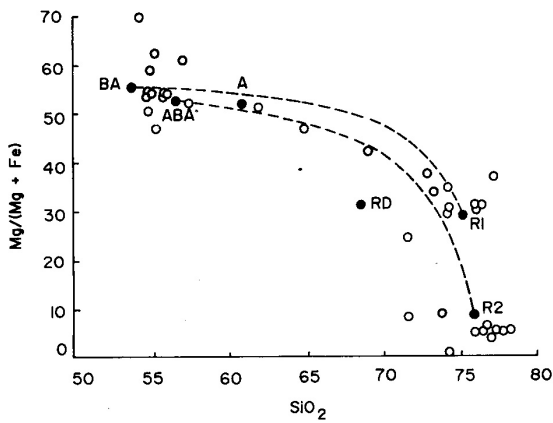


Fig. C.59: Plot of SiO_2 vs. $\text{Mg}/(\text{Mg} + \text{Fe})$ for HFF volcanics. Mixing curves (broken lines) between basaltic andesites (BA and ABA) and rhyolites (R1 and R2) have been calculated according to Langmuir *et al.* (1978).

bers in this mixing process are suggested by the following lines of evidence in eruptive rocks of the HFF:

- (i) Xenoliths (possibly flattened pumice) of basaltic andesite in pyroclastic rhyolite flows.
- (ii) Xenocrysts of quartz together with pseudomorphs after olivine in basaltic andesite.
- (iii) Light coloured (more silica-rich) globules in rhyodacite.
- (iv) Composite dykes consisting of cores of rhyolite and margins of dolerite.

Since the dykes are considered to be significantly younger than the HFF volcanic succession, the end members chosen for evaluation of the mixing process are basaltic andesite/acid basaltic andesite (BA/ABA) and rhyolite (R1 and R2). The proportions of these end members which best fit the target compositions of andesite (A) and rhyodacite (RD) were first approximated by using a least squares computation on the major elements. The proportions thus estimated are then used in the general mixing equation to predict trace element abundances in the target compositions (Tables C.22 to C.25). Discussion below is largely restricted to trace elements due to their greater variation, but it should be noted that major element predictions are invariably worse than previously discussed models.

6.4.1 Mixing to generate andesite (A)

Mixing of basaltic andesite (BA) and rhyolite (R1) in order to produce andesite (A) enables direct comparison with the stage BA-A in both FC and AFC models. Mixing BA and R1 in the approximate proportion 2:1 yields an andesitic mixture with trace element abundances which compare favourably to those predicted by a FC model.

Comparison of Table C.9 with C.22 shows that for the trace elements modelled, only Co and Ba concentrations can be more successfully modelled by a FC process. It should, however, be noted that FC modelling over the smaller compositional range ABA-A predicts better agreement for Y, Ba, Th and all the compatible elements than does mixing (cf. Tables C.11 and C.22). Furthermore, the preferred model for the stage BA-A is an AFC process (using R1 as assimilant) which predicts better agreement for all the trace

elements except Nb, Sr, Rb and V when compared with mixing (cf. Tables C.16 and C.22).

A mixture of ABA and R2 in the approximate proportion 2:1 produces an andesite in which the trace element concentrations predicted again compare favourably with the values obtained by FC modelling for the comparable stage ABA-A (cf. Tables C.11 and C.23). Concentrations of trace elements which are better predicted by the latter model include Y, Co, V, Ba and LREE. Although not strictly comparable, trace element abundances predicted by the AFC model for the stage BA-A using R2 as assimilant (not presented here) are similar to slightly worse in the case of Nb, Sr, Ni, Co and Ba than those obtained by the mixing of ABA and R2 (Table C.23).

Reasonably good mixing models (especially with respect to the HFSE predictions) may also be obtained for combinations of basaltic andesite/acid basaltic andesite (BA/ABA) and rhyodacite (RD). These mixes are, however, probably hypothetical and do not appear to be substantiated by field or petrographic evidence. Accordingly, these models will not be discussed further in this study.

6.4.2 Mixing to generate rhyodacite (RD)

Mixing of basaltic andesite (BA) and rhyolite (R1) produces rhyodacite in which major element fits are not acceptable, particularly when one considers relatively immobile oxides such as TiO_2 (Tables C.24 and C.25). Mixing of BA and R1 in the approximate proportion 1:4 predicts trace element values which are generally worse than in the FC stage (A-RD) and provides sufficient grounds for rejection of this mixing model (cf. Tables C.12 and C.24).

Mixing of acid basaltic andesite (ABA) and rhyolite (R2) in the approximate proportion 1:3 predicts trace element abundances which are in better agreement than the predictions of a FC model with respect to Rb, Co, V, Sc and LREE (cf. Tables C.12 and C.24). However, poor major element agreement was again used to calculate the mixing proportions.

Poor model fits (not presented here) were also obtained for the mixing combinations of andesite (A) and rhyolite (R1/R2).

6.4.3 Discussion

Magma mixing is difficult to evaluate due to the compositional variation (scatter) within end members of the HFF volcanic suite. While a non-linear relationship in several variation diagrams (e.g. Al_2O_3 - SiO_2 , Y- SiO_2) indicates that simple mixing could not have occurred between specific samples, choice of other samples does allow the process to have taken place. The plot of SiO_2 versus $\text{Mg}/(\text{Mg} + \text{Fe})$ (Fig. C.59) illustrates that a family of such mixing curves may exist in order to satisfy this process. Where the specific samples chosen for modelling are examined in different variation diagrams, it is evident that the proportions of mixing are not consistent between the plots. This observation is partly reflected in the larger residual sums of squares obtained by least squares approximation of the major elements.

TABLE C.22: Magma mixing: basaltic andesite and rhyolite to yield andesite (BA + R1 = A).

(a) Least squares mixing approximation for MM model				(b) Predicted trace element abundances in andesite magma using parameters in (a) and equations of Langmuir <i>et al.</i> (1978).						
Target Composition (A)			Starting Compositions (BA + R1)							
Actual	Estimated	Diff.	Magma Proportions		BA	R1	A	Magma	%Diff.	
SiO ₂	60.89	60.74	0.15	BA : 67.54%	Nb	6.1	16.1	9.9	9.4	-5.6
TiO ₂	0.77	0.70	0.07	R1 : 32.46%	Zr	123	266	198	169	-14.4
Al ₂ O ₃	15.35	14.27	1.08		Y	23	94	39	46	18.1
FeO*	6.40	6.93	-0.53		Ba	578	208	959	458	-52.2
MnO	0.14	0.13	0.01		Sr	590	55	427	416	-2.5
MgO	3.87	4.52	-0.65		Rb	51	212	117	103	-11.7
CaO	6.19	6.28	-0.09		Th	0.5	25	10.1	8.4	-16.3
Na ₂ O	3.36	3.68	-0.32		Ni	48	9.0	26	35	35.9
K ₂ O	2.82	2.58	0.24		Co	26	0.5	25	17.7	-29.1
P ₂ O ₅	0.21	0.17	0.04		V	170	42	127	128	1.1
Total	100.00	100.00								
Residual sum of squares = 2.072										

TABLE C.23: Magma mixing: acid basaltic andesite and rhyolite to yield andesite (BA + R2 = A).

(a) Least squares mixing approximation for MM model				(b) Predicted trace element abundances in andesite magma using parameters in (a) and equations of Langmuir <i>et al.</i> (1978).						
Target Composition (A)			Starting Compositions (ABA + R2)							
Actual	Estimated	Diff.	Magma Proportions		ABA	R2	A	Magma	%Diff.	
SiO ₂	60.89	62.89	-2.00	ABA : 67.72%	Nb	5.6	16.0	9.9	9.0	-9.5
TiO ₂	0.77	0.72	0.05	R2 : 32.28%	Zr	164	317	198	213	7.8
Al ₂ O ₃	15.35	14.47	0.88		Y	27	78	39	43	11.4
FeO*	6.40	6.34	0.06		Ba	527	1310	959	780	-18.7
MnO	0.14	0.14	0.00		Sr	736	29	427	508	18.9
MgO	3.87	3.54	0.33		Rb	38	187	117	86	-26.4
CaO	6.19	5.63	0.56		Th	5.7	19	10.1	10.0	-1.1
Na ₂ O	3.36	3.54	-0.18		Ni	39	2.5	26	27	4.7
K ₂ O	2.82	2.49	0.33		Co	31	0.9	25	21	14.9
P ₂ O ₅	0.21	0.24	-0.03		Cr	131	21	119	95	-19.8
Total	100.00	100.00			V	162	4.1	127	111	-12.6
Residual sum of squares = 5.338										
					Sc	26	5.7	21	19.4	-7.4
					La	19	48	26	28	9.1
					Ce	44	103	48	63	31.3
					Nd	29	62	31	40	27.9

Several trace element abundances (e.g. Nb, Sr) in andesite may be more successfully modelled by mixing of basaltic andesite (*sensu lato*) and rhyolite than by such processes as fractional crystallisation and assimilation- fractional crystallisation. A similar observation is made for abundances of certain trace elements (e.g. Co, V) in rhyodacite. The implication of these models is that although mixing processes are not capable of producing completely the desired

intermediate compositions in volcanics of the HFF, such processes may have acted in conjunction with fractional crystallisation and assimilation in producing the observed liquid line(s) of descent.

Choice of end members in the mixing process has not been rigorous largely due to the metamorphic character of the intermediate rocks, especially the andesites. Furthermore, the study suffers from the lack of such diagnostic evidence

TABLE C.24: Magma mixing: basaltic andesite and rhyolite to yield rhyodacite (BA + R1 = RD).

(a) Least squares mixing approximation for MM model				(b) Predicted trace element abundances in rhyodacite magma using parameters in (a) and equations of Langmuir <i>et al.</i> (1978).						
Target Composition (RD)			Starting Compositions (BA + R1)							
Actual	Estimated	Diff.	Magma Proportions		BA	R1	RD	Magma	%Diff.	
SiO ₂	68.50	70.93	-2.43	BA : 20.28%	Nb	6.1	16.1	14.8	14.1	-4.9
TiO ₂	0.63	0.30	0.33	R1 : 79.72%	Zr	123	266	234	237	1.3
Al ₂ O ₃	14.57	12.69	1.88		Y	23	94	56	80	42.2
FeO*	4.25	3.51	0.74		Ba	578	208	628	283	-54.9
MnO	0.11	0.05	0.06		Sr	590	55	340	164	-51.9
MgO	1.08	1.69	-0.61		Rb	51	212	146	179	22.8
CaO	2.74	2.39	0.35		Th	(0.5)	25	17.7	20	13.2
Na ₂ O	4.25	4.46	-0.21		Ni	48	9.0	2.1	16.9	705.2
K ₂ O	3.68	3.92	-0.24		Co	26	0.5	6.5	5.7	-12.8
P ₂ O ₅	0.19	0.06	0.13		V	170	42	58	68	17.2
Total	100.00	100.00								

Residual sum of squares = 10.691

TABLE C.25: Magma mixing: acid basaltic andesite and rhyolite to yield rhyodacite (ABA + R2 = RD).

(a) Least squares mixing approximation for MM model				(b) Predicted trace element abundances in rhyodacite magma using parameters in (a) and equations of Langmuir <i>et al.</i> (1978).						
Target Composition (RD)			Starting Compositions (ABA + R2)							
Actual	Estimated	Diff.	Magma Proportions		ABA	R2	RD	Magma	%Diff.	
SiO ₂	68.50	70.90	-2.40	ABA : 26.33%	Nb	5.6	16.0	14.8	13.3	-10.4
TiO ₂	0.63	0.40	0.23	R2 : 73.67%	Zr	164	317	234	277	18.2
Al ₂ O ₃	14.57	12.89	1.68		Y	27	78	56	65	15.3
FeO*	4.25	3.87	0.38		Ba	527	1310	628	1104	75.8
MnO	0.11	0.11	0.00		Sr	736	29	340	215	-36.7
MgO	1.08	1.45	0.37		Rb	38	187	146	148	1.2
CaO	2.74	2.52	0.22		Th	5.7	19	17.7	15.5	-12.4
Na ₂ O	4.25	3.97	0.28		Ni	39	2.5	2.1	12.1	476.7
K ₂ O	3.68	3.78	-0.10		Co	31	(0.9)	6.5	8.8	35.8
P ₂ O ₅	0.19	0.10	0.09		Cr	131	21	21	50	137.9
Total	100.00	99.99			V	162	4.1	58	46	-21.2
					Sc	26	5.7	8.5	11.0	29.9
					La	19	48	40	40	0.9
					Ce	44	103	87	87	0.5
					Nd	29	62	49	53	8.8

Residual sum of squares = 9.061

as disequilibrium phenocryst assemblages and isotopic data for the intermediate members. The likelihood of extensive mixing between basaltic andesite and rhyolite must take into account the inhibiting viscosity difference (cf. Turner and Campbell, 1986) between these liquids. Sakuyama (1984) suggested that such mixing may occur if basic magma is injected into an acidic magma chamber, thereby creating the motive force for convection. Experimental work (Kouchi and Sunagawa, 1985) has shown that basaltic and dacitic magmas may be easily mixed. By analogy (i.e. similar viscosity contrast) basaltic andesite-rhyolite mixes in the HFF may have resulted in the occasional presence of unmixed felsic globules in rhyodacite (cf. Section C.2).

Given the above evidence and the rather poor data constraints, it is clear that magma mixing (*sensu lato*) cannot be excluded as a process in the petrogenesis of the HFF eruptive rocks. However, the binary mixing models used in this study are probably unrealistic in view of accompanying fractional crystallisation and crystal dissolution (Gill, 1981). While Sparks (1983) maintains that the majority of volcanic rocks show evidence of magma mixing, Sakuyama (1984) is more specific in regarding magma mixing between highly contrasted compositions as one of the important characteristics of arc volcanic rocks.

6.5 PARTIAL MELTING (PM)

The difficulty in relating basaltic andesites and rhyolites of the HFF to each other by FC and AFC processes strongly suggests independent derivation of these magma types. The relative uniformity in composition of most basaltic andesites infers a broadly homogeneous source, while the compositional diversity of the rhyolites is more compatible with a heterogeneous source composition. Emphasis on the average R_0 values for the HFF eruptive rocks finds a ready explanation in mantle and crustal sources for mafic and felsic magmas, respectively. However, magmas produced by partial melting undergo fractional crystallisation en route to the surface, thereby making it difficult to separate discussion of these processes. Partial melting models will be considered for each end member of the HFF before considering what, if any, modification of the initial melts is needed in order to derive the observed compositions of the final liquids.

6.5.1 Basaltic andesites

(i) Basaltic andesite as a primary magma

Mantle-derivation of HFF basaltic andesite (*sensu lato*) parental magmas is indicated by the low R_0 (0.70305 ± 17). The primary nature of basaltic andesite may be questioned in view of Mg-numbers which are generally less than required values of ≥ 67 (Gill, 1981, p.110) for melts in equilibrium with upper mantle olivines ($Fo \geq 87$), given the Fe/Mg Kd olivine/liquid = 0.3 (Roeder and Emslie, 1970). However, calculated Mg-numbers depend on the chosen Fe_2O_3/FeO ratio, a ratio known to show significant variation in andesites. Gill (1981) recommended adoption of a

pre-eruption Fe_2O_3/FeO ratio of 0.3, which yields a mean Mg-number of 62 ± 5 for the basaltic andesites. A higher Fe_2O_3/FeO ratio of between 0.6 and 0.7 is determined by using the method of Le Maitre (1976) and will lead to Mg-numbers which are commonly greater than 67. Such high Mg-numbers probably reflect oxidation as a result of alteration and so Gill's (1981) recommended Fe_2O_3/FeO ratio of 0.3 has been adopted.

The composition of BH 694 (BA), a "high-Mg andesite" ($MgO = 6.47\%$), satisfies none of the criteria for being a peridotite-derived primary melt, viz. $FeO^*/MgO < 1$, Mg-number > 67 , and Ni content > 100 ppm (Gill, 1981, p.255). Nevertheless, consideration of all basaltic andesites in the HFF indicates that several samples do satisfy these criteria, but are unfortunately more intensely metamorphosed. The high-Mg basaltic andesite BH 598 (MBA) exhibits all the above properties of a primary melt and will therefore be discussed along with BA.

Moderately high Ni and Cr contents (see Section C.4.3.1.3) in many basaltic andesites imply that substantial fractional crystallisation of olivine and pyroxene has not occurred. Although plagioclase fractionation is suggested by slightly negative Eu anomalies for both MBA and ABA, Sr abundances appear too high for this to have been a major process, thereby inferring the susceptibility of Eu to alteration (Glikson, pers. comm., 1989).

The possibility of generating a primary partial melt of basaltic andesitic composition from a mantle source derives support from the experimental work of Mysen and Boettcher (1975). These workers have shown that oversaturated andesitic magma can be produced by low degrees of partial melting of garnet lherzolite under vapour present conditions at pressures of up to 25 kb.

A pyrolite source composition (Ringwood, 1979) was chosen in order to approximate the degree of melting required to produce a basaltic andesite magma. Degrees of melting of 2% and 1% for BA and MBA, respectively, were calculated for K_2O on the assumption that all the K_2O enters the melt. These estimates are regarded as low and would typically result in magmas of more alkaline (and undersaturated) compositions than are observed. In view of probable mobility of K in the basaltic andesites, possibly as a result of alteration, melt factors of between 5% and 20% were adopted in the modelling of both BA and MBA as partial melts.

A model pyrolite source composition of 58% olivine, 15% orthopyroxene, 14% clinopyroxene and 13% garnet was determined by using the least squares approach of Bryan *et al.* (1969) to estimate the source mineralogy (Table C.26). Phase compositions used in this calculation are listed in Table C.8 and were obtained from peridotite xenoliths in kimberlite pipes from southern Africa (Boyd and Nixon, 1973; MacGregor, 1979; Erlank *et al.*, 1987). Phlogopite and ilmenite, although present in the pyrolite source, constitute insignificant proportions which are unlikely to remain in the residuum over the melting range being considered. These phases are not, therefore, included in the putative pyrolite source. One feature of the above calculation is that it utilises $FeO^* + MgO$ rather than the individual oxides in an attempt to make allowance for the partitioning of Fe

TABLE C.26: Least squares approximation to determine the phase proportions in a putative pyrolite mantle source (pyrolite and phase compositions from Tables C.7 and C.8, respectively).

Dependent vector: Pyrolite					
	Observed	Calculated	Difference	Phase	Proportions
SiO ₂	45.85	45.88	0.03	Fo 90	0.5793
TiO ₂	0.20	0.20	0.00	Opx 2	0.1453
Al ₂ O ₃	3.36	3.36	0.00	Cpx 3	0.1434
MnO	0.15	0.14	-0.01	Gt	0.1296
MgO+FeO*	46.86	46.89	0.03	Phg	0.0024
CaO	3.15	3.16	0.01	Ilm	0.0001
Na ₂ O	0.40	0.35	-0.05		
K ₂ O	0.03	0.03	0.00	Total	1.0000

Sum of squares of differences = 0.01

TABLE C.27: Comparison of observed and predicted trace element abundances for 5-20% batch melts of "chondritic" and "enriched" pyrolite source composition (Kd's listed in Appendix III).

Pyrolite phase assemblage: ol (58%), opx (15%), cpx (14%), gt (13%) - Table C.26.

Melt proportions: ol (0%), opx (20%), cpx (40%), gt (40%) - see text.

	<i>Chondritic</i> Pyrolite source	5% melting	10% melting	15% melting	20% melting	BA	MBA
Nb	0.35	3.8	2.5	1.9	1.5	6.1	5.2
Zr	6.2	29	26	24	22	123	115
Y	2.2	8.3	7.9	7.6	7.3	23	23
Ba	3.5	70	35	23	17	578	709
Sr	11	220	110	73	55	590	470
Rb	1	20	10	6.7	5.0	51	74
Ni	2000	298	300	302	304	48	358
Co	110	59	60	62	63	26	54
V	75	256	259	262	265	170	166

	<i>Enriched</i> Pyrolite source	5% melting	10% melting	15% melting	20% melting	BA	MBA
Nb	0.9	9.8	6.4	4.8	3.8	6.1	5.2
Zr	15.5	72	65	60	55	123	115
Y	5.5	21	20	19	18	23	23
Ba	8.8	176	88	57	44	578	709
Sr	27.5	549	275	183	137	590	470
Rb	2.5	50	25	17	12	51	74
Ni	2000	298	300	302	304	48	358
Co	110	59	60	62	63	26	54
V	75	256	259	262	265	170	166

and Mg between the melt and restite during melting of the source mineral assemblage (Cox *et al.*, 1984).

Quantitative trace element modelling of partial melting has been carried out based on the model pyrolite source composition in Table C.26, while melt proportions are approximations based on realistic melting modes (Erlank, pers. comm., 1989). The exclusion of olivine from the melting mode is based on the assumption that this phase will not contribute significantly to the melt and that its inclusion merely complicates the calculation. Results presented in Table C.26 are based on Kd's from Frey *et al.* (1978) and Le Roex (1980), and have been calculated according to the equilibrium partial melting equations of Shaw (1970). It is realised that more elegant models can be used but that the ranges in trace element variation do not warrant such approaches. Trace element abundances in the pyrolite source (Table C.7) are assumed to be chondritic, except for Rb and Nb, and are based on data published by Frey *et al.* (1978) and from Erlank (pers. comm., 1989).

Trace element data presented in Table C.27 illustrate poor agreement between observed (BA and MBA) and predicted abundances for between 5% and 20% melting of a "chondritic" pyrolite source. Incompatible elements display insufficient enrichment in these melts, while compatible elements (Ni, Co) are insufficiently depleted in the case of BA, but show reasonable agreement with MBA. While the data do not allow for rejection of a pyrolite source, the probability of basaltic andesite (in particular BA) representing a primary liquid in equilibrium with a "chondritic" composition seems small.

Mantle enrichment has been invoked by numerous workers in order to explain both observed and calculated abundances of primary partial melts (e.g. Frey *et al.*, 1978; Boettcher *et al.*, 1979; Menzies and Murthy, 1980; Erlank *et al.*, 1987). An arbitrary value of 2.5 times chondritic is adopted for the enrichment of incompatible elements (including the volatile element Rb) in the pyrolite source (see Frey *et al.*, 1978). Trace element data for 5-20% melting of this "enriched" source is presented in Table C.27, showing that while predicted abundances are considerably better than those for the same range of melting of a "chondritic" source, most of the incompatible element abundances (except Nb and Y) are still too low.

(ii) Basaltic andesite derived from a parental melt

The poor correspondence in composition between primary mantle (both "chondritic" and "enriched") melts and HFF basaltic andesites suggests that the latter may be derived by fractional crystallisation of a parental magma. The derivative nature of basaltic andesite is difficult to evaluate quantitatively in view of the wide choice of model parameters. Gill (1981) concluded that by far the most common and extensive process of andesite derivation is by 5-40% crystal fractionation of the phenocryst phases plag + opx/ol + cpx + mt from basaltic magma.

While abundances of compatible elements in basaltic andesite (especially the high-Mg type) appear too high (Table C.7) to be the result of extensive pyroxene and olivine removal, the moderately high Sr contents and slightly negative Eu anomalies argue against the removal of large amounts of

plagioclase. Alternatively, a basaltic magma parental to the HFF basaltic andesites must be assumed to be characterised by relatively high abundances of MgO (>> 6.5 wt. %) and the compatible elements and low Al₂O₃ (< 15 wt. %). Such basaltic magmas, although reported from primitive island arcs (Cox and Bell, 1972), appear to be absent from most island arcs and active continental margins. Fractional crystallisation of such anomalous magma using the assemblage plag + ol + cpx + mt would probably produce a derivative liquid similar in composition to HFF basaltic andesite. The relatively high K-contents of HFF basaltic andesites further suggest that the parental magma was not a primary magma, since the latter would require a very low degree of partial melting of an "enriched" pyrolite source with only 0.07 wt.% K₂O.

(iii) REE considerations

As argued above, HFF basaltic andesites display compositional features which suggest that no extensive fractionation of the assemblage plag + ol + cpx + mt has occurred in the parental magma. Separation of considerably less than 40% solids (the maximum considered by Gill, 1981) is, therefore, likely to have occurred and this would not, especially in the absence of hornblende as a fractionating phase, have a major effect on the REE pattern. Since REE behave as incompatible elements, it is possible to back-calculate the mantle source composition in the absence of a primary magma. The results of these back-calculations, assuming 5-20% batch melting, are presented in Table C.28 for high-Mg basaltic andesite and illustrated in a chondrite-normalised plot (Fig. C.60). The similarity in REE patterns between MBA and ABA suggests that these magmas were derived from the same source, albeit by slightly different degrees of melting and accompanying fractional crystallisation.

Chondrite-normalised REE patterns show that for about 10% partial melting (i.e. intermediate to the patterns illustrated in Fig. C.60), the mantle source is enriched in both LREE (3-5x) and HREE (2-7x) relative to chondritic abundances. While LREE enrichment is of a similar order to that commonly quoted for enriched mantle in the literature (e.g. Frey *et al.*, 1978), the HREE enrichment (particularly Lu) is noticeably higher. Despite assuming a greater contribution by garnet to the melt, the source remains anomalously enriched in HREE relative to chondrites and may indicate that the amount of residual garnet is less than assumed. Garnet must, however, be residual in order to account for the relatively steep REE patterns displayed by the basaltic andesites in Fig. C.60.

Although relative REE abundances in chondrites may differ by up to 20% (Nakamura, 1974), the REE enrichment of 2-7x chondrites in the putative mantle source remains considerably higher than concentration levels of 2-4x predicted by other workers for the upper mantle (Gast, 1968; Frey, 1969; Frey and Green, 1974). This discrepancy infers that the upper mantle below the AMT may have been modified by processes resulting in strong enrichment and fractionation of REE.

The above model is problematic in that the assumed 2.5x chondrite enrichment in incompatible elements is low rela-

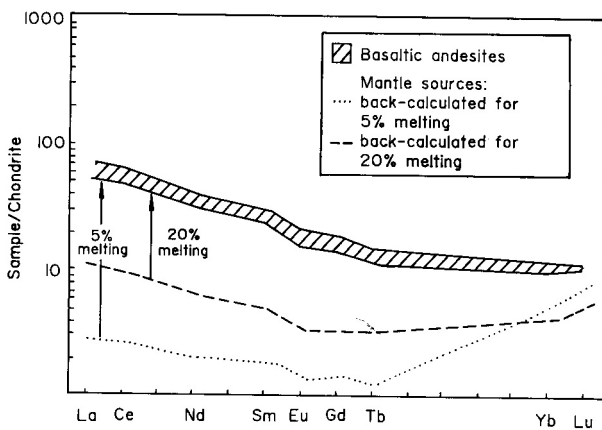
TABLE C.28: Back-calculation to derive REE abundances in a mantle source to high-Mg basaltic andesite (MBA) magma assuming 5-20% batch melting.

Pyrolite source assemblage: ol (58%), opx (15%), cpx (14%), gt (12%) - Table C.26.

Melting mode: ol (0%), opx (20%), cpx (40%), gt (40%) - see text.

Calculated source compositions after degrees of melting indicated below:

	MBA	5% melting	10% melting	15% melting	20% melting
La	16.7	0.883	1.71	2.54	3.37
Ce	37.9	2.13	4.01	5.89	7.77
Nd	18.1	1.16	2.02	2.89	3.75
Sm	4.42	0.342	0.543	0.744	0.946
Eu	1.14	0.097	0.148	0.198	0.248
Gd	3.81	0.362	0.524	0.685	0.847
Tb	0.57	0.059	0.082	0.106	0.129
Yb	2.14	1.11	1.04	0.967	0.893
Lu	0.38	0.269	0.243	0.217	0.191

Kd's used are from Frey *et al.* (1978) - Appendix III.**Fig. C.60:** Chondrite-normalised REE patterns for HFF basaltic andesites (lower boundary of shaded area represents high-Mg basaltic andesite, MBA; upper boundary represents acid basaltic andesite, ABA) compared with the back-calculated mantle source compositions assuming 5 and 20% batch melting (non-modal).

tive to the high REE enrichment (2-7x chondrite). Furthermore, the concave-upward REE pattern of the calculated mantle source and La_N/Yb_N ratio of 1.1 for 10% batch melting constitute unusual features for a mantle source. This may imply the mixing of at least two distinct geochemical components (cf. Frey and Green, 1974), a possibility difficult to evaluate in this study in view of the paucity of REE data and relatively poor model constraints.

An alternative source to the high-Mg basaltic andesite of the HFF is provided by the presence of pillowed me-

tabasalt in the early-stage crust of the AMT. This Kairab Complex amphibolite has compositional characteristics of arc or back-arc tholeiite (Section C.4) and could conceivably have been in an environment suitable for transformation into eclogite. The REE pattern for pillowed metabasalt from the Kairab Complex is presented in Fig. C.61 and as explained above, the incompatible REE can be modelled in the absence of a primary magma. Modelling of 10-20% batch melting of an eclogite source (62% clinopyroxene, 38% garnet; Yoder and Tilley, 1962) with the REE composition of Kairab metabasalt is presented in Table C.29 and Fig. C.61. Melting of eclogite results in LREE abundances which show some overlap with basaltic andesite, but patterns are significantly different and unacceptably high depletion of HREE is predicted. Consequently melting of an eclogitic source is considered as unlikely to have resulted in magmas of basaltic andesite composition. Glikson (pers. comm., 1989) further points out that such a model would require subduction of large volumes of early AMT basaltic crust and production of basaltic andesite by > 70% remelting - a tectonically and petrogenetic ally unlikely process since liquids would segregate from residue upon much smaller degrees of partial melting.

(iv) Discussion

Despite poor constraints on the quantitative modelling carried out above, several important features emerge with respect to the petrogenesis of the HFF basaltic andesites. These are as follows:

(a) Basaltic andesites (including high-Mg types) are not primary melts of unmodified pyrolite or eclogite.

TABLE C.29: Comparison of observed and predicted REE abundances in high-Mg basaltic andesite magma for 10-20% batch melting of Kairab Complex metabasalt assuming the mineralogy of eclogite.

Source mode: cpx (62%), gt (38%) - after Yoder and Tilley, (1962)

Melting mode: cpx (70%), gt (30%) - after Zielinski and Lipman (1976).

	Eclogite source	MBA	10% melting	15% melting	20% melting
La	2.66	16.7	23.9	16.6	12.7
Ce	5.84	37.9	47.4	34.0	26.5
Nd	4.65	18.1	29.8	23.0	18.7
Sm	1.22	4.42	5.93	4.89	4.16
Eu	0.46	1.14	1.96	1.66	1.44
Gd	1.27	3.81	4.75	4.12	3.64
Tb	0.21	0.57	0.71	0.63	0.56
Yb	1.03	2.14	0.64	0.65	0.66
Lu	0.18	0.38	0.082	0.084	0.085

Kd's used are from Frey *et al.* (1978) - Appendix III.

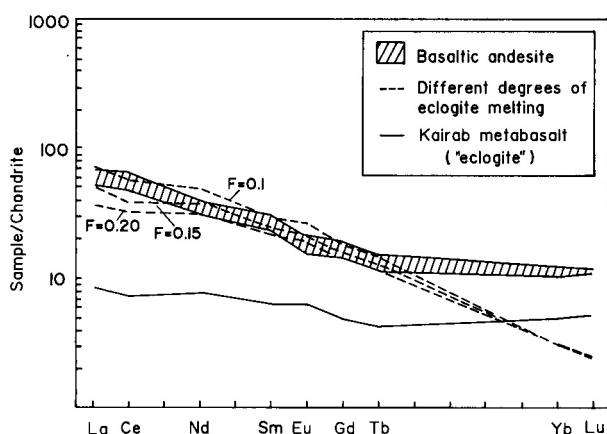


Fig. C.61: Chondrite-normalised REE patterns generated by different degrees of batch melting (10-20%) of an eclogite source with the composition of Kairab Complex metabasalt. These melt-derived patterns show poor correspondence to REE patterns for the HFF basaltic andesites MBA (lower boundary of shaded area) and ABA (upper boundary of shaded area).

(b) Precursors to the basaltic andesites require incompatible element enrichment of the mantle source region.

(c) Enrichment in the incompatible elements Ba, Sr and Rb suggests the involvement of continental crust, a feature not easily reconciled with the low R_0 in the HFF basaltic andesites.

(d) The proposed model of 10% melting of "enriched" pyroxenite followed by a moderate degree (< 40%) of fractional crystallisation of the assemblage plag + 01 + cpx + mt is similar to the model proposed by Gill (1981) for the production of a calc-alkaline trend.

(e) The high Ni and Co contents displayed by high-Mg andesite could reflect accumulation of ferromagnesian phases.

(f) REE compositions of high-Mg basaltic andesite (and acid basaltic andesite) produced by the proposed model in (d) require enrichment of a single mantle source composition (LREE 3-5x chondrite, HREE 2-7x chondrite).

(g) REE preclude the derivation of high-Mg basaltic andesite (and acid basaltic andesite) from an eclogitic source with the REE composition of pillow-bearing amphibolite in the Kairab Complex.

6.5.2 Rhyolites

(i) General

The apparently large volume of rhyolites relative to basaltic andesites in the HFF argues against a genetic relationship by fractional crystallisation since this process should result in a felsic end-product which is volumetrically much smaller than the basic magma, even if the process involved substantial crustal assimilation (Kleeman, 1965; Hyndman, 1972). Any melting model for the genesis of the HFF rhyolites must, however, take into account their intimate and interbedded relationship with volumetrically subordinate basaltic andesites as well as the underlying continental crust.

Although the uncertainties in R_0 preclude any model which relies solely on these data, it should be noted that these ratios are in all probability different if rhyolites and basaltic andesites are regarded as cogenetic, with rhyolites having much higher R_0 values (0.718 ± 15) compared to the basaltic andesites (0.70305 ± 17). Such high initial ratios cannot be explained by fractional crystallisation alone, but

are consistent with an origin by anatexis of older continental crust or by AFC with crust characterised by much higher R_0 values. Rb/Sr ratios in the rhyolites also appear to argue against fractional crystallisation as the dominant process in their derivation, since much higher ratios are usually exhibited by extensive fractional crystallisation of feldspars in a granite melt (McCarthy and Hasty, 1976).

The suggestion by Loiselle and Wones (1979) that A-type magmas may be produced by fractional crystallisation of a basaltic parent magma is not considered seriously here in view of the lack of variety of felsic derivatives in the HFF and the volumetric considerations discussed above. A-type compositional characteristics of the HFF rhyolites may, by analogy with similar magma types in southeastern Australia (e.g. Collins *et al.*, 1982), suggest an origin by partial melting of an anhydrous or granulitic crustal source from which melt has previously been removed. The problem with exposed granulite terrains is that they rarely consist of highly refractory residues (Sheraton and Black, 1988), thereby implying that it is the anhydrous character that makes granulites a suitable source for A-type magmas. Although Anderson (1983) has suggested a tonalitic to granodioritic meta-igneous source as an alternative to granulite, A-type melts are essentially the result of the low K_d 's of LILE and HFSE in melts derived under anhydrous conditions (Glikson, pers. comm., 1989).

Relatively mafic I-type granites are thought to represent about 25% melting of a dioritic lower crust (Compston and Chappell, 1979), the water required for such melting probably being provided by the breakdown of hydrous phases such as biotite and amphibole. H_2O -undersaturated melts generated in the crust may vary in composition from tonalite to granite (Wyllie, 1977), the more felsic compositions being characteristic of lower pressures. While Chappell and White (1974) imply that this compositional range may exist at relatively low temperatures ($< 850^\circ\text{C}$), Wyllie (1977) infers temperatures of up to 1100°C for the more mafic compositions even under relatively hydrous (≈ 2 wt. % H_2O) conditions.

Although the presence of some water and volatiles in the HFF rhyolites is indicated by the occasional presence of biotite and the widespread occurrence of ash-flow tuffs, the magma must have been sufficiently hot and anhydrous to rise to a shallow level in the crust and result in significant welding of the tuffs. The assumption of an essentially anhydrous nature of the rhyolites allows the representation of their normative compositions in the dry ternary system Qz-Ab-An (Fig. C.62). The rhyolite compositions (R1 and R2) plot close to the 5 kb liquidus surface and in the proximity of putative minimum melt. Although an increasing Ab/An ratio will result in displacement of the cotectic line away from the Qz apex (Von Platen, 1965), this effect may also be the result of post-eruptive processes, e.g. albitisation.

The inferred liquidus temperature of 1000 – 1100°C appears too high for high-silica rhyolites and may suggest that an anhydrous system is not strictly applicable. Collins *et al.* (1982) suggest that such “minimum” or “near-minimum” melts are I-type and may be controlled by the release of volatiles and the melting of plagioclase, K-feldspar and

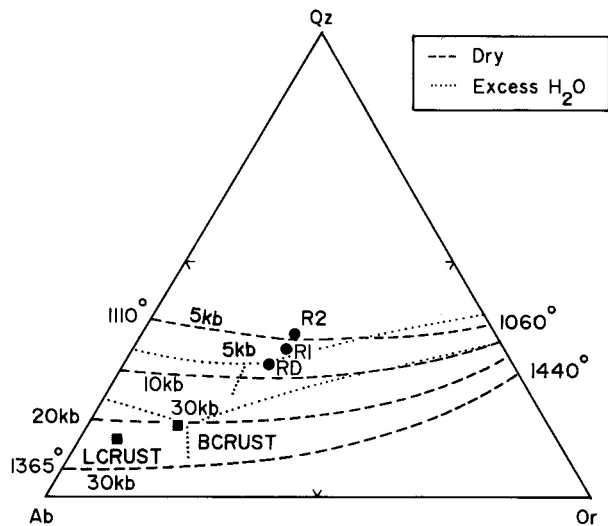


Fig. C.62: Ternary system Qz-Ab-Or (H_2O) illustrating the positions of rhyodacite (RD) and rhyolites (R1 and R2) of the HFF relative to liquidus field boundaries at different pressures (after Wyllie, 1977).

quartz. The residual rock is a granulite and this composition may be approximated by using Taylor and McLennan's (1985) average for the lower crust. An origin for Sinclair-age felsic rocks by partial fusion of lower crustal material has been previously proposed (Watters, 1978), but this idea has not been quantitatively tested. It should be noted that the maximum pressure of rhyolite generation is about 7 kb (Fig. C.62) and thus somewhat shallow for an origin in the lower most crust. Accordingly, the modelling exercise also takes into account the possibility that the source composition of the rhyolites may be closer to Taylor and McLennan's (1985) estimate for “bulk crust”.

(ii) Quantitative modelling

Three assumptions are made in the quantitative assessment of partial melting in the crust:

(a) The melt and solid residue are in equilibrium until the melt separates, i.e. so-called “batch melting” (Shaw, 1970).

(b) The source must contain quartz, K-feldspar and plagioclase in order to form melt of a “granitic” composition (see position of “Lower Crust” and “Bulk Crust” in Fig. C.62).

(c) K and Rb have been affected by magmatic processes only and can be used to estimate, respectively, the maximum and minimum degrees of melt. This is achieved by assuming complete incompatibility (not strictly true) of these elements such that $D=0$ and C_L/C_0 approaches $1/F$, where D is the bulk distribution coefficient, C_L/C_0 is the concentration of a trace element in the melt relative to its concentration in the source, and F is the weight fraction of melt relative to the parent.

Consideration of K_2O and Rb (see (c) above) suggests that the rhyolite compositions R1 and R2 can be generated by 3–8% melting of a lower crustal source or 15–25% melting of a bulk crustal source. Anatexis in the upper crust is precluded by the high degrees (53–76%) of melt which would be required to generate rhyolitic compositions. Compositionally similar rhyolites in the Sinclair type area suggest

a large volume of felsic magma which, for the degrees of melting considered above, imply derivation from a source 4-33 times greater in size than the melt volume. Source regions of this size are unlikely to be homogeneous (although minimum melts may be similar) and hence support the use of crustal averages in modelling rather than any specific rock type. Furthermore, the apparent absence of granulite facies rocks from the AMT basement (although underlying granulites may be present) does not allow the choice of an existing lithology to be made in the case of lower crustal melting.

Different degrees of melting of a given source material will result in a change in the proportions of the residual phases and the parameter D will vary accordingly. Knowledge of the proportions of the source minerals and their contribution to the melt (so-called "melting mode") enables the determination of the restite mineralogy for a specific degree of melting. The melting mode was calculated by using the least squares approximation of Bryan *et al.* (1969) and then subtracted from the source mineralogy to yield the restite mineralogy. The expression used to calculate the proportion of a given phase is as follows:

$$\text{Restite} = [\text{Source} - (F \times \text{Melt})]/(1 - F)$$

The normative compositions of lower and bulk crustal sources are essentially the same as those used by Taylor and McLennan (1985) and are based on the major oxides excluding P_2O_5 . The inference that P_2O_5 is negligible in amount is important from the point of view that normative apatite (and its potential effect on REE distribution) will be absent. If P_2O_5 contents in the lower and bulk crust are sufficiently high to result in the saturation value of 0.14% P_2O_5 (Watson and Capobianco, 1981), then P_2O_5 saturation is expected for relatively low degrees of crustal melting (< 25%; Stern and Gottfried, 1986). However, HFF rhyolites

are commonly undersaturated in P_2O_5 (< 0.1 %), thereby indicating that crustal anatexis is only likely in the event of the source containing a negligible amount of P_2O_5 .

The melting modes determined for R1 and R2 are very similar and have, therefore, been averaged for the purpose of determining the restite mineralogy. The melting modes incorporate two simplifying procedures, viz. the addition of FeO^* and MgO because of element partitioning by certain phases (see Section C.6.5.1) and the treatment of plagioclase as Ab and An prior to summation in the final melting mode. Restite compositions generated by melt removal after varying degrees of fusion of both lower and bulk crustal sources are presented in Table C.30. For the maximum degrees of melting of lower and bulk crust sources (8% and 25%, respectively), it is important to note that certain phases are no longer present in the residue and can therefore not exert any effect on the trace element composition of the melt (Hanson, 1978). Furthermore, exhaustion of K-feldspar \pm quartz will require a higher temperature phase to melt and a "non-minimum" melt must result (Collins *et al.*, 1982). The simplifying assumption has been made that this melt will be a "near-minimum" melt and approximately granitic in composition. This is not critical here since most discussion refers to the "average" amount of melt in each case, viz. 5% and 20% for the lower and bulk crust, respectively.

Partition coefficients used in the modelling procedure are presented in Appendix III and have, where possible, been chosen from dacitic bulk compositions. The predicted trace element abundances for varying degrees of melting of the lower and bulk crust sources are compared with rhyolites R1 and R2 in Table C.31 and Fig. C.63 (a) and (b). Given the flexibility in choice of K_d 's, it can be stated that both sources are acceptable for explaining the HFSE abundances, although the model fit is better for the lower crust. Ba

TABLE C.30: Restite compositions generated by melt removal after varying degrees of fusion of both lower and bulk crustal sources. Crustal averages from Taylor and McLennan (1985).

a) 3-8% fusion of lower crust

Phases	Lower Crust Norm	Melting Mode	Restite (3% melting)	Restite (5% melting)	Restite (8% melting)
Quartz	3.75	28.70	2.98	2.44	1.58
K-feldspar	2.00	26.60	1.24	0.71	0.00
Plagioclase	54.11	37.80	54.61	54.97	55.46
Orthopyroxene	28.96	3.15	29.76	30.32	31.16
Clinopyroxene	9.27	3.46	9.45	9.58	9.77
Ilmenite	1.90	0.31	1.95	1.98	2.04

b) 15-25% fusion of bulk crust

Phases	Bulk Crust Norm	Melting Mode	Restite (15% melting)	Restite (20% melting)	Restite (25% melting)
Quartz	6.13	28.70	2.15	0.49	0.00
K-feldspar	6.50	26.60	2.95	1.48	0.00
Plagioclase	52.76	37.80	55.40	56.50	56.84
Orthopyroxene	24.73	3.15	28.54	30.13	31.42
Clinopyroxene	8.18	3.46	9.01	9.36	9.60
Ilmenite	1.71	0.31	1.96	2.06	2.15

TABLE C.31: Calculated trace element abundances in the melt for varying degrees of fusion of lower and bulk crustal sources. Predicted abundances are compared with observed abundances in R1 and R2 (selected trace elements) and BH 669 (REE). Kd's listed in Appendix III (Table VI).

	Lower Crust			Bulk Crust			HFF rhyolites	
	3% melting	5% melting	8% melting	15% melting	20% melting	25% melting	R1	R2
Nb	16.6	15.8	14.7	25	23	21	16.1	16.0
Zr	286	267	243	294	261	236	266	317
Y	86	79	71	64	56	49	94	78
Ba	480	503	533	512	555	598	208	1310
Sr	95	96	98	111	115	121	55	29
Rb	85	66	49	175	140	117	212	187
Ni	23	23	23	21	21	21	9.0	2.5
Co	9.3	9.2	9.2	8.7	8.7	8.8	0.5	0.9
V	247	245	241	205	200	198	42	4.1
								BH 669
La	24	24	22	31	29	27		47
Ce	50	48	45	63	58	55		110
Nd	24	23	22	27	26	24		46
Sm	5.4	5.2	5.0	5.6	5.2	5.0		10.1
Eu	0.82	0.82	0.82	0.79	0.79	0.81		0.81
Gd	5.2	5.1	4.9	5.2	4.8	4.6		10.5
Tb	0.92	0.90	0.87	0.90	0.84	1.81		1.71
Yb	4.2	4.1	3.9	3.9	3.6	3.4		7.11
Lu	0.50	0.48	0.47	0.49	0.45	0.43		1.13

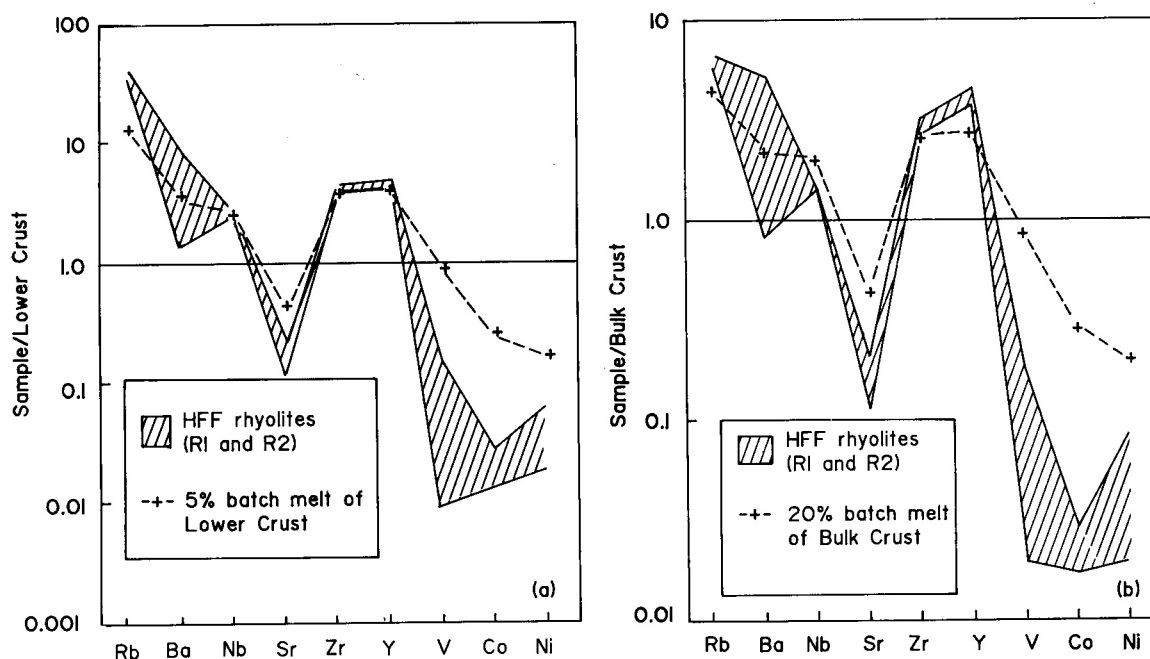


Fig. C.63: Comparison between trace element compositions of HFF rhyolites (R1 and R2) normalised to crustal averages (after Taylor and McLennan, 1985) and 5 and 20% batch melts of (a) Lower Crust, and (b) Bulk Crust, respectively.

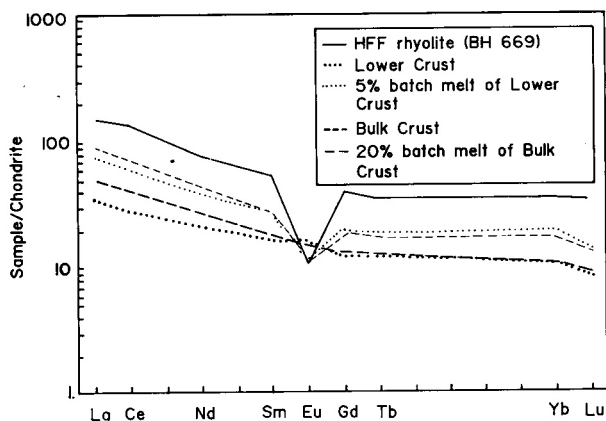


Fig. C.64: Chondrite-normalised REE patterns for HFF rhyolite and 5 and 20% batch melts of Lower and Bulk Crust, respectively.

for melts of both source compositions is within the range of values expected, while better agreement is demonstrated by bulk crust for the remaining trace elements except Sr and Rb. REE predictions, although only testable against sample BH 669 (a rhyolite which is compositionally similar to R2), demonstrate insufficient enrichment in all elements except Eu (Fig. C.64). While bulk crust melting is better able to match the abundances of the LREE, lower crust melting better satisfies Eu and the HREE. In general, however, the modelling does not enable a confident choice to be made between sources of average lower and bulk crust composition.

(iii) Discussion

Discrepancies between observed and predicted trace element abundances in the rhyolites (Table C.31) illustrate the following important features:

(a) The higher than predicted Rb/Sr ratio is compatible with the operation of fractional crystallisation, although much higher ratios are usually exhibited by extensive fractionation of feldspars in a granitic melt (McCarthy and Hasty, 1976).

(b) Abundances for elements with bulk D 's significantly greater than unity (Sr, Ni, Co, V) are lower than predicted and their variable concentration in the rhyolites strongly supports a dominant fractional crystallisation process (cf. Hanson, 1978).

(c) Feldspar-dominated fractional crystallisation is capable of explaining both general REE enrichment in the rhyolites and the large negative Eu anomaly. Metasomatic or hydrothermal processes cannot be easily invoked to explain REE (especially HREE) enrichment since these processes would be expected to disrupt regular igneous-type REE patterns and result in excessive enrichment in the HFSE.

Hanson (1978) has illustrated the very different compositional effects on the melt that result from low degrees of melting ($F < 0.3$) depending on whether K-feldspar or biotite are residual phases. Clemens and Vielzeuf (1987), however, consider that biotite will react with quartz and plagioclase on melting to form K-feldspar \pm orthopyroxene \pm garnet \pm cordierite, in which event the melt composition would not be significantly affected. If hydrous phases

survive in the residue, their volatile contents should enable melting in vapour-absent conditions. However, with the exception of biotite, the high K_d 's for REE in possible residual phases such as amphibole, garnet, apatite, magnetite, sphene and zircon will lead to even lower REE abundances than those predicted by the melting of a normative residue and a much steeper than observed REE pattern. One must assume, therefore, that such REE-rich phases are relatively soluble in A-type melts.

Melting of F- and Cl-rich amphiboles and biotites in the residue would cause enrichment in highly charged cations and REE (Collins *et al.*, 1982). The possibility that such enrichment is the result of late-stage residual fluids derives support from such features as widespread enrichment in many (though not all) rhyolites in the HFF with respect to the elements K, Rb and Ba. Similar enrichment in Zr and the REE may be attributed to stabilisation of these elements by excess alkali cations (Collins *et al.*, 1982) rather than a F-rich fluid phase.

Although not undersaturated, the HFF rhyolites exhibit a mean agpaitic index (molecular $[\text{Na}_2\text{O} + \text{K}_2\text{O}]/\text{Al}_2\text{O}_3$) of 1.03, thereby displaying sufficient alkalinity to accommodate the above suggestions. The presence of occasional fluorite in the rhyolites suggests that F abundances were probably high. Although the HFF rhyolites demonstrate many so-called A-type chemical characteristics, it is perhaps better to restrict this definition in the strict sense to peralkaline (or near-peralkaline) magmas which show extreme enrichment in highly charged cations (Sheraton and Black, 1988).

Back-calculation of REE abundances in BH 669 allows the determination of the source composition assuming similar degrees of melting and the same residual assemblages used for lower and bulk crustal sources. The source compositions determined, although broadly similar to HFF basaltic andesites with respect to LREE abundances (especially for 3% melting of a lower crust mineralogy), show much greater enrichment in HREE. It is, therefore, unlikely that the rhyolites were derived from a source similar in composition to the basaltic andesites.

While geochemical considerations are equivocal with regard to a lower or bulk crustal composition of the source for the HFF rhyolites, additional constraints can be used to indicate the most likely source region. The degree of melting required in the lower crust may be too low ($< 20\%$) to enable segregation and ascent of the melt according to Clemens and Vielzeuf (1987). Furthermore, if the source is indeed the granulitic residue produced by 25% melting of the lower crust (Compston and Chappell, 1979), then the siliceous and alkaline HFF rhyolites must represent less than 25% melting. If the HFF rhyolites were derived from a source at a depth of 18 to 25 km (5-7 kb), then in a continental crust at least 30 km thick (Watters, 1978), the source would be situated in the lower to middle part of the crust. A deeper crustal source may well apply to more rhyodacitic compositions which indicate a pressure of 8 kb (≈ 30 km) in Fig. C.62.

In conclusion it appears likely that the HFF rhyolites were produced by $\pm 20\%$ fusion of a source of intermediate composition situated within the lower third of the con-

tinental crust. While fractional crystallisation may result in the observed enrichment in many of the incompatible elements, including Y and Zr but excluding Nb, the high REE abundances require an additional process of enrichment, possibly late-stage residual fluids involving volatile transfer. Such late-stage enrichment has probably been superimposed on a process of feldspar-dominated fractional crystallisation which would have resulted in enrichment of the incompatible elements, but depletion of Eu and Sr. The additional separation of biotite \pm orthopyroxene from the melt would have caused significant depletion in the elements Ni, Co and V (due to the high K_d 's) while assisting in the enrichment in REE.

6.6 GENERAL DISCUSSION

6.6.1 Petrogenesis of the basaltic andesites and andesites

While it is well established that orogenic andesites are not primary melts of subducted ocean-floor basalt (Gill, 1981), the case for slab recycling is much better. $^{87}\text{Sr}/^{86}\text{Sr}$ initial ratios (R_0 values) are too low to accommodate a major input from either subducted sediment or continental crust, despite Sr/Nd and Ba/La ratios (averages of 15 and 31, respectively) which are too high to be accommodated by slab-only derivation (Gill, 1981). As noted in Section C.5, however, $^{238}\text{U}/^{204}\text{Pb}$ ratios do indicate crustal involvement in the genesis of basaltic andesites and this may also reflect sediment involvement.

Both REE patterns and variable abundances of Ni, Co, Cr and V in the HFF argue against any equilibrium between basaltic andesite and eclogite. Similarly, residual clinopyroxene and garnet in eclogite have low K_d 's for HFSE and cannot explain the relatively low abundances in basaltic andesites. Attempts to model these flows as primary melts of "chondritic" or "enriched" mantle have also been largely unsuccessful. What seems certain, however, is that the parental magma to the HFF basaltic andesites was derived from a relatively enriched mantle source. While such enrichment may be the result of interaction between partial melts (and derivative fluids) of the asthenosphere and overlying lithospheric mantle, a tempting explanation is provided by the situation of the mantle wedge above a fluid-rich subduction zone.

Mantle enrichment may have been fluid-related and slab dehydration would certainly provide a source of not only water, but also incompatible elements, radiogenic isotopes and SiO_2 (so-called IRS fluid of Gill, 1981). Even HFSE, especially Nb, could be leached by CO_2 -bearing fluid (subducted carbonate?) and then migrate into the overlying mantle wedge. If this environment contained sufficient non-radiogenic Sr (likely if carbonates are subducted), then the low R_0 value of HFF basaltic andesite could not be used to preclude crustal recycling. Partial melts may also migrate upwards from the slab into the mantle wedge, although Gill (1981) considers the high-temperature parental melts of basic andesites to require melting of both slab and overlying wedge. Fluid is a critical ingredient not only to provide the means of enriching the mantle source, but especially to enable melting by depression of the solidus.

The combination of partial melting and fluid movement in the mantle wedge is able to explain two important features of the petrogenetic modelling. Firstly, the "IRS fluid" accounts for the introduction of accessory phases which have high K_d 's (> 1) for Ti-group elements and hence low abundances of most of these elements in the HFF basaltic andesites. If, however, one assumes that these accessory phases have low melting points and hence enter the melt, then it becomes necessary to invoke a previous melting episode. Secondly, the moderate degree of fractional crystallisation of a primary melt required to produce basaltic andesite may be attributed to the more siliceous nature of unfractionated melts in the mantle wedge than elsewhere (Gill, 1981). The oxidising nature of this fluid-rich environment, in addition to the high pressure (Osborn, 1969, 1979), may further suggest the early stabilisation and fractionation of magnetite and thereby contribute to significant depletion in such elements as V, Ti, Cr and Ni.

The existence of a 30-40 km thick crust prior to eruption of the HFF volcanics is indicated by the high metamorphic grade of the existing early-stage crust or basement, the relatively high Sr and Rb abundances within the HFF basaltic andesites (Condie, 1973) and a relatively low CaO content at 6% MgO (Plank and Langmuir, 1988). These features are important in view of the strong correlation between crustal thickness and the compositional characteristics of orogenic volcanic associations noted worldwide (Coulon and Thorpe, 1981). A thick crust will promote fractional crystallisation, irrespective of whether AFC operates or not, in a basaltic (parental?) liquid and hence explains the absence of basaltic eruptive rocks from the AMT.

Crustal influence is strongly suggested by the relative success of AFC modelling for the progression from basaltic andesite to andesite in the HFF. While several LILE are too enriched in the lavas to be explained without invoking participation of the crust, low R_0 values for the basaltic andesites indicate that either crustal recycling (a mantle process) was dominant or that crustal interaction (in a crustal environment) has been largely restricted to more andesitic liquids. In this regard, it is interesting to note that andesites from the oceanic Marianas arc are isotopically unaffected by subduction, but volatile and trace elements require slab recycling (Gill, 1981). The implication is that in the HFF, where crust is present, both slab recycling and crustal contamination may have taken place.

In conclusion, the favoured process for the genesis of the compositional range basaltic andesite-andesite in the HFF is by partial melting of mantle pyrolite (peridotite) which has been enriched by fluid migration from below, possibly a hydrous subducted slab, and subsequent fractional crystallisation of the parental melt. In the crustal environment the basaltic andesitic liquid underwent assimilation-fractional crystallisation and mixing with cogenetic rhyolite (and/or older crust) to produce an andesitic liquid.

6.6.2 Petrogenesis of rhyolite and rhyodacite

Several features mitigate against rhyodacites and rhyolites being derived by fractional crystallisation of andesite in the HFF. These are the large volume of rhyolitic rocks,

assumed high R_0 values (0.718 ± 15) and the compositional heterogeneity which virtually precludes rigorous petrogenetic modelling. All these features may, however, be explained by derivation of the rhyolites from older continental crust. In particular, a heterogeneous crustal source implied by the elemental and isotopic compositions of the rhyolites is capable of producing a variety of minimum, near-minimum and non-minimum melts which would account for considerable compositional variation in the end product.

Fractional crystallisation does, however, appear to have operated in the genesis of the rhyolites as indicated by relatively high Rb/Sr ratios (cf. McCarthy and Hasty, 1976), low abundances of compatible elements and a large negative Eu anomaly. While the negative Eu anomaly may be explained by major residual plagioclase in the source, the accompanying Sr and often extreme CaO depletion (Fig. C.64; Table C.7) suggest that fractional crystallisation was probably still an important process. Furthermore, a high Kd for Eu in the source implies a low oxygen fugacity (Drake and Weill, 1975) which is probably not likely in a crustal source. However, under oxidising conditions, albitisation of plagioclase will preferentially enrich the fluid in Eu relative to other REE and hence contribute to a negative Eu anomaly (Fowler and Doig, 1983). Significantly, pronounced negative Eu anomalies in Proterozoic rhyolites and tuffs have previously been attributed entirely to a combination of sodium and potassium metasomatism (White and Martin, 1980). Metasomatic processes which may have affected some of the rhyolites, e.g. the low-Ba types which tend to fall close to the "anomalous granite" field in the ternary plot Rb-Ba-Sr, are attributed to late-stage residual fluids and can hence be regarded as part of the magmatic system.

Cann (1970) has shown that relatively dry partial melts of felsic crust tend to rise to high crustal levels. Even less hydrous A-type melts (as represented by the HFF rhyolites with their paucity of hydrous phases) should therefore be able to reach the surface and erupt. Melting of essentially anhydrous felsic granulites requires high temperatures (Wyllie, 1977), thereby implying deep crustal levels unless an additional source of heat is invoked. Experimental work by the same worker indicates that such melts tend to be alkaline and poor in silica especially in the presence of CO_2 -rich fluid. The silica-rich nature of the HFF rhyolites clearly implies a different source (i.e. at a shallower level) or some process whereby silica could be enriched.

Experimental and modelling considerations suggest that the source of HFF rhyolites was probably in the middle to lower crust, thereby inferring that additional heat was needed for melting. Two processes capable of inducing melting within the crust may be considered. Firstly, co-genetic basaltic andesite infers high liquidus temperatures which would enable some melting of the crust if intrusion and ponding of the magma took place. Secondly, the release of pressure in an extensional regime (Section D.3) would assist melting and reduce the viscosity of the melt. It is this stress regime which Clemens and Vielzeuf (1987) regard as the most critical factor influencing the ascent and ultimate emplacement of a magma.

While fractional crystallisation within the rhyolitic suite is seen as essential to producing much of the observed geochemical variation (e.g. low abundances of compatible elements), this process may not be the dominant control. Sharp compositional gradients within stratified felsic magma chambers are thought to be the result of thermogravitational diffusion (McBirney, 1980; Hildreth, 1981), a mechanism which could explain such features as the nearly three-fold variation in Nb in the range 73-78% SiO_2 . So although crustal anatexis is capable of explaining many of the overall features exhibited by the HFF rhyolites, in detail one must also consider the effects of fractional crystallisation, late-stage residual fluids involving volatile transfer, and possible thermogravitational diffusion (Hildreth, 1981).

6.6.3 Petrogenesis of the HFF volcanic succession

Wyllie (1977) has shown experimentally that although tonalitic (andesitic) melts can be derived by the melting of wet peridotite alone, these melts can not be generated at pressures typical of the mantle below continental crust which is in the order of 35 km in thickness. In order to generate andesite directly from the mantle, one might speculate that an extensional environment is required in order to reduce pressure. In an intracontinental environment, such crustal thinning should enable primary basaltic andesitic melts to reach the surface with minimal fractional crystallisation, thereby preserving the low R_0 values indicative of mantle derivation. However, this poses a problem with regard to the more differentiated andesitic liquids and geochemical evidence for crustal involvement. In a convergent margin, these characteristics may be related, at least in part, to a source in the mantle wedge.

While major element compositions of arc basalts appear to favour a source in the mantle wedge (Plank and Langmuir, 1988), it is the trace element abundances which enable assessment of the relative roles of subcontinental lithosphere (mantle wedge) and subduction zone (Pearce, 1983). "Average" basaltic andesite of the HFF has been normalised to MORB in Fig. C.65 and illustrates that K-group elements

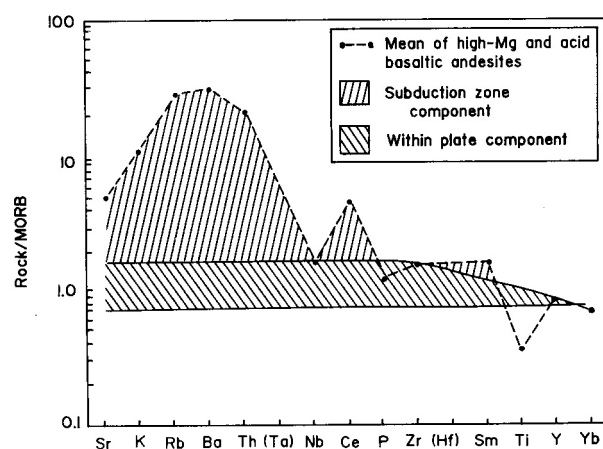


Fig. C.65: MORB-normalised trace element pattern for HFF basaltic andesites (mean of MBA and ABA) illustrating the relative contributions to the source region of subduction zone and within-plate mantle components. Procedure according to Pearce (1983).

and Ce may owe their enrichment almost entirely to a subduction zone, while HFSE, Sm and Yb appear to be derived from metasomatised subcontinental lithosphere. The negative anomalies displayed by P and Ti may reflect both the lithospheric composition and the effect of fractional crystallisation in the crust. Enrichment in LILE is characteristic of volcanic arcs such as central Chile (Section C.4), although similar enrichment is displayed by some intercontinental Karoo basalts (Cox, 1983).

The ascent of basaltic andesitic melt would be retarded in a compressional environment, thereby allowing both cooling and fractional crystallisation. The net result would be an increasing proportion of andesitic derivative liquids and probably a relatively small volume of erupted basaltic andesite and andesite compared with rhyolite erupted in an extensional environment. In addition, such retardation of the magma at depth and raising of isotherms could allow melting of the lower to middle crust and the production of granitic (rhyolitic) minimum melts. Progression of the stress regime towards a more tensional environment would enable the rhyolitic melts to segregate and possibly ascend in large volumes by magma fracturing, the most likely mechanism of magma ascent according to Clemens and Vielzeuf (1987). Fractional crystallisation of the rising felsic melts superimposed on compositional variation in the source would account for much of the variation in composition of rhyodacitic, low- and high-silica rhyolites in the HFF.

6.7 SUMMARY

(i) Neither closed system fractional crystallisation (FC) nor assimilation-fractional crystallisation (AFC) is able to fully account for the compositional variation from basaltic andesite to rhyolite unless allowance is made for considerable latitude in the model parameters. However, in view of the effects of deformation and possible alteration, it is conceivable that FC could account for the variation from basaltic andesite to andesite (and possibly rhyodacite).

(ii) Using immobile HFSE alone, the HFF demonstrates a change in fractionating mafic phases from clinopyroxene-dominated (basaltic andesite-andesite) to amphibole \pm biotite-dominated (andesite-rhyodacite) which appears to reflect the increasing involvement of continental crust (Pearce and Norry, 1979).

(iii) AFC is considered as a viable process to account for the variation from basaltic andesite to andesite by utilising an assimilant with the composition of HFF rhyolite and moderate degrees of assimilation ($r=0.46$) and fractional crystallisation ($F=0.81$). Admixtures of an assimilant similar in composition to average lower crust are able to further improve compatible element predictions. However, in the progression from andesite to rhyolite, AFC is unable to improve substantially on the predictions of FC even for a wide variety of assimilants. The broad compositional variation in HFF rhyolites is difficult to reproduce by either FC or AFC modelling.

(iv) Magma mixing between basaltic andesite and rhyolite to produce andesite and/or rhyodacite is difficult to as-

sess in view of considerable compositional variation within the end members. Maintenance of constant proportions of end members in mixing models is less easily achieved for rhyodacite compared with andesite. Since some trace element abundances (Nb, Sr in andesite; Co, V in rhyodacite) are better predicted by magma mixing than FC or AFC, it appears likely that magma mixing operated to some extent in the petrogenesis of the HFF.

(v) 5-20% melting of "chondritic" and "enriched" pyrolyte sources do not produce liquids with trace element compositions similar to those of HFF basaltic andesites (including high-Mg types). Consequently the latter are unlikely to be primary mantle melts.

(vi) REE indicate that for 10% melting, the calculated mantle source for high-Mg basaltic andesite shows an unusual concave-upward REE pattern (2-7x chondrite enrichment) that could imply the mixing of at least two distinct geochemical components. REE further preclude the derivation of basaltic andesites from an eclogitic source with the composition of pillow-bearing amphibolite in the Kairab Complex.

(vii) Basaltic andesites have probably been derived by fractional crystallisation of a basaltic magma involving moderate amounts of plagioclase, olivine, pyroxene and magnetite as shown by the moderately high Ni, Cr and Sr contents and slightly negative Eu anomalies in the former.

(viii) HFF rhyolites may have been produced by \pm 20% partial melting of a source of intermediate composition (e.g. average lower or bulk crust; Taylor and McLennan, 1985) situated within the lower third of a 30-40 km thick continental crust.

(ix) Feldspar-dominated fractional crystallisation in crustal melts is able to account for the incompatible element enrichment (excluding Nb) in rhyolites and depletion in Eu and Sr, but the high abundances of HREE require an additional process of enrichment, possibly late-stage fluids involving volatile transfer. The depletion in Ni, Co and V suggests the additional separation of biotite \pm orthopyroxene from the melt.

(x) It is concluded that the HFF volcanic suite was erupted at a continental margin. Early basaltic andesites display low R_0 values which suggest that there was only a limited input of subducted sediment or continental crust at this stage. Moderate fractional crystallisation of a primary melt to produce basaltic andesite (probably via parental basaltic magma) is compatible with the occurrence of more siliceous unfractionated melts in the mantle wedge than elsewhere. Enrichment of the mantle source is attributed to IRS fluid (Gill, 1981) from a hydrous subducted slab. In the crustal environment the basaltic andesite underwent AFC and mixing with cogenetic rhyolite (and/or older crust) to produce an andesitic liquid. The large volume of rhyolites, their high R_0 values and their compositional heterogeneity all suggest that they have been derived by anatexis of heterogeneous continental crust. Melting took place as a result of heat transfer by conduction in response to the ponding of basaltic magma at the base of the crust and the release of pressure with the development of intra-arc extensional tectonics.

PART D: SYNTHESIS

1. INTRODUCTION

The aim of Part D is to integrate the data presented in Parts Band C into a model for the crustal evolution of the AMT. The nature and timing of the formation of early- and late-stage crust in the AMT are important to an understanding of the regional relationship between the Sinclair Sequence and the NMC. The popular concept of a metamorphic basement overlain by undeformed and unmetamorphosed supracrustals is in need of revision in view of the continuity of crustal development from the middle to late Proterozoic. No detailed discussion is given on the geotectonic evolution of the early-stage crust, but the salient features are treated briefly in order to provide the necessary framework for discussion of the controversial tectonic setting of Sinclair-age magmatism.

2. ISOTOPIC EVOLUTION

2.1 STRONTIUM ISOTOPES

R_0 values for all the suites analysed in this study are plotted against their calculated Rb-Sr ages in a Sr evolution diagram (Fig. D.1). A Sr-isotopic evolution line for "Bulk Earth" is drawn through BABI (basaltic achondrite best initial ratio of 0.69898; Papanastassiou and Wasserburg, 1969) and the present-day "Bulk Earth" average of 0.7045

(O'Nions *et al.*, 1979). Also shown in Fig. D.1 is the oceanic mantle evolution line, which represents a mantle source depleted in Rb relative to "Bulk Earth", and the subcontinental mantle source region for southern Africa (shaded area; Erlank *et al.*, 1980). Model ages may be derived by extrapolating the Sr-isotopic vectors (defined by the average rate of increase in $^{87}\text{Sr}/^{86}\text{Sr}$, or the time-integrated Rb/Sr ratio, with time for each rock type) to the latter line. Assuming closed system behaviour with respect to Rb and Sr, such model ages reflect the maximum age at which a magma could have separated from its mantle source.

A very low Rb/Sr ratio for metabasalt in the Kairab Complex does not allow extrapolation of the Sr-isotopic evolution vector to the mantle evolution lines. However, the R_0 value of 0.7027 is intermediate relative to these lines and hence supports derivation from a mantle source. Intermediate values of 0.7029 and 0.7030 for the Aunis Tonalite Gneiss and HFF basaltic andesite, respectively, likewise argue for mantle derivation of their parental magmas.

The low R_0 value for the Aunis Tonalite Gneiss also falls within the 95% confidence limits placed on a mantle growth curve constructed by Peterman (1979) for Archaean to Cretaceous tonalities and trondhjemites. While this low R_0 value could conceivably be related to partial melting of an older crustal source region characterised by low Rb/Sr ratio, this is probably not likely in view of the apparent absence of basement rocks which are sufficiently Rb-poor and the

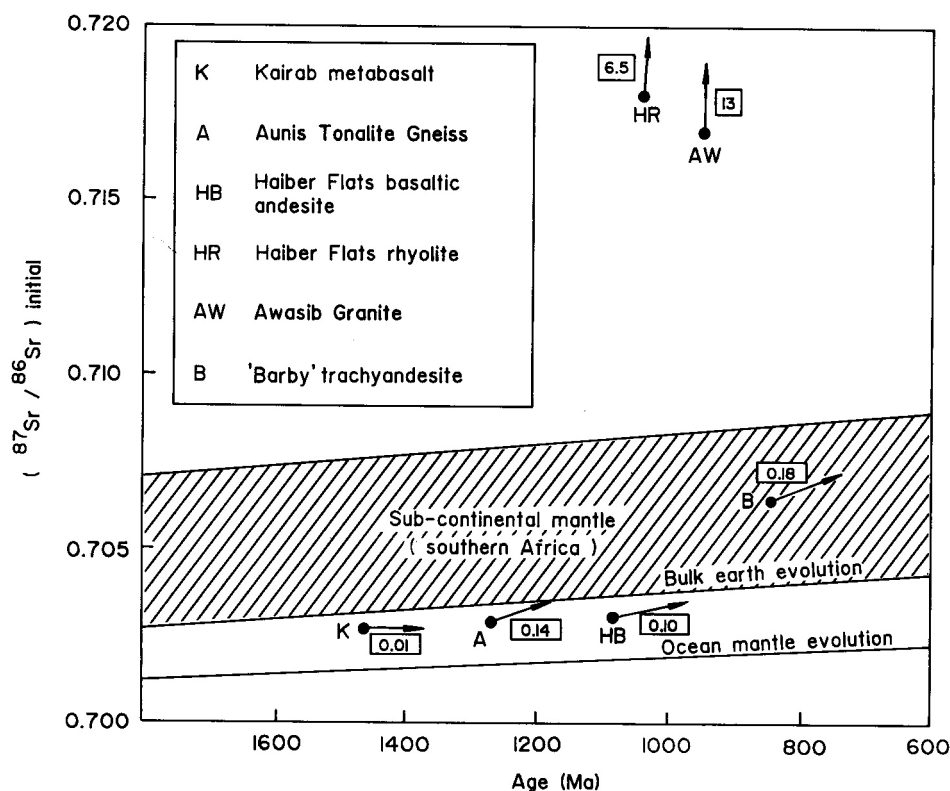


Fig. D.1: Sr-isotope evolution diagram for lithologic units from the Awasib Mountain terrain and Sinclair Sequence. Arrows represent the average rate of increase in $^{87}\text{Sr}/^{86}\text{Sr}$ with time for each unit, while the average Rb/Sr ratios are indicated alongside in boxes. The shaded area corresponds to the subcontinental mantle below southern Africa as determined by Erlank *et al.* (1980) and is bounded on the lower side by the "Bulk Earth" evolution line of O'Nions *et al.* (1979).

large volume of the tonalite. The relatively low R_0 values for a variety of rock types in both the early- and late-stage crust of the AMT suggest juvenile additions to the crust from the mantle in the period 1460-1086 Ma.

Rb-Sr data for the HFF rhyolite and Awasib Granite plot significantly above the mantle evolution lines in Fig. D.1. While the Sr-isotopic vectors exhibit steep trends which are compatible with an interpretation of crustal melting or metamorphic resetting (Davies and Allsopp, 1976), the large uncertainties in regression analyses (Table D.1) do not allow acceptable constraints to be placed on maximum model ages. In other words, the extrapolation of the Sr-isotopic vectors to the mantle curves cannot be reliably used to estimate the age of pre-existing rocks or precursors which have been subjected to crustal reworking. Nevertheless, the very high average Rb/Sr ratios of both HFF rhyolite (≈ 6.5) and Awasib Granite (≈ 13) could indicate derivation from high Rb/Sr sources in a crustal protolith not much older than the derivatives themselves. Significantly, the period between 1000 and 1100 Ma (the approximate age of these A-type magmas) occurs immediately after the Namaqua tectogenesis which has been bracketed in the interval 1300 to 1100 Ma by Barton and Burger (1983).

The R_0 value of 0.7064 for the "Barby Formation" trachyandesite plots well above the mantle evolution lines but within the shaded area designated by Erlank *et al.* (1980) as subcontinental mantle in southern Africa. This suggests derivation from either subcontinental mantle or lower crust. If this trachyandesite is a post-tectonic sill, then the relatively high R_0 is compatible with emplacement into an already thickened crust.

Pb data for all suites analysed are compared in Fig. D.2 with both the two-stage Pb evolution model of Stacey and Kramers (1975) and the reservoir growth curves derived from the plumbotectonics model of Zartman and Doe (1981). The latter authors invoke dynamic mixing between the mantle and continental crust during orogenesis in order to explain the μ values inferred for the mantle and lower crust (< 9.7) and the upper crust (≥ 10.1).

Data for the Kairab Complex metabasalt, whose parental magmas are inferred to be of mantle origin, define a Pb-Pb isochron with a μ value of approximately 9.87 for the source. This μ_2 value is only slightly higher than the μ value of 9.74 for the second stage of the Pb evolution model of Stacey and Kramers (1975) and hence approximates "Bulk Earth" evolution. Fig. D.2 illustrates that this source μ_2 value also conforms to the well-mixed orogene environment of Zartman and Doe (1981).

Relatively high μ_{12} values for both "Barby Formation" trachyandesite (≈ 10.1) and HFF basaltic andesite (≈ 10.2) data suggest partial to complete crustal derivation of the Pb. In the case of the trachyandesite, samples plot between growth curves for the orogene and upper crust, thereby implying derivation from a source more enriched than that of the orogene. A high source U/Pb ratio is not inconsistent with the origin in the lower crust or subcontinental mantle inferred from Rb-Sr data (Fig. D.1). However, basaltic andesite samples of the HFF plot above the upper crust reservoir growth curve and therefore suggest derivation from a source with an even higher U/Pb ratio than the source

TABLE D.1: Summary of Rb-Sr and Pb-Pb regression results.

	Rb-Sr			Pb-Pb		
	Age (ma)	$(^{87}\text{Sr}/^{86}\text{Sr})_0$	MSUM (n)	Age (Ma)	$^{238}\text{U}/^{204}\text{Pb}$	MSUM (n)
Kairab Complex metabasalt	1461 \pm 169	0.70269 \pm 12	2.48 (10)	1467 +201/ -215	9.87 +.14/ -.15	1.1 (4)
Aunis Tonalite Gneiss	1271 \pm 62	0.7029 \pm 3	1.3 (9)			
Haiber Flats Formation basaltic andesite	1086 \pm 44	0.70305 \pm 17	0.82 (8)	563 +2196/ -8820	10.18 +.36/ -.62	0.21 (4)
Haiber Flats Formation rhyolite	1038 \pm 74	0.718 \pm 15	7.0 (10)			
Awasib Granite	957 \pm 50	0.717 \pm 8	15 (10)			
"Barby Formation" trachyandesite	844 \pm 35	0.70641 \pm 25	1.1 (7)	1271 +836/ -1154	10.06 +.27/ -.33	1.4 (4)

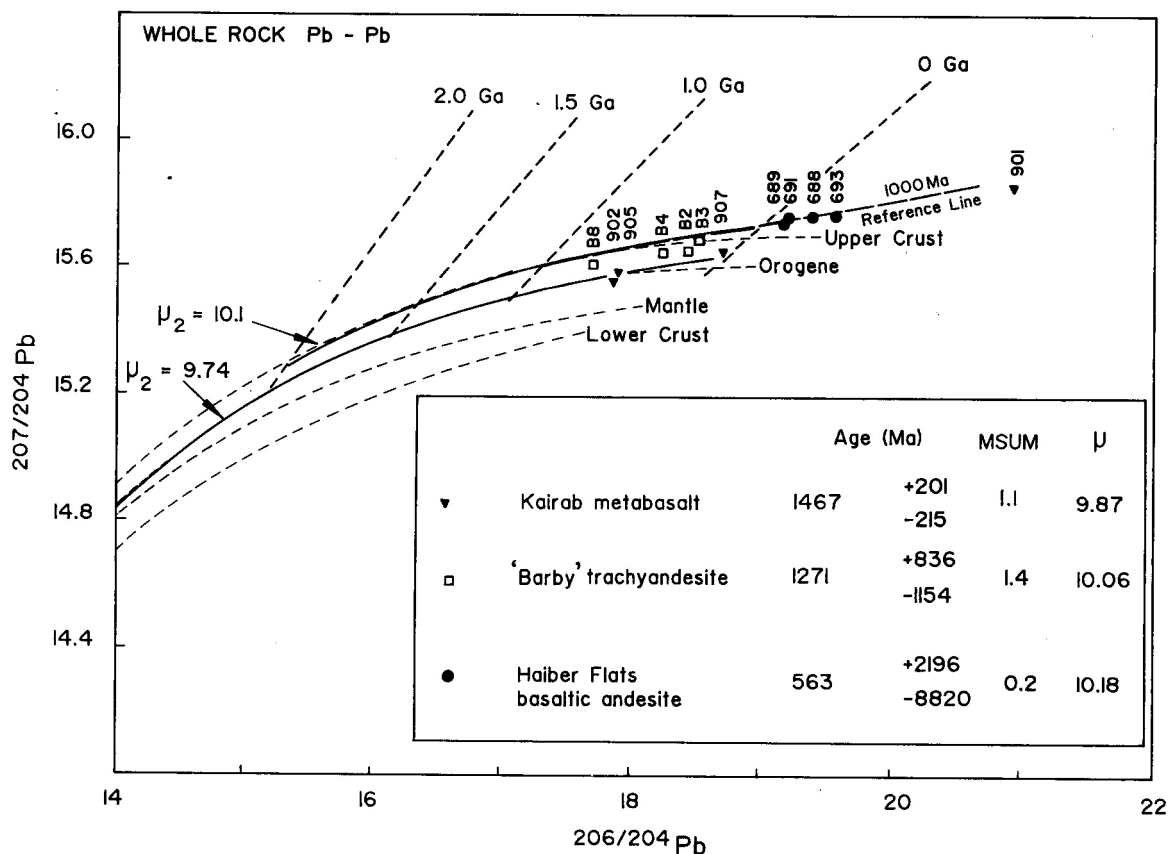


Fig. D.2: Pb-Pb isochron diagram for volcanic rocks from the Kairab Complex, Haiber Flats Formation and "Barby Formation". Pb isotopic compositions are interpreted in terms of the two-stage Pb growth model of Stacey and Kramers (1975); second-stage Pb growth curves for μ_2 values of 9.74 and 10.1 are indicated. Dashed lines represent Pb growth curves calculated for various mantle and crustal reservoirs by Zartman and Doe (1981).

of the "Barby Formation" trachyandesite. The upper crustal source indicated by Pb data for the HFF basaltic andesite is not compatible with the mantle source implied by Rb-Sr data.

If more reliance is placed on the constraints provided by the Rb-Sr data, then the high μ_2 values indicated for the sources of both "Barby Formation" trachyandesite and HFF basaltic andesite may, instead of reflecting crustal sources, indicate the existence of a mantle source region with a high U/pb ratio. Ancient enriched reservoirs may, according to Anderson (1982b), require episodic or continuous differentiation rather than simple two-stage growth. Such a mantle reservoir clearly implies that the Zartman and Doe (1981) model of Pb-isotope evolution may not be applicable to the subcontinental mantle in southwestern Africa, a distinct possibility in view of both mantle heterogeneity and the paucity of Pb data from southern Africa in the compilation of their model.

Anderson (1982a) has shown that mixing between depleted and enriched mantle reservoirs can result in an increase in U/pb ratios relative to the primitive mantle, but a decrease in $^{87}\text{Sr}/^{86}\text{Sr}$ ratios. In this author's "dynamically stratified" Earth, the shallow mantle reservoir is enriched at various times by both the upward migration of melts and subduction of oceanic crust and sediments. The apparent increase in μ_2 values of the mantle source from early- to late-stage crust in the AMT could also reflect a trend towards increasing source enrichment with respect to "Bulk Earth". While

several workers (Chase, 1981; Cohen and O'Nions, 1982; McKenzie, 1986) maintain that significant source enrichment, as indicated by some mid-ocean ridge basalts, should persist as a mantle heterogeneity for a minimum of 1000 Ma, this view is difficult to reconcile with the short-lived heterogeneities envisaged by Hawkesworth *et al.* (1984) in a convecting upper mantle.

The use of low R_0 values to infer a mantle source may be incorrect where non-radiogenic Sr is sufficiently abundant to act as a buffer and obscure the effects of mixing between crust and mantle (Armstrong, 1981). High Sr contents in the mantle will, therefore, result in a greater sensitivity of any magma source to Pb as opposed to Sr crustal contamination (Anderson, 1982a). This would allow for significant crustal recycling to have taken place undetected by Rb-Sr data alone, a process which is substantiated by the imbalance between the rate of magma emplacement relative to crustal growth in both modern plate margins and ancient greenstone belts (Dimroth, 1985). Nd isotopic data from southern Africa infer a high continental growth rate prior to 1400 Ma with < 10% of continental crust being formed from mantle precursors and processes in the last 1000 Ma (Harris *et al.*, 1987). While these data do not exclude crustal growth after 1400 Ma, the implied predominance of crustal recycling and reworking is consistent with the high μ values obtained for the HFF basaltic andesite and "Barby" trachyandesite. Assuming, then, that the high μ_2 of 10.2 in the case of the HFF basaltic andesite is an indication of

substantial crustal recycling, the most likely environment for such mixing would be at an active continental margin. As shown in Section C.4, such an environment is strongly supported by trace element data.

3. GEOTECTONIC SETTING

3.1 BACKGROUND

The environment of formation for the NMC adjacent to the Sinclair Sequence is poorly known, although Tankard *et al.* (1982) suggest that the Garub Sequence (including pelites, carbonates and basic rocks) may form part of a back-arc basin. The correlation of basic volcanics in the Garub Sequence and Kairab Complex with similar rock types in the Areachap Group near Upington, South Africa (Geringer *et al.*, 1986), suggests that all of these successions may have formed part of an active continental margin approximately 850 km long.

Watters (1974) was first to interpret the Sinclair Sequence as part of a much larger active continental margin which he designated the "Rehoboth Magmatic Arc". This interpretation has been refuted by subsequent workers (Kröner, 1977; Mason, 1981; Brown and Wilson, 1986; Borg, 1988) who consider a model of intracontinental rifting to better ac-

commodate both geological and geochemical features. An anorogenic character for felsic magmatism in the Sinclair Sequence was, however, implied much earlier on by Von Brunn (1967), who likened several of the high-level granites to the alkaline Younger Nigerian Granites.

Central to the geochemical part of this controversy is the K-rich nature of many rocks within the Barby Formation, a criterion which is difficult to use as diagnostic of a particular tectonic setting (Burke and Kidd, 1980). Detailed studies of K-rich (but presumably not peralkaline) rocks do, however, appear to be "earmarks" of two specific tectonic settings according to Ryan *et al.* (1987), viz. subduction-related (above the deepest parts of a subducted slab or when compression is relaxed) and post-collisional (in fault-bounded basins on thickened continental crust). Plume-related activity is an additional possibility but usually attended by the presence of voluminous peralkaline rocks and an identifiable trace of magmatic migration.

While earliest Sinclair -age magmatism appears to be about 100 Ma younger than its pre-tectonic "basement" (this study), it is significant that the youngest manifestations of tectonic activity in the adjacent NMC occur at *ca.* 1000 Ma and hence overlap with this magmatism. The AMT, which is situated along the western margin of the Sinclair Sequence, clearly occupies a key area with regard to any solution of the "orogenic versus anorogenic" controversy.

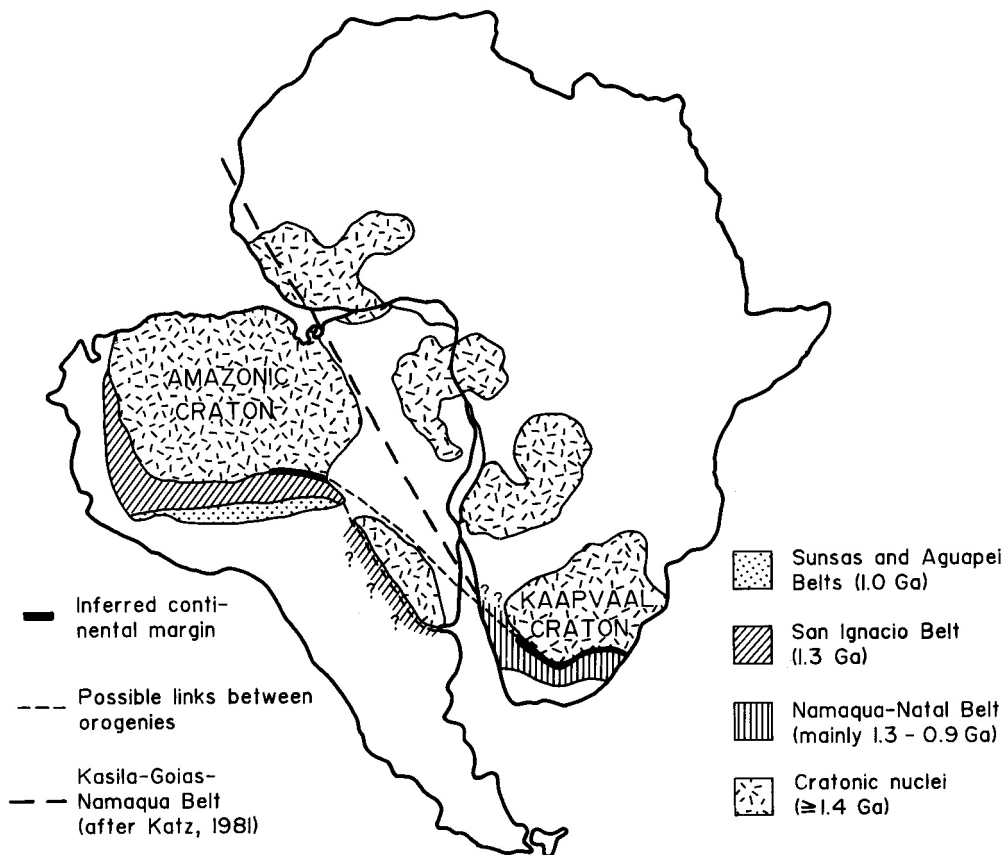


Fig. D.3: Proposed link between inferred continental margins in southern Africa and South America at *ca.* 1.3 Ga compared with the "Kasila-Goias-Namaqua Belt" as proposed by Katz (1981). South American data from Litherland *et al.* (1985). Fit of South America and Africa according to alternative model of De Wit *et al.* (1988).

3.2 EARLY-TO LATE-STAGE CRUSTAL EVOLUTION OF THE NMC

De Beer and Meyer (1984) have shown that the gravity signature along the northern margin of the Namaqua-Natal Belt may be accommodated by a model of uplift associated with differential movement along a faulted transition to the older Kaapvaal Craton. This model is consistent with the final stages of development of an Andean mountain belt with northward subduction of lithosphere below a continental margin. Available gravity, magnetic and geoelectrical data indicate the possible presence of oceanic crust at a relatively shallow depth, thus inferring that the NMC did not form intracatonically. This belt may continue in a northwesterly direction into South America and join up with a line of 1300 Ma old mafic and ultramafic intrusions which have been described as part of the Ciriquire arc (Litherland *et al.*, 1985). This arc is situated adjacent to the Amazonic Craton and is thought to mark the limit of the San Ignacio Orogeny. The overall similarity to the NMC is heightened by the presence of the spatially associated 1000 Ma Sunsas Orogeny. This reconstruction differs somewhat from that of Katz (1981) in that it implies a continuation of the Namaqua orogeny (*sensu lato*) along the west rather than the east side of the Amazonic Craton (Fig. D.3).

Similarities between the early-stage crust of the AMT and the western margin of the Kheis Belt include an abundance of mafic schist and amphibolite of volcanic origin and overlapping age ranges, viz. 1485-1268 Ma (U-Pb model ages; Barton and Burger, 1983) and 1460-1270 Ma (Rb-Sr and Pb-Pb isochron ages - Hoal *et al.*, 1989; this study). Hartnady *et al.* (1985) suggest that the Namaqua orogeny was initiated by the collision of the 1300 Ma old Jannelsepan arc complex with a continent. This suggestion is consistent with recent data on the volcano-sedimentary Copperton Formation which indicate an active continental margin or island-arc setting at *ca.* 1350 Ma (Cornell *et al.*, 1986).

Late-tectonic Namaqua granites (1200-1100 Ma) overlap in age with granulite facies metamorphism and retrograde shearing, both dated at *ca.* 1100 Ma (Hartnady *et al.*, 1985). The northwest-trending Gordonia subprovince was initially a zone of convergent thrusting and folding, followed by an estimated minimum of 140 km dextral shearing, e.g. Brakbos-Dagbreek-Straussburg line (Stowe, 1984). Elsewhere major thrusts have been turned on edge and reactivated as transcurrent shears, e.g. the Doornberg Line (Hartnady *et al.*, 1985).

Jackson (1976) estimated the peak of amphibolite metamorphism in the Gordonia subprovince to be at about 800°C and 6 kb, with a maximum geothermal gradient of 50°C/km. Further south Clifford *et al.* (1981) determined PT conditions of 900°C and 6-7 kb for 1200 Ma granulites and dated the main regional event (D_2) at 1187 ± 22 Ma (Rb-Sr whole-rock isochron). Associated hypersthene-bearing intrusives are related to the granulite facies metamorphism and were emplaced some 1100 Ma ago, while biotite-bearing garnet-sillimanite rocks yielded a K-Ar age of *ca.* 950 Ma (Clifford *et al.*, 1981). The latter age conceivably reflects uplift and cooling. Ar-Ar data on hornblendes in the NMC and Marydale Group date cooling below 600°C at 1080 Ma,

suggesting that Namaqua tectogenesis ended at about that time (Cornell *et al.*, 1986).

De Beer and Meyer (1984) have attributed the younger 1100 Ma events in the NMC to activation of a new, north-dipping, Cordilleran-type subduction zone along the Southern Cape Conductive Belt. Shearing at the boundary between the Gordonia subprovince and Kaapvaal Craton appears to have been accompanied by uplift of extensive high-grade regions (Hartnady *et al.*, 1985). According to Joubert (1981), thermal metamorphism in the NMC outlasted the 1100 Ma old shearing and may be defined as an event at about 1000 Ma. This event was post-granulite facies metamorphism, probably coeval with and younger than D_3 (and $D_4?$), and clearly contemporaneous with magnetism in the Sinclair Sequence and Koras Group. Accompanying deformation probably affected marginal parts of the AMT and Sinclair equivalents situated further west, e.g. the Konipberg Formation (McDaid, 1978).

Evidence for a major tectonomagmatic event at *ca.* 1100-1000 Ma in the NMC led Hartnady *et al.* (1985) to suggest terrane juxtaposition along the Brakbos and Doornberg shears, emplacement of late-tectonic granites and the formation of the Koras Group "pull-apart" basins.

Blignault *et al.* (1974) suggest that the basement to the Sinclair Sequence (Kumbis Complex; Watters, 1974) is part of the Kheis System, thereby allowing for the possibility of continuity with the Kaapvaal Craton. While this study does not address this possibility, the position of a craton boundary is difficult to establish due to extensive cover, the possible juxtaposition of allochthonous terranes and the fact that geophysical signatures tend to record the most recent event. Indications are that much of the early-stage crust in the AMT, and basement to the Sinclair Sequence, is lithologically similar to the NMC.

The positioning of the Namaqua front northeast of the "Excelsior-Lord Hill Mylonite Belt" by Blignault *et al.* (1974) is questionable in view of Vajner's (1974) description of this front as a zone which could vary from a metamorphic transition to an oblique-slip fault, but is essentially an interface between an older (> 2.5 Ga) and younger (1.25-0.9 Ga) province. Amphibolites which occur on either side of the Namaqua "front" are medium-grade and therefore not compatible with Blignault *et al.*'s (1974) concept of a northern marginal zone. Similar medium-grade amphibolites also occur well within their designated "northern low-stage zone".

The Excelsior-Lord Hill shear zone (Fig. AA) is, however, a well-defined feature and may be an important tectonostratigraphic terrane boundary for the following reasons:

(a) Uplift of deep-level granulites immediately south of the shear zone suggest that this is a major crustal discontinuity.

(b) A major metamorphic boundary is evident across the Lord Hill mylonite belt near Narubis and is probably less obvious across the Excelsior shear due to a general decrease in metamorphic grade towards the northwest.

(c) The southeastward continuation of this shear zone appears to link up with anyone of several shear zones in the vicinity of Upington, thereby forming a continuous zone of

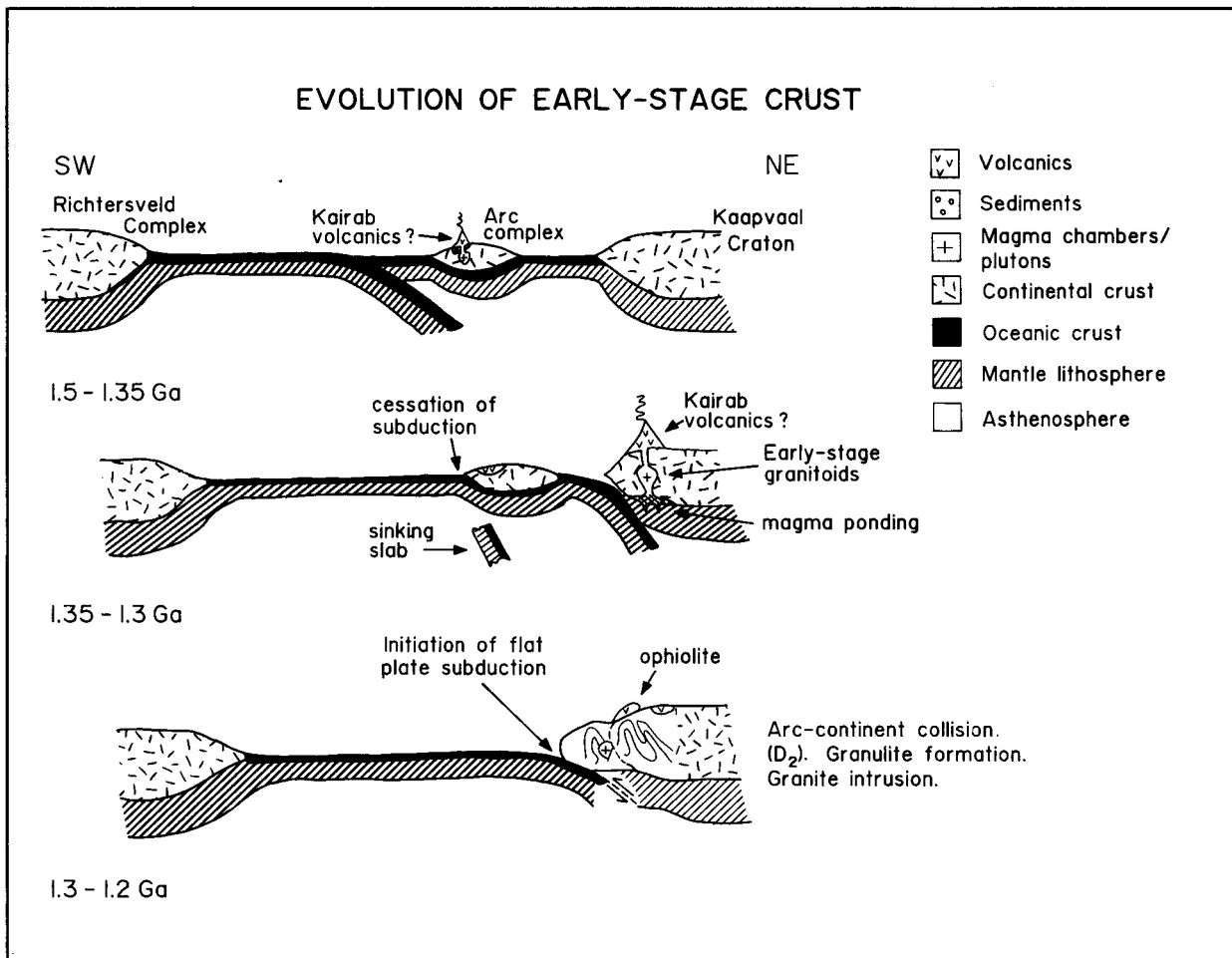


Fig. D.4: Proposed tectonic model for the evolution of the early-stage crust of the Awasi Mountain terrain.

faulting and shearing which follows an approximate line of gravity highs along the margin of an ancient craton.

(d) Northwestward extension of this shear zone as a major terrane boundary (the "EHL") was considered by Hoal (1987, 1989b) on the basis of aeromagnetic data and a line of mafic and ultramafic intrusions (Fig. A.4).

On the basis of the above considerations, the early-stage (≥ 1.3 Ga) crust in the AMT may have been formed in part by an arc-continent (or arc-arc) collision similar to the collision of the Jannelsepan arc complex and Kaapvaal Craton proposed by Hartnady *et al.* (1985). Younger Khorasib granites (< 1.3 Ga) represent late- to post-tectonic intrusions but may incorporate collisional S-types as well. This model (Fig. D.4) implies the operation of subduction at least 100 Ma prior to the earliest magmatism in the Sinclair Sequence and AMT.

A younger tectonomagmatic event within the NMC is marked by metamorphism and shearing at 1.1-1.0 Ga. As suggested by De Beer and Meyer (1984), this event may be attributed to a new subduction zone along the Southern Cape Conductive Belt. Subduction of similar timing and orientation could have affected the AMT and adjacent NMC by causing significant uplift south of the Excelsior-Lord Hill shear zone and propagating shears well within the Rehoboth subprovince. The close temporal and spatial association between this late tectonic event and magmatism in the Sinclair Sequence and late-stage AMT crust is significant and will be discussed below.

3.3 GEOTECTONIC EVOLUTION OF LATE-STAGE CRUST IN THE AMT AND THE TYPE AREA OF THE SINCLAIR SEQUENCE

3.3.1 A model of anorogenic rifting

The major evidence cited in favour of a rift-related origin for the Sinclair Sequence may be summarised as follows:

(a) Volcano-sedimentary successions are undeformed and unmetamorphosed (Kröner, 1977).

(b) The cyclicity of Sinclair deposition is attributed to repeated down sagging of intracratonic grabens along near-vertical fault margins (Kröner, 1977).

(c) Small yoked basins in the Sinclair Sequence are analogous to those in the East African Rift (Mason, 1981).

(d) Radiometric ages indicate a distinct lateral younging along a linear trend marked by positive Bouguer gravity anomalies (Borg, 1988).

(e) Continental red-bed sediments occur together with bimodal volcanics and high-level granite intrusions (Borg, 1988).

(f) Continental tholeiites predominate over calc-alkaline and alkaline basalts (Borg, 1988).

(g) Compositional features of volcanics such as high Zr/Y ratios of the calc-alkaline Barby Formation (Brown and Wilson, 1986) and peralkalinity of some rhyolites (Borg, 1988).

(h) Low $^{87}\text{Sr}/^{86}\text{Sr}$ initial ratios of high-K and shoshonitic volcanics are the product of fusion of an upper mantle source rather than a source in subducted oceanic lithosphere (Kröner, 1977).

The debate as to whether or not plate tectonics operated in the middle to late Proterozoic (e.g. Kröner, 1981; Hynes, 1987) will not form part of this discussion, particularly in view of the probability that such a mechanism already operated in pre-Sinclair times. Late-stage crust is only undeformed and unaltered in the type area of the Sinclair Sequence, an increasing degree of deformation and metamorphism being observed towards the AMT or "palaeomargin". Nevertheless, large parts of the cover are unaffected by any typical orogeny as a result of the nature of deformation, i.e. vertical tectonics combined with strike-slip movement along the faulted margins of grabens. Such "ice-floe" tectonics are better able to explain the greatly variable crustal levels encountered in the province than a model of repeated down sagging.

Small yoked basins, where present, are probably the result of the uplift of basement blocks along cross faults. Such basins, although commonly a feature of continental rifts, are unlikely to be confined to them. Furthermore, volcanics of the Barby Formation appear to extend well beyond the confines of their eruptive centres and, by implication, their "host" basins.

A linear trend of lateral younging defined by positive Bouguer gravity anomalies is highly speculative. Firstly, the age data compiled by Borg (1988) in defining this "younging" is poorly constrained and incorporates both pre-Sinclair and errorchron ages. Secondly, the entire age range is evident within a comparatively small region of the Sinclair Sequence alone. Thirdly, the trend of positive gravity anomalies is an extension of a linear trend of pre-Sinclair age which extends from southern Namibia to Natal (Fig. A.3). Fourthly, the link up of gravity anomalies between southern and northern Namibia is not justified by existing data.

Red-bed sedimentation in the Sinclair Sequence is a reflection of vertical tectonics which have resulted in the uplift of crustal blocks and rapid deposition of immature detritus into adjacent basins. Great thicknesses of sediments of local volcanic provenance are, however, also important in the Sinclair. Bimodal magmatic associations cannot be used as unequivocal evidence of "anorogenic" rifting. In reference to North Island in New Zealand, Hamilton (1988) states that "Were this strongly bimodal magmatic assemblage met in an ancient setting, it would be regarded by most petrologists as evidence against a subduction setting - yet, it is in fact forming in a magmatic arc". The large volume of granite (*sensu stricto*) magmatism in the Sinclair and its occurrence late in each magmatic cycle are difficult to reconcile with the progressive thinning of the crust in a rift setting.

Although tholeiitic affinities might be dominant amongst basalts (*sensu stricto*) in the Sinclair Sequence, this has to be seen in the context of the overall predominance of calc-alkaline basaltic andesites (including andesites) and the restriction of the basalts to a linear zone furthest from the palaeomargin. These basalts and their associated rhyolites

resemble the anorogenic associations described by Ewart (1979; 1982). Particularly diagnostic of this association is the aphyric nature of the Sinclair basalts (Brown and Wilson, 1986) and their enrichment in HFSE relative to the calc-alkaline lavas.

Magma compositions in active continental margins, cannot, compared with island arcs, be easily distinguished from their counterparts in continental rift settings. Hence high ratios of Zr/Y for the calc-alkaline Barby Formation volcanics may reflect a "within-plate" component, a feature not unique to anorogenic settings. This is borne out by the equally high Zr/Y ratios evident in published analyses of volcanics from high-K orogenic suites (e.g. Western USA; Ewart, 1982). The peralkaline rhyolites which Borg (1988) compares with silicic rhyolites in Ethiopia show alkali indices which are lower (by about 10%) and very close to unity on average.

Low R_0 values are recorded in both high-K and more calc-alkaline eruptive rocks in both the Sinclair and AMT. These ratios infer a mantle origin, but must be reconciled with the high concentrations of LILE which partly reflect metasomatism of the source (Section C.6). While such source characteristics are not unique to a particular tectonic setting, it should be noted that the K enrichment, if in the source mantle, would have had to be of short-term nature or the high associated Rb/Sr would have resulted in high R_0 values.

In summary, it is the occurrence of a great volume of chemically "orogenic" volcanic rocks together with repeated cycles of magmatism, major granitic plutonism, a compositional polarity away from and increasing degree of metamorphism and deformation towards a palaeomargin, and the absence of any significant volume of undersaturated rocks that militate most strongly against the formation of the Sinclair Sequence and the late-stage AMT in a rift setting.

3.3.2 A subduction-related model

(i) Geotectonic features

The model discussed is broadly similar to that proposed by Watters (1974), but differs markedly in many respects, particularly in terms of the linkage between contemporaneous Sinclair magmatism and Namaqua tectonics. The portrayal of the Sinclair Sequence as part of a curvilinear feature or extended rift at the margin of an ancient craton does not form part of this discussion, but correlations along this "arc" are in need of revision.

The major objection to the formation of the Sinclair Sequence and late-stage AMT crust along an active continental margin is the apparent absence of a widespread orogeny. Since isostatic uplift and erosion of thickened crust are normal consequences of subduction, a further objection to this model is the remarkable preservation of high-level cover close to the assumed site of convergence.

Deposition of volcano-sedimentary successions took place in a largely tensional environment which may be expected behind the accretionary wedge in an overriding plate provided that no collision is underway (Hamilton, 1988). More typically, however, extension in a convergent margin is associated with either back-arc spreading or intra-arc rift-

ing. While the bimodal and high-K nature of Sinclair volcanics is not incompatible with these settings, a bimodal tholeiitic association is typically encountered furthest from the margin and appears to be volumetrically subordinate to the calc-alkaline association.

The most important features of the subduction-related model are summarised in Fig. D.5 and listed below:

(a) The dip of the subducting slab was shallow in order to account for the expression of lateral compression in vertical "ice-floe" tectonics as discussed for the Laramide Orogeny by Rodgers (1987). This analogy explains why "conventional" compressional features are not more widespread as generally observed for "Chilean-type" margins (Uyeda, 1981). Central to this style of tectonics was the utilisation of pre-existing structural weaknesses (northwest-trending) in the continental crust. The early development of high-angle normal faults is not inconsistent with this model since tangential stresses are first accumulated by vertical deformations (Brunn, 1983).

(b) Subduction took place at an oblique angle to the continental margin, thereby resulting in strike-slip movement and the probable creation of pull-apart basins. While Jarrard (1986) has estimated that two-thirds of modern active continental margins have active strike-slip motion near the arc, the apparent confinement of many of the volcano-sedimentary successions in the Sinclair to basins is analogous to the graben-hosted stratovolcanoes of the High Cascades described by McBirney and White (1982).

(c) Subduction could have been accompanied by sufficient continental retreat to create a multi-rift environment similar to that observed in Japan (Tamaki, 1985). Although not essential to the model, divergence between the back-arc plate and fore-arc sliver would allow extension independent of the dip of the subducting plate.

(d) Later steepening of the subducting slab caused a form of back-arc spreading or foreland rifting to take place furthest from the continental margin. The bimodal tholeiitic association of volcanics in this back-arc was formed contemporaneously with, or slightly earlier than, the more marginal high-K calc-alkaline HFF volcanics. A distinct zonal arrangement in the compositions of volcanic rocks is evident and implies subduction to the northeast. The more central situation of apparently older calc-alkaline and shoshonitic rocks of the Barby Formation appears to belong to an earlier episode of magmatism. Such slab steepening may be the result of cessation of subduction (Le Pichon and Angelier, 1979) and would induce extension due to asthenospheric flow. Rapid transition from calc-alkaline to A-type magmatism has been recorded in part of the Pan-African Trans-Saharan belt (Liégeois and Black, 1987), where extension is attributed to the rise of asthenospheric mantle to shallow depth beneath the continental lithosphere after rupture of the cold plunging plate.

(e) Oblique collision between this active continental margin and a continent to the southeast took place at *ca.* 1100-1000 Ma, resulting in major dextral transcurrent movement and uplift. This event deformed supracrustal Sinclair Sequence equivalents in the Konipberg (fore-arc?), removed the accretionary complex, and uplifted granulites (root of

arc?) adjacent to the Excelsior-Lord Hill shear zone. Jarrard (1986) has estimated that fore-arc slivers occur in about 50% of modern subduction zones and that their transport along strike-slip faults is expected as a normal consequence of subduction, particularly under conditions of oblique convergence, strong interplate coupling and a continental overriding plate. While translational movement alone could explain the disruption of any paired metamorphic belt, the high geothermal gradient (particularly in the Precambrian) would also militate against the preservation of blueschists.

(f) Late- to post-collisional granite magmatism resulted in the voluminous granites which typically close off the Sinclair magmatic event. The post-kinematic style of emplacement of the youngest I- and A-type plutons in the Sinclair are typical of Pitcher's (1983) late uplift stage of orogenesis. Late-stage extensional tectonism may have been partly responsible for the coalescence of crustal partial melts and the intrusion of batholiths similar to the intercontinental silicic batholiths described by Hildreth (1981). Uplift and erosion were mainly confined to that portion of the arc to the southwest of the Excelsior shear zone and its extensions to the northwest and southeast. This crustal break may be explained by a magmatic arc being the weakest part of an overriding plate as a result of higher thermal gradients, decreased lithospheric thickness due to heating and increased crustal thickness due to plutonism (Jarrard, 1986).

The cyclical nature of the Sinclair sedimentation and magmatism may be explained by pulsing of the subduction. As in the Chilean Andes, episodic phases of extension and compression result from a changing roll-back velocity combined with changes in the motion of the overriding plate (Dewey, 1980). Periods of compression initially resulted in increased vertical uplift, strike-slip movement and mainly sedimentation. Mafic volcanism could also have been a feature of these compressive periods but generally characterised the waning stages when reduced stress enabled ponding of the magmas at the base of the crust. Relaxation of lateral compression was responsible for major crustal fusion and the production of mainly A-type rhyolites and their batholithic equivalents. In subduction zones, the source material (mantle or crust) is renewed so that there is *repetition* of magma types during volcano-plutonic episodes (Bateman, 1983).

Isostatic uplift and subsequent erosion of magmatic arcs must be expected as a natural consequence of magma input and thermal expansion. Preservation of high-level features in an ancient continental margin requires extension to proceed at a greater rate than magma input (e.g. North Island, New Zealand; Adams and Ware, 1977). While different in form and origin from non-extensional volcano-sedimentary synclines in Chile (Levi and Aguirre, 1981), Sinclair basins may show similar down warping as a result of material lost by air fall associated with voluminous ash-flow tuff eruptions (cf. Wopmay orogen; Hildebrand and Bowering, 1984). The paucity of air-fall deposits in the Sinclair Sequence could indicate enormous loss of ash which would need to exceed magma input into the crust in order to allow subsidence due to this mechanism alone.

While strike-slip shearing and uplift appear to be more

common towards the palaeomargin of the Sinclair, stretching and subsidence are more widespread in the foreland. This polarity is not unlike that observed in the Rocky Mountains and Basin and Range of North America, features most recently explained as being compatible with the subduction of a spreading ridge (Wilson, 1988). Although attractive, this possibility has not been pursued in view of the absence of distinctive geochemical features (see below).

(ii) *Geochemical and isotopic features*

Compositional characteristics of the late-stage AMT crust are discussed in detail in Section C.4 along with the geochemical features displayed by the HFF volcanic rocks which are thought to be most characteristic of a subduction-related source. The calc-alkaline nature of the basic to intermediate part of the succession is reflected in both whole-rock and phenocryst (especially augite) compositions' while rhyolites tend to show more alkaline (though not undersaturated) compositions. The large volume of calc-alkaline rocks in the Sinclair Sequence is well documented (Watters, 1974) and important, despite the lack of andesite (*sensu stricto*) domination, with regard to Miyashiro's (1974) contention that calc-alkaline eruptions are restricted almost exclusively to volcanic arcs.

Tectonic discrimination diagrams (e.g. Pearce and Cann, 1973) have been avoided in this discussion in view of growing evidence that such diagrams are indications of source characteristics rather than geotectonic settings (e.g. Prestvik, 1982; Duncan, 1987). In particular, Morrison (1978) has shown that based on immobile trace element abundances alone, tectonomagmatic discriminant diagrams attributed the volcanic products of a single tectonic environment in Skye (Scotland) to several different tectonic settings.

Bimodal volcanism recognised in modern arcs is apparently restricted in space and time (Hildreth, 1981) and volcanics from a large segment of an arc system rarely show bimodality (Condie, 1987). In the ancient rock record, such bimodality could reflect a preservation bias towards back-arc successions, e.g. southwest USA (Condie, 1987). Within the single well-studied HFF suite, incorporation of the closely associated Haisib Intrusive Suite (unerupted intermediate compositions of the HFF?) indicates that bimodality may not be a marked feature.

While low $^{87}\text{Sr}/^{86}\text{Sr}$ initial ratios in HFF basaltic andesites are compatible with a relationship to a subducting mid-ocean ridge, high K contents and low TiO_2 contents differ from the compositions of tholeiitic andesites thought to be characteristic of mid-ocean ridge-continental margin interactions (Hurst, 1982). Basalts from the northern part of the "Barby Formation" have been analysed by Brown and Wilson (1986) and several flows indicate low K (<0.5 wt.% K_2O) and high TiO_2 (> 1.8 %) contents. These compositions probably reflect the influence of upwelling asthenosphere below a zone of tension in the foreland.

While several incompatible trace elements (Zr, Y, Zn) display typical within-plate enrichment in tholeiitic mafic lavas of the "northern Barby Formation", it is noteworthy that Nb abundances are typically low (< 13 ppm; Brown and Wilson, 1986; Fig. 15). This may reflect an inherent

characteristic of the upper mantle which is shared by the presumably older calc-alkaline mafic lavas of the "southern Barby Formation". The latter, however, show relative enrichment in Ba, K and Rb which is probably the result of subduction-related metasomatism of the upper mantle. This suggests that the subduction signature was lost due to mantle convection and no longer existed as a source characteristic for the younger tholeiitic lavas. Smedley (1986) has inferred a similar relationship between Palaeozoic calc-alkaline and alkaline lavas in Scotland.

Shoshonites are typically found in volcanoes farthest from the plate boundary or in areas of uplift following cessation of subduction, while boninites may belong to an early stage in subduction zone development (Gill, 1982). The distribution of shoshonites in the Barby Formation is consistent with Gill's observation, while the single flow of boninitic affinity in the HFF is situated amongst the most westerly volcanic outcrops of the Sinclair. The alkaline affinities of some magmas in the Sinclair should be viewed in the context of observed compositional gradients from calc-alkaline to alkaline (and peralkaline) rocks in subduction-related suites, e.g. Trans-Pecos province, Texas (Barker, 1987). Available data (Watters, 1974; Kröner, unpublished) further indicate that Sinclair "trachybasalts" do not display the characteristically strong "positive" Nb-Ta anomaly of typical alkaline basalts (Weaver and Tarney, 1982).

Considerable volumes of erupted and emplaced felsic magmas show A-type chemical features compatible with crustal derivation. Heat was provided by the arrival of mafic magmas at the base of the crust, thereby suggesting that a large portion of the lower part of the crust was molten. This suggests that the more mafic "mantle-derived" magmas must have been affected by the crust and that the low $^{87}\text{Sr}/^{86}\text{Sr}$ initial ratios are the result of equilibration of the upper mantle with the lower crust, e.g. San Juan volcanic field (Lipman *et al.*, 1978). Such equilibration of magma and crust is invoked by Ewart (1982) to explain the high-K signature of orogenic magmas, particularly those situated along continental margins.

Calc-alkaline basaltic andesites of the HFF exhibit an R_0 value consistent with derivation from the "Bulk Earth" source inferred for modern island-arc extrusive rocks (Cox *et al.*, 1979, p.365). The more enriched source implied by Pb data may be a consequence of significant crustal recycling into the mantle source, a process more likely to occur at an active continental margin than within an intracratonic rift. The enriched mantle source could, however, represent a long-lived heterogeneity inherited from an earlier event (cf. Hoal, 1987).

3.4 DISCUSSION

In the debate on the "orogenic versus anorogenic" geotectonic setting for the Sinclair Sequence, the obvious objection to the mobilist viewpoint is that too much weight has been placed on a geochemical subduction signature which may have been inherited from a more ancient event (Hoal, 1987). Significantly, it has been shown in this study that at least part of the early-stage AMT crust appears to have

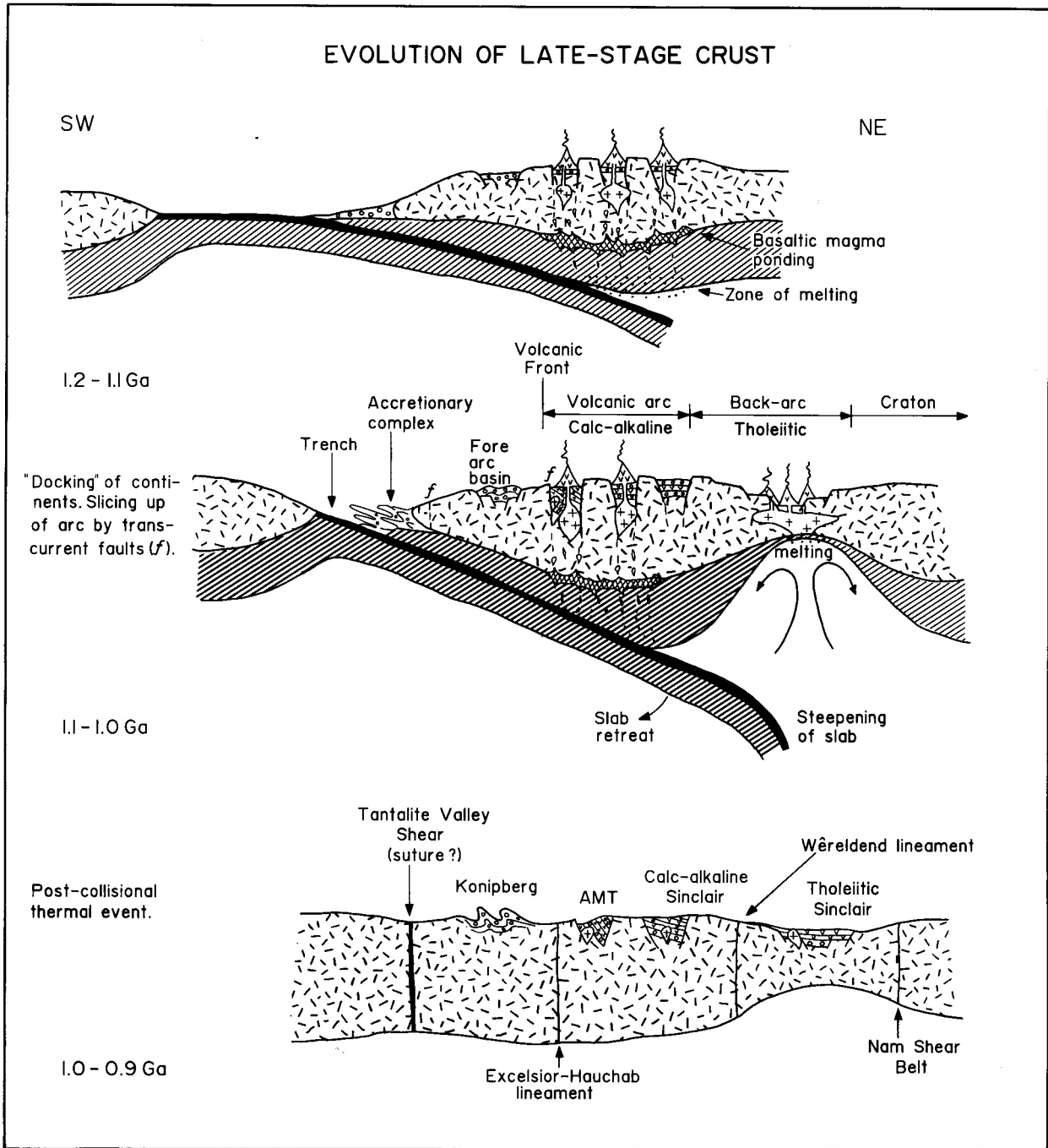


Fig. D.5: Proposed tectonic model for the evolution of the Sinclair Sequence and late-stage crust of the Awasi Mountain terrain. Legend as for Fig. D.4.

formed in a subduction setting itself. Thirlwall (1988) is more definite in his claim that it is chemically impossible to deduce a relationship to active subduction.

Metasomatism of the mantle by a subducting slab is considered by Thirlwall (1988) to continue as long as the slab is available and this signature will remain for a significant period after subduction ceases. Age constraints in the Sinclair Sequence suggest that such metasomatised mantle would have come into being prior to *ca.* 1.3 Ga and was sampled continually from about 1.2 Ga (Barby Formation magmatism) to about 1.1 Ga (HFF and possibly Guperas

Formation magmatism). This would require the subduction signature to survive at least 200 Ma of mantle convection. One possible way of shielding such metasomatised mantle would be by its incorporation into the lithospheric keel of the continent.

Apart from the problem of sustaining a mantle "anomaly", its non-renewable nature poses a major obstacle in the way of explaining the repetition of orogenic magmatism within the Sinclair and late-stage AMT. A mantle plume or zone of mantle upwelling is required by the anorogenic model, but initial melting of this source will deplete it dramatically

in LILE- and incompatible elements. The expected source depletion in subsequent magmas is, however, not observed and this suggests that metasomatism must be a continual process. By contrast, active subduction offers a continuous means of metasomatising the mantle. While so-called arc-terminating transform volcanism is characterised by source enrichment in incompatible (alkalis) and refractory elements (Mg, Ni, Cr) alone, more typical arc magmas include a slab-derived silicate melt as well (Gill, 1982).

The above arguments are restricted to the mafic rocks of the Sinclair Sequence and late-stage crust of the AMT. Associated felsic rocks are typically A-type and their crustal derivation indicates that they are not strictly part of a calc-alkaline suite. However, it is important to draw a distinction between rhyolites derived by fractional crystallisation of mafic magmas in island arcs and anatectic rhyolites which are not uncommon in active continental margins. It is the nature of the pre-existing continental crust that will influence most strongly the compositions of these rhyolites. Accordingly, A-type magma compositions cannot be used in any tectonomagmatic sense. Nevertheless, the implied crustal source and similar age to interbedded basaltic andesites suggest periodic shifts in source region from mantle (\pm recycled crust) to crust.

The great diversity in magmatism in the Sinclair is not only a reflection of source renewal, but also the result of crustal heterogeneity and thickness. The cyclical development of this region is influenced primarily by subduction, but also by prevailing stress and the effect of previous melting episodes in the crust. This situation is demonstrably different from that of isolated non-arc andesites which may occur well within a continental interior and are not obviously related to subduction.

The actual site of subduction which influenced the formation of the Sinclair Sequence (and probably also the Koras Group) is uncertain but any suture could have been rendered cryptic by major dextral shearing as suggested by Harnady *et al.* (1985). It is considered that this subduction was, in effect, initiated by the earlier 1.3 Ga collision (cf. Hamilton, 1988) and was situated either along the 700 km long Tantalite Valley-Haalenberg Lineament (Hoal, 1987) or to the southwest of this lineament along an extension of the zone designated as the Southern Cape Conductive Belt by De Beer and Meyer (1984).

The culmination of the late-stage magmatism was marked by an extensional phase during which there was widespread intrusion of late- to post-Sinclair dykes. Both Rb-Sr and Pb-Pb data for a trachyandesite sill indicate derivation from an enriched source, either in the subcontinental mantle or lower crust. This source may have preserved its heterogeneity from an earlier orogenic event but Pb data provide evidence for reduced crustal recycling into the mantle relative to earlier basaltic andesite of the HFF. Cessation of crust-mantle mixing related to subduction may be reflected by a μ_2 value which is lower than the value for the HFF. This may further be the result of a trend towards increasing extensional tectonics prior to Pan-African rifting.

4. SUMMARY

The main findings of this study are summarised below.

- The AMT crust is made up of early- and late-stage lithologies which are correlated with the Namaqualand Metamorphic Complex (NMC) and Sinclair Sequence, respectively.
- The oldest part of the early-stage crust is represented by the Kairab Complex which comprises a diverse group of schists, gneisses, metaquartzites and amphibolites. These rocks have undergone three episodes of deformation (D_1 - D_3), the earliest stages being associated with migmatitisation. Compositions of hornblende, biotite and epidote within the amphibolites are compatible with low-medium grade amphibolite facies metamorphism, a feature also displayed by Garub Sequence metabasites in the NMC. High-alumina pillow-bearing basalts form part of a tholeiitic basalt-rhyolite volcanic succession which exhibits few compositions in the basaltic andesite-dacite range. Basalts yield a primary age of *ca.* 1460 Ma (Rb-Sr, Pb-Pb) with a low $^{87}\text{Sr}/^{86}\text{Sr}$ initial (R_0) of 0.7027 ± 1 and are characterised by the low contents of Ti, Nb, Zr, Y, Ni and Cr typical of island-arc or back-arc settings. Low- and high-silica pyroclastic rhyolites display chondrite-normalised patterns (especially negative Th anomalies) which are consistent with a subduction-related environment.
- Largely metaluminous granitoid intrusive suites within the early-stage crust are mostly younger than the Kairab Complex and have undergone D_3 deformation. The primary igneous mineralogy is often well preserved although gneissic textures suggest low-medium grade metamorphism. There is a close spatial association between the Kairab metavolcanic succession and both gabbroic and granitic (*sensu lato*) rocks. Cumulate-textured gabbros are compositionally similar to the basalts, but lack high-alumina types and show relatively enriched MORB-normalised trace element abundance patterns. The association between gabbro, a mafic dyke swarm, pillow-bearing basalt, pyroclastic rhyolite and tonalite-trondhjemite southwest of Chowachasib Mountain resembles that of a dismembered ophiolite complex.
- The Aunis Tonalite Gneiss (dated at 1270 ± 62 Ma; Rb-Sr) shows similar ORG-normalised trace element abundance patterns to low-silica rhyolite in the Kairab Complex. The association between the Aunis Tonalite Gneiss and Kairab gabbro may follow a poorly defined gabbro-trondhjemite (or calcic) rather than calc-alkaline trend. The generally younger Khorasib Granite Gneiss consists of a tonalite-granite association which follows a calc-alkaline to alkali-calcic trend similar to that of the Sierra Nevada batholith. The progression from Aunis Tonalite Gneiss to Khorasib Granite Gneiss reflects juvenile ($R_0 = 0.7029 \pm 3$) magma input followed by an increasing contribution from subcontinental within-plate mantle lithosphere and heterogeneous crust. ORG-normalised patterns are typical of arc granites (i.e. enrichment in K, Rb, Ba and Th relative to Nb, Zr and Y) and suggest that the change in granitoid compositions records a progression from a primitive to

- mature (continental) arc or post-orogenic environment.
- The late-stage crust of the AMT is made up of both volcano-sedimentary successions and high-level intrusions. With the possible exception of the youngest granites, these rocks have undergone three main episodes of deformation (D_4 - D_6), the most intense phase (D_5) being associated with greenschist facies metamorphism. Late bimodal dyke swarms constitute the youngest expression of magmatism in the AMT, but these dykes have been affected by a late episode of folding (D_7).
 - The oldest sediments in the late-stage crust are represented by the Urusib Formation and have been deposited in fault-bounded troughs and pull-apart basins which reflect separate, but broadly synchronous, periods of uplift and quiescence. While periods of active uplift have resulted in the formation of braided streamflow fans (immature and poorly-sorted clastic rocks), more stable crustal conditions were required for the formation of associated lake deposits (shales and siltstones). There is an increase in the ratio of volcanic to granitic clasts with time. A maximum thickness of 2400 m was recorded at the type locality of the Urusib Formation.
 - The predominantly volcanic Haiber Flats Formation (HFF) overlies the Urusib Formation disconformably and is confined to the same northwest-trending troughs. The volcanic succession has a minimum thickness of 3000 m and the existence of at least three volcanic centres is suggested by regional compositional variations, changes in thickness of flows, proximal agglomerates and the presence of subvolcanic intrusions. The eruptive rocks are typically porphyritic, commonly pyroclastic, and made up predominantly of basaltic andesite-andesite and rhyodacite-rhyolite with volumetrically minor andesite-dacite. The earliest volcanics were largely basaltic andesites but the increasing volume of rhyolites eventually exceeded the former by a factor of three. Stratified tuffites and volcanoclastic and clastic rocks make up less than 10% of the HFF. Lithologically similar basaltic andesites and tuffites of the Barby Formation crop out in the eastern part of the AMT, but are not in contact with the HFF.
 - Metamorphic biotites in basaltic andesites of the HFF and the associated late-stage Haisib Intrusive Suite (monzonite to granite) are unrelated to the younger Pan-African orogeny and suggest a regional metamorphic temperature of 400-450°C. Compositions of relict plagioclase, pyroxene and titanomagnetite phenocrysts are similar to their counterparts in orogenic basaltic andesites. This is in agreement with the whole-rock compositions of the HFF which indicate a strong similarity to calc-alkaline or high-K (not shoshonitic) volcanic suites from active continental margins such as western North America and Chile. These distinctive compositional features include high abundances of K, Rb, LREE, Th and Zr (and sometimes Nb and Y), and low abundances of the HFSE (except Nb and Y in the rhyolites). For the basaltic andesites (including high-Mg types), both MORB-normalised trace element and chondrite-normalised REE patterns support an active margin setting and are similar to patterns obtained for andesites of the Barby Formation. Rhyolites, however, are fractionated crustal melts and therefore exhibit the high abundances of silica and alkalis and low MgO and CaO typical of suites unrelated to subduction. Such A-type characteristics are further illustrated by the similarity of chondrite-normalised trace element patterns to patterns from intracontinental rift- or hot spot-related rhyolite suites, but the similarity of REE patterns to patterns displayed by subduction-related suites suggests the possibility of intra-arc extension in an active continental margin setting.
 - HFF basaltic andesite yields an age of 1086 ± 44 Ma and R_0 of 0.7030 ± 2 indicating derivation from a mantle source region which is slightly depleted relative to "Bulk Earth". The errorchron age estimate of $1038 \pm 74^*$ Ma (R_0 of $0.718 \pm 15^*$) obtained for a rhyolite porphyry from the HFF is within error of that deduced for the basaltic andesite. The high R_0 for the rhyolite is consistent with the crustal origin inferred from A-type characteristics. Petrogenetic modelling suggests that basaltic andesite (including high-Mg types) evolved from a mantle-derived basaltic parent by fractional crystallisation and subsequently underwent assimilation-fractional crystallisation and mixing with rhyolite (or rhyolitic crust) to form andesite. Rhyolites are fractionated, near-minimum partial melts of a basic to intermediate source in the lower to middle crust. Heat was supplied by cogenetic basaltic andesite. Compositional variability in the rhyolites may be attributed to source heterogeneity, fractionational crystallisation, volatile transfer (late-stage magmatic fluids) and thermogravitational diffusion. Rhyodacites appear to have a similar origin to the rhyolites, but possibly underwent some mixing with basic magma in addition.
 - The post-HFF Haisib Intrusive Suite (HIS) and Awasib Granite show close spatial and compositional associations with the volcanics, despite relative enrichment in K, Rb, LREE, Th, Zr, Nb, Ni and Cr at intermediate silica levels. ORG-normalised patterns for the calc-alkaline HIS show enrichments typical of volcanic arcs (e.g. Chile), while patterns for the slightly peralkaline Awasib Granite are typical of "crust-dominated" within-plate granites such as the Sabaloka Complex in Sudan. These changes reflect the increasing crustal and within-plate influences noted for the HFF. The A-type Awasib Granite yields an errorchron age of $957 \pm 50^*$ Ma and R_0 of $0.717 \pm 8^*$, both features being compatible with field relationships and the inferred crustal source. REE patterns do not, however, support a subvolcanic relationship between the HFF rhyolite and Awasib Granite.
 - Other late-stage intrusive units include the gabbroic to syenitic Saffier Intrusive Suite (SIS) and Bushman Hill Quartz Diorite (which are broadly contemporaneous with the HIS), and the young Chowachasib Granite Suite. Original igneous mineral phases are better preserved in those intrusive suites which are situated to the east of the HIS and Awasib Granite. Together, these late-stage granitoids show a change in composition from calc-alkaline to alkali-calcic, which is compatible

with an overall increase in arc maturity.

- When compared with the type area of the Sinclair Sequence, the late-stage AMT shows a higher degree of metamorphism and deformation. The development of the Sinclair Sequence took place in three major cycles, the late-stage AMT being accommodated largely within the second cycle. Radiometric dating, however, places the AMT development closer to “late” Sinclair times. Trachyandesite within the “Barby Formation” yielded a young isochron age of 844 ± 35 Ma and R_0 of 0.7064 ± 2 . This age resembles that of the post-Sinclair, early Pan-African, Gannakouriep dyke swarm.
- Evolution of the AMT crust is considered to have taken place in two major tectonomagmatic events. Formation of the early-stage crust started around 1460 Ma ago as a primitive arc (or back-arc) and ended as a relatively mature arc or active continental margin about 1270 Ma ago. Continental collision (coinciding with D_2 in the NMC) triggered renewed subduction with a different polarity. This oblique subduction initiated both compressional (“ice-floe”) and tensional (pull-apart) tectonics at an active continental margin before 1200 Ma (the preferred age of the Barby Formation). Alternation of compression and tension resulted in calc-alkaline mafic and felsic magmatism in the arc, while bimodal tholeiitic volcanism took place in a developing back-arc basin. Transcurrent movements resulted in slicing up and removal of part of the volcanic arc and accretionary complex, but extensional tectonics enabled the preservation of thick volcano-sedimentary successions which now constitute the Sinclair Sequence. The evolution of the late-stage crust of the AMT was terminated by granite plutonism at *ca.* 934 Ma. Post-tectonic dyke swarms utilised a conjugate fracture pattern which may be related to earlier dextral shearing.

5. CONCLUDING REMARKS

This study has dealt with a variety of volcano-sedimentary and intrusive lithologies in the AMT and has presented data on, and interpretation of, lithostratigraphic, mineralogical, whole-rock compositional and isotopic aspects. It has been shown that the early- and late-stage crust in the AMT can be correlated with the NMC and Sinclair Sequence, respectively, and that the crust has evolved continually from the middle to late Proterozoic.

The extended history (*ca.* 1.5–1.0 Ga) of subduction-related tectonomagmatic activity recorded by the AMT is important in the southern African context with regard to the development of the regionally extensive Namaqualand Metamorphic Complex and Sinclair Sequence. Thus correlation between the Kairab Complex, Garub Sequence and Areachap Group (South Africa) enables the reconstruction of an active continental margin at *ca.* 1.3 Ga that extends some 800 km along the eastern margin of the NMC and may demarcate the boundary between the latter and an older craton (possibly part of the Kaapvaal Craton). Continental collision is considered to have taken place between *ca.* 1.3 and 1.2 Ga in an event which is widely represented by deforma-

tion (D_2 episode?) and granitoid emplacement in the NMC.

Magmatism in the Sinclair Sequence was initiated at least as early as 1.2 Ga and is related to the initiation of subduction in response to continental collision. The oblique component and low angle of subduction enabled preservation of high-level volcano-sedimentary successions in both pull-apart and extensional basins. Correlation between the Sinclair Sequence and Koras Group (South Africa) suggests that this active margin may, like its predecessor at 1.3 Ga, extend over a considerable distance (about 770 km) in a northwest-trending direction. The HFF forms the most westerly outcrop of this subduction-related volcanism and reveals a history of deformation and metamorphism that pre-dates the Pan-African orogeny. The broadly synchronous tectonomagmatic activity in the Sinclair Sequence (including the AMT) and the adjacent Central Zone of the NMC may, in part, be related to activity at different crustal levels. Termination of subduction and crustal stabilisation appear to have taken place by *ca.* 0.9 Ga, not long before earliest Pan-African rifting.

Outstanding issues that have not been addressed in any detail by this study provide the following opportunities for future research:

(i) A detailed structural and lithostratigraphic study of the Excelsior-Hauchab Lineament and adjacent zones in order to fully assess the importance of this lineament as a major tectonostratigraphic terrane boundary between the Gonderia and Rehoboth subprovinces.

(ii) A petrological and geochronological study of the “basement” in the type area of the Sinclair Sequence to determine whether these underlying rocks are part of the NMC or an older craton (Kaapvaal Craton?).

(iii) Quantitative modelling of the petrogenesis of the Kairab Complex volcanic suite and associated intrusive rocks to provide a better understanding of the evolution of the early-stage crust of the AMT.

(iv) A comprehensive study (mapping, petrology and isotope chemistry) of the proposed ophiolite complex within the Kairab Complex.

(v) Geochronological and isotopic studies of undeformed and unmetamorphosed lithologies of the lower most Sinclair Sequence (Nagatis Formation and Naisib River Igneous Suite) in order to better constrain the Sinclair-NMC relationship and to determine the source characteristics of early-Sinclair magmatism.

(vi) A geochemical investigation of Sinclair Sequence outliers at Hauchab and Konipberg, since these occurrences may provide important information on volcanism in a fore-arc or along the volcanic front of an active continental margin.

(vii) A regional geochemical study of the bimodal dyke swarm in the AMT and Sinclair Sequence to determine whether this magmatism is part of late-Sinclair crustal consolidation or represents, instead, the earliest manifestation of Pan-African magmatism.

(viii) A lithostratigraphic, geochemical and geochronological compilation of data on Irumide-age rocks in the Rehoboth area with a view to establishing the significance of the so-called “Rehoboth Magmatic Arc”.

REFERENCES

- Adams, R.D. and Ware, D.E. (1977). Subcrustal earthquakes beneath New Zealand; locations determined with a laterally inhomogeneous velocity model. *New Zealand J. Geol. Geophys.*, **20**, 59-83.
- Ahrendt, H., Hunziker, J.C. and Weber, K. (1977). Age and degree of metamorphism and time of nappe emplacement along the southern margin of the Damara Orogen/Namibia (SW-Africa). *Geol. Rndschr.*, **67**, 719-742.
- Albat, H.-M. (1984). The Proterozoic granulite facies terrane around Kliprand, Namaquaian and Metamorphic Complex. *Bull. Precam. Res. Unit, Univ. Cape Town*, **33**, 382 pp.
- Anderson, D.L. (1982a). Isotopic evolution of the mantle: the role of magma mixing. *Earth Planet. Sci. Lett.*, **57**, 1-12.
- Anderson, D.L. (1982b). Isotopic evolution of the mantle: a model. *Earth Planet. Sci. Lett.*, **57**, 13-24.
- Anderson, M. (1983). Proterozoic anorogenic granite plutonism of North America, 133-154. In: Medaris, L.G., Byers, C.W., Mickelson, D.M. and Shanks, W.C. (Eds) *Proterozoic geology*. Geol. Soc. Am. Mem., **161**, 315 pp.
- Arculus, R.J. (1976). Geology and geochemistry of the alkali basalt-andesite association of Grenada, Lesser Antilles island arc. *Geol. Soc. Am. Bull.*, **87**, 612-624.
- Armstrong, R.L. (1981). Radiogenic isotopes: the case for crustal recycling on a near-steady-state no-continental-growth Earth. *Phil. Trans. R. Soc. Lond.*, **A301**, 443-472.
- Arth, J.G. (1976). Behaviour of trace elements during magmatic processes - a summary of theoretical models and their applications. *J. Res. U.S. Geol. Surv.*, **4**, 41-47.
- Bacon, C.R. and Duffield, W.A. (1981). Late Cenozoic rhyolites from the Kern Plateau, southern Sierra Nevada, California. *Am. J. Sci.*, **281**, 1-34.
- Bailey, J.C. (1981). Geochemical criteria for a refined tectonic discrimination of orogenic andesites. *Chem. Geol.*, **32**, 139-154.
- Bard, J.P. (1970). Composition of hornblendes formed during the Hercynian progressive metamorphism of the Aracena metamorphic belt (SW Spain). *Contrib. Mineral. Petrol.*, **28**, 117-134.
- Barker, D.S. (1987). Tertiary alkaline magmatism in Trans-Pecos Texas, 415-431. In: Fitton, J.G. and Upton, B.G.J. (Eds) *Alkaline Igneous Rocks*. Spec. Publ. geol. Soc. Lond., **30**, 568 pp.
- Barker, F. (1979). Trondhjemite: definition, environment and hypotheses of origin, 1-12. In: Barker, F. (Ed.) *Trondhjemites, dacites and related rocks*. Elsevier, Amsterdam, 659 pp.
- Barker, F. and Arth, J.G. (1976). Generation of trondhjemitic-tonalitic liquids and Archean bimodal trondhjemite-basalt suites. *Geology*, **4**, 596-600.
- Barton, E.S. and Burger, A.J. (1983). Reconnaissance isotopic investigations in the Namaqua mobile belt and implications for Proterozoic crustal evolution - Upington geotraverse, 173-191. In: Botha, B.J.V. (Ed.) *Namaqualand Metamorphic Complex*. Spec. Publ. geol. Soc. S. Afr., **10**, 198 pp.
- Bateman, P.C. (1983). A summary of critical relations in the central part of the Sierra Nevada batholith, California, U.S.A. *Geol. Soc. Am. Mem.*, **159**, 241-259.
- Bates, R.L. and Jackson, J.A. (1980). *Glossary of Geology*. 2nd Ed. American Geological Institute, Falls Church, 751 pp.
- Beetz, W. (1923). The Konkiep Formation on the borders of the Namib Desert north of Aus. *Trans. geol. Soc. S. Afr.*, **25**, 23-40.
- Beetz, W. (1924). On a great trough-valley in the Namib. *Trans. geol. Soc. S. Afr.*, **27**, 1-38.
- Beswick, A.E. and Soucie, G. (1978). A correction procedure for metasomatism in an Archaean greenstone belt. *Precam. Res.*, **6**, 235-248.
- Binns, R.A. (1965). The mineralogy of metamorphosed basic rocks from the Willyama Complex, Broken Hill District, New South Wales, Part 1. Hornblendes. *Mineralog. Mag.*, **35**, 306-326.
- Blignault, H.J., Jackson, M.P.A., Beukes, G.J. and Toogood, D.J. (1974). The Namaqua tectonic province in South West Africa, 15-29. In: Kröner, A. (Ed.) *Contributions to the Precambrian Geology of southern Africa*. Bull. Precam. Res. Unit, Univ. Cape Town, **15**, 213 pp.
- Bloomer, S.H. and Hawkins, J.W. (1987). Petrology and geochemistry of boninite series volcanic rocks from the Mariana trench. *Contrib. Mineral. Petrol.*, **97**, 361-377.
- Boardman, S.J. and Condie, K.C. (1986). Early Proterozoic bimodal volcanic rocks in central Colorado, U.S.A., Part II: geochemistry, petrogenesis and tectonic setting. *Precam. Res.*, **34**, 37-68.
- Boettcher, A.L., O'Neil, J.R., Windom, K.E., Stewart, D.C. and Wilshire, H.G. (1979). Metasomatism of the upper mantle and the genesis of kimberlites and alkali basalts, 173-182. In: Boyd, F.R. and Meyer, H.O.A. (Eds) *The Mantle Sample*. Proc. Second Int. Kimberlite Conf., Washington, **2**, 423 pp.
- Borg, G. (1988). The Koras-Sinclair-Ghanzi Rift in southern Africa. Volcanism, sedimentation, age relationships and geophysical signature of a late middle Proterozoic rift system. *Precam. Res.*, **38**, 75-90.
- Borg, J.Y. (1963). On conventional calculations of amphibole formulae from chemical analyses with inaccurate H₂O (+) and F determinations. *Mineralog. Mag.*, **36**, 583-590.
- Boyd, F.R. and Nixon, P.H. (1973). Origin of the ilmenite-silicate nodules in kimberlites from Lesotho and South Africa, 254-268. In: Nixon, P.H. (Ed) *Lesotho Kimberlites*. Lesotho Nat. Dev. Corp., Maseru, 350 pp.
- Braun, E. and Muller, G. (1975). Zur chemischen Variabilität regional-metamorph gebildeter Plagioklase, Epidote und Granate. *Contrib. Mineral. Petrol.*, **52**, 193-211.
- Brooks, C., Hart, S.R. and Wendt, I. (1972). Realistic use of two-error regression treatments applied to rubidium data. *Rev. Geophys. Space Phys.*, **10**, 551-577.
- Brophy, J.G. (1986). The Cold Bay Volcanic Center, Aleutian Volcanic Arc. I. Implications for the origin of Hi-Alumina Arc Basalt. *Contrib. Mineral. Petrol.*, **93**, 368-380.
- Brophy, J.G. (1987). The Cold Bay Volcanic Center, Aleutian Volcanic Arc. II. Implications for fractionation and mixing mechanism in calc-alkaline andesite genesis. *Contrib. Mineral. Petrol.*, **97**, 378-388.
- Brophy, J.G. and Marsh, B.D. (1986). On the origin of high-alumina arc basalt and the mechanics of melt extraction. *J. Petrol.*, **27**, 763-789.
- Brown, G.C. (1977). Mantle origin of Cordilleran granites. *Nature*, **265**, 21-24.
- Brown, G.C. (1982). Calc-alkaline intrusive rocks: their diversity, evolution, and relation to volcanic arcs, 437-461. In: Thorpe, R.S. (Ed.) *Andesites: Orogenic Andesites and Related Rocks*. Wiley, Chichester, 724 pp.
- Brown, G.C., Thorpe, R.S. and Webb, P.C. (1984). The geochemical characteristics of granitoids in contrasting arcs and comments on magma sources. *J. geol. Soc. Lond.*, **141**, 413-426.
- Brown, G.J. and Wilson, A.H. (1986). The petrology and geochemistry of the Barby Formation, Sinclair Sequence. *Communs. geol. Surv. S.W. Africa/Namibia*, **2**, 93-108.
- Brown, G.M., Holland, J.G., Sigurdsson, H., Tomblin, J.F. and Arculus,

- R.J. (1977). Geochemistry of the Lesser Antilles volcanic island arc. *Geochim. Cosmochim. Acta*, **41**, 785-801.
- Brunn, J.H. (1983). Oceans, continents and orogens. *Tectonophysics*, **99**, 1-29.
- Bryan, W.B., Finger, L.W. and Chayes, F. (1969). Estimating proportions in petrographic mixing equations by least-squares approximation. *Science*, **163**, 926-927.
- Burke, K.C.A and Kidd, W.S.F (1980). Volcanism on Earth through time, 503-522. In: Strangway, D.W. (Ed.) *The Continental Crust and Its Mineral Deposits*. Spec. Pap. Geol. Assoc. Canada, **28**, 804 pp.
- Cahen, L. and Snelling N.J. (1984). *The Geochronology and Evolution of Africa*. Clarendon Press, Oxford, 512 pp.
- Cameron, M. and Papike, J.J. (1980). Crystal chemistry of silicate pyroxenes, 5-92. In: Prewitt, C.T. (Ed.) *Pyroxenes*. Mineralog. Soc. Am., Reviews in Mineralogy, **7**, 525 pp.
- Cameron, W.E., Nisbet, E.G. and Dietrich, V.J. (1979). Boninites, komatiites and ophiolitic basalts. *Nature*, **280**, 550-553.
- Cann, J.R. (1970). Upward movement of granitic magma. *Geol. Mag.*, **107**, 335-340.
- Carmichael, I.S.E. (1964). The petrology of Thingmuli, a Tertiary volcano in eastern Iceland. *J. Petrol.*, **5**, 435-460.
- Chappel, B.W. and White, A.J.R. (1974). Two contrasting granite types. *Pacific Geology*, **8**, 173-174.
- Chase, C.G. (1981). Oceanic island Pb: two-stage histories and mantle evolution. *Earth Planet. Sci. Lett.*, **52**, 277-284.
- Chayes, F. (1964). A petrographic distinction between Cenozoic volcanics in and around the open oceans. *J. Geophys. Res.*, **69**, 1573-1588.
- Clemens, J.D. and Vielzeuf, D. (1987). Constraints on melting and magma production in the crust. *Earth Planet. Sci. Lett.*, **86**, 287-306.
- Clifford, T.N., Stumpfl, E.F., Burger, A.J., McCarthy, T.S. and Rex, D.C. (1981). Mineral chemical and isotopic studies of Namaqualand granulites, South Africa: a Grenville analogue. *Contrib. Mineral. Petrol.*, **77**, 225-250.
- Cohen, R.S. and O'Nions, R.K. (1982). Identification of recycled continental material in the mantle from Sr, Nd, and Pb isotope investigations. *Earth Planet. Sci. Lett.*, **61**, 73-84.
- Coleman, R.G. (1977). *Ophiolites: Ancient Oceanic Lithosphere?* Springer-Verlag Berlin, 229 pp.
- Collins, W.J., Beams, S.D., White, A.J.R and Chappell, B.W. (1982). Nature and origin of A-type granites with particular reference to southeastern Australia. *Contrib. Mineral. Petrol.*, **80**, 189-200.
- Compston, W. and Chappell, B.W. (1979). Strontium isotopic evolution of granitoid source rocks, 377-424. In: McElhinney, M.W. (Ed.) *The Earth: Its Origin, Structure and Evolution*. Academic Press, London, 597 pp.
- Condie, K.C. (1973). Archean magmatism and crustal thickening. *Geol. Soc. Am. Bull.*, **84**, 2981-2992.
- Condie, K.C. (1986). Geochemistry and tectonic setting of early Proterozoic supracrustal rocks in the southwestern United States. *J. Geol.*, **94**, 845-864.
- Condie, K.C. (1987). Early Proterozoic volcanic regimes in southwestern North America, 211-218. In: Pharaoh, T., Beckinsale, R.D. and Rickard, D. (Eds) *Geochemistry and Mineralization of Proterozoic Volcanic Suites*. Spec. Publ. geol. Soc. Lond., **33**, 575 pp.
- Consolidated Diamond Mines (CDM) Mineral Surveys (1981). Airborne magnetic and radiometric survey - Sinclair Block, Namibia. *Geol. Surv. S.W. Africa/Namibia Open File Rep.* CDM 81/1.
- Cooper, A.F. (1972). Progressive metamorphism of metabasic rocks from the Haast Schist Group of southern New Zealand. *J. Petrol.*, **13**, 457-492.
- Cornell, D.H., Hawkesworth, C.J., Van Calsteren, P. and Scott, W.D. (1986). Sm-Nd study of Precambrian crustal development in the Prieska-Copperton region, Cape Province. *Trans. geol. Soc. S. Afr.*, **89**, 17-28.
- Coulon, C. and Thorpe, R.S. (1981). Role of continental crust in petrogenesis of orogenic volcanic associations. *Tectonophysics*, **77**, 79-93.
- Cox, K.G. (1983). The Karoo Province of southern Africa: Origin of trace element enrichment patterns, 139-157. In: Hawkesworth, C.J. and Norry, M.J. (Eds) *Continental Basalts and Mantle Xenoliths*. Shiva, Nantwich, 272 pp.
- Cox, K.G. and Bell, J.D. (1972). A crystal fractionation model for basaltic rocks of the New Georgia Group, British Solomon Islands. *Contrib. Mineral. Petrol.*, **37**, 1-13.
- Cox, K.G., Bell, J.D. and Pankhurst, R.J. (1979). *The Interpretation of Igneous Rocks*. George Allen and Unwin, London, 450 pp.
- Cox, K.G., Duncan, A.R., Bristow, J.W., Taylor, S.R. and Erlank, A.J. (1984). Petrogenesis of the basic rocks of the Lebombo, 149-169. In: Erlank, A.J. (Ed.) *Petrogenesis of the Volcanic Rocks of the Karoo Province*. Spec. Publ. geol. Soc. S. Afr., **13**, 396 pp.
- Crawford, A. and Keays, R.R. (1978). Cambrian greenstone belt in Victoria: marginal sea-crust slices in the Lachlan Fold Belt of southern Australia. *Earth Planet. Sci. Lett.*, **41**, 197-208.
- Cullers, R.L. and Graf, M. (1984). Rare earth elements in igneous rocks of the continental crust: intermediate and silicic rocks - ore petrogenesis, 275-316. In: P. Henderson (Ed.) *Rare Earth Element Geochemistry*. Developments in geochemistry, **2**. Elsevier, Amsterdam, 510 pp.
- Davies, R.D. and Allsopp, H.L. (1976). Strontium isotopic evidence relating to the evolution of the lower Precambrian granitic crust in Swaziland. *Geology*, **4**, 553-556.
- Davis, A., Blackburn, W.H., Brown, W.R. and Ehmann, W.D. (1978). *Trace element geochemistry and origin of late Precambrian - early Cambrian Catocin greenstones of the Appalachian Mountains*. Rep. (unpubl.), Univ. of California, Davies, California.
- De Albuquerque, C.A.R. (1973). Geochemistry of biotites from granitic rocks, northern Portugal. *Geochim. Cosmochim. Acta*, **37**, 1779-1802.
- De Beer, J.H. and Meyer, R. (1984). Geophysical characteristics of the Namaqua-Natal belt and its boundaries, South Africa. *J. Geodynamics*, **1**, 473-494.
- Deer, W.A., Howie, R.A. and Zussman, J. (1966). *An Introduction to the Rock-forming Minerals*. Longman London, 528 pp.
- De Paolo, D.J. (1981). Trace element and isotopic effects of combined wallrock assimilation and fractional crystallization. *Earth Planet. Sci. Lett.*, **53**, 189-202.
- Dewey, J.F. (1980). Episodicity, sequence, and style at convergent plate boundaries, 553-573. In: Strangway, D.W. (Ed.) *The Continental Crust and Its Mineral Deposits*. Spec. Pap. Geol. Assoc. Canada, **20**, 804 pp.
- De Wit, M., Jeffery, M., Bergh, H. and Nicolaysen, L. (1988). *Geological map of sectors of Gondwana reconstructed to their disposition ~ 150 Ma. Scale 1:10 000 000 Lambert equal area projection centred at 20°S, 40°E*. Bernard Price Inst. Geophys. Res., Univ. Witwatersrand, and Am. Ass. Petrol. Geol.
- Dimroth, E. (1985). A mass balance between Archean and Phanerozoic rates of magma emplacement, crustal growth and erosion: implications for recycling of the continental crust. *Chem. Geol.*, **53**, 17-24.
- Dodge, F.C.W., Papike, J.J. and Mays, R.E. (1968). Hornblendes from granitic rocks of the central Sierra Nevada batholith. California. *J. Petrol.*, **9**, 378-410.
- Dostal, J., Dupuy, C. and Venturelli, G. (1982). Geochemistry of volcanic rocks from the Monte Arci (west Sardinia, Italy). *Chem. Geol.*, **35**, 247-264.

- Drake, M.J. and Weill, D.F. (1975). Partition of Sr, Ba, Ca, Y, Eu²⁺, Eu³⁺, and other REE between plagioclase feldspar and magmatic liquid: an experimental study. *Geochim. Cosmochim. Acta*, **39**, 689-712.
- Duncan, A.R. (1987). The Karoo igneous province - a problem area for inferring tectonic setting from basalt geochemistry, 13-34. In: Weaver, S.D. and Johnson, R.W. (Eds) *Tectonic Controls on Magma Chemistry*. J. Volcanol. Geotherm. Res., **32**, 285 pp.
- Duncan, A.R., Erlank, A.J. and Betton, P.S. (1984). Appendix I: analytical techniques and database descriptions, 389-395. In: Erlank, A.J. (Ed.) *Petrogenesis of the Volcanic Rocks of the Karoo Province*. Spec. Publ. geol. Soc. S. Afr., **13**, 396 pp.
- Dupuy, C., Dostal, J., Capredri, S. and Lefevre, C. (1976). Petrogenetic implications of uranium abundances in volcanic rocks from southern Peru. *Bull. Volcanol.*, **39**, 363-370.
- Eglinton, B.M., Harmer, R.E. and Kerr, A. (1986). Petrographic, Rb-Sr isotope and geochemical characteristics of intrusive granitoids from the Port Edward - Port Shepstone area, Natal. *Trans. geol. Soc. S. Afr.*, **89**, 199-213.
- Engel, A.E.J. and Engel, C.G. (1960). Progressive metamorphism and granitization of the major paragneiss, Northwest Adirondacks Mountains, New York. Part II: Mineralogy. *Geol. Soc. Am. Bull.*, **71**, 1-58.
- Engel, A.E.J. and Engel, C.G. (1962). Hornblendes formed during progressive metamorphism of amphibolites, northwest Adirondack Mountains, New York. *Geol. Soc. Am. Bull.*, **73**, 1499-1514.
- Erlank, A.J., Allsopp, H.L., Duncan, A.R. and Bristow, J.W. (1980). Mantle heterogeneity beneath southern Africa: evidence from the volcanic record. *Phil. Trans. R. Soc. Lond.*, **297**, 295-307.
- Erlank, A.J., Waters, F.G., Hawkesworth, C.J., Haggerty, S.E., Allsopp, H.L., Rickard, R.S. and Menzies, M.A. (1987). Evidence for mantle metasomatism in peridotite nodules from the Kimberley pipes, South Africa, 211-311. In: Menzies, M.A. and Hawkesworth, C.J. (Eds) *Mantle Metasomatism*. Academic Press, London, 472 pp.
- Ewart, A. (1976). Mineralogy and chemistry of modern orogenic lavas - some statistics and implications. *Earth Planet. Sci. Lett.*, **31**, 417-432.
- Ewart, A. (1979). A review of the mineralogy and chemistry of Tertiary-Recent dacitic, rhyolitic, and related salic volcanic rocks, 13-121. In: Barker, F. (Ed.) *Trondhjemites, Dacites and Related Rocks*. Elsevier, Amsterdam, 659 pp.
- Ewart, A. (1982). The mineralogy and petrology of Tertiary-Recent orogenic volcanic rocks: with special reference to the andesitic-basaltic compositional range, 25-95. In: Thorpe, R.S. (Ed) *Andesites: Orogenic Andesites and Related Rocks*. John Wiley & Sons, Chichester, 724 pp.
- Fisher, R.V. and Schmincke, H.-U. (1984). *Pyroclastic Rocks*. Springer-Verlag, Berlin, 472 pp.
- Floyd, P.A. (1976). Geochemical variation in the greenstones of S.W. England. *J. Petrol.*, **17**, 522-545.
- Floyd, P.A. and Winchester, J.A. (1975). Magma type and tectonic setting discrimination using immobile elements. *Earth Planet. Sci. Lett.*, **27**, 211-218.
- Fowler, A.D. and Doig, R. (1983). The significance of europium anomalies in the REE spectra of granites and pegmatites, Mont Laurier, Quebec. *Geochim. Cosmochim. Acta*, **47**, 1131-1137.
- Frey, F.A. (1969). Rare earth abundances in a high-temperature peridotite intrusion. *Geochim. Cosmochim. Acta*, **33**, 1429-1447.
- Frey, F.A. and Green, D.H. (1974). The mineralogy, geochemistry and origin of olivine inclusions in Victorian basanites. *Geochim. Cosmochim. Acta*, **38**, 1023-1059.
- Frey, F.A., Green, D.H. and Roy, S.D. (1978). Integrated models of basalt petrogenesis: a study of quartz tholeiites to olivine melilitites from southeastern Australia utilizing geochemical and experimental petrological data. *J. Petrol.*, **19**, 463-513.
- Garrison, J.R., Jr. (1978). Plagioclase compositions from metabasalts, southeastern Llano uplift: plagioclase unmixing during amphibolite-grade metamorphism. *Am. Miner.*, **63**, 143-149.
- Gass, I.G. (1977). The evolution of the Pan-African crystalline basement in N.E. Africa and Arabia. *J. geol. Soc. Lond.*, **134**, 129-138.
- Gast, P.W. (1968). Trace element fractionation and the origin of tholeiitic and alkaline magma types. *Geochim. Cosmochim. Acta.*, **33**, 1057-1086.
- Geological map of South West Africa/Namibia (1980). Scale 1: 1 000 000. *Geol. Surv. S. Afr.*
- Geringer, G.J., Botha, B.J.V., Pretorius, U. and Ludick, D.J. (1986). Calc-alkaline volcanism along the eastern margin of the Namaqua mobile belt, South Africa - a possible middle Proterozoic volcanic arc. *Precam. Res.*, **33**, 139-170.
- Gill, J.B. (1970). Geochemistry of Viti Levu, Fiji, and its evolution as an island arc. *Contrib. Mineral. Petrol.*, **27**, 179-203.
- Gill, J.B. (1981). *Orogenic Andesites and Plate Tectonics*. Springer-Verlag, Berlin, 390 pp.
- Gill, J.B. (1982). Mountain building and volcanism, 13-17. In: Hsu, K.J. (Ed.) *Mountain Building Processes*. Academic Press, London, 263 pp.
- Gill, R.C.O. (1979). Comparative petrogenesis of Archaean and modern low K tholeiites. A critical review of some geochemical aspects, 431-447. In: Ahrens, L.H. (Ed.) *Origin and Distribution of the Elements*. Proc. second Symp. Paris - UNESCO, May 1977. Pergamon Press, Oxford, 909 pp.
- Goldsmith, J.R. (1982). Review of the behaviour of plagioclase under metamorphic conditions. *Am. Miner.*, **67**, 643-652.
- Gorton, M. (1977). The geochemistry and origin of Quaternary volcanism in the New Hebrides. *Geochim. Cosmochim. Acta*, **41**, 1257-1270.
- Grapes, R.H. (1975). Actinolite-hornblende pairs in metamorphosed gabbros, Hidaka Mountains, Hokkaido. *Contrib. Mineral. Petrol.*, **49**, 125-140.
- Grapes, R.H. and Graham, C.M. (1978). The actinolite-hornblende series in metabasites and the so-called miscibility gap: a review. *Lithos*, **11**, 85-97.
- Grapes, R.H., Hashimoto, S. and Miyashita, S. (1977). Amphiboles of a metagabbro-amphibolite sequence, Hidaka Metamorphic Belt, Hokkaido. *J. Petrol.*, **18**, 285-318.
- Greenman, L. (1966). *The geology of Area 2515C Lüderitz, South West Africa*. M.Sc. thesis (unpubl.), Univ. CapeTown, 105 pp.
- Grove, T.L. (1977). Structural characterization of labradorite-bytownite plagioclase from volcanic, plutonic and metamorphic environments. *Contrib. Mineral. Petrol.*, **64**, 273-302.
- Grove, T.L. and Donnelly-Nolan, J.M. (1986). The evolution of young silicic lavas at Medicine Lake volcano, California: implications for the origin of compositional gaps in calc-alkaline series lavas. *Contrib. Mineral. Petrol.*, **92**, 281-302.
- Guidotti, C.V. (1984). Micas in metamorphic rocks, 357-467. In: Bailey, S.W. (Ed.) *Micas*. Mineralog. Soc. Am., Reviews in Mineralogy, **13**, 584 pp.
- Gunn, B.M. (1974). Systematic petrochemical difference in andesite suites. *Bull. Volcanol.*, **38**, 481-489.
- Gust, D.A. and Perfit, M.R. (1987). Phase relations of a high-Mg basalt from the Aleutian Island Arc: implications for primary island arc basalts and high-Al basalts. *Contrib. Mineral. Petrol.*, **97**, 7-18.
- Hamilton, W.B. (1988). Plate tectonics and island arcs. *Geol. Soc. Am. Bull.*, **100**, 1503-1527.

- Hanson, G.N. (1978). The application of trace elements to the petrogenesis of igneous rocks of granitic composition. *Earth Planet. Sci. Lett.*, **38**, 26-43.
- Harmer, R.E. (1985). Rb-Sr isotopic study of units of the Pienaars River Alkaline Complex, north of Pretoria, South Africa. *Trans. geol. Soc. S. Afr.*, **88**, 207-214.
- Harmer, R.E. and Sharpe, M.R. (1985). Field relations and strontium isotope systematics of the marginal rocks of the Eastern Bushveld Complex. *Econ. Geol.*, **80**, 813-837.
- Harris, N.B.W., Hawkesworth, C.J., Van Clasteren, P., McDermott, F. (1987). Evolution of continental crust in southern Africa. *Earth Planet. Sci. Lett.*, **83**, 85-93.
- Harrison, P.A. (1979). *The structure and sedimentology of the Sinclair Group in the Awasi Mountains, Diamond Area No. 2, South West Africa/Namibia*. B.Sc. (Hons.) thesis (unpubl.), Rhodes University, Grahamstown, 69 pp.
- Hartnady, C., Joubert, P. and Stowe, C. (1985). Proterozoic crustal evolution in southwestern Africa. *Episodes*, **8**, 236-244.
- Hawkesworth, C.J., Rogers, N.W., Van Calsteren, P.W.C. and Menzies, M.A. (1984). Mantle enrichment processes. *Nature*, **311**, 331-335.
- Hawthorne, F.C. (1981). Crystal chemistry of the amphiboles, 1-102. In: Veblen, D.R. (Ed.) *Amphiboles and other hydrous pyriboles - mineralogy*. Mineralog. Soc. Am., Reviews in Mineralogy, **9A**, 372 pp.
- Hay, R.L., Hildreth, W. and Lambe, R.N. (1979). Globule ignimbrite of Mount Suswa, Kenya, 167-175. In: Chapin, C.E. and Elston, W.E. (Eds) *Ashflow tuffs*. Geol. Soc. Am. Spec. Pap., **180**.
- Henderson, P. (1984). General geochemical properties and abundances of the rare earth elements, 1-32. In: Henderson, P. (Ed.) *Rare Earth Element Geochemistry*. Developments in Geochemistry, **2**. Elsevier, Amsterdam. 510 pp.
- Hey, M.H. (1954). A new review of the chlorites. *Mineralog. Mag.*, **30**, 277-292.
- Hickey, R.L. and Frey, F.A. (1982). Geochemical characteristics of boninite series volcanics: implications for their source. *Geochim. Cosmochim. Acta*, **46**, 2099-2115.
- Hietanen, A. (1974). Amphibole pairs, epidote minerals, chlorite and plagioclase in metamorphic rocks, Northern Sierra Nevada, California. *Am. Miner.*, **59**, 22-40.
- Hildebrand, R.S. and Bowring, S.A. (1984). Continental intra-arc depressions, a non extensional model for their origin, with a Proterozoic example from Wopmay orogen. *Geology*, **12**, 73-77.
- Hildreth, W. (1981). Gradients in silicic magma chambers: implications for lithospheric magmatism. *J. Geophys. Res.*, **86**, 10153-10192.
- Hoal, B.G. (1985). Preliminary report on the geology of the south-eastern part of Diamond Area No.2, South West Africa/Namibia. *Communs geol. Surv. S. W. Africa/Namibia*, **1**, 9-21.
- Hoal, B.G. (1987). Terrane significance of the boundary between the Rehoboth and Gordonia subprovinces in southern Namibia, 42-45. In: Hartnady, C.J.H. (Ed.) *Proceedings and Abstracts of the Alex L. du Toit Golden Jubilee Conference on Tectonostratigraphic Terrane Analysis*. Precam. Res. Unit., Univ. Cape Town, 69 pp.
- Hoal, B.G. (1989a). *Proterozoic crustal evolution of the Awasi Mountain terrain, southern Namibia, with special reference to the volcanic Haiber Flats Formation*. Ph.D. thesis (unpubl.), Univ. Cape Town, 257 pp.
- Hoal, B.G. (1989b). The geological history of the Awasi Mountain terrain and its relationship to the Sinclair Sequence and Namaqualand Metamorphic Complex. *Communs geol. Surv. Namibia*, **5**, 41-51.
- Hoal, B.G., Harmer, R.E. and Eglington, B.M. (1986). Rb-Sr geochronology of the Middle to Late Proterozoic Awasi Mountain terrane. *Communs geol. Surv. S.W. Africa/Namibia*, **2**, 53-59.
- Hoal, B.G., Harmer, R.E. and Eglington, B.M. (1989). Isotopic evolution of the Middle to Late Proterozoic Awasi Mountain terrain in southern Namibia. *Precam. Res.*, **45**, 175-189.
- Hoffmann, K.H. (1989). New aspects of lithostratigraphic subdivision and correlation of late Proterozoic to early Cambrian rocks of the southern Damara Belt and their correlation with the central and northern Damara Belt and the Gariep Belt. *Communs geol. Surv. Namibia*, **5**, 59-67.
- Holdaway, M.J. (1965). Basic regional metamorphic rocks in part of the Klamath Mountains, northern California. *Am. Miner.*, **50**, 953-977.
- Humphris, S.E. (1984). The mobility of the rare earth elements in the crust, 317-373. In: Henderson, P. (Ed.) *Rare Earth Element Geochemistry*. Developments in Geochemistry, **2**. Elsevier Amsterdam, 510 pp.
- Hurst, R.W. (1982). Petrogenesis of the Conejo volcanic suite, southern California: evidence for mid-ocean ridge - continental margin interactions. *Geology*, **10**, 267-272.
- Hyndman, D.W. (1972). *Petrology of igneous and metamorphic rocks*. McGraw-Hill, San Francisco, 533 pp.
- Hynes, A. (1982). A comparison of amphiboles from medium- and low-pressure metabasites. *Contrib. Mineral. Petrol.* **81**, 119-125.
- Hynes, A. (1987). Back-arc spreading in the Proterozoic - a theoretical approach. *Precam. Res.*, **36**, 189-199.
- Innocenti, F., Manetti, P., Peccerillo, A. and Poli, G. (1981). South Aegean volcanic arc: geochemical variations and geotectonic implications. *Bull. Volcanol.*, **44**, 377-391.
- Irvine, T.N. and Baragar, W.R.A. (1971). A guide to the chemical classification of the common volcanic rocks. *Can. J. Earth Sci.*, **8**, 523-548.
- Jackson, M.P.A. (1975). Field relations between key lithological units of the Namaqualand Metamorphic Complex and the Naisib River Complex in the eastern Lüderitz district. *12th Ann. Rep. Precam. Res. Unit, Univ. Cape Town*, 33-40.
- Jackson, M.P.A. (1976). High-grade metamorphism and migmatization of the Namaqua Metamorphic Complex around Aus in the southern Namib Desert, South West Africa. *Bull. Precam. Res. Unit, Univ. Cape Town*, **18**, 299 pp.
- Jacobs, J.W., Korotev, R.L., Blanchard, D.P. and Haskin, L.A. (1977). A well tested procedure for instrumental neutron activation analysis of silicate rocks and minerals. *J. Radioanal. Chem.*, **40**, 93-114.
- Jakeš, P. and Gill, J. (1970). Rare earth elements and the island arc tholeiite series. *Earth Planet. Sci. Lett.*, **9**, 17-28.
- Jakeš, P. and Smith, I.E.M. (1970). High potassium calc-alkaline rocks from Cape Nelson, Eastern Papua. *Contrib. Mineral. Petrol.*, **28**, 259-271.
- Jakeš, P. and White, A.J.R. (1972). Major and trace element abundances in volcanic rocks of orogenic areas. *Geol. Soc. Am. Bull.*, **83**, 29-40.
- Jamieson, R.A. (1981). Metamorphism during ophiolite emplacement - the petrology of the St Anthony complex. *J. Petrol.*, **22**, 397-449.
- Jarrard, R.D. (1986). Terrane motion by strike-slip faulting of forearc slivers. *Geology*, **14**, 780-783.
- Jenner, G.A. (1981). Geochemistry of high-Mg andesites from Cape Vogel, Papua New Guinea. *Chem. Geol.*, **33**, 307-332.
- Jolly, W.T. (1972). Degradation (hydration) - aggradation (dehydration) and low-rank metamorphism of mafic volcanic sequences. *24th Int. Geol. Congress*, **2**, 11-18.
- Jolly, W.T. (1987). Geology and geochemistry of Huronian rhyolites and low- Ti continental tholeiites from the Thessalon region, central Ontario. *Can. J. Earth Sci.*, **24**, 1360-1385.

- Joubert, P. (1981). The Namaqualand Metamorphic Complex, 671-705. In: Hunter, D.R. (Ed.) *Precambrian of the Southern Hemisphere*. Developments in Precambrian Geology, 2. Elsevier, Amsterdam, 882 pp.
- Juteau, M., Michard, A., Zimmerman, J. and Albaredé, F. (1984). Isotopic heterogeneities in the granitic intrusion of Monte Capanne (Elba Island, Italy) and dating concepts. *J. Petrol.*, **25**, 532-545.
- Kaiser, E. (1926). *Die Diamantenwüste Südwestafrikas. Mit Beiträgen von W. Beetz, J. Bohm, R. Martin, R. Raujff, M. Storz, E. Stromer, W. Weissermel und K. Willman*. 2 vol. Dietrich Reimer, Berlin.
- Karig, D.E. and Moore, G.F. (1975). Tectonically controlled sedimentation in marginal basins. *Earth Planet. Sci. Lett.*, **26**, 233-238.
- Katz, M.B. (1981). A shear-mobile transform belt in the Precambrian Gondwanaland of Africa - South America. *Geol. Rundsch.*, **70**, 1012-1019.
- Key, R.M. and Rundle, C.C. (1981). The regional significance of new isotopic ages from Precambrian windows through the "Kalahari Beds" in north-western Botswana. *Trans. geol. Soc. S. Afr.*, **84**, 51-66.
- Kleeman, A.W. (1965). The origin of granitic magmas. *J. geol. Soc. Aust.*, **12**, 35-52.
- Kleywegt, R.J. (1967). *The gravity survey of South West Africa*. Ph.D. thesis (unpubl.), Univ. Natal, Pietermaritzburg, 98 pp.
- Kouchi, A. and Sunagawa, I. (1985). A model for mixing basaltic and dacitic magmas as deduced from experimental data. *Contrib. Mineral. Petrol.*, **89**, 17-23.
- Kröner, A. (1975). Geochronology. *13th a. Rep. Precam. Res. Unit, Univ. Cape Town*, 139-143.
- Kröner, A. (1977). The Sinclair aulacogen - a late Proterozoic volcano-sedimentary association along the Namib Desert of southern Namibia (SWA). *Abstr. 9th Colloquium Afr. Geol.*, Göttingen, 82-83.
- Kröner, A. (1981). Precambrian crustal evolution and continental drift. *Geol. Rundsch.*, **70**, 412-428.
- Kröner, A. and Jackson, M.P.A. (1974). Geological reconnaissance of the coast between Lüderitz and Marble Point, South West Africa, 79-97. In: Kröner, A. (Ed.) *Contributions to the Precambrian Geology of southern Africa*. Bull. Precam. Res., Univ. Cape Town, 15,213 pp.
- Kröner, A., Vajner, V. and Burger, A.J. (1977). Geotectonic significance of radiometric age data from the late Proterozoic Koras Group, northern Cape Province, South Africa. *Abstr. 9th Colloquium Afr. Geol.*, Göttingen, 80-81.
- Kuno, H. (1960). High-alumina basalt. *J. Petrol.*, **1**, 121-145.
- Kuno, H. (1968). Differentiation of basalt magmas, 623-688. In: Hess, H.H. and Poldervaart, J. (Eds) *Basalts*. Interscience, New York, **2**, 380 pp.
- Kushiro, I. (1960). Si-Al relation in clinopyroxene from igneous rocks. *Am. J. Sci.*, **258**, 548-554.
- Kushiro, I. (1975). On the nature of silicate melt and its significance in magma genesis: regularities in the shift of the liquidus boundaries involving olivine, pyroxene, and silica minerals. *Am. J. Sci.*, **275**, 411-431.
- Laird, J. (1982). Amphiboles in metamorphosed basaltic rocks: greenschist facies to amphibolite facies, 113-137. In: Veblen, D.R. and Ribbe, P.H. (Eds) *Amphiboles: petrology and experimental phase relations*. Mineralog. Soc. Am., Reviews in Mineralogy, **98**, 390 pp.
- Langmuir, C.H., Vocke, R.D., Jr., Hanson, G.N. and Hart, S.R. (1978). A general mixing equation with applications to Icelandic basalts. *Earth Planet. Sci. Lett.*, **37**, 380-392.
- Leake, B.E. (1965). The relationship between composition of calciferous amphibole and grade of metamorphism, 299-317. In: Pitcher, W.S. and Flinn, G.W. (Eds) *Controls of Metamorphism*. Oliver and Boyd, Edinburgh, 368 pp.
- Leake, B.E. (1968). A catalog of analysed calciferous and subcalciferous amphiboles together with their nomenclature and associated minerals. *Spec. Pap. geol. Soc. Am.*, **98**, 210 pp.
- Le Bas, M.J. (1962). The role of aluminium in igneous rocks. *Am. J. Sci.*, **260**, 267-288.
- Le Bas, M.J., Le Maitre, R.W., Streckeisen, A. and Zanettin, B. (1986). A chemical classification of volcanic rocks based on the total alkali-silica diagram. *J. Petrol.*, **27**, 745-750.
- Le Maitre, R.W. (1976). Some problems of the projection of chemical data into mineralogical classifications. *Contrib. Mineral. Petrol.*, **56**, 181-189.
- Le Maitre, R.W. (1981). GENMIX - a generalized petrological mixing model program. *Computers and Geosciences*, **7**, 229-247.
- Le Maitre, R.W. (1984). A proposal by the IUGS Subcommittee on the Systematics of Igneous Rocks for a chemical classification of volcanic rocks based on the total alkali silica (TAS) diagram. *Austral. J. Earth Sci.*, **31**, 243-255.
- Le Pichon, X. and Angeier, J. (1979). The Hellenic arc and trench system: a key to the Neotectonic evolution of the Eastern Mediterranean area. *Tectonophys.*, **60**, 1-42.
- Le Roex, A.P. (1980). *Geochemistry and mineralogy of selected Atlantic Ocean basalts*. Ph.D. thesis (unpubl.). Univ. Cape Town, 281 pp.
- Leterrier, J., Maury, R.C., Thonon, P., Girard, D. and Marchal, M. (1982). Clinopyroxene composition as a method of identification of the magmatic affinities of paleo-volcanic series. *Earth Planet. Sci. Lett.*, **59**, 139-154.
- Levi, B. and Aguirre, L. (1981). Ensilic spreading-subsidence in the Mesozoic and Paleogene of central Chile. *J. geol. Soc. Lond.*, **138**, 76-81.
- Liégeois, J.P. and Black, R. (1987). Alkaline magmatism subsequent to collision in the Pan-African belt of the Adrar des Iforas (Mali), 381-401. In: Fitton, F.G. and Upton, B.G.J. (Eds) *Alkaline Igneous Rocks*. Spec. Publ. geol. Soc. Lond., **30**, 568 pp.
- Lindsley, D.H. (1983). Pyroxene thermometry. *Am. Miner.*, **68**, 477-493.
- Lindstrom, D.J. and Korotev, R.L. (1982). TEABAGS: Computer programs for Instrumental Neutron Activation analysis. *J. Radioanal. Chem.*, **70**, 439-458.
- Liou, J.G. (1973). Synthesis and stability relations of epidote, $\text{Ca}_2\text{Al}_2\text{FeSi}_3\text{O}_{12}(\text{OH})$. *J. Petrol.*, **14**, 381-413.
- Lipman, P.W., Doe, B.R., Hedge, C.E. and Stevens, T.A. (1978). Petrologic evolution of the San Juan volcanic field, southwestern Colorado: Pb and Sr isotopic evidence. *Geol. Soc. Am. Bull.*, **89**, 59-82.
- Litherland, M., Klinck, B.A., O'Connor, E.A. and Pitfield, P.E.J. (1985). Andean-trending mobile belts in the Brazilian Shield. *Nature*, **314**, 345-348.
- Loiselle, M.C. and Wones, D.R. (1979). Characteristics and origin of anorogenic granites. *Geol. Soc. Am. Abstr. Progr.*, **11**, 468.
- Lopez-Escobar, L., Frey, F.A. and Vergara, M. (1976). Andesites from central-south Chile: trace-element abundances and petrogenesis, 725-761. In: *Proc. Symp. Andean Antarct. Volcanol. Probl.*, IAV-CEI.
- Ludwig, K.R. (1980). Calculation of uncertainties of U-Pb isotope data. *Earth Planet. Sci. Lett.*, **46**, 212-220.
- MacGregor, I.D. (1979). Mafic and ultramafic xenoliths from the Kao kimberlite pipe, 156-172. In: Boyd, F.R. and Meyer, H.O.A. (Eds) *Proc. Second Int. Kimberlite Conf., Washington*, **2**, 423 pp.
- MacLean, W.H., St. Seymour, K. and Prabhu, M.K. (1982). Sr, Y, Zr, Nb, Ti, and REE in Grenville amphibolites at Montauban-Ils-Mines, Quebec. *Can. J. Earth Sci.*, **19**, 633-644.
- Martin, H. (1965). *The Precambrian Geology of South West Africa and*

- Namaqualand*. Precam. Res. Unit., Univ. Cape Town, 159 pp.
- Martin, R.F. and Bonin, B. (1976). Water and magma genesis: the association hypersolvus granite - subsolvus granite. *Can. Miner.*, **14**, 228-237.
- Maruyama, S., Suzuki, K. and Liou, J.G. (1983). Greenschist-amphibolite transition equilibria at low pressures. *J. Petrol.*, **24**, 583-604.
- Mason, B. (1966). *Principles of Geochemistry*. 3rd edition. Wiley, New York. 329 pp.
- Mason, R. (1981). The Damara Mobile Belt in South West Africa/Namibia, 754-802. In: Hunter, D.R. (Ed.) *Precambrian of the Southern Hemisphere*. Developments in Precambrian Geology, **2**. Elsevier, Amsterdam, 882 pp.
- Masuda, Y., Nishimura, S., Ikeda, T. and Katsui, Y. (1975). Rare-earth and trace elements in the Quaternary volcanic rocks of Hokkaido, Japan. *Chem. Geol.*, **15**, 251-271.
- McBirney, A.R. (1980). Mixing and unmixing of magmas. *J. Volcanol. Geotherm. Res.*, **7**, 357-371.
- McBirney, A.R. and White, C.M. (1982). The Cascade Province, 115-135. In: Thorpe, R.S. (Ed.) *Andesites: Orogenic Andesites and Related Rocks*. Wiley, Chichester, 724 pp.
- McCarthy, T.S. and Hasty, R.A. (1976). Trace element distribution patterns and their relationship to the crystallization of granitic melts. *Geochim. Cosmochim. Acta.*, **40**, 1351-1358.
- McDaid, J. (1976). Preliminary report on the geology of the northern part of Diamond Area No.1, South West Africa. *13th Ann. Rep. Precam. Res. Unit, Univ. Cape Town*, 89-96.
- McDaid, J. (1978). The geology of the northern part of Diamond Area No.1, South West Africa. *14th and 15th a. Repts. Precam. Res. Unit, Univ. Cape Town*, 124-140.
- McKenzie, D. (1986). Mantle mixing still a mystery. *Nature*, **323**, 297.
- Menzies, M. and Murthy, V.R. (1980). Mantle metasomatism as a precursor to the genesis of alkaline magmas - isotopic evidence. *Am. J. Sci.*, **280**, 622-638.
- Middlemost, E.A.K. (1975). The basalt clan. *Earth-Sci. Rev.*, **11**, 337-364.
- Milner, S.C. (1988). *The geology and geochemistry of the Etendeka Formation quartz latites, Namibia*. Ph.D. thesis (unpubl.). Univ. Cape Town, 263 pp.
- Miyashiro, A. (1953). Calcium poor garnet in relation to metamorphism. *Geochim. Cosmochim. Acta*, **4**, 179-208.
- Miyashiro, A. (1973). *Metamorphism and Metamorphic Belts*. George, Allen and Unwin, London, 492 pp.
- Miyashiro, A. (1974). Volcanic rock series in island arcs and active continental margins. *Am. J. Sci.*, **274**, 321-355.
- Miyashiro, A., Shido, F. and Ewing, M. (1969). Diversity and origin of abyssal tholeiite from the Mid-Atlantic Ridge near 24° and 30° north latitude. *Contrib. Mineral. Petrol.*, **23**, 38-52.
- Morrison, M.A. (1978). The use of 'immobile' trace elements to distinguish the palaeotectonic affinities of metabasalts: applications to the Palaeocene basalts of Mull and Skye, northwest Scotland. *Earth Planet. Sci. Lett.*, **39**, 407-416.
- Myers, J.D., Marsh, B.D. and Krishna Sinha, A. (1986). Geochemical and strontium isotopic characteristics of parental Aleutian Arc magmas: evidence from the basaltic lavas of Atka. *Contrib. Mineral. Petrol.*, **94**, 1-11.
- Mysen, B.O. and Boettcher, A.L. (1975). Melting of a hydrous mantle. II. Geochemistry of crystals and liquids formed by anatexis of mantle peridotite at high pressures and temperatures as a function of controlled activity of water, hydrogen and carbon dioxide. *J. Petrol.*, **16**, 549-593.
- Nakamura, N. (1974). Determination of REE, Ba, Fe, Mg, Na and K in carbonaceous and ordinary chondrites. *Geochim. Cosmochim. Acta*, **38**, 757-775.
- Nash, W.P. and Crecraft, H.R. (1985). Partition coefficients for trace elements in silicic magmas. *Geochim. Cosmochim. Acta*, **49**, 2309-2322.
- Nisbet, E.G. and Pearce, L.A. (1977). Clinopyroxene composition in mafic lavas from different tectonic settings. *Contrib. Mineral. Petrol.*, **63**, 149-160.
- Norrish, K. and Hutton, J.T. (1969). An accurate X-ray spectrographic method for the analysis of a wide range of geological samples. *Geochim. Cosmochim. Acta*, **33**, 431-453.
- O'Nions, R.K., Carter, S.R., Eversen, N.M. and Hamilton, P.J. (1976). Geochemical and cosmochemical applications of Nd isotope analysis. *Ann. Rev. Earth Planet. Sci.*, **7**, 11-38.
- Osborn, E.F. (1969). The complementariness of orogenic andesite and alpine peridotite. *Geochim. Cosmochim. Acta*, **33**, 307-324.
- Osborn, E.F. (1979). The reaction principle, 133-170. In: Yoder, H.S., Jr. (Ed) *The evolution of the igneous rocks - fiftieth anniversary perspectives*. Univ. Press, Princeton, 588 pp.
- Papanastassiou, D.A. and Wasserburg, G.J. (1969). Initial strontium isotopic abundances and the resolution of small time differences in the formation of planetary objectives. *Earth Planet. Sci. Lett.*, **5**, 361-376.
- Peacock, M.A. (1931). Classification of igneous rock series. *J. Geol.*, **39**, 54-67.
- Pearce, J.A. (1982). Trace element characteristics of lavas from destructive plate boundaries, 525-548. In: Thorpe, R.S. (Ed.) *Andesites: Orogenic Andesites and Related Rocks*. Wiley, Chichester, 724 pp.
- Pearce, J.A. (1983). Role of the sub-continental lithosphere in magma genesis at active continental margins, 230-249. In: Hawkesworth, C.J. and Norry, M.J. (Eds) *Continental Basalts and Mantle Xenoliths*. Shiva, Nantwich, 272 pp.
- Pearce, J.A. and Cann, J.R. (1973). Tectonic setting of basic volcanic rocks determined using trace element analyses. *Earth Planet. Sci. Lett.*, **19**, 290-300.
- Pearce, J.A., Harris, N.B.W. and Tindle, A.G. (1984). Trace element discrimination diagrams for the tectonic interpretation of granitic rocks. *J. Petrol.*, **25**, 956-983.
- Pearce, J.A. and Norry, M.J. (1979). Petrogenetic implications of Ti, Zr, Y, and Nb variations in volcanic rocks. *Contrib. Mineral. Petrol.*, **69**, 33-47.
- Peccerillo, A. and Taylor, S.R. (1976). Geochemistry of Eocene calc-alkaline volcanic rocks from the Kastamonu area, northern Turkey. *Contrib. Mineral. Petrol.*, **58**, 63-81.
- Peterman, Z.E. (1979). Strontium isotope geochemistry of late Archean to late Cretaceous tonalities and trondhjemites, 133-147. In: Barker, F. (Ed.) *Trondhjemites, dacites and related rocks*. Elsevier, Amsterdam, 659 pp.
- Pitcher, W.S. (1983). Granite type and tectonic environment, 9-40. In: Hsu, K.J. (Ed.) *Mountain Building Processes*. Academic Press, New York, 263 pp.
- Plank, T. and Langmuir, C.H. (1988). An evaluation of the global variations in the major element chemistry of arc basalts. *Earth Planet. Sci. Lett.*, **90**, 349-370.
- Prestvik, T. (1982). Basic volcanics and tectonic setting. A discussion of the Zr-Ti-Y discrimination diagram and its suitability for classification purposes. *Lithos*, **15**, 241-247.
- Raase, P. (1974). Al and Ti contents of hornblende, indicators of pressure and temperature of regional metamorphism. *Contrib. Mineral. Petrol.*, **45**, 231-236.
- Range, P. (1910). Zur Geologie des Namalandes, Deutsch-Südwestafrika. *Mn. Z. Dtsch. geol. Ges.*, **62**, 462-468.
- Range, P. (1912). Geologie des deutschen Namalandes. *Beitr. geol. Erf. Dtsch. Schutzgeb.*, **2**, 13.
- Reid, D.L. (1977). Geochemistry of Precambrian igneous rocks in the lower Orange River region. *Bull. Precam. Res. Unit., Univ. Cape Town*, **22**, 397 pp.
- Reid, D.L. (1982). Age relationships within the Vooldsdrif batholith, low-

- er Orange River region II. A two stage emplacement history and the extent of Kibaran overprinting. *Trans. geol. Soc. S. Afr.*, **85**, 105-110.
- Reid, D.L., Mailing, S. and Allsopp, H.L. (1988). Rb-Sr ages of granitoids in the Rehoboth-Nauchas area, South West Africa/Namibia. *Communs. geol. Surv. S. W. Africa/Namibia*, **4**, 19-27.
- Reid, D.L., Welke, H.I., Erlank, A.J. and Betton, P.I. (1987). Composition, age and tectonic setting of amphibolites in the central Bushmanland Group, Western Namaqua Province, southern Africa. *Precam. Res.*, **36**, 99-126.
- Ringwood, A.E. (1979). Composition and origin of the Earth, 1-58. In: McElhinney, M.W. (Ed.) *The Earth: Its Origin, Structure and Evolution*. Academic Press, London, 597 pp.
- Rodgers, J. (1987). Chains of basement uplifts within cratons marginal to orogenic belts. *Am. J. Sci.*, **287**, 661-692.
- Roeder, P.L. and Emslie, R.F. (1970). Olivine-liquid equilibrium. *Contrib. Mineral. Petrol.*, **29**, 275-289.
- Rogers, J.J.W. and Greenberg, J.K. (1981). Trace elements in continental-margin magmatism. Part III. Alkali granites and their relationship to cratonization: summary. *Geol. Soc. Am. Bull.*, **92**, 6-9.
- Ross, C.S. and Smith, R.L. (1961). Ash-flow tuffs: their origin, geologic relations and identification. *U.S. geol. Surv. Prof. Pap.*, **366**, 1-77.
- Ross, M. and Huebner, J.S. (1979). Temperature-composition relationships between naturally occurring augite, pigeonite, and orthopyroxene at one bar pressure. *Am. Miner.*, **64**, 1133-1155.
- Ryan, A.B., Baragar, W.R.A. and Kontak, D.J. (1987). Geochemistry, tectonic setting, and mineralization of high-potassium middle Proterozoic rocks in central Labrador, Canada, 241-254. In: Pharaoh, T.C., Beckinsale, R.D. and Rickard, D. (Eds) *Geochemistry and Mineralization of Proterozoic Volcanic Suites*. Spec. Publ. geol. Soc. Lond., **33**, 575 pp.
- Saunders, A.D. (1984). The rare earth element characteristics of igneous rocks from the ocean basins, 205-236. In: Henderson, P. (Ed.) *Rare Earth Element Geochemistry*. Developments in Geochemistry, **2**. Elsevier Amsterdam, 510 pp.
- Sakuyama, M. (1984). Magma mixing and magma plumbing systems in island arcs. *Bull. Volcanol.*, **47**, 685-703.
- Schmid, R. (1981). Descriptive nomenclature and classification of pyroclastic deposits and fragments: Recommendations of the IUGS Subcommittee on the Systematics of Igneous Rocks, *Geology*, **9**, 41-43.
- Sethuraman, K. and Moore, J.M. (1973). Petrology of metavolcanic rocks in the Bishop Corners - Donaldson area, Grenville Province, Ontario. *Can. J. Earth Sci.*, **10**, 589.
- Shand, S.J. (1927). *Eruptive Rocks*. T. Murby & Co., London, 360 pp.
- Shaw, D.M. (1970). Trace element fractionation during anatexis. *Geochem. Cosmochim. Acta*, **34**, 237-242.
- Sheraton, J.W. and Black, L.P. (1988). Chemical evolution of granitic rocks in the East Antarctic Shield, with particular reference to post-orogenic granites. *Lithos*, **21**, 37-52.
- Shervais, J.W. (1982). Ti-V plots and the petrogenesis of modern and ophiolitic lavas. *Earth Planet. Sci. Lett.*, **59**, 101-118.
- Shido, F. (1958). Plutonic and metamorphic rocks of the Nakaso and Iritono districts in the central Abukuma Plateau. *J. Fac. Sci. Tokyo Univ.*, **II**, **11**, 131-217.
- Shido, F. and Miyashiro, A. (1959). Hornblendes of the basic metamorphic rocks. *J. Fac. Sci. Tokyo Univ.*, **II**, **12**, 85-102.
- Smedley, P.L. (1986). The relationship between calc-alkaline volcanism and within-plate continental rift volcanism: evidence from Scottish Palaeozoic lavas. *Earth Planet. Sci. Lett.*, **76**, 113-128.
- Smith, J.V. (1974). *Feldspar Minerals. J. Crystal Structure and Physical Properties*. Springer-Verlag, Heidelberg, 627 pp.
- Smith, R.E. (1968). Redistribution of major elements in the alteration of some basic lavas during burial metamorphism. *J. Petrol.*, **9**, 191-219.
- Smith, R.E. (1969). Zones of progressive regional burial metamorphism in part of the Tasman Geosyncline, eastern Australia. *J. Petrol.*, **10**, 144-163.
- Smith, R.E. and Smith, S.E. (1976). Comments on the use of Ti, Zr, Y, Sr, K, P and Nb in classification of basaltic magmas. *Earth Planet. Sci. Lett.*, **32**, 114-120.
- South African Committee for Stratigraphy - SACS (1980). Kent, L.E. (Comp.) Stratigraphy of South Africa. Part I: *Lithostratigraphy of the Republic of South Africa, South West Africa/Namibia and the Republics of Bophutatswana, Transkei and Venda*. *Handb. geol. Surv. S. Afr.*, **8**, 690 pp.
- Sparks, R.S.J. (1983). Mixed-upmagmas. *Nature*, **306**, 315-316.
- Speer, J.A. (1981). Petrology of cordierite- and almandine-bearing granitoid plutons of the southern Appalachian Piedmont, U.S.A. *Can. Miner.*, **19**, 35-46.
- Speer, J.A. (1984). Micas in igneous rocks, 299-356. In: Bailey, S.W. (Ed.) *Micas*. Mineralog. Soc. Am., Reviews in Mineralogy, **13**, 584 pp.
- Stacey, J.S. and Kramers, J.D. (1975). Approximation of terrestrial lead isotope evolution by a two stage model. *Earth Planet. Sci. Lett.*, **26**, 207-221.
- Stern, R.I. and Gottfried, D. (1986). Petrogenesis of a Late Precambrian (575-600 Ma) bimodal suite in Northeast Africa. *Contrib. Mineral. Petrol.*, **92**, 492-501.
- Stowe, C.W. (1984). Explanation of the Upington Geotraverse, South Africa, 35-44. In: Rast, N. and Delany, F.M. (Eds) *Profiles of Orogenic Belts*. Am. Geophys. Union, Geodynamics Series, **10**, 310 pp.
- Stumpfl, E.F., Clifford, T.N., Burger, A.J. and Van Zyl, D. (1976). The copper deposits of the O'Okiep District, South Africa: new data and concepts. *Mineral. Deposita*, **11**, 46-70.
- Sylvester, P.J., Attoh, K. and Schulz, K.J. (1987). Tectonic setting of late Archean bimodal volcanism in the Michipicoten (Wawa) greenstone belt, Ontario. *Can. J. Earth Sci.*, **24**, 1120-1134.
- Tamaki, K. (1985). Two modes of back-arc spreading. *Geology*, **13**, 475-478.
- Tankard, A.J., Jackson, M.P.A., Eriksson, K.A., Hobday, D.K., Hunter, D.R. and Minter, W.E.L. (1982). *Crustal Evolution of Southern Africa. 3.8 Billion Years of Earth History*. Springer-Verlag, New York, 523 pp.
- Taylor, S.R., Capp, A.C., Graham, A.L. and Blake, D.H. (1969). Trace element abundances in andesites, II. Saipan, Bougainville and Fiji. *Contrib. Mineral. Petrol.*, **23**, 1-26.
- Taylor, S.R. and Gorton, M.P. (1977). Geochemical application of spark source mass spectrography, III. Element sensitivity, precision and accuracy. *Geochim. Cosmochim. Acta*, **41**, 1375-1380.
- Taylor, S.R. and McLennan, S.M. (1985). *The continental crust: Its composition and evolution*. Blackwell, Oxford, 312 pp.
- Taylor, S.R. and White, A.J.R. (1966). Trace element abundances in andesites. *Bull. Volcanol.*, **29**, 177-194.
- Terakado, Y. and Masuda, A. (1988). Trace-element variations in acidic rocks from the Inner Zone of southwest Japan. *Chem. Geol.*, **67**, 227-241.
- Thirwall, M.P. (1988). Wenlock to mid-Devonian volcanism of the Caledonian-Appalachian orogen, 415-428. In: Harris, A.L. and Fettes, D.J. (Eds) *The Caledonian-Appalachian Orogen*. Spec. Publ. geol. Soc. Lond., **38**, 643 pp.
- Thirwall, M.F. and Jones, N.W. (1983). Isotope geochemistry and contamination mechanics of Tertiary lavas from Skye, Northwest Scotland, 186-208. In: Hawkesworth, C.J. and Norry, M.J. (Eds) *Continental Basalts and Mantle Xenoliths*. Shiva, Nantwich, 272 pp.
- Thompson, R.N., Morrison, M.A., Hendry, G.L. and Parry, S.J. (1984).

- An assessment of the relative roles of crust and mantle in magma genesis: an elemental approach. *Phil. Trans. R. Soc. Lond.*, **A310**, 549-590.
- Thornton, C.P. and Tuttle, O.F. (1960). Chemistry of igneous rocks, I. Differentiation Index. *Am. J. Sci.*, **258**, 664-684.
- Thorpe, R.S., Potts, P.J. and Francis, P.W. (1976). Rare earth data and petrogenesis of andesite from the North Chilean Andes. *Contrib. Mineral. Petrol.*, **54**, 65-78.
- Turner, J.S. and Campbell, I.H. (1986). Convection and mixing in magma chambers. *Earth-Sci. Rev.*, **23**, 255-352.
- Uyeda, S. (1981). Subduction zones and back arc basins - a review. *Geol. Rundsch.*, **70**, 552-569.
- Vajner, V. (1974). The tectonic development of the Namaqua mobile belt and its foreland in parts of the Northern Cape. *Bull. Precam. Res. Unit, Univ. Cape Town*, **14**, 201 pp.
- Van Niekerk, C.B. and Burger, A.J. (1967). Radiometric dating of the Koras Formation. *Ann. geol. Surv. Dep. Min. S. Afr.*, **6**, 77-82.
- Vernon, R.H. and Williams, P.F. (1988). Distinction between intrusive and extrusive or sedimentary parentage of felsic gneisses: Examples from the Broken Hill Block, NSW. *Austral. J. Earth Sci.*, **35**, 379-388.
- Von Brunn, V. (1967). *Acid and basic igneous rock associations west of Helmeringhausen, South West Africa*. Ph.D. thesis (unpubl.), Univ. Cape Town, 170 pp.
- Von Platen, H. (1965). Experimental anatexis and genesis of migmatites, 203-218. In: Pitcher, W.S. and Flinn, G.W. (Eds) *Controls of metamorphism*. Oliver & Boyd, Edinburgh, 368 pp.
- Walraven, F. (1984). Geochemistry of the Timbavati Gabbro of the Eastern Transvaal Lowveld, South Africa. *Trans. geol. Soc. S. Afr.*, **87**, 211-223.
- Watson, E.B. and Capobianco, C.J. (1981). Phosphorus and the rare earth elements in felsic magmas: An assessment of the role of apatite. *Geochim. Cosmochim. Acta*, **45**, 2349-2358.
- Watters, B.R. (1974). Stratigraphy, igneous petrology and evolution of the Sinclair Group in southern South West Africa. *Bull. Precam. Res. Unit., Univ. Cape Town*, **16**, 235 pp.
- Watters, B.R. (1976). Possible late Precambrian subduction zone in South West Africa. *Nature*, **259**, 471-473.
- Watters, B.R. (1978). Petrogenesis of the felsic rock units of the late-Precambrian Sinclair Group, South West Africa. *Geol. Rd-sch.*, **67**, 743-773.
- Watters, B.R. (1982). A Sr-isotopic study of a suite of Precambrian shoshonites from the Sinclair Group in southern Namibia. *Trans. geol. Soc. S. Afr.*, **85**, 81-86.
- Weaver, B.L. and Tarney, J. (1982). Andesitic magmatism and continental growth, 115-135. In: Thorpe, R.S. (Ed.) *Andesites: Orogenic Andesites and Related Rocks*. Wiley, Chichester, 724 pp.
- Whalen, J.B., Currie, K.L. and Chappell, B.W. (1987). A-type granites: geochemical characteristics, discrimination and petrogenesis. *Contrib. Mineral. Petrol.*, **95**, 407-419.
- White, M.V.W. and Martin, R.F. (1980). The metasomatic changes that accompany uranium mineralization in the nonorogenic rhyolites of the Upper Aillik Group, Labrador. *Can. Miner.*, **18**, 459-479.
- Williams-Jones, I.E. (1984). *The petrology of the basalts of the Dordabis Formation, in the vicinity of Dordabis in central S.W.A./Namibia*. M.Sc. thesis (unpubl.), Rhodes University, Grahamstown, 114 pp.
- Wilson, T.J. (1988). Convection tectonics: some possible effects upon the Earth's surface of flow from the deep mantle. *Can. J. Earth Sci.*, **25**, 1199-1208.
- Winchester, J.A. and Floyd, P.A. (1977). Geochemical discrimination of different magma series and their differentiation products using immobile elements. *Chem. Geol.*, **20**, 325-343.
- Winkler, G.F. (1976). *Petrogenesis of Metamorphic Rocks*. Springer-Verlag, Berlin, 334 pp.
- Wones, D.R. and Gilbert, M.C. (1982). Amphiboles in the igneous environment, 355-390. In: Veblen, D.R. and Ribbe, P.H. (Eds) *Amphiboles: petrology and experimental phase relations*. Mineralog. Soc. Am., Reviews in Mineralogy, **9B**, 390 pp.
- Wood, D.A. (1979). A variably-veined sub-oceanic upper mantle: genetic significance for mid-ocean ridge basalts from geochemical evidence. *Geology*, **7**, 499-503.
- Wyllie, P.J. (1977). Crustal anatexis: an experimental review, 41-71. In: Green, D.H. (Ed.) *Experimental Petrology Related to Extreme Metamorphism*. Tectonophys., **43**.
- Yoder, H.S., Jr. and Tilley, C.E. (1962). Origin of basalt magmas: an experimental study of natural and synthetic rock systems. *J. Petrol.*, **3**, 342-532.
- York, D. (1966). Least-squares fitting of a straight line. *Can. J. Phys.*, **44**, 1079-1086.
- York, D. (1969). Least-squares fitting of a straight line with correlated errors. *Earth Planet. Sci. Lett.*, **5**, 320-324.
- Zartman, R.E. and Doe, B.R. (1981). Plumbotectonics - the model. *Tectonophys.*, **75**, 135-162.
- Zielinski, R.A. and Lipman, P.W. (1976). Trace-element variations at Summer Coon volcano, San Juan Mountains, Colorado, and the origin of continental-interior andesite. *Geol. Soc. Am. Bull.*, **87**, 1477-1485.

APPENDIX

I. SAMPLE LOCALITIES

Sample localities have been plotted on the 1:100 000 geological map of the Awasi Mountain terrain located in the map pocket.

II. ANALYTICAL TECHNIQUES

i. SAMPLE PREPARATION

Whole-rock sample preparation was carried out in the laboratory of the Geological Survey of Namibia (Windhoek). Samples were initially split in a hydraulic splitter before being crushed in a jaw crusher with carbon-steel jaws and finally ground to -300# powder in a carbon-steel grinding vessel on a Siebtechnik swing mill. An agate grinding vessel was used for all powders intended for isotopic analyses. Polishing and carbon-coating of thin sections for electron microprobe analyses were carried out at the Geochemistry Department of the University of Cape Town.

ii. WHOLE-ROCK ANALYSES

a. X-ray fluorescence spectrometry

X-ray fluorescence (XRF) analyses of whole-rock samples were carried out by the author at the Geochemistry Department of the University of Cape Town (UCT). Procedures are described in detail by Duncan *et al.* (1984) and will not be repeated here. Additional analytical data (largely on samples of the early-stage crust of the AMT) have been obtained from XRF facilities at the Geological Survey of South Africa in Pretoria (GS) and the University of Natal in Pietermaritzburg (UN).

International rock standards, including the USGS standard set, were used for calibration in all cases in addition to "in-house" and national rock standards (e.g. NIM). Estimates of precision and detection limit are provided in Duncan *et al.* (1984, their Tables II and III) for UCT analyses and Table I for UN analyses, but estimates of precision and reproducibility are available for only a limited number of elements in the case of GS analyses (Walraven, 1984; Appendix A). Accordingly, duplicate samples were analysed at both the GS and UCT for a range of elements compared in Fig. 1 and Table II. Interlaboratory correlation, although poor for certain elements (e.g. Co), is acceptable for the majority of elements used in this study and does not adversely affect the conclusions reached. However, because interelement ratios can vary significantly (e.g. 22.6% difference in Rb/Sr in Table II), no GS analyses were used in the construction of isochrons. XRF spectrometers used were Philips PW1400 and Siemens SRS-1 machines at UCT, Rigaku Denki and Philips PW1600 machines at GS, and a Philips PW1410 machine at UN.

All major elements (except Na, and K in GS samples) were analysed using the flux fusion method of Norrish and Hutton (1969). Na (and K in GS samples) was analysed on

pressed powder briquettes. Volatile constituents (H_2O^- and loss on ignition, LOI) were determined for UCT samples by drying the sample at 110°C (H_2O^-) followed by roasting for 12 hours in a muffle furnace at 900°C (LOI). CO_2 analyses in the case of GS samples were carried out by infra-red spectroscopy on a Leco analyser. UN analyses do not include any estimates of volatile constituents.

All trace elements were analysed on pressed powder briquettes and are listed in Table III for the three laboratories. Trace elements determined in all samples were Nb, Zr, Y, Sr, Rb, Zn, Ni, V and Ba.

b. Rare earth element (REE) analyses

REE data (excluding La, Ce and Nd determined by XRF) were made available for selected samples by D.L. Reid (pers. comm., 1987; Table IV). These INAA analyses were carried out at the New Mexico Institute of Mining and Metallurgy, using techniques described by Jacobs *et al.* (1977) and Lindstrom and Korotev (1982).

c. Radiogenic isotope analyses

The analytical procedures applied at the National Physical Research Laboratory (NPRL) for Sr isotope analysis have been described by Harmer and Sharpe (1985) and Harmer (1985) and involve standard cation-exchange extraction of Sr following sample dissolution in $\text{HF-HNO}_3\text{-HCl}$. Blanks were in the order of 1 ng. Isotopic analyses were carried out by the author on a VG 354 mass spectrometer equipped with a multi-collector array and automatic computer control of the analytical procedure. All ratios are normalised to $^{86}\text{Sr}/^{88}\text{Sr} = 0.1194$ and are relative to a value of 0.71023 ± 4 (2 standard deviations on 28 measurements) for NBS standard Sr salt SRM 987. Sample Sr ratios are reproducible to 0.01%.

Data were regressed using the method of York (1969) with blanket weighting factors based on one-sigma uncertainties of 1.5% and 0.01% in X ($^{87}\text{Rb}/^{86}\text{Sr}$) and Y ($^{87}\text{Sr}/^{86}\text{Sr}$) respectively in the case of XRF analyses, and 0.8% and 0.02% in X and Y respectively in the case of isotope dilution (ID) determinations. Goodness-of-fit of the regression line was tested by the value $\text{MSUM} = \text{SUMS}/(n-2)$ as described by Brooks *et al.* (1972); scatter in the data in excess of the analytical uncertainty is reflected by $\text{MSUM} > 2.5$. In cases of excess, or "geological scatter", the regression line is termed an "errorchron" and the errors for the age estimate are calculated by York (1966), which augments the errors to account for the scatter. Errorchron age estimates are identified in the text and figures by an asterisk ("*"). All errors are given at the two-sigma level.

Sample preparation for Pb isotopes at the NPRL involved anion exchange in small quartz-glass columns and elution using HBr and $\text{H}_2\text{O}^{\text{XRX}}$. Total method blanks of less than 1 ng were considered negligible. The Pb fraction was loaded on single Re filaments with 1M HNO_3^{XX} and 1N H_3PO_4 , and isotopic analyses carried out on a VG

TABLE I: Major and trace element analysis by XRF - University of Natal (A. Wilson, pers. comm., 1988).

				Precision (%)					Detection Limit (D.L.)				
Major elements (>1 wt.%)				1					<0.001 wt.%				
Minor elements (<1 wt.%)				5					<0.001 wt.%				
Trace elements:	Nb	Zr	Y	Sr	Rb	Zn	Cu	Ni	Cr	V	Sc	Ba	La
Precision (%)	5	2	5	5	2	2	2	2	5	5	10	15	10
D.L. ($\times 10^{-1}$ ppm)	1	1	1	1	1	.1	.1	.1	10	10	10	20	20

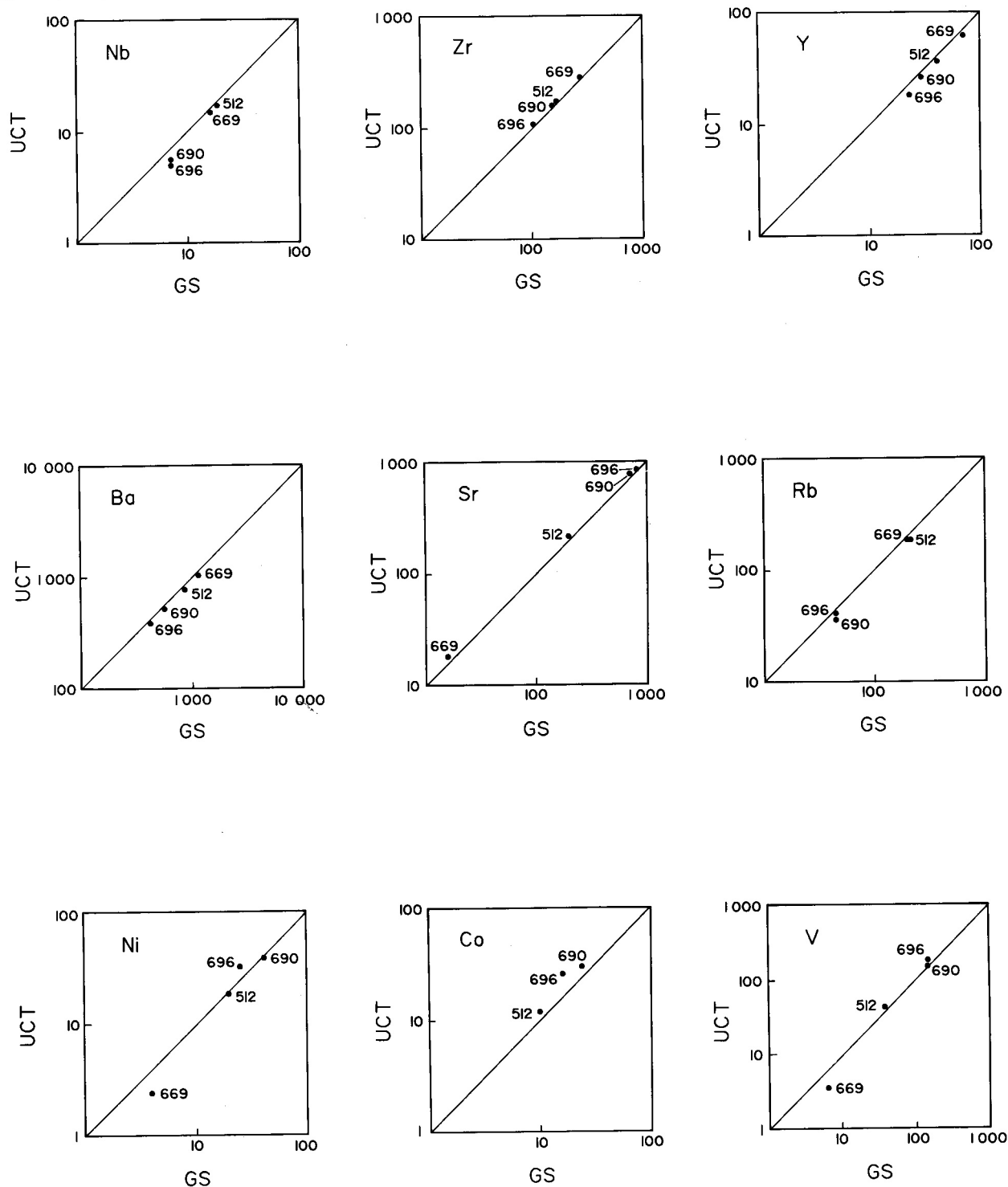
**Fig. I:** Comparative log-log plots of trace element analyses performed on four sets of duplicate samples (BH 512, 669, 690, 696) at the University of Cape Town (UCT) and Geological Survey of South Africa (GS). Good agreement is shown for those analyses which lie close to the 45° line.

TABLE II: Comparison between analyses performed on duplicate powders of basaltic andesite (BH 690) at Geological Survey (GS) and the University of Cape Town (UCT).

Oxide	GS	UCT	(%Diff.)	Element	GS	UCT	(%Diff.)
SiO ₂	55.02	55.88	-1.54	Nb	7	6	16.67
TiO ₂	0.92	0.96	-4.17	Zr	152	162	-6.17
Al ₂ O ₃	15.62	15.49	0.84	Y	29	26	11.54
Fe ₂ O ₃	9.25	9.06	2.10	Sr	688	726	-5.23
MnO	0.16	0.17	-5.88	Rb	43	37	16.22
MgO	5.28	5.10	3.53	Zn	83	71	16.90
CaO	7.97	7.94	0.38	Cu	92	64	43.75
Na ₂ O	3.51	3.15	11.43	Ni	41	38	7.89
K ₂ O	1.49	1.47	1.36	Co	24	31	-22.58
P ₂ O ₅	0.34	0.34	0.00	V	146	160	-8.75
H ₂ O	0.16	0.12	33.33	Ba	559	520	7.50
LOI	0.53	0.54	-1.85	%Diff. = % difference of GS relative to UCT analysis			

TABLE III: Trace elements routinely analysed at the University of Cape Town (UCT; n=21), Geological Survey (GS; n=15) and the University of Natal (UN; n=13).

UCT	Mo	Nb	Zr	Y	Sr	U	Rb	Th	Pb	Zn	Cu	Ni	Co	Cr	V	Ba	Sc	La	Ce	Nd	Cs
GS	Mo	Nb	Zr	Y	Sr	U	Rb	Th	Pb	Zn	Cu	Ni	Co		V	Ba					
UN		Nb	Zr	Y	Sr		Rb			Zn	Cu	Ni		Cr	V	Ba	Sc	La			

TABLE IV: Rare earth element data for selected samples (NMIMT; Reid, pers. comm., 1987).

	BH 770 (Kairab metabasalt)	BH 598 (HFF high-Mg basaltic andesite)	BH 690 (HFF acid basaltic andesite)	BH 669 (HFF rhyolite)	BH 668 (Awasib Granite)
La	2.66	16.7	21.7	46.7	71.5
Ce	5.84	37.9	51.0	110	169
Nd	4.65	18.1	23.4	45.7	86.0
Sm	1.22	4.42	5.91	10.1	20.3
Eu	0.46	1.14	1.51	0.81	0.32
Gd	1.27	3.81	4.97	10.5	22.5
Tb	0.21	0.57	0.74	1.71	3.80
Yb	1.03	2.14	2.54	7.11	9.53
Lu	0.18	0.38	0.41	1.13	1.42

MM30 mass spectrometer. Five runs of the NBS 981 Pb standard yielded mean values of $206/204 = 16.897 \pm 5$, $207/204 = 15.441 \pm 7$, and $208/204 = 36.539 \pm 24$. A reproducibility in $206/204$ and $207/204$ of 0.09% was achieved and data were regressed using the technique of York (1969). A correlation coefficient of 0.946 was determined from five runs of NBS 981 and by using the formulation of Ludwig (1980).

iii. MINERAL ANALYSES

Analyses of individual minerals were carried out by the author at UCT using a Cameca Camebax Microbeam Electron Microscope. An accelerating voltage of 15 kV was used for most analyses. However, the beam current and focussing were changed from 40 nA and 2-5 μm for pyroxenes and olivines to 20 nA and 10-30 μm for feldspars and micas. Raw counts were corrected for dead-time losses and background, and the intensity-concentration relationship was calibrated by using a variety of natural and synthetic mineral standards listed in Duncan *et al.* (1984). Matrix corrections were corrected using the ZAF technique. Typical two-sigma counting errors and lower limits of detection are given in Milner (1988; Appendix 2).

III. DATABASE DESCRIPTION

The whole-rock and mineral database used in this study is contained on the accompanying Microfiche card (42X format).

i. WHOLE-ROCK DATA

The whole-rock database for the Awasib Mountain terrain incorporates geochemical data for 190 samples obtained at three analytical institutions, UCT (n = 87), GS (n

= 74) and UN (n = 29). Data are tabulated and indexed on Microfiche and are organised according to analytical institution and sample number. All data are reported as obtained with total Fe expressed as Fe_2O_3 . Table V presents the same whole-rock data recalculated to 100% (volatile-free) and arranged according to lithologic group and compositional affinity within a specific group. Values close to the lower limit of detection (D.L.) in this table have been arbitrarily set at $0.5 \times \text{D.L.}$

ii. MINERAL DATA

A total of 23 sets of EMP analyses have been used in this study and correspond to the following lithologic groupings: Kairab metabasalt (n = 2), Kairab metagabbro (n = 1), Aunis Tonalite Gneiss (n = 2), Haiber Flats Formation basaltic andesite-andesite (n = 5), Haiber Flats Formation rhyolite (n = 2), Barby Formation basaltic andesite (n = 1), Haisib Intrusive Suite (n = 3), Awasib Granite (n = 2) and Chowachasib Granite Suite (n = 5). Each data set comprises analyses for a variety of phases (e.g. feldspar, pyroxene, amphibole, mica, chlorite, epidote and oxide minerals) which are tabulated and indexed on the accompanying Microfiche card. All data are reported as determined with total Fe expressed as FeO. Concentrations below detection limit are indicated by the abbreviation "ND" (Not Detected).

iii. DISTRIBUTION COEFFICIENT DATA

Distribution coefficients (Kd's) and their data sources used in petrogenetic modelling (Section C.6) are presented in Table VI. Kd's have been independently selected for the compositional ranges shown; accordingly, Kd's may not show strong compositional dependence (see discussion in Section C.6.1 - Introduction).

TABLE V: Normalised whole-rock data for the Awasisb Mountain terrain (all Fe as Fe₂O₃; n.a. = not analysed).

	BH546	BH554	BH740	BH757	BH770A	BH774A	BH783	BH785	BH786	BH791	BH792	BH830	BH831	BH843	BH883	BH901	BH902	BH903	BH904	BH905
SiO ₂	48.92	50.27	52.04	46.92	48.61	45.78	47.58	48.45	50.34	48.61	49.02	48.22	47.93	47.74	49.28	46.51	48.42	48.21	48.23	48.39
TiO ₂	.41	.25	.78	.43	.40	.33	.45	.40	.31	.34	.27	.35	.37	.41	.27	.32	.49	.47	.36	.40
Al ₂ O ₃	17.37	17.59	17.58	16.11	20.32	18.60	20.89	15.43	17.38	14.85	17.50	14.79	15.98	14.62	19.88	18.60	18.13	19.20	22.03	20.74
Fe ₂ O ₃	11.09	7.73	12.55	11.03	12.89	11.94	12.96	10.57	10.06	12.70	10.81	12.53	12.72	13.09	12.03	12.93	14.41	13.70	10.46	12.74
MnO	.19	.14	.22	.21	.25	.32	.21	.24	.26	.26	.20	.20	.32	.30	.14	.34	.20	.22	.32	.22
MgO	7.55	6.47	3.70	7.06	2.79	4.90	3.38	7.20	5.30	8.44	6.94	8.08	8.00	7.07	4.71	6.09	4.19	4.31	4.76	2.96
CaO	13.17	13.85	10.39	16.30	13.22	13.82	11.83	15.64	15.21	13.08	13.76	13.15	12.51	14.17	12.22	13.09	12.03	11.34	9.96	12.99
Na ₂ O	1.04	3.51	2.39	1.49	1.35	3.51	2.45	1.96	1.04	1.41	1.31	2.03	1.66	2.14	1.37	1.91	1.92	2.29	3.44	1.33
K ₂ O	.24	.17	.23	.38	.09	.75	.10	.00	.00	.21	.11	.53	.40	.31	.00	.13	.10	.14	.38	.10
P ₂ O ₅	.03	.02	.13	.06	.07	.05	.14	.12	.10	.10	.08	.11	.11	.14	.10	.07	.10	.11	.08	.12
TOTAL 100.00	100.00	100.00	100.00	100.00	100.00	100.00	100.00	100.00	100.00	100.00	100.00	100.00	100.00	100.00	100.00	100.00	100.00	100.00	100.00	100.00
Mo	n.a.	n.a.	5	5	1	.5	n.a.	2	1	.5	.5	.5	.5	2	.5	.5	2	.5	.5	.5
Nb	2	1	1.0	1	7	7	n.a.	7	8	8	7	7	7	8	8	7	8	8	7	8
Zr	16	8	49	13	36	39	n.a.	41	38	42	34	42	44	46	40	33	38	36	32	37
Y	8	8	18	11	9	6	n.a.	11	9	11	6	12	12	16	7	7	12	11	6	10
Sr	184	240	197	214	284	235	n.a.	411	235	196	196	246	204	201	249	245	276	306	356	281
U	n.a.	n.a.	2	2	.5	.5	n.a.	.5	.5	.5	.5	.5	.5	.5	.5	.5	2	.5	.5	.5
Rb	2	1.0	4	8	5	15	n.a.	5	5	8	7	12	13	9	4	5	5	5	10	7
Th	n.a.	n.a.	3	3	.5	.5	n.a.	.5	.5	.5	.5	.5	.5	1	.5	.5	2	.5	.5	.5
Pb	n.a.	n.a.	3	3	10	14	n.a.	16	16	11	6	15	14	15	5	4	11	8	4	8
Cu	94	61	97	76	83	93	n.a.	32	74	89	54	114	101	115	88	61	128	93	115	91
Zn	7	219	86	199	109	2	n.a.	8	62	14	2	80	20	59	29	16	162	101	129	105
Ni	39	61	10	103	13	36	n.a.	244	40	60	36	99	67	87	19	5	9	10	16	3
Co	n.a.	n.a.	38	59	30	40	n.a.	25	33	48	33	51	45	36	35	28	30	50	34	22
Cr	153	135	13	324	n.a.															
V	346	252	250	248	385	347	n.a.	348	345	370	390	362	356	359	368	363	441	434	369	423
Ba	22	8	63	55	77	293	n.a.	115	94	85	92	137	116	125	137	65	105	101	137	121
Sc	50	51	38	52	n.a.															
Cs	n.a.	2	2	n.a.																
La	3	1	7	4	n.a.															
Ce	n.a.	n.a.	10	3	n.a.															
Nd	n.a.	n.a.	9	2	n.a.															
BH546	:	Kairab Metabasalt																		
BH554	:	Kairab Metabasalt																		
BH740	:	Kairab Metabasalt																		
BH757	:	Kairab Metabasalt																		
BH770A	:	Kairab Metabasalt																		
BH774A	:	Kairab Metabasalt																		
BH783	:	Kairab Metabasalt																		
BH785	:	Kairab Metabasalt																		
BH786	:	Kairab Metabasalt																		
BH791	:	Kairab Metabasalt																		
BH792	:	Kairab Metabasalt																		
BH830	:	Kairab Metabasalt																		
BH831	:	Kairab Metabasalt																		
BH843	:	Kairab Metabasalt																		
BH883	:	Kairab Metabasalt																		
BH901	:	Kairab Metabasalt																		
BH902	:	Kairab Metabasalt																		
BH903	:	Kairab Metabasalt																		
BH904	:	Kairab Metabasalt																		
BH905	:	Kairab Metabasalt																		

TABLE V (continued)

	BH906	BH907	BH743	BH742	BH738	BH739	BH741	BH772	BH780	BH793	BH534	BH544	BH561	BH664	BH736	BH761	BH762	BH781	BH833	BH839
SiO ₂	47.84	48.58	58.62	64.78	72.70	72.16	76.29	71.43	76.89	73.81	48.15	49.53	49.85	49.70	49.36	50.02	46.08	49.85	49.48	46.77
TiO ₂	.31	.43	.67	.58	.31	.30	.25	.22	.10	.14	1.00	.24	1.04	1.00	.39	.50	.73	1.08	.58	.34
Al ₂ O ₃	20.01	20.03	19.89	16.00	12.40	12.68	12.46	13.57	10.83	11.74	10.63	15.13	16.22	14.64	14.52	11.50	15.44	15.19	15.23	16.22
Fe ₂ O ₃	12.52	12.94	6.71	8.07	5.65	4.42	2.40	5.16	4.86	6.08	11.61	8.19	10.32	11.01	11.67	10.15	12.71	10.54	14.23	11.42
MnO	.21	.24	.13	.08	.15	.12	.05	.14	.23	.25	.19	.17	.16	.19	.20	.16	.22	.16	.42	.32
MgO	3.90	3.22	1.18	1.56	.59	.40	.14	.89	.00	.00	17.26	8.93	8.20	10.70	9.19	17.06	10.87	10.41	6.13	8.27
CaO	13.81	13.18	10.08	4.21	2.55	4.56	2.67	3.12	2.69	2.20	8.33	17.32	9.09	9.25	13.22	7.48	11.86	8.84	11.19	14.14
Na ₂ O	1.11	1.03	2.38	3.62	4.43	4.13	4.24	4.04	1.84	4.57	.19	.39	2.80	1.92	1.18	2.31	1.50	2.12	1.98	1.67
K ₂ O	.16	.21	.15	.93	1.15	1.15	1.44	1.38	2.55	1.13	2.40	.09	2.09	1.41	.20	.65	.50	1.59	.60	.69
P ₂ O ₅	.11	.13	.19	.16	.08	.10	.06	.05	.03	.08	.25	.01	.23	.19	.07	.18	.08	.22	.16	.17
TOTAL	100.00	100.00	100.00	100.00	100.00	100.00	100.00	100.00	100.00	100.00	100.00	100.00	100.00	100.00	100.00	100.00	100.00	100.00	100.00	100.00
Mo	.5	1	4	2	3	2	2	2	4	3	n.a.	n.a.	n.a.	n.a.	4	3	4	3	5	5
Nb	8	8	.9	5	5	4	3	3	10	8	5	1	9	4	1	1.0	1	2	2	8
Zr	37	40	56	125	99	96	110	98	114	86	49	3	108	74	11	64	15	72	58	41
Y	9	11	25	36	37	22	20	49	57	40	13	7	25	20	10	16	11	20	22	11
Sr	252	323	301	251	178	193	20	579	67	150	77	179	283	418	221	837	211	567	177	275
U	.5	.5	2	2	2	2	2	2	.5	.5	n.a.	n.a.	n.a.	n.a.	2	2	2	6	5	.5
Rb	6	10	1	30	22	16	19	31	52	27	105	n.a.	78	67	4	16	14	38	11	16
Th	.5	.5	3	3	3	2	2	3	.5	.5	n.a.	n.a.	n.a.	n.a.	3	3	3	6	5	.5
Pb	13	13	3	3	3	3	3	3	11	10	n.a.	n.a.	n.a.	n.a.	3	3	3	7	10	14
Zn	88	88	68	116	77	44	36	57	79	57	79	42	100	88	80	73	109	74	71	161
Cu	152	137	84	6	1	1	3	9	.5	4	4	105	81	34	148	39	75	53	11	131
Ni	20	18	5	2	2	2	2	1	.5	.5	519	76	194	177	644	128	198	132	32	68
Co	38	36	16	6	1	7	4	3	23	14	n.a.	n.a.	n.a.	59	73	64	54	48	39	n.a.
Cr	n.a.	n.a.	15	10	10	19	16	15	n.a.	n.a.	1581	196	285	509	400	1283	83	556	n.a.	n.a.
V	379	396	173	23	.9	24	17	.9	20	10	224	238	196	206	248	129	205	222	451	241
Ba	69	107	33	174	629	330	408	132	326	349	450	24	355	434	55	135	82	348	142	203
Sc	n.a.	n.a.	34	26	17	13	7	16	n.a.	n.a.	29	61	27	35	54	25	48	33	n.a.	n.a.
Cs	n.a.	n.a.	1	3	3	1	1	4	n.a.	n.a.	n.a.	n.a.	n.a.	n.a.	5	2	4	2	n.a.	n.a.
La	n.a.	n.a.	1	11	9	10	8	12	n.a.	n.a.	n.a.	n.a.	22	8	4	12	2	6	n.a.	n.a.
Ce	n.a.	n.a.	10	24	22	23	20	29	n.a.	n.a.	n.a.	n.a.	n.a.	n.a.	8	18	3	13	n.a.	n.a.
Nd	n.a.	n.a.	10	18	19	13	13	21	n.a.	n.a.	n.a.	n.a.	n.a.	n.a.	5	12	5	13	n.a.	n.a.

BH906 : Kairab Metabasalt
 BH907 : Kairab Metabasalt
 BH743 : Kairab Meta-andesite
 BH742 : Kairab Metadacite
 BH738 : Kairab Metarhyolite
 BH739 : Kairab Metarhyolite
 BH741 : Kairab Metarhyolite
 BH772 : Kairab Metarhyolite
 BH780 : Kairab Metarhyolite
 BH793 : Kairab Metarhyolite
 BH534 : Kairab Metagabbro
 BH544 : Kairab Metagabbro
 BH561 : Kairab Metagabbro
 BH664 : Kairab Metagabbro
 BH736 : Kairab Metagabbro
 BH761 : Kairab Metagabbro
 BH762 : Kairab Metagabbro
 BH781 : Kairab Metagabbro
 BH833 : Kairab Metagabbro
 BH839 : Kairab Metagabbro

TABLE V (continued)

	BH768	BH784	BH727A	BH745	BH746	BH747	BH748	BH749	BH750	BH751A	BH752	BH753A	BH759	BH878	BH888	BH542	BH549	BH557	BH539	BH624
SiO ₂	71.19	64.04	74.07	71.44	69.75	70.31	71.90	71.71	71.21	72.07	73.69	71.22	72.28	72.22	73.51	64.60	63.31	63.27	69.24	62.96
TiO ₂	.45	.33	.20	.24	.32	.34	.26	.28	.28	.27	.27	.30	.30	.20	.45	.75	.85	.94	.37	1.04
Al ₂ O ₃	13.51	15.67	12.72	13.62	13.97	13.83	13.42	13.39	13.90	13.19	12.62	13.49	13.16	12.97	12.17	16.57	16.59	15.66	15.63	15.98
Fe ₂ O ₃	5.56	8.49	3.47	3.71	5.21	4.95	4.15	4.44	4.21	4.26	3.80	4.81	4.44	5.13	5.12	5.08	6.22	7.64	3.26	6.66
MnO	.14	.16	.10	.90	.15	.12	.04	.12	.10	.11	.02	.15	.10	.07	.25	.08	.13	.19	.08	.11
MgO	.52	1.68	.76	1.18	1.29	1.29	1.13	1.23	1.17	1.25	1.19	1.32	.69	.34	.29	2.06	1.72	1.30	1.15	1.94
CaO	3.15	3.81	2.43	3.05	4.30	4.29	3.92	3.84	4.07	3.57	3.21	4.15	3.11	3.73	2.74	3.71	3.29	3.54	3.06	3.95
Na ₂ O	3.43	5.57	4.56	4.46	3.92	3.91	3.95	3.83	3.84	3.92	3.98	3.58	4.13	3.84	4.05	3.39	4.22	4.50	4.81	4.45
K ₂ O	1.95	.07	1.57	1.30	.98	.85	1.15	1.06	1.13	1.33	1.14	.86	1.72	1.38	1.34	3.50	3.43	2.63	2.29	2.55
P ₂ O ₅	.11	.18	.12	.10	.11	.11	.06	.11	.08	.02	.08	.12	.08	.12	.08	.27	.24	.34	.11	.36
TOTAL	100.00	100.00	100.00	100.00	100.00	100.00	100.00	100.00	100.00	100.00	100.00	100.00	100.00	100.00	100.00	100.00	100.00	100.00	100.00	100.00
Mo	3	2	2	.5	.5	.5	.5	.5	.5	.5	.5	.5	.5	.7	6	n.a.	n.a.	n.a.	n.a.	n.a.
Nb	4	9	9	4	6	6	6	5	5	6	6	6	4	8	15	12	18	66	4	24
Zr	145	78	151	99	147	95	73	73	69	84	105	86	113	89	46	271	582	439	127	583
Y	46	30	51	25	27	31	23	25	22	28	26	24	42	26	37	30	31	158	14	50
Sr	173	214	130	214	218	235	197	208	214	200	192	215	139	176	381	580	337	174	420	300
U	2	.5	.5	.5	.5	.5	.5	.5	.5	.5	.5	.5	2	.5	5	n.a.	n.a.	n.a.	n.a.	n.a.
Rb	35	8	38	36	31	26	31	31	32	36	32	26	38	33	42	64	70	162	55	120
Th	3	.5	1	.5	.5	3	.5	.5	.5	.5	.5	.5	2	.5	5	n.a.	n.a.	n.a.	n.a.	n.a.
Pb	3	6	18	29	10	184	26	4	.5	1	21	8	3	11	5	n.a.	n.a.	n.a.	n.a.	n.a.
Zn	79	71	49	50	71	74	57	61	60	60	53	64	52	56	75	68	96	153	41	104
Cu	3	9	4	2	.5	10	.5	4	6	6	2	.5	8	20	3	14	15	8	2	34
Ni	1	.5	.5	.5	.5	.5	.5	.5	.5	.5	.5	.5	2	.5	2	23	21	5	17	23
Co	5	24	.5	.5	2	3	3	3	1	.5	.5	2	6	19	2	n.a.	n.a.	n.a.	n.a.	n.a.
Cr	10	n.a.	18	n.a.	n.a.	n.a.	n.a.	n.a.	n.a.	17	n.a.	14	15	n.a.	9	33	30	5	30	48
V	5	49	26	59	56	42	56	46	57	46	46	58	24	66	3	85	77	37	40	10
Bb	629	113	353	495	468	360	437	417	406	462	538	401	627	410	1377	2365	514	782	1206	1206
Sc	13	n.a.	10	n.a.	n.a.	n.a.	n.a.	n.a.	n.a.	11	n.a.	16	10	n.a.	21	11	19	23	5	13
Cs	1	n.a.	4	n.a.	1	n.a.	n.a.	n.a.	n.a.	n.a.										
La	13	n.a.	12	n.a.	n.a.	n.a.	n.a.	n.a.	n.a.	2	n.a.	2	12	n.a.	14	65	128	85	27	151
Ce	30	n.a.	23	n.a.	37	n.a.	n.a.	n.a.	n.a.	n.a.										
Nd	22	n.a.	19	n.a.	26	n.a.	n.a.	n.a.	n.a.	n.a.										

BH768	:	Kairab Metateisite	BH752	:	Aunis Tonalite Gneiss
BH784	:	Kairab Metateisite	BH753A	:	Aunis Tonalite Gneiss
BH727A	:	Aunis Tonalite Gneiss	BH759	:	Aunis Tonalite Gneiss
BH745	:	Aunis Tonalite Gneiss	BH878	:	Aunis Tonalite Gneiss
BH746	:	Aunis Tonalite Gneiss	BH888	:	Aunis Tonalite Gneiss
BH747	:	Aunis Tonalite Gneiss	BH542	:	Khorasib Tonalite Gneiss
BH748	:	Aunis Tonalite Gneiss	BH549	:	Khorasib Tonalite Gneiss
BH749	:	Aunis Tonalite Gneiss	BH557	:	Khorasib Tonalite Gneiss
BH750	:	Aunis Tonalite Gneiss	BH539	:	Khorasib Granodiorite Gneiss
BH751A	:	Aunis Tonalite Gneiss	BH624	:	Khorasib Granodiorite Gneiss

TABLE V (continued)

	BH801	BH892	BH537	BH538	BH556	BH723	BH550	BH562	BH471	BH625	BH710	BH724	BH725	BH899	BH900	BH481	BH535	BH564	BH500	BH501
SiO ₂	65.93	67.07	72.78	74.68	76.35	69.51	78.79	68.37	74.74	78.02	74.09	74.25	74.70	72.49	73.34	76.15	74.44	77.05	54.73	56.86
TiO ₂	.42	.53	.39	.23	.17	.56	.10	.54	.15	.07	.18	.15	.15	.10	.11	.14	.15	.01	1.38	1.18
Al ₂ O ₃	15.82	15.98	13.97	13.01	12.48	14.49	11.51	14.80	13.95	11.24	14.02	13.60	13.60	14.27	13.14	12.67	13.86	12.83	16.23	16.07
Fe ₂ O ₃	4.62	3.94	2.47	2.23	1.84	3.97	1.32	4.94	1.45	1.70	1.93	1.98	1.88	2.41	2.70	1.65	1.67	1.07	9.95	8.78
MnO	.14	.06	.11	.05	.04	.08	.02	.09	.06	.03	.06	.04	.05	.13	.22	.04	.03	.03	.14	.15
MgO	.63	1.49	.56	.40	.24	1.06	.09	.48	.19	.08	.29	.39	.32	.00	.00	.16	.27	.08	4.49	4.88
CaO	2.82	3.61	1.21	1.38	1.03	2.48	.75	2.08	.76	.32	1.56	1.61	1.46	1.64	1.55	.63	1.07	.43	7.29	6.72
Na ₂ O	5.17	4.32	4.36	3.19	3.09	3.15	2.90	3.06	4.16	1.89	3.36	2.95	2.96	3.68	3.70	3.50	2.51	4.63	2.51	2.40
K ₂ O	4.16	2.82	4.07	4.79	4.72	4.53	4.52	5.52	4.51	6.64	4.46	4.93	4.84	5.20	5.16	5.04	5.97	3.87	2.96	2.67
P ₂ O ₅	.28	.19	.08	.04	.03	.18	.01	.13	.02	.01	.04	.03	.04	.10	.07	.01	.02	n.a.	.33	.30
TOTAL	100.00	100.00	100.00	100.00	100.00	100.00	100.00	100.00	100.00	100.00	100.00	100.00	100.00	100.00	100.00	100.00	100.00	100.00	100.00	100.00
Mo	7	4	n.a.	6	5	n.a.	n.a.	n.a.	5	3										
Nb	11	6	13	5	8	18	3	24	17	5	11	6	9	12	11	33	3	29	10	8
Zr	244	158	305	196	120	299	105	572	139	204	138	138	135	148	164	171	98	120	231	218
Y	20	12	48	22	15	48	3	51	47	88	38	16	21	31	27	83	8	239	32	29
Sr	1187	669	136	274	52	197	131	157	85	41	140	204	143	180	196	38	403	9	422	470
U	6	5	n.a.	.5	.5	n.a.	n.a.	n.a.	2	2										
Rb	87	58	81	81	127	150	39	106	147	133	171	125	140	172	157	186	78	248	99	106
Th	36	5	n.a.	21	16	n.a.	n.a.	n.a.	11	7										
Pb	46	5	n.a.	32	32	n.a.	n.a.	n.a.	19	3										
Zn	67	49	69	31	33	63	6	77	23	33	39	31	34	42	47	55	11	35	108	83
Cu	7	4	4	17	3	5	10	9	6	18	3	22	1	8	3	5	2	9	6	6
Ni	.5	17	10	12	10	18	10	7	11	9	10	10	10	.5	.5	11	10	9	71	88
Co	32	12	n.a.	16	.5	n.a.	n.a.	n.a.	40	38										
Cr	n.a.	30	16	23	18	30	17	9	19	17	16	16	12	n.a.	n.a.	21	18	22	78	123
V	113	50	19	22	10	44	15	19	6	3	17	13	12	49	52	5	15	.9	188	157
Ba	2634	1358	1343	1317	227	963	1798	1854	633	212	666	1459	947	1075	982	195	4700	17	1293	1012
Sc	n.a.	6	5	2	3	7	2	9	5	1	4	3	3	n.a.	n.a.	2	2	1	23	20
Cs	n.a.	1	n.a.	4	4															
La	n.a.	20	61	47	53	91	22	146	40	48	36	58	45	n.a.	n.a.	74	111	n.a.	33	31
Ce	n.a.	46	n.a.	70	62															
Nd	n.a.	24	n.a.	40	33															
BH801 :	Khorasib Granodiorite Gneiss																			
BH892 :	Khorasib Granodiorite Gneiss																			
BH537 :	Khorasib Monzogranite Gneiss																			
BH538 :	Khorasib Monzogranite Gneiss																			
BH556 :	Khorasib Monzogranite Gneiss																			
BH723 :	Khorasib Monzogranite Gneiss																			
BH550 :	Khorasib Syenogranite Gneiss																			
BH562 :	Khorasib Syenogranite Gneiss																			
BH471 :	Khorasib Monzogranite																			
BH625 :	Khorasib Monzogranite																			
BH710 :	Khorasib Monzogranite																			
BH724 :	Khorasib Monzogranite																			
BH725 :	Khorasib Monzogranite																			
BH899 :	Khorasib Monzogranite																			
BH900 :	Khorasib Monzogranite																			
BH481 :	Khorasib Syenogranite																			
BH535 :	Khorasib Syenogranite																			
BH564 :	Khorasib Syenogranite																			
BH500 :	HFF Basaltic Andesite																			
BH501 :	HFF Basaltic Andesite																			

TABLE V (continued)

	BH509	BH519	BH598	BH604	BH687	BH688	BH689	BH690B	BH691	BH692	BH693	BH694	BH696B	BH574	BH576	BH575	BH512	BH660	BH498	BH504
SiO ₂	56.63	54.52	53.79	54.83	55.62	55.34	54.21	56.12	54.12	54.44	54.41	53.19	55.21	60.46	61.67	64.62	68.74	68.17	71.42	72.82
TiO ₂	1.11	1.21	.82	.95	.93	.94	.92	.96	.99	.75	.92	.97	1.09	.77	.72	.64	.35	.63	.34	.20
Al ₂ O ₃	17.14	16.49	13.05	14.59	15.06	15.10	15.26	15.56	15.66	14.19	15.38	15.19	16.38	15.24	15.21	15.35	14.85	14.50	13.88	13.47
Fe ₂ O ₃	6.44	9.43	9.27	8.70	9.09	8.99	10.36	9.10	9.69	9.87	9.59	10.19	8.03	7.06	6.64	5.62	3.82	4.70	3.68	2.24
MnO	.09	.12	.13	.17	.19	.21	.15	.17	.14	.15	.20	.18	.12	.14	.06	.05	.09	.11	.05	.28
MgO	5.10	5.71	10.84	7.31	5.45	5.40	5.36	5.12	5.65	7.19	5.92	6.41	4.61	3.85	3.53	2.53	1.41	1.08	.16	.68
CaO	6.01	7.87	6.84	5.81	7.74	7.29	7.36	7.98	5.48	8.80	7.89	8.86	8.40	6.14	4.79	2.87	3.15	2.72	1.24	.90
Na ₂ O	5.26	3.17	2.57	4.05	3.64	3.80	3.54	3.17	4.55	2.97	3.39	3.10	4.94	3.34	4.13	4.51	3.79	4.23	3.76	4.31
K ₂ O	1.98	1.21	2.39	3.19	1.96	2.58	2.44	1.47	3.23	1.28	1.90	1.65	.94	2.80	3.04	3.61	3.71	3.66	5.37	4.59
P ₂ O ₅	.25	.27	.30	.40	.33	.35	.40	.34	.49	.34	.39	.25	.27	.21	.20	.20	.09	.19	.09	.50
TOTAL	100.00	100.00	100.00	100.00	100.00	100.00	100.00	100.00	100.00	100.00	100.00	100.00	100.00	100.00	100.00	100.00	100.00	100.00	100.00	100.00
Mo	3	3	3	2	2	.5	2	4	2	.5	1	.5	3	2	3	2	4	4	3	5
Nb	8	7	5	8	8	7	8	6	7	7	7	6	5	10	9	10	17	15	24	15
Zr	204	197	114	162	149	157	151	163	158	124	141	122	109	197	214	233	178	232	498	267
Y	25	29	22	26	30	30	30	26	27	25	29	23	18	39	37	36	38	55	63	82
Sr	356	427	466	239	679	618	609	729	522	615	586	584	845	424	385	309	217	338	110	54
U	2	2	2	2	3	5	4	5	1	.5	2	.5	5	2	5	2	8	4	5	.5
Rb	138	52	74	171	75	90	80	38	104	34	53	50	40	116	137	147	187	145	208	179
Th	10	3	3	3	8	3	5	6	5	1	5	.5	5	10	10	13	18	18	28	25
Pb	3	12	15	3	17	39	26	6	21	25	17	27	6	35	10	20	11	27	27	44
Zn	30	87	106	126	58	40	61	72	51	66	61	44	29	92	6	39	29	83	46	41
Cu	2	2	2	459	23	.5	81	64	10	16	50	19	2	2	2	1	1	12	1	4
Ni	91	132	354	143	36	45	34	39	40	54	40	47	32	25	30	23	19	2	2	6
Co	29	47	53	40	19	23	22	31	28	30	25	26	26	25	17	17	12	6	2	.5
Cr	130	185	712	362	n.a.	n.a.	n.a.	130	n.a.	n.a.	n.a.	n.a.	94	118	105	54	34	21	19	36
V	149	167	165	164	148	142	140	161	129	149	168	169	188	126	114	89	42	58	8	36
Ba	507	521	703	624	605	808	660	523	821	445	653	572	386	952	892	1135	787	625	1274	301
Sc	19	23	25	23	n.a.	n.a.	n.a.	25	n.a.	n.a.	n.a.	n.a.	29	20	16	11	7	8	5	n.a.
Cs	7	5	4	5	n.a.	n.a.	n.a.	3	n.a.	n.a.	n.a.	n.a.	2	2	4	4	5	5	3	n.a.
La	28	27	18	23	n.a.	n.a.	n.a.	19	n.a.	n.a.	n.a.	n.a.	11	25	26	29	34	40	78	n.a.
Ce	50	54	32	44	n.a.	n.a.	n.a.	43	n.a.	n.a.	n.a.	n.a.	25	48	50	56	63	87	153	n.a.
Nd	26	30	23	28	n.a.	n.a.	n.a.	29	n.a.	n.a.	n.a.	n.a.	18	31	30	33	29	49	76	n.a.

BH509	: HFF Basaltic Andesite
BH519	: HFF Basaltic Andesite
BH598	: HFF Basaltic Andesite
BH604	: HFF Basaltic Andesite
BH687	: HFF Basaltic Andesite
BH688	: HFF Basaltic Andesite
BH689	: HFF Basaltic Andesite
BH690B	: HFF Basaltic Andesite
BH691	: HFF Basaltic Andesite
BH692	: HFF Basaltic Andesite
BH693	: HFF Basaltic Andesite
BH694	: HFF Basaltic Andesite
BH696B	: HFF Basaltic Andesite (tuff)
BH574	: HFF Andesite
BH576	: HFF Andesite
BH575	: HFF Dacite
BH512	: HFF Rhyodacite
BH660	: HFF Rhyodacite
BH498	: HFF Rhyolite
BH504	: HFF Rhyolite

TABLE V (continued)

	BH505	BH513	BH583	BH585	BH607	BH608	BH611	BH614	BH615	BH616	BH617	BH620	BH669	BH697	BH705	BH706	BH707	BH708	BH709
SiO ₂	71.40	73.16	76.07	77.16	74.00	76.48	74.08	76.61	77.51	77.82	76.38	73.59	76.91	75.14	74.17	74.05	76.36	75.95	75.97
TiO ₂	.37	.16	.08	.10	.30	.09	.10	.08	.08	.05	.16	.21	.16	.13	.13	.12	.05	.07	.07
Al ₂ O ₃	14.65	12.87	12.16	11.84	13.03	12.06	12.83	11.97	11.42	11.21	11.89	12.61	11.75	11.99	12.46	12.66	11.53	11.80	11.99
Fe ₂ O ₃	2.77	2.41	2.14	1.76	2.62	2.13	1.98	1.94	2.08	2.08	2.28	3.07	2.15	2.28	2.27	2.32	1.75	1.88	1.92
MnO	.09	.12	.02	.07	.02	.02	.14	.05	.06	.05	.06	.14	.02	.02	.13	.08	.01	.05	.09
MgO	.46	.63	.06	.52	.01	.06	.53	.06	.06	.06	.06	.15	.04	.47	.51	.48	.39	.43	.43
CaO	1.14	.77	.39	.62	1.18	.38	.46	.44	.26	.22	.37	1.14	.30	.72	.55	.37	.52	.46	.50
Na ₂ O	5.60	5.29	4.80	3.47	4.65	5.06	4.84	4.36	3.59	4.03	4.37	5.11	4.11	4.78	4.23	5.37	4.36	4.93	4.75
K ₂ O	3.43	4.32	4.50	4.32	4.16	3.93	4.82	4.66	5.10	4.66	4.60	3.94	4.73	4.49	4.67	4.49	5.03	4.34	4.18
P ₂ O ₅	.08	.27	.02	.14	.09	.02	.21	.01	.01	.00	.02	.04	.01	.00	.00	.06	.00	.09	.10
TOTAL	100.00	100.00	100.00	100.00	100.00	100.00	100.00	100.00	100.00	100.00	100.00	100.00	100.00	100.00	100.00	100.00	100.00	100.00	100.00
Mo	5	8	2	2	1	2	5	3	3	.7	2	2	3	5	8	6	5	3	5
Nb	21	13	29	16	18	34	17	28	26	31	16	13	15	16	13	13	25	22	24
Zr	318	404	250	235	278	238	254	251	237	206	305	487	293	266	408	398	223	220	219
Y	53	80	106	107	61	102	108	106	92	107	83	69	64	93	80	77	130	127	131
Sr	135	45	69	36	110	38	54	46	45	36	40	41	18	55	40	30	24	53	33
U	4	.5	8	.5	2	7	2	10	5	8	5	2	2	.5	3	.5	4	.5	2
Rb	110	170	132	205	123	138	206	213	219	219	150	148	188	212	186	180	328	276	285
Th	21	24	30	24	28	31	11	31	27	29	22	15	22	25	27	23	40	32	37
Pb	3	33	23	40	9	7	11	15	33	15	17	28	34	7	30	16	26	11	48
Zn	10	3	7	51	11	7	7	18	64	9	6	81	41	28	8	11	25	44	53
Cu	4	3	77	18	1	3	7	3	12	10	4	4	1	.5	18	18	7	.5	10
Ni	7	5	4	7	4	2	5	3	2	2	3	3	2	9	.5	4	5	16	7
Co	2	5	.9	.5	.9	9	5	.9	.9	2	.9	1.0	.9	.5	.5	.5	.5	.5	.5
Cr	25	n.a.	18	n.a.	16	26	n.a.	30	19	20	20	20	20	n.a.	n.a.	n.a.	n.a.	n.a.	n.a.
V	12	28	4	41	23	15	39	6	4	4	6	4	4	42	32	38	27	39	27
Ba	1286	830	125	113	529	277	157	186	148	94	1274	1083	1066	2081	858	827	88	166	107
Sc	5	n.a.	.4	n.a.	5	.4	n.a.	.4	.4	.4	6	5	6	n.a.	n.a.	n.a.	n.a.	n.a.	n.a.
Cs	1	n.a.	1	n.a.	1	1	n.a.	1	1	1	3	3	4	n.a.7	n.a.	n.a.	n.a.	n.a.	n.a.
La	50	n.a.	64	n.a.	54	36	n.a.	57	57	48	53	57	43	n.a.	n.a.	n.a.	n.a.	n.a.	n.a.
Ce	101	n.a.	130	n.a.	114	87	n.a.	118	125	99	109	117	102	n.a.	n.a.	n.a.	n.a.	n.a.	n.a.
Nd	54	n.a.	73	n.a.	62	47	n.a.	68	69	55	66	67	56	n.a.	n.a.	n.a.	n.a.	n.a.	n.a.

BH505 : HFF Rhyolite
 BH513 : HFF Rhyolite
 BH583 : HFF Rhyolite
 BH585 : HFF Rhyolite
 BH607 : HFF Rhyolite
 BH608 : HFF Rhyolite
 BH611 : HFF Rhyolite
 BH614 : HFF Rhyolite
 BH615 : HFF Rhyolite
 BH616 : HFF Rhyolite
 BH617 : HFF Rhyolite
 BH620 : HFF Rhyolite
 BH669 : HFF Rhyolite
 BH697 : HFF Rhyolite
 BH699 : HFF Rhyolite
 BH705 : HFF Rhyolite
 BH706 : HFF Rhyolite
 BH707 : HFF Rhyolite
 BH708 : HFF Rhyolite
 BH709 : HFF Rhyolite

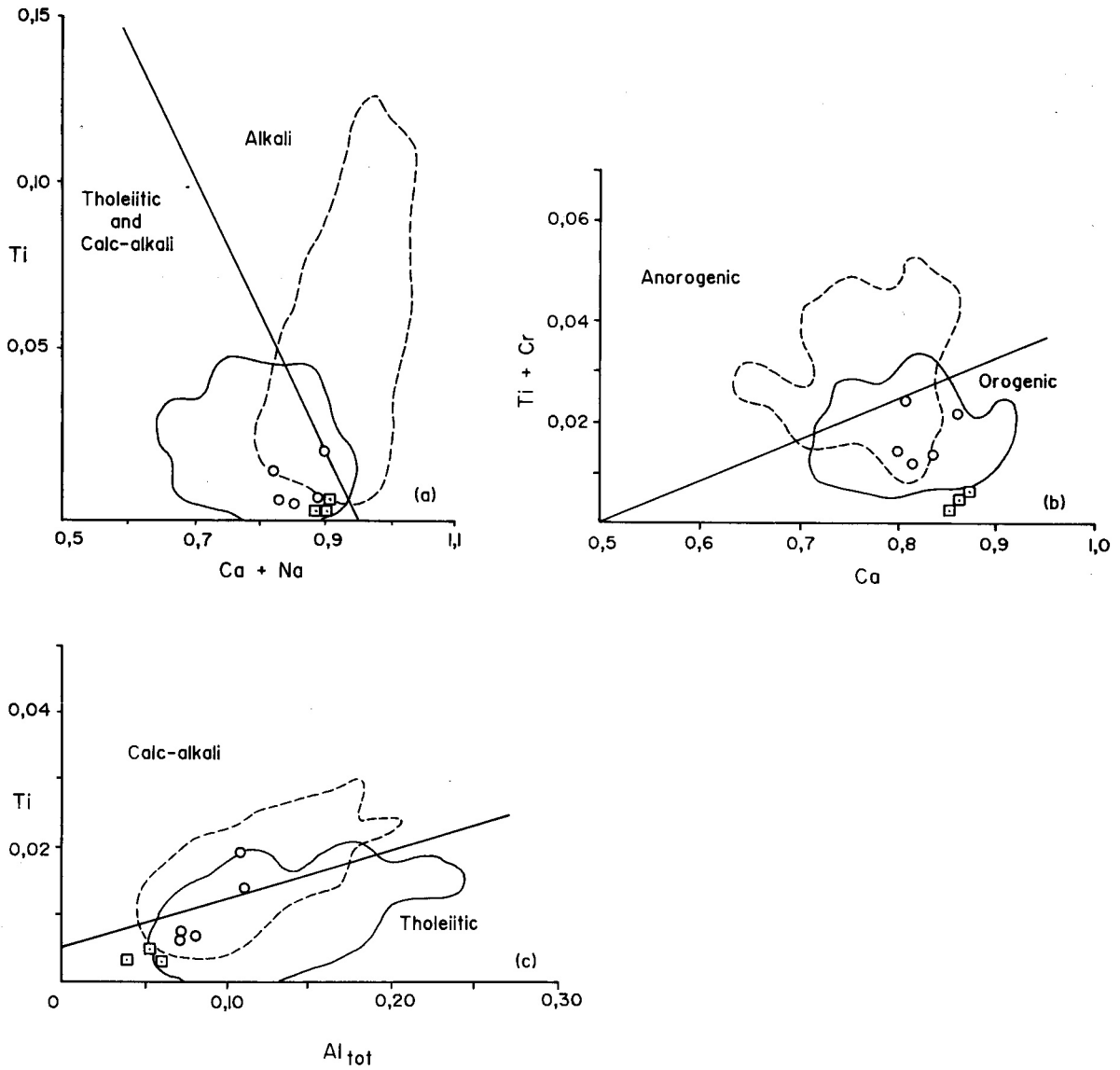


Fig. C.11: Magmatic affinities of clinopyroxene phenocrysts in the HFF and Barby Formation according to the discrimination diagrams of Leterrier *et al.* (1982). Each diagram shows the dividing line between, and outermost contours of, the fields distinguished.

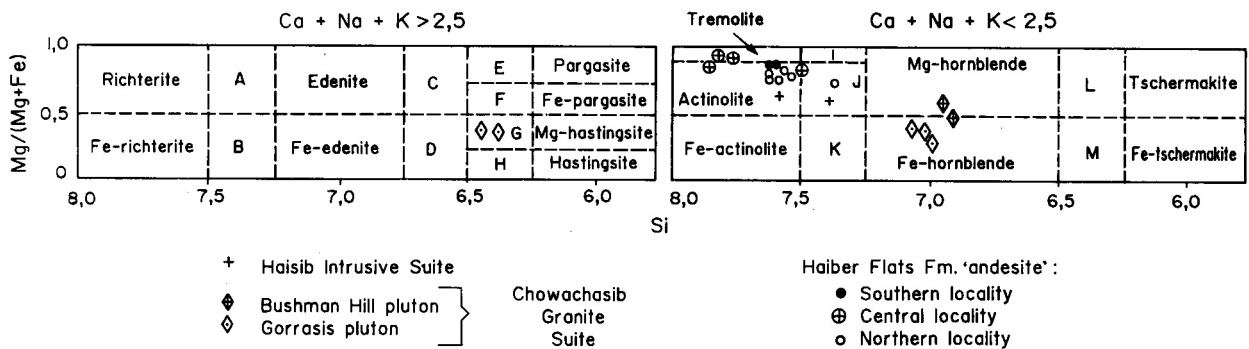


Fig. C.12: Amphibole compositions in HFF "andesite" and post-HFF granitoids plotted in terms of the classification of Leake (1968). All data normalised to 23 oxygens. Only hornblendes from the Chowachasib Granite Suite are igneous in origin. Fields as in Fig. B.4.

TABLE V (continued)

	BH596	BH658	BH499	BH703	BH529	BH847	BH569	BH817	BH818	BH819	BH820	BH821	BH822	BH865	BH866	BH823	BH491	BH868	BH893	BH527
SiO ₂	64.61	63.28	66.06	67.85	70.22	45.72	51.56	48.29	49.39	47.87	48.57	47.77	46.79	50.30	49.51	52.08	53.30	54.47	52.42	53.70
TiO ₂	.74	.85	.60	.43	.57	.73	.80	.48	.41	.23	.22	.28	.13	.79	.80	.23	1.00	.82	1.01	.97
Al ₂ O ₃	15.15	15.53	15.42	15.47	14.22	7.53	13.28	13.50	15.27	18.69	27.27	16.00	21.74	11.98	13.34	19.95	15.70	21.08	14.39	15.58
Fe ₂ O ₃	4.81	4.76	4.55	4.05	3.67	12.34	10.36	8.03	8.82	7.51	4.56	8.05	7.76	11.23	11.31	6.66	9.40	5.98	9.68	9.34
MnO	.07	.08	.10	.07	.07	.20	.19	.17	.16	.14	.07	.14	.11	.19	.18	.13	.16	.08	.16	.16
MgO	2.35	2.52	1.70	1.38	.73	21.40	10.50	8.80	10.29	9.70	3.77	11.70	10.13	13.59	11.29	8.35	6.95	2.40	7.56	6.84
CaO	2.86	3.10	3.31	3.24	2.00	10.18	8.43	19.12	14.11	14.05	12.42	14.76	11.71	8.90	9.69	9.79	7.92	7.99	8.12	8.25
Na ₂ O	3.66	3.86	4.37	4.37	3.82	1.13	2.61	1.50	1.40	1.76	2.68	1.28	1.22	2.17	2.63	2.71	2.92	4.08	3.46	2.75
K ₂ O	5.48	5.72	3.72	2.97	4.57	.54	1.75	.13	.14	.04	.37	.04	.38	.52	.98	.09	2.38	2.48	2.69	2.15
P ₂ O ₅	.27	.29	.17	.17	.13	.23	.51	.00	.02	.02	.06	.00	.03	.34	.26	.02	.27	.62	.50	.27
TOTAL	100.00	100.00	100.00	100.00	100.00	100.00	100.00	100.00	100.00	100.00	100.00	100.00	100.00	100.00	100.00	100.00	100.00	100.00	100.00	100.00
Mo	5	3	3	2	n.a.	5	4	2	4	3	1	4	3	1	5	5	n.a.	5	5	n.a.
Nb	18	19	17	8	14	15	.9	2	2	2	2	2	2	2	2	2	6	3	5	5
Zr	346	402	270	178	360	83	45	19	16	13	25	15	17	35	58	17	126	112	140	140
Y	33	31	43	23	50	14	23	16	11	7	2	10	2	24	14	2	24	19	17	26
Sr	363	279	291	312	177	409	736	324	380	374	683	323	558	661	792	565	521	1266	860	536
U	7	7	2	2	n.a.	6	2	6	6	5	5	5	5	6	6	5	n.a.	5	5	n.a.
Rb	297	309	124	109	111	12	31	2	2	2	5	2	7	7	21	2	79	57	87	54
Th	27	29	13	6	n.a.	6	3	6	6	6	5	6	6	6	6	5	n.a.	5	6	n.a.
Pb	33	24	26	11	n.a.	7	11	7	7	6	6	6	6	7	7	6	n.a.	6	6	n.a.
Zn	44	52	57	52	62	78	83	59	62	39	50	43	60	94	80	45	77	48	76	86
Cu	59	67	10	11	5	35	13	12	88	91	21	97	10	76	37	6	63	155	68	64
Ni	48	53	11	11	12	714	254	93	128	121	54	209	171	385	207	39	71	22	80	65
Co	14	14	12	7	n.a.	96	49	45	53	52	29	59	64	59	54	33	n.a.	17	39	n.a.
Cr	116	117	43	33	20	1493	657	288	678	403	6	671	101	873	599	203	277	38	232	271
V	78	86	65	47	30	151	166	225	134	74	37	93	30	156	190	51	207	160	158	207
Ba	1151	736	1047	818	1111	201	1299	49	35	18	70	13	74	573	527	30	790	951	933	809
Sc	9	11	10	9	8	42	25	49	49	33	7	44	13	30	29	21	28	11	21	27
Cs	4	11	1	3	n.a.	2	2	2	2	2	2	2	2	2	2	2	n.a.	2	2	n.a.
La	46	39	45	24	113	18	22	1	1	1	1	1	1	12	11	1	27	24	19	26
Ce	90	83	87	51	n.a.	49	41	3	3	3	5	3	3	29	28	2	n.a.	55	47	n.a.
Nd	45	40	48	27	n.a.	37	30	6	5	2	3	2	2	23	21	1	n.a.	35	33	n.a.

BH596 : Haisib Quartz Syenite
 BH658 : Haisib Quartz Syenite
 BH499 : Haisib Granodiorite
 BH703 : Haisib Granodiorite
 BH529 : Haisib Monzogranite
 BH847 : Saffier Picrite
 BH569 : Saffier Gabbro
 BH817 : Saffier Monzogabbro
 BH818 : Saffier Gabbro
 BH819 : Saffier Monzogabbro
 BH820 : Saffier Gabbro
 BH821 : Saffier Gabbro
 BH822 : Saffier Gabbro
 BH865 : Saffier Gabbro
 BH866 : Saffier Gabbro
 BH823 : Saffier Norite
 BH491 : Saffier Monzogabbro
 BH868 : Saffier Monzogabbro
 BH893 : Saffier Monzonite
 BH527 : Saffier Diorite

TABLE V (continued)

	BH814	BH845	BH850	BH851	BH854	BH856	BH874	BH618	BH619	BH661	BH677	BH678	BH679	BH680	BH681	BH682	BH683	BH684
SiO ₂	57.65	55.22	57.23	59.41	59.63	54.01	55.07	73.48	76.86	76.79	76.36	75.78	76.29	77.05	76.72	76.36	75.12	76.72
TiO ₂	.77	.90	.94	.87	.65	.78	.89	.22	.10	.16	.09	.02	.01	.02	.03	.06	.11	.04
Al ₂ O ₃	17.53	17.53	18.35	18.64	19.49	15.94	17.45	12.45	11.24	11.90	11.72	11.76	11.57	11.45	11.62	11.51	12.02	11.26
Fe ₂ O ₃	5.82	5.92	5.44	4.14	3.41	6.93	5.95	2.66	1.81	2.07	1.80	1.92	1.80	1.71	1.99	1.61	1.73	1.80
MnO	.09	.08	.08	.06	.06	.11	.09	.03	.07	.02	.02	.10	.07	.04	.06	.11	.42	.07
MgO	2.54	3.83	2.19	1.53	1.32	6.75	4.14	.63	.47	.04	.38	.40	.38	.34	.39	.45	.52	.36
CaO	4.26	4.77	3.99	3.10	3.04	5.62	4.73	.94	.67	.37	.37	.40	.45	.31	.34	.40	.52	.47
Na ₂ O	3.65	3.90	3.75	3.99	3.82	2.81	3.91	4.97	4.49	4.11	4.02	5.00	4.84	4.44	3.40	5.19	4.88	4.95
K ₂ O	7.13	7.08	7.35	7.78	8.13	6.23	7.02	4.47	4.29	4.71	4.63	4.62	4.59	4.61	5.38	4.15	4.26	4.35
P ₂ O ₅	.56	.77	.69	.49	.45	.80	.76	.15	.00	.03	.00	.01	.00	.03	.06	.15	.41	.00
TOTAL 100.00	100.00	100.00	100.00	100.00	100.00	100.00	100.00	100.00	100.00	100.00	100.00	100.00	100.00	100.00	100.00	100.00	100.00	100.00
Mo	6	5	6	6	7	5	8	5	.5	2	4	5	5	2	9	.5	4	6
Nb	6	7	10	6	6	2	9	13	9	13	17	23	22	17	28	10	21	30
Zr	142	189	149	98	129	100	183	362	235	290	226	221	210	183	200	166	200	233
Y	17	19	18	13	7	14	14	78	99	65	104	146	147	131	135	116	120	178
Sr	509	884	922	911	1240	944	878	77	48	22	12	17	18	34	61	29	20	16
U	5	5	5	5	5	5	5	.5	.5	2	5	.5	.5	.5	2	19	.5	4
Rb	432	416	412	369	382	358	437	133	150	162	199	324	319	325	190	235	274	314
Th	12	12	14	5	5	6	12	20	26	22	15	43	36	45	34	50	35	47
Pb	39	33	29	30	26	31	33	25	13	63	35	7	100	369	27	271	168	61
Cu	78	41	47	35	26	48	42	49	14	20	59	90	124	37	.5	60	150	170
Zn	74	45	146	168	102	37	110	.5	.5	2	3	10	.5	3	7	3	3	3
Ni	28	62	14	8	11	186	77	4	.5	2	3	9	21	8	.5	3	13	12
Co	14	15	12	8	7	27	17	.5	.5	.9	.5	.5	.5	.5	7	.5	.5	.5
Cr	25	112	13	9	7	312	132	n.a.	n.a.	15	22	n.a.						
V	160	187	167	137	105	143	172	38	23	8	3	27	39	28	19	27	38	27
Ba	1111	1699	1758	1933	2888	1787	1677	393	114	1149	353	66	103	135	244	107	101	61
Sc	14	10	8	6	4	12	9	n.a.	n.a.	5	n.a.							
Cs	4	14	9	6	9	12	15	n.a.	n.a.	2	n.a.							
La	17	32	31	29	22	28	33	n.a.	n.a.	49	n.a.							
Ce	39	66	66	57	46	56	68	n.a.	n.a.	112	n.a.							
Nd	26	40	38	31	26	36	39	n.a.	n.a.	62	n.a.							

BH814 : Saffier Syenite
 BH845 : Saffier Syenite
 BH850 : Saffier Syenite
 BH851 : Saffier Syenite
 BH854 : Saffier Syenite
 BH856 : Saffier Syenite
 BH874 : Saffier Syenite
 BH618 : Awasib Granite
 BH619 : Awasib Granite
 BH661 : Awasib Granite
 BH677 : Awasib Granite
 BH678 : Awasib Granite
 BH679 : Awasib Granite
 BH680 : Awasib Granite
 BH681 : Awasib Granite
 BH682 : Awasib Granite
 BH683 : Awasib Granite
 BH684 : Awasib Granite
 BH668 : Awasib Granite
 BH671 : Awasib Granite
 BH677 : Awasib Granite
 BH678 : Awasib Granite
 BH679 : Awasib Granite
 BH680 : Awasib Granite
 BH681 : Awasib Granite
 BH682 : Awasib Granite
 BH683 : Awasib Granite
 BH684 : Awasib Granite

TABLE V (continued)

	BH685	BH700	BH797	BH848	BH880	BH894	BH662	BH760	BH807	BH835
SiO ₂	76.57	74.56	75.38	70.00	75.38	74.26	77.34	74.92	75.04	73.90
TiO ₂	.06	.20	.18	.38	.13	.20	.10	.28	.29	.32
Al ₂ O ₃	11.66	12.43	13.13	15.39	13.13	13.49	11.77	12.64	12.61	12.94
Fe ₂ O ₃	1.78	2.67	1.49	2.63	1.36	1.78	1.59	2.49	2.11	2.51
MnO	.10	.05	.02	.02	.05	.04	.02	.05	.00	.06
MgO	.56	.19	.17	.72	.23	.39	.11	.39	.41	.30
CaO	.48	.75	.88	2.10	1.18	1.43	.69	.96	1.09	.96
Na ₂ O	4.42	4.19	4.53	3.91	4.11	3.93	3.39	4.19	3.69	4.76
K ₂ O	4.32	4.90	4.26	4.80	4.41	4.43	5.04	4.03	4.71	4.21
P ₂ O ₅	.05	.04	.03	.11	.03	.04	.02	.05	.06	.04
TOTAL	100.00	100.00	100.00	100.00	100.00	100.00	100.00	100.00	100.00	100.00
Mo	.5	3	4	7	3	4	2	2	4	6
Nb	16	15	9	8	8	7	16	13	9	6
Zr	214	305	170	323	74	97	120	294	173	248
Y	145	70	24	27	10	21	49	48	40	33
Sr	42	39	108	476	132	182	19	78	97	124
U	10	4	4	4	4	4	4	2	4	4
Rb	205	165	108	129	103	74	223	124	128	58
Th	50	18	29	11	10	5	36	16	17	5
Pb	193	35	24	25	23	19	29	20	24	13
Zn	32	112	13	39	25	30	22	41	34	52
Cu	15	7	2	4	2	1	1	2	4	2
Ni	16	4	3	7	4	5	3	4	6	3
Co	.5	.9	2	4	2	3	.9	2	3	3
Cr	n.a.	22	12	16	11	10	15	17	13	7
V	40	10	3	23	9	13	2	14	14	7
Ba	107	318	1515	2665	429	738	83	535	747	2054
Sc	n.a.	2	2	3	4	3	2	6	4	3
Cs	n.a.	5	1	1	1	1	4	5	3	1
La	n.a.	77	50	49	21	39	53	42	42	71
Ce	n.a.	156	90	100	41	63	111	85	77	125
Nd	n.a.	83	42	50	16	26	51	42	35	64

- BH685 : Awasib Granite
- BH700 : Awasib Granite
- BH797 : Chowachasib Monzogranite
- BH848 : Chowachasib Monzogranite
- BH880 : Chowachasib Monzogranite
- BH894 : Chowachasib Monzogranite
- BH662 : Chowachasib Syenogranite
- BH760 : Chowachasib Syenogranite
- BH807 : Chowachasib Syenogranite
- BH835 : Chowachasib K-feldspar Granite

TABLE VI: Partition coefficients used in petrogenetic modelling.

(a) Closed system fractional crystallisation (FC) and assimilation-fractional crystallisation (AFC) models.

<i>Kd's for basaltic andesites</i>										<i>Kd's for andesites</i>							
	Plag	Oi	Cpx	Mt	Ap		Plag	Opx	Cpx	Mt	Ap		Plag	Opx	Cpx	Mt	Ap
Nb	0.160	0.010	0.390	10.000	0.100		0.025	0.350	0.200	1.000	0.100		0.025	0.350	0.200	1.000	0.100
Zr	0.030	0.010	0.200	0.200	0.100		0.100	0.080	0.300	0.200	0.100		0.100	0.080	0.300	0.200	0.100
Y	0.060	0.010	1.500	0.200	30.000		0.045	0.450	0.700	0.200	30.000		0.045	0.450	0.700	0.200	30.000
Sr	1.270	0.010	0.070	0.100	3.000		2.700	0.040	0.070	0.600	3.000		2.700	0.040	0.070	0.600	3.000
Rb	0.360	0.010	0.050	0.004	0.100		0.020	0.015	0.013	0.004	0.100		0.020	0.015	0.013	0.004	0.100
Th	0.010	0.250	0.152	0.040	0.100		0.004	0.054	0.035	0.040	0.100		0.004	0.054	0.035	0.040	0.100
Ni	0.050	16.800	2.110	1.200	0.200		0.111	5.200	5.200	4.000	0.200		0.111	5.200	5.200	4.000	0.200
Co	0.027	4.110	1.220	6.100	0.200		0.280	4.000	1.800	5.200	0.200		0.280	4.000	1.800	5.200	0.200
Cr	0.027	1.650	21.680	22.000	0.200		0.024	9.300	9.700	5.000	0.200		0.024	9.300	9.700	5.000	0.200
V	0.010	0.085	1.000	17.000	0.100		0.010	0.557	1.000	17.000	0.100		0.010	0.557	1.000	17.000	0.100
Ba	1.050	0.040	0.100	0.050	0.100		0.083	0.060	0.038	0.050	0.100		0.083	0.060	0.038	0.050	0.100
Sc	0.010	0.155	2.940	1.600	0.220		0.017	2.700	6.880	1.740	0.220		0.017	2.700	6.880	1.740	0.220
La	0.690	0.010	0.100	0.400	15.000		0.127	0.238	0.140	0.446	15.000		0.127	0.238	0.140	0.446	15.000
Ce	0.710	0.010	0.200	0.400	25.000		0.300	0.301	0.508	0.419	25.000		0.300	0.301	0.508	0.419	25.000
Nd	0.370	0.010	0.400	0.400	45.000		0.240	0.144	0.645	0.435	45.000		0.240	0.144	0.645	0.435	45.000

<i>Kd's for dacites</i>										<i>Kd's for rhyodacites and rhyolites</i> (specifically models incorporating R1 rhyolite)													
	Plag	Cpx	Hbl	Biot	Mt	Ap	Qtz		Plag	K-spar	Cpx	Biot	Mt	Ap	Qtz		Plag	K-spar	Cpx	Biot	Mt	Ap	Qtz
Nb	0.025	0.210	0.800	1.655	1.000	0.100	0.010		0.060	0.006	0.200	3.100	10.700	0.100	0.010		0.060	0.006	0.200	3.100	10.700	0.100	0.010
Zr	0.020	1.000	1.600	1.500	1.800	0.100	0.075		0.370	0.290	2.720	4.190	1.200	0.100	0.075		0.370	0.290	2.720	4.190	1.200	0.100	0.075
Y	0.040	0.700	1.390	0.240	1.440	30.000	0.010		0.040	0.006	1.500	0.990	1.300	30.000	0.010		0.040	0.006	1.500	0.990	1.300	30.000	0.010
Sr	2.700	0.650	0.630	0.145	0.500	3.000	0.010		2.960	5.100	0.516	0.290	10.000	3.000	0.010		2.960	5.100	0.516	0.290	10.000	3.000	0.010
Rb	0.032	0.090	0.070	5.000	0.004	0.100	0.008		0.150	1.000	0.047	3.530	0.004	0.100	0.015		0.150	1.000	0.047	3.530	0.004	0.100	0.015
Th	0.050	0.250	0.140	0.563	0.070	0.100	0.120		0.040	0.070	3.937	1.540	0.320	0.100	0.018		0.040	0.070	3.937	1.540	0.320	0.100	0.018
Ni	0.217	6.000	12.200	1.220	13.100	0.200	0.010		1.100	1.440	0.870	1.220	1.190	0.200	0.001		1.100	1.440	0.870	1.220	1.190	0.200	0.001
Co	0.035	3.700	7.750	27.000	11.000	0.200	0.010		0.080	0.610	11.000	27.750	35.000	0.200	0.001		0.080	0.610	11.000	27.750	35.000	0.200	0.001
Cr	0.030	1.000	35.500	3.960	5.000	0.200	0.010		0.030	0.560	2.868	11.480	20.000	0.200	0.001		0.030	0.560	2.868	11.480	20.000	0.200	0.001
V	0.460	2.300	6.450	25.000	34.300	0.100	0.010		0.460	0.550	1.600	25.000	20.000	0.100	0.001		0.460	0.550	1.600	25.000	20.000	0.100	0.001
Ba	0.650	0.036	0.189	6.360	0.199	0.100	0.032		1.200	4.900	0.131	3.000	0.850	0.100	0.009		1.200	4.900	0.131	3.000	0.850	0.100	0.009
Sc	0.013	6.200	9.540	4.100	2.200	0.220	0.016		0.030	0.050	23.350	10.802	4.475	0.220	0.016		0.030	0.050	23.350	10.802	4.475	0.220	0.016
La	0.140	0.160	0.191	0.030	0.880	15.000	0.006		0.288	0.155	4.695	0.744	0.670	15.000	0.006		0.288	0.155	4.695	0.744	0.670	15.000	0.006
Ce	0.127	0.231	0.339	0.037	0.117	25.000	0.006		0.194	0.020	1.600	0.786	0.745	25.000	0.006		0.194	0.020	1.600	0.786	0.745	25.000	0.006
Nd	0.123	0.455	0.879	0.044	0.250	45.000	0.012		0.165	0.020	3.133	0.800	1.200	45.000	0.012		0.165	0.020	3.133	0.800	1.200	45.000	0.012

TABLE VI (continued)

Kd's for rhyodacites and rhyolites (specifically models incorporating R2 rhyolite)

	Plag	K-spar	Hbl	Biot	Mt	Ap	Qtz
Nb	0.060	0.006	2.500	3.100	6.500	0.100	0.010
Zr	0.370	0.290	1.600	2.000	1.200	0.100	0.075
Y	0.040	0.006	5.800	0.990	1.300	30.000	0.010
Sr	4.400	6.223	0.630	1.110	10.000	3.000	0.010
Rb	0.150	1.000	0.070	3.530	0.004	0.100	0.015
Th	0.040	0.070	0.154	1.540	0.320	0.100	0.018
Ni	1.100	1.440	8.500	1.220	1.190	0.200	0.001
Co	0.080	0.610	7.750	28.500	35.000	0.200	0.001
Cr	0.030	0.560	11.000	3.960	20.000	0.200	0.001
V	0.460	0.550	45.000	25.000	20.000	0.100	0.001
Ba	0.370	1.190	0.100	3.000	0.850	0.100	0.009
Sc	0.010	0.010	13.500	10.802	4.475	0.220	0.016
La	0.288	0.155	2.000	0.744	0.670	15.000	0.006
Ce	0.205	0.020	0.899	1.210	0.745	25.000	0.006
Nd	0.120	0.020	2.800	0.800	1.200	45.000	0.012

Data sources:
 FC & AFC models utilise Kd's from an unpublished compilation by Ewart and Duncan (pers. comm., 1987).
 Partial melting models for pyrolyte utilise Kd's from Frey *et al.* (1978) and Le Roex (1980).
 Partial melting models for Lower and Bulk crust utilise Kd's from Hanson (1978), Pearce and Norry (1979), Henderson (1984), Nash and Crecraft (1985), and an unpublished compilation by Ewart and Duncan (pers. comm., 1987).
Mineral abbreviations:
 Plag (plagioclase), K-spar (K-feldspar), Ol (olivine), Cpx (clinopyroxene), Opx (orthopyroxene), Hbl (hornblende), Biot (biotite), Mt (magnetite), Ilm (ilmenite), Ap (apatite), Qtz (quartz), Gt (garnet).

(b) Partition coefficients for partial melting (PM) models.

Kd's for pyrolyte

	Ol	Opx	Cpx	Gt	Plag	Opx	Cpx	Ilm	K-spar	Qtz
Nb	0.0500	0.0100	0.0900	0.0100	Nb	0.025	0.350	10.000	0.010	0.001
Zr	0.0100	0.0100	0.2200	1.2000	Zr	0.200	0.080	3.000	0.150	0.010
Y	0.0020	0.0090	0.5000	1.4000	Y	0.040	0.400	0.100	0.006	0.001
Ba	0.0001	0.0001	0.0001	0.0001	Ba	0.369	0.038	0.010	6.120	0.009
Sr	0.0001	0.0001	0.0001	0.0001	Sr	4.400	0.040	0.010	3.870	0.001
Rb	0.0001	0.0001	0.0001	0.0001	Rb	0.032	0.010	0.010	0.340	0.002
Ni	10.0000	4.0000	1.8000	0.8000	Ni	0.217	16.950	10.000	1.820	0.001
Co	2.0000	2.0000	1.2000	2.0000	Co	0.051	10.520	10.000	0.610	0.001
V	0.0100	0.3000	1.5000	0.2700	V	0.460	1.425	10.000	0.550	0.001
La	0.0005	0.0005	0.0200	0.0010	La	0.245	0.422	7.100	0.100	0.018
Ce	0.0008	0.0009	0.0400	0.0033	Ce	0.200	0.456	7.800	0.040	0.014
Nd	0.0013	0.0019	0.0900	0.0184	Nd	0.162	0.571	7.600	0.030	0.016
Sm	0.0019	0.0028	0.1400	0.0823	Sm	0.127	0.702	6.900	0.020	0.017
Eu	0.0019	0.0036	0.1600	0.1333	Eu	2.000	0.507	2.500	1.130	0.080
Gd	0.0019	0.0063	0.1800	0.1951	Gd	0.090	0.950	6.700	0.011	0.018
Tb	0.0019	0.0089	0.1900	0.2568	Tb	0.114	0.835	6.500	0.010	0.019
Yb	0.0040	0.0286	0.2000	4.0000	Yb	0.044	0.867	4.100	0.012	0.017
Lu	0.0048	0.0380	0.1900	5.7000	Lu	0.113	0.922	3.600	0.006	0.011

Kd's for Lower and Bulk Crust

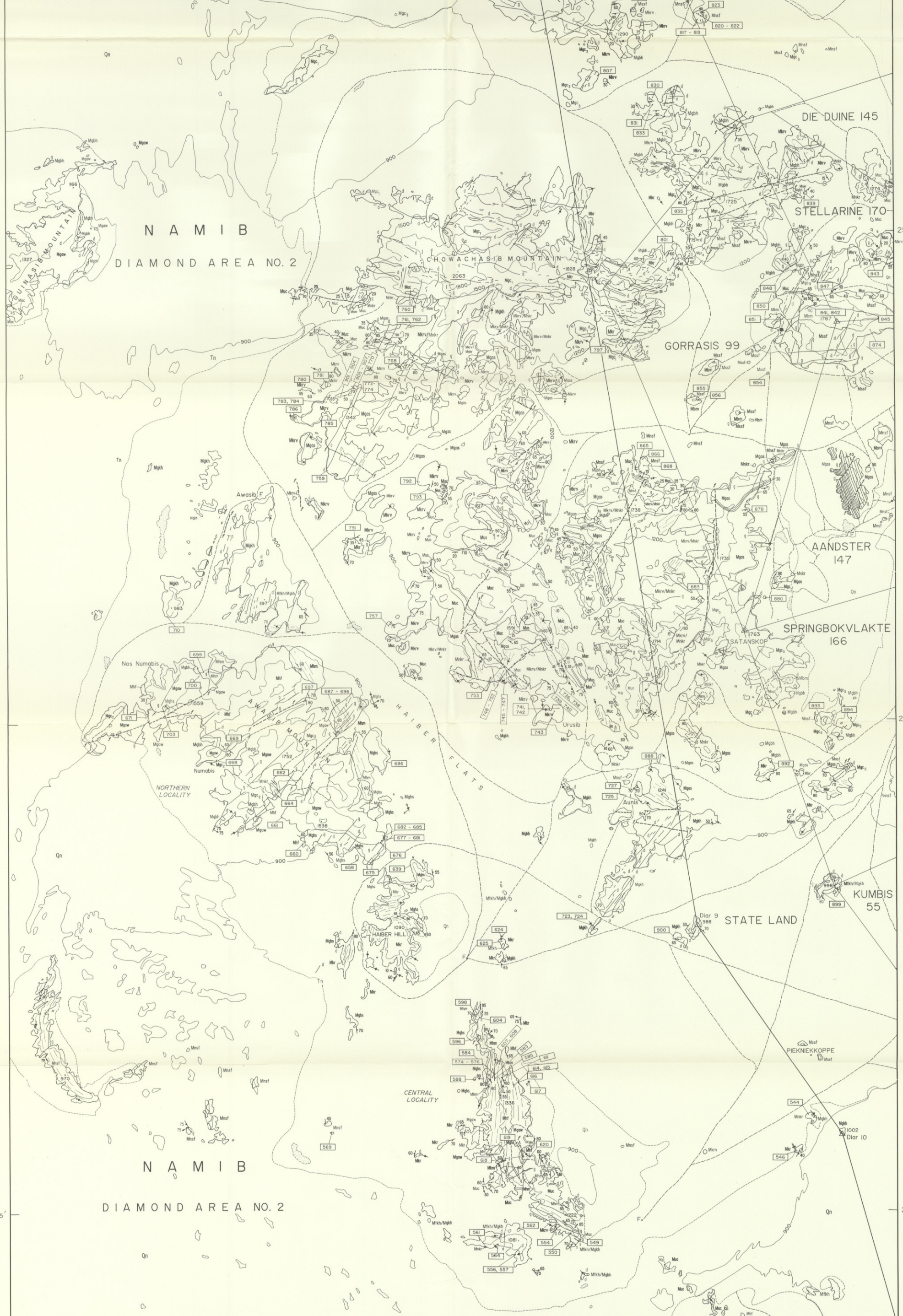
**GEOLOGICAL MAP OF THE AWASIB MOUNTAIN TERRAIN,
SOUTHERN NAMIBIA**

LOCALITY MAP



- Mean magnetic declination
1975 West of True North
(1979.0). Mean annual change
7 Eastwards (1971 - 1975)
- Trigonometrical beacon with height in metres
 - Spot height in metres
 - Farm house
 - Tracks
 - Dune margin
 - Cadastral boundary
 - Diamond area boundary
 - Waterholes and wells
 - Contour lines (intervals 300 metres)
 - Dry pan
 - Geochronological sample locality (All numbers prefixed by 50)

Mapping, compilation and drawing by B.G. Hoel
Final draughting by S.P. Cloete
Geological Survey of Namibia, Windhoek (1989)



LITHOSTRATIGRAPHIC UNITS		STRUCTURAL SYMBOLS	
Surficial deposits, mainly alluvium, sand, gravel and calcareate	Partially consolidated (Tn) and unconsolidated (Qn) dune deposits of the Namib Desert	Lithological contact or limit of outcrop	Inferred, approximate or gradational lithological contact
Phonolite dyke	Felsic dyke, sill or plug (various ages)	Mafic dyke, sill or plug (various ages)	Strike and dip of bedding or primary layering
Mgpc	Mgmv	Mgh	Strike and dip of overturned bedding or primary layering
Mghs	Mgh	Mgh	Strike and dip of foliation or cleavage
Mgh	Mgh	Mgh	Strike and dip of bedding-parallel foliation or cleavage
Mgh	Mgh	Mgh	Strike and dip of spaced foliation or cleavage
Mgh	Mgh	Mgh	Strike and dip of bedding-parallel or primary layering-parallel foliation
Mgh	Mgh	Mgh	Trend and plunge of lineation
Mgh	Mgh	Mgh	Trend and plunge of pebble stretching lineation
Mgh	Mgh	Mgh	Trend and plunge of lineation combined with strike and dip of foliation or cleavage
Mgh	Mgh	Mgh	Syncline axis
Mgh	Mgh	Mgh	Anticline axis
Mgh	Mgh	Mgh	Fault
Mgh	Mgh	Mgh	Thrust
Mgh	Mgh	Mgh	Shear
Mgh	Mgh	Mgh	Dip of shear plane
Mgh	Mgh	Mgh	Form lines representing bedding, primary layering or foliation

MINISTRY OF MINES
AND ENERGY
GEOLOGICAL SURVEY LIBRARY
WINDHOEK
Class: NAM SUR P48
Access No.: 1733